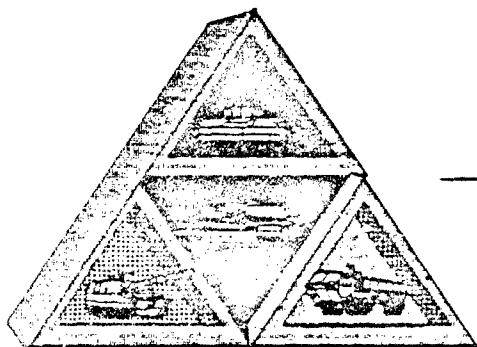


AD-A265 255



20030226119

ARDEC



Technical Report

No. 13568

DTIC

ELECTE
MAY 14 1993

S

E

D

Luminance, Contrast and Polarization of White Light
Reflected from Ground Combat Vehicles

May, 1990 - July, 1992

93 5 00 100

93-1016



By

Roy M. Matchko
Grant R. Gerhart

Approved for public release.
Distribution is unlimited.



U.S. Army Tank-Automotive Command
Research, Development, and Engineering Center
Warren, Michigan 48397-5000

NOTICES

This report is not to be construed as an official Department of the Army position:

Mention of any trade names or manufacturers in this report shall not be construed as an official endorsement or approval of such products or companies by the U.S. Government.

DTIC QUALITY INSPECTED 8

Accession For	
NTIS CRA&I	<input checked="checked" type="checkbox"/>
DTIC TAB	<input type="checkbox"/>
Unannounced	<input type="checkbox"/>
Justification	
By	
Distribution /	
Availability Codes	
Dist	Avail and/or Special
A-1	

Destroy this report when it is no longer needed. Do not return it to the originator.

REPORT DOCUMENTATION PAGE			Form Approved OMB No. 0704-0188	
<small>Public reporting burden for this collection of information is estimated to average 1 hour per response, including the time for reviewing instructions, searching existing data sources, gathering and maintaining the data needed, and completing and reviewing the collection of information. Send comments regarding this burden estimate or any other aspect of this collection of information, including suggestions for reducing this burden, to Washington Headquarters Services, Directorate for Information Operations and Reports, 1215 Jefferson Davis Highway, Suite 1204, Arlington, VA 22202-4302, and to the Office of Management and Budget, Paperwork Reduction Project (0704-0188), Washington, DC 20503.</small>				
1. AGENCY USE ONLY (Leave blank)	2. REPORT DATE June, 1992	3. REPORT TYPE AND DATES COVERED Final Report. July, 1990 - May, 1992		
4. TITLE AND SUBTITLE Luminance, Contrast and Polarization of White Light Reflected from Ground Combat Vehicles			5. FUNDING NUMBERS	
6. AUTHOR(S) Roy M. Matchko and Grant R. Gerhart				
7. PERFORMING ORGANIZATION NAME(S) AND ADDRESS(ES) U.S. Army Tank-Automotive Command AMSTA - RSA Warren, MI 48397-5000			8. PERFORMING ORGANIZATION REPORT NUMBER	
9. SPONSORING / MONITORING AGENCY NAME(S) AND ADDRESS(ES)			10. SPONSORING / MONITORING AGENCY REPORT NUMBER	
11. SUPPLEMENTARY NOTES				
12a. DISTRIBUTION / AVAILABILITY STATEMENT			12b. DISTRIBUTION CODE	
13. ABSTRACT (Maximum 200 words) This document presents the results of a comprehensive study for the luminance and polarization characteristics of three selected combat vehicles. The objective was to measure and analyze bi-directional reflectance data for the M60 tank, the Marine Corps amphibious Light Armored Vehicle (LAV25), the M1 tank and various background scenes. The goal was to understand the passive, visual signatures of these vehicles in terms of phenomenological parameters such as angles of incidence and reflection, polarization angles, material properties, diurnal changes, vehicle geometry and shape, and scene content. The primary illumination sources were the sun, sky and background reflections, and a laboratory xenon arc lamp. The analysis relied primarily upon the Fresnel equations for the polarization work and geometric optics for the luminance data. Important results include the identification of elevated vehicle regions as the primary sources of specular reflected solar illuminance, sky illumination as the principal source of intensely polarized reflected light, temporal variations in contrast across the target as a function of diurnal time period and vehicle orientation, and the aging characteristics of the chemical agent resistant coating (CARC) paints used on the vehicle surfaces. This work is volume one of an extended effort to analyze ground combat vehicle signatures.				
14. SUBJECT TERMS CARC paint, contrast, LAV25, luminance, M1, M60, polarization, reflectance			15. NUMBER OF PAGES 332	
			16. PRICE CODE	
17. SECURITY CLASSIFICATION OF REPORT Unclassified	18. SECURITY CLASSIFICATION OF THIS PAGE Unclassified	19. SECURITY CLASSIFICATION OF ABSTRACT Unclassified	20. LIMITATION OF ABSTRACT Unlimited	

NSN 7540-01-280-5500

Standard Form 298 (Rev 2-89)
Prescribed by ANSI Std Z39-18
298-102

ACKNOWLEDGEMENT

Mr. Matchko acknowledges the support of the Army Research Office (ARO) High School Science and Mathematics Faculty Program for providing the financial support to complete this work. In particular, he would like to thank Mr. Gary Hill from Battelle for facilitating both the summer and STAS academic year programs.

CONTENTS

FIGURES.	vii
TABLES.	xix
SUMMARY	1
INTRODUCTION	3
 M60 STUDIES	 8
Study 09 July, 1990	9
M60 Study of 12 July, 1990	13
M60 Study A on 17 July, 1990	16
M60 Study B on 17 July, 1990	19
SUMMARY OF M60 STUDIES.	22
 M1 STUDIES	 27
Study 19 July, 1990	27
M1 Study A on 19 July, 1990	30
M1 Study B on 19 July, 1990	33
Study 1 August, 1990	37
Study 6 August, 1990	53
SUMMARY OF M1 STUDIES	66
THE TURRET.	66
THE SKIRT.	69
TRACK AND SUSPENSION.	70
LUMINANCE DURING CLEAR SKIES.	71
CONTRAST DURING CLEAR SKIES.	75
RANGE.	79
PHOTOGRAPHIC DECEPTION.	80
LAV25 STUDIES.	85
Study 23 July, 1990	88
Study 24 July, 1990	92
Study 26 July, 1990	96
SUMMARY OF LAV25 STUDIES.	102
WHEEL AREAS.	102
AVERAGE LAV25 LUMINANCE	107
TREELINE LUMINANCE	108
CONTRAST.	110
SHADING.	112
 GLARE AND EDGE EFFECT.	 113

HORIZONTAL AND VERTICAL POLARIZATION OF THE MIA1.	117
ANALYSIS OF 20 JUNE, 1991 STUDY.	149
SUMMARY OF 20 JUNE, 1991 STUDY.	153
LUMINANCE, POLARIZATION AND CHROMATICITY	
STUDY ON 15 JULY, 1991.	154
ANALYSIS OF 15 JUNE, 1991 STUDY.	193
SUMMARY OF CHROMATICITY STUDY.	195
LUMINANCE OF NEW AND OLD CARC PAINTED SURFACES	196
ANALYSIS AND SUMMARY OF NEW/OLD CARC SURFACE STUDY	202
GONIOPHOTOMETRIC STUDIES OF A CARC PAINTED SURFACE.	203
AZIMUTHAL STUDY.	203
SUMMARY.	205
GONIOPHOTOMETRIC READINGS IN THE PLANE OF INCIDENCE. . .	206
SUMMARY.	218
GONIOPHOTOMETRIC READINGS PERPENDICULAR TO	
THE PLANE OF INCIDENCE.	219
SUMMARY.	226
LUMINANCE FROM A CARC PAINTED SAMPLE USING	
XENON LIGHT.	227
SUMMARY.	230
POLARIZATION AXIS OF REFLECTED WHITE LIGHT FROM	
A CARC PAINTED SAMPLE.	234
FRESNEL MODEL.	241
SUMMARY.	278
CONCLUSIONS.	281
LUMINANCE.	281
CONTRAST.	283
POLARIZATION.	285
CHROMATICITY.	287
RECOMMENDATIONS.	288
APPENDIX A - OPTICAL DENSITY AND TRANSMITTANCE.	289
APPENDIX B - POLARIZATION AXIS FINDER.	295
APPENDIX C - THE ASTONOMICAL TRIANGLE.	297
APPENDIX D - ANGLE BETWEEN SUN'S RAYS AND PLANE.	301
APPENDIX E - EQUATIONS FOR REFLECTED SUN RAY.	303

FIGURES

Figure 1.	Minolta Luminance Meter LS-100 and Data Printer DF-10	4
Figure 2.	Setup Used to Obtain Luminance Readings for M60 Studies	8
Figure 3.	Position and Area of Luminance Readings for M60 Studies	9
Figure 4.	M60 Tank Luminance (09 Jul 90)	10
Figure 5.	Background Luminance (09 Jul 90)	10
Figure 6.	Contrast between M60 and Sky (09 Jul 90)	11
Figure 7.	Contrast between M60 and Concrete (09 Jul 90)	11
Figure 8.	Contrast between M60 and Dirt-Gravel (09 Jul 90)	11
Figure 9.	Contrast between M60 and Grass (09 Jul 90)	11
Figure 10.	M60 Tank Luminance (12 Jul 90)	13
Figure 11.	Background Luminance(12 Jul 90)	13
Figure 12.	Contrast between M60 and Sky (12 Jul 90)	14
Figure 13.	Contrast between M60 and Concrete (12 Jul 90)	14
Figure 14.	Contrast between M60 and Dirt-Gravel (12 Jul 90)	14
Figure 15.	Contrast between M60 and Grass (12 Jul 90)	14
Figure 16.	M60 Tank Luminance (17 Jul 90)	16
Figure 17.	Background Luminance(17 Jul 90)	16
Figure 18.	Contrast between M60 and Sky (17 Jul 90)	17
Figure 19.	Contrast between M60 and Concrete (17 Jul 90)	17
Figure 20.	Contrast between M60 and Dirt-Gravel (17 Jul 90)	17
Figure 21.	Contrast between M60 and Grass (17 Jul 90)	17
Figure 22.	Position and Area of Lum,inance Readings for M60 Study B (17 Jul 90)	19
Figure 23.	M60 Luminance at 10:35 (17 Jul 90 Study B)	19
Figure 24.	Contrast between M60 and Grass at 10:35 (17 Jul 90 Study B)	19
Figure 25.	M60 Luminance at 10:35 (17 Jul 90 Study B)	21
Figure 26.	M60 Luminance at 11:35 (17 Jul 90 Study B)	21
Figure 27.	Contrast between M60 and Grass at 10:35 (17 Jul 90 Study B)	21
Figure 28.	Contrast between M60 and Grass at 11:35 (17 Jul 90 Study B)	21
Figure 29.	M60 Luminance Ratios (12 Jul 90)	24
Figure 30.	M60 Luminance Ratios (17 Jul 90)	24
Figure 31.	Contrast between M60 and Trees (09 Jul 90)	26
Figure 32.	Contrast between M60 and Trees (12 Jul 90)	26
Figure 33.	Contrast between M60 and Trees (17 Jul 90)	26
Figure 34.	MI Luminance Reading Setup for Study A and Study B on 19 Jul 90	28
Figure 35.	Position and Area of MI Luminance Readings for Study A (19 Jul 90)	29
Figure 36.	Position and Area of MI Luminance Readings for Study B (19 Jul 90)	29
Figure 37.	MI Luminance (19 Jul 90)	30
Figure 38.	Background Luminance(19 Jul 90)	30
Figure 39.	Contrast between MI and Sky (19 Jul 90)	31
Figure 40.	Contrast between MI and Concrete (19 Jul 90)	31
Figure 41.	Contrast between MI and Dirt-Gravel (19 Jul 90)	31
Figure 42.	Contrast between MI and Grass (19 Jul 90)	31

Figure 43.	M1 Luminance at 10:05 (19 Jul 90)	33
Figure 44.	M1 Luminance at 10:35 (19 Jul 90)	33
Figure 45.	M1 Luminance at 11:05 (19 Jul 90)	33
Figure 46.	M1 Luminance at 11:35 (19 Jul 90)	33
Figure 47.	M1 Luminance at 12:05 (19 Jul 90)	34
Figure 48.	M1 Luminance at 12:35 (19 Jul 90)	34
Figure 49.	M1 Luminance at 13:05 (19 Jul 90)	34
Figure 50.	M1 Luminance at 13:35 (19 Jul 90)	34
Figure 51.	M1 Luminance at 14:05 (19 Jul 90)	35
Figure 52.	M1 Luminance at 14:35 (19 Jul 90)	35
Figure 53.	M1 Luminance at 15:05 (19 Jul 90)	35
Figure 54.	Average M1 Luminance between 10:05 and 15:05 (19 Jul 90)	35
Figure 55.	Contrast between M1 and Trees (19 Jul 90) Study A	36
Figure 56.	Average Contrast (19 Jul 90) Study B	36
Figure 57.	M1 Luminance Study B (19 Jul 90)	36
Figure 58.	Position and Surroundings of M1 for Studies 1 Aug 90 and 6 Aug 90	37
Figure 59.	M1 Measurement Area (1 Aug 90 and 6 Aug 90). Range 36 feet	38
Figure 60.	M1 Measurement Area (1 Aug 90 and 6 Aug 90). Range 100 feet	38
Figure 61.	M1 Measurement Area (1 Aug 90 and 6 Aug 90). Range 200 feet	39
Figure 62.	M1 Measurement Area (1 Aug 90 and 6 Aug 90). Range 330 feet	39
Figure 63.	M1 Luminance at 10:00 (1 Aug 90). Range 36 feet	40
Figure 64.	M1 Luminance at 11:00 (1 Aug 90). Range 36 feet	40
Figure 65.	M1 Luminance at 12:00 (1 Aug 90). Range 36 feet	40
Figure 66.	M1 Luminance at 13:00 (1 Aug 90). Range 36 feet	40
Figure 67.	M1 Luminance at 14:00 (1 Aug 90). Range 36 feet	41
Figure 68.	M1 Luminance at 15:00 (1 Aug 90). Range 36 feet	41
Figure 69.	Average M1 Luminance (1 Aug 90). 10:00-15:00. Range 36 feet	41
Figure 70.	M1 Luminance at 10:10 (1 Aug 90). Range 100 feet	42
Figure 71.	M1 Luminance at 11:10 (1 Aug 90). Range 100 feet	42
Figure 72.	M1 Luminance at 12:10 (1 Aug 90). Range 100 feet	42
Figure 73.	M1 Luminance at 13:10 (1 Aug 90). Range 100 feet	42
Figure 74.	M1 Luminance at 14:10 (1 Aug 90). Range 100 feet	43
Figure 75.	M1 Luminance at 15:10 (1 Aug 90). Range 100 feet	43
Figure 76.	Average M1 Luminance (1 Aug 90). 10:10-15:10. Range 100 feet	43
Figure 77.	Average M1 Luminance (1 Aug 90). Different Ranges	44
Figure 78.	Average Luminance of Trees (1 Aug 90). Different Ranges	44
Figure 79.	Luminance of Grass (1 Aug 90). Different Ranges	44
Figure 80.	Luminance of Sky (1 Aug 90). Different Ranges	44
Figure 81.	Average Contrast of M1/Trees (1 Aug 90). Different Ranges	45
Figure 82.	Average Contrast of M1/Grass (1 Aug 90). Different Ranges	45
Figure 83.	Average Contrast of M1/Sky (1 Aug 90). Different Ranges	45
Figure 84.	Average Contrast of M1/Trees/Grass/Sky (1 Aug 90). Range 36 feet	46
Figure 85.	Average Contrast of M1/Trees/Grass/Sky (1 Aug 90). Range 100 feet	46
Figure 86.	Average Contrast of M1/Trees/Grass/Sky (1 Aug 90). Range 200 feet	46

Figure 87.	Average Contrast of M1/Trees/Grass/Sky (1 Aug 90). Range 330 feet	46
Figure 88.	Photograph of M1 on 1 Aug 90 at 10:00	47
Figure 89.	Photograph of M1 on 1 Aug 90 at 11:00	47
Figure 90.	Photograph of M1 on 1 Aug 90 at 12:00	47
Figure 91.	Photograph of M1 on 1 Aug 90 at 13:00	47
Figure 92.	Photograph of M1 on 1 Aug 90 at 14:00	47
Figure 93.	Photograph of M1 on 1 Aug 90 at 15:00	47
Figure 94.	M1 Luminance at 10:00 (6 Aug 90). Range 36 feet	54
Figure 95.	M1 Luminance at 11:00 (6 Aug 90). Range 36 feet	54
Figure 96.	M1 Luminance at 12:00 (6 Aug 90). Range 36 feet	54
Figure 97.	M1 Luminance at 13:00 (6 Aug 90). Range 36 feet	54
Figure 98.	M1 Luminance at 14:00 (6 Aug 90). Range 36 feet	55
Figure 99.	M1 Luminance at 15:00 (6 Aug 90). Range 36 feet	55
Figure 100.	Average M1 Luminance (6 Aug 90). 10:00-15:00. Range 36 feet	55
Figure 101.	M1 Luminance at 10:10 (6 Aug 90). Range 100 feet	56
Figure 102.	M1 Luminance at 11:10 (6 Aug 90). Range 100 feet	56
Figure 103.	M1 Luminance at 12:10 (6 Aug 90). Range 100 feet	56
Figure 104.	M1 Luminance at 13:10 (6 Aug 90). Range 100 feet	56
Figure 105.	M1 Luminance at 14:10 (6 Aug 90). Range 100 feet	57
Figure 106.	M1 Luminance at 15:10 (6 Aug 90). Range 100 feet	57
Figure 107.	Average M1 Luminance (6 Aug 90). 10:10-15:10. Range 100 feet	57
Figure 108.	Average M1 Luminance (6 Aug 90). Different Ranges	58
Figure 109.	Average Luminance of Trees (6 Aug 90). Different Ranges	58
Figure 110.	Luminance of Grass (6 Aug 90). Different Ranges	58
Figure 111.	Luminance of Sky (6 Aug 90). Different Ranges	58
Figure 112.	Average Contrast of M1/Trees (6 Aug 90). Different Ranges	59
Figure 113.	Average Contrast of M1/Grass (6 Aug 90). Different Ranges	59
Figure 114.	Average Contrast of M1/Sky (6 Aug 90). Different Ranges	59
Figure 115.	Average Contrast of M1/Trees/Grass/Sky (6 Aug 90). Range 36 feet	60
Figure 116.	Average Contrast of M1/Trees/Grass/Sky (6 Aug 90). Range 100 feet	60
Figure 117.	Average Contrast of M1/Trees/Grass/Sky (6 Aug 90). Range 200 feet	60
Figure 118.	Average Contrast of M1/Trees/Grass/Sky (6 Aug 90). Range 330 feet	60
Figure 119.	Average M1 Luminance (19 Jul 90). 10:05-15:05. Range 36 feet	67
Figure 120.	Average M1 Luminance (1 Aug 90). 10:00-15:00. Range 36 feet	67
Figure 121.	Average M1 Luminance (6 Aug 90). 10:00-15:00. Range 36 feet	67
Figure 122.	Contrast of M1 Targets/Trees (1 Aug 90). Range 36 feet	73
Figure 123.	Contrast of M1 Targets/Grass (1 Aug 90). Range 36 feet	73
Figure 124.	Contrast of M1 Targets/Sky (1 Aug 90). Range 36 feet	73
Figure 125.	Average M1 Target Luminance (1 Aug 90). Range 36 feet	73
Figure 126.	Contrast of M1 Targets/Trees (1 Aug 90). Range 100 feet	74
Figure 127.	Contrast of M1 Targets/Grass (1 Aug 90). Range 100 feet	74
Figure 128.	Contrast of M1 Targets/Sky (1 Aug 90). Range 100 feet	74
Figure 129.	Average M1 Target Luminance (1 Aug 90). Range 100 feet	74
Figure 130.	Contrast of M1 Targets/Trees (19 Jul 90). Range 36 feet	77

Figure 131.	Contrast of M1 Targets/Grass (19 Jul 90). Range 36 feet	77
Figure 132.	Contrast of M1 Targets/Sky (19 Jul 90). Range 36 feet	77
Figure 133.	Average M1 Target Luminance (19 Jul 90). Range 36 feet	77
Figure 134.	Contrast of M1 Targets/Trees (6 Aug 90). Range 36 feet	78
Figure 135.	Contrast of M1 Targets/Grass (6 Aug 90). Range 36 feet	78
Figure 136.	Contrast of M1 Targets/Sky (6 Aug 90). Range 36 feet	78
Figure 137.	Average M1 Target Luminance (6 Aug 90). Range 36 feet	78
Figure 138.	Complete, Uncropped Scene of Figure 92	81
Figure 139.	Complete, Uncropped Scene of Figure 93	81
Figure 140.	Checker Board Grid with Equal Number of Black and White Squares	83
Figure 141.	Photograph of Figure 140	83
Figure 142.	Checker Board Grid with Three Black Squares and Thirty White Squares	84
Figure 143.	Photograph of Figure 142	84
Figure 144.	Position and Surroundings of the LAV25	85
Figure 145.	LAV25 Measurement Area. Range 36 feet	86
Figure 146.	LAV25 Measurement Area. Range 100 feet	86
Figure 147.	LAV25 Measurement Area. Range 200 feet	87
Figure 148.	LAV25 Measurement Area. Range 330 feet	87
Figure 149.	LAV25 Luminance at 10:00 (23 Jul 90). Range 36 feet	88
Figure 150.	LAV25 Luminance at 10:30 (23 Jul 90). Range 36 feet	88
Figure 151.	LAV25 Luminance at 11:30 (23 Jul 90). Range 36 feet	88
Figure 152.	LAV25 Luminance at 12:45 (23 Jul 90). Range 36 feet	88
Figure 153.	LAV25 Luminance at 13:30 (23 Jul 90). Range 36 feet	89
Figure 154.	LAV25 Luminance at 14:05 (23 Jul 90). Range 36 feet	89
Figure 155.	Average Luminance of LAV25 and Trees (23 Jul 90). Range 36 feet	89
Figure 156.	Average Contrast of LAV25/Trees (23 Jul 90). Range 36 feet	89
Figure 157.	LAV25 Luminance at 10:45 (23 Jul 90). Range 100 feet	90
Figure 158.	LAV25 Luminance at 11:45 (23 Jul 90). Range 100 feet	90
Figure 159.	LAV25 Luminance at 13:00 (23 Jul 90). Range 100 feet	90
Figure 160.	LAV25 Luminance at 13:30 (23 Jul 90). Range 100 feet	90
Figure 161.	LAV25 Luminance at 14:14 (23 Jul 90). Range 100 feet	91
Figure 162.	LAV25 Average Luminance (23 Jul 90). Different Ranges	91
Figure 163.	LAV25 Luminance at 9:00 (24 Jul 90). Range 36 feet	92
Figure 164.	LAV25 Luminance at 9:30 (24 Jul 90). Range 36 feet	92
Figure 165.	LAV25 Luminance at 10:00 (24 Jul 90). Range 36 feet	92
Figure 166.	LAV25 Luminance at 10:30 (24 Jul 90). Range 36 feet	92
Figure 167.	LAV25 Luminance at 11:00 (24 Jul 90). Range 36 feet	93
Figure 168.	Average LAV25 and Background Luminance (24 Jul 90). Range 36 feet	93
Figure 169.	Tree Line Luminance (24 Jul 90). Range 36 feet and 200 feet	93
Figure 170.	Average Contrast of LAV25/Grass/Concrete/Sky/Trees (24 Jul 90).	93
Figure 171.	LAV25 Luminance at 9:15 (24 Jul 90). Range 100 feet	94
Figure 172.	LAV25 Luminance at 9:45 (24 Jul 90). Range 100 feet	94
Figure 173.	LAV25 Luminance at 10:15 (24 Jul 90). Range 100 feet	94
Figure 174.	LAV25 Luminance at 10:45 (24 Jul 90). Range 100 feet	94

Figure 175.	LAV25 Luminance at 11:15 (24 Jul 90). Range 100 feet	9
Figure 176.	Average LAV25 Luminance (24 Jul 90). Different Ranges	9
Figure 177.	Average Contrast of LAV25/Trees (24 Jul 90). 36 feet and 200 feet	9
Figure 178.	LAV25 Luminance at 9:30 (26 Jul 90). Range 36 feet	9
Figure 179.	LAV25 Luminance at 10:30 (26 Jul 90). Range 36 feet	9
Figure 180.	LAV25 Luminance at 11:30 (26 Jul 90). Range 36 feet	9
Figure 181.	LAV25 Luminance at 12:30 (26 Jul 90). Range 36 feet	9
Figure 182.	LAV25 Luminance at 13:30 (26 Jul 90). Range 36 feet	9
Figure 183.	LAV25 Luminance at 14:30 (26 Jul 90). Range 36 feet	9
Figure 184.	Average LAV25 Luminance (26 Jul 90). Different Ranges	9
Figure 185.	Average Tree Line Luminance (26 Jul 90). Different Ranges	9
Figure 186.	LAV25 Luminance at 9:40 (26 Jul 90). Range 100 feet	9
Figure 187.	LAV25 Luminance at 10:40 (26 Jul 90). Range 100 feet	9
Figure 188.	LAV25 Luminance at 11:40 (26 Jul 90). Range 100 feet	9
Figure 189.	LAV25 Luminance at 12:40 (26 Jul 90). Range 100 feet	9
Figure 190.	LAV25 Luminance at 13:40 (26 Jul 90). Range 100 feet	9
Figure 191.	LAV25 Luminance at 14:40 (26 Jul 90). Range 100 feet	9
Figure 192.	Luminance of Grass (26 Jul 90). Different Ranges	9
Figure 193.	Luminance of Sky (26 Jul 90). Different Ranges	9
Figure 194.	Average Contrast of LAV25/Trees (26 Jul 90). Different Ranges	10
Figure 195.	Average Contrast of LAV25/Grass (26 Jul 90). Different Ranges	10
Figure 196.	Average Contrast of LAV25/Sky (26 Jul 90). Different Ranges	10
Figure 197.	Average Contrast of LAV25/Concrete (26 Jul 90). Different Ranges	10
Figure 198.	Photograph of LAV25 on 26 Jul 90 at 9:30	10
Figure 199.	Photograph of LAV25 on 26 Jul 90 at 10:30	10
Figure 200.	Photograph of LAV25 on 26 Jul 90 at 11:30	10
Figure 201.	Photograph of LAV25 on 26 Jul 90 at 12:30	10
Figure 202.	Photograph of LAV25 on 26 Jul 90 at 13:30	10
Figure 203.	Photograph of LAV25 on 26 Jul 90 at 14:30	10
Figure 204.	Average LAV25 Area Luminance (23 Jul 90). Range 36 feet	10
Figure 205.	Average LAV25 Luminance Ratios (23 Jul 90). Range 36 feet	10
Figure 206.	Average LAV25 Area Luminance (23 Jul 90). Range 100 feet	10
Figure 207.	Average LAV25 Luminance Ratios (23 Jul 90). Range 100 feet	10
Figure 208.	Average LAV25 Area Luminance (24 Jul 90). Range 36 feet	10
Figure 209.	Average LAV25 Luminance Ratios (24 Jul 90). Range 36 feet	10
Figure 210.	Average LAV25 Area Luminance (24 Jul 90). Range 100 feet	10
Figure 211.	Average LAV25 Luminance Ratios (24 Jul 90). Range 100 feet	10
Figure 212.	Average LAV25 Area Luminance (26 Jul 90). Range 36 feet	10
Figure 213.	Average LAV25 Luminance Ratios (26 Jul 90). Range 36 feet	10
Figure 214.	Average LAV25 Area Luminance (26 Jul 90). Range 100 feet	10
Figure 215.	Average LAV25 Luminance Ratios (26 Jul 90). Range 100 feet	10
Figure 216.	LAV25 Turret Area at 14:30 on 26 Jul 90	11
Figure 217.	M113A3. Viewing Toward the North	114
Figure 218.	M113A3. Viewing Toward the Southwest	114

Figure 219.	Photograph of Side of M113A3. No Polaroid in Front of Camera	115
Figure 220.	Photograph of Side of M113A3. Polaroid in Front of Camera	115
Figure 221.	Photograph of Top of M113A3. No Polaroid in Front of Camera	116
Figure 222.	Photograph of Top of M113A3. Polaroid in Front of Camera	116
Figure 223.	Positioning of Polarizer in Front of LS-100	117
Figure 224.	Measurement Areas on M1A1	117
Figure 225.	M1A1 at 08:30	118
Figure 226.	M1A1 at 09:00	118
Figure 227.	M1A1 at 09:30	118
Figure 228.	M1A1 at 10:00	119
Figure 229.	M1A1 at 10:30	119
Figure 230.	M1A1 at 11:00	119
Figure 231.	M1A1 at 11:30	120
Figure 232.	M1A1 at 12:00	120
Figure 233.	M1A1 at 12:30	120
Figure 234.	M1A1 at 13:00	121
Figure 235.	M1A1 at 13:30	121
Figure 236.	M1A1 at 14:00	121
Figure 237.	M1A1 at 14:30	122
Figure 238.	M1A1 at 15:00	122
Figure 239.	M1A1 at 15:30	122
Figure 240.	M1A1 at 16:00	123
Figure 241.	M1 LUMINANCE AT 08:00 (20 JUN 91)	127
Figure 242.	M1 LUMINANCE AT 09:00 (20 JUN 91)	127
Figure 243.	M1 LUMINANCE AT 09:30 (20 JUN 91)	127
Figure 244.	M1 LUMINANCE AT 10:00 (20 JUN 91)	127
Figure 245.	M1 LUMINANCE AT 10:30 (20 JUN 91)	128
Figure 246.	M1 LUMINANCE AT 11:00 (20 JUN 91)	128
Figure 247.	M1 LUMINANCE AT 11:30 (20 JUN 91)	128
Figure 248.	M1 LUMINANCE AT 12:00 (20 JUN 91)	128
Figure 249.	M1 LUMINANCE AT 12:30 (20 JUN 91)	129
Figure 250.	M1 LUMINANCE AT 13:00 (20 JUN 91)	129
Figure 251.	M1 LUMINANCE AT 13:30 (20 JUN 91)	129
Figure 252.	M1 LUMINANCE AT 14:00 (20 JUN 91)	129
Figure 253.	M1 LUMINANCE AT 14:30 (20 JUN 91)	130
Figure 254.	M1 LUMINANCE AT 15:00 (20 JUN 91)	130
Figure 255.	M1 LUMINANCE AT 15:30 (20 JUN 91)	130
Figure 256.	M1 LUMINANCE AT 16:00 (20 JUN 91)	130
Figure 257.	LUMINANCE RATIO (L_v/L_n). AREA #1 (20 JUN 91)	132
Figure 258.	LUMINANCE RATIO (L_v/L_n). AREA #2 (20 JUN 91)	132
Figure 259.	LUMINANCE RATIO (L_v/L_n). AREA #3 (20 JUN 91)	132
Figure 260.	LUMINANCE RATIO (L_v/L_n). AREA #4 (20 JUN 91)	132
Figure 261.	LUMINANCE RATIO (L_v/L_n). AREA #5 (20 JUN 91)	133

Figure 262.	LUMINANCE RATIO (LV/Ln).	AREA #6 (20 JUN 91)	133
Figure 263.	LUMINANCE RATIO (LV/Ln).	AREA #7 (20 JUN 91)	133
Figure 264.	LUMINANCE RATIO (LV/Ln).	AREA #8 (20 JUN 91)	133
Figure 265.	LUMINANCE RATIO (LV/Ln).	AREA #9 (20 JUN 91)	134
Figure 266.	LUMINANCE RATIO (LV/Ln).	AREA #10 (20 JUN 91)	134
Figure 267.	LUMINANCE RATIO (LV/Ln).	AREA #11 (20 JUN 91)	134
Figure 268.	LUMINANCE RATIO (LV/Ln).	AREA #12 (20 JUN 91)	134
Figure 269.	LUMINANCE RATIO (LV/Ln).	AREA #13 (20 JUN 91)	135
Figure 270.	LUMINANCE RATIO (LV/Ln).	AREA #14 (20 JUN 91)	135
Figure 271.	LUMINANCE RATIO (LV/Ln).	AREA #15 (20 JUN 91)	135
Figure 272.	LUMINANCE RATIO (Lh/Ln).	AREA #1 (20 JUN 91)	137
Figure 273.	LUMINANCE RATIO (Lh/Ln).	AREA #2 (20 JUN 91)	137
Figure 274.	LUMINANCE RATIO (Lh/Ln).	AREA #3 (20 JUN 91)	137
Figure 275.	LUMINANCE RATIO (Lh/Ln).	AREA #4 (20 JUN 91)	137
Figure 276.	LUMINANCE RATIO (Lh/Ln).	AREA #5 (20 JUN 91)	138
Figure 277.	LUMINANCE RATIO (Lh/Ln).	AREA #6 (20 JUN 91)	138
Figure 278.	LUMINANCE RATIO (Lh/Ln).	AREA #7 (20 JUN 91)	138
Figure 279.	LUMINANCE RATIO (Lh/Ln).	AREA #8 (20 JUN 91)	138
Figure 280.	LUMINANCE RATIO (Lh/Ln).	AREA #9 (20 JUN 91)	139
Figure 281.	LUMINANCE RATIO (Lh/Ln).	AREA #10 (20 JUN 91)	139
Figure 282.	LUMINANCE RATIO (Lh/Ln).	AREA #11 (20 JUN 91)	139
Figure 283.	LUMINANCE RATIO (Lh/Ln).	AREA #12 (20 JUN 91)	139
Figure 284.	LUMINANCE RATIO (Lh/Ln).	AREA #13 (20 JUN 91)	140
Figure 285.	LUMINANCE RATIO (Lh/Ln).	AREA #14 (20 JUN 91)	140
Figure 286.	LUMINANCE RATIO (Lh/Ln).	AREA #15 (20 JUN 91)	140
Figure 287.	LUMINANCE DIFFERENCE (Lh-LV).	AREA #1 (20 JUN 91)	142
Figure 288.	LUMINANCE DIFFERENCE (Lh-LV).	AREA #2 (20 JUN 91)	142
Figure 289.	LUMINANCE DIFFERENCE (Lh-LV).	AREA #3 (20 JUN 91)	142
Figure 290.	LUMINANCE DIFFERENCE (Lh-LV).	AREA #4 (20 JUN 91)	142
Figure 291.	LUMINANCE DIFFERENCE (Lh-LV).	AREA #5 (20 JUN 91)	143
Figure 292.	LUMINANCE DIFFERENCE (Lh-LV).	AREA #6 (20 JUN 91)	143
Figure 293.	LUMINANCE DIFFERENCE (Lh-LV).	AREA #7 (20 JUN 91)	143
Figure 294.	LUMINANCE DIFFERENCE (Lh-LV).	AREA #8 (20 JUN 91)	143
Figure 295.	LUMINANCE DIFFERENCE (Lh-LV).	AREA #9 (20 JUN 91)	144
Figure 296.	LUMINANCE DIFFERENCE (Lh-LV).	AREA #10 (20 JUN 91)	144
Figure 297.	LUMINANCE DIFFERENCE (Lh-LV).	AREA #11 (20 JUN 91)	144
Figure 298.	LUMINANCE DIFFERENCE (Lh-LV).	AREA #12 (20 JUN 91)	144
Figure 299.	LUMINANCE DIFFERENCE (Lh-LV).	AREA #13 (20 JUN 91)	145
Figure 300.	LUMINANCE DIFFERENCE (Lh-LV).	AREA #14 (20 JUN 91)	145
Figure 301.	LUMINANCE DIFFERENCE (Lh-LV).	AREA #15 (20 JUN 91)	145
Figure 302.	LUMINANCE DIFFERENCE (Lh-LV).	LEFT SIDE OF MI TURRET	146
Figure 303.	LUMINANCE DIFFERENCE (Lh-LV).	MIDDLE OF MI TURRET	147
Figure 304.	LUMINANCE DIFFERENCE (Lh-LV).	RIGHT SIDE OF MI TURRET	148
Figure 305.	MIN POLARIZATION ANGLE - MIAI FACETS		150

Figure 306.	MAX POLARIZATION ANGLE - MIA1 FACETS	150
Figure 307.	The Eastern Hemispherical Sky at 30° Altitude	152
Figure 308.	MIA1, LS-100 and CS-100 Positions for 15 July, 1991 Study	154
Figure 309.	Location of the Grass Area Metered on 15 July, 1991	155
Figure 310.	Location of the Tree Areas Metered on 15 July, 1991	155
Figure 311.	LUMINANCE OF AREA #12 (15 JUL 91)	158
Figure 312.	LUMINANCE OF AREA #13 (15 JUL 91)	159
Figure 313.	LUMINANCE OF AREA #15 (15 JUL 91)	160
Figure 314.	LUMINANCE OF MIA1 FACETS (15 JUL 91)	161
Figure 315.	MIN POLARIZATION ANGLE - MIA1 FACETS	162
Figure 316.	MAX POLARIZATION ANGLE - MIA1 FACETS	163
Figure 317.	L_{\min}/L_n POLARIZATION RATIO - MIA1 FACETS	166
Figure 318.	L_{\max}/L_n POLARIZATION RATIO - MIA1 FACETS	167
Figure 319.	L_{\min}/L_{\max} POLARIZATION RATIO - MIA1 FACETS	168
Figure 320.	DEGREE OF POLARIZATION - MIA1 FACETS	169
Figure 321.	POLARIZATION MIN - MAX DIFFERENCE - MIA1 FACETS	170
Figure 322.	MIN - MAX POLARIZATION ANGLE DIFFERENCE (enlarged)	171
Figure 323.	MIN - MAX POLARIZATION ANGLE DIFFERENCE	172
Figure 324.	ALTITUDE AND AZIMUTH (15 JUL 91)	177
Figure 325.	ANGLE BETWEEN I AND METER	178
Figure 326.	DIURNAL CHANGES IN $\langle i \rangle$ AND $\langle RL \rangle$. AREA #12	179
Figure 327.	DIURNAL CHANGES IN $\langle i \rangle$ AND $\langle RL \rangle$. AREA #13	180
Figure 328.	DIURNAL CHANGES IN $\langle i \rangle$ AND $\langle RL \rangle$. AREA #15	181
Figure 329.	LUMINANCE vs ANGLE RL . MIA1 AREAS (15 JUL 91)	182
Figure 330.	LUMINANCE vs SUM METER ANGLE (15 JUL 91)	183
Figure 331.	LUMINANCE vs ANGLE OF INCIDENCE (15 JUL 91)	184
Figure 332.	LUMINANCE vs $\cos i$. MIA1 AREAS (15 JUL 91)	185
Figure 333.	LUMINANCE OF AREA #12, #13 and #15; LUMINANCE vs $\cos i$ (15 JUL 91)	186
Figure 334.	LUMINANCE OF MIA1 FACETS; LUMINANCE vs ANGLE OF INCIDENCE; LUMINANCE vs SUM METER ANGLE; LUMINANCE vs ANGLE RL (15 JUL 91)	187
Figure 335.	DIURNAL CHANGES IN $\langle i \rangle$ AND $\langle RL \rangle$. AREA #12; DIURNAL CHANGES IN $\langle i \rangle$ AND $\langle RL \rangle$. AREA #13; DIURNAL CHANGES IN $\langle i \rangle$ AND $\langle RL \rangle$. AREA #15; ANGLE BETWEEN I AND METER	188
Figure 336.	CHROMATICITY DIAGRAM. MIA1 AREA #12, #13, #15 and GRASS (15 JUL 91)	191
Figure 337.	CHROMATICITY DIAGRAM. TREE AREA #1, #2 and #3	192
Figure 338.	Camcorder with Rotating Linear Polarizer	194
Figure 339.	Position of CARC Painted Steel Plate (#12') Near Area #12	197
Figure 340.	Position of CARC Painted Steel Plate (#15') Near Area #15	197
Figure 341.	LUMINANCE OF AREA #12; MIA1 AND CARC SAMPLE	198

Figure 342.	LUMINANCE OF AREA #15; M1A1 AND CARC SAMPLE	199
Figure 343.	LUMINANCE RATIOS; M1A1/CARC SAMPLE	200
Figure 344.	LUMINANCE OF AREA #12; LUMINANCE OF AREA #15; LUMINANCE RATIOS; M1A1/CARC SAMPLE	201
Figure 345.	Experimental Setup for Azimuth Study	203
Figure 346.	GONIOPHOTOMETRIC RECORD OF CARC PAINTED STEEL PLATE	204
Figure 347.	Goniometric Support	206
Figure 348.	Allignment to the Plane of Incidence	206
Figure 349.	Goniometric Equipment for Readings in the Plane of Incidence	207
Figure 350.	Positive and Negative CARC Slopes	210
Figure 351.	Calculation of Meter Angle θ	211
Figure 352.	Calculation of the Angle of Incidence	212
Figure 353.	Area B = Area A/Cos i	212
Figure 354.	Luminance vs Cos i for Reflected Sunlight from CARC Sample. (Metering in the plane of incidence)	213
Figure 355.	Luminance vs Cos i . Meter \angle 's: 5°, 10° and 15°	214
Figure 356.	Luminance vs Cos i . Meter \angle 's: 20°, 25°, 30° and 35°	214
Figure 357.	Luminance vs Cos i . Meter \angle 's: 40°, 45°, 50° and 55°	214
Figure 358.	Luminance vs Cos i . Meter \angle 's: 60°, 65°, 70° and 75°	214
Figure 359.	Goniophotometric Record of CARC Sample. i \approx 90°	215
Figure 360.	Goniophotometric Record of CARC Sample. i \approx 85°	215
Figure 361.	Goniophotometric Record of CARC Sample. i \approx 80°	215
Figure 362.	Goniophotometric Record of CARC Sample. i \approx 75°	215
Figure 363.	Goniophotometric Record of CARC Sample. i \approx 70°	216
Figure 364.	Goniophotometric Record of CARC Sample. i \approx 65°	216
Figure 365.	Goniophotometric Record of CARC Sample. i \approx 60°	216
Figure 366.	Goniophotometric Record of CARC Sample. i \approx 55°	216
Figure 367.	Goniophotometric Record of CARC Sample. i \approx 50°	217
Figure 368.	Goniophotometric Record of CARC Sample. i \approx 45°	217
Figure 369.	Goniophotometric Record of CARC Sample. i \approx 40°	217
Figure 370.	Goniophotometric Record of CARC Sample. i \approx 35°	217
Figure 371.	Geometry for Calculating Meter Angle θ	223
Figure 372.	Luminance vs Cos i for Reflected Sunlight from CARC Sample (Metering perpendicular to the plane of incidence)	224
Figure 373.	Luminance vs Cos i . Meter \angle 's: 20°, 25°, 30° and 35°	225
Figure 374.	Luminance vs Cos i . Meter \angle 's: 0°, 5°, 10° and 15°	225
Figure 375.	Luminance vs Cos i . Meter \angle 's: -5°, -10°, -15° and -20°	225
Figure 376.	Luminance vs Cos i . Meter \angle 's: -25°, -30°, -35° and -40°	225
Figure 377.	Luminance vs Cos i . Meter \angle 's: -45°, -50°, -55°	226
Figure 378.	Geometry of Experimental Setup for Luminance From a CARC Painted Sample Using Xenon Light	227

Figure 379.	Photograph of Experimental Setup for Luminance From a CARC Painted Sample Using Xenon Light	227
Figure 380.	Geometry Defining α , β , γ and ψ	229
Figure 381.	Geometry Relating to Unit Vector R	229
Figure 382.	Geometry Relating to Rotation of Sample (α , β and ψ)	231
Figure 383.	Luminance vs $\cos i$ for Reflected Polarized Xenon Light from CARC Painted Sample	232
Figure 384.	Luminance vs $\cos i$ for Reflected Unpolarized Xenon Light from CARC Painted Sample	233
Figure 385.	Geometry of Experimental Setup for Polarization Axis of Reflected White Light from a CARC Painted Sample	234
Figure 386.	Photograph of Experimental Setup for Polarization Axis of Reflected White Light from a CARC Painted Sample	234
Figure 387.	Method for Measuring Polarizer Transmission Axis θ	235
Figure 388.	Use of Camera and Mirror to Measure azimuth angle α	235
Figure 389.	Method Used to Measure Azimuth Angle α	235
Figure 390.	Polarization Axis of Reflected Xe Light from CARC Painted Sample. $\theta = 0^\circ$ to 90° ; $\alpha = 180^\circ$ and 160°	236
Figure 391.	Polarization Axis of Reflected Xe Light from CARC Painted Sample. $\theta = 0^\circ$ to 90° ; $\alpha = 140^\circ$ and 120°	237
Figure 392.	Polarization Axis of Reflected Xe Light from CARC Painted Sample. $\theta = 0^\circ$ to 90° ; $\alpha = 100^\circ$ and 80°	238
Figure 393.	Polarization Axis of Reflected Xe Light from CARC Painted Sample. $\theta = 0^\circ$ to 90° ; $\alpha = 60^\circ$ and 40°	239
Figure 394.	Polarization Axis of Reflected Xe Light from CARC Painted Sample. $\theta = 0^\circ$ to 90° ; $\alpha = 20^\circ$	240
Figure 395.	Geometry Relating to Definition of ϕ , ψ , E , E_s , E_p , R , R_s and R_p	242
Figure 396.	Geometry Relating to Definition of I and r	242
Figure 397.	Geometry Relating to Description of E	243
Figure 398.	Geometry Relating to Definition of C and D	243
Figure 399.	ψ' vs θ for $\alpha = 180^\circ$	254
Figure 400.	ψ' vs θ for $\alpha = 160^\circ$	255
Figure 401.	ψ' vs θ for $\alpha = 140^\circ$	256
Figure 402.	ψ' vs θ for $\alpha = 120^\circ$	257
Figure 403.	ψ' vs θ for $\alpha = 100^\circ$	258
Figure 404.	ψ' vs θ for $\alpha = 80^\circ$	259
Figure 405.	ψ' vs θ for $\alpha = 60^\circ$	260
Figure 406.	ψ' vs θ for $\alpha = 40^\circ$	261
Figure 407.	ψ' vs θ for $\alpha = 20^\circ$	262
Figure 408.	Predicted Polarization Axis Values and Experimental Results	263
Figure 409.	Angular Difference between Predicted and Experimental Polarization Axis Values	263
Figure 410.	Relative Reflection Intensities; $n = 1.2$; $\alpha = 100^\circ - 180^\circ$	274
Figure 411.	Relative Reflection Intensities; $n = 1.2$; $\alpha = 20^\circ - 80^\circ$	275

Figure 412.	Relative Reflection Intensities; $n = 1.7$; $\alpha = 100^\circ - 180^\circ$	276
Figure 413.	Relative Reflection Intensities; $n = 1.7$; $\alpha = 20^\circ - 80^\circ$	277
Figure 414.	Macbeth TD 502 Densitometer	290
Figure 415.	Measuring Luminance of Polarized Light (Step 1)	291
Figure 416.	Measuring Luminance of Polarized Light (Step 2)	291
Figure 417.	Experimental Setup for Measuring Luminance of Polarized Light with the Minolta LS-100 Luminance Meter	291
Figure 418.	Measuring Luminance of Polarized Light (Step 1)	292
Figure 419.	Measuring Luminance of Polarized Light (Step 2)	292
Figure 420.	Measuring Luminance of Polarized Light (Step 3)	292
Figure 421.	Luminance vs Angle Between Axis of Polarizer	293
Figure 422.	Luminance Ratios vs Angle Between Axis of Polarizer	294
Figure 423.	The Axis Finder is a Polarizer with Circular Concentric Transmission Axes	295
Figure 424.	Axis Finder Used to Locate the Transmission Axis of a Linear Polarizer	295
Figure 425.	The Astronomical Triangle ZRP	296
Figure 426.	Astronomical Triangle, with Heavenly Body R West of Meridian	297
Figure 427.	Astronomical Triangle, with Heavenly Body R East of Meridian	297
Figure 428.	Spherical Triangle	298
Figure 429.	Angle Between Sun's Rays and Plane	300
Figure 430.	Case 1: Horizontal Surfaces ($S = \gamma = 0$)	307
Figure 431.	Case 2: Vertical Surfaces Facing South ($S = 90^\circ$, $\gamma = 0$)	308

TABLES

Table 1.	Summary of Study Content and Conditions (First Nine Studies)	5
Table 2.	Summary of M60 Luminance Readings for 9 July, 1990	10
Table 3.	Summary of M60 Contrast Calculations for 9 July, 1990	12
Table 4.	Summary of M60 Luminance Readings for 12 July, 1990	13
Table 5.	Summary of M60 Contrast Calculations for 12 July, 1990	15
Table 6.	Summary of M60 Luminance Readings for 17 July, 1990	16
Table 7.	Summary of M60 Contrast Calculations for 17 July, 1990	18
Table 8.	M60 Luminance Study for StudyB On 17 July, 1990	20
Table 9.	Largest Difference in M60 Luminance Readings for 9 July, 1990	23
Table 10.	Summary of M60 Luminance Readings (Excluding Study B of 17 Jul 90)	24
Table 11.	Summary of M1 Luminance Readings for Study A of 19 Jul y, 1990	30
Table 12.	Summary of M1 Contrast Calculations for Study A on 19 July, 1990	32
Table 13.	M1 Area Luminance Analysis for Times 10:00-15:00 on 1 Aug 90	48
Table 14.	M1 Area Luminance Analysis for Times 10:00-15:00 on 1 Aug 90	49
Table 15.	Average Tree Line Luminance on 1 Aug 90	49
Table 16.	Summary of M1 Diurnal Luminance Averages for 1 August, 1990	50
Table 17.	Analysis of M1 Turret Luminance Readings on 1 Aug 90. R = 36'	51
Table 18.	Analysis of M1 Turret Luminance Readings on 1 Aug 90. R = 100'	51
Table 19.	Analysis of M1 Skirt Luminance Readings on 1 Aug 90. R = 36'	52
Table 20.	Analysis of M1 Skirt Luminance Readings on 1 Aug 90. R = 100'	52
Table 21.	M1 Area Luminance Analysis for Times 10:00-15:30 on 6 Aug 90	61
Table 22.	M1 Area Luminance Analysis for Times 10:00-15:30 on 6 Aug 90	62
Table 23.	Average Tree Line Luminance on 6 Aug 90	62
Table 24.	Summary of M1 Diurnal Luminance Averages for 6 August, 1990	63
Table 25.	Analysis of M1 Turret Luminance Readings on 6 Aug 90. R = 36'	64
Table 26.	Analysis of M1 Turret Luminance Readings on 6 Aug 90. R = 100'	64
Table 27.	Analysis of M1 Skirt Luminance Readings on 6 Aug 90. R = 36'	65
Table 28.	Analysis of M1 Skirt Luminance Readings on 6 Aug 90. R = 100'	65
Table 29.	M1 Luminance Averages for Turret, Skirt and Tractor Areas. R=36'	66
Table 30.	Summary Analysis of M1 Turret Luminance Readings on 19 Jul 90	68
Table 31.	Summary Analysis of M1 Skirt Luminance Readings on 19 Jul 90	69
Table 32.	Summary Analysis of M1 Road Wheel Luminance Readings	70
Table 33.	M1, Tree and Grass Luminance Analysis for 1 Aug 90	71
Table 34.	Average Turret, Skirt and Road Wheel Luminance Analysis for 1 Aug 90. Range = 36 feet	72
Table 35.	Average Turret, Skirt and Road Wheel Luminance Analysis for 1 Aug 90. Range = 100 feet	72
Table 36.	M1 Contrast for Tree and Grass Backgrounds on 1 Aug 90.	75
Table 37.	Contrast Analysis of M1 Turret, Skirt and Road Wheels on 1 Aug 90. Range = 36 feet	76
Table 38.	Contrast Analysis of M1 Turret, Skirt and Road Wheels on 1 Aug 90. Range = 100 feet	76

Table 39.	Average MI Luminance for 1 Aug 90 for Different Ranges	79
Table 40.	Average Contrast of MI for 1 Aug 90 for Different Ranges	79
Table 41.	Contrast of LAV25 Wheels Using Surrounding Wheel Area as Background 23 July, 1990. Range = 36 feet	106
Table 42.	LAV25 Average Luminance Analysis. Range = 36 feet	107
Table 42.	LAV25 Average Luminance Analysis. Range = 36 feet	107
Table 43.	Average LAV25 Luminance on 26 July, 1990. Different Ranges	107
Table 44.	LAV25 Average Luminance Analysis for 26 Jul 90. Different Ranges	108
Table 45.	Average Treeline Luminance for 23 Jul 90 and 24 Jul 90	108
Table 46.	Summary and Analysis of Treeline Luminance for 26 Jul 90	109
Table 47.	Average LAV25 Luminance and Contrast for Ranges of 36 feet and 200 feet on 24 July, 1990	110
Table 48.	Summary of Average LAV25 Contrast Using a Treeline as a Background	110
Table 49.	Summary of Average LAV25 Contrast Using Grass as a Background	111
Table 50.	MIAl Luminance Ln (No Polarizer) on 20 June, 1991	124
Table 51.	MIAl Luminance Lv on 20 June, 1991 (Polarizer's Axis Vertical)	125
Table 52.	MIAl Luminance Lh on 20 June, 1991 (Polarizer's Axis Horizontal)	126
Table 53.	MIAl Luminance Ratio LV/Lh (20 Jun 91)	131
Table 54.	MIAl Luminance Ratio Lh/Ln (20 Jun 91)	136
Table 55.	MIAl Luminance Difference Lh - Lh (20 Jun 91)	141
Table 56.	Sun's Position and Angles of Incidence for 20 June, 1991	149
Table 57.	MIAl Luminance and Polarization Data for Area #12 (15 Jul 91)	156
Table 58.	MIAl Luminance and Polarization Data for Area #13 (15 Jul 91)	156
Table 59.	MIAl Luminance and Polarization Data for Area #15 (15 Jul 91)	157
Table 60.	MIAl Luminance and Polarization Calc. for Area #12 (15 Jul 91)	164
Table 61.	MIAl Luminance and Polarization Calc. for Area #13 (15 Jul 91)	164
Table 62.	MIAl Luminance and Polarization Calc. for Area #15 (15 Jul 91)	165
Table 63.	Sun's Position and Angles of Incidence for 15 July, 1991	173
Table 64.	Angles from Coordinate Axis for MIAl Area #12 on 15 July, 1991	174
Table 65.	Angles from Coordinate Axis for MIAl Area #13 on 15 July, 1991	175
Table 66.	Angles from Coordinate Axis for MIAl Area #15 on 15 July, 1991	176
Table 67.	CIE Coordinates for MIAl Facets on 15 July, 1991	189
Table 68.	CIE Coordinates for Grass and Trees on 15 July, 1991	190
Table 69.	Maximum Luminance for MIAl on 15 July, 1991	193
Table 70.	Luminance of MIAl (Area #12 and #13) and CARC-Painted Steel Plate on 31 July, 1991	196
Table 71.	Data for Azimuthal Study of 13 August, 1991	203
Table 72.	Luminance Readings When Metering Parallel to the Incident Plane on 15 July, 1991	208
Table 73.	Luminance Readings When Metering Parallel to the Incident Plane on 15 July, 1991; CARC Slope = 5° and 10°	208
Table 74.	Luminance Readings When Metering Parallel to the Incident Plane on 15 July, 1991; CARC Slope = 15° and -5°	208

Table 75.	Luminance Readings When Metering Parallel to the Incident Plane on 15 July, 1991; CARC Slope = -10° and -15°	209
Table 76.	Luminance Readings When Metering Parallel to the Incident Plane on 15 July, 1991; CARC Slope = -20° and -25°	209
Table 77.	Luminance Readings When Metering Parallel to the Incident Plane on 15 July, 1991; CARC Slope = -30° and -35°	209
Table 78.	Luminance Readings When Metering Parallel to the Incident Plane on 15 July, 1991; CARC Slope = -40° and -45°	210
Table 79.	Luminance Readings When Metering Parallel to the Incident Plane on 15 July, 1991; CARC Slope = -50° and -55°	210
Table 80.	Luminance Readings When Metering Parallel to the Incident Plane. Data Arranged According to Metering Angle θ .	211
Table 81.	Luminance Readings When Metering Parallel to the Incident Plane. Data Arranged According to Metering Angle θ .	212
Table 82.	Luminance Readings When Metering Perpendicular to the Incident Plane; CARC Slopes = 0° , 5° , 10° , 15° , 20° and 25°	220
Table 83.	Luminance Readings When Metering Perpendicular to the Incident Plane; CARC Slopes = 30° , 35° , 0° , -5° , -10° and -15°	221
Table 84.	Luminance Readings When Metering Perpendicular to the Incident Plane; CARC Slopes = -20° , -25° , -30° , -35° , -40° , -45° , -50° and -55°	222
Table 85.	Meter Angle θ as a Function of Rotation Angle ϕ	223
Table 86.	Luminance Readings from a CARC Painted Sample Using Xe Light. $\alpha = 40^\circ$; $\delta = 10^\circ$, 20° and 30°	228
Table 87.	Luminance Readings from a CARC Painted Sample Using Xe Light. $\alpha = 40^\circ$ and 60° ; $\delta = 0^\circ$	228
Table 88.	Angle β Between Meter and Sample	230
Table 89.	Orientation of Polarization Axis for Reflected Xe Light from a CARC Painted Sample	240
Table 90.	Degree of Polarization Axis from Horizontal (ψ) for Reflected Xe Light from a CARC Painted Sample	241
Table 91.	Calculations. $C+/C- = \cos(\phi+\phi')/\cos(\phi-\phi')$. $\psi' = \psi + \epsilon$	245
Table 92.	Calculations of Relative Intensities for Reflected Xe Light from a CARC-Painted Sample for $n = 1.2$	265
Table 93.	Calculations of Relative Intensities for Reflected Xe Light from a CARC-Painted Sample for $n = 1.7$	269
Table 94.	Range of Angles of Incidence i , Angles of Refraction r and Reflectances r_p and r_s	279
Table 95.	Approximate Average Luminance	282
Table 96.	Average M1 Contrast Using Tree and Grass Backgrounds on 1 August, 1990	284
Table 97.	Average LAV25 Contrast Using Tree and Grass Backgrounds on 1 August, 1990	284

Table 98.	Luminance (L) and Luminance Ratios Using Polarized and Unpolarized Light with the Minolta LS-100 Luminance Meter	290
Table 99.	Luminance (L) and Luminance Ratios Using Polarized Light with the Minolta LS-100 Luminance Meter	291

SUMMARY

The primary purpose of this work is to study the visual signature of several representative ground combat vehicles. The principal focus is the acquisition and analysis of luminance and polarization data for reflected light from the target and background surfaces. A major goal is to characterize vehicle visual signatures in terms of regions with high luminance contrast. These high contrast areas in turn increase vehicle detectability and in many cases become prominent cue features for threat observers. Three vehicles were selected for extensive data acquisition and analysis: the M60 tank, the Marine Corps amphibious Light Armored Vehicle (LAV25), and the M1 Abrahms tank. In addition, luminance reflectance measurements were made on several sample plates with chemical agent resistant coating (CARC) paints.

The scope of this work included several thousand luminance measurements for the three vehicles relative to sky, concrete, dirt-gravel, grass and tree backgrounds. Extensive measurements were made over the diurnal time period between 08:00 and 15:00 hours. Several different sky conditions including cloud cover, haze, overcast and clear were conducted during the summer months at the U.S. Army Tank-Automotive Command (TACOM) in Warren, Michigan. Luminance data was acquired for four different ranges at 30, 100, 200 and 330 feet. Several different vehicle orientations were used for diurnal data acquisition. Additional data included laboratory reflectance measurements using a xenon arc lamp on an optical table. Other investigations included a diurnal photographic record of relative contrast variations as a function of solar position and vehicle orientation.

The data acquisition process included point by point luminance measurements made with a Minolta luminance meter LS-100 with a one-degree acceptance angle. A polarization axis finder, consisting of circular concentric linear polarizers, determined quantitatively the polarization angle and qualitatively the degree of polarization. A diurnal record of the sky polarization was recorded using the polarization axis finder.

Additional investigations included a comparison of reflected luminance data for new and old CARC painted surfaces. Specifically, the older painted surfaces were approximately 25 percent brighter than a freshly-painted panel prepared in an otherwise identical fashion.

An analysis of the photographic data shows that many edges with high luminance contrast result from specular reflections. Furthermore, the specular reflected light is in many cases highly polarized. The specular glare is reduced by adjusting the transmission axis of the viewing polarizer perpendicular to the polarization vector of the reflected light. Similarly, the apparent edge contrast increases by adjusting the polarizer parallel to the polarization vector. Edges with different paint colors have similar specular reflection coefficients. The specular reflected light shows characteristics of "whitening" with very little absorption by the pigment material. Controlling edge contrast is important for limiting recognition and identification capabilities of threat observers.

A linear polarizer was attached to the shaft of small DC motor rotating at 32 rpm. The entire unit was positioned in front of a video camcorder to determine the angular position for minimum and maximum transmission through the polarization filter. When the degree of polarization is large, an "apparent flashing" was observed for the reflected light originating from certain regions on the vehicle. Subsequent analysis indicated that this phenomena was more pronounced on shaded regions not directly illuminated by the sun. The indirect sky illumination emanating 90° from the orientation of the sun is highly polarized and accounts for the large variations in camcorder intensity. Direct solar illumination has a small degree of polarization; consequently, most observations of sunlit surfaces show very little "flashing" except for specular reflections. The degree of polarization for this case is greatest at the Brewster angle and less pronounced at the angle of specular reflection. If the incident light, however, is highly polarized, then the "flashing" effect is more pronounced even at nonspecular angles. An important feature is that shadowed regions on the vehicle have a lower average luminance while the "flashing" effect is more pronounced, resulting in a high contrast temporal cue feature.

INTRODUCTION

Contrast is one of many factors which influences the ability to detect targets. All successful models which predict the probability of detecting targets will contain a contrast term.

The following equation was used to calculate contrast throughout this report:

$$C = \frac{L_T - L_B}{L_B}$$

where C = Contrast

L_T = Luminance of target

L_B = Luminance of background

Luminance is defined as:

1. The quality or state of being luminous
2. A measure of the brightness of a luminous surface, measured in candela (cd) per unit area
3. The photometric analog of radiance
4. A measure of the amount of visible light emitted from an extended source into a given solid angle and incident on a receiving surface (measurements are weighted via the CIE curve)
5. The luminous flux (lumens) per unit solid angle emitted per unit projected area of the source

The luminance unit cd/m^2 is used exclusively throughout this study. The following are conversions to other units:

Units for Luminance

$$1 \text{ cd}/\text{m}^2 = 1 \text{ nit} = 0.292 \text{ footlambert}$$

$$1 \text{ lambert} = 1 \text{ cd}/\pi \text{ cm}^2 = 1 \times 10^4 \text{ cd}/\pi \text{ m}^2 = 3183 \text{ nit}$$

$$1 \text{ footlambert} = 1 \text{ cd}/\pi \text{ ft}^2 = 3.426 \text{ nit}$$

The candela (cd) is an international unit for luminous intensity. It is one sixtieth of the luminous intensity of a square centimeter of fused thoria, a white oxide of the element thorium, maintained at 2046 K, the temperature of freezing platinum under a pressure of 101.325 newtons per square meter.

Figure 1 shows the luminance meter used for all studies. The settings used for the Minolta Luminance Meter LS-100 were as follows:

Calibration: PRESET
Measuring Mode: ABS
Response: FAST (two seconds)

The LS-100 has a one percent acceptance angle and measurements are virtually unaffected by light sources outside the measurement area. The photocell measures light received by the lens and is filtered to closely match the CIE Relative Photopic Luminosity Response.

A tripod was used to stabilize the meter.

A Minolta Data Printer DP-10 was used to reduce the time required between successive readings and to produce a hard copy of the data. The DP-10 was placed inside the holding strap of the LS-100 to eliminate the need for a table or an extra pair of hands.

The first nine studies include:

1. Diurnal measurements of the luminance from an M60, an M1 and a LAV25
2. Diurnal measurements of the luminance from sky, trees, grass, concrete and dirt-gravel
3. Calculations of the contrast between these vehicles and the backgrounds measured
4. An analysis of the contrasts obtained
5. Analysis of diurnal photographs of an M1

Three days were devoted to the acquisition of luminance data for reflected light from each of the three vehicles. Table 1 gives a summary of the content and conditions of each study. The cardinal directions within the parentheses of Table 1 refer to the orientation of the vehicle. For example, (north) indicates that the metered side of the vehicle was facing north during metering. The luminance meter pointed in the opposite direction.

These nine studies, as a whole, were not planned in advance but were done "on the run." After luminance data was collected and analyzed for one study, the next study was designed. Each study began as a phenomenological study; a search for high contrast areas which can become prominent cue features for threat observers.

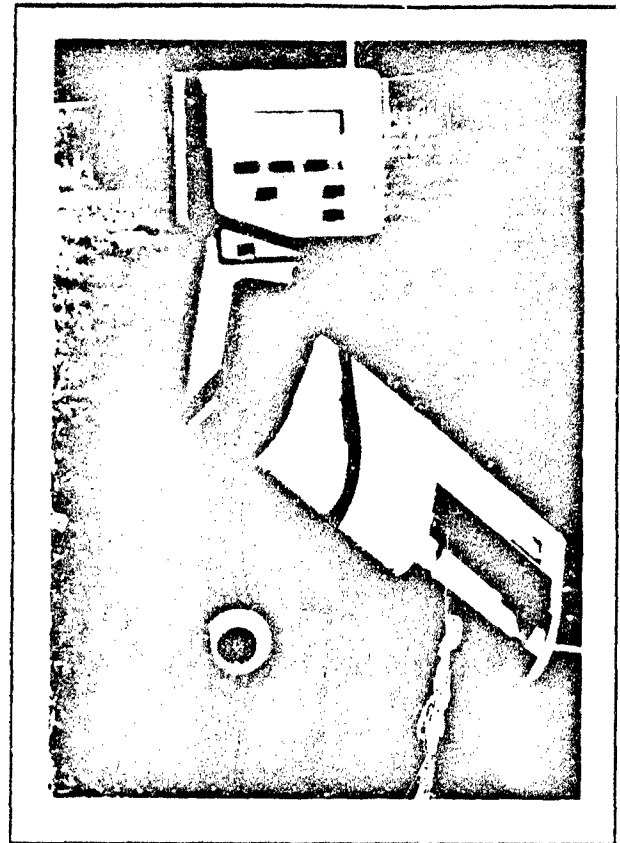


Figure 1
Minolta Luminance Meter LS-100 and
Data Printer DP-10

In all of the studies where the metered side of the vehicle was facing east, 50 luminance readings were taken randomly of a wooded area directly behind the vehicle. Readings were acquired from left to right using an up and down scanning pattern.

Table 1. Summary of Study Content and Conditions

Vehicle/Backgrounds	Date/Sky Conditions	Meter Range(s)
M60 (north) Sky, Grass, Trees, Concrete and Dirt	09 JULY, 1990 Clear 10:30-11:30, Cloudy 11:30-15:30	36'
M60 (north) Sky, Grass, Trees, Concrete and Dirt	12 JULY, 1990 Overcast 9:30-15:00	36'
M60 (north) Sky, Grass, Trees, Concrete and Dirt	17 JULY, 1990 Hazy, Cloudy, Overcast 9:00-15:15	36'
M1 (north) Sky, Grass, Trees, Concrete and Dirt	07 JULY, 1990 Hazy 9:00-12:00, Overcast 12:00-15:00	36'
M1 (east) Sky, Grass and Trees	01 AUGUST, 1990 Clear Skies 10:00-15:30	36, 100, 200 and 330'
M1 (east) Sky, Grass and Trees	06 AUGUST, 1990 Overcast 10:00-15:30	36, 100, 200 and 330'
LAV25 (east) Trees	23 JULY, 1990 Clear 10:00-11:00, Cloudy 11:00-15:00	36, 100, 200 and 330' Trees 36' only
LAV25 (east) Sky, Grass, Concrete and Trees	24 JULY, 1990 Clear Skies 9:00-11:30	36, 100, 200 and 330' Trees 36 & 200'
LAV25 (east) Sky, Grass, Concrete and Trees	26 JULY, 1990 Hazy 9:30-12:30, 12:30-14:30	36, 100, 200 and 330' Concrete 36 & 100'

All studies were conducted at the U.S. Army Tank-Automotive Research, Development and Engineering Center in Warren, Michigan in the vicinity of building 200C and were conducted during Eastern Daylight Standard Time.

All photographs were taken with a Canon A1 set for automatic exposure. The camera was fitted with a Canon Zoom Lens FD 28-85 mm and loaded with Kodak TMAX 400 film.

When two nonparallel surfaces of a vehicle meet, a rounded edge is formed. Under the right conditions, this edge may appear as a white line and can be used as a cue feature for threat observers. The "Glare and Edge Effect" study represents an initial investigation of the factors producing this phenomena and the nature of the light leaving the rounded edge.

In the study "Horizontal and Vertical Polarization of the M1A1", diurnal luminance readings and photographs were acquired for the M1A1 turret and skirt areas from 08:30 to 16:00 at thirty minute intervals under clear skies. The photographs show pictorially how luminance, contrast, shadows and shading vary diurnally over the elevated areas of the vehicle. The luminance data includes readings both without a polarizer and through a polarizer with its transmission axis oriented horizontally and vertically. This study also includes photographs of the Eastern hemispherical sky at a 30° altitude taken through a polarization axis finder. This study initiates the idea that the polarization of the sky is the major source of polarized light reflected from the M1A1.

The "Luminance, Polarization and Chromaticity Study on 15 July, 1991" was conducted to determine the degree and nature of linearly polarized reflected light from a CARC-painted M1A1. The study was also designed to determine how the three coordinates of the CIE Chromaticity Diagram vary diurnally for three different facets on the M1A1 and two backgrounds; a grass area and three tree areas. Data was collected simultaneously by two researchers. One used the Minolta LS-100 luminance meter fitted with a linear polarizer and the other used the Minolta CS-100 chromaticity meter. The range of the M1A1 and grass area was 36 feet. The range of the tree area was approximately 1000 feet. Data was collected at 30-minute intervals from 08:00 to 14:30. Skies were clear until 12:00; cloudy and overcast after 12:00. This study also describes the results of video tapes obtained by positioning a rotating (32 rpm) linear polarizer in front of a camcorder. This study was designed to determine when and where the greatest degree of reflected polarized light can be detected from a ground vehicle. When polarized light passes through the rotating linear polarizer a "flicker" effect is produced. The degree of "flicker" is a measure of the degree of polarization.

To obtain a more comprehensive understanding of the luminance and polarization of reflected light from a CARC-painted surface, under controlled conditions, a nine-by-ten inch steel plate was prepared and painted using the same procedures and materials as would be used for a combat-prepared M1A1. A luminance comparison test was conducted using two weathered M1A1 areas and the newly painted surface. Diurnal measurements of the luminance from the two M1A1 areas and the CARC-painted steel plate positioned adjacent to these areas can be found in the study "Luminance of New and Old CARC-Painted Surfaces." Data was collected from 08:00 to 15:00 at 30-minute intervals under clear skies at a range of 36 feet.

Three goniophotometric studies of the CARC-painted steel plate were designed to acquire information on the light distributing properties of the sample illuminated by sunlight. The first, "Azimuthal Study", shows how luminance is affected by changes in the azimuthal viewing angle when the altitude of the viewing angle (30°) is constant. Data was acquired at 12:00 under clear skies. The study "Goniophotometric Readings in the Plane of Incidence" shows how luminance is affected by changes in the surface altitude of the viewing angle for readings in the plane of incidence. The study "Goniophotometric Readings Perpendicular to the Plane of Incidence" shows how luminance is affected by changes in the surface altitude of the viewing angle for readings perpendicular to the plane of incidence.

The last two studies of this report were designed to acquire information on the light distributing properties of the CARC-painted steel plate without the influence of sky conditions. These studies were conducted inside, in a darkroom setting, using a Xenon light source as the only source of illumination.

The study "Luminance from a CARC-Painted Sample Using Xenon Light" consists of two different kinds of measurement. In the first part of the study, luminance readings were acquired outside the plane of incidence using a linear polarizer in front of the Xenon light source with its transmission axis horizontal. The collimated Xenon light rays made a 40° angle with the horizontal and the meter slope was adjusted to produce luminance readings at angles of 0° , 10° , 20° and 30° from the horizontal. The CARC-painted sample was positioned in a vertical plane at all times and was rotated about a vertical axis producing a range of azimuthal angles between 0° and 90° in 10-degree increments. The azimuthal angle of the meter was held constant at 40° . In the second part of the study, luminance measurements were acquired in the plane of incidence using horizontal, unpolarized light from the Xenon light source. The luminance meter was also positioned to acquire readings from the horizontal. The CARC-painted sample was positioned in a vertical plane at all times and was rotated about a vertical axis producing a range of azimuthal angles between 0° and 90° in 10-degree increments. The luminance meter was positioned to produce azimuthal angles of 40° and 60° .

The purpose of the study "Polarization Axis of Reflected White Light from a CARC-Painted Sample" was to determine how the degree of polarization and the polarization angle are affected by changes in azimuthal viewing angle when the altitude of the viewing angle is constant. The source of light for this study was a collimated Xenon light source with a linear polarizer placed in front of the collimating lens. Both the luminance meter and the Xenon light source were positioned with a 40° slope. Azimuthal angles ranged from 20° to 180° in 20-degree increments. The polarization axis of the incident light ranged from 0° to 90° in 10-degree increments. All of the data for this study is in the form of photographs of reflected light passing through a polarization axis finder. The polarization axis finder determines the polarization axis of linear polarized light and visually indicates the intensity of polarization. As a first attempt at quantifying observations, this study compares experimental results with a modified version of Fresnel's laws of reflection.

M60 STUDIES

Figure 2 shows the setup used to obtain luminance readings for the three studies involving the M60 tank. The LS-100 was positioned 36 feet from a stationary M60. The M60 was not moved during the three days of data collection. The M60 side was facing north and the LS-100 was pointed toward the south.

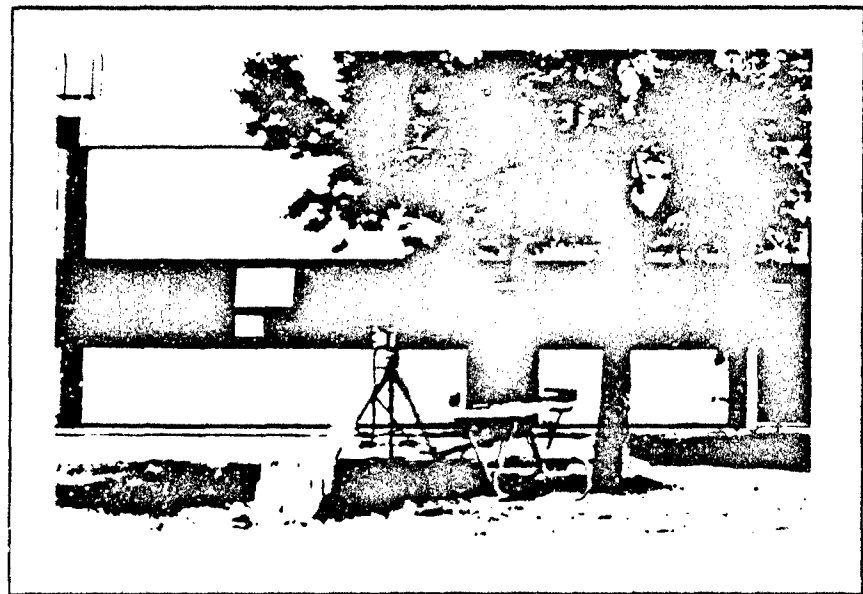
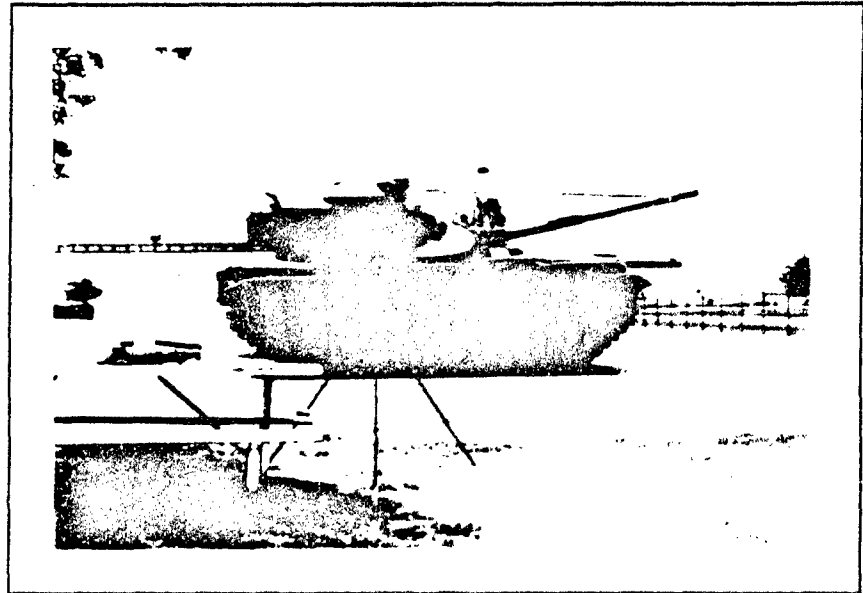


Figure 2
Setup Used to Obtain Luminance Readings for M60 Studies

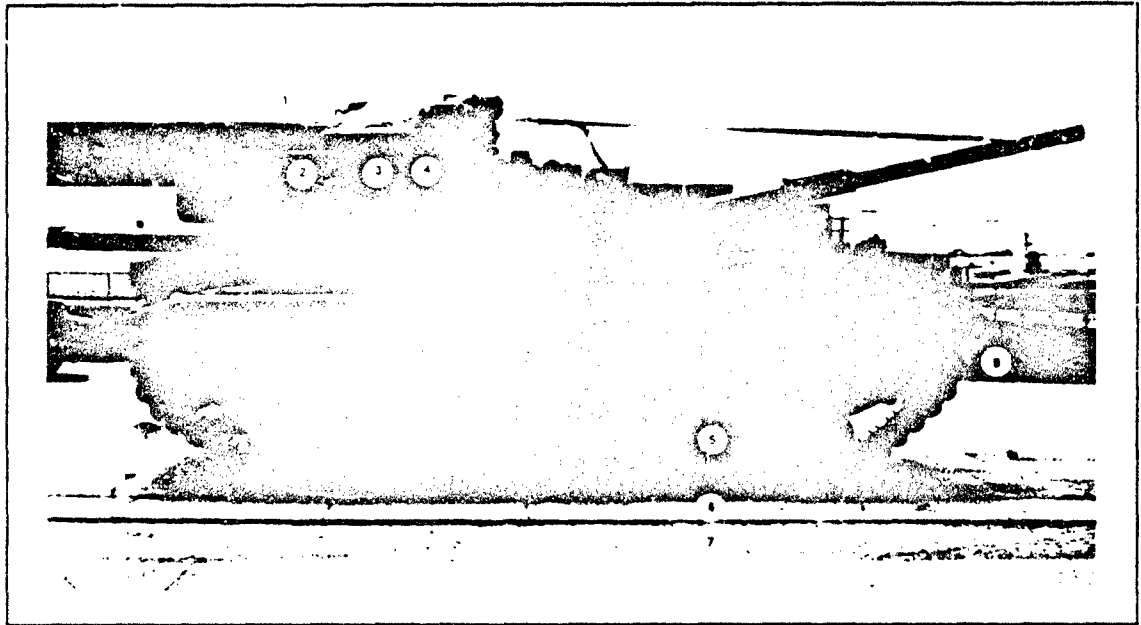


Figure 3
Position and Area of Luminance Readings for M60 Studies

The circled numbers of Figure 3 show the position and measurement area used for all M60 studies. The LS-100 measurement area is approximately the same as is circled on the photograph.

Area #9, tree background, does not show in the photograph. Area #9 is located to the far right (west) of the M60. This tree line is oriented along a north-south line. The LS-100 meter pointed toward the west when area #9 was measured.

The M60 side was facing north and metering was toward the south.

Two studies were conducted on 17 July, 1990. To distinguish between them, they will be referred to as Study A and Study B. Study A consisted of 10 luminance readings taken every 15 minutes. Study B consisted of 44 luminance readings taken at 10:35, 11:35 and 13:05.

Study 09 July, 1990 Overcast 10:30 - 11:00, Partly Cloudy 11:30 - 15:30

This is the only study for which the DP-10 Data Printer was not used. Luminance readings for the same area were observed during a 15-second time interval and only the minimum and maximum values were recorded. Graphs, contrast calculations and analysis for this study are based on the averages of these minimum and maximum readings.

M60 Study of 09 July, 1990

Table 2. Summary of Luminance Readings for 09 July, 1990
(Clear Skies 10:30 - 11:30, Cloudy 11:30 - 15:30)

Measurement Area	Range of Measurements (cd/m ²)	Average Luminance (cd/m ²)	Standard Deviation
#1 (Sky)	5,500 - 14,600	10,509	2,903
#2 (M60 Turret)	574 - 1,400	917	176
#3 (M60 Turret)	640 - 1,150	857	135
#4 (M60 Turret)	380 - 660	508	84
#5 (M60 Wheel)	210 - 466	336	68
#6 (Concrete)	1,100 - 6,100	3,405	1,533
#7 (Dirt-Gravel)	1,320 - 5,900	3,816	1,523
#8 (Grass)	1,020 - 2,780	2,011	632
#9 (Trees)	250 - 1,000	558	166

M60 TANK LUMINANCE
RANGE = 36 FEET

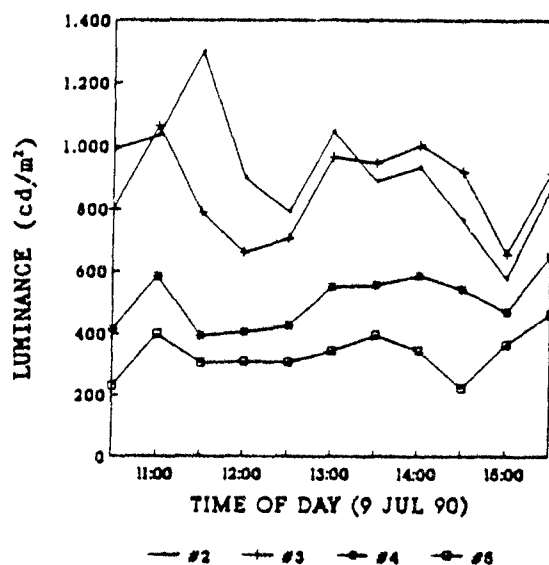


Figure 4

BACKGROUND LUMINANCE

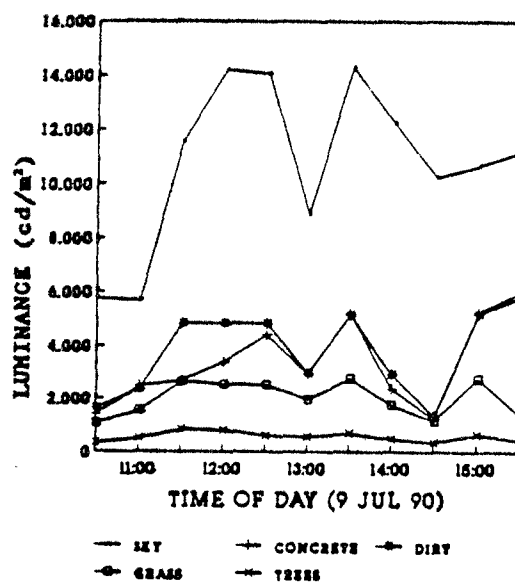


Figure 5

M60 Study of 09 July, 1990 (Clear Skies 10:30 - 11:30, Cloudy 11:30 - 15:30)

M60 TANK
SKY BACKGROUND

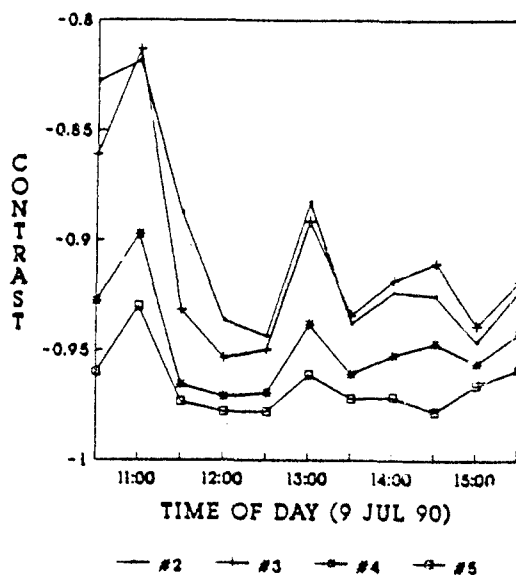


Figure 6

M60 TANK
CONCRETE BACKGROUND

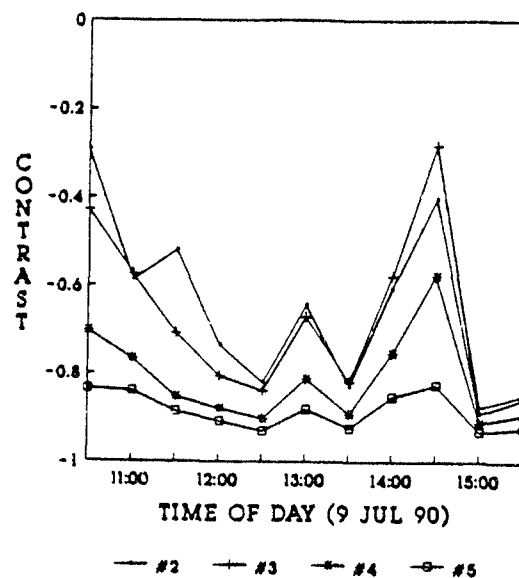


Figure 7

M60 TANK
DIRT-GRAVEL BACKGROUND

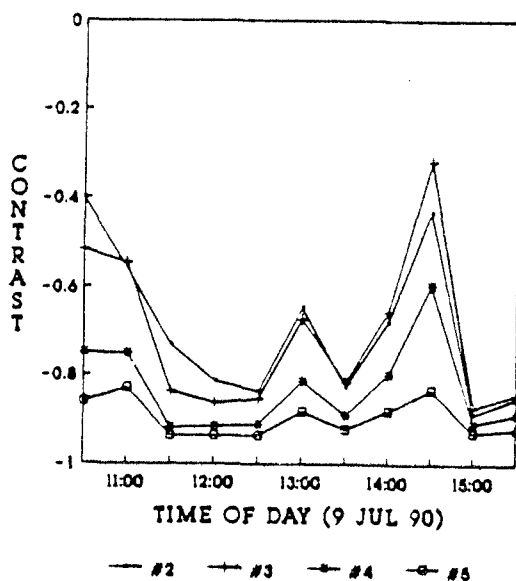


Figure 8

M60 TANK
GRASS BACKGROUND

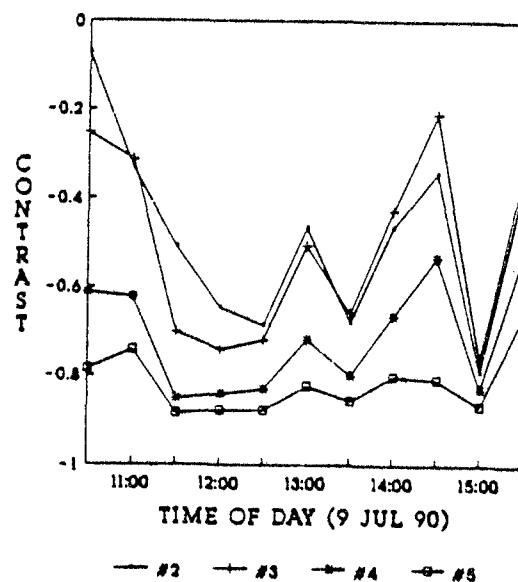


Figure 9

Table 3. Summary of Contrast Calculations for 09 July, 1990
(Clear Skies 10:30 - 11:30, Cloudy 11:30 - 15:30)

Targ./Backg.	#2/Sky	#3/Sky	#4/Sky	#5/Sky
Minimum	-0.946	-0.954	-0.971	-0.978
Maximum	-0.818	-0.813	-0.897	-0.930
Average	-0.905	-0.911	-0.948	-0.966
Std. Dev.	0.043	0.040	0.021	0.013
Targ./Backg.	#2/Concrete	#3/Concrete	#4/Concrete	#5/Concrete
Minimum	-0.890	-0.875	-0.910	-0.930
Maximum	-0.293	-0.280	-0.574	-0.825
Average	-0.652	-0.675	-0.813	-0.885
Std. Dev.	0.187	0.184	0.101	0.039
Targ./Backg.	#2/Dirt	#3/Dirt	#4/Dirt	#5/Dirt
Minimum	-0.889	-0.874	-0.919	-0.937
Maximum	-0.402	-0.317	-0.596	-0.830
Average	-0.697	-0.709	-0.832	-0.898
Std. Dev.	0.163	0.176	0.097	0.040
Targ./Backg.	#2/Grass	#3/Grass	#4/Grass	#5/Grass
Minimum	-0.791	-0.762	-0.851	-0.885
Maximum	-0.075	-0.211	-0.527	-0.663
Average	-0.488	-0.512	-0.712	-0.817
Std. Dev.	0.197	0.203	0.120	0.065
Targ./Backg.	#2/Trees	#3/Trees	#4/Trees	#5/Trees
Minimum	-0.084	-0.175	-0.535	-0.641
Maximum	2.046	1.724	0.611	0.143
Average	0.783	0.713	0.015	-0.354
Std. Dev	0.587	0.639	0.384	0.205

M60 Study of 12 July, 1990

Table 4. Summary of Luminance Readings for 12 July, 1990
(Overcast 9:30-15:00)

Measurement Area	Range of Measurements (cd/m ²)	Average Luminance (cd/m ²)	Standard Deviation
#1 (Sky)	3,570 - 15,400	10,177	4,396
#2 (M60 Turret)	440 - 1,110	769	167
#3 (M60 Turret)	470 - 1,170	853	187
#4 (M60 Turret)	255 - 730	475	129
#5 (M60 Wheel)	125 - 503	297	98
#6 (Concrete)	630 - 5,100	2,647	1,346
#7 (Dirt-Gravel)	440 - 5,500	2,479	1,603
#8 (Grass)	550 - 3,060	1,946	839
#9 (Trees)	170 - 1,150	672	312

M60 TANK LUMINANCE
RANGE = 36 FEET

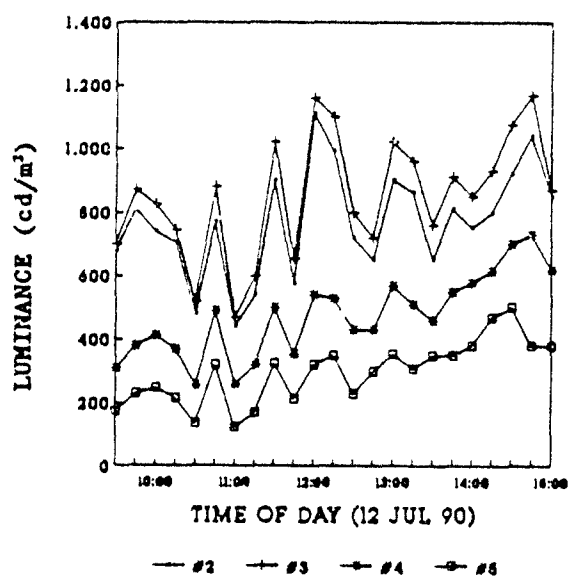


Figure 10

BACKGROUND LUMINANCE

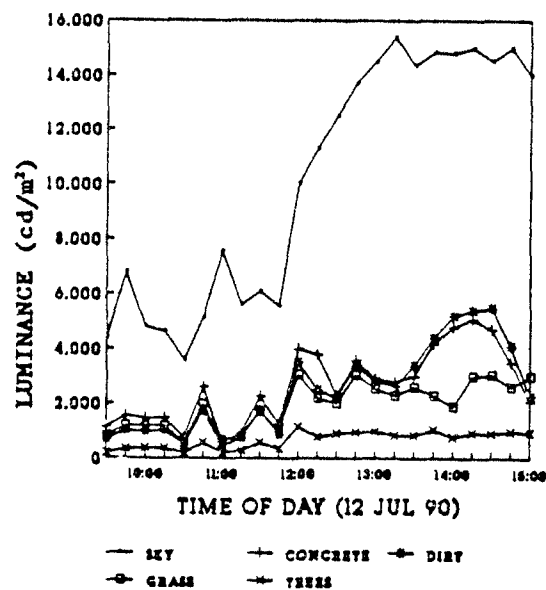


Figure 11

M60 Study of 12 July, 1990 (Overcast 9:30-15:00)

M60 TANK
SKY BACKGROUND

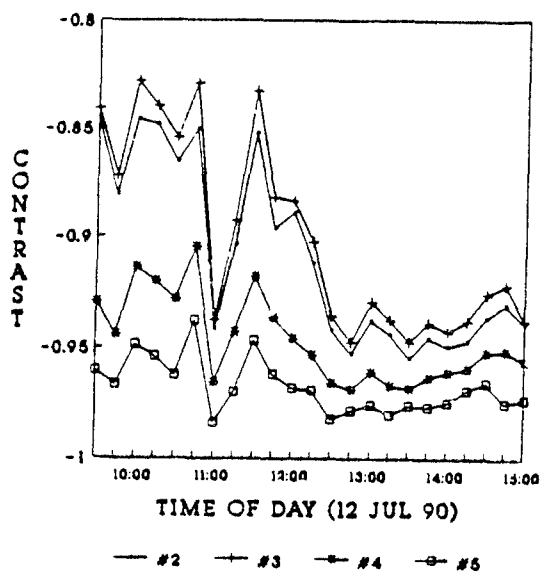


Figure 12

M60 TANK
CONCRETE BACKGROUND

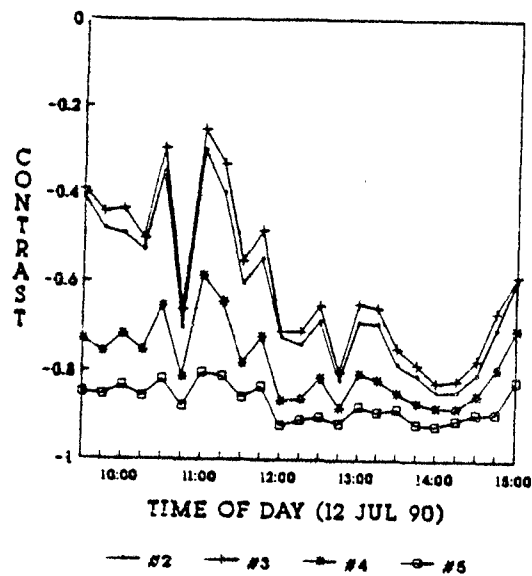


Figure 13

M60 TANK
DIRT-GRAVEL BACKGROUND

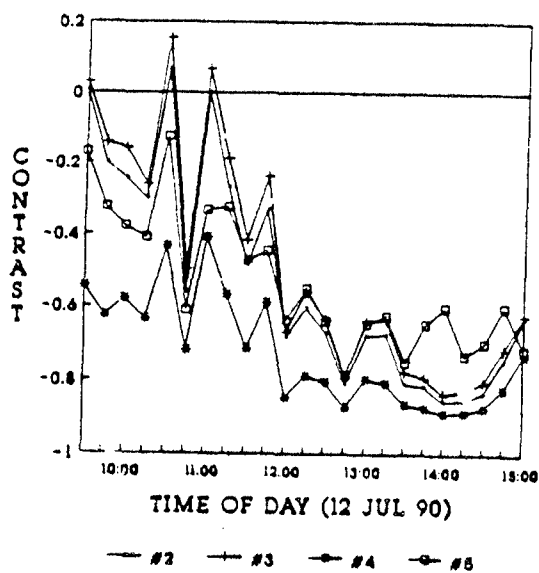


Figure 14

M60 TANK
GRASS BACKGROUND

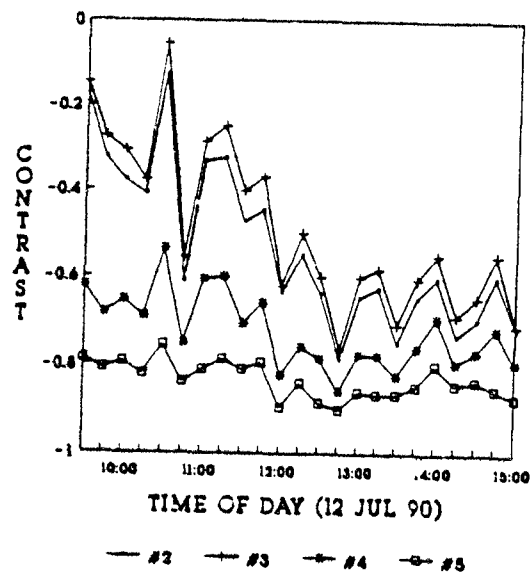


Figure 15

Table 5. Summary of Contrast Calculations for 12 July, 1990
(Overcast 9:30-15:00)

Targ./Backg.	#2/Sky	#3/Sky	#4/Sky	#5/Sky
Minimum	-0.955	-0.947	-0.969	-0.983
Maximum	-0.845	-0.828	-0.905	-0.938
Average	-0.909	-0.900	-0.947	-0.967
Std. Dev.	0.040	0.043	0.019	0.012
Targ./Backg.	#2/Concrete	#3/Concrete	#4/Concrete	#5/Concrete
Minimum	-0.844	-0.823	-0.881	-0.921
Maximum	-0.303	-0.254	-0.587	-0.802
Average	-0.633	-0.597	-0.784	-0.871
Std. Dev.	0.162	0.170	0.081	0.038
Targ./Backg.	#2/Dirt	#3/Dirt	#4/Dirt	#5/Dirt
Minimum	-0.856	-0.837	-0.888	-0.927
Maximum	0.067	0.156	-0.409	-0.700
Average	-0.521	-0.476	-0.725	-0.838
Std. Dev.	0.292	0.309	0.145	0.073
Targ./Backg.	#2/Grass	#3/Grass	#4/Grass	#5/Grass
Minimum	-0.787	-0.764	-0.859	-0.902
Maximum	-0.127	-0.055	-0.536	-0.755
Average	-0.532	-0.485	-0.724	-0.834
Std. Dev.	0.182	0.190	0.081	0.038
Targ./Backg.	#2/Trees	#3/Trees	#4/Trees	#5/Trees
Minimum	-0.316	-0.242	-0.547	-0.747
Maximum	2.400	2.500	0.550	-0.125
Average	0.440	0.581	-0.159	-0.493
Std. Dev.	0.711	0.740	0.312	0.159

M60 Study A on 17 July, 1990.

Table 6. Summary of Luminance Readings for Study A on 17 July, 1990
(Hazy, Cloudy, Overcast 9:00-15:15)

Measurement Area	Range of Measurements (cd/m ²)	Average Luminance (cd/m ²)	Standard Deviation
#1 (Sky)	5,850 - 16,600	10,575	3,134
#2 (M60 Turret)	690 - 1,520	1,081	276
#3 (M60 Turret)	690 - 1,575	1,032	265
#4 (M60 Turret)	305 - 950	478	165
#5 (M60 Wheel)	192 - 510	310	94
#6 (Concrete)	2,700 - 5,100	3,673	639
#7 (Dirt-Gravel)	1,325 - 4,280	2,669	832
#8 (Grass)	2,200 - 3,700	2,964	348
#9 (Trees)	685 - 1,120	836	102
#10 (M60 Base)	101 - 321	180	50

M60 TANK LUMINANCE
RANGE = 36 FEET

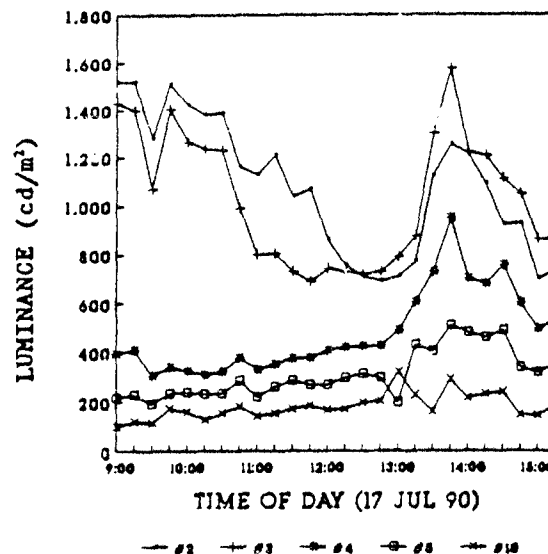


Figure 16

BACKGROUND LUMINANCE

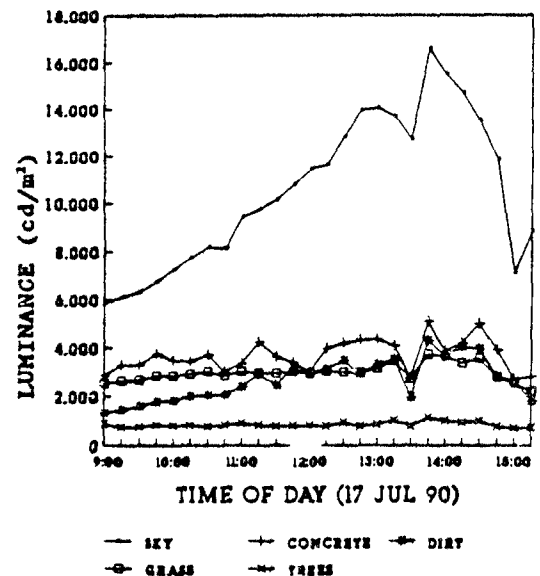


Figure 17

M60 Study A on 17 July, 1990 (Hazy, Cloudy, Overcast 9:00-15:15)

M60 TANK
SKY BACKGROUND

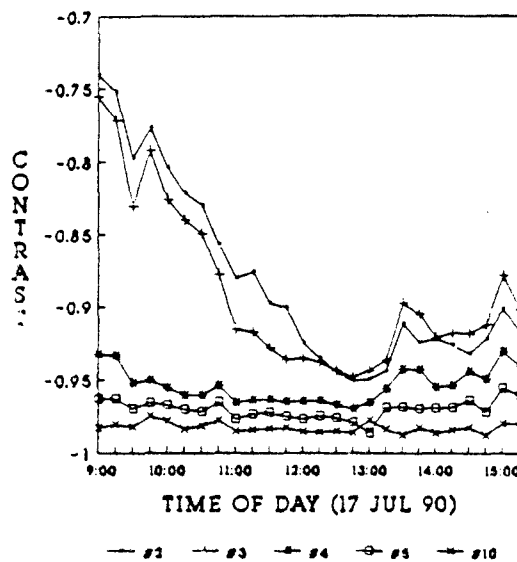


Figure 18

M60 TANK
CONCRETE BACKGROUND

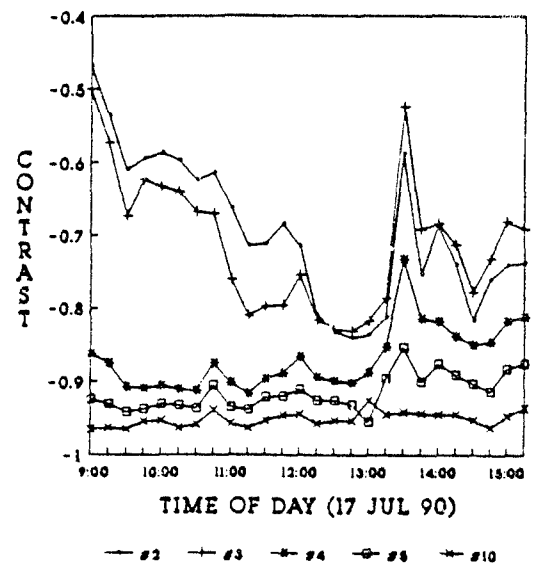


Figure 19

M60 TANK
DIRT-GRAVEL BACKGROUND

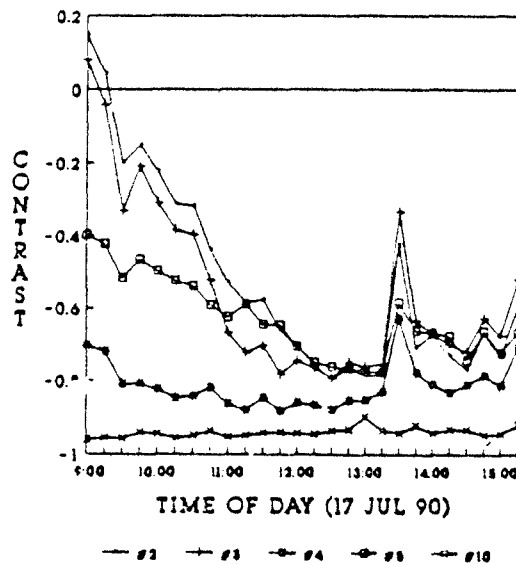


Figure 20

M60 TANK
GRASS BACKGROUND

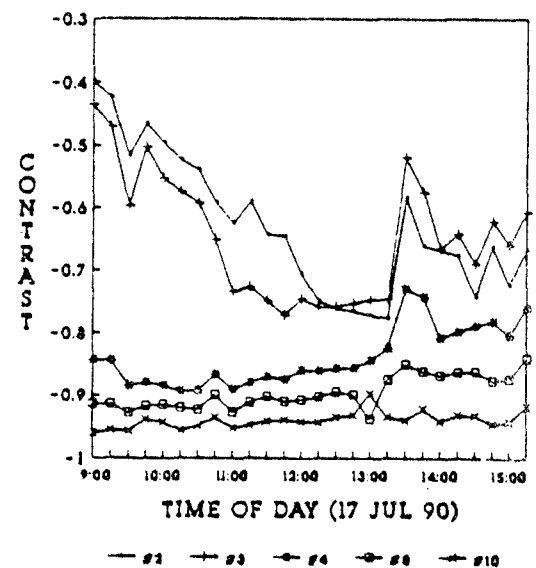


Figure 21

Table 7. Summary of Contrast Calculations for Study A on 17 July, 1990
(Hazy, Cloudy, Overcast 9:00-15:15)

Targ/Backg	#2/Sky	#3/Sky	#4/Sky	#5/Sky	#10/Sky
Minimum	-0.951	-0.948	-0.970	-0.986	-0.988
Maximum	-0.740	-0.756	-0.930	-0.955	-0.974
Average	-0.882	-0.890	-0.954	-0.970	-0.983
Std. Dev.	0.063	0.055	0.011	0.006	0.003
Targ/Backg	#2/Concr.	#3/Concr.	#4/Concr.	#5/Concr.	#10/Concr.
Minimum	-0.840	-0.831	-0.917	-0.955	-0.965
Maximum	-0.469	-0.500	-0.733	-0.853	-0.926
Average	-0.695	-0.710	-0.869	-0.915	-0.951
Std. Dev.	0.099	0.091	0.043	0.024	0.010
Targ/Backg	#2/Dirt	#3/Dirt	#4/Dirt	#5/Dirt	#10/Dirt
Minimum	-0.794	-0.791	-0.880	-0.941	-0.947
Maximum	0.147	0.079	-0.626	-0.794	-0.900
Average	-0.526	-0.555	-0.813	-0.879	-0.930
Std. Dev.	0.264	0.237	0.061	0.032	0.014
Targ/Backg	#2/Grass	#3/Grass	#4/Grass	#5/Grass	#10/Grass
Minimum	-0.777	-0.772	-0.894	-0.937	-0.960
Maximum	-0.399	-0.435	-0.730	-0.841	-0.897
Average	-0.630	-0.648	-0.839	-0.896	-0.940
Std. Dev.	0.108	0.098	0.047	0.026	0.013
Targ/Backg	#2/Trees	#3/Trees	#4/Trees	#5/Trees	#10/Trees
Minimum	-0.244	-0.218	-0.627	-0.771	-0.884
Maximum	1.040	0.879	-0.052	-0.478	-0.625
Average	0.310	0.243	-0.433	-0.632	-0.786
Std. Dev.	0.366	0.318	0.159	0.088	0.047

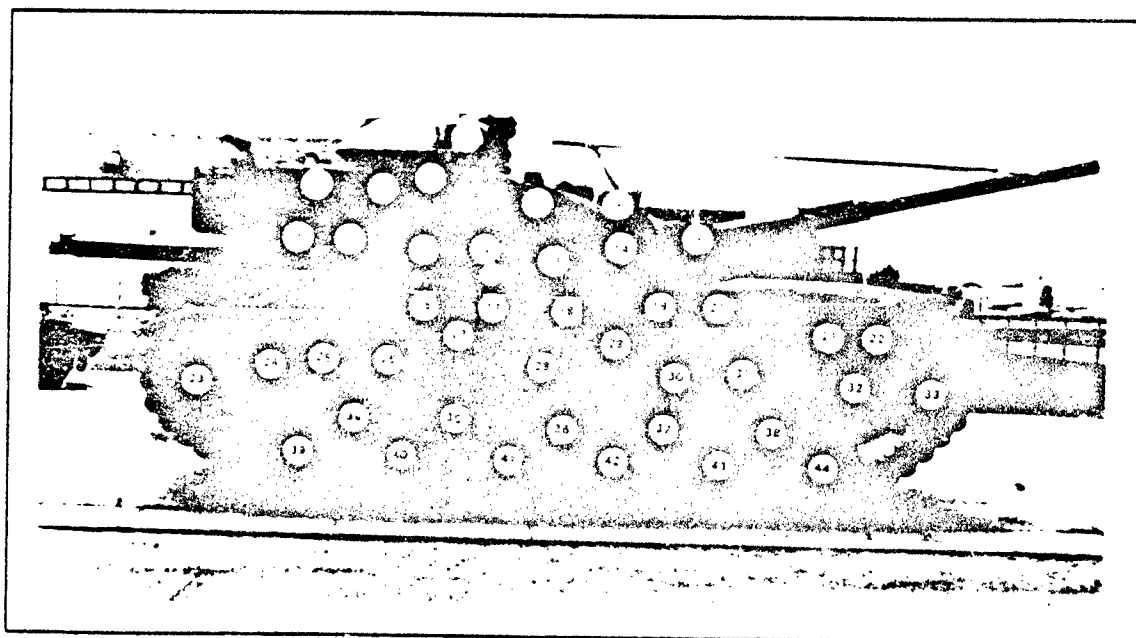


Figure 22
Position and Area of Luminance Readings for Study B on 17 July, 1990

The circled numbers of Figure 22 show the position of the 44 luminance measurements acquired at 10:35, 11:35 and 13:05 on 17 July, 1990. The LS-100 measurement area is approximately the same as is circled on the photograph.

M60 LUMINANCE
RANGE • 36 FEET
10:35 AM, 17 JULY 1990

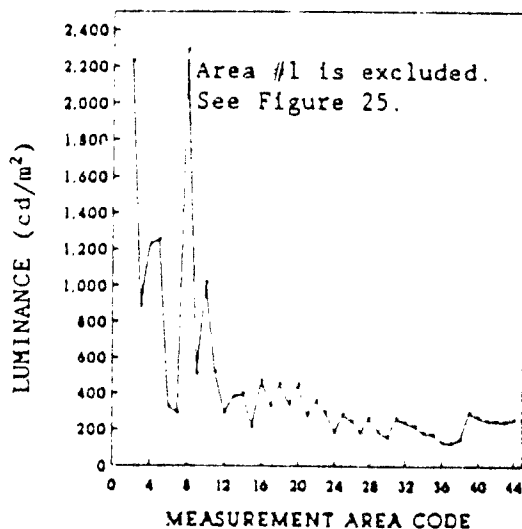


Figure 23

M60 TANK
GRASS BACKGROUND
10:35, 17 JULY 1990

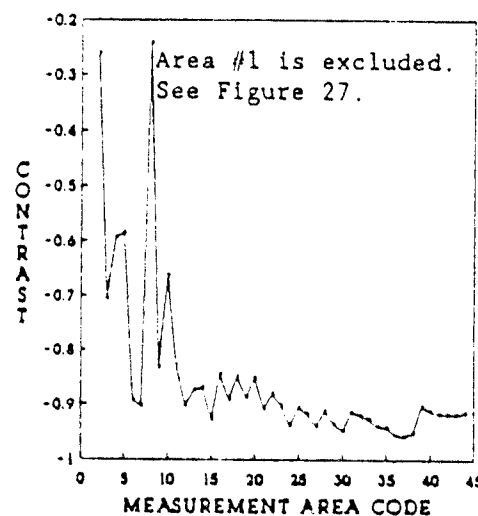


Figure 24

Table 8. M60 Luminance Study for Study B on 17 July, 1990

Area #	Luminance (cd/m ²)			Contrast Calculations (M60/Grass)		
	10:35	11:35	13:05	10:35	11:35	13:05
1	5541	14000	5969	0.835	3.795	0.907
2	2232	3249	5551	-0.261	0.113	0.773
3	857	587	1723	-0.706	-0.799	-0.450
4	1227	851	694	-0.594	-0.709	-0.778
5	1253	773	789	-0.585	-0.735	-0.748
6	325	365	500	-0.892	-0.875	-0.840
7	291	359	550	-0.904	-0.877	-0.824
8	2290	1699	1295	-0.242	-0.418	-0.586
9	507	441	569	-0.832	-0.849	-0.818
10	1016	845	734	-0.664	-0.711	-0.765
11	519	519	636	-0.828	-0.822	-0.797
12	293	320	484	-0.903	-0.890	-0.845
13	382	487	844	-0.874	-0.833	-0.730
14	396	506	1337	-0.869	-0.827	-0.573
15	214	561	806	-0.929	-0.808	-0.742
16	469	574	957	-0.845	-0.803	-0.694
17	328	423	361	-0.891	-0.855	-0.885
18	453	546	480	-0.850	-0.813	-0.847
19	340	334	408	-0.887	-0.886	-0.870
20	449	501	517	-0.851	-0.828	-0.835
21	278	336	237	-0.908	-0.885	-0.924
22	360	442	285	-0.881	-0.849	-0.909
23	295	322	397	-0.902	-0.890	-0.873
24	186	219	282	-0.938	-0.925	-0.910
25	283	312	395	-0.906	-0.893	-0.874
26	249	234	364	-0.918	-0.920	-0.884
27	182	221	289	-0.940	-0.924	-0.908
28	265	303	384	-0.912	-0.896	-0.877
29	191	205	290	-0.937	-0.930	-0.907
30	155	238	316	-0.949	-0.918	-0.899
31	261	297	407	-0.914	-0.898	-0.870
32	238	257	354	-0.921	-0.912	-0.887
33	218	252	315	-0.928	-0.914	-0.899
34	179	189	256	-0.941	-0.935	-0.918
35	174	151	219	-0.942	-0.948	-0.930
36	130	142	213	-0.957	-0.951	-0.932
37	127	145	223	-0.958	-0.950	-0.929
38	147	185	267	-0.951	-0.937	-0.915
39	295	307	377	-0.902	-0.895	-0.880
40	263	283	341	-0.913	-0.903	-0.891
41	248	265	342	-0.918	-0.909	-0.891
42	249	268	359	-0.918	-0.908	-0.885
43	245	261	354	-0.919	-0.911	-0.887
44	258	280	366	-0.915	-0.904	-0.883
MINIMUM	127	142	213	-0.958	-0.951	-0.932
MAXIMUM	5541	14000	5969	0.835	3.795	0.907
AVERAGE	566	774	746	-0.813	-0.735	-0.762
ST. DEV.	893	2078	1139	0.296	0.712	0.364

M60 Luminance for Study 8 on 17 July, 1990

M60 LUMINANCE
RANGE = 36 FEET
10:35 AM, 17 JULY 1990

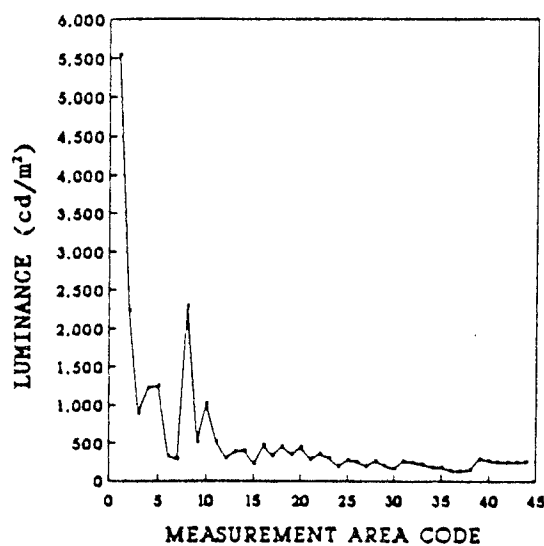


Figure 25

M60 LUMINANCE
RANGE = 36 FEET
11:35 AM, 17 JULY 1990

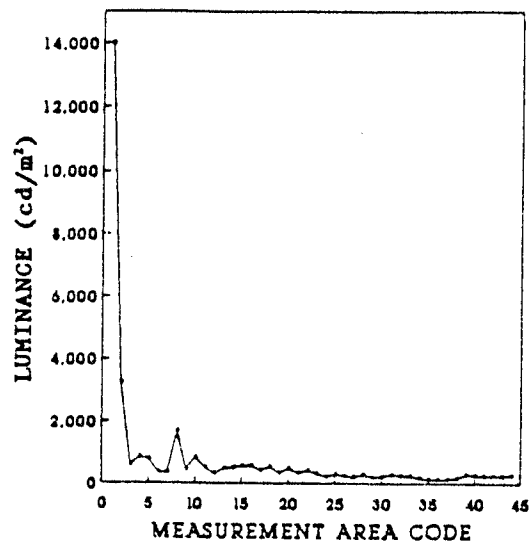


Figure 26

M60 TANK
GRASS BACKGROUND
10:35, 17 JULY 1990

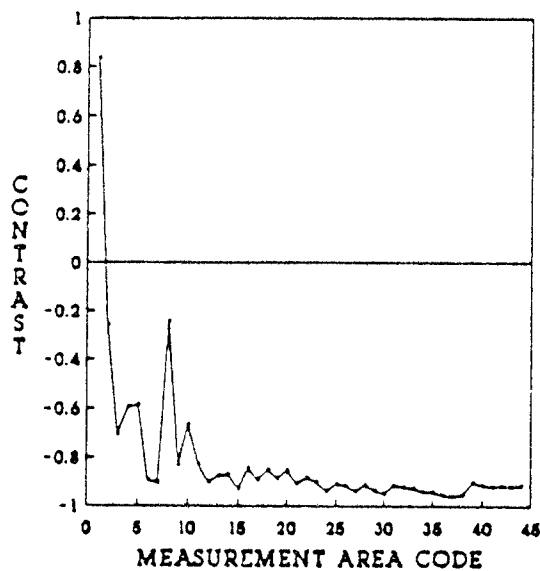


Figure 27

M60 TANK
GRASS BACKGROUND
11:35 AM, 17 JULY 1990

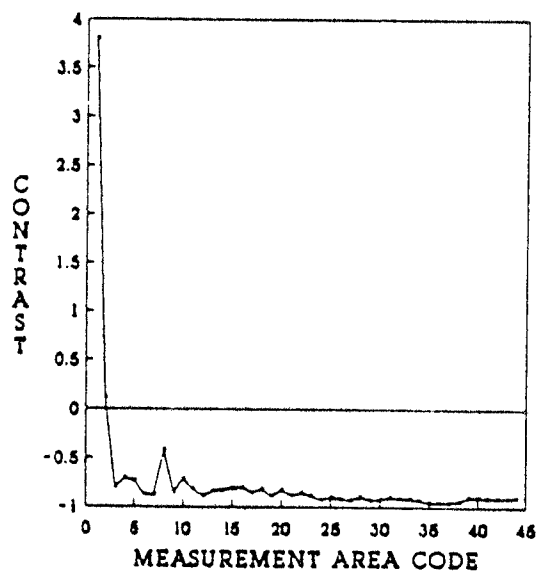


Figure 28

SUMMARY OF M60 STUDIES

The largest luminance measurement for the M60 was 14,000 cd/m². This reading was acquired for area #1 (Figure 22 and Figure 26; Study B on 17 July, 1990; 11:35). Since the majority of the luminance readings for the M60 were below 1,000 cd/m², readings above 1,000 cd/m² are most likely due to intense specular reflection.

Specular reflection exists when the majority of the light incident on a surface reflects sharply away from the surface. The majority of the light leaving the surface travels in the same general direction. Diffuse reflection exists when reflected light travels in many different directions.

Specular reflection by an M60 area is enhanced by the following conditions:

1. Smooth surface
2. Elevated position
3. Beveled, rounded shape
4. Light color
5. Location on east side of vehicle
6. Clearance from shadows

Area #1, area #2,... area #5 (Figure 22) satisfy these conditions and account for the very large luminance readings acquired from them.

As the sun, relative to the M60, rises from the east and moves toward the west, different areas on the M60 exhibit intense specular reflection at different times. For example, the luminance of area #3, located on the west side of the turret, increases from 10:35 to 13:05. Whereas, area #4, located on the east side of the turret, decreases in luminance for the same period of time.

Luminance readings for the M60 decrease, in general, for areas closer to the ground (Figure 23, Figure 25 and Figure 26; Table 8).

The alternating high and low luminance readings for area #16, area #17,... area #22 (Figure 22 and Figure 23; Table 8) are due to the alternating colors in the camouflage pattern.

The alternating high and low luminance readings for area #23, area #24,... area #44 (Figure 22 and Figure 23; Table 8) are primarily due to some areas being located in cavities. For example, area #34, area #35,...area #38 are located in cavities close to the bottom base of the M60. These cavity areas produced the lowest luminance readings (minimum = 127 cd/m²; maximum = 267 cd/m²).

Figure 16, which relates to the regular study on 17 July, 1990, also suggests intense specular reflection from turret areas during the morning hours (9:00 - 12:00). There is a significant diurnal change in luminance for area #2 (turret) and area #3 (turret; Figure 3). Area #4 (turret) and area #5 (wheel) do not show this kind of change. Although area #4 is also on the turret, it is located on the west side of the turret on a flatter, darker area. Area #5 is close to the ground, located to the west of the luminance meter and is not smooth. Luminance readings from area #4 and area #5 are less likely to be affected by specular reflection.

Figure 30 illustrates how specular reflection from area #2 and area #3 (Figure 3) decreased as the sun rose and passed behind the M60. The luminance ratio of area #2 (turret) or area #3 (turret) to area #5 (wheel) decreased by nearly 1.3/hr from 9:00 to 12:00 on 17 July, 1990. The sky condition for this period of time was hazy.

Figure 29 illustrates how specular reflection from area #2 and area #3 was reduced by the overcast sky condition on 12 July, 1990. The luminance ratio of area #4 (turret) to area #5 (wheel) not only remained nearly constant throughout the day on both days, but also was nearly the same value on both days. The average luminance ratio, area #4/area #5, on 12 July, 1990 was 1.64. On 17 July, 1990 the average ratio was 1.55.

Sky conditions also contribute to variance in luminance. During the study of 9 July, 1990, luminance readings were observed for 15-second intervals for each target and background measured. Even though the sky condition did not appear to change visually during this time interval, variance in luminance occurred to the extent shown in Table 10 below.

Table 10. Largest Difference in Luminance Readings for 9 July, 1990

Meas. Area	#1 Sky	#2 Turret	#3 Turret	#4 Turret	#5 Wheel	#6 Concr.	#7 Dirt	#8 Grass	#9 Trees
Minimum (cd/m ²)	8600	830	980	540	280	2000	5100	1450	600
Maximum (cd/m ²)	9200	1150	1150	630	330	3000	5300	1650	1000
Average (cd/m ²)	8900	990	1065	585	305	2500	5200	1550	800
Diff. (cd/m ²)	600	320	170	90	50	1000	200	200	400
% Diff.	7	32	16	15	16	40	4	13	50
Time	13:00	10:30	11:00	11:00	11:30	11:00	15:00	11:00	12:00

The '% Diff.' row of Figure 10 was obtained using: $\frac{\text{Max} - \text{Min}}{\text{Average}} \times 100$

The 'Time row' indicates the time when the largest luminance difference occurred on 9 July, 1990 during the 15-second observing interval.

An interesting phenomenon was observed when cumulus clouds approached the sun. Luminance readings were observed to increase. The clouds, behaving as mirrors, reflected more light onto a target area than would be produced by light coming directly from the sun alone.

Figure 10 also illustrates the effect of sky conditions on luminance readings. Openings in the cloud cover on 12 July, 1990 produced considerable variance in the luminance readings. As mentioned earlier, overcast sky conditions do, however, tend to make the luminance ratios more constant (Figure 29 and Figure 30).

Table 9. Summary of M60 Luminance Readings (excluding Study B of 17 July 1990)

Measurement Area (Targets)	Luminance (cd/m ²)			Measurement Area (Backgrounds)	Luminance (cd/m ²)		
	Min	Max	Avg		Min	Max	Avg
#2 (Turret)	440	1,520	922	#1 (Sky)	3,570	16,600	10,520
#3 (Turret)	470	1,575	914	#6 (Concrete)	630	6,100	3,242
#4 (Turret)	305	950	487	#7 (Dirt)	440	5,900	2,988
#5 (Wheel)	125	730	314	#8 (Grass)	550	3,700	2,307
#10 (Base)	101	321	180	#9 (Trees)	101	1,150	689

M60 LUMINANCE RATIOS

OVERCAST

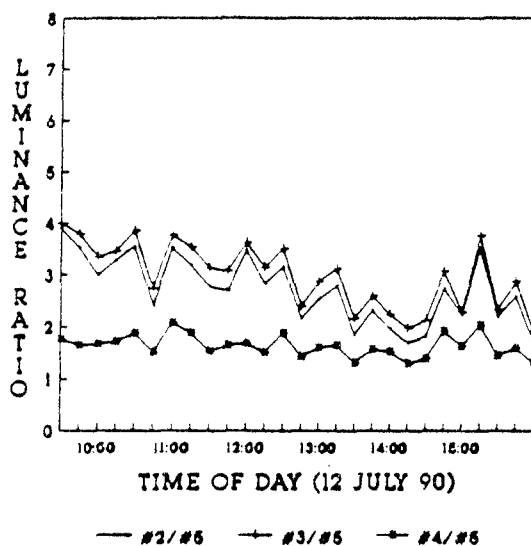


Figure 29

M60 LUMINANCE RATIOS

HAZY - CLOUDY - OVERCAST

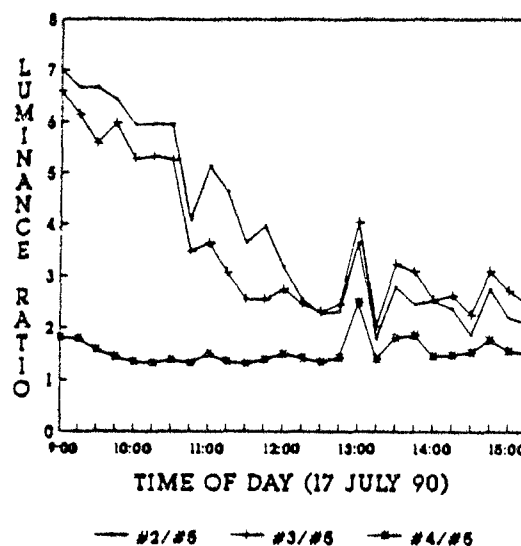


Figure 30

Contrast values for the M60 varied considerably; for a given area and for the entire vehicle. From Table 8, using grass as a background, the largest variance in contrast for a single area was acquired from area #1 (Figure 22; Range of contrast: +0.835 to +3.795). The higher elevated eastern turret areas always produced the greatest variance in contrast. When considering the contrast of the M60 as whole, using a grass background, the range of contrast extends from -0.951 (area #36; Figure 22) to +3.795 (area #1; Figure 22).

The range of contrast, using trees as a background, extends from -0.242 to +2.50 for area #3 (Figure 3; Table 5). Of the five backgrounds measured, the trees produced the greatest variance in contrast. As mentioned earlier, the tree line was oriented along a north-south line and the M60 along an east-west line. This orthogonal relationship does not appear to have any relevance to the shape of the tree background contrast curves of Figure 31, Figure 32 or Figure 33. The shapes of the contrast graphs for M60 targets and grass background, Figures 9, Figure 15 and Figure 21, look similar to the corresponding tree background contrast graphs of Figures 31, Figure 32 and Figure 33. As will be seen in later studies, the range of luminance readings for the trees in the M60 studies (100 - 1000 cd/m²) are similar to those obtained in studies for the M1 and LAV25.

The least variance in contrast occurred between the M60 and the sky. This is expected, since the sky luminance is approximately 10 times greater than the M60. The range of contrast values, using a sky background on 17 July, 1990, was from -0.74 to -0.95 (Table 7; area #2/Sky).

M60 TANK
TREE BACKGROUND

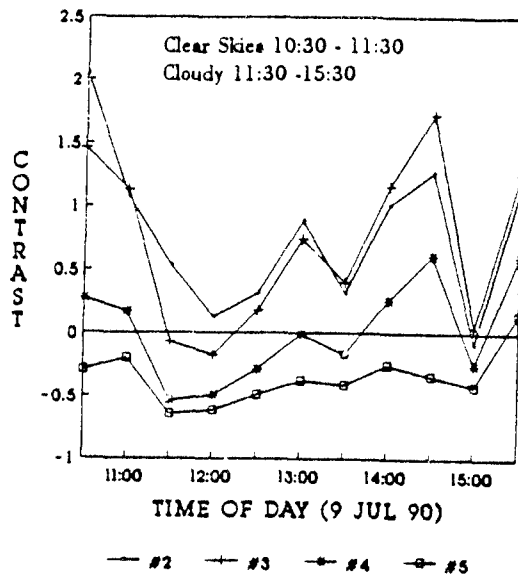


Figure 31

M60 TANK
TREE BACKGROUND

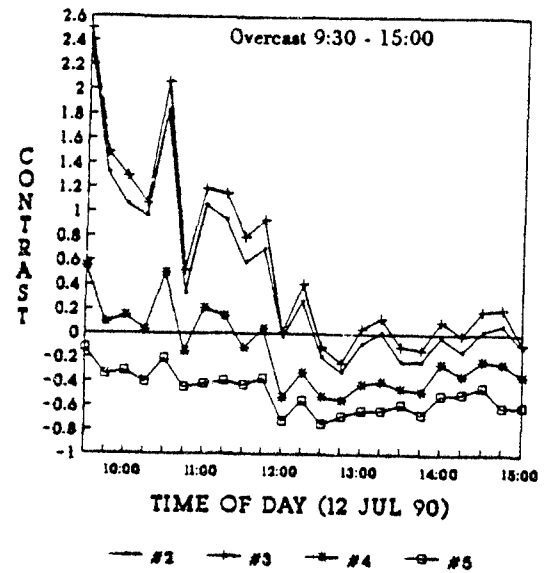


Figure 32

M60 TANK
TREE BACKGROUND

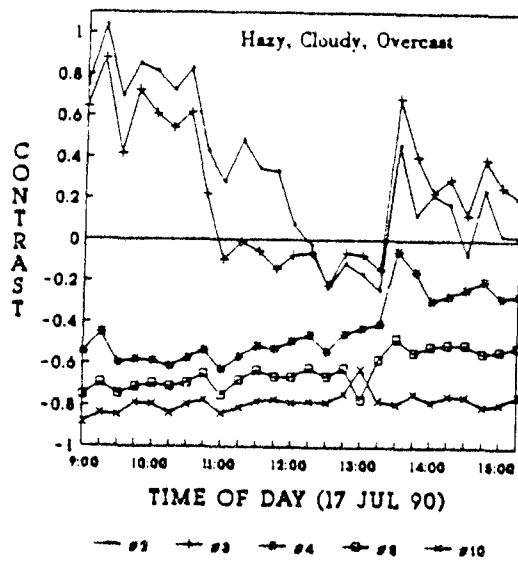


Figure 33

M1 STUDIES

Study 19 July, 1990 Hazy 9:00-12:00, Overcast 12:00-15:00

Two studies were conducted on 19 July, 1990. To distinguish between them, they will be referred to as Study A and Study B. Study A consisted of 11 luminance readings taken every 15 minutes from 9:00 to 15:00. Study B consisted of 45 luminance readings taken every 30 minutes from 10:05 to 15:05.

Figure 34 shows the setup used to obtain luminance readings for the two studies involving the M1 on 19 July, 1990. The LS-100 was positioned 36 feet from a stationary M1. The M1 was not moved during data collection. The M1 side was facing north and the LS-100 was pointed toward the south.

The circled numbers of Figure 35 and Figure 36 show the position and measurement areas used for the 19 July, 1990 M1 studies. The LS-100 measurement area is approximately the same as is circled on the photograph.

Area #11 of Study A (tree background) does not show in the photograph. Area #11 is located to the far right (west) of the M1. This tree line is oriented along a north-south line. The LS-100 meter pointed toward the west when area #11 was measured.

The M1 side was facing north and metering was toward the south.

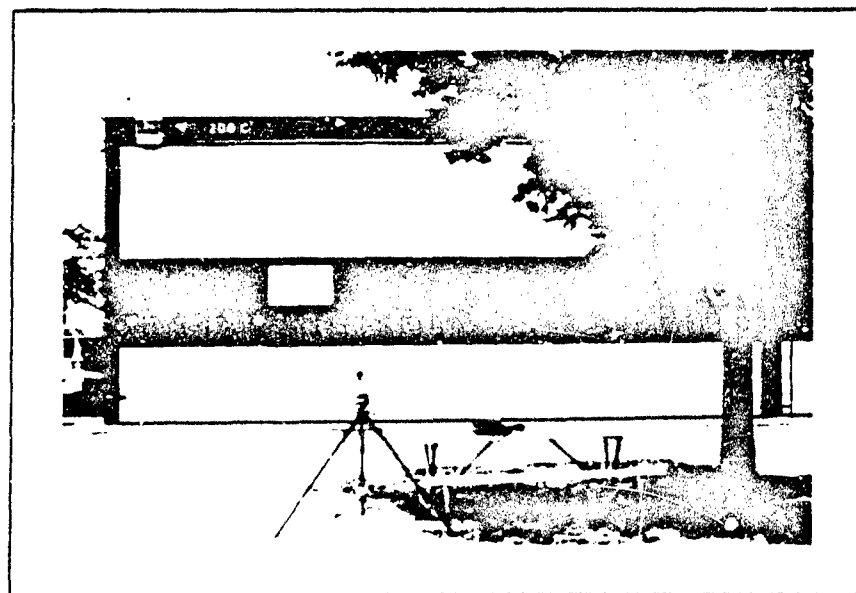
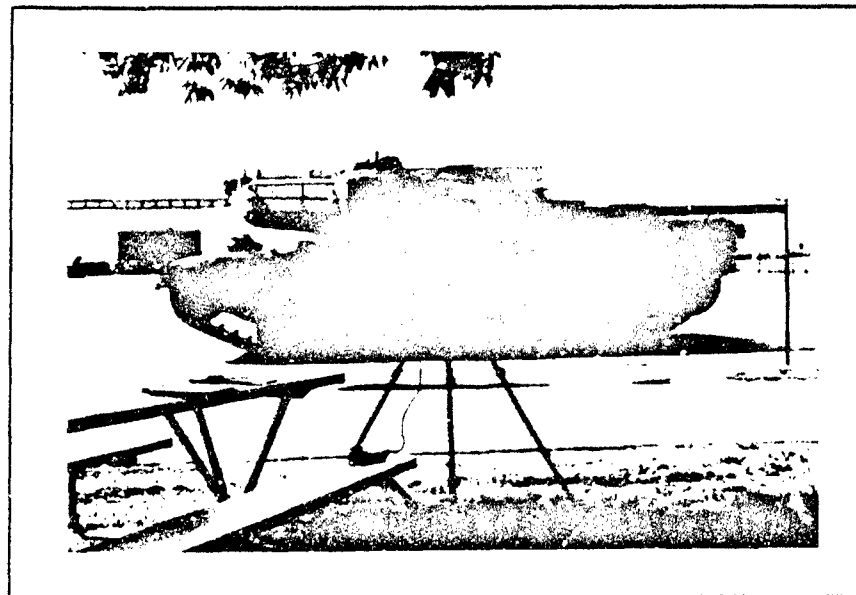


Figure 34
M1 Luminance Reading Setup for Study A and Study B on 19 July, 1990

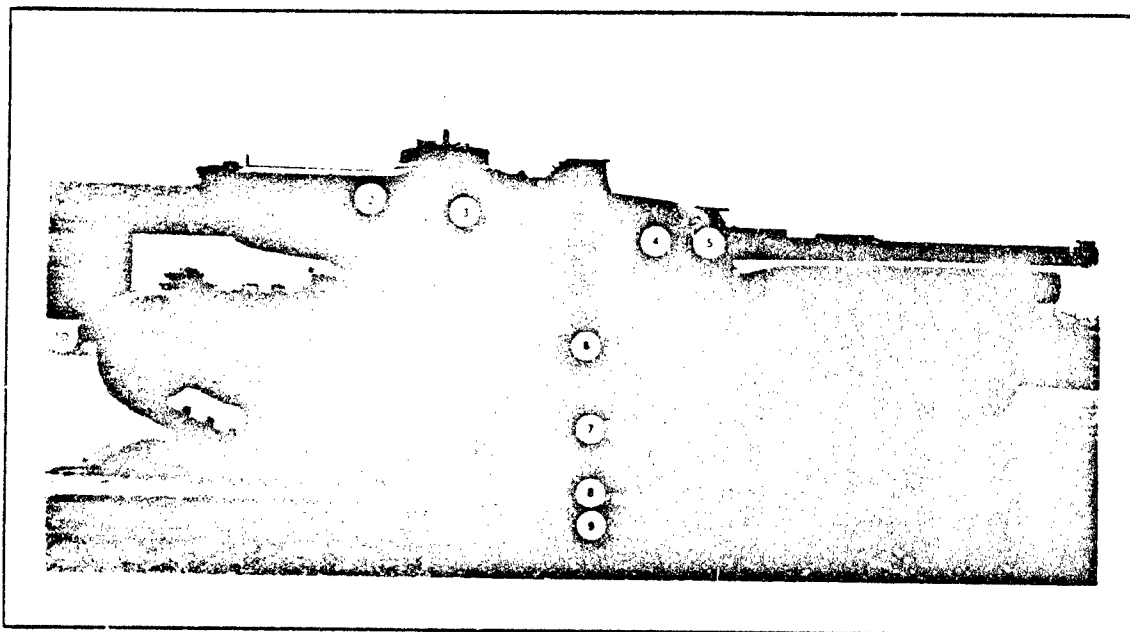


Figure 35
Position and Area of M1 Luminance Readings for Study A on 19 July, 1990

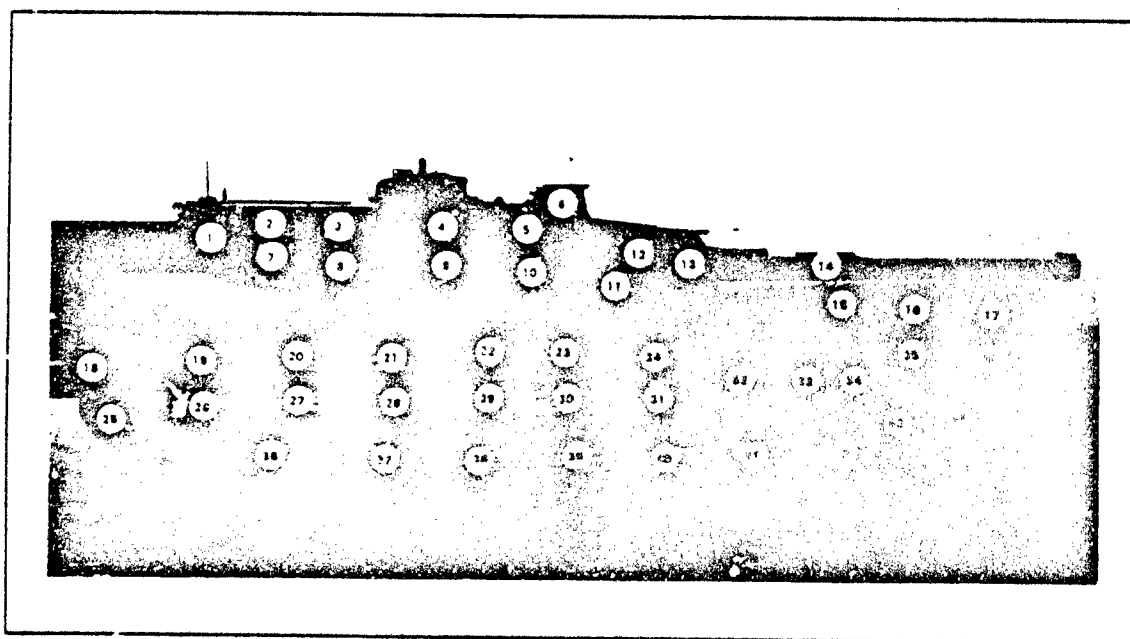


Figure 36
Position and Area of M1 Luminance Readings for Study B on 19 July, 1990

M1 Study A on 19 July, 1990.

Table 11. Summary of Luminance Readings for Study A on 19 July, 1990
(Hazy 9:00-12:00, Overcast 12:00-15:00)

Measurement Area	Range of Measurements (cd/m ²)	Average Luminance (cd/m ²)	Standard Deviation
#1 (Sky)	5,523 - 14,270	9,9005	2,659
#2 (M1 Turret)	639 - 1,763	1,354	306
#3 (M1 Turret)	381 - 952	710	131
#4 (M60 Turret)	690 - 1,950	1,401	297
#5 (M1 Turret)	569 - 4,106	1,554	959
#6 (M1 Skirt)	387 - 989	719	130
#7 (M1 Wheel)	151 - 447	322	66
#8 (Concrete)	1,110 - 5,440	3,200	1,106
#9 (Dirt-Gravel)	875 - 4,293	2,205	856
#10 (Grass)	899 - 3,311	2,503	629
#11 (Trees)	385 - 1,350	1,064	270

M1 LUMINANCE
RANGE - 36 FEET

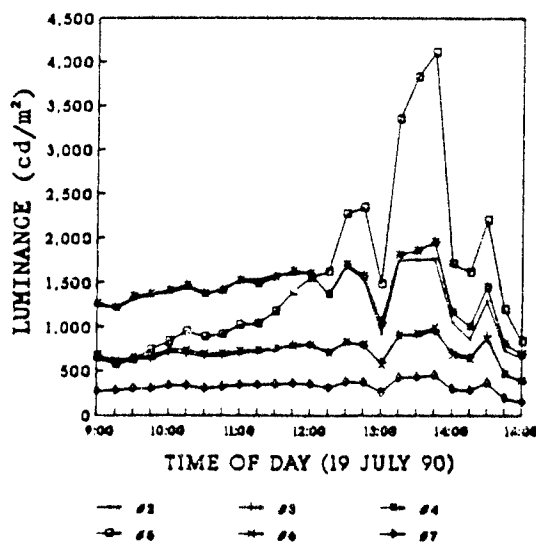


Figure 37

BACKGROUND LUMINANCE

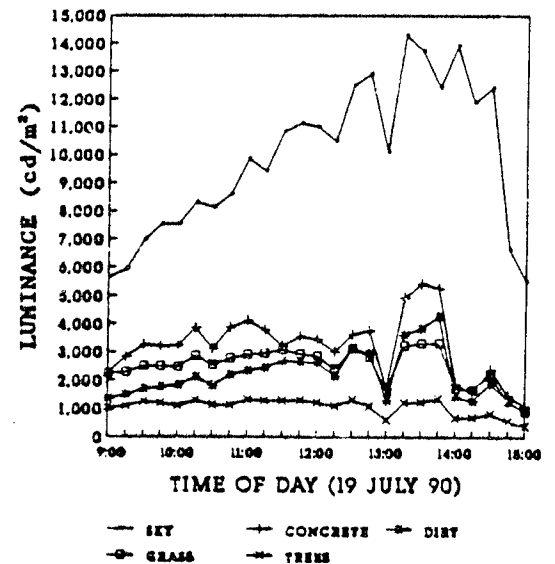


Figure 38

M1 Study A on 19 July, 90 (Hazy 9:00-12:00, Overcast 12:00-15:00)

M1 CONTRAST
SKY BACKGROUND

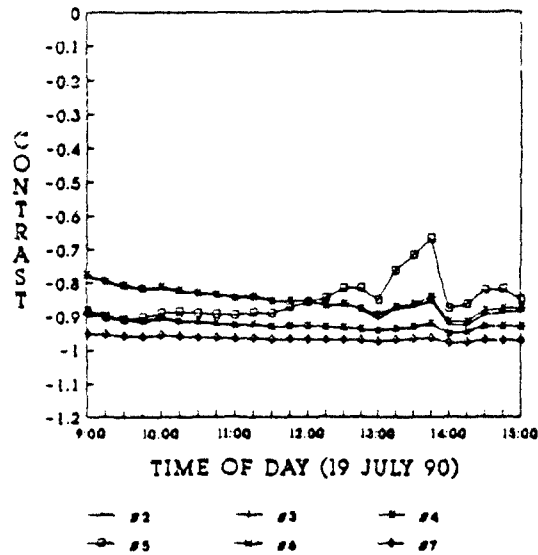


Figure 39

M1 CONTRAST
CONCRETE BACKGROUND

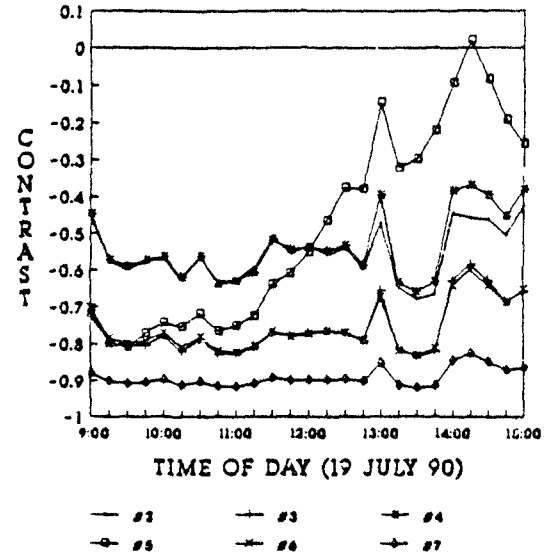


Figure 40

M1 CONTRAST
DIRT-GRAVEL BACKGROUND

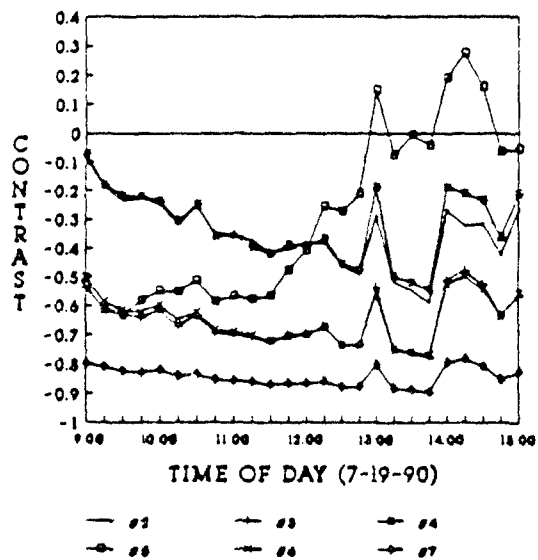


Figure 41

M1 CONTRAST
GRASS BACKGROUND

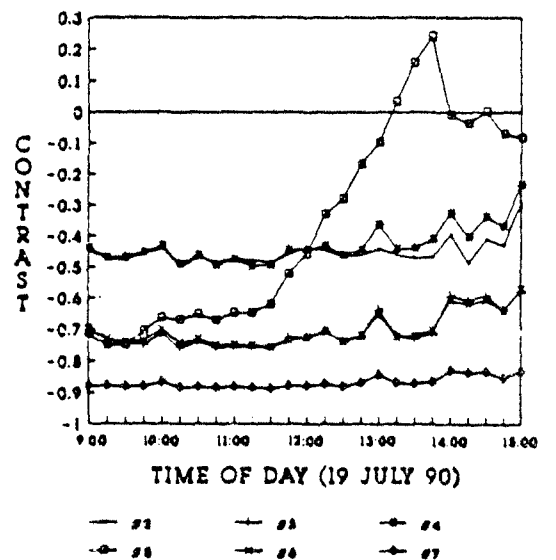


Figure 42

Table 12. Summary of Contrast Calculations for Study A on 19 July, 1990
(Hazy 9:00-12:00, Overcast 12:00-15:00)

Targ./Backg.	#2/Sky	#3/Sky	#4/Sky	#5/Sky	#6/Sky	#7/Sky
Minimum	-0.928	-0.949	-0.916	-0.910	-0.951	-0.979
Maximum	-0.781	-0.889	-0.777	-0.669	-0.880	-0.952
Average	-0.857	-0.926	-0.853	-0.852	-0.924	-0.966
Std. Dev.	0.037	0.013	0.034	0.058	0.016	0.007
Targ./Backg.	#2/Concr	#3/Concr	#4/Concr	#5/Concr	#6/Concr	#7/Concr
Minimum	-0.678	-0.834	-0.658	-0.209	-0.830	-0.921
Maximum	-0.424	-0.583	-0.368	0.020	-0.597	-0.825
Average	-0.554	-0.754	-0.534	-0.486	-0.755	-0.892
Std. Dev.	0.072	0.072	0.091	0.266	0.067	0.026
Targ./Backg.	#2/Dirt	#3/Dirt	#4/Dirt	#5/Dirt	#6/Dirt	#7/Dirt
Minimum	-0.589	-0.778	-0.546	-0.635	-0.770	-0.896
Maximum	-0.086	-0.479	-0.072	0.275	-0.497	-0.782
Average	-0.348	-0.650	-0.322	-0.294	-0.646	-0.843
Std. Dev.	0.116	0.084	0.123	0.295	0.081	0.032
Targ./Backg.	#2/Grass	#3/Grass	#4/Grass	#5/Grass	#6/Grass	#7/Grass
Minimum	-0.500	-0.760	-0.497	-0.751	-0.756	-0.887
Maximum	-0.289	-0.576	-0.232	0.241	-0.570	-0.830
Average	-0.452	-0.705	-0.428	-0.365	-0.702	-0.868
Std. Dev.	0.041	0.058	0.061	0.323	0.052	0.018
Targ./Backg.	#2/Trees	#3/Trees	#4/Trees	#5/Trees	#6/Trees	#7/Trees
Minimum	0.046	-0.488	0.072	-0.500	-0.475	-0.761
Maximum	0.660	0.081	0.792	2.124	0.039	-0.560
Average	0.298	-0.297	0.357	0.551	-0.291	-0.686
Std. Dev.	0.155	0.173	0.211	0.874	0.155	0.061

M1 Study B on 19 July, 1990 (Hazy 9:00-12:00, Overcast 12:00-15:00)

M1 LUMINANCE AT 10:05
RANGE = 36 FEET
19 JULY 1990

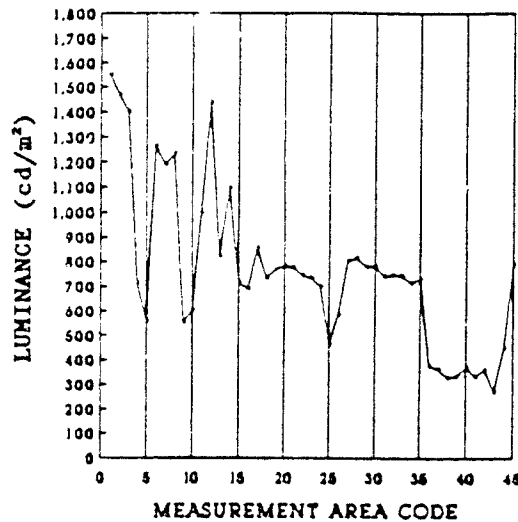


Figure 43

M1 LUMINANCE AT 10:35
RANGE = 36 FEET
19 JULY 1990

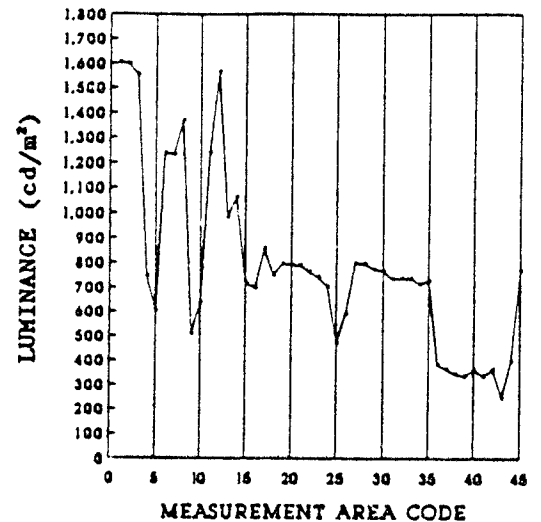


Figure 44

M1 LUMINANCE AT 11:05
RANGE = 36 FEET
19 JULY 1990

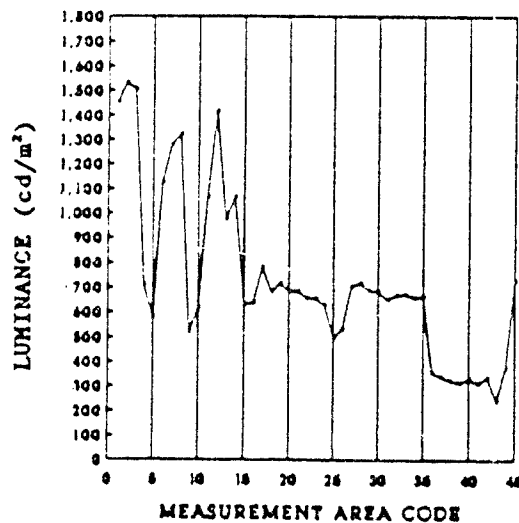


Figure 45

M1 LUMINANCE AT 11:35
RANGE = 36 FEET
19 JULY 1990

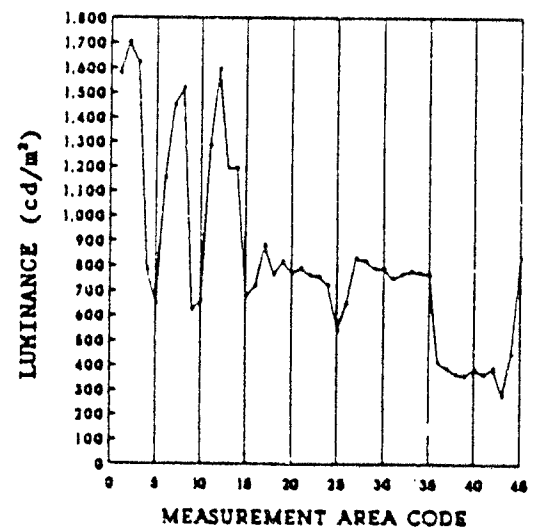


Figure 46

M1 Study B on 19 July, 1990 (Hazy 9:00-12:00, Overcast 12:00-15:00)

M1 LUMINANCE AT 12:05
RANGE = 36 FEET
19 JULY 1990

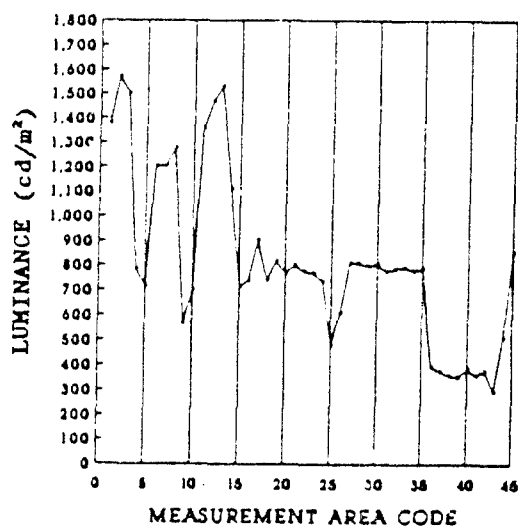


Figure 47

M1 LUMINANCE AT 12:35
RANGE = 36 FEET
19 JULY 1990

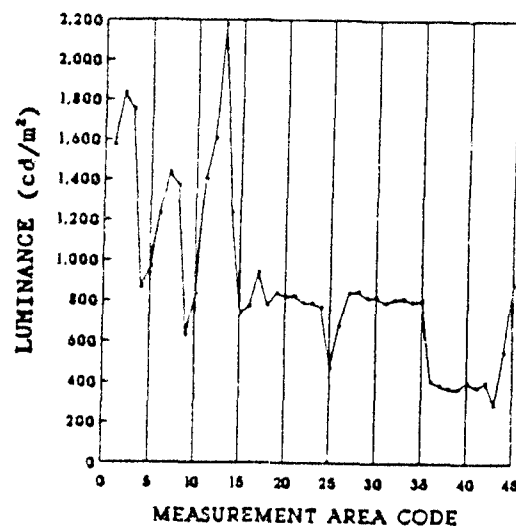


Figure 48

M1 LUMINANCE AT 13:05
RANGE = 36 FEET
19 JULY 1990

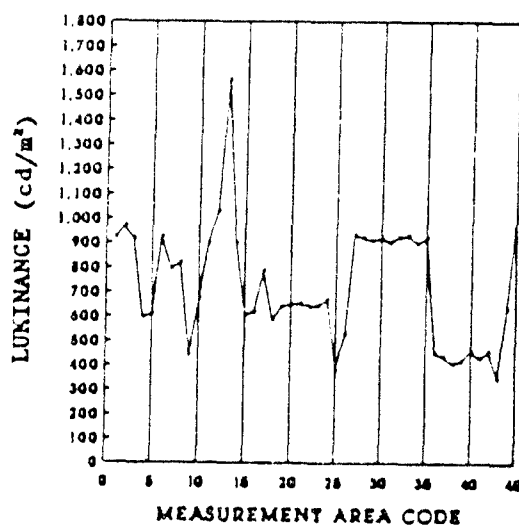


Figure 49

M1 LUMINANCE AT 13:35
RANGE = 36 FEET
19 JULY 1990

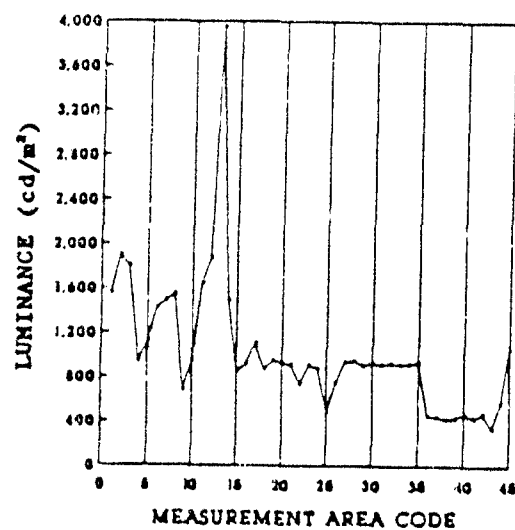


Figure 50

M1 Study B on 19 July, 1990 (Hazy 9:00-12:00, Overcast 12:00-15:00)

M1 LUMINANCE AT 14:05
RANGE = 36 FEET
19 JULY 1990

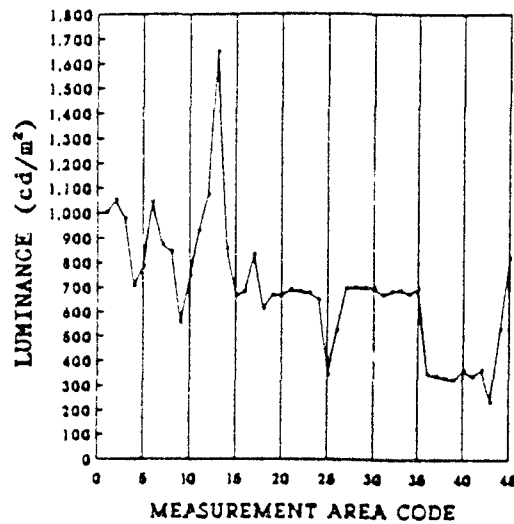


Figure 51

M1 LUMINANCE AT 14:35
RANGE = 36 FEET
19 JULY 1990

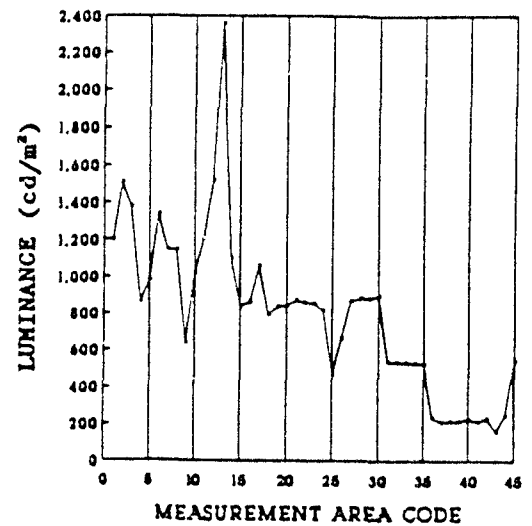


Figure 52

M1 LUMINANCE AT 15:05
RANGE = 36 FEET
19 JULY 1990

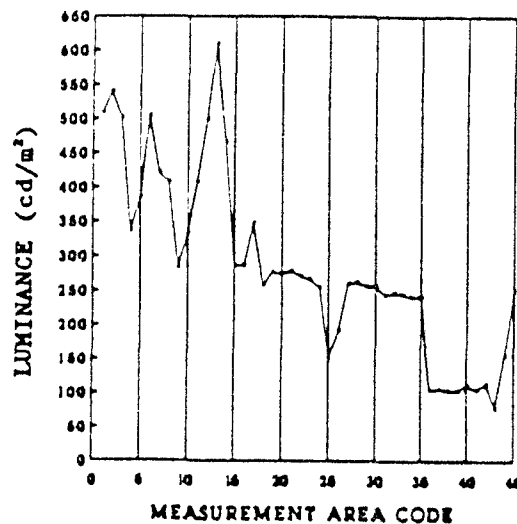


Figure 53

AVERAGE M1 LUMINANCE
RANGE = 36 FEET
19 JULY 1990: 10:05 - 15:05

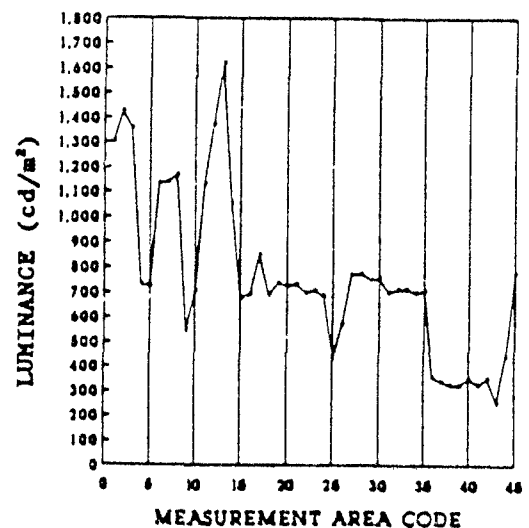


Figure 54

M1 Study on 19 July, 90 (Hazy 9:00-12:00, Overcast 12:00-15:00)

M1 CONTRAST
TREE BACKGROUND
STUDY A

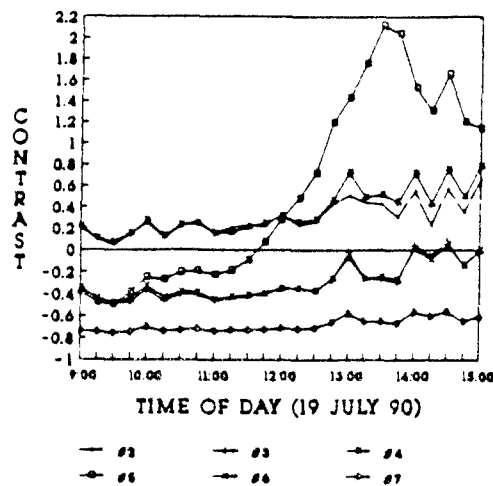


Figure 55

AVERAGE CONTRAST OF M1
RANGE = 36 FEET
STUDY B

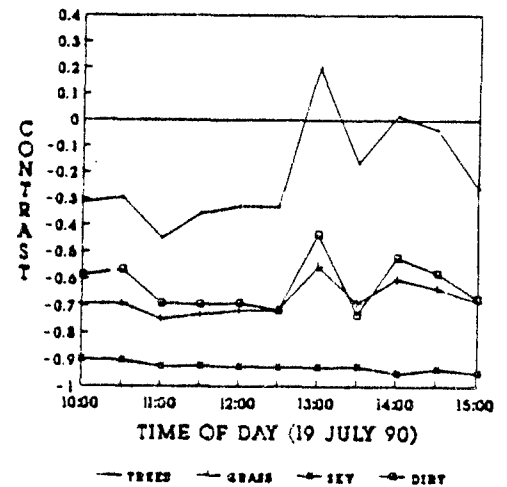


Figure 56

M1 LUMINANCE
RANGE = 36 FEET
STUDY B

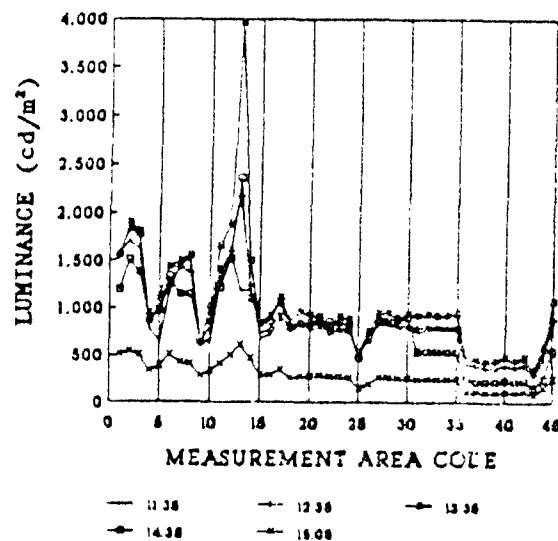


Figure 57

Study 1 August, 1990 Clear skies 10:00 - 15:30

Figure 58 shows the position and surroundings of the M1 used for studies 1 August, 1990 and 6 August, 1990. The M1 and tree line were facing east. The LS-100 meter was pointed west while luminance data was collected.

Luminance readings were acquired for the M1 and tree line using four different ranges from the M1: 36 feet, 100 feet, 200 feet and 330 feet. Figure 59, Figure 60,...Figure 62 show the approximate M1 measurement area for these four ranges.

Fifty different luminance readings were selected from the tree line between the poles in Figure 58. Readings were acquired from left to right using an up-down scanning pattern.

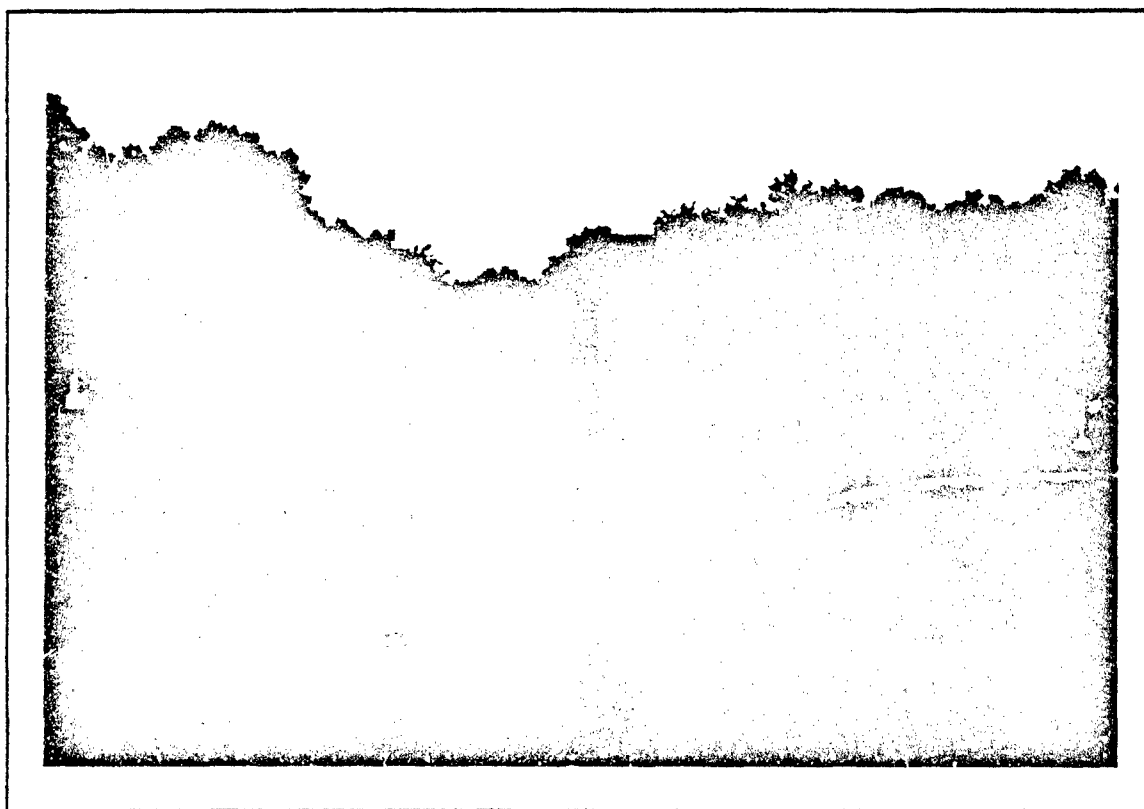


Figure 58

Position and surroundings of the M1 used for studies 1 August, 1990 and 6 August, 1990. The M1 and tree line were facing east. The LS-100 meter was pointed west while luminance data was collected.

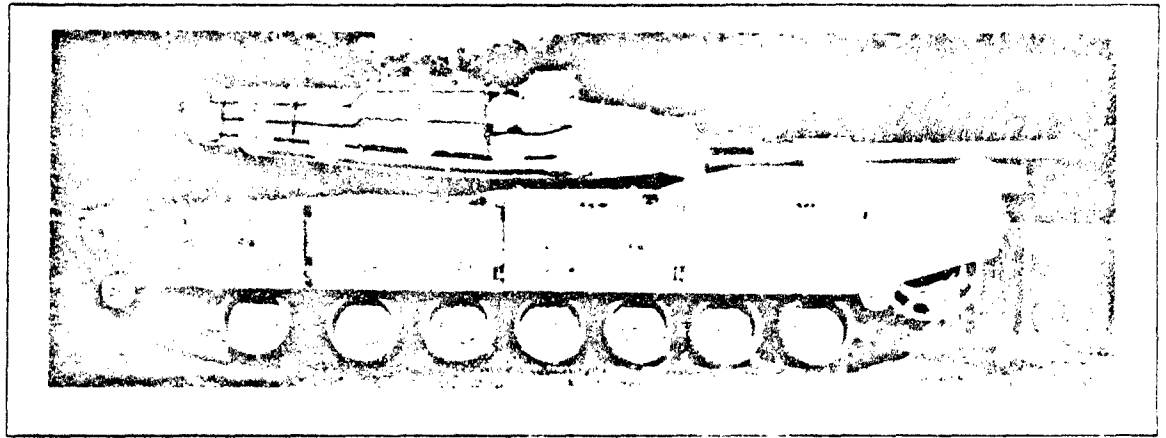


Figure 59

Approximate M1 Measurement Area for Study 1 August and 6 August, 1990.
Range = 36 feet

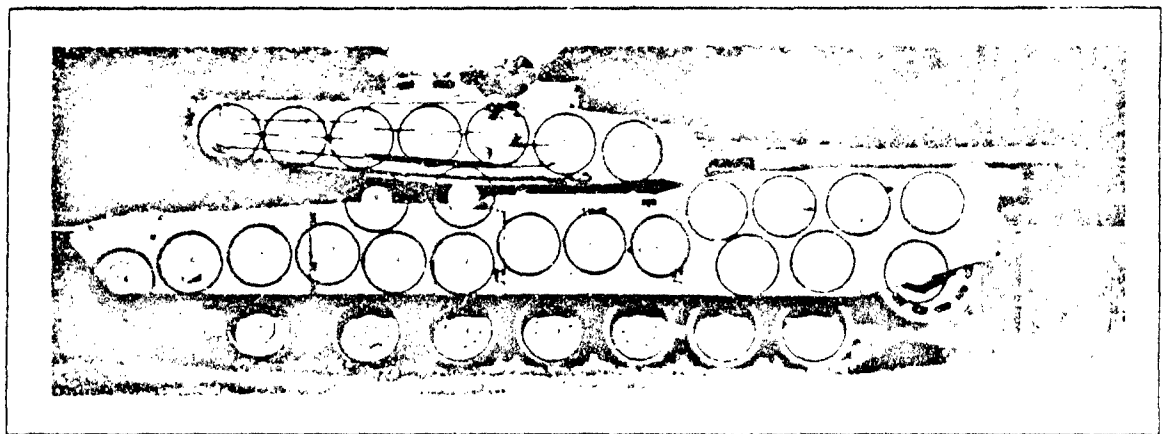


Figure 60

Approximate M1 Measurement Area for Study 1 August and 6 August, 1990.
Range = 100 feet

As the LS-100 Luminance Meter was moved farther from the M1, the luminance area measured on the M1 increased. The luminance area increases as the square of the range. If the range is doubled, the measurement area increases by a factor of four.

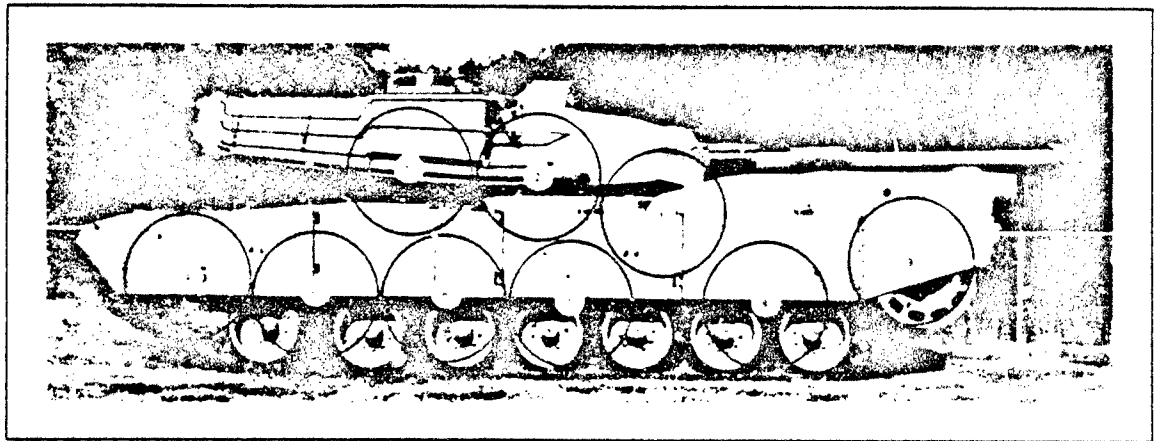


Figure 61

Approximate M1 Measurement Area for Study 1 August and 6 August, 1990.
Range = 200 feet

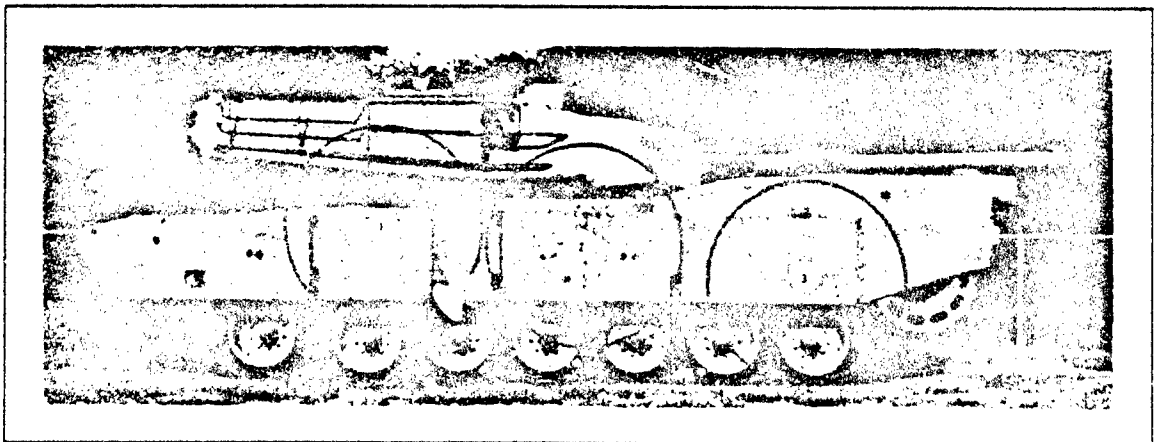


Figure 62

Approximate M1 Measurement Area for Study 1 August and 6 August, 1990.
Range = 330 feet

When the word "average" occurs in the title for the graphs that follow, it will indicate that the average luminance was used for constructing the graph.

All graphs involving the tree line were constructed using the average luminance of fifty random tree line luminance readings.

M1 Study on 1 August, 1990 (Clear Skies 10:00-15:30)

M1 LUMINANCE AT 10:00

RANGE = 36 FEET
1 AUGUST, 1990

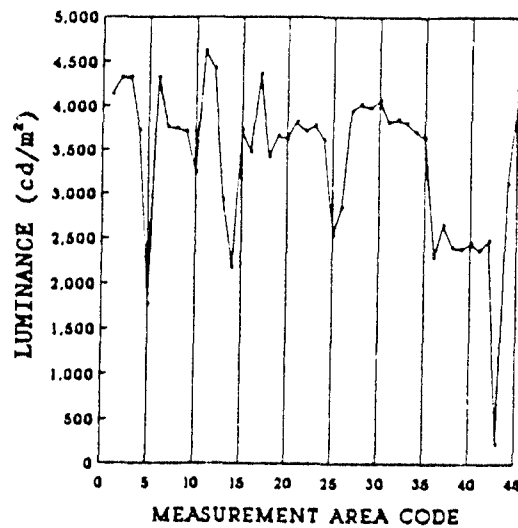


Figure 63

M1 LUMINANCE AT 11:00

RANGE = 36 FEET
1 AUGUST, 1990

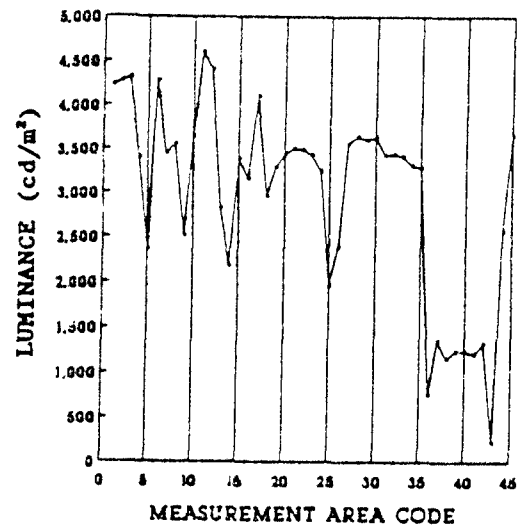


Figure 64

M1 LUMINANCE AT 12:00

RANGE = 36 FEET
1 AUGUST, 1990

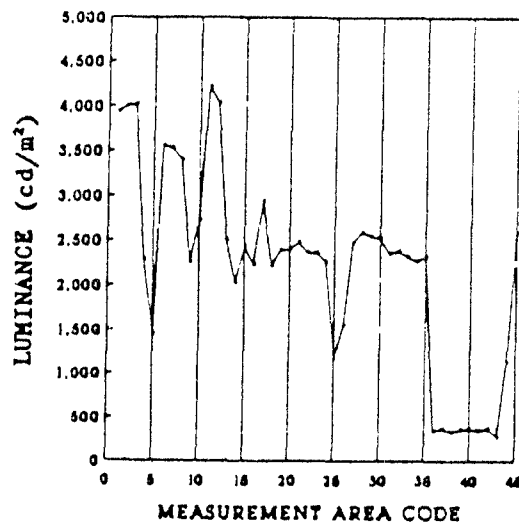


Figure 65

M1 LUMINANCE AT 13:00

RANGE = 36 FEET
1 AUGUST, 1990

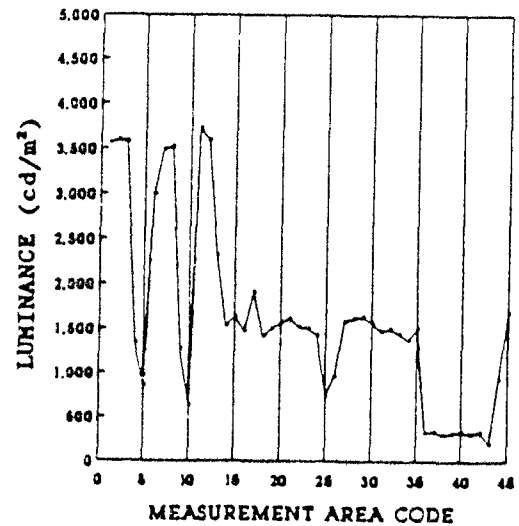


Figure 66

M1 Study on 1 August, 1990 (Clear Skies 10:00-15:30)

M1 LUMINANCE AT 14:00
RANGE = 36 FEET
1 AUGUST, 1990

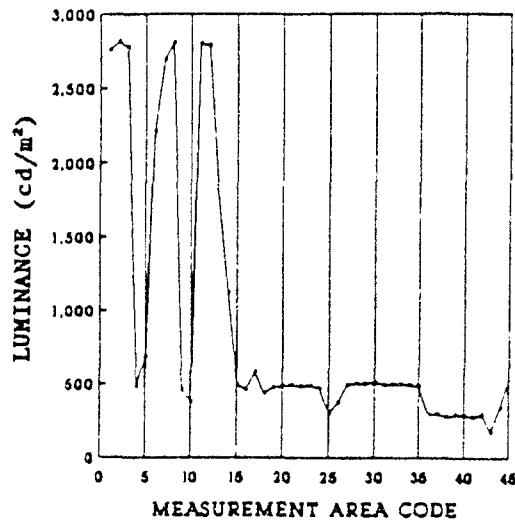


Figure 67

M1 LUMINANCE AT 15:00
RANGE = 36 FEET
1 AUGUST, 1990

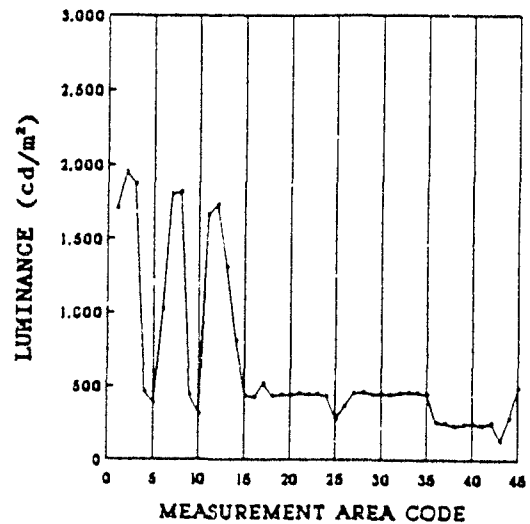


Figure 68

AVERAGE M1 LUMINANCE
RANGE = 36 FEET
1 AUGUST, 1990: 10:00 - 15:00

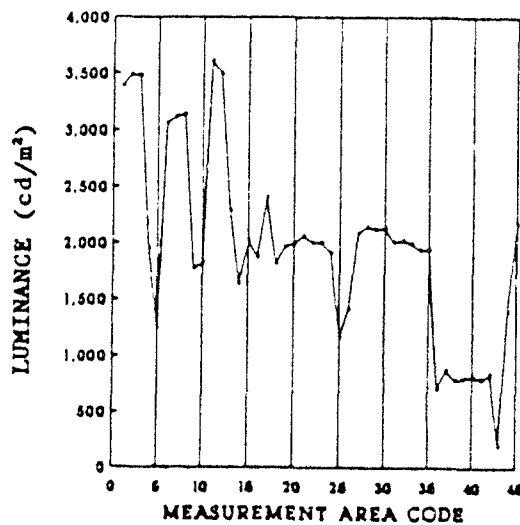


Figure 69

M1 Study on 1 August, 1990 (Clear Skies 10:00-15:30)

MI LUMINANCE AT 10:10
RANGE = 100 FEET
1 AUGUST, 1990

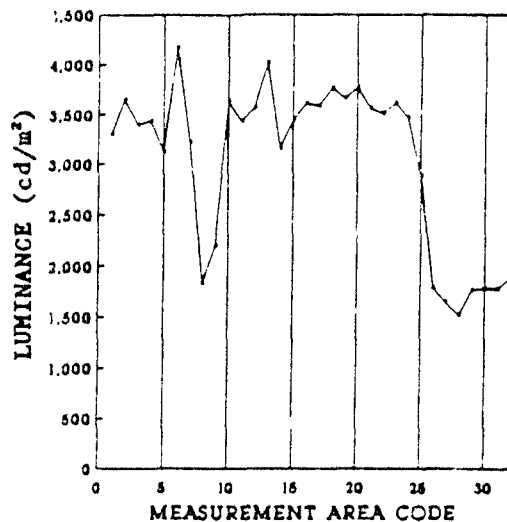


Figure 70

MI LUMINANCE AT 11:10
RANGE = 100 FEET
1 AUGUST, 1990

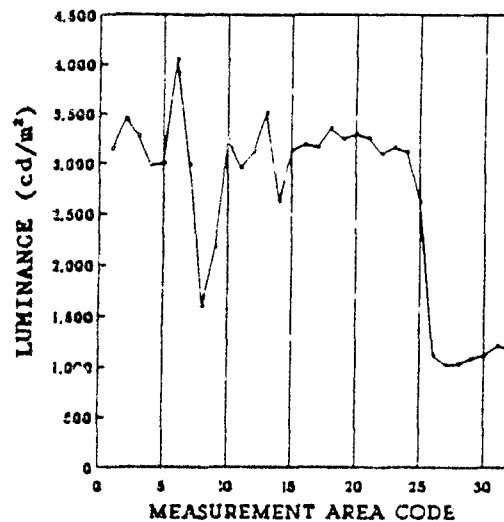


Figure 71

MI LUMINANCE AT 12:10
RANGE = 100 FEET
1 AUGUST, 1990

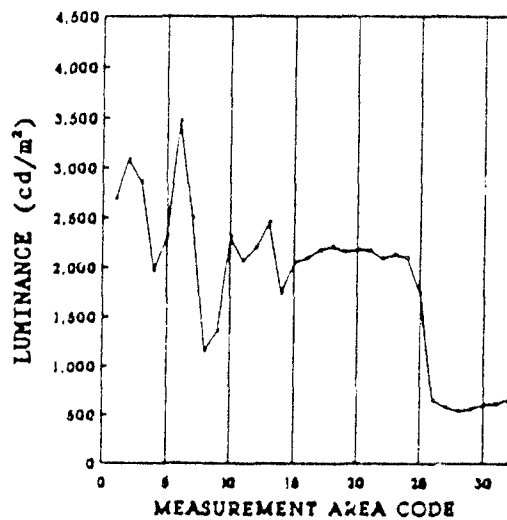


Figure 72

MI LUMINANCE AT 13:10
RANGE = 100 FEET
1 AUGUST, 1990

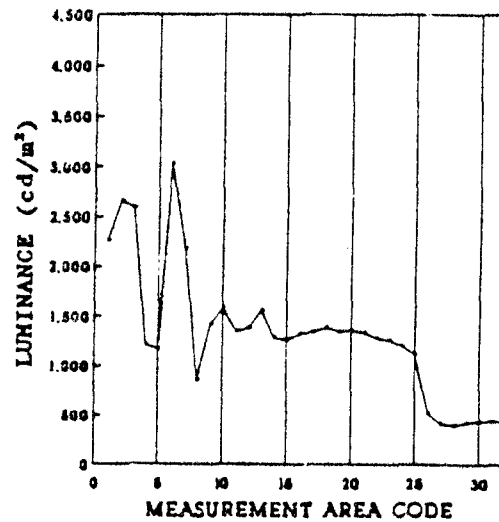


Figure 73

MI Study on 1 August, 1990 (Clear Skies 10:00-15:30)

MI LUMINANCE AT 14:10
RANGE • 100 FEET
1 AUGUST, 1990

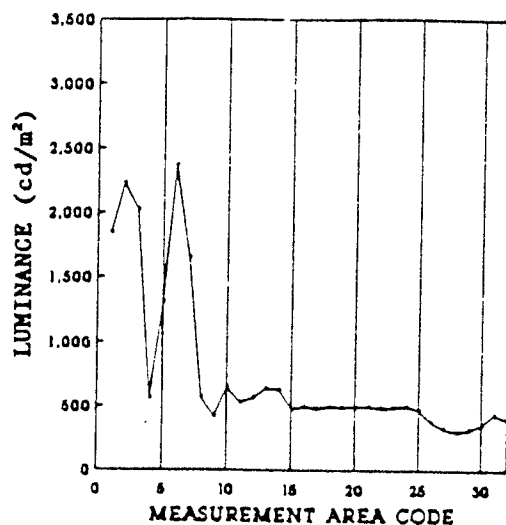


Figure 74

MI LUMINANCE AT 15:10
RANGE • 100 FEET
1 AUGUST, 1990

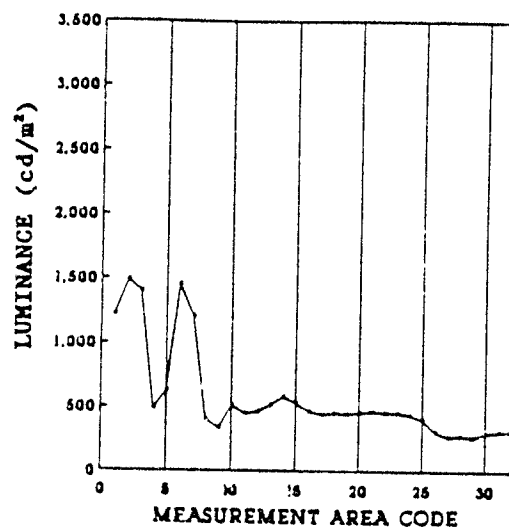


Figure 75

AVERAGE MI LUMINANCE
RANGE • 100 FEET
1 AUGUST, 1990: 10:10 - 15:10

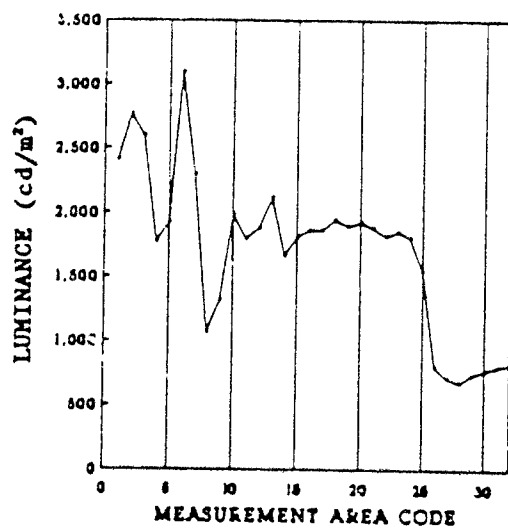


Figure 76

M1 Study on 1 August, 1990 (Clear Skies 10:00-15:30)

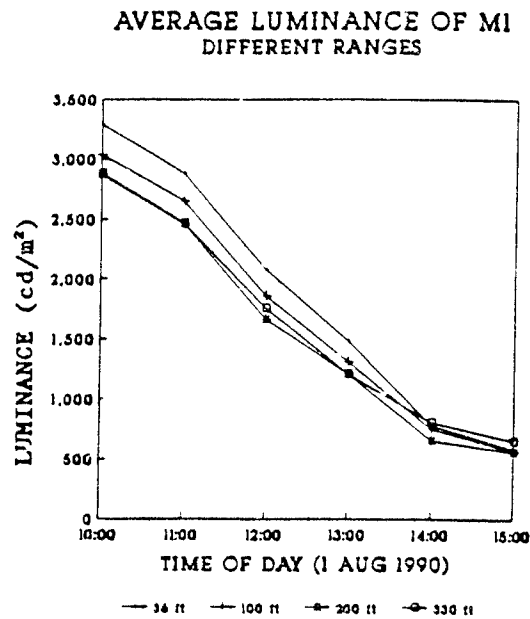


Figure 77

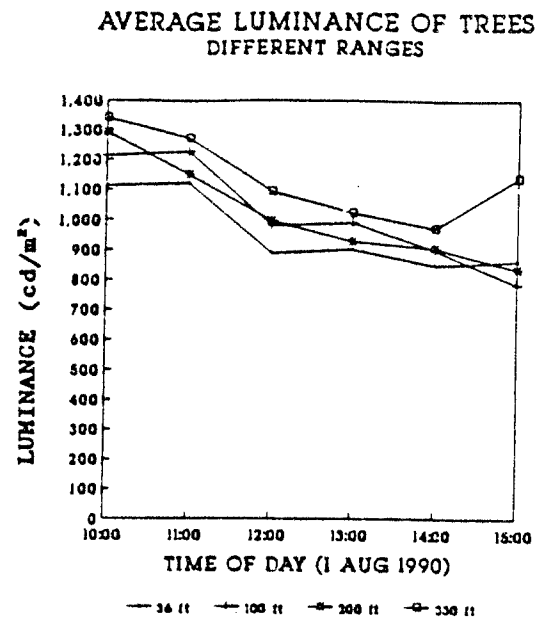


Figure 78

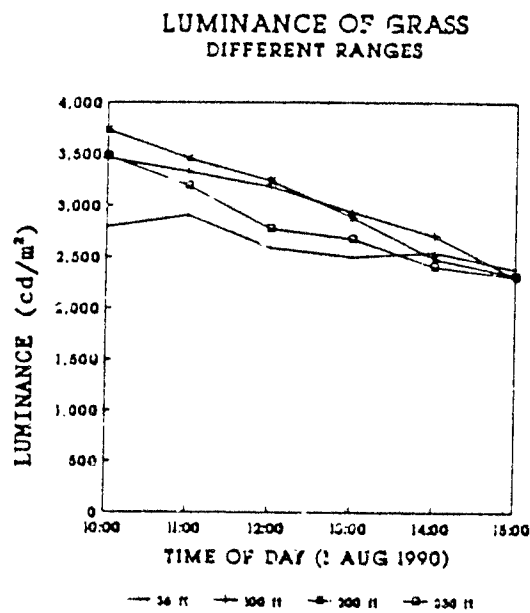


Figure 79

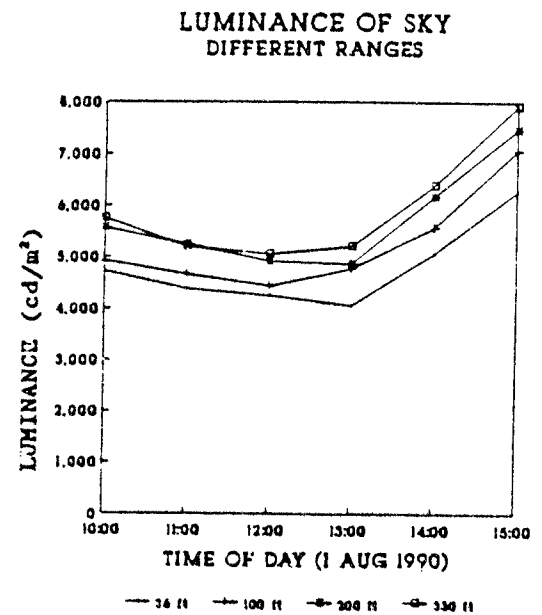


Figure 30

M1 Study on 1 Aug, 1990 (Clear Skies 10:00-15:30)

AVERAGE CONTRAST OF M1
AVERAGE TREE BACKGROUND
DIFFERENT RANGES

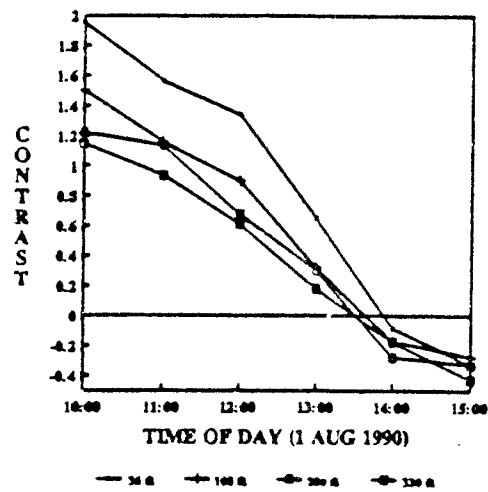


Figure 81

AVERAGE CONTRAST OF M1
GRASS BACKGROUND
DIFFERENT RANGES

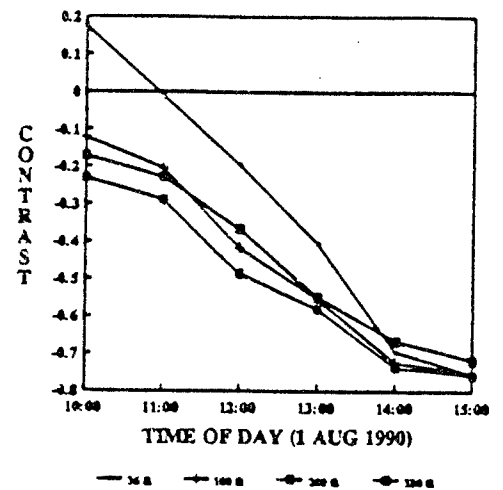


Figure 82

AVERAGE CONTRAST OF M1
SKY BACKGROUND
DIFFERENT RANGES

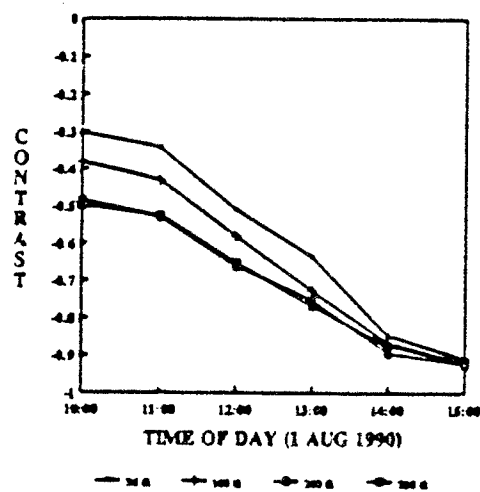


Figure 83

M1 Study on 1 August, 1990 (Clear Skies 10:00-15:30)

AVERAGE CONTRAST OF M1
RANGE = 36 FEET

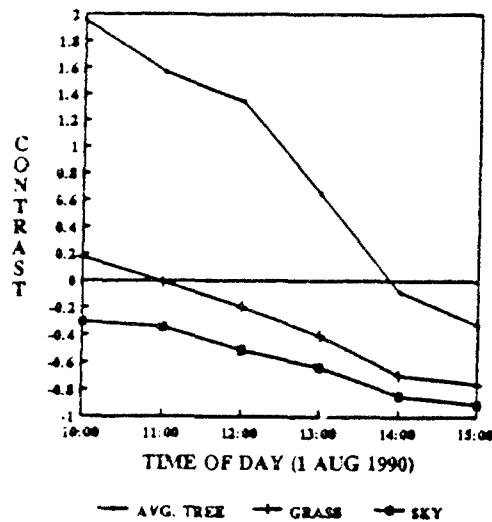


Figure 84

AVERAGE CONTRAST OF M1
RANGE = 100 FEET

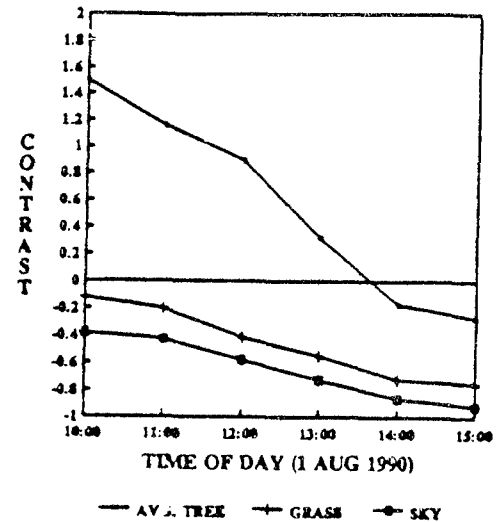


Figure 85

AVERAGE CONTRAST OF M1
RANGE = 100 FEET

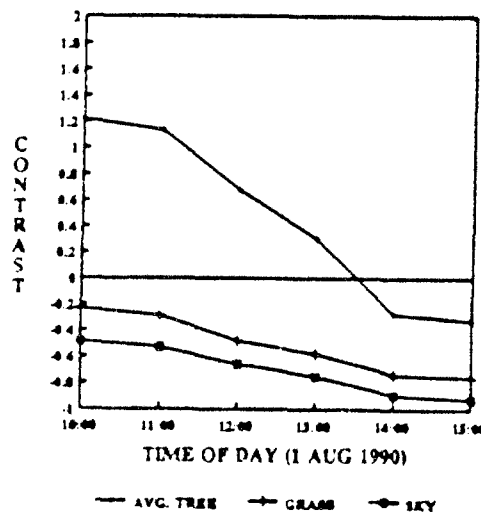


Figure 86

AVERAGE CONTRAST OF M1
RANGE = 330 FEET

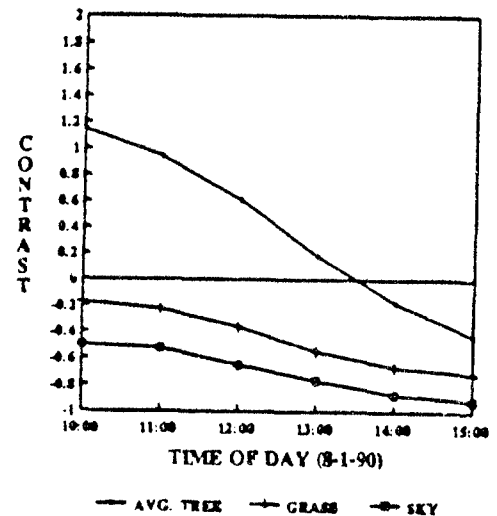


Figure 87

M1 Study on 1 August, 1990 (Clear Skies 10:00-15:30)

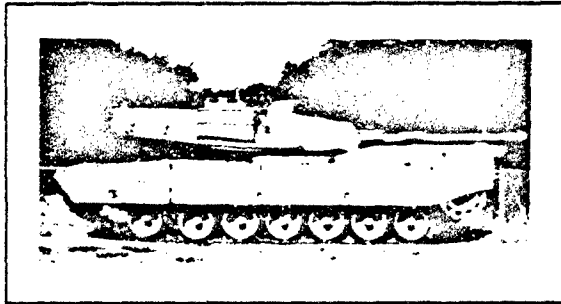


Figure 88

10:00 1 August, 1990

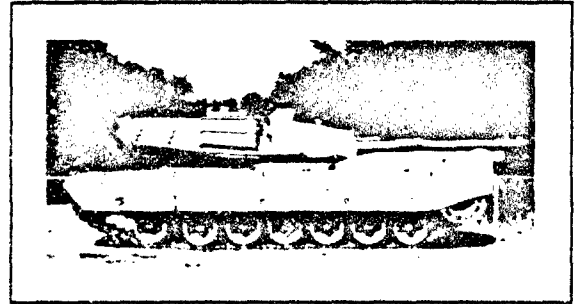


Figure 89

11:00 1 August, 1990

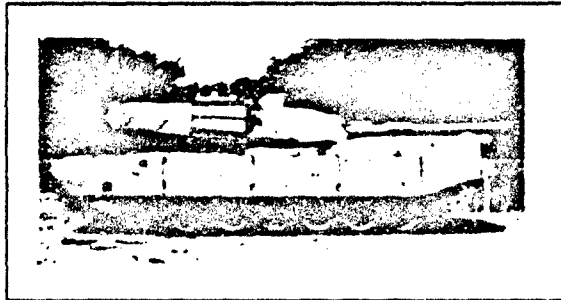


Figure 90

12:00 1 August, 1990

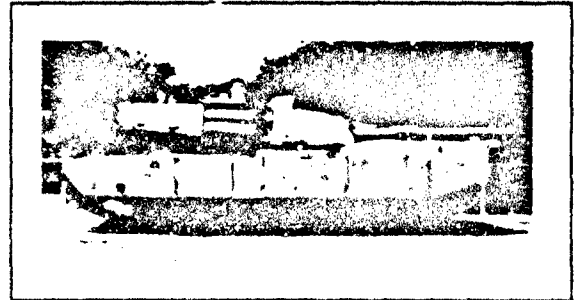


Figure 91

13:00 1 August, 1990

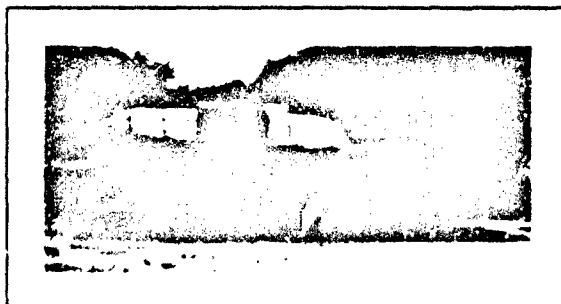


Figure 92

14:00 1 August, 1990

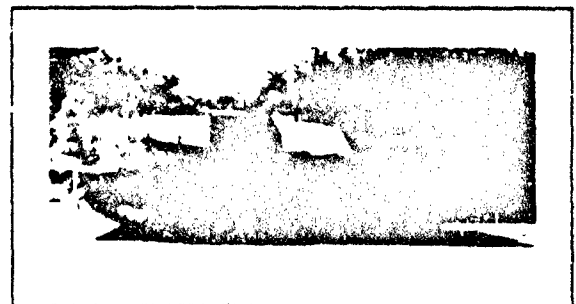


Figure 93

15:00 1 August, 1990

Table 13. M1 Area Luminance Analysis For Times 10:00 - 15:00 on 1 August, 1990

Range - 36 feet			Range - 100 feet		
Area #	Avg.	St. Dev.	Area #	Avg.	St. Dev.
1	3388	897	1	2410	726
2	3493	856	2	2762	740
3	3480	895	3	2589	698
4	1946	1297	4	1774	1132
5	1249	677	5	1924	945
6	3064	1168	6	3090	951
7	3119	675	7	2291	705
8	3142	659	8	1066	517
9	1774	1174	9	1315	742
10	1822	1413	10	1985	1192
11	3605	1066	11	1795	1134
12	3496	966	12	1881	1187
13	2282	567	13	2117	1338
14	1637	530	14	1664	961
15	2021	1286	15	1811	1168
16	1870	1198	16	1864	1224
17	2402	1535	17	1864	1222
18	1813	1156	18	1945	1293
19	1961	1262	19	1890	1251
20	1995	1280	20	1927	1286
21	2061	1331	21	1879	1226
22	2002	1308	22	1818	1188
23	2001	1311	23	1851	1229
24	1908	1246	24	1800	1190
25	1161	839	25	1537	966
26	1413	948	26	792	516
27	2087	1370	27	709	486
28	2142	1403	28	678	452
29	2117	1386	29	740	534
30	2127	1411	30	771	529
31	2005	1322	31	800	526
32	2022	1326	32	817	561
33	1989	1311			
34	1933	1273			
35	1946	1253			
36	709	723			
37	876	880			
38	781	790			
39	807	782			
40	820	801			
41	791	780			
42	843	817			
43	205	46			
44	1396	1079			
45	2165	1393			
Avg.	1952	1060	Avg.	1692	932
St. Dev.	325	311	St. Dev.	616	301

Table 14. M1 Area Luminance Analysis For Times 10:00 - 15:00 on 1 August, 1990
Clear Skies All Day.

Range - 200 feet			Range - 330 feet		
Area #	Avg.	St. Dev.	Area #	Avg.	St. Dev.
1	1546	766	1	1529	801
2	1679	949	2	1748	871
3	2091	921	3	1600	808
4	1557	709			
5	1398	808			
6	1380	863			
7	1455	906			
8	1387	829			
9	1614	1040			
<hr/>			<hr/>		
Avg.	1567	866	Avg.	1626	827
St. Dev.	210	95	St. Dev.	91	32

The column heading 'Avg.' in Table 13 and Table 14 refers to the averages of six luminance readings acquired between the times 10:00 and 15:00 for each measurement area.

The column heading 'St. Dev.' refers to the standard deviation.

Table 13 relates to Figure 59 and Figure 60. Table 14 relates to Figure 61 and Figure 62.

Table 15. Average Tree Line Luminance (cd/m^2) on 1 August, 1990

Range	10:00	11:00	12:00	13:00	14:00	15:00	Avg.
36'	1113	1121	888	901	849	863	956
100'	1213	1226	979	991	899	786	1016
200'	1291	1150	995	923	906	837	1018
330'	1341	1272	1092	1024	972	1140	1140
Avg.	1240	1192	989	961	907	907	1033
S. D.	86	60	72	49	44	138	75

Table 16. Summary of Diurnal Luminance Averages (cd/m^2) for 1 August, 1990
Clear Skies All Day.

Range	Time	Avg. M1	Avg. Tree	Grass	Sky
36 feet	10:00	2295	1113	2797	4724
36 feet	11:00	2872	1121	2907	4382
36 feet	12:00	2075	888	2584	4256
36 feet	13:00	1481	901	2497	4071
36 feet	14:00	777	849	2546	5072
36 feet	15:00	579	863	2383	6272
36 feet	Average	1845	956	2619	4796
36 feet	Std. Dev.	1005	115	179	736
100 feet	10:00	3035	1213	3461	4914
100 feet	11:00	2643	1226	3327	4657
100 feet	12:00	1855	979	3123	4440
100 feet	13:00	1308	991	2935	4784
100 feet	14:00	745	899	2703	5576
100 feet	15:00	569	786	2307	7072
100 feet	Average	1693	1016	2986	5241
100 feet	Std. Dev.	917	159	393	891
200 feet	10:00	2866	1291	3729	5567
200 feet	11:00	2453	1150	3454	5242
200 feet	12:00	1665	993	3237	4922
200 feet	13:00	1207	928	2881	4866
200 feet	14:00	653	906	2482	6189
200 feet	15:00	560	837	2323	7473
200 feet	Average	1567	1018	3018	5710
200 feet	Std. Dev.	862	156	505	905
330 feet	10:00	2879	1341	3477	5753
330 feet	11:00	2441	1272	3190	5201
330 feet	12:00	1756	1092	2774	5057
330 feet	13:00	1206	1024	2676	5211
330 feet	14:00	801	972	2405	6389
330 feet	15:00	631	1140	2306	7928
330 feet	Average	1626	1140	2805	5923
330 feet	Std. Dev.	826	130	414	1004

Table 17. Analysis of M1 Turret Luminance Readings (cd/m^2) on 1 August, 1990
Range = 36 feet. Clear Skies All Day.

Area #	10:00	11:00	12:00	13:00	14:00	15:00	Avg.	Sd. Dev
1	4138	4226	3935	3563	2761	1704	3388	897
2	4317	4275	3999	3598	2817	1951	3493	856
3	4325	4317	4015	3581	2776	1867	3480	895
4	3719	3397	2282	1342	480	457	1946	1297
5	1767	2357	1446	854	685	386	1249	677
6	4318	4279	3557	2996	2212	1023	3064	1168
7	3750	3447	3525	3494	2695	1800	3119	675
8	3740	3560	3398	3524	2807	1820	3142	659
9	3707	2512	2254	1269	463	436	1774	1174
10	3243	3649	2726	624	376	312	1822	1413
11	4618	4606	4211	3732	2800	1665	3605	1066
12	4421	4414	4027	3593	2789	1732	3496	966
13	2924	2827	2500	2316	1815	1307	2282	567
<hr/>								
Avg.	3768	3682	3221	2653	1960	1266	2758	947
St. Dev.	744	723	848	1154	1013	625	789	255

Table 18. Analysis of M1 Turret Luminance Readings (cd/m^2) on 1 August, 1990
Range = 100 feet. Clear Skies All Day.

Area #	10:10	11:10	12:10	13:10	14:10	15:10	Avg.	St. Dev.
1	3300	3144	2688	2261	1846	1220	2410	726
2	3650	3452	3083	2662	2230	1488	2762	740
3	3394	3275	2852	2587	2023	1400	2589	698
4	3439	2976	1962	1220	562	483	1774	1132
5	3118	3004	2311	1170	1313	628	1924	945
6	4166	4049	3470	3032	2367	1455	3090	951
7	3220	2984	2501	2182	1652	1209	2291	705
<hr/>								
Avg.	3470	3269	2696	2159	1713	1126	2406	842
St. Dev.	325	358	463	662	573	376	426	156

Table 19. Analysis of M1 Skirt Luminance Readings (cd/m^2) on 1 August, 1990
Range = 36 feet. Clear Skies All Day.

Area #	10:00	11:00	12:00	13:00	14:00	15:00	Avg.	St. Dev.
18	3416	2962	2217	1417	435	429	1813	1156
19	3656	3297	2390	1504	475	443	1961	1262
20	3625	3449	2401	1574	481	437	1995	1280
21	3815	3513	2484	1616	489	450	2061	1331
22	3712	3493	2364	1516	482	442	2002	1308
23	3777	3434	2364	1501	485	446	2001	1311
24	3615	3247	2258	1430	466	431	1908	1246
27	3944	3569	2477	1584	493	453	2087	1370
28	4022	3652	2595	1618	503	459	2142	1403
29	3977	3612	2542	1632	498	443	2117	1386
30	4063	3647	2524	1564	512	451	2127	1411
31	3813	3444	2361	1479	489	441	2005	1322
32	3846	3449	2383	1503	495	454	2022	1326
33	3800	3421	2319	1440	497	457	1989	1311
34	3700	3316	2265	1376	489	454	1933	1273
35	3636	3294	2320	1507	479	442	1946	1253
45	4034	3667	2584	1690	528	489	2165	1393
Avg.	3791	3439	2403	1527	488	448	2016	1314
St. Dev.	172	174	111	83	19	13	90	65

Table 20. Analysis of M1 Skirt Luminance Readings (cd/m^2) on 1 August, 1990
Range = 100 feet. Clear Skies All Day.

Area #	10:10	11:10	12:10	13:10	14:10	15:10	Avg.	St. Dev.
15	3438	3130	2042	1260	473	525	1811	1168
16	3607	3199	2092	1326	494	467	1864	1224
17	3579	3172	2170	1345	478	441	1864	1222
18	3766	3363	2204	1389	494	452	1945	1293
19	3654	3252	2154	1344	488	445	1890	1251
20	3772	3308	2174	1358	493	454	1927	1286
21	3559	3257	2168	1334	493	464	1879	1226
22	3501	3098	2087	1279	485	456	1818	1188
23	3614	3164	2125	1261	487	456	1851	1229
24	3460	3119	2088	1197	498	438	1800	1190
Avg.	3595	3206	2130	1309	488	460	1865	1228
St. Dev.	109	82	49	55	7	23	45	39

Study 6 August, 1990 Overcast skies 10:00 - 15:30.

The only difference between this study and Study 1 conducted on August, 1990 is sky condition. The overcast sky condition during this study produced no sharp shadows.

Figure 58 shows the the M1 position and its background. The M1's position and orientation was not altered during the time interval between the Study 1 on August, 1990 and the Study 6 on August, 1990.

Figure 59, Figure 60,...Figure 62 show the approximate M1 measurement areas used for this study.

M1 Study on 6 August, 1990 (Overcast 10:00-15:30)

MI LUMINANCE AT 10:00

RANGE = 36 FEET
6 AUGUST, 1990

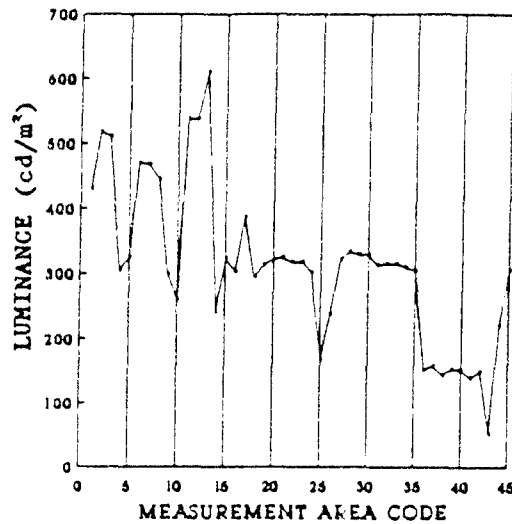


Figure 94

MI LUMINANCE AT 11:00

RANGE = 36 FEET
6 AUGUST, 1990

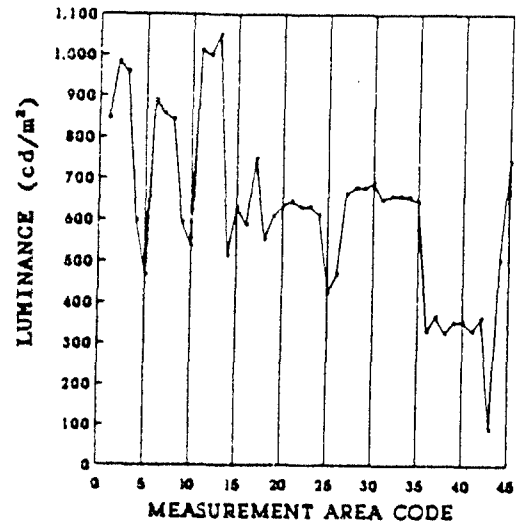


Figure 95

MI LUMINANCE AT 12:00

RANGE = 36 FEET
6 AUGUST, 1990

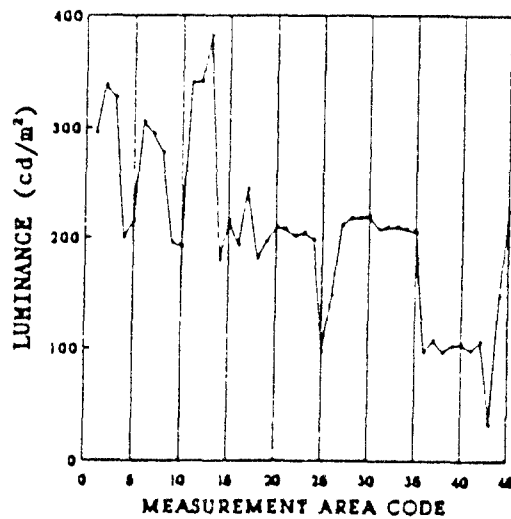


Figure 96

MI LUMINANCE AT 13:00

RANGE = 36 FEET
6 AUGUST, 1990

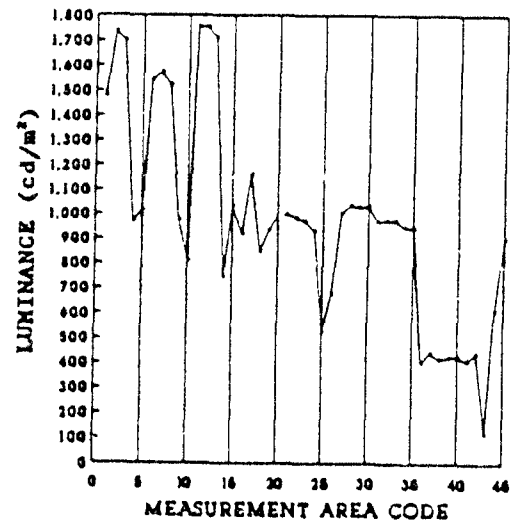


Figure 97

M1 Study on 6 August, 1990 (Overcast 10:00-15:30)

M1 LUMINANCE AT 14:00
RANGE = 36 FEET
6 AUGUST, 1990

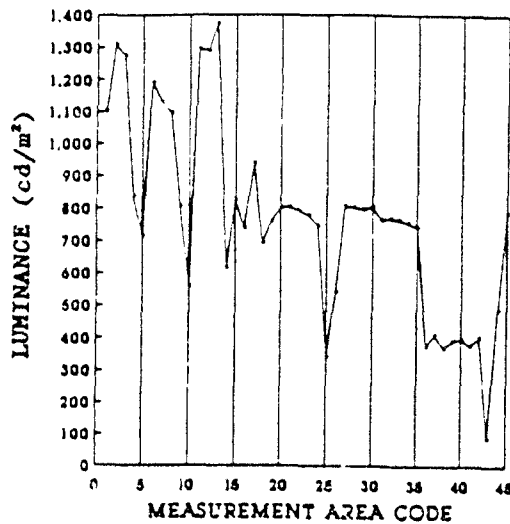


Figure 98

M1 LUMINANCE AT 15:00
RANGE = 36 FEET
6 AUGUST, 1990

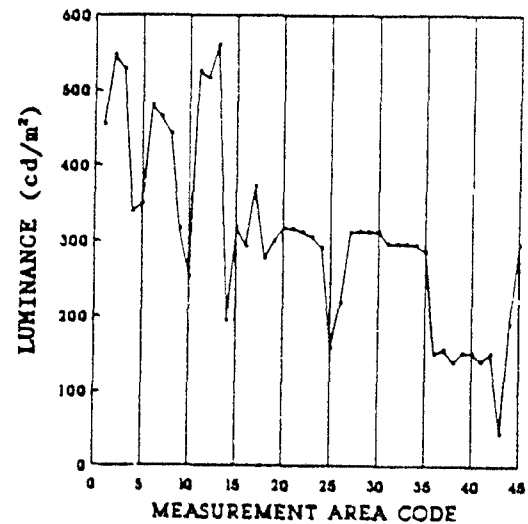


Figure 99

AVERAGE M1 LUMINANCE
RANGE = 36 FEET
6 AUGUST, 1990; 10:00 - 15:00

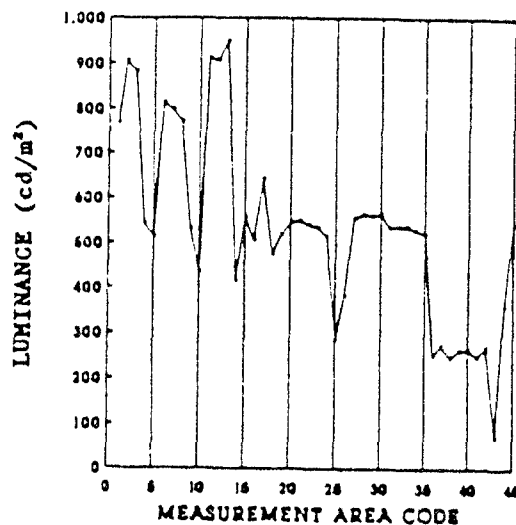


Figure 100

M1 Study on 6 August, 1990 (Overcast 10:00-15:30)

M1 LUMINANCE AT 10:10
RANGE = 100 FEET
6 AUGUST, 1990

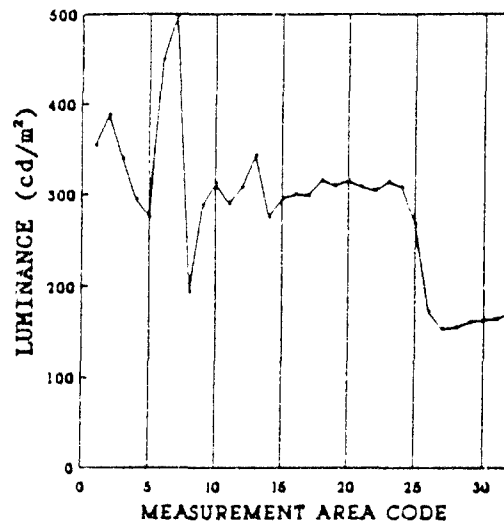


Figure 101

M1 LUMINANCE AT 11:10
RANGE = 100 FEET
6 AUGUST, 1990

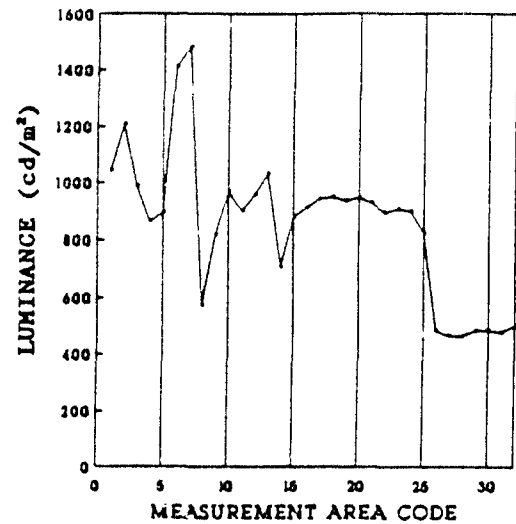


Figure 102

M1 LUMINANCE AT 12:10
RANGE = 100 FEET
6 AUGUST, 1990

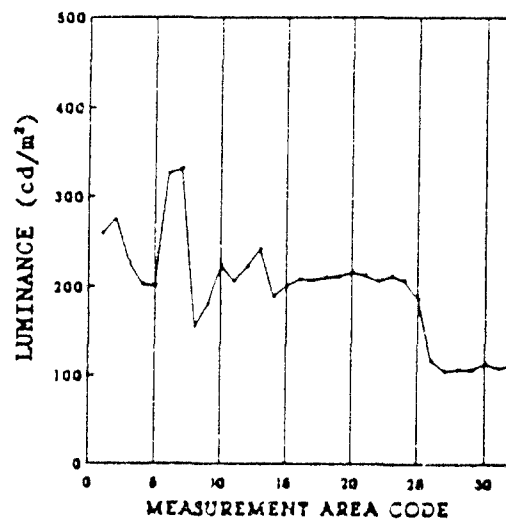


Figure 103

M1 LUMINANCE AT 13:10
RANGE = 100 FEET
6 AUGUST, 1990

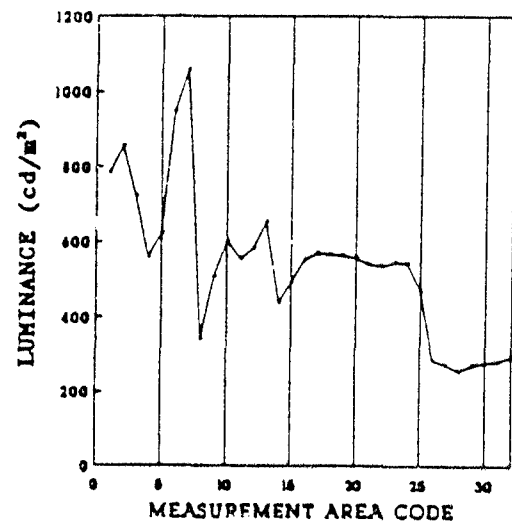


Figure 104

M1 Study on 6 August, 1990 (Overcast 10:00-15:30)

MI LUMINANCE AT 14:10
RANGE = 100 FEET
6 AUGUST, 1990

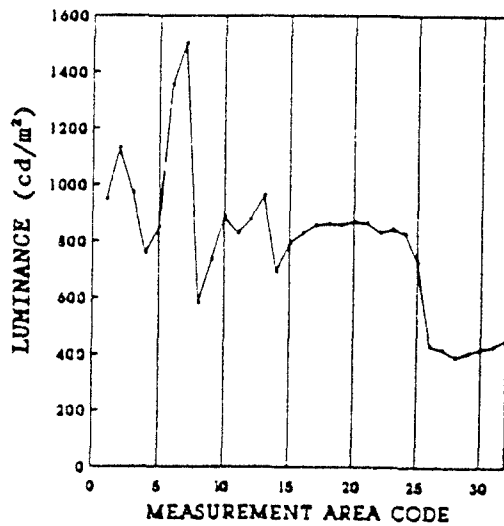


Figure 105

MI LUMINANCE AT 15:10
RANGE = 100 FEET
6 AUGUST, 1990

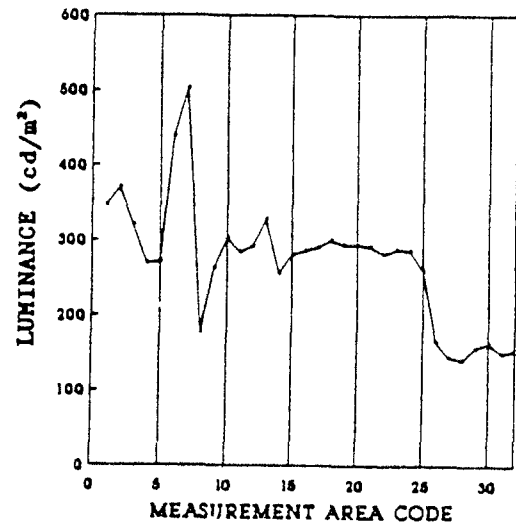


Figure 106

AVERAGE MI LUMINANCE
RANGE = 100 FEET
6 AUGUST, 1990

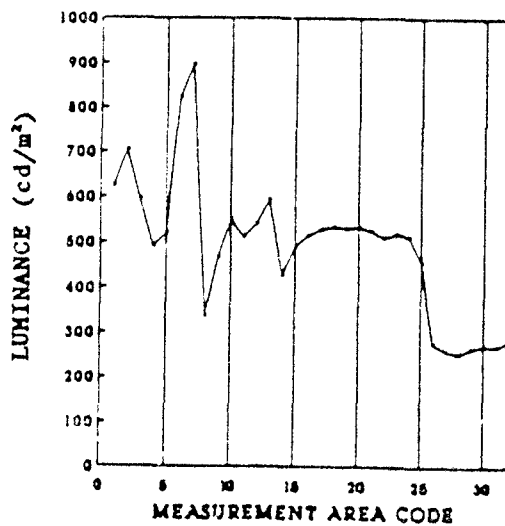


Figure 107

M1 Study on 6 August, 1990 (Overcast 10:00-15:30)

AVERAGE LUMINANCE of M1
DIFFERENT RANGES

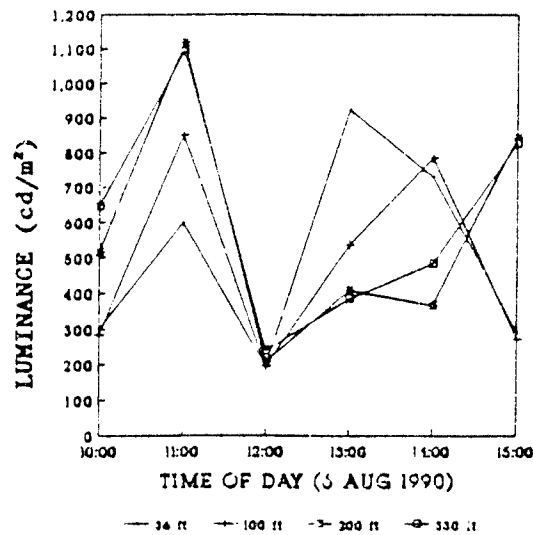


Figure 108

AVERAGE LUMINANCE of TREES
DIFFERENT RANGES

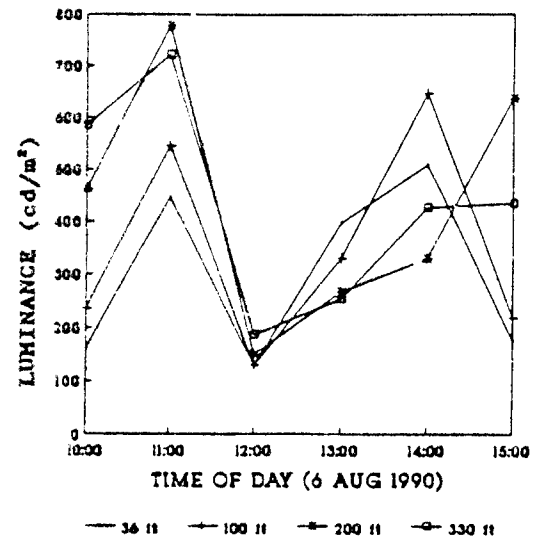


Figure 109

LUMINANCE of GRASS
DIFFERENT RANGES

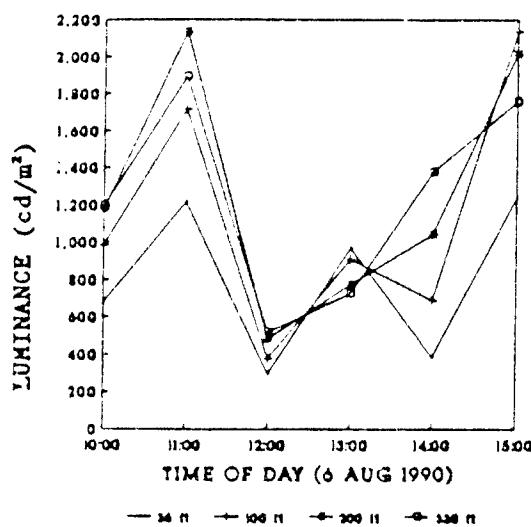


Figure 110

LUMINANCE of SKY
DIFFERENT RANGES

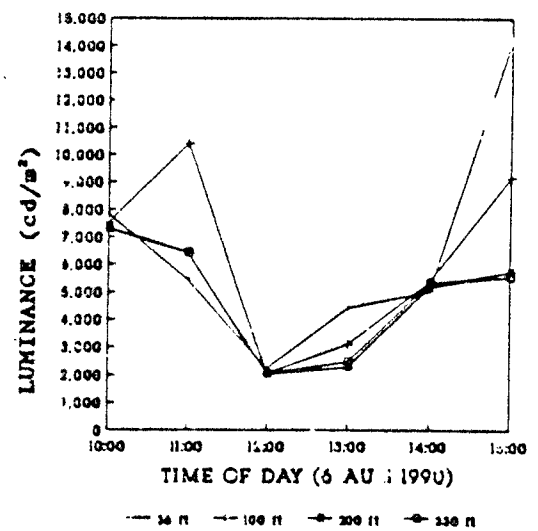


Figure 111

M1 Study on 6 August, 1990 (Overcast 10:00-15:30)

AVERAGE CONTRAST OF MI
AVERAGE TREE BACKGROUND
DIFFERENT RANGES

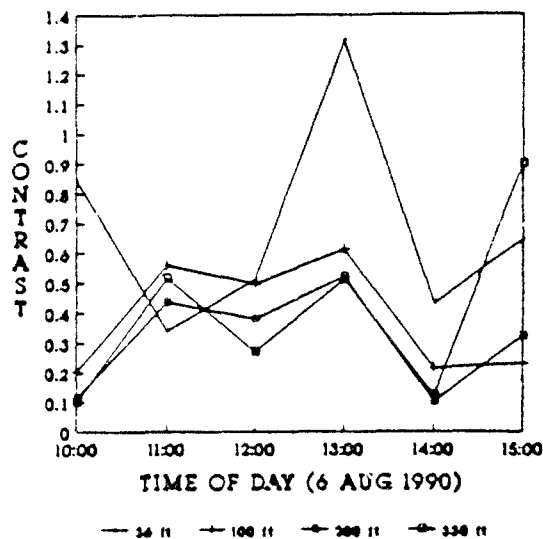


Figure 112

AVERAGE CONTRAST OF MI
GRASS BACKGROUND
DIFFERENT RANGES

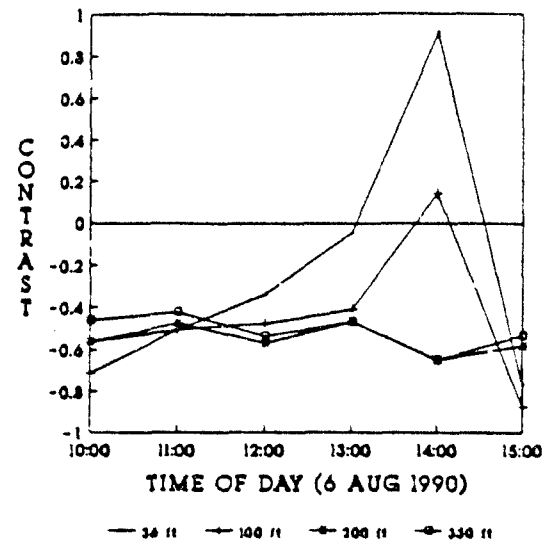


Figure 113

AVERAGE CONTRAST OF MI
SKY BACKGROUND
DIFFERENT RANGES

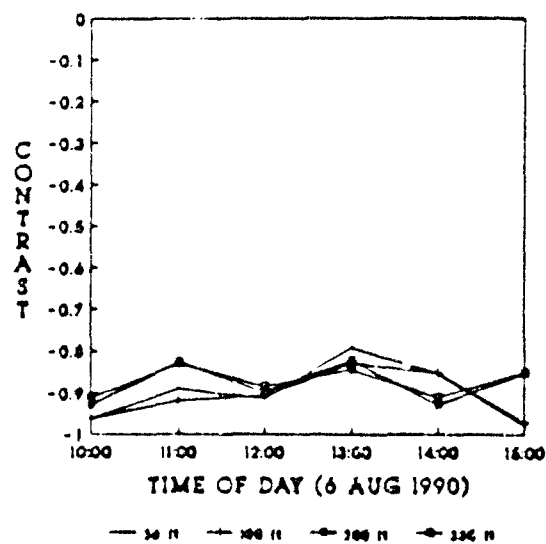


Figure 114

M1 Study on 6 August, 1990 (Overcast 10:00-15:30)

AVERAGE CONTRAST OF M1
RANGE = 36 FEET

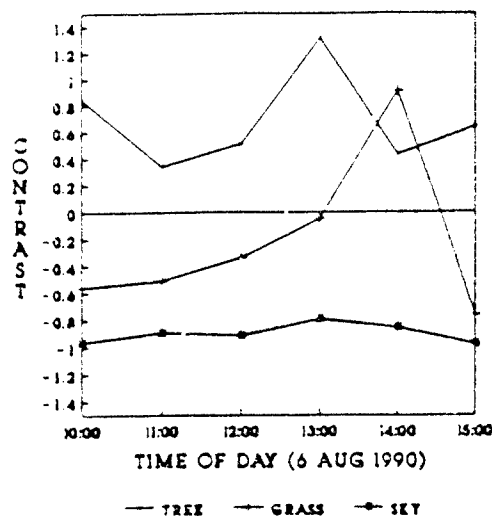


Figure 115

AVERAGE CONTRAST OF M1
RANGE = 100 FEET

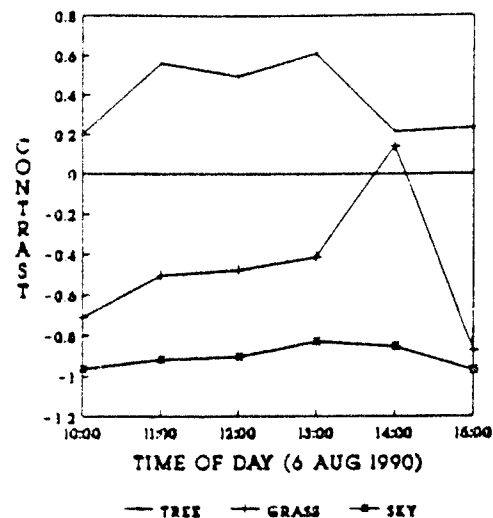


Figure 116

AVERAGE CONTRAST OF M1
RANGE = 200 FEET

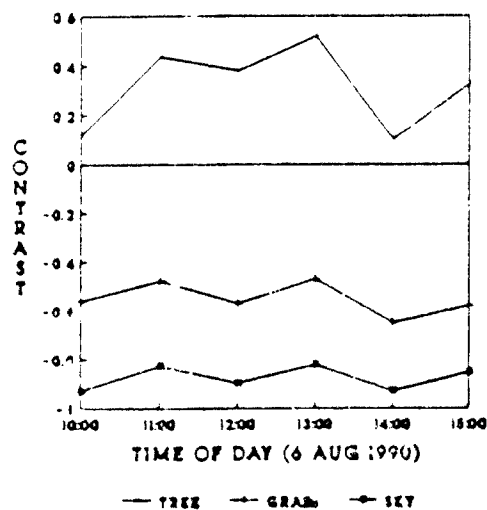


Figure 117

AVERAGE CONTRAST OF M1
RANGE = 330 FEET

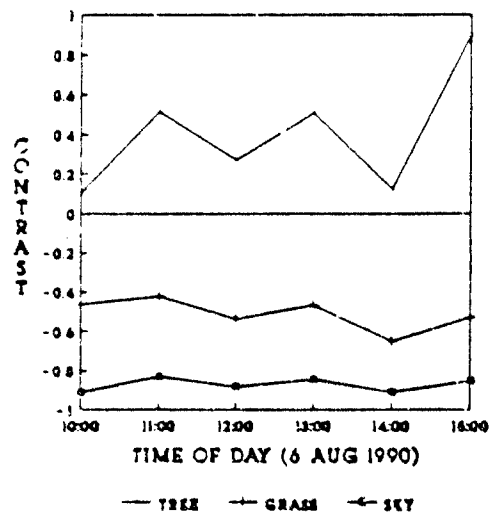


Figure 118

Table 21. M1 Area Luminance Analysis For Times 10:00 - 15:30 on 6 August, 1990

Range - 36 feet			Range - 100 feet		
Area #	Avg.	St. Dev.	Area #	Avg.	St. Dev.
1	767	420	1	623	313
2	905	493	2	704	377
3	883	483	3	594	313
4	541	285	4	491	253
5	514	272	5	520	284
6	813	441	6	822	443
7	797	445	7	896	478
8	770	435	8	337	179
9	531	285	9	466	243
10	435	220	10	550	294
11	911	497	11	511	273
12	906	497	12	540	291
13	948	476	13	594	313
14	415	221	14	426	207
15	557	297	15	490	261
16	505	263	16	515	274
17	642	333	17	528	287
18	474	241	18	534	285
19	519	269	19	529	283
20	546	286	20	534	286
21	549	287	21	524	282
22	539	284	22	509	270
23	534	278	23	519	272
24	513	268	24	512	270
25	285	156	25	456	243
26	382	193	26	276	139
27	553	292	27	260	139
28	564	297	28	253	134
29	560	294	29	265	139
30	565	297	30	271	139
31	533	279	31	269	142
32	537	281	32	282	151
33	536	280			
34	528	272			
35	520	272			
36	251	121			
37	273	135			
38	248	125			
39	263	129			
40	265	131			
41	249	125			
42	269	136			
43	71	30			
44	361	180			
45	543	273			
Avg.	506	264			
St. Dev.	210	116			
			Avg.	487	257
			St. Dev.	154	83

Table 22. M1 Area Luminance Analysis For Times 10:00 - 15:30 on 6 August, 1990
Overcast 10:00 - 15:30.

Range - 200 feet			Range - 330 feet		
Area #	Avg.	St. Dev.	Area #	Avg.	St. Dev.
1	523	260	1	572	269
2	628	310	2	658	306
3	776	383	3	607	281
4	529	285			
5	509	273			
6	527	296			
7	549	317			
8	567	344			
9	583	347			
Avg.			Avg.		
St. Dev.			St. Dev.		
	577	310		612	285
	86	41		35	16

The column heading 'Avg.' in Table 21 and Table 22 refers to the averages of six luminance readings acquired between the times 10:00 and 15:00 for each measurement area.

The column heading ' St. Dev.' refers to the standard deviation.

Table 21 relates to Figure 59 and Figure 60. Table 22 relates to Figure 61 and Figure 62.

Table 23. Average Tree Line Luminance (cd/m²) on 6 August, 1990

Range	10:00	11:00	12:00	13:00	14:00	15:00	Avg.
36'	162	446	129	399	510	177	304
100'	236	546	131	332	647	220	352
200'	461	778	150	269	332	638	438
330'	585	722	188	255	428	436	436
Avg.	361	623	150	314	479	368	382
S. D.	170	133	24	57	116	184	66

Table 24. Summary of Diurnal Luminance Averages (cd/m²) for 6 August, 1990
Overcast 10:00 - 15:30.

Range	Time	Avg. M1	Avg. Tree	Grass	Sky
36 feet	10:00	299	162	679	7824
36 feet	11:00	598	446	1214	5463
36 feet	12:00	195	129	294	2238
36 feet	13:00	924	399	949	4446
36 feet	14:00	730	510	382	5046
36 feet	15:00	291	177	1237	14190
36 feet	Average	506	304	796	6535
36 feet	Std. Dev.	264	152	373	3796
100 feet	10:00	284	236	985	7526
100 feet	11:00	852	546	1717	10410
100 feet	12:00	196	131	376	2070
100 feet	13:00	535	332	907	3123
100 feet	14:00	786	647	688	5384
100 feet	15:00	271	220	2139	9160
100 feet	Average	487	352	1135	6279
100 feet	Std. Dev.	257	185	605	3039
200 feet	10:00	515	461	1176	7285
200 feet	11:00	1118	778	2136	6435
200 feet	12:00	207	150	482	2032
200 feet	13:00	409	269	773	2282
200 feet	14:00	366	332	1044	5193
200 feet	15:00	845	638	2014	5731
200 feet	Average	577	438	1271	4826
200 feet	Std. Dev.	310	216	610	1994
330 feet	10:00	645	585	1195	7301
330 feet	11:00	1095	722	1693	6453
330 feet	12:00	239	188	517	2057
330 feet	13:00	385	255	725	2481
330 feet	14:00	481	428	1378	5353
330 feet	15:00	827	436	1759	5547
330 feet	Average	612	436	1245	4865
330 feet	Std. Dev.	285	182	501	1946

Table 25. Analysis of M1 Turret Luminance Readings (cd/m²) on 6 August, 1990
Range = 36 feet. Overcast 10:00 - 15:30.

Area #	10:00	11:00	12:00	13:00	14:00	15:00	Avg.	St. Dev.
1	429	845	295	1477	1101	455	767	420
2	518	982	338	1735	1310	547	905	493
3	510	958	327	1698	1275	528	883	483
4	305	597	200	970	835	339	541	285
5	326	467	215	1013	714	349	514	272
6	470	889	305	1543	1192	480	813	441
7	468	856	294	1573	1127	464	797	445
8	444	842	277	1522	1095	442	770	435
9	299	593	195	975	805	316	531	285
10	261	537	192	811	558	252	435	220
11	537	1011	340	1756	1294	526	911	497
12	537	1000	341	1753	1290	516	906	497
13	610	1050	383	1712	1374	561	948	476
<hr/>								
Avg.	440	817	285	1426	1075	444	748	404
St. Dev.	105	192	62	337	252	95	172	96

Table 26. Analysis of M1 Turret Luminance Readings (cd/m²) on 6 August, 1990
Range = 100 feet. Overcast 10:00 - 15:30.

Area #	10:10	11:10	12:10	13:10	14:10	15:10	Avg.	St. Dev.
1	354	1043	259	785	948	347	623	313
2	388	1207	276	856	1129	370	704	377
3	339	988	226	722	970	320	594	313
4	294	864	202	560	754	269	491	253
5	275	897	201	625	849	272	520	284
6	450	1414	326	948	1354	440	822	443
7	498	1483	331	1059	1502	503	896	478
<hr/>								
Avg.	371	1128	260	794	1072	360	664	352
St. Dev.	75	228	50	163	252	80	140	78

Table 27. Analysis of M1 Skirt Luminance Readings (cd/m²) on 6 August, 1990
Range = 36 feet. Clear Skies All Day.

Area #	10:00	11:00	12:00	13:00	14:00	15:00	Avg.	St. Dev.
18	294	551	181	846	692	277	474	241
19	313	608	196	935	760	300	519	269
20	322	632	209	995	802	317	546	286
21	325	644	207	996	804	316	549	287
22	317	628	201	983	791	311	539	284
23	318	630	204	968	778	305	534	278
24	301	611	197	930	747	291	513	268
27	322	663	211	1005	808	311	553	292
28	334	677	217	1037	804	313	564	297
29	329	676	217	1026	798	312	560	294
30	329	689	219	1032	805	313	565	297
31	313	649	207	970	764	297	533	279
32	315	659	209	973	769	297	537	281
33	315	659	209	972	765	297	536	280
34	310	655	207	944	754	295	528	272
35	304	643	204	941	744	286	520	272
45	306	741	224	900	789	297	543	273
<hr/>								
Avg.	316	648	207	968	775	302	536	280
St. Dev.	10	39	10	48	30	11	21	13

Table 28. Analysis of M1 Skirt Luminance Readings (cd/m²) on 6 August, 1990
Range = 100 feet. Clear Skies All Day.

Area #	10:10	11:10	12:10	13:10	14:10	15:10	Avg.	St. Dev.
15	295	880	201	494	791	281	490	261
16	300	914	208	553	827	287	515	274
17	299	945	207	571	855	292	528	287
18	315	950	210	568	860	301	534	285
19	309	936	211	565	859	294	529	283
20	315	949	216	558	869	295	534	286
21	308	928	212	540	863	292	524	282
22	304	895	206	536	830	282	509	270
23	314	907	212	547	843	289	519	272
24	307	899	206	543	827	287	512	270
<hr/>								
Avg.	307	920	209	548	842	290	519	277
St. Dev.	7	24	4	21	23	6	13	8

SUMMARY OF M1 STUDIES

One of the more important results of the M1 studies is that the M1 has three distinguishing luminance areas: the turret, the skirt and the track and suspension areas. The graphs of Figure 119, Figure 120 and Figure 121 support this idea.

Figure 119 relates to the M1 side facing north and metering toward the south on a hazy, overcast day. Figure 120 and Figure 121 relate to the M1 side facing east and metering toward the west. Figure 120 relates to a clear day. Figure 121 relates to an overcast day. Note: Figure 59 relates the measurement area code to the position on the M1.

The turret, skirt and track and suspension areas remain distinguishing features regardless of M1 orientation, time of daylight or sky condition.

Table 29. M1 Luminance Averages for Turret, Skirt and Tractor Areas (cd/m^2).
Range: 36 feet.

M1 Area	Hazy-Overcast 19 July, 1990	Clear Skies 1 August, 1990	Overcast 6 August, 1990
Turret	1104	2758	748
Skirt	719	2016	536
Wheels	340	804	260

THE TURRET

The turret, which is the most elevated M1 region, produces the largest luminance readings. It consists of beveled, flat areas and obtuse corners which join together to form a three-dimensional figure. Also, there are areas (area #4 and area #9 of Figure 59) which extend out from other areas. These extensions produce shadows and undergo strong specular reflection at different times than other turret areas. The photographs of Figure 88, Figure 89,... Figure 93 illustrate the diurnal changes in luminance which result from the turret geometry.

Table 30 also illustrates that luminance readings from the turret areas show large variances in luminance compared to other areas of the M1. The standard deviation for luminance of turret areas between 10:00 and 15:00 on 19 July, 1990 varied from 21 percent to 34 percent of the average luminance. On 1 August, 1990 it varied from 20 percent to 52 percent of the average luminance. On 6 August, 1990 the standard deviation varied from 21 percent to 24 percent of the average luminance. Even on an overcast day, turret areas show large variances in luminance compared to other areas of the M1.

AVERAGE M1 LUMINANCE

RANGE = 36 FEET

19 JULY 1990; 10:05 - 15:05

METERING SOUTH HAZY-OVERCAST

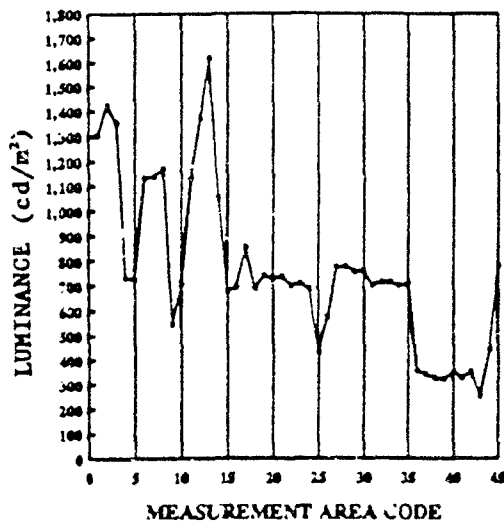


Figure 119

AVERAGE M1 LUMINANCE

RANGE = 36 FEET

1 AUGUST, 1990; 10:00 - 15:00

METERING WEST CLEAR SKIES

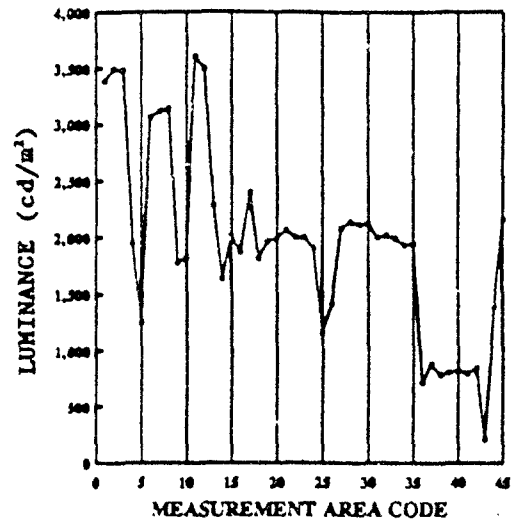


Figure 120

AVERAGE M1 LUMINANCE

RANGE = 36 FEET

6 AUGUST, 1990; 10:00 - 15:00

METERING WEST OVERCAST

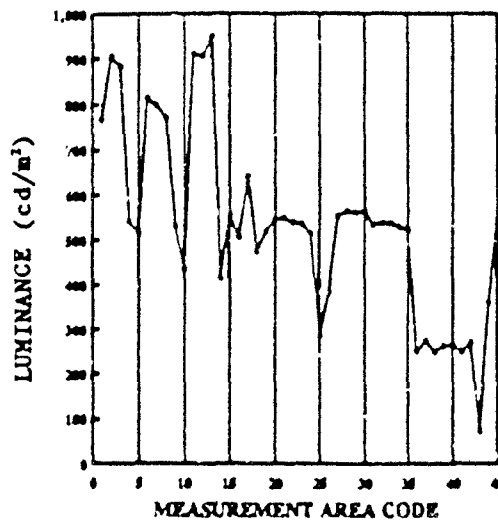


Figure 121

The greatest variance in luminance occurred for turret area #13 (Figure 59) during Study B on 19 July, 1990. Figure 49 and Figure 50 illustrate the dramatic diurnal changes in luminance for area #13.

The lowest luminance reading from the M1 turret was 192 cd/m². This was acquired from area #10 (Figure 59) during overcast skies, range 36 feet, at 12:00 on 6 August, 1990.

The largest luminance reading from the M1 turret was 4,618 cd/m². This was acquired from area #11 (Figure 59) during clear skies, range 36 feet, at 10:00 on 1 August, 1990.

Table 30. Summary Analysis of M1 Turret Luminance Readings (cd/m²).

Note:

$$\% \text{ of Average} = \frac{\text{Standard Deviation}}{\text{Average}} \times 100$$

19 July, 1990. Hazy - Overcast. Range - 36 feet						
	10:00	11:00	12:00	13:00	14:00	15:00
Average	1061	1084	1173	859	941	441
Standard Dev.	357	358	343	262	252	91
% of Average	34	33	29	31	27	21
1 August, 1990. Clear Skies All Day. Range - 36 feet						
	10:00	11:00	12:00	13:00	14:00	15:00
Average	3768	3682	3221	2653	1960	1266
Standard Dev.	744	723	848	1154	1013	625
% of Average	20	20	26	44	52	49
6 August, 1990. Overcast. Range - 36 feet						
	10:00	11:00	12:00	13:00	14:00	15:00
Average	440	817	285	1426	1075	444
Standard Dev.	105	192	62	337	252	95
% of Average	24	24	22	24	23	21

THE SKIRT

The skirt areas produce luminance readings between the turret and track and suspension areas.

The skirt of the M1 is essentially a vertical plane. Two areas of measurement on the skirt (area #25 and area #26) differed from all other skirt areas. Area #25 is partly on the skirt and partly on the idler wheel. Area #26 is a square opening in the skirt which exposes a part of the track and suspension area. The luminance from these two areas was significantly lower than other skirt areas.

The luminance readings from the skirt areas show small variances in luminance compared to the M1 turret. Points on the diurnal luminance graphs (Figure 119, Figure 120 and Figure 121), which correspond to the skirt areas, form nearly horizontal segments on the graphs.

Table 31 also illustrates that luminance readings from the skirt areas show small variances in luminance compared to the turret areas of the M1. The standard deviation for luminance of skirt areas between 10:00 and 15:00 on 19 July, 1990 varied from 4 percent to 18 percent of the average luminance. On 1 August, 1990 it varied from 3 percent to 5 percent of the average luminance. On 6 August, 1990 the standard deviation varied from 3 percent to 6 percent of the average luminance.

Table 31. Summary Analysis of M1 Skirt Luminance Readings (cd/m²).

19 July, 1990. Hazy - Overcast. Range - 36 feet						
	10:00	11:00	12:00	13:00	14:00	15:00
Average	757	680	787	809	687	258
Standard Dev.	32	26	28	144	40	12
% of Average	4	4	4	18	6	5
1 August, 1990. Clear Skies All Day. Range - 36 feet						
	10:00	11:00	12:00	13:00	14:00	15:00
Average	3791	3439	2403	1527	488	488
Standard Dev.	172	174	111	83	19	13
% of Average	5	5	5	5	4	3
6 August, 1990. Overcast. Range - 36 feet						
	10:00	11:00	12:00	13:00	14:00	15:00
Average	316	648	207	968	755	302
Standard Dev.	10	39	10	48	30	11
% of Average	3	6	5	5	4	4

TRACK AND SUSPENSION

The only track and suspension areas studied were the road wheels. These areas are the lowest areas on the M1 and produced the lowest luminance readings. As Figure 88, Figure 89,... Figure 93 illustrate, they are very susceptible to shading from areas above them.

The luminance readings from the road wheel areas show small variances in luminance compared to the M1 turret. Points on the diurnal luminance graphs which correspond to the wheel areas form nearly horizontal segments on the graphs.

Table 32 also illustrates that luminance readings from the wheel areas show small variances in luminance compared to the turret areas of the M1. The standard deviation for luminance of wheel areas between 10:00 and 15:00 on 19 July, 1990 varied from 4 percent to 5 percent of the average luminance. On 1 August, 1990 it varied from 3 percent to 16 percent of the average luminance. On 6 August, 1990 the standard deviation varied from 3 percent to 5 percent of the average luminance.

Table 32. Summary Analysis of M1 Road Wheel Luminance Readings (cd/m²).

19 July, 1990. Hazy - Overcast. Range = 36 feet						
	10:00	11:00	12:00	13:00	14:00	15:00
Average	351	330	370	438	343	107
Standard Dev.	18	14	15	19	14	4
% of Average	5	4	4	4	4	4
1 August, 1990. Clear Skies All Day. Range = 36 feet						
	10:00	11:00	12:00	13:00	14:00	15:00
Average	2425	1185	258	325	286	244
Standard Dev.	107	186	14	13	8	9
% of Average	4	16	4	4	3	4
6 August, 1990. Overcast. Range = 36 feet						
	10:00	11:00	12:00	13:00	14:00	15:00
Average	149	347	102	422	389	149
Standard Dev.	6	16	4	14	15	6
% of Average	4	5	4	3	4	4

LUMINANCE DURING CLEAR SKIES

The study of 1 August, 1990 was the only M1 study conducted during clear skies. This study is very important since cloud conditions do not muddle analysis. One of the interesting results of this study is that average M1 luminance, average tree luminance and grass luminance readings can be described by linear equations. As will be seen in a later study (Study 24 July, 1990), similar results were obtained for the LAV25 during clear skies.

Table 33 provides expressions for luminance (L) in terms of time (t = 0 corresponds to 10:00) for different ranges. Correlation coefficients are included to show how close the relationships fit collected data.

Figure 77, Figure 78 and Figure 79 show the collected data in graphical form.

Table 33. M1, Tree and Grass Luminance Analysis for 1 August, 1990 (Clear Skies)
Note: t in hours. Metering toward the west.

Average M1 Luminance Analysis for 1 August, 1990 (10:00 to 15:00)		
Range	Luminance (cd/m ²)	Corr. Coefficient
36 feet	$L = 3303 - 583 t$	0.9912
100 feet	$L = 3019 - 530 t$	0.9887
200 feet	$L = 2809 - 497 t$	0.9840
330 feet	$L = 2816 - 476 t$	0.9850
Average Tree Luminance Analysis for 1 August, 1990 (10:00 to 15:00)		
Range	Luminance (cd/m ²)	Corr. Coefficient
36 feet	$L = 1102 - 59 t$	0.8696
100 feet	$L = 1237 - 89 t$	0.9532
200 feet	$L = 1237 - 88 t$	0.9604
330 feet	$L = 1281 - 56 t$	0.7391
Grass Luminance Analysis for 1 August, 1990 (10:00 to 15:00)		
Range	Luminance (cd/m ²)	Corr. Coefficient
36 feet	$L = 2850 - 93 t$	0.8843
100 feet	$L = 3654 - 254 t$	0.9918
200 feet	$L = 3754 - 294 t$	0.9946
330 feet	$L = 3398 - 237 t$	0.9801

It was shown earlier that the M1 has three distinguishing luminance areas: the turret, the skirt and the track and suspension areas. During clear skies, there are time intervals for which the luminance of these areas can be described by linear equations. Table 34 (range 36 feet) and Table 35 (range 100 feet) introduce these equations and the times for which they are appropriate. Correlation coefficients are also included.

Figure 125 (range 36 feet) and Figure 129 (range 100 feet) show the collected data in graphical form. The very abrupt change in luminance of the road wheels after 12:00 is clearly due to shading by areas above the track and suspension area as can be seen in the photographs of Figure 88, Figure 89,...Figure 93. These photographs also support the data of Figure 125 and Figure 129 with regard to the abrupt change in luminance of the skirt area after 14:00.

The equations for average luminance from Table 34 show that the rate at which average luminance decreases for the turret ($609 \text{ cd/m}^2/\text{hr}$) is approximately 40 percent less than the rate at which luminance decreases for the skirt ($972 \text{ cd/m}^2/\text{hr}$) and road wheels ($1033 \text{ cd/m}^2/\text{hr}$).

Table 34. Average Turret, Skirt and Road Wheel Luminance Analysis for 1 August, 1990. Clear Skies. Range = 36 feet. t in hours. Metering toward the west

M1 Area	Luminance (cd/m^2)	Time Interval	Corr. Coeff.
Turret	$L = 3775 - 609 t$	11:00 - 15:00	0.9965
Skirt	$L = 3424 - 972 t$	11:00 - 14:00	0.9994
Road Wheels	$L = 2356 - 1033 t$	10:00 - 12:00	0.9934

The equations for average luminance from Table 35 show that the rate at which average luminance decreases for the turret ($484 \text{ cd/m}^2/\text{hr}$) is also approximately 40 percent less than the rate at which luminance decreases for the skirt area ($811 \text{ cd/m}^2/\text{hr}$).

Table 35. Average Turret, Skirt and Road Wheel Luminance Analysis for 1 August, 1990. Clear Skies. Range = 100 feet. t in hours. Metering toward the west

M1 Area	Luminance (cd/m^2)	Time Interval	Corr. Coeff.
Turret	$L = 3614 - 484 t$	10:00 - 15:00	0.9941
Skirt	$L = 3767 - 811 t$	10:00 - 14:00	0.9929
Road Wheels	$L = 1720 - 570 t$	10:00 - 12:00	0.9981

M1 Turret, Skirt and Road Wheel Analysis for 1 August, 1990 (Range = 36 feet)

CONTRAST OF M1 TARGETS
TREE BACKGROUND
RANGE = 36 FEET

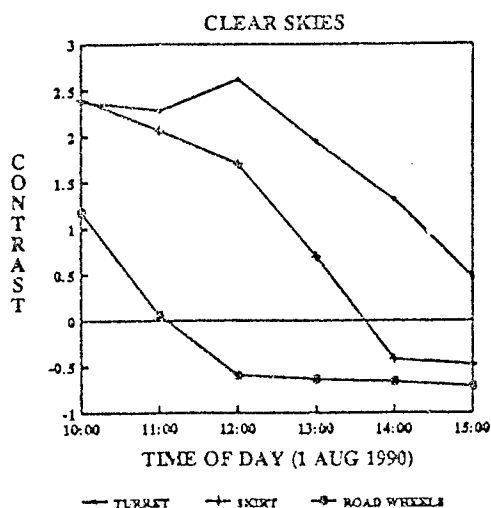


Figure 122

CONTRAST OF M1 TARGETS
GRASS BACKGROUND
RANGE = 36 FEET

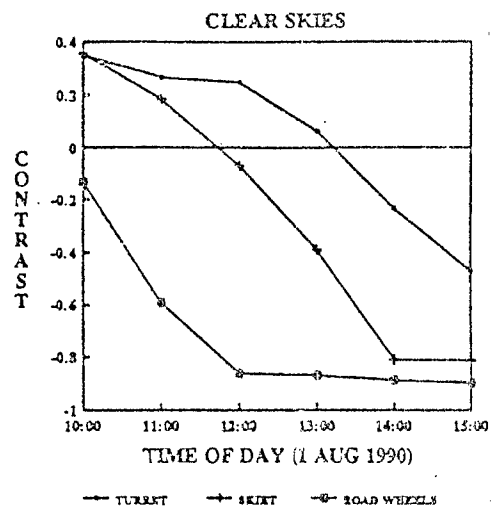


Figure 123

CONTRAST OF M1 TARGETS
SKY BACKGROUND
RANGE = 36 FEET

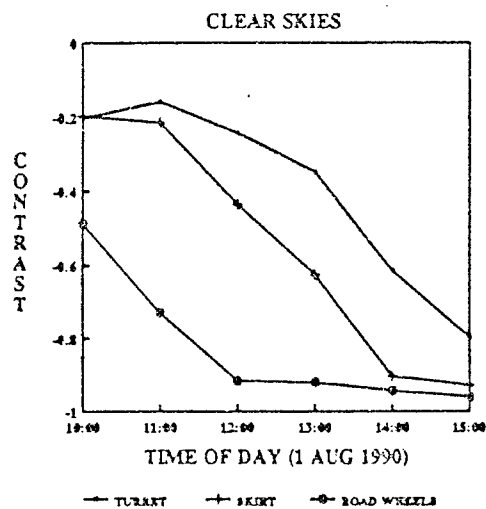


Figure 124

AVERAGE M1 LUMINANCE
RANGE = 36 FEET
CLEAR SKIES

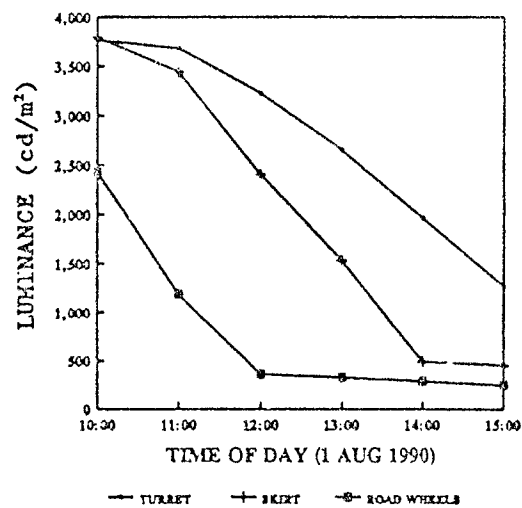


Figure 125

M1 Turret, Skirt and Road Wheel Analysis for 1 August, 1990 (Range = 100 feet)

CONTRAST OF M1 TARGETS
TREE BACKGROUND
RANGE = 100 FEET

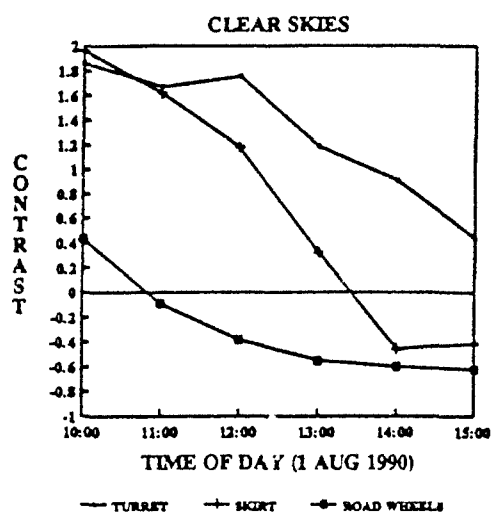


Figure 126

CONTRAST OF M1 TARGETS
GRASS BACKGROUND
RANGE = 100 FEET

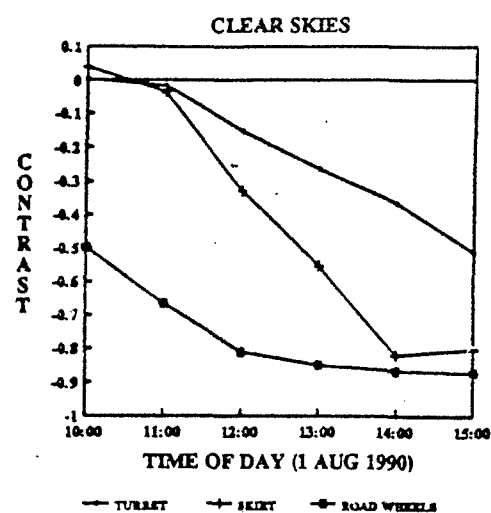


Figure 127

CONTRAST OF M1 TARGETS
SKY BACKGROUND
RANGE = 100 FEET

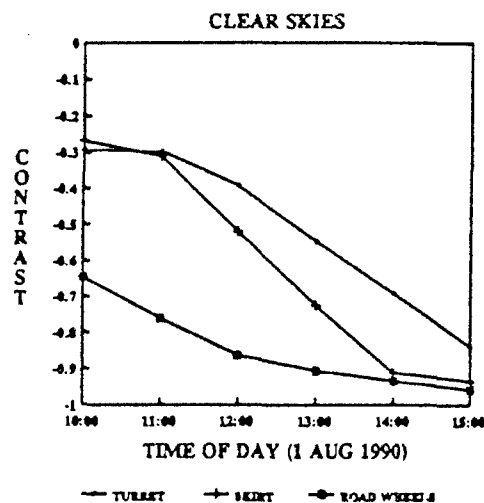


Figure 128

AVERAGE M1 LUMINANCE
RANGE = 100 FEET
CLEAR SKIES

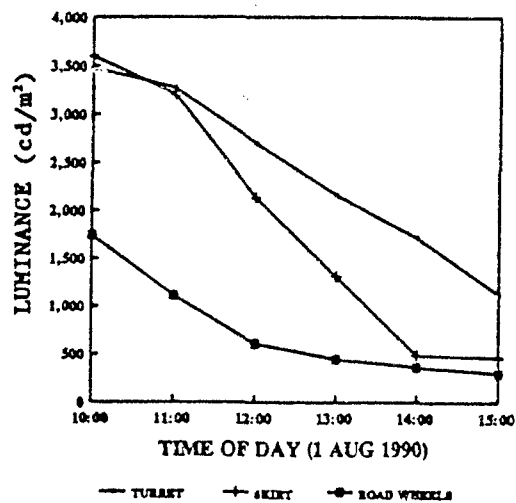


Figure 129

CONTRAST DURING CLEAR SKIES

Since both the average luminance of the M1 and the background can be expressed as linear equations during clear skies, it would appear that contrast between the M1 and background would not result in a linear equation since

$$CONTRAST = \frac{L_T - L_B}{L_B}$$

where L_T = luminance of M1 and L_B = luminance of background.

The ratio of two linear equations can not, in general, be a linear equation. However, since the luminance of tree and grass backgrounds is nearly constant (small coefficients of the first degree term), contrast between the M1 and trees and between the M1 and grass, during clear skies, can be expressed as linear equations to a high degree of precision. Table 36 provides expressions for contrast (C) in terms of time (t = 0 corresponds to 10:00) for different ranges. Correlation coefficients are included to show how close the relationships fit collected data.

Figure 81 and Figure 82 show the collected data in graphical form.

Table 36. M1 Contrast for Tree and Grass Backgrounds on 1 August, 1990 (Clear Skies)

Note: t in hours. Metering toward the west.

Contrast of M1 using Tree Background on 1 August, 1990 (10:00 - 15:00)		
Range	Contrast	Corr. Coefficient
36 feet	$C = 2.06 - 0.487 t$	0.9861
100 feet	$C = 1.53 - 0.384 t$	0.9882
200 feet	$C = 1.34 - 0.353 t$	0.9802
330 feet	$C = 1.21 - 0.333 t$	0.9959
Contrast of M1 using Grass Background on 1 August, 1990 (10:00 - 15:00)		
Range	Contrast	Corr. Coefficient
36 feet	$C = 0.376 - 0.198 t$	0.9926
100 feet	$C = 0.021 - 0.138 t$	0.9861
200 feet	$C = -0.106 - 0.116 t$	0.9837
330 feet	$C = -0.028 - 0.121 t$	0.9873

During clear skies, there are time intervals for which the contrast of the turret, skirt and road wheels can be described by linear equations. Table 37 (range 36 feet) and Table 38 (range = 100 feet) introduce these equations and the times for which they are appropriate. Correlation coefficients are also included. Figure 122, Figure 123, Figure 124, Figure 126, Figure 127, Figure 127 and Figure 128 show the collected data in graphical form.

Table 37. Contrast Analysis of M1 Turret, Skirt and Road Wheels on 1 August, 1990
Clear Skies. Range = 36 feet. Metering toward the west. t in hours

Contrast of M1 Targets using Tree Background			
M1 Area	Contrast	Time Interval	Corr. Coeff.
Turret	$C = 2.65 - 0.71 t$	12:00 - 15:00	0.9982
Skirt	$C = 1.73 - 1.07 t$	12:00 - 14:00	0.9996
Road Wheels	$C = 1.10 - 0.89 t$	10:00 - 12:00	0.9891
Contrast of M1 Targets using Grass Background			
M1 Area	Contrast	Time Interval	Corr. Coeff.
Turret	$C = 0.27 - 0.25 t$	12:00 - 15:00	0.9971
Skirt	$C = -0.05 - 0.37 t$	12:00 - 14:00	0.9970
Road Wheels	$C = -0.16 - 0.36 t$	10:00 - 12:00	0.9889

Table 38. Contrast Analysis of M1 Turret, Skirt and Road Wheels on 1 August, 1990
Clear Skies. Range = 100 feet. Metering toward the west. t in hours

Contrast of M1 Targets using Tree Background			
M1 Area	Contrast	Time Interval	Corr. Coeff.
Turret	$C = 1.70 - 0.42 t$	12:00 - 15:00	0.9916
Skirt	$C = 1.16 - 0.81 t$	12:00 - 14:00	0.9996
Road Wheels	$C = 0.40 - 0.41 t$	10:00 - 12:00	0.9862
Contrast of M1 Targets using Grass Background			
M1 Area	Contrast	Time Interval	Corr. Coeff.
Turret	$C = -0.02 - 0.12 t$	11:00 - 15:00	0.9983
Skirt	$C = -0.05 - 0.26 t$	11:00 - 14:00	0.9987
Road Wheels	$C = -0.50 - 0.16 t$	10:00 - 12:00	0.9990

M1 Turret, Skirt and Road Wheel Analysis for 19 July, 1990 (Range = 36 feet)

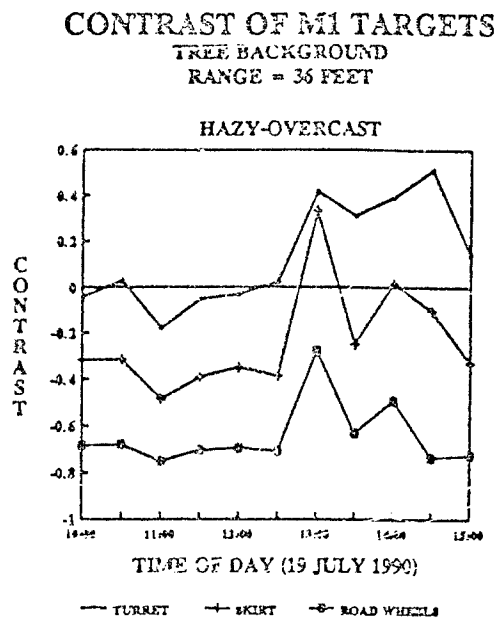


Figure 130

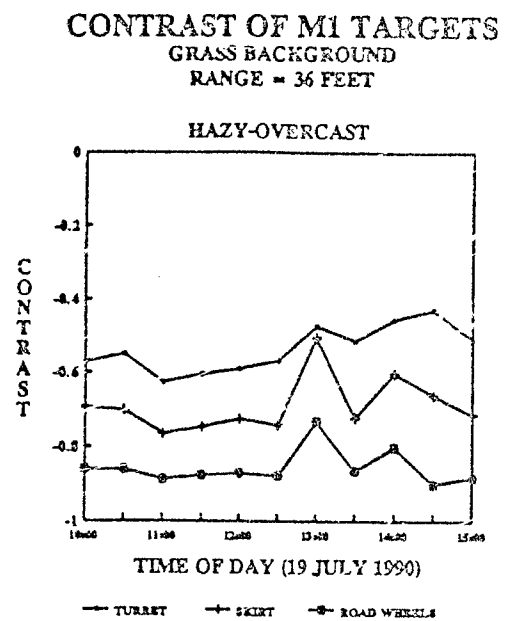


Figure 131

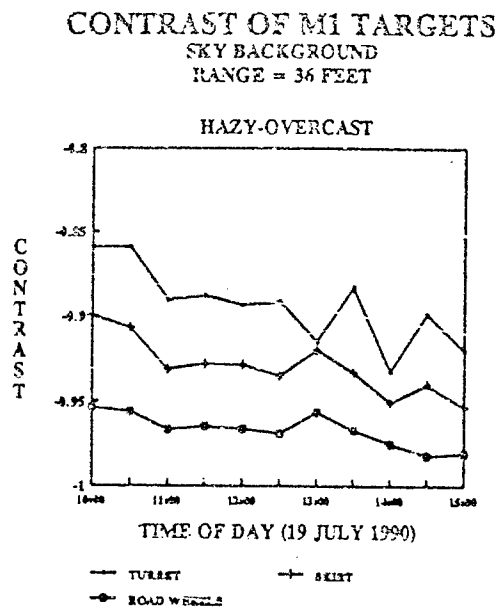


Figure 132

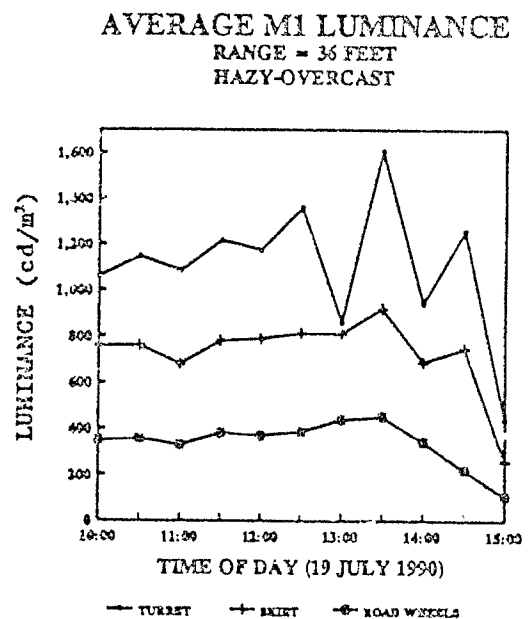


Figure 133

M1 Turret, Skirt and Road Wheel Analysis for 6 August, 1990 (Range = 36 feet)

CONTRAST OF M1 TARGETS
TREE BACKGROUND
RANGE = 36 FEET

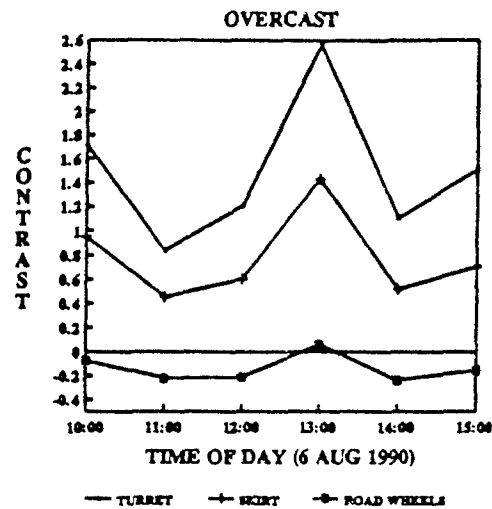


Figure 134

CONTRAST OF M1 TARGETS
GRASS BACKGROUND
RANGE = 36 FEET

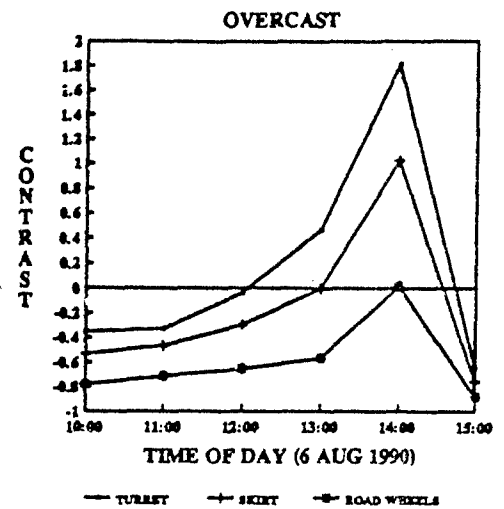


Figure 135

CONTRAST OF M1 TARGETS
SKY BACKGROUND
RANGE = 36 FEET

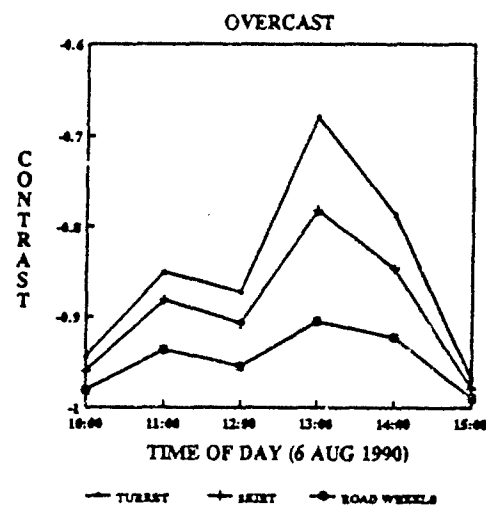


Figure 136

AVERAGE M1 LUMINANCE
RANGE = 36 FEET
OVERCAST

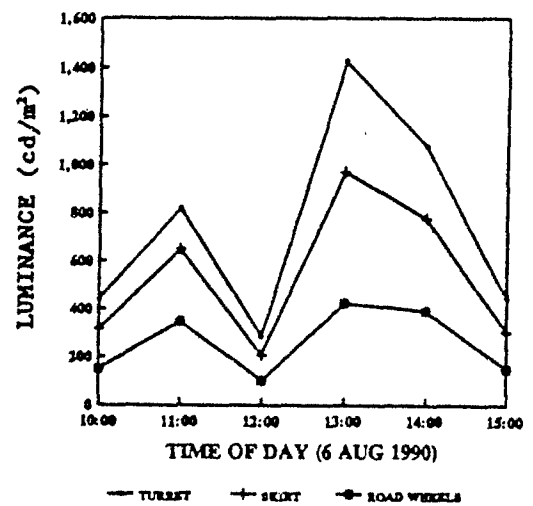


Figure 137

RANGE

The average luminance of the M1, as measured from ranges of 36, 100, 200 and 330 feet, is represented by the graph of Figure 77 and Table 33. There is very little difference in the average M1 luminance readings using different ranges. As Table 33 illustrates, the expression for average luminance at 36 feet, using 45 M1 luminance readings, is nearly the same as the expression for average luminance at 330 feet where only three M1 luminance readings were used. As Table 33 also illustrates, there is a small change in the rate at which average M1 luminance decreases when the range increases. This is due to more recessed areas being included in the measurement area at greater ranges (see Figure 59, Figure 60,... Figure 62).

During clear skies, the rate at which average contrast decreases for the M1 (Table 36) also changes slightly for different ranges. The reason for this small decrease in the rate at which contrast decreases for increasing ranges is the same as given above.

Table 39. Average Luminance (cd/m^2) for the Day of 1 August, 1990 for Different Ranges. Clear Skies. Averages based on the time interval from 10:00 to 15:00.

Measurement Area	Range 36 feet	Range 100 feet	Range 200 feet	Range 330 feet
M1	1845	1693	1567	1626
Trees	956	1016	1018	1140
Grass	2619	2986	3018	2805
Sky	4796	5241	5710	5923

Table 40. Average Contrast of M1 for the Day of 1 August, 1990 for Different Ranges. Clear Skies. Averages based on the time interval from 10:00 to 15:00.

Background	Range 36 feet	Range 100 feet	Range 200 feet	Range 330 feet
Trees	0.847	0.571	0.453	0.377
Grass	-0.315	-0.463	-0.514	-0.450
Sky	-0.592	-0.652	-0.708	-0.707

PHOTOGRAPHIC DECEPTION

Figure 88, Figure 89,...Figure 93 show photographs of the M1 for the six times luminance readings were made on 1 August, 1990. It was discovered that these photographs are very misleading with regard to how the luminance of the M1 changes with time.

Note:

Figure 88, Figure 89,...Figure 93 were taken with a Canon A1 set for automatic exposure. The camera was loaded with Kodak TMAX 400 film. The pictures were developed consecutively on the same day, using the same paper stock and the same chemicals. The enlarger was not changed for any of the exposures and the same time was used for all prints.

Example 1: It appears that the luminance of the turret increases from 10:00 to 13:00. In fact, as Figure 129 illustrates, the luminance of the turret decreases continuously throughout this time interval.

Example 2: It appears that Figure 92 and Figure 93 should be switched. The average luminance of the M1 appears to be greater at 15:00 than at 14:00. In fact, as Figure 77 illustrates, the average M1 luminance continuously decreases from 10:00 to 15:00.

Evidently, in Example 1, the rate of decrease in luminance of the turret areas was less than the rate of decrease in the average luminance for the entire scene. The luminance of the turret areas was progressively greater than the average luminance of the scene as the day progressed from 10:00 to 13:00. It can be seen from Table 34 that the rate of decrease in luminance of the skirt and road wheels is greater than the turret.

All objects in a scene with average luminance are printed as middle gray. The turret was printed progressively lighter than middle gray since its luminance was greater than the average luminance of the scene.

The explanation of the deception in Example 2 is illustrated in Figure 138 and Figure 139. When the photographs of Figure 92 and Figure 93 were taken, the camera was inadvertently positioned to include more sky background in Figure 92 than in Figure 93. This produced a higher average luminance for Figure 92 than for Figure 93. Therefore, since there are areas on the M1 with luminance below the average luminance of the scene, those areas on the M1 printed darker in Figure 92 than in Figure 93.

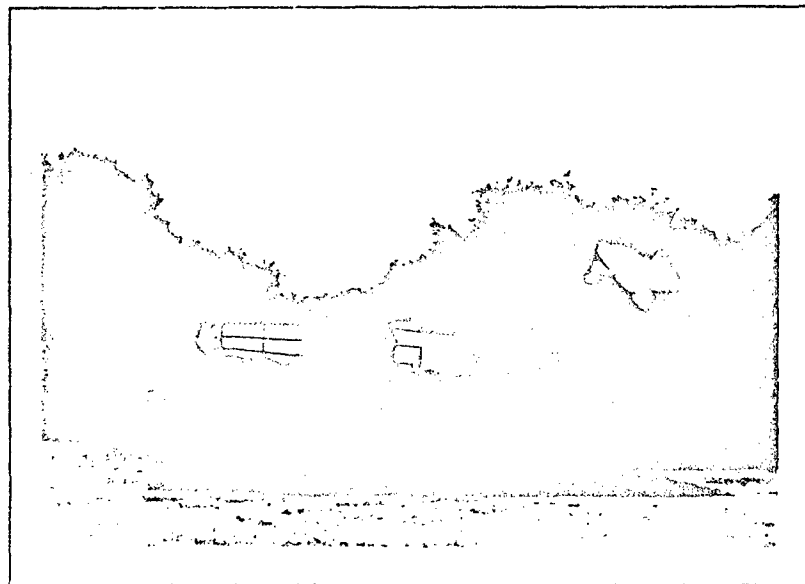


Figure 138
Complete, Uncropped Scene of Figure 92

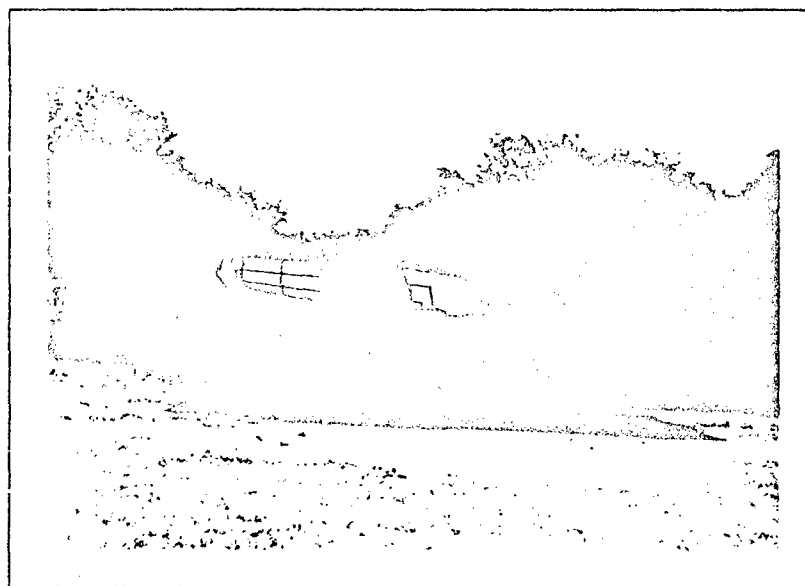


Figure 139
Complete, Uncropped Scene of Figure 93

Whenever a reflected light exposure meter of a camera is used to obtain an exposure setting of an evenly illuminated single toned surface, the resultant camera setting will produce a negative density which will produce a "middle gray" in the print. A photograph of a completely black or completely white card will produce a print which is completely "middle gray."

Figure 140, Figure 141,...Figure 143 illustrate this idea. Figure 140 was produced using a laser printer. Figure 141 is a photograph of Figure 140. It was obtained using a reflected light exposure meter. The black squares appear black and the white squares appear white. The white squares had a luminance far above the average luminance for the scene (Figure 140). Therefore, the white squares printed much lighter than "middle gray." The black squares had a luminance far below the average luminance for the scene (Figure 140). Therefore, the black squares printed much darker than "middle gray."

Figure 142 was also produced using a laser printer. Figure 143 is a photograph of Figure 142. This photograph was obtained using the same reflected light exposure meter as was used for Figure 141. The black squares appear very black but the white squares appear gray. Since Figure 142 contains many more white squares than black squares, the average luminance for this scene is higher than for Figure 140. The white squares had a luminance close to the average luminance for the scene (Figure 142). Therefore, the white squares printed a little lighter than "middle gray." The black squares had a luminance far below the average luminance for the scene (Figure 142). Therefore, the black squares printed much darker than "middle gray."

Both pictures, Figure 141 and Figure 143, were developed consecutively on the same day, using the same paper stock and the same chemicals. The enlarger was not changed for either exposure and the same time was used for both prints.

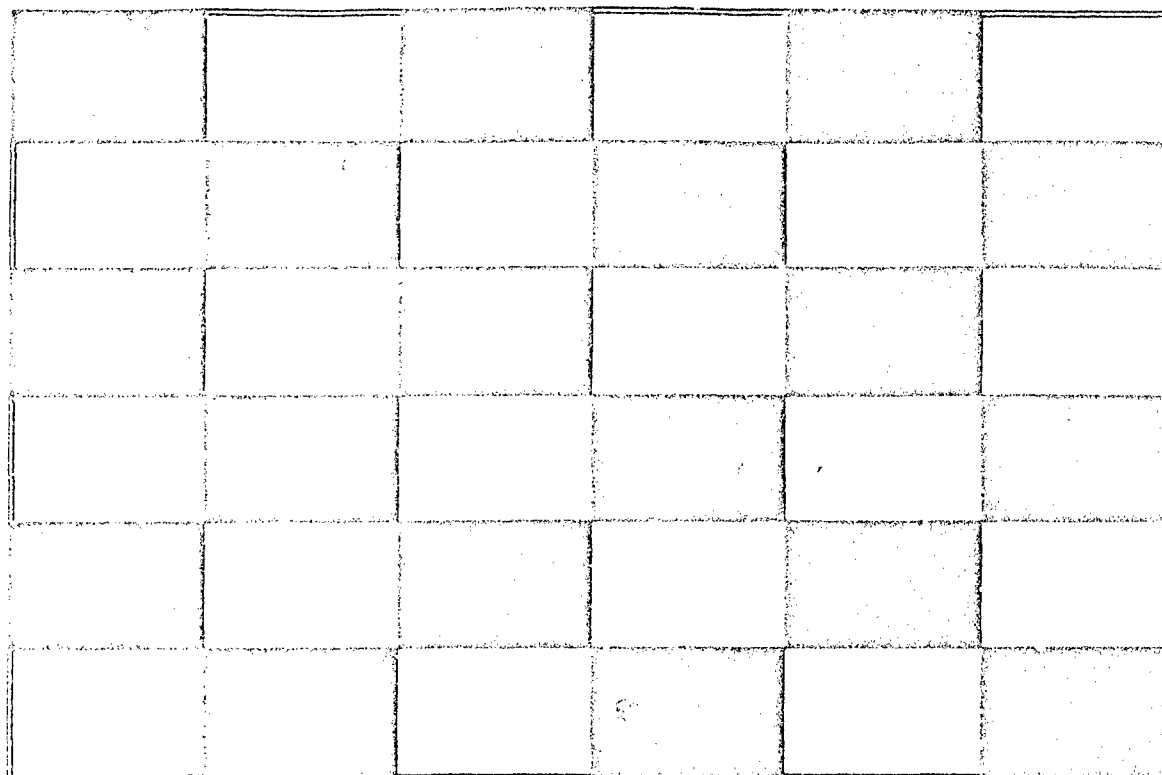


Figure 140
Checker Board Grid with Equal Number of Black and White Squares

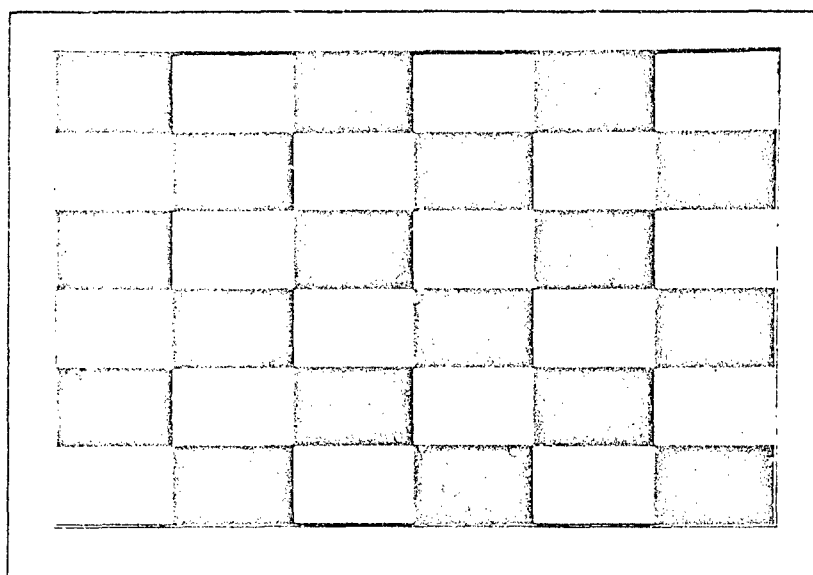


Figure 141
Photograph of Figure 140

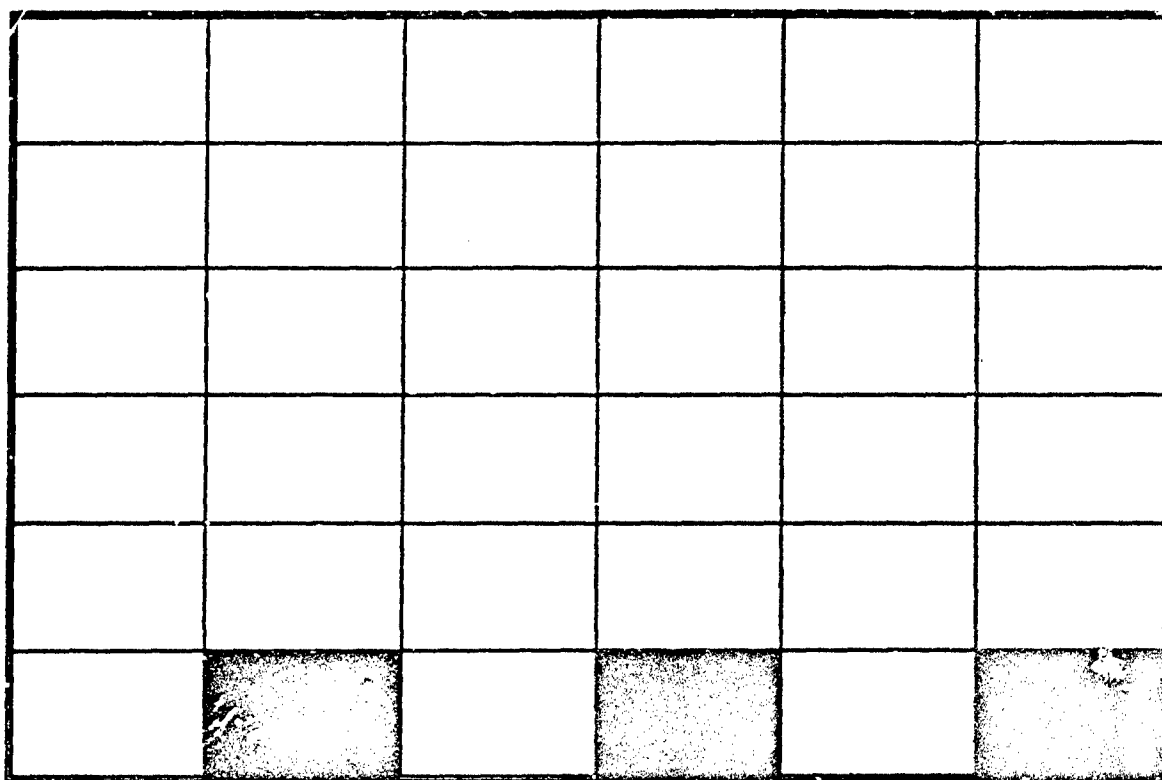


Figure 142
Checker Board Grid with Three Black Squares and Thirty Three White Squares

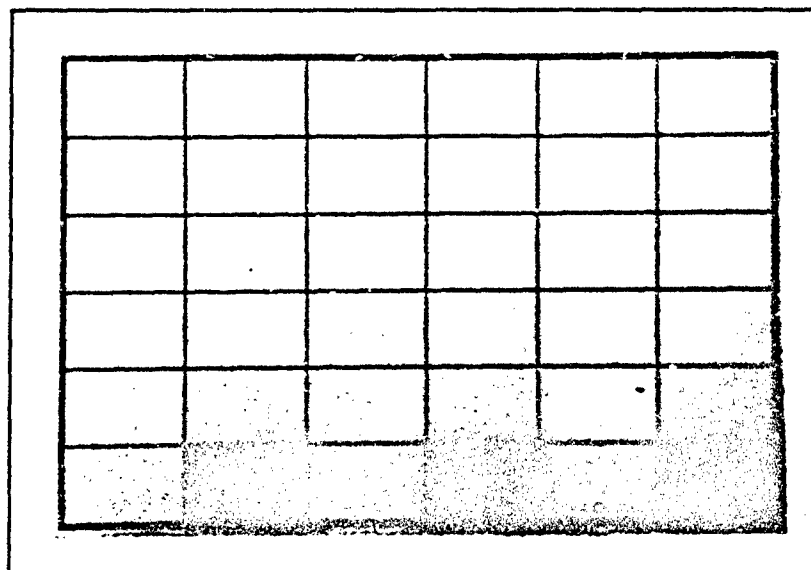


Figure 143
Photograph of Figure 142

LAV25 STUDIES

Figure 144 shows the position and surroundings of the LAV25 used for all studies of the LAV25. The LAV25 and tree line were facing east. The LS-100 meter was pointed west while luminance data was collected.

Luminance readings were acquired for the LAV25 and tree line using four different ranges from the LAV25: 36 feet, 100 feet, 200 feet and 330 feet. Figure 145, Figure 146,...Figure 148 show the approximate LAV25 measurement area for these four ranges.

When the word "average" occurs in the title for the graphs that follow, the average luminance was used for constructing the graph.

All graphs involving the tree line were constructed using the average luminance of 50 random tree line luminance readings between the poles in Figure 144. Tree line luminance readings were acquired from left to right using an up-down scanning pattern.

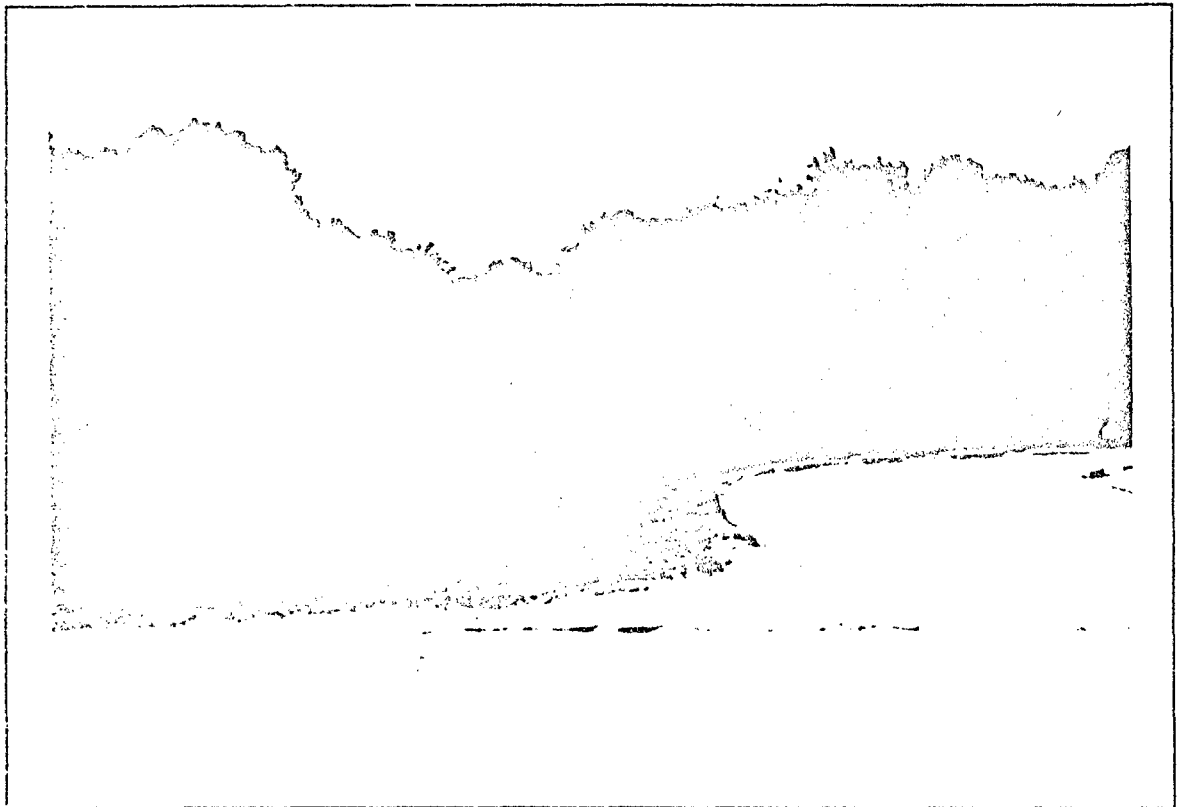


Figure 144

Position and Surroundings of the LAV25.
Metering Toward the West.

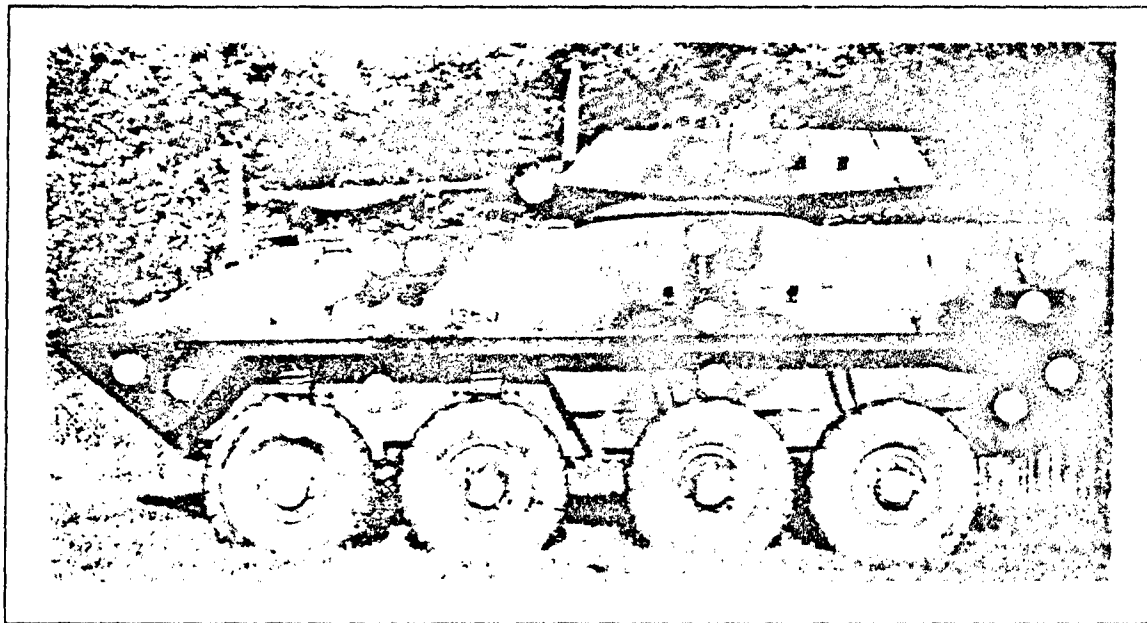


Figure 145

Approximate LAV25 Measurement Area. Range = 36 feet.

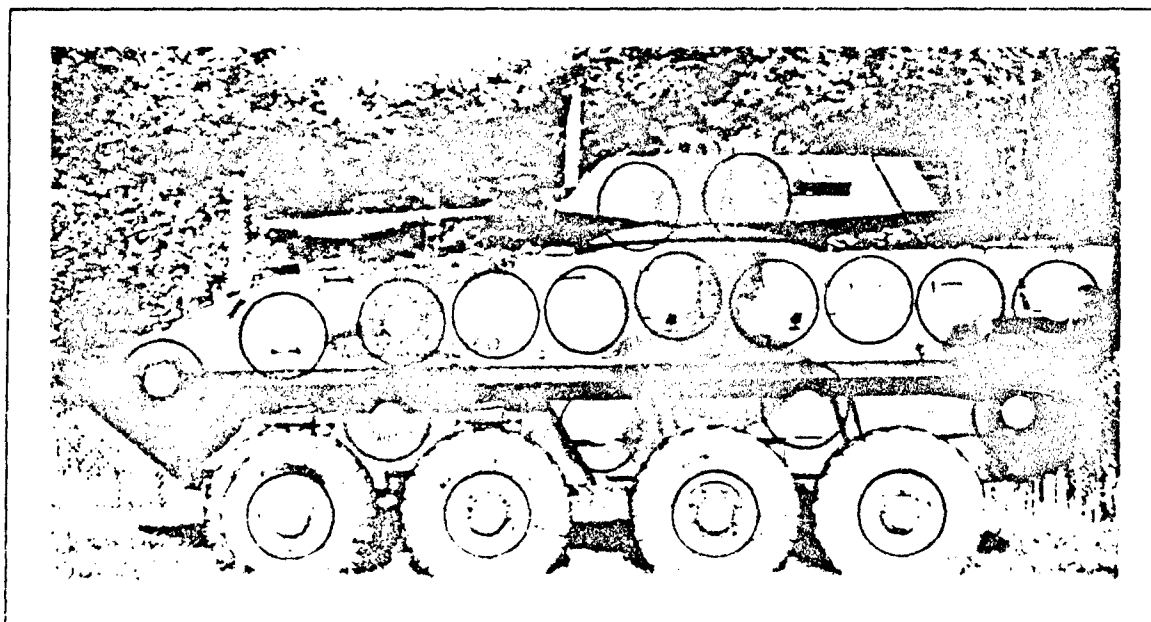


Figure 146

Approximate LAV25 Measurement Area. Range = 100 feet.

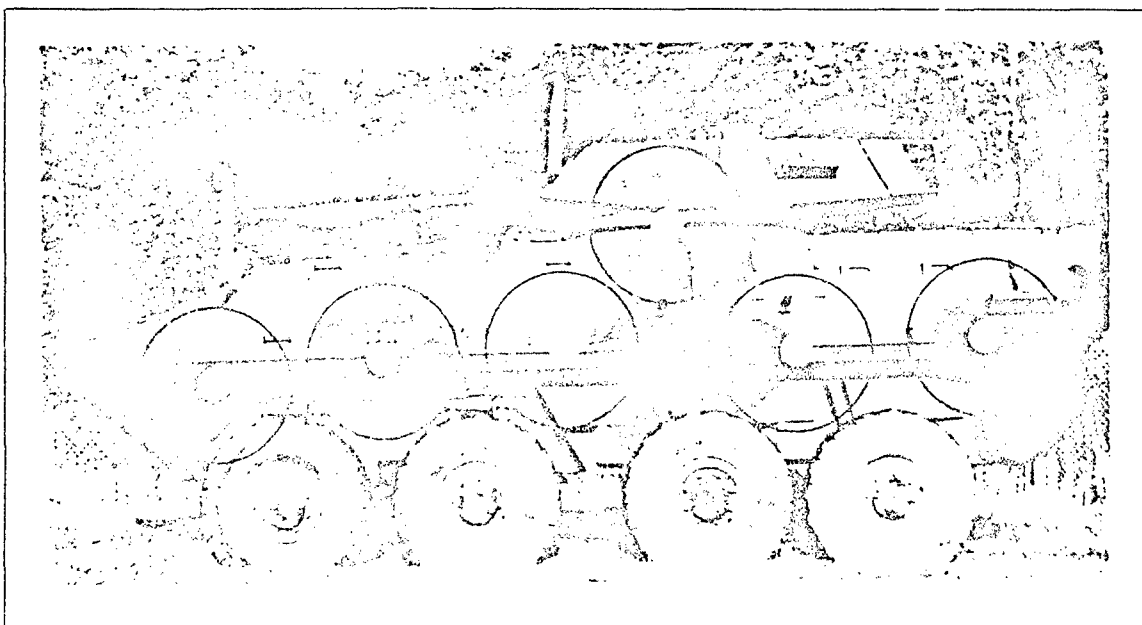


Figure 147

Approximate LAV25 Measurement Area. Range = 200 feet.

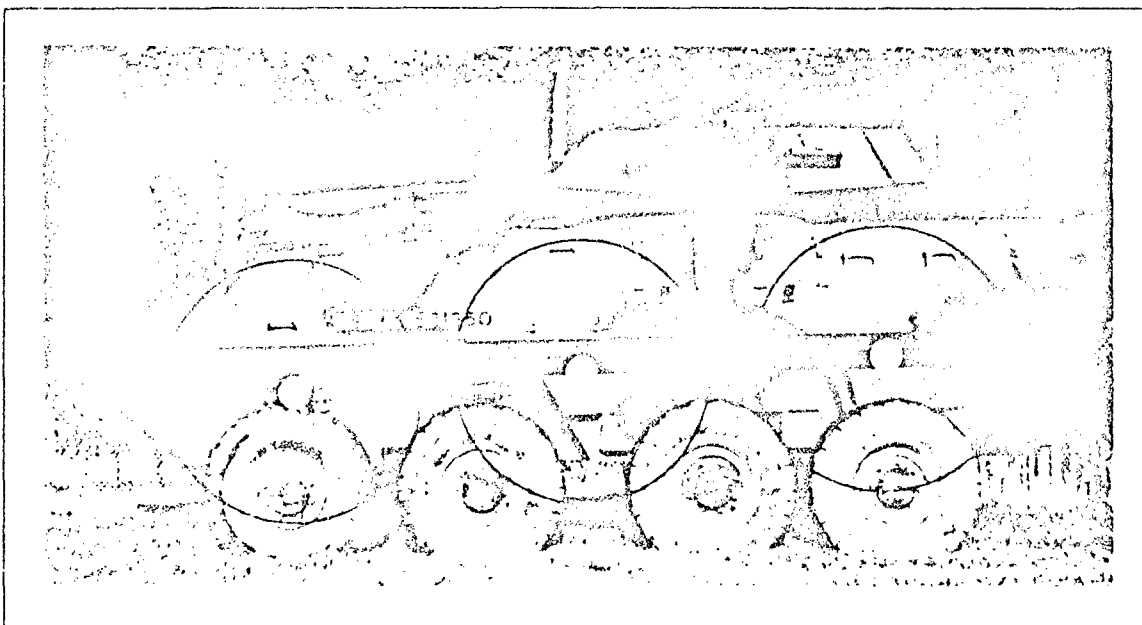


Figure 148

Approximate LAV25 Measurement Area. Range = 330 feet.

Study 23 July, 1990 Clear Skies 10:00-11:00, Cloudy 11:00-15:00

LAV25 LUMINANCE AT 10:00
METERING WEST AT 36 FEET
23 JULY, 1990; CLEAR SKIES

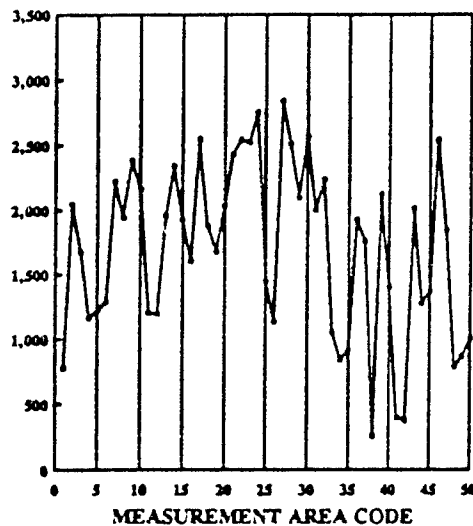


Figure 149

LAV25 LUMINANCE AT 10:30
METERING WEST AT 36 FEET
23 JULY, 1990; CLEAR SKIES

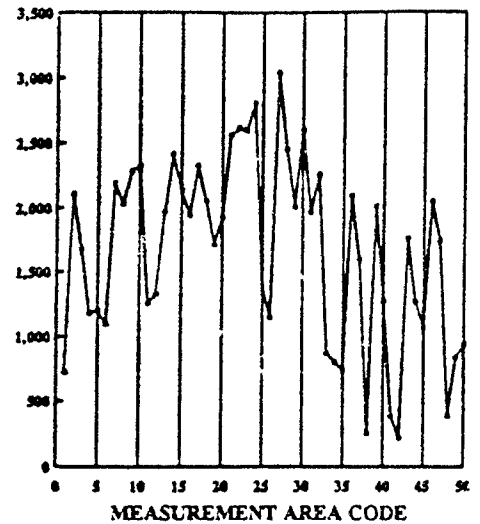


Figure 150

LAV25 LUMINANCE AT 11:30
METERING WEST AT 36 FEET
23 JULY, 1990; CLOUDY

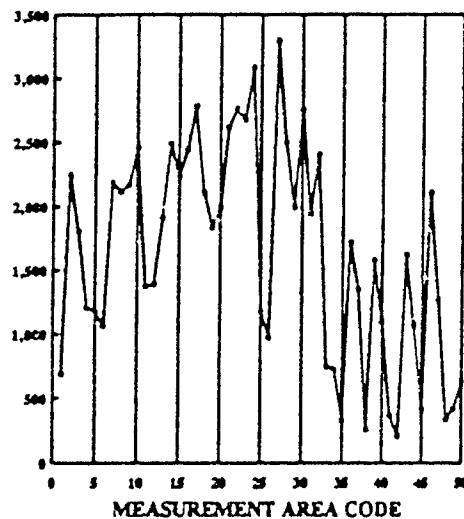


Figure 151

LAV25 LUMINANCE AT 12:45
METERING WEST AT 35 FEET
23 JULY, 1990; CLOUDY

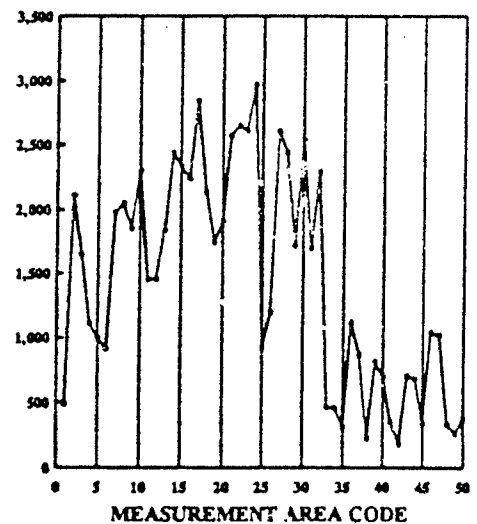


Figure 152

Study 23 July, 1990 Clear Skies 10:00-11:00, Cloudy 11:00-15:00

LAV25 LUMINANCE AT 13:30
METERING WEST AT 36 FEET
23 JULY, 1990; CLOUDY

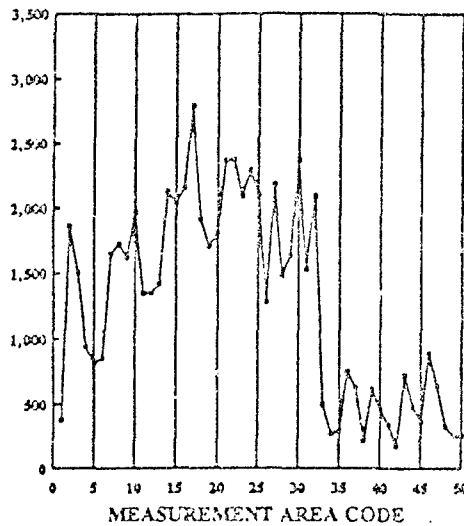


Figure 153

LAV25 LUMINANCE AT 14:05
METERING WEST AT 36 FEET
23 JULY, 1990; CLOUDY

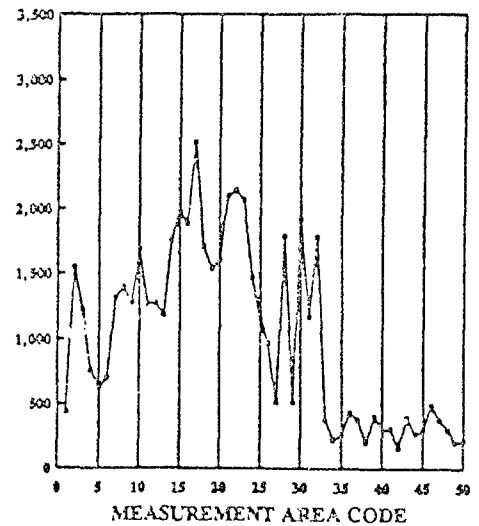


Figure 154

AVERAGE LUMINANCE
METERING AT 36 FEET

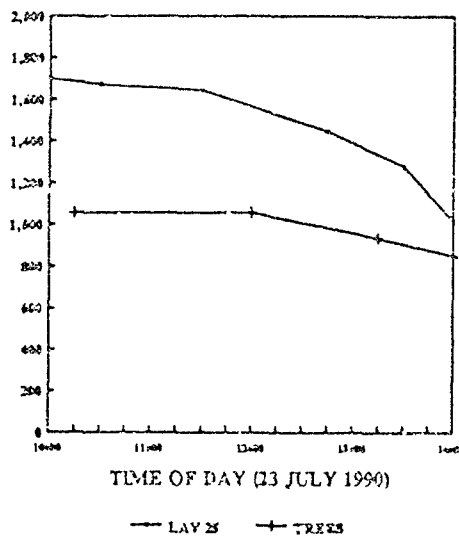


Figure 155

AVERAGE LAV25 CONTRAST
TREE BACKGROUND
METERING WEST AT 36 FEET

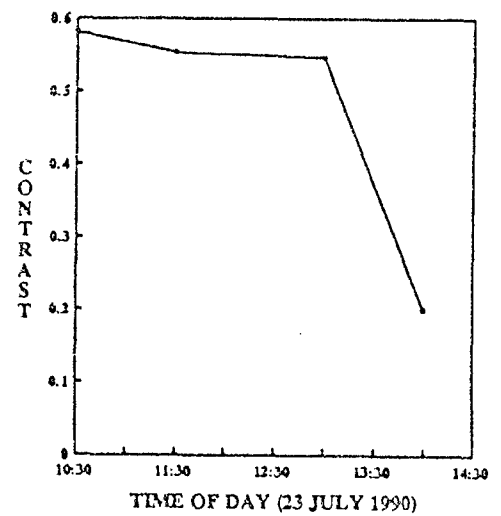


Figure 156

Study 23 July, 1990 Clear Skies 10:00-11:00, Cloudy 11:00-15:00

LAV25 LUMINANCE AT 10:45
METERING WEST AT 100 FEET
23 JULY, 1990; CLEAR SKIES

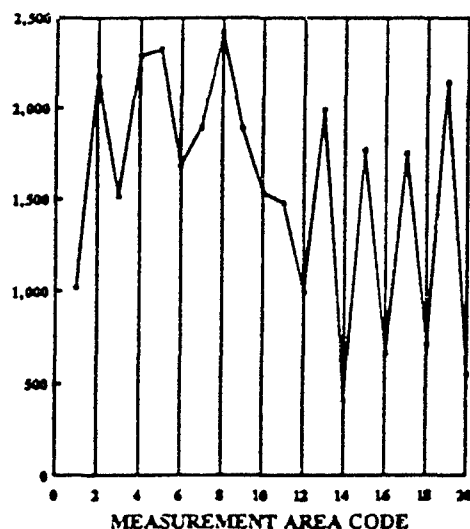


Figure 157

LAV25 LUMINANCE AT 11:45
METERING WEST AT 100 FEET
23 JULY, 1990; CLOUDY

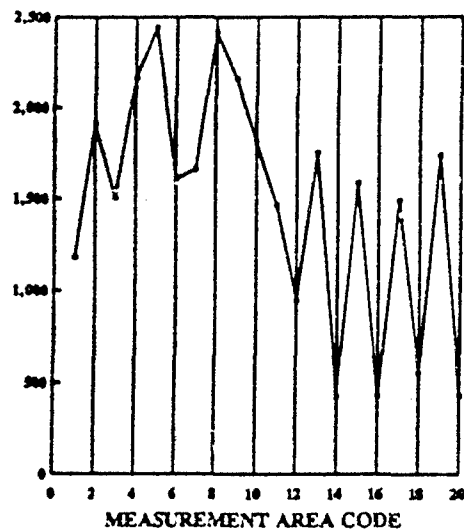


Figure 158

LAV25 LUMINANCE AT 13:00
METERING WEST AT 100 FEET
23 JULY, 1990; CLOUDY

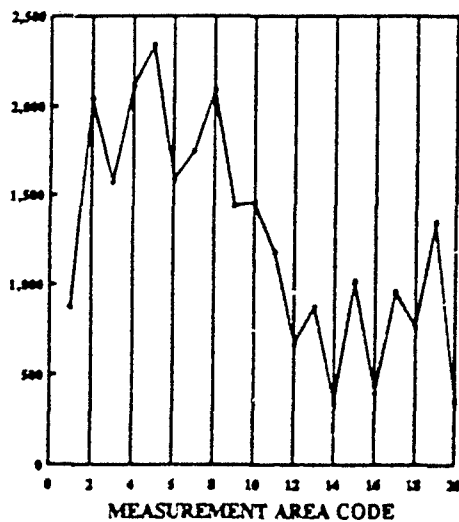


Figure 159

LAV25 LUMINANCE AT 13:30
METERING WEST AT 100 FEET
23 JULY, 1990; CLOUDY

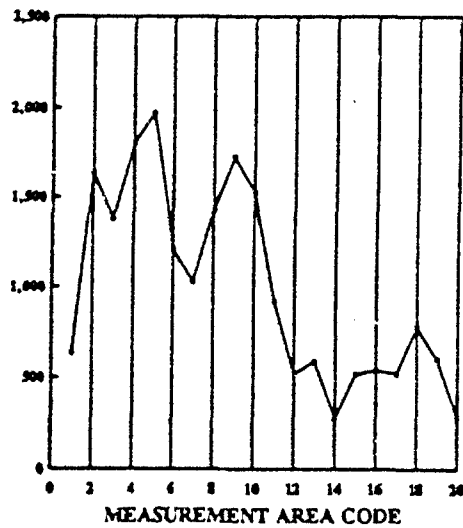


Figure 160

Study 23 July, 1990 Clear Skies 10:00-11:00, Cloudy 11:00-15:00

LAV25 LUMINANCE AT 14:15
METERING WEST AT 100 FEET
23 JULY, 1990; CLOUDY

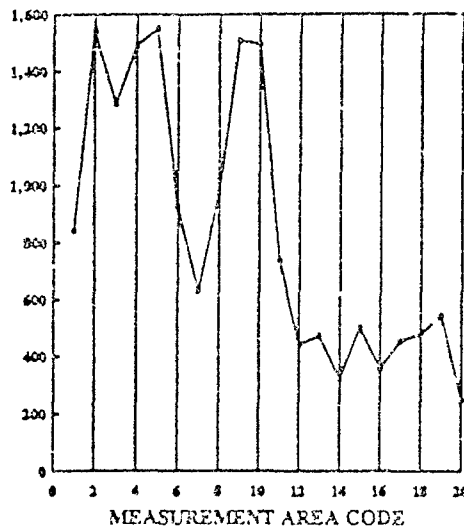


Figure 161

LAV25 AVERAGE LUMINANCE
METERING WEST
CLEAR UNTIL 11:00, CLOUDY AFTER 11:00

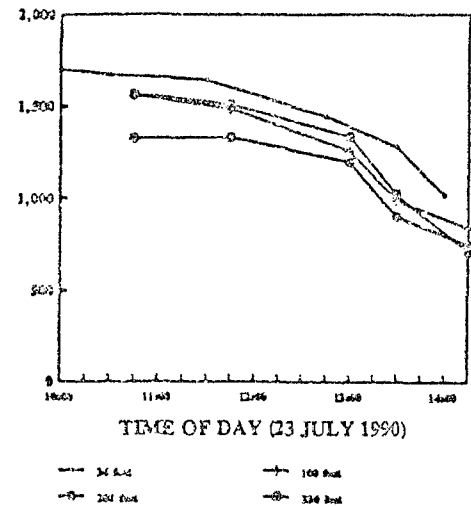


Figure 162

Study 24 July, 1990 Clear Skies

LAV25 LUMINANCE AT 9:00
METERING WEST AT 36 FEET
24 JULY, 1990; CLEAR SKIES

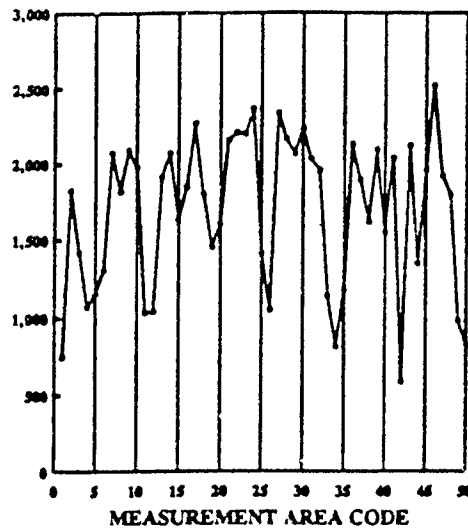


Figure 163

LAV25 LUMINANCE AT 9:30
METERING WEST AT 36 FEET
24 JULY, 1990; CLEAR SKIES

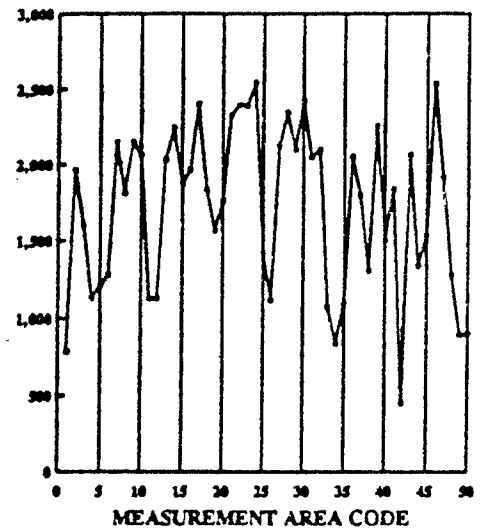


Figure 164

LAV25 LUMINANCE AT 10:00
METERING WEST AT 36 FEET
24 JULY, 1990; CLEAR SKIES

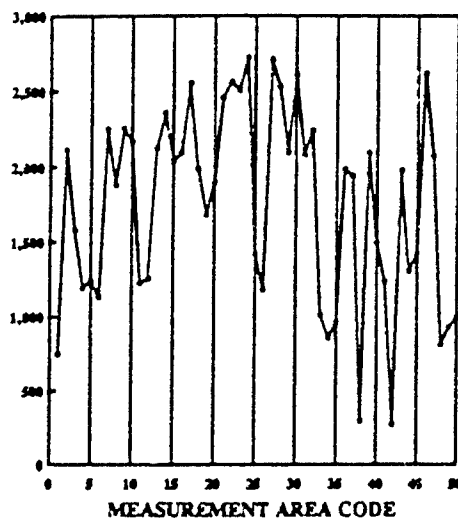


Figure 165

LAV25 LUMINANCE AT 10:30
METERING WEST AT 36 FEET
24 JULY, 1990; CLEAR SKIES

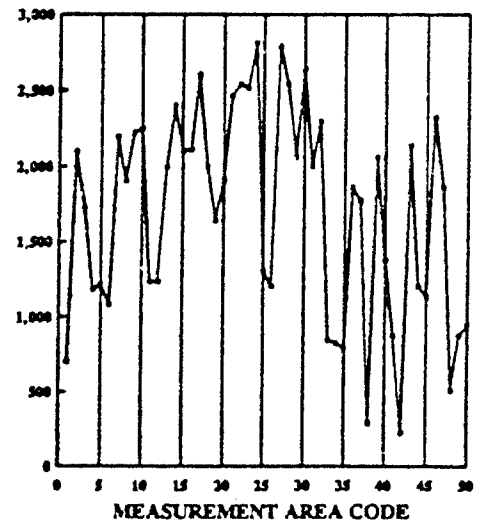


Figure 166

Study 24 July, 1990 Clear Skies

LAV25 LUMINANCE AT 11:00
METERING WEST AT 36 FEET
24 JULY, 1990; CLEAR SKIES

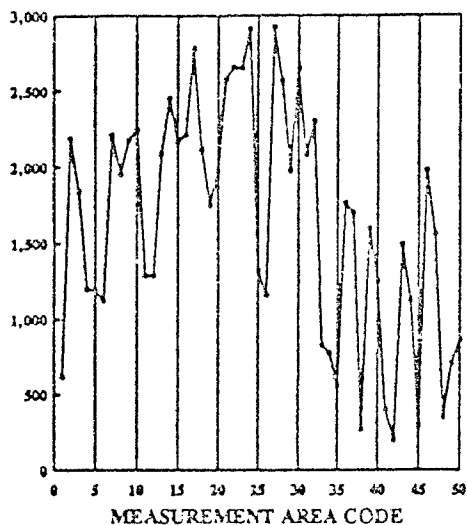


Figure 167

AVERAGE LUMINANCE
METERING AT 36 FEET
CLEAR SKIES

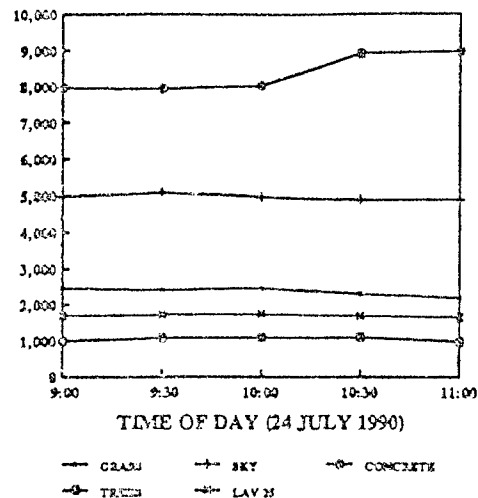


Figure 168

TREE LINE LUMINANCE
CLEAR SKIES

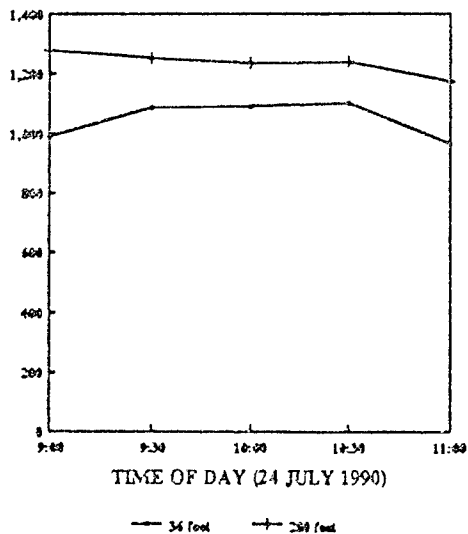


Figure 169

AVERAGE LAV25 CONTRAST
METERING AT 36 FEET
CLEAR SKIES

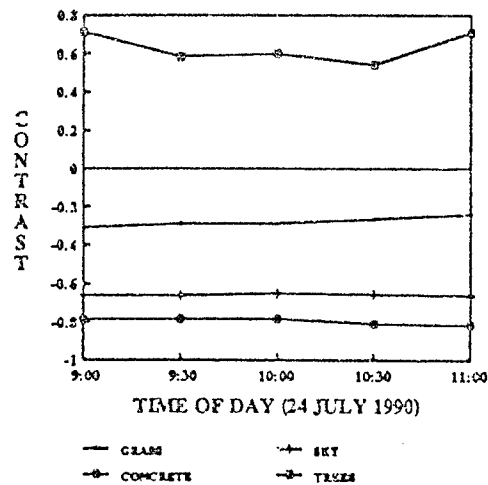


Figure 170

Study 24 July, 1990 Clear Skies

LAV25 LUMINANCE AT 9:15
METERING WEST AT 100 FEET
24 JULY, 1990; CLEAR SKIES

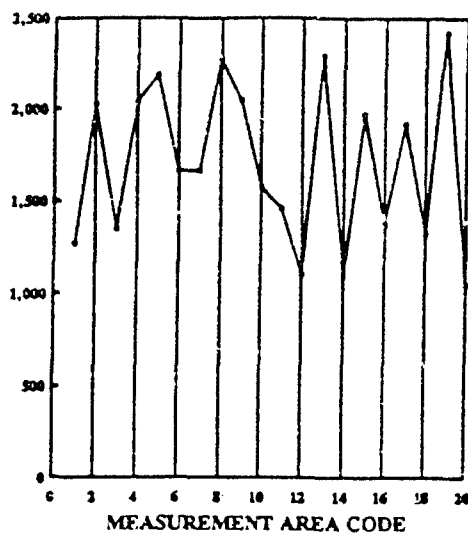


Figure 171

LAV25 LUMINANCE AT 9:45
METERING WEST AT 100 FEET
24 JULY, 1990; CLEAR SKIES

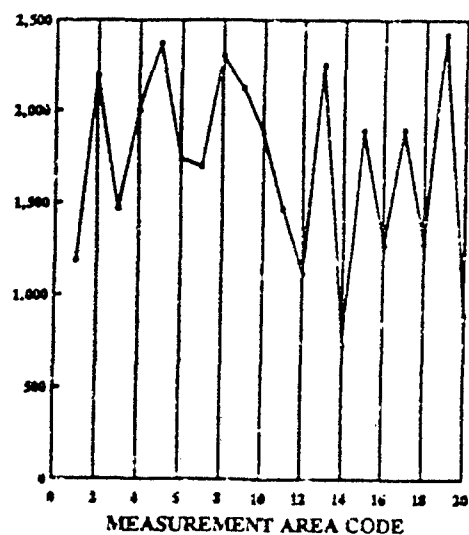


Figure 172

LAV25 LUMINANCE AT 10:15
METERING WEST AT 100 FEET
24 JULY, 1990; CLEAR SKIES

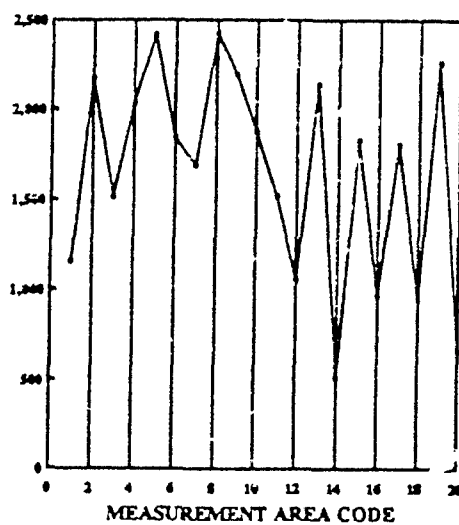


Figure 173

LAV25 LUMINANCE AT 10:45
METERING WEST AT 100 FEET
24 JULY, 1990; CLEAR SKIES

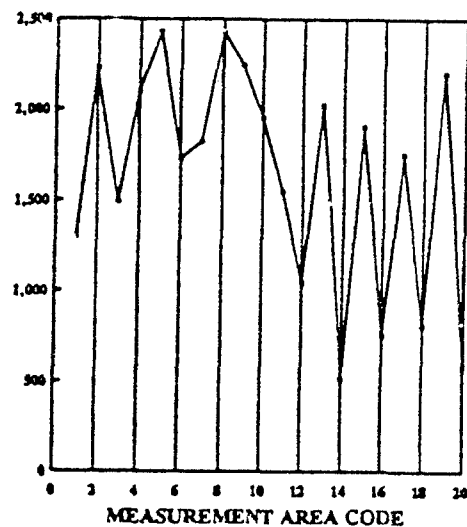


Figure 174

Study 24 July, 1990 Clear Skies

LAV25 LUMINANCE AT 11:15
METERING WEST AT 100 FEET
24 JULY, 1990; CLEAR SKIES

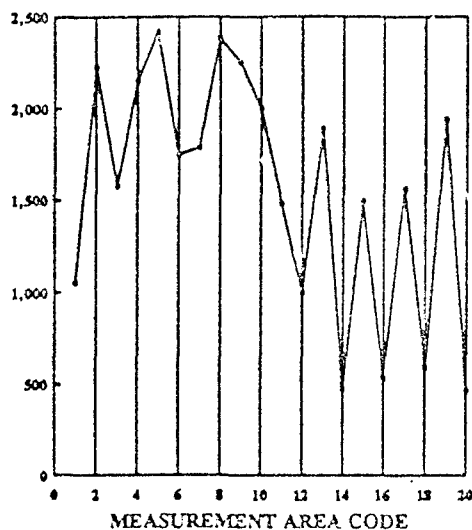


Figure 175

AVERAGE LAV25 LUMINANCE
CLEAR SKIES

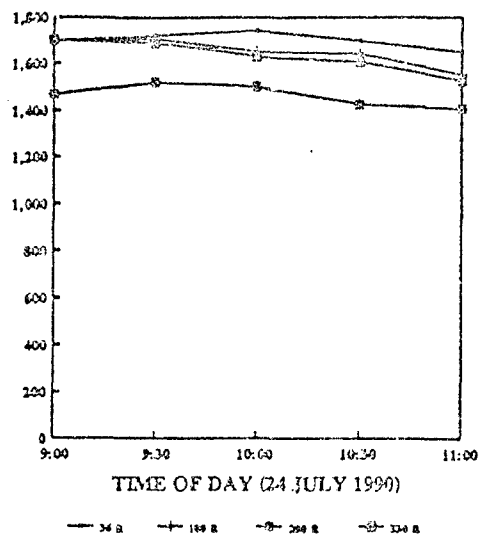


Figure 176

AVERAGE LAV25 CONTRAST
TREE BACKGROUND
CLEAR SKIES

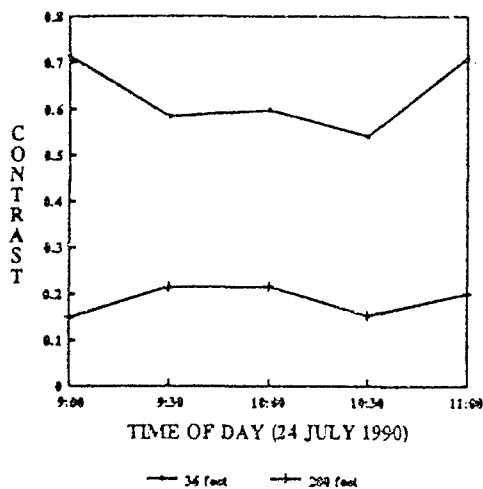


Figure 177

Study 26 July, 1990 Hazy 9:30-12:30, Cloudy 12:30-14:30

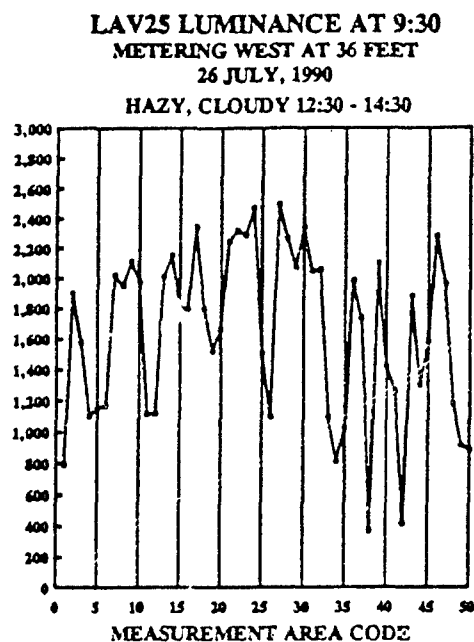


Figure 178

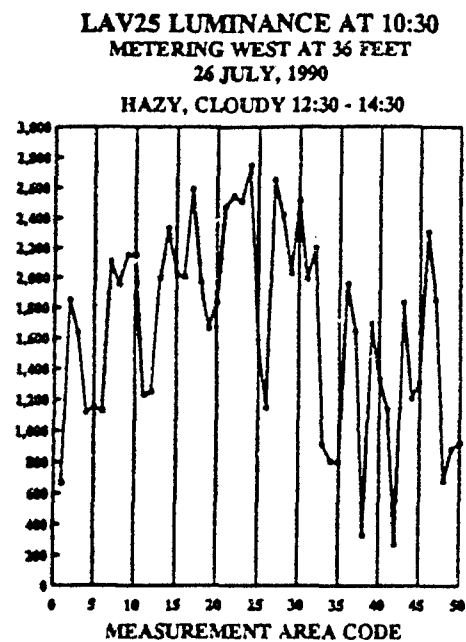


Figure 179

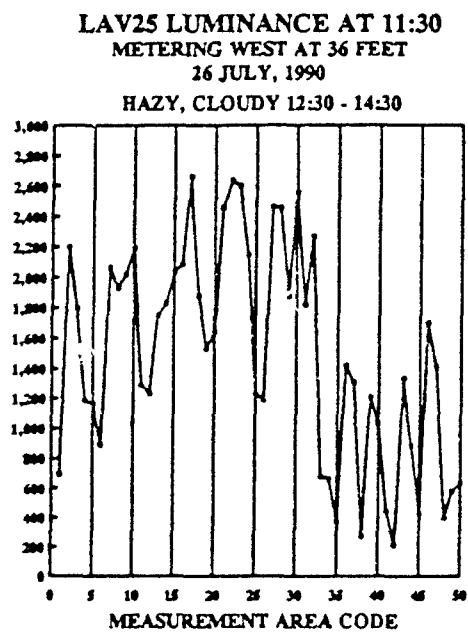


Figure 180

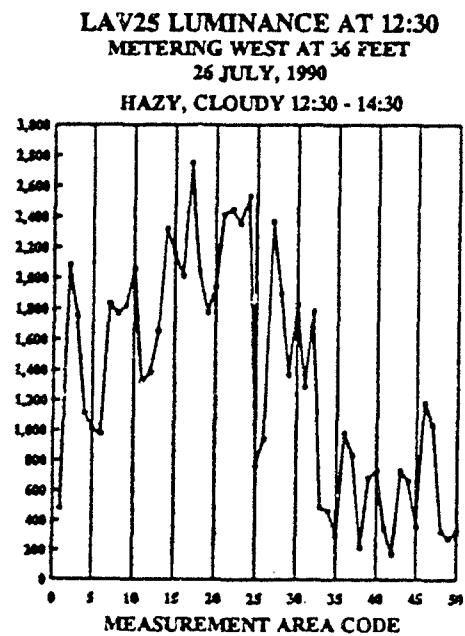


Figure 181

Study 26 July, 1990 Hazy 9:30-12:30, Cloudy 12:30-14:30

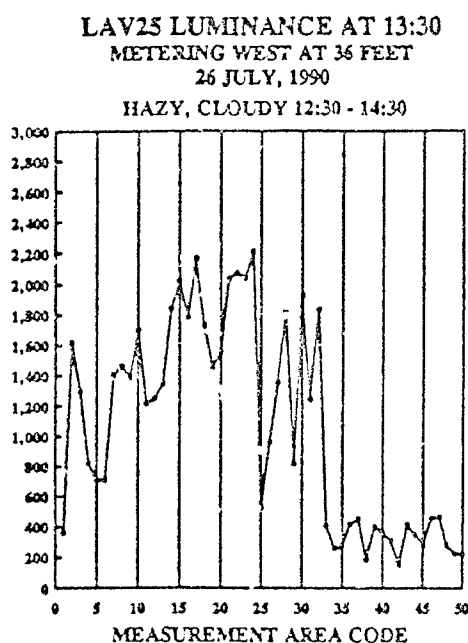


Figure 182

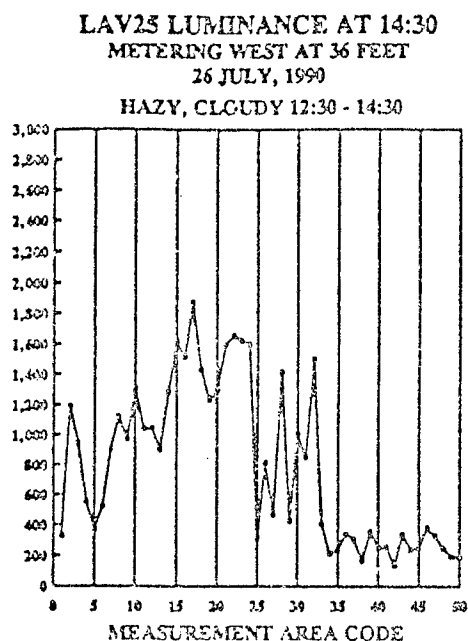


Figure 183

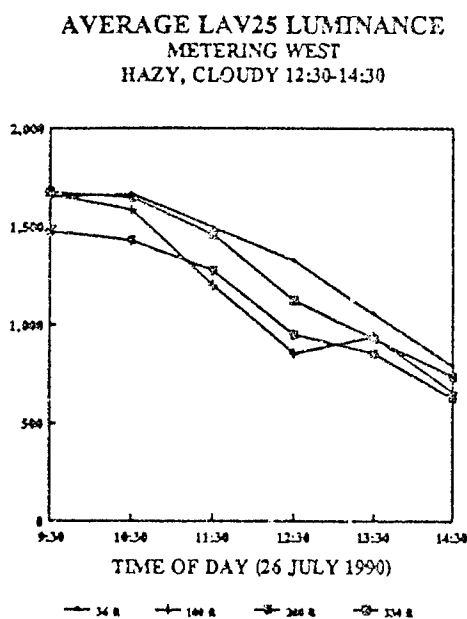


Figure 184

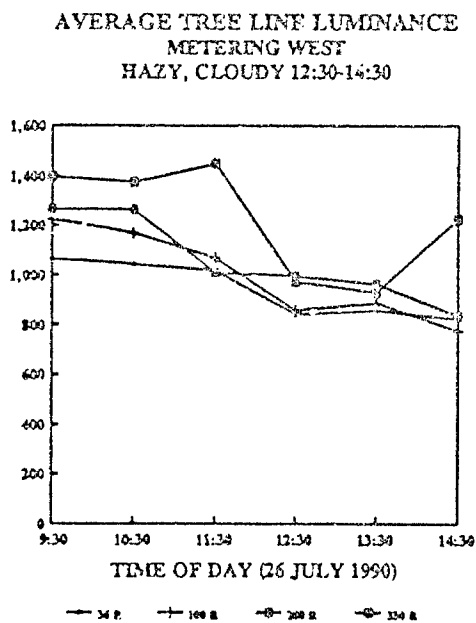


Figure 185

Study 26 July, 1990 Hazy 9:30-12:30, Cloudy 12:30-14:30

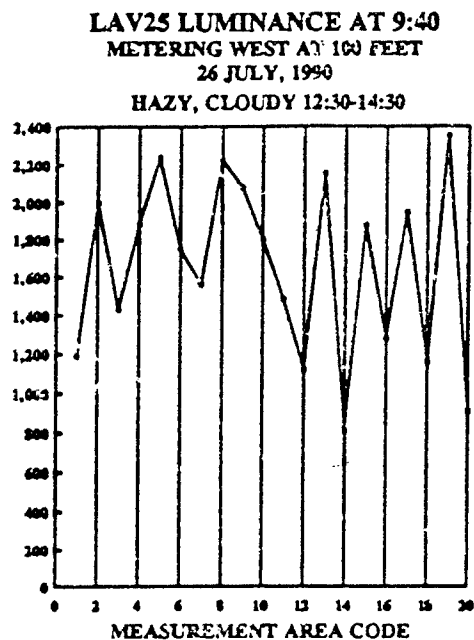


Figure 186

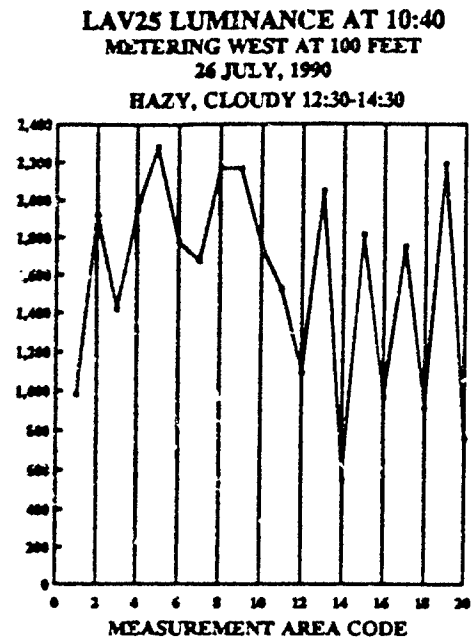


Figure 187

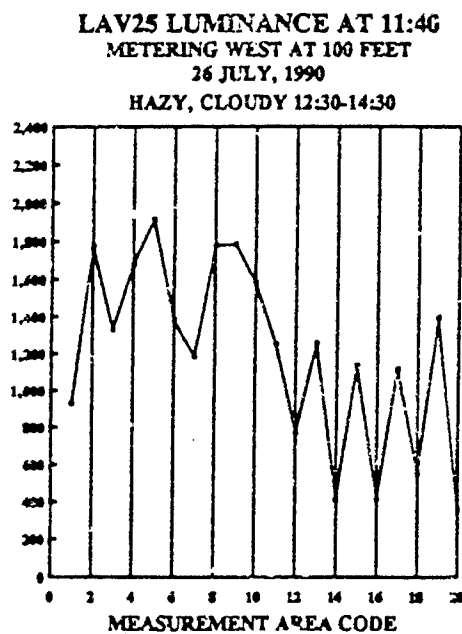


Figure 188

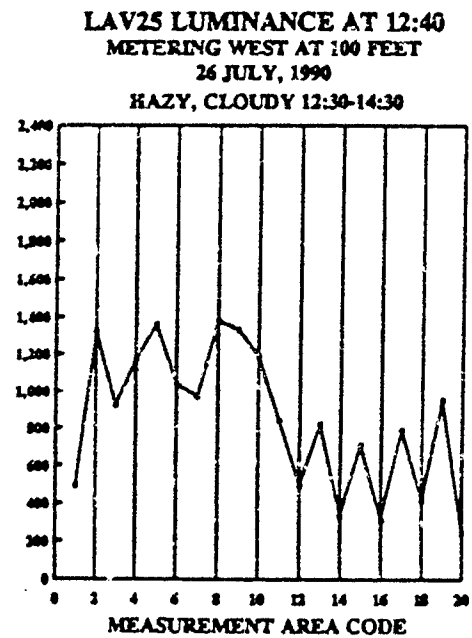


Figure 189

Study 26 July, 1990 Hazy 9:30-12:30, Cloudy 12:30-14:30

LAV25 LUMINANCE AT 13:40
METERING WEST AT 100 FEET
26 JULY, 1990
HAZY, CLOUDY 12:30-14:30

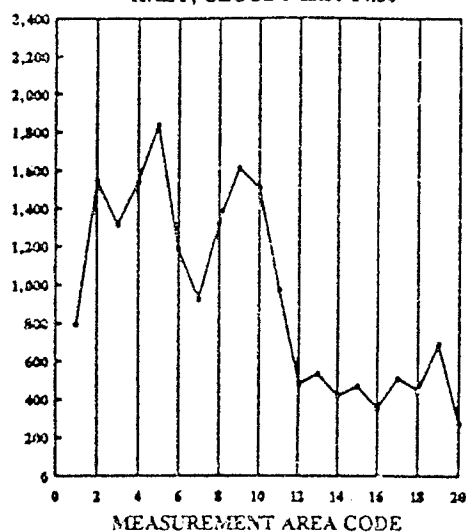


Figure 190

LAV25 LUMINANCE AT 14:40
METERING WEST AT 100 FEET
26 JULY, 1990
HAZY, CLOUDY 12:30-14:30

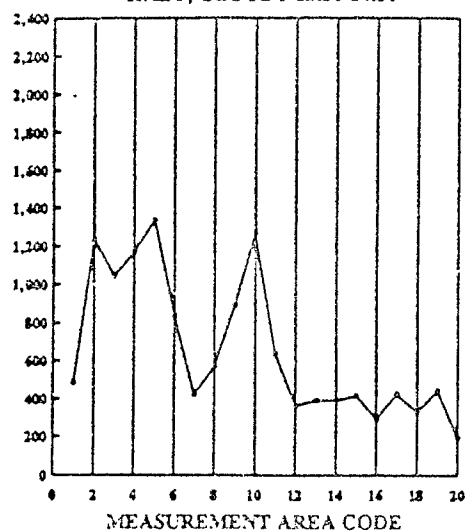


Figure 191

LUMINANCE OF GRASS
HAZY, CLOUDY 12:30-14:30

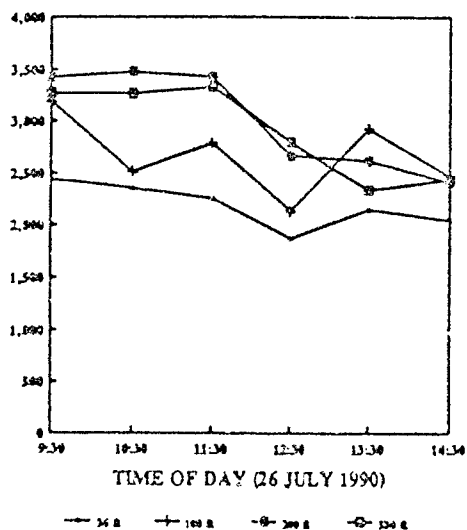


Figure 192

LUMINANCE OF SKY
HAZY, CLOUDY 12:30-14:30

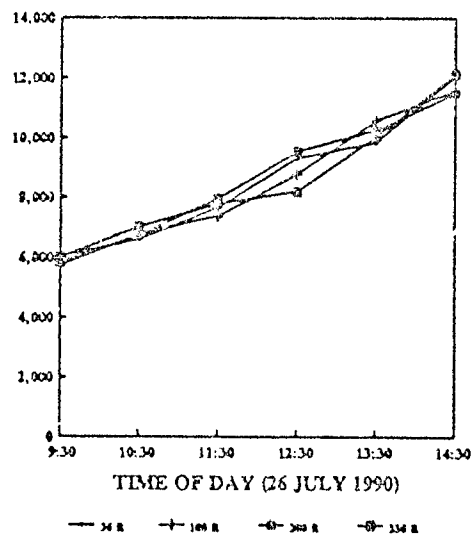


Figure 193

Study 26 July, 1990 Hazy 9:30-12:30, Cloudy 12:30-14:30

AVERAGE LAV25 CONTRAST
TREE BACKGROUND
HAZY, CLOUDY 12:30-14:30

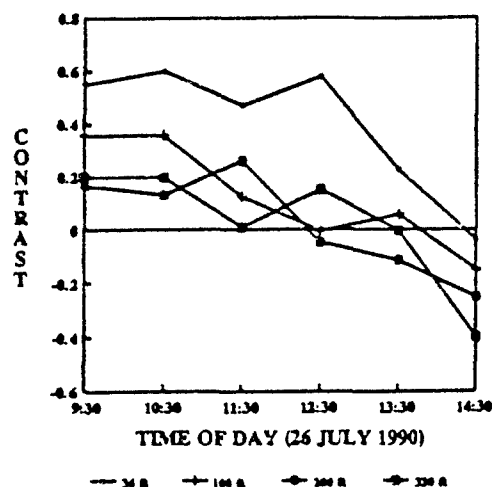


Figure 194

AVERAGE LAV25 CONTRAST
GRASS BACKGROUND
HAZY, CLOUDY 12:30-14:30

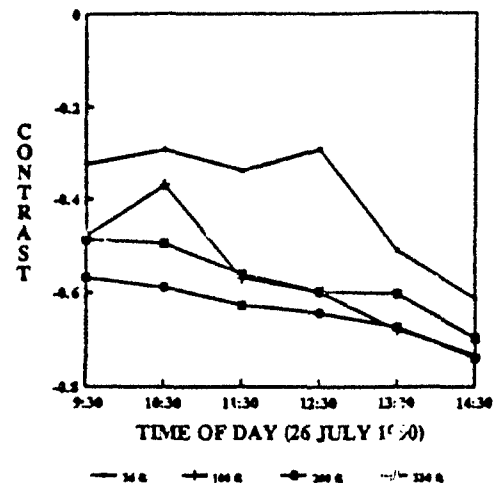


Figure 195

AVERAGE LAV25 CONTRAST
SKY BACKGROUND
HAZY, CLOUDY 12:30-14:30

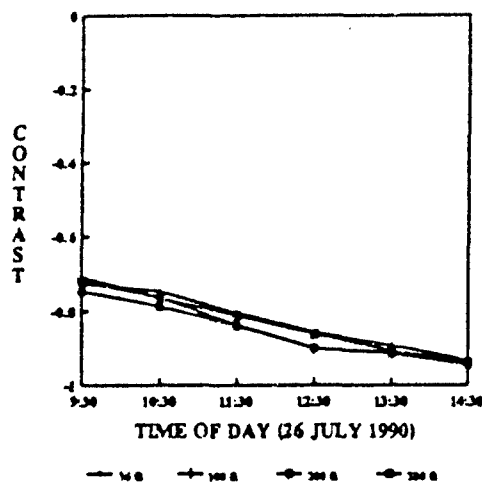


Figure 196

AVERAGE LAV25 CONTRAST
CONCRETE BACKGROUND
HAZY, CLOUDY 12:30-14:30

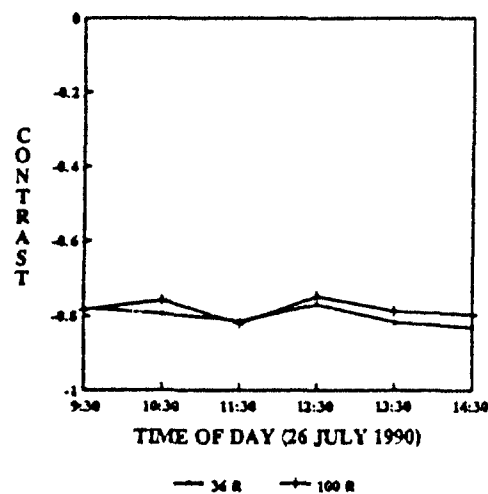


Figure 197

LAV25 Study on 26 July, 1990 (Hazy 9:00-12:30, Cloudy 12:30-14:30; Viewing Toward West)

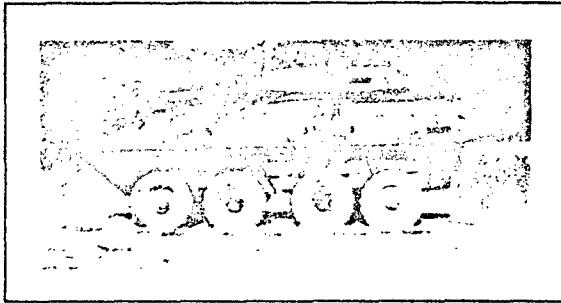


Figure 198

LAV25 at 9:30

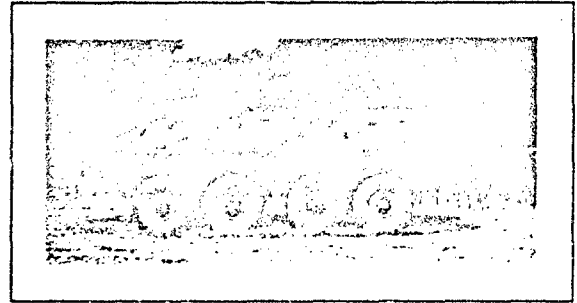


Figure 199

LAV25 at 10:30

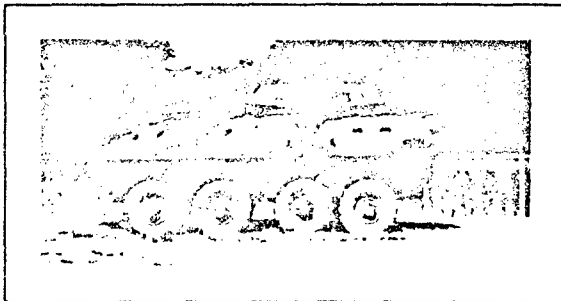


Figure 200

LAV25 at 11:30

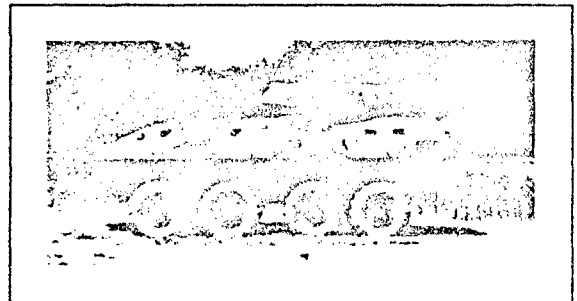


Figure 201

LAV25 at 12:30

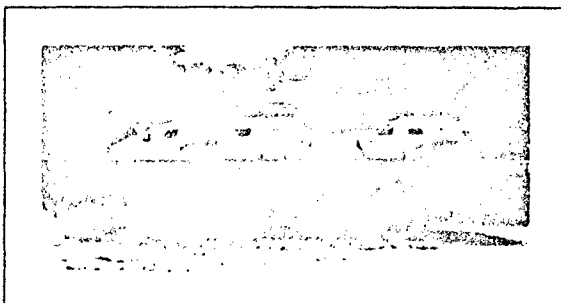


Figure 202

LAV25 at 13:30

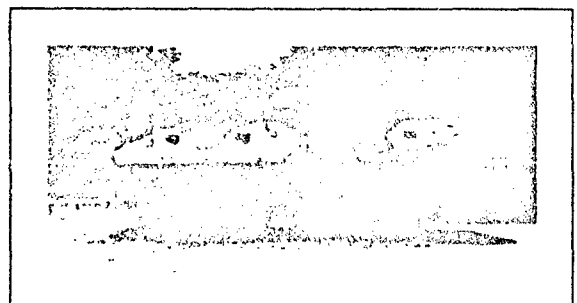


Figure 203

LAV25 at 14:30

SUMMARY OF LAV25 STUDIES

All LAV25 studies were conducted with the vehicle oriented along a north-south line with luminance metering toward the west. Figure 144 shows the position of the vehicle and its surroundings during the times measurements were acquired. All conclusions in this study are based on this vehicle orientation and setup.

Luminance readings were acquired from four different ranges: 36, 100, 200 and 330 feet. The approximate measurement areas on the LAV25 for these ranges are shown in Figure 145, Figure 146,...Figure 148.

WHEEL AREAS

The most obvious luminance feature of the LAV25 relates to the vehicle's wheels and the surrounding wheel areas. In terms of luminance, the LAV25 is a bi-sectional vehicle. Its high stature, when positioned on the ground, produces significant shading of the wheel areas between 10:30 and 14:30. The photographs of Figure 198, Figure 199,...Figure 203 illustrate how shading and shadows develop between 9:30 and 14:30. Shadows in the wheel areas begin at 10:30 and complete shading occurs at 14:30.

The graphs of Figure 149, Figure 150,...Figure 154 (range = 36 feet) illustrate clearly the bi-sectional luminance nature of the LAV25. The variance in luminance for measurement areas 34-50 (wheel areas) is greater than for measurement areas 1-33. As time elapses, the two sections graphically separate.

The graphs of Figure 157, Figure 158,...Figure 161 (range = 100 feet) also illustrate clearly the bi-sectional luminance nature of the LAV25. The variance in luminance for measurement areas 13-20 (wheel areas) is much greater than for measurement areas 1-12. As time elapses, the two sections graphically separate.

The graphs of Figure 204, Figure 205,...Figure 215 compare the average luminance of the wheel areas to the average luminance of those areas above them for ranges of 36 feet and 100 feet. At approximately 9:00, the average luminance of both areas is approximately 1700 cd/m². At approximately 12:00, the average luminance of the wheel areas is approximately 50 percent of the average luminance of the area above the wheels. The ratio of the average luminance of the wheel areas to the average luminance of the area above the wheels decreases at the approximate rate of 0.15 per hr.

Table 41 gives the luminance of the LAV25 wheels, the luminance of the immediate surrounding areas and the contrast between them. There is considerable contrast between the LAV25 wheels and the immediate LAV25 surrounding areas. The average contrast between the LAV25 and tree background is approximately 0.6 (Figure 156, Figure 170 and Figure 194). However, the contrast between the LAV25 wheels and the immediate surrounding LAV25 areas varies from 0.57 to 2.61.

Study 23 July, 1990 Clear Skies 10:00-11:00, Cloudy 11:00-15:00

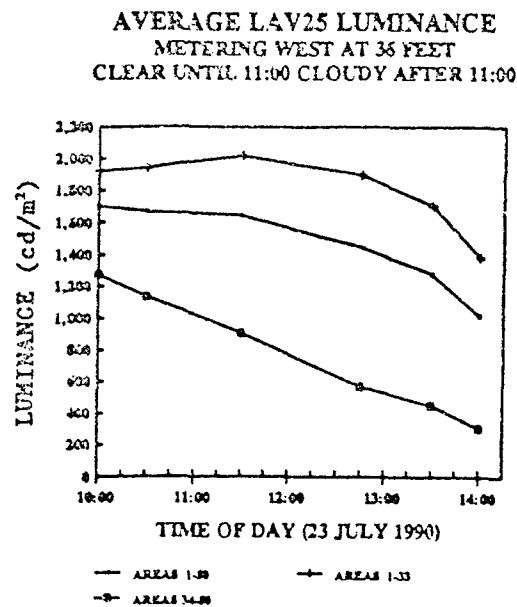


Figure 204

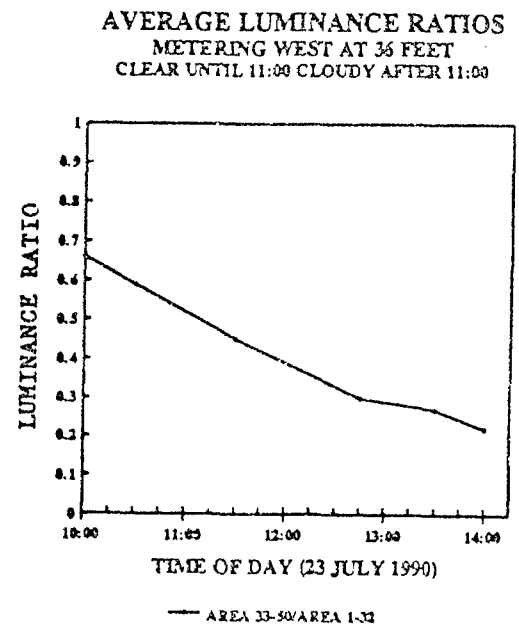


Figure 205

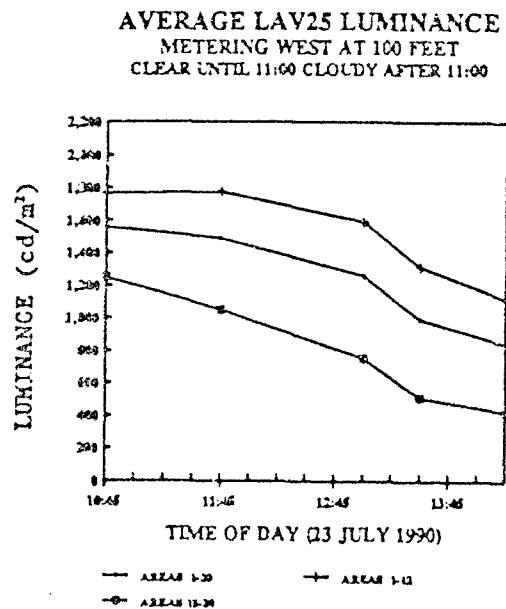


Figure 206

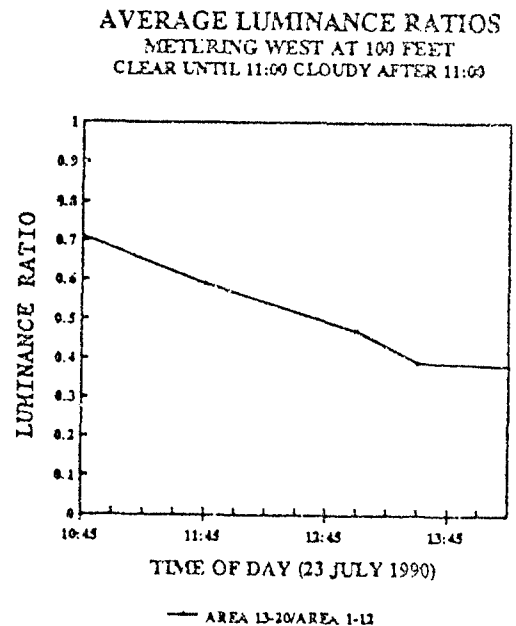


Figure 207

Study 24 July, 1990 Clear Skies

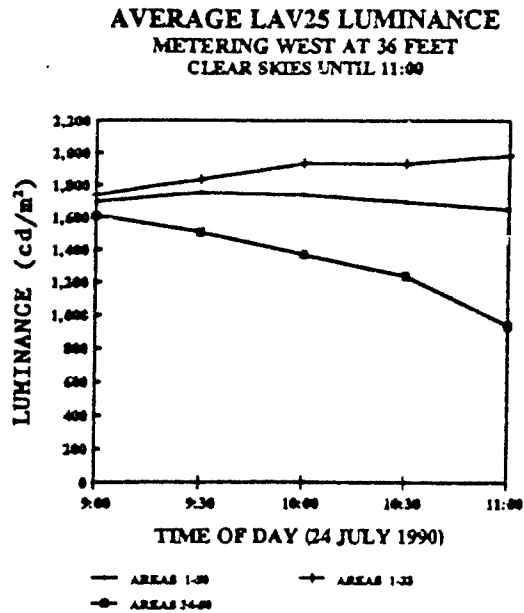


Figure 208

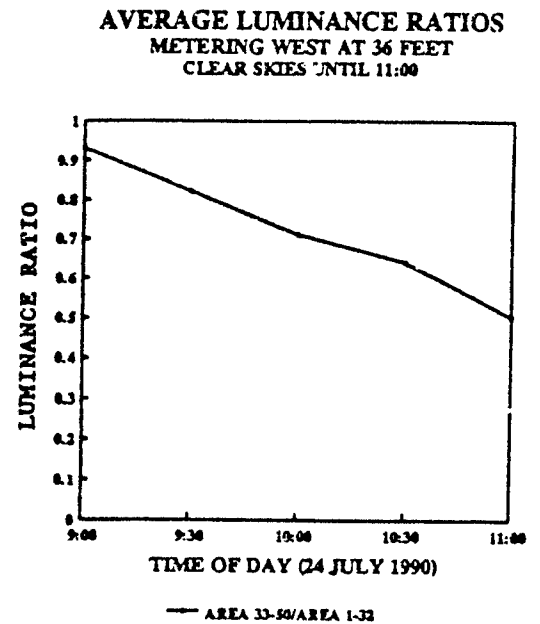


Figure 209

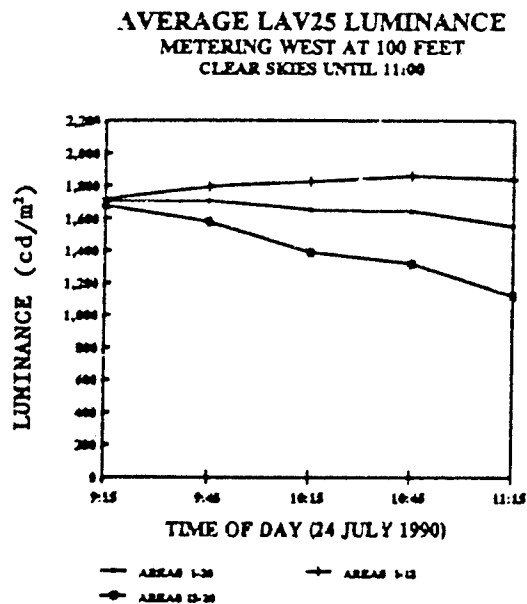


Figure 210

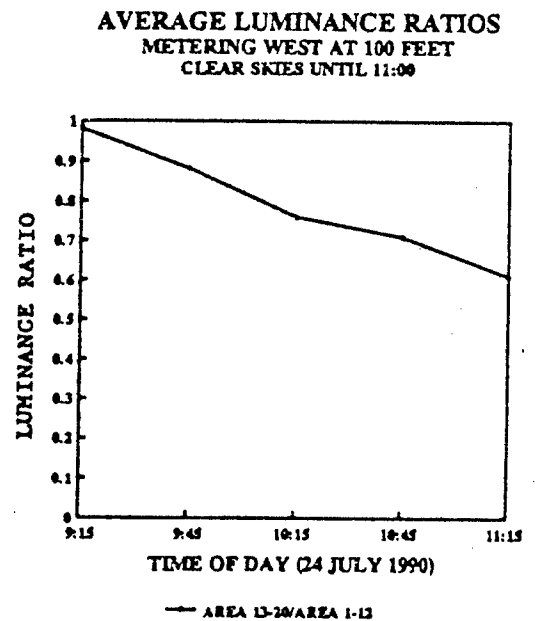


Figure 211

Study 26 July, 1990 Hazy 9:30-12:30, Cloudy 12:30-14:30

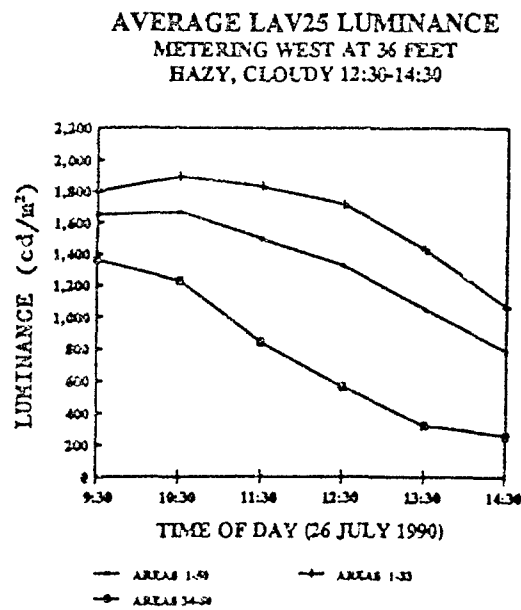


Figure 212

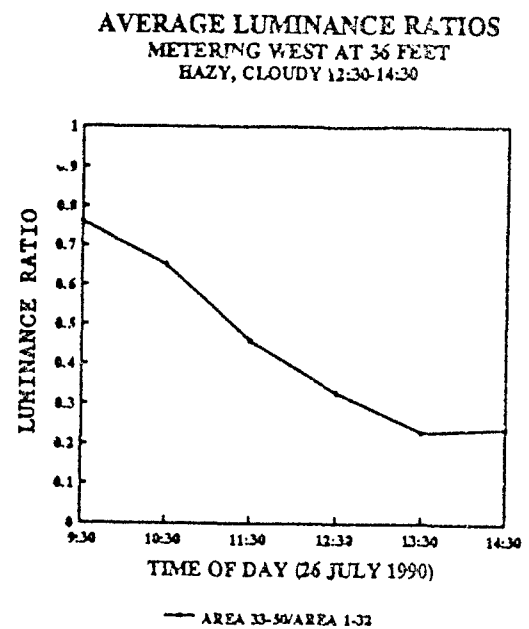


Figure 213

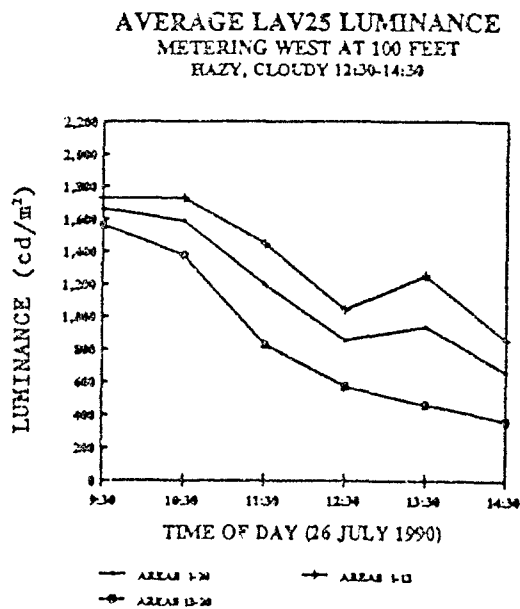


Figure 214

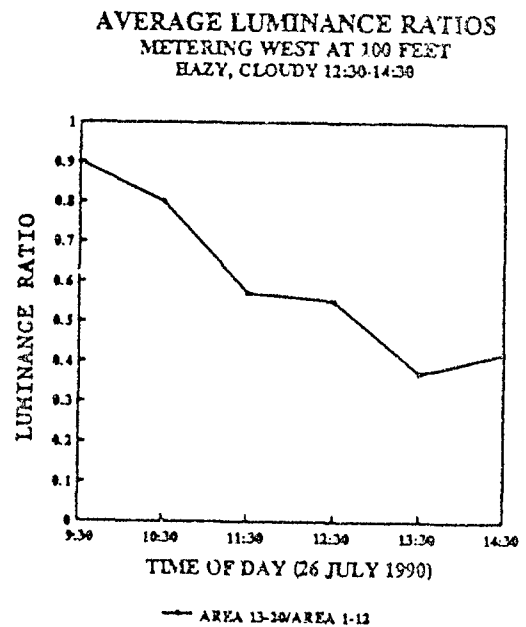


Figure 215

Table 41. Contrast of LAV25 Wheels Using Surrounding Wheel Area as Background.
23 July, 1990. Range = 36 feet. Clear Until 11:00, Cloudy after 11:00

Luminance (cd/m ²) of LAV25 Wheels						
Area #	10:00	10:30	11:30	12:45	13:30	14:00
36	1924	2090	1718	1118	753	432
37	1760	1590	1349	860	625	378
39	2123	2011	1578	813	616	403
40	1400	1270	1088	691	461	305
43	2014	1756	1619	701	724	396
44	1274	1264	1068	679	481	271
46	2543	2047	2109	1036	892	495
47	1843	1741	1263	1016	641	380
Average	1860	1721	1474	865	649	383
Luminance of LAV25, Surrounding Wheel Areas						
34	836	800	721	454	270	222
35	914	732	328	307	303	266
38	256	251	260	222	220	206
41	398	383	366	345	341	308
42	374	216	204	180	174	160
45	1367	1059	407	332	362	304
48	780	384	336	325	326	301
49	863	833	419	258	252	204
50	1003	934	631	375	256	224
Average	755	621	408	311	278	244
Contrast	1.47	1.77	2.61	1.78	1.33	0.57

AVERAGE LAV25 LUMINANCE

The LAV25 was made available for measurement for five days. Unfortunately, it rained one of the days and the cloud conditions were extremely variable on another. None of the days provided clear skies for the entire day. During those time periods for which the skies were not completely clear, luminance readings were only taken when the sun was not eclipsed by clouds. During the study of 26 July, the sky conditions after 12:30 were hazy, overcast and cloudy.

In all three studies of the LAV25, there are extended periods of time for which the average luminance of the LAV25 can be expressed by linear equations. Table 42 provides expressions for average luminance (L) in terms of time (t) for the three days data was acquired. Correlation coefficients (r) are included to show how close the relationships fit collected data. Figure 155, Figure 168 and Figure 184 show graphically the data used to obtain Table 42.

Table 42. LAV25 Average Luminance Analysis. Range = 36 feet

t - 0	Time Range; Date	Luminance (cd/m ²)	r
10:00	10:00 - 13:30; 23 July	L = 1740 - 117 t	0.957
9:30	9:30 - 11:00; 24 July	L = 1767 - 52 t	0.837
10:30	10:30 - 14:30; 26 July	L = 1705 - 220 t	0.993

Table 43 gives the average luminance acquired for the LAV25 on 26 July, 1990 for different ranges. The far left column titled "Average" represents the average LAV25 luminance for a specific time. The row titled "Average" represents the average LAV25 luminance for the entire time period data was collected. Figure 184 shows the data in graphical form.

Table 43. Average LAV25 Luminance (cd/m²) on 26 July, 1990 for Different Ranges

Range	36 feet	100 feet	200 feet	330 feet	Average
9:30	1649	1661	1476	1677	1616
10:30	1667	1585	1427	1646	1581
11:30	1494	1198	1273	1458	1356
12:30	1326	853	947	1121	1062
13:30	1052	935	851	926	941
14:30	789	657	625	734	701
Average	1330	1148	1100	1260	1209

Table 44 provides expressions for average luminance (L) in terms of time (t) for four different ranges. Correlation coefficients (r) are included to show how close the relationships fit collected data.

Table 44. LAV25 Average Luminance Analysis for 26 July, 1990 (t = 0 at 9:30)

Range	Luminance (cd/m ²)	r
36 feet	$L = 1780 - 180 t$	0.964
100 feet	$L = 1670 - 209 t$	0.960
200 feet	$L = 1550 - 180 t$	0.982
330 feet	$L = 1775 - 206 t$	0.983
Average	$L = 1694 - 194 t$	0.986

TREELINE LUMINANCE

The photograph of Figure 144 shows the surrounding treeline background used for the three studies conducted for the LAV25. All graphs and tables relating to the treeline were constructed using the average luminance of 50 random luminance readings between the poles shown in Figure 144.

Table 45 and Table 46 provide a summary and an analysis of the average treeline luminance readings acquired during the LAV25 studies. Figure 155, Figure 169 and Figure 185 show the results in graphical form

Table 45. Average Treeline Luminance (cd/m²) for 23 July, 1990 and 24 July, 1990

23 July; Range - 36'		24 July; Range - 36'		24 July; Range - 200'	
Time	Luminance	Time	Luminance	Time	Luminance
10:15	1056	9:05	989	9:20	1277
12:00	1057	9:35	1086	9:50	1251
13:15	934	10:05	1090	10:20	1235
14:00	849	10:35	1101	10:45	1238
		11:05	964	11:15	1173
Average	974	Average	1046	Average	1235
$L = 1091 - 55 t$ $r = 0.889$		$L = 1053 - 7 t$ $r = 0.086$		$L = 1279 - 44 t$ $r = 0.912$	

Table 46. Summary and Analysis of Average Treeline Luminance (cd/m^2) for 26 July, 1990

Time	Luminance R = 36'	Luminance R = 100'	Luminance R = 200'	Luminance R = 330'	Average Luminance
9:30	1064	1224	1265	1397	1238
10:30	1042	1168	1263	1375	1212
11:30	1017	1067	1010	1448	1136
12:30	840	857	994	973	916
13:30	857	885	961	929	908
14:30	821	774	836	1224	914
Average	940	996	1055	1224	1054
Range = 36 feet		L = 1079 - 56 t		r = 0.929	
Range = 100 feet		L = 1232 - 94 t		r = 0.966	
Range = 200 feet		L = 1274 - 88 t		r = 0.947	
Range = 330 feet		L = 1415 - 77 t		r = 0.636	
AVERAGE LUMINANCE		L = 1250 - 79 t		r = 0.929	

Table 45 and Table 46 indicate that the average diurnal treeline luminance can be expressed as linear equations. With one exception, range R = 330 feet, the correlation coefficients are above 0.92.

These tables also indicate that the average treeline luminance is greater for larger ranges. The reason for this is unknown. Some considerations are:

1. Approximatel five minutes were required to transport and set up the equipment for each new range position. It also takes time to acquire the luminance readings for each range. Sun position and sky conditions can change during this time.
2. The treeline luminance averages were obtained from a random sampling of trees and bushes. Each average represents a different collection of targets.
3. The luminance measurement area becomes larger the farther the meter gets from the target.

This difference in treeline luminance for different ranges contributes significantly to contrast differences for the LAV25 when the treeline is used as a background for different ranges. The graph of Figure 177 shows an average contrast of approximately 0.6 for a range 36 feet. When the range was 200 feet, the average contrast was approximately 0.2. This significant contrast difference is also due to the difference in measurement areas (Figure 145 and Figure 147) used for the two ranges. The wheels of the LAV25, which increase the average luminance of the LAV25, were not included in the measurement areas for a range of 200 feet.

Table 47. Average Luminance and Contrast for Ranges of 36 feet and 200 feet on 24 July, 1990

Range (feet)	Average LAV25 Luminance (cd/m ²)	Average Treeline Luminance (cd/m ²)	Average Contrast
36	1700	1046	0.62
200	1464	1235	0.19

Similar results were obtained for the LAV25 study of 26 July, 1990. Figure 194 illustrates that a higher contrast is obtained at a range of 36 feet than is obtained for higher ranges at the same time of day.

CONTRAST

Four different backgrounds were used to acquire contrast values for the LAV25: grass, sky, concrete and trees. Of the three studies conducted for the LAV25, the study of 26 July, 1990 was the most extensive. This study involved all four backgrounds for four different ranges.

Table 48 gives a summary of the average contrasts obtained for the three LAV25 studies using a treeline as background. The following symbols are used: R = range in feet, C = contrast, r = correlation coefficient and t = time in hours (t = 0 at the start of the time interval). In those instances where the contrast was approximately constant, the average contrast is given for the time interval. For many time intervals the best fit curve through the data points is a straight line.

Table 48. Summary of Average LAV25 Contrast Using a Treeline as a Background

R (feet)	Time Interval	Date	Contrast Description	r
36	10:30 - 12:30	23 July, 1990	C = 0.56	
36	12:30 - 14:00	23 July, 1990	C = 0.56 - 0.28 t	1.000
36	9:00 - 11:00	24 July, 1990	C = 0.63	
36	9:30 - 12:30	26 July, 1990	C = 0.55	
36	12:30 - 14:30	26 July, 1990	C = 0.57 - 0.31 t	0.992
100	9:30 - 14:30	26 July, 1990	C = 0.33 - 0.11 t	0.839
200	9:00 - 11:00	24 July, 1990	C = 0.19	
200	9:30 - 14:30	26 July, 1990	C = 0.25 - 0.09 t	0.865
330	9:30 - 14:30	26 July, 1990	C = 0.27 - 0.10 t	0.813

Figure 198, Figure 199,...Figure 203 lend support to the results shown in Table 48. After 12:30 there is significant shading in the LAV25 wheels. Table 48 illustrates this for a range of 36 feet. Both studies, 23 July and 26 July, show a drastic change in the description of contrast after 12:30. The contrast is constant, approximately 0.55 until 12:30. After 12:30, the contrast is best described by the linear equation: $C = 0.57 - 0.3 t$. Contrast decreases at the rate of 0.3/hour from 12:30 to 14:30 due to shading of the LAV25 wheels. Figure 156 and Figure 194 illustrate this graphically.

Table 49. Summary of Average LAV25 Contrast Using Grass as a Background.

R (feet)	Time Interval	Date	Contrast Description	r
36	9:00 - 11:00	24 July, 1990	$C = - 0.28$	
36	9:30 - 12:30	26 July, 1990	$C = - 0.31$	
36	12:30 - 14:30	26 July, 1990	$C = - 0.31 - 0.16 t$	
100	9:30 - 14:30	26 July, 1990	$C = - 0.41 - 0.06 t$	0.900
200	9:30 - 14:30	26 July, 1990	$C = - 0.56 - 0.03 t$	0.978
300	9:30 - 14:30	26 July, 1990	$C = - 0.47 - 0.04 t$	0.966

Shading of the LAV25 wheels is also evident in the contrast calculations using a grass background. Table 49 gives two descriptions for the contrast of the LAV25 on 26 July when the range was 36 feet. From 9:30 to 12:30 the contrast is approximately constant (-0.31). From 12:30 to 14:30 the contrast is best described by: $C = -0.41 - 0.06 t$. After 12:30 the contrast decreases at the rate of 0.06/hour. The negative contrast values obtained using a grass background indicate that the luminance of the grass was greater than the average luminance of the LAV25.

The description of contrast values acquired for the LAV25 using sky as a background were nearly the same for all ranges on 24 July (9:00 - 11:00) and 26 July, 1990 (9:30 - 14:30):

$$C = - 0.73 - 0.04 t$$

The contrast of the LAV25 using concrete as a background was nearly constant ($C = - 0.79$) for all ranges on 24 July (9:00 - 11:00) and also 26 July, 1990 (9:30 - 14:30).

SHADING

Figure 198, Figure 199,...Figure 203 reveal those areas susceptible to diurnal shading. As these photographs illustrate, the wheel areas constitute more than 50 percent of the vehicle's side surface area and undergo the greatest amount of shading. As discussed in an earlier section, contrast variations are highest for the wheel areas.

The LAV25 turret also produces shading in the areas below it. In fact, the greatest contrast variation was obtained for measurement area #27 (see Figure 145). The range of luminance for this area was 3299 cd/m² (11:30, 23 July, 1990) to 516 cd/m² (14:00, 23 July, 1990).

Figure 216 shows an enlarged view of the turret area at 14:30 on 26 July, 1990. This photograph illustrates the extent of shading produced by the turret.

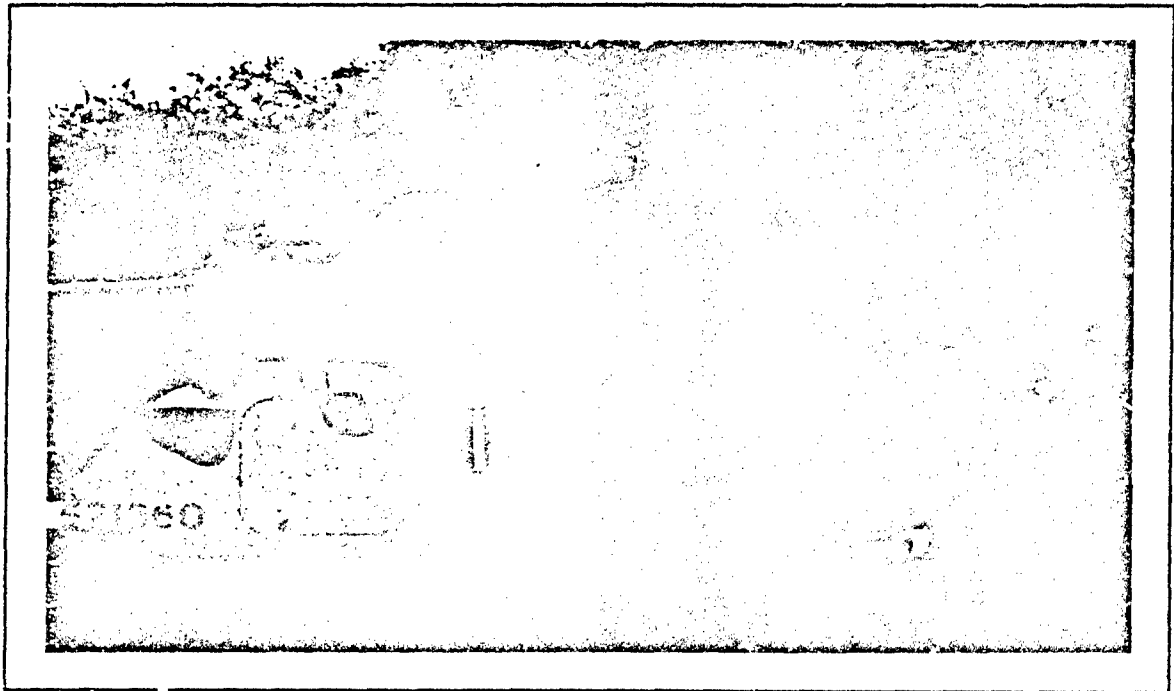


Figure 216
LAV Turret Area at 14:30 on 26 July, 1990

GLARE AND EDGE EFFECT

When two nonparallel surfaces of a vehicle meet, a rounded edge is formed. This edge may be formed by a single metal plate, a weld joint or a bend. In most instances, the width of this edge will be greater than several hundred microns. Under the right conditions, an edge may appear as a white line.

Arrow 1 and Arrow 3 in Figure 217 indicate places on the M113A3 where a white line occurs along an edge. Arrow 2 in Figure 217 indicates a place on the M113A3 where a white line is not visible along an edge.

Arrow 2 in Figure 218 indicates another edge on the M113A3 which shows a white line. Arrow 3 of Figure 218 indicates a shaded place along the top edge of the M113A3 where there is a break in the white line. Arrow 1 in Figure 218 indicates a place along a cylindrical rod which also produces a white line.

The white lines in the photographs are produced by a mirror like reflection called specular reflection. Because of the roundness of the edge, the white outline can be observed from many different directions, especially for edges near the top of the vehicle. Most of the light reflected off edges near the ground is reflected toward the ground and away from an observer.

Arrow 1, Arrow 2 and Arrow 3 in Figure 219 indicate places where glare occurs along an edge at the top of the M113A3. Figure 220 shows the same view using a polarizer in front of the camera lens. The polarizer is effective in reducing glare because the specularly reflected light from the edges is linearly polarized to a considerable extent. The degree of glare extinction depends on the angle between the transmission axis of the polarizer and the plane of polarization of the reflected light. The photograph of Figure 219 was obtained by rotating a polarizer in front of the camera lens until the glare from the edge, indicated by Arrow 3, was a minimum.

The painted metal objects, indicated by Arrow 1 and Arrow 2 of Figure 221, show significant glare along their edges and on their adjacent surfaces. Again, a polarizer is able to reduce the glare significantly as shown in Figure 222.

Arrow 1, Arrow 2 and Arrow 3 of Figure 221 indicate an edge that has been painted with three different colors, one of the colors being flat black. Figure 222 illustrates that the different colors of paint have little effect on the degree of glare. The entire illuminated edge appears white. Evidently, the glare is associated with light that has not interacted with the paint pigments.

An important consequence of the edge effect is an increase in contrast between the edge and surrounding surfaces. This increase in contrast increases the visibility of the vehicle.

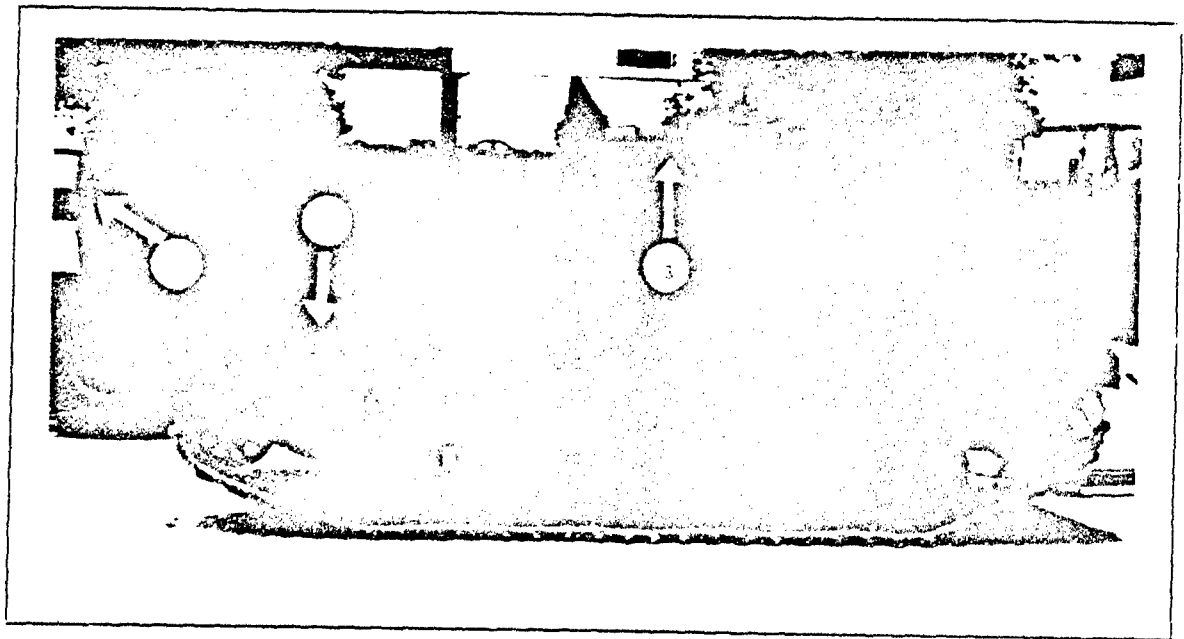


Figure 217
M113A3. Viewing Toward the North.

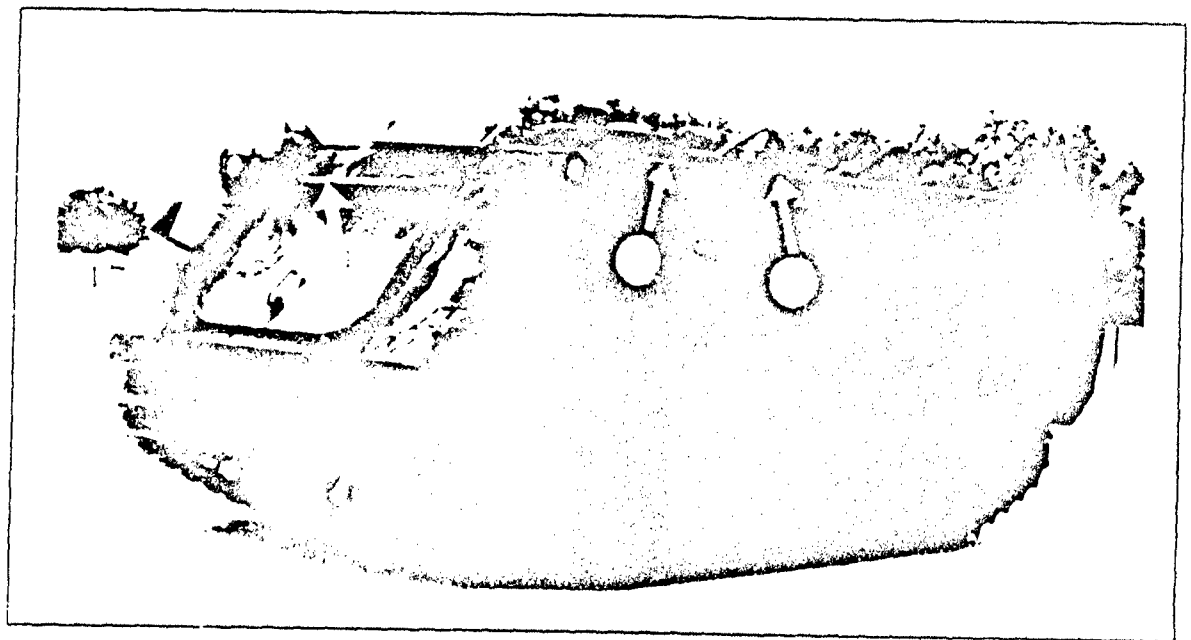


Figure 218
M113A3. Viewing Toward the Southwest.

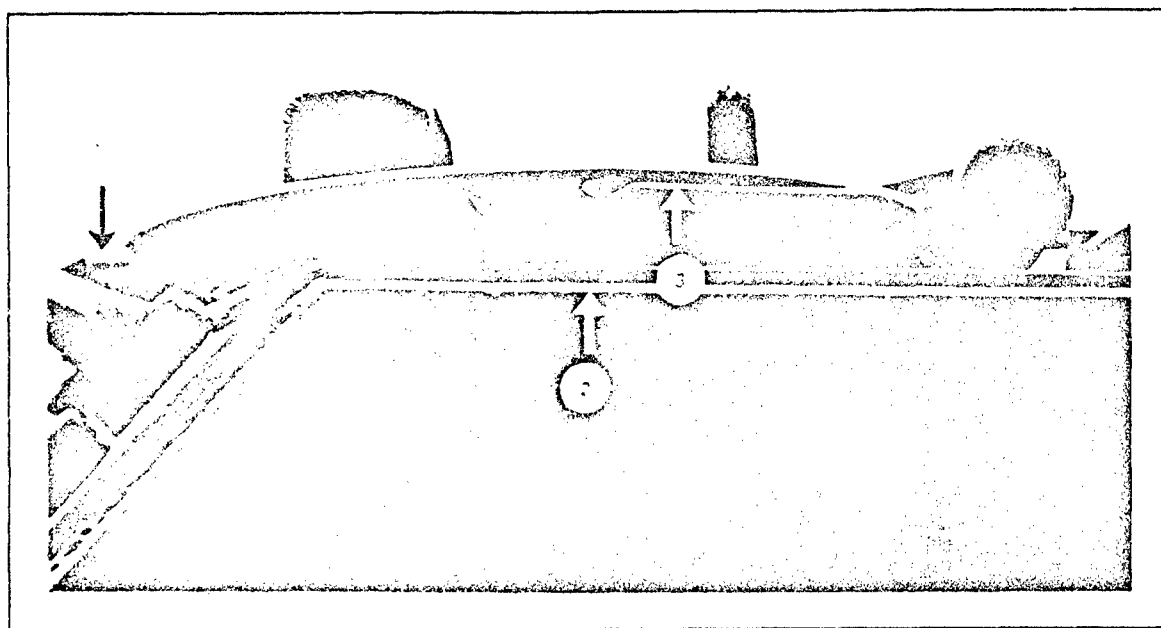


Figure 219
Photograph of Side of M113A3 - No Polaroid in Front of Camera.

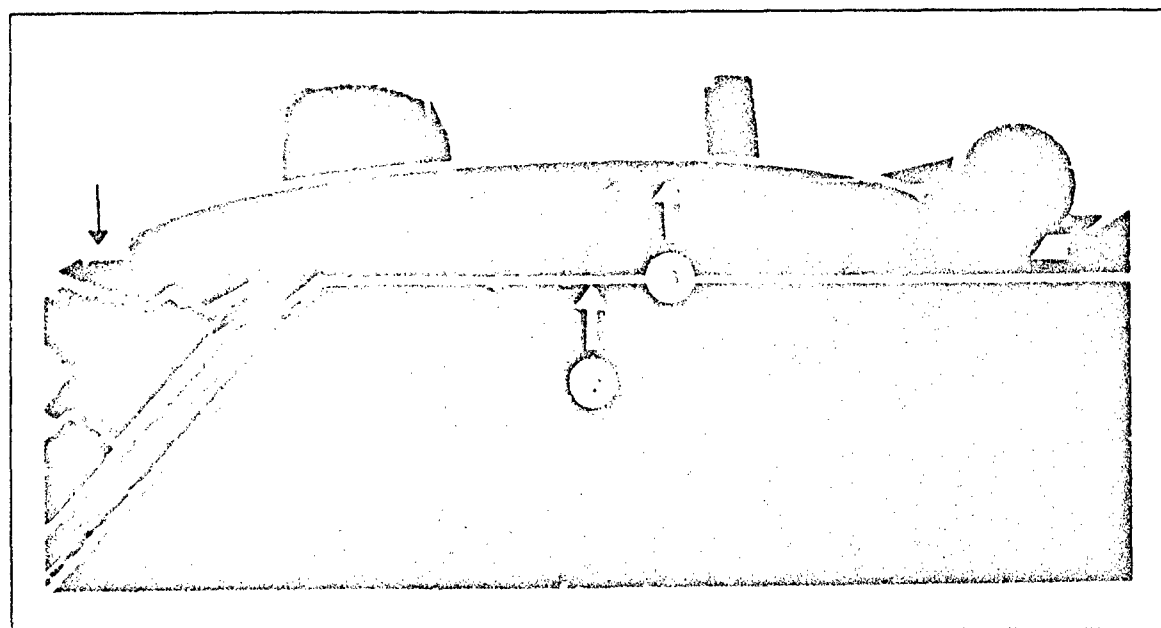


Figure 220
Photograph of Side of M113A3 - Polaroid in Front of Camera.

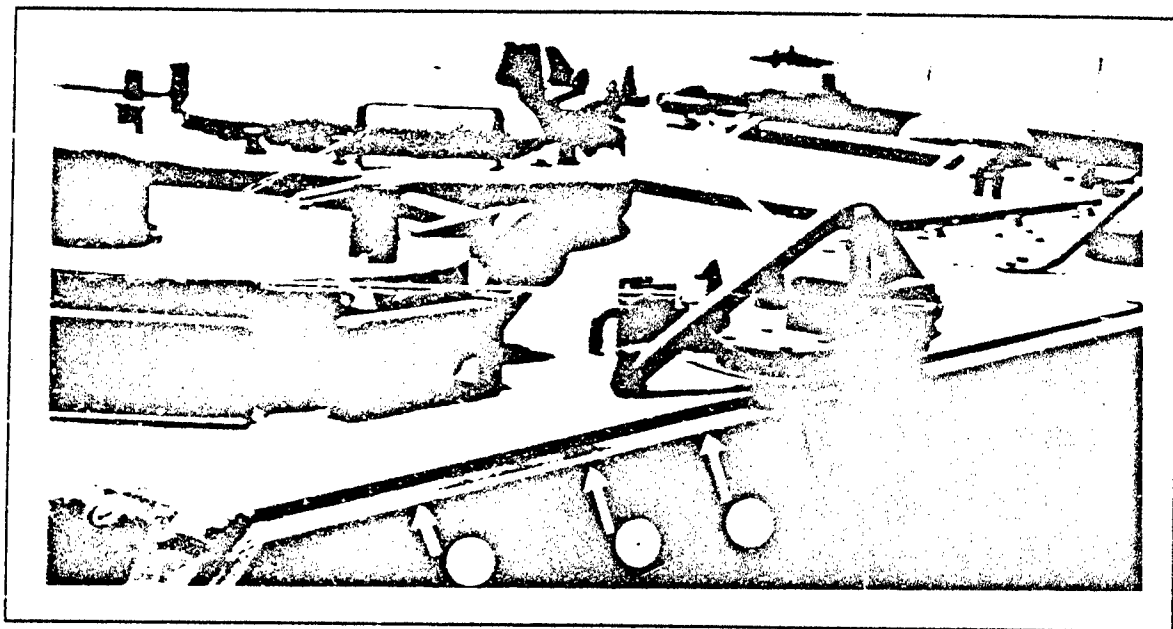


Figure 221
Photograph of Top of M113A3 - No Polaroid in Front of Camera.

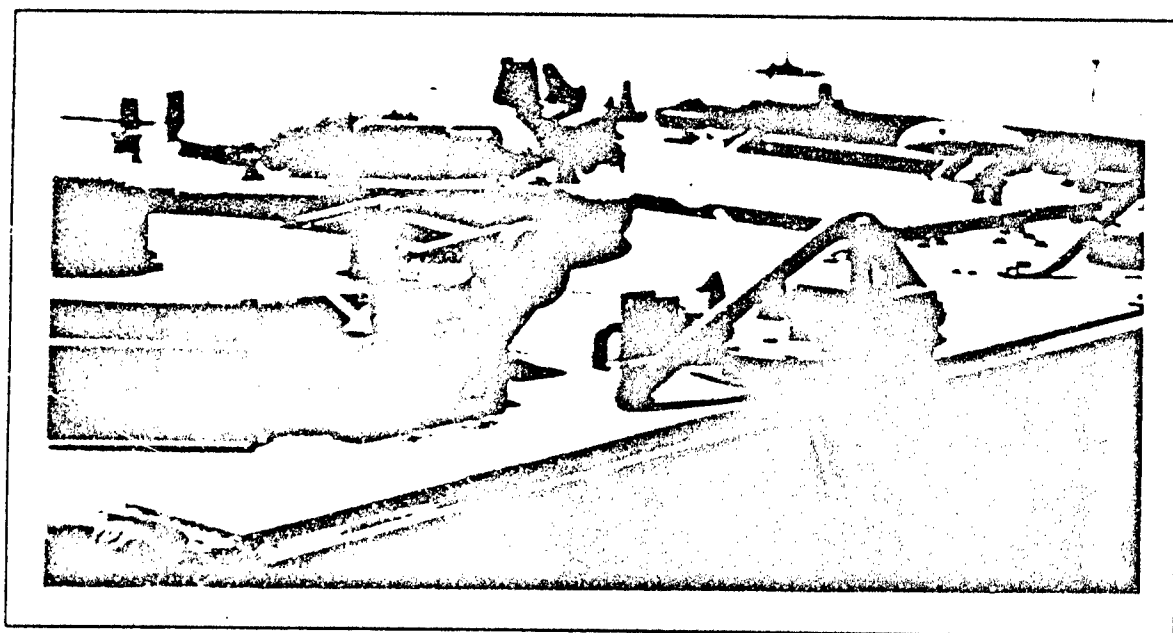


Figure 222
Photograph of Top of M113A3 - Polaroid in Front of Camera.

HORIZONTAL AND VERTICAL POLARIZATION OF THE M1A1

On June 20, 1991, diurnal luminance readings and photographs were acquired for the M1A1 turret area from 08:30 to 16:00. The M1A1 was positioned along a north-south line and metering was to the west. A Minolta LS-100 Luminance Meter was used to make the readings. Three different luminance readings were made at 30 minute time intervals. For the first reading, no polarizer was used in front of the LS-100. For the second reading, a polarizer was positioned in front of the LS-100 with its transmission axis vertical. For the third reading, a polarizer was positioned in front of the LS-100 with its transmission axis horizontal, as shown in Figure 223. The entire study was conducted under clear skies.

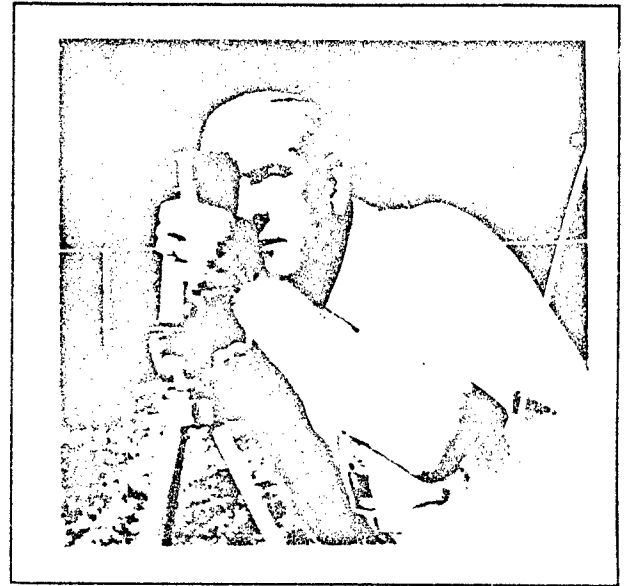


Figure 223
Positioning of Polarizer in Front of LS-100

Figure 224 shows the fifteen measurement areas for which diurnal luminance readings were acquired.

Figure 225, Figure 226,...Figure 240 show the diurnal photographs acquired for the M1A1.

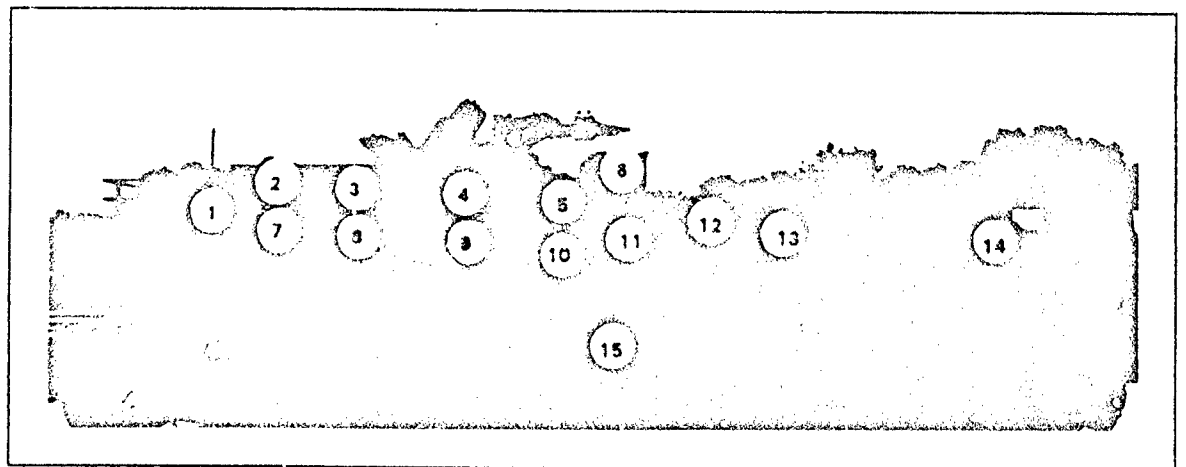


Figure 224
Measurement Areas on M1A1

M1 on 20 June, 1991. Clear Skies. M1 Positioned North-South. Metering West.

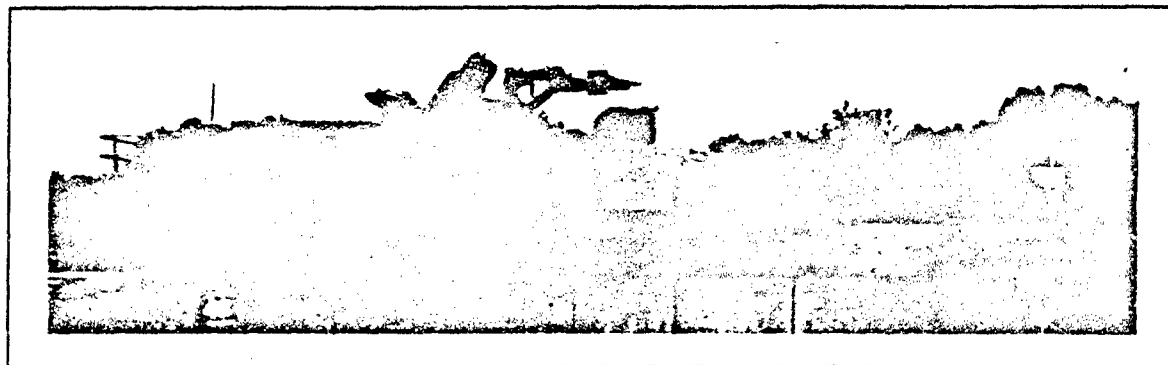


Figure 225
M1A1 at 08:30

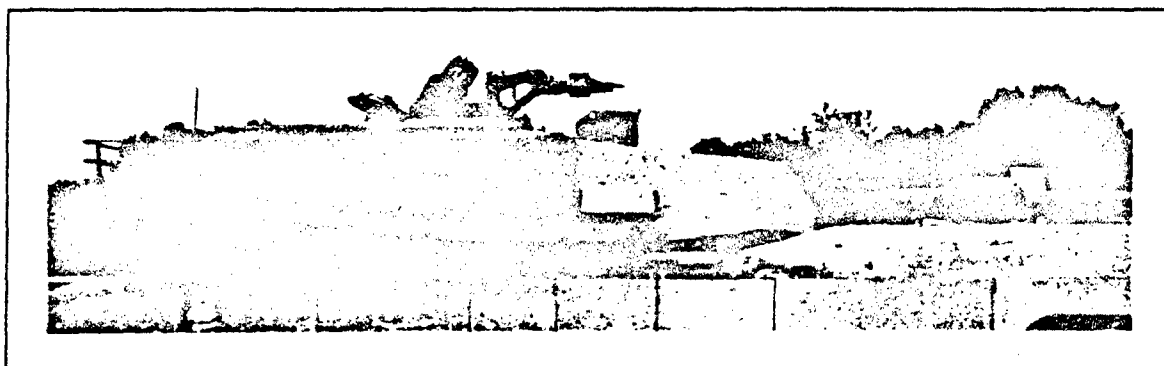


Figure 226
M1A1 at 09:00

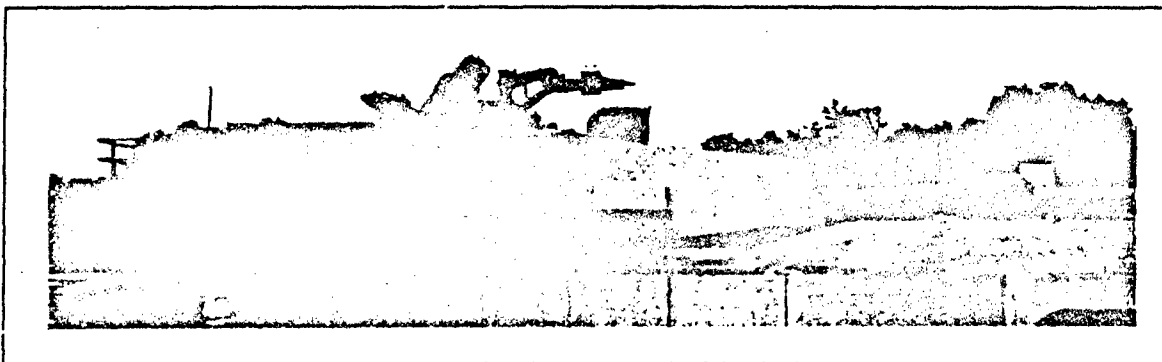


Figure 227
M1A1 at 09:30

M1 on 20 June, 1991. Clear Skies. M1 Positioned North-South. Metering West.

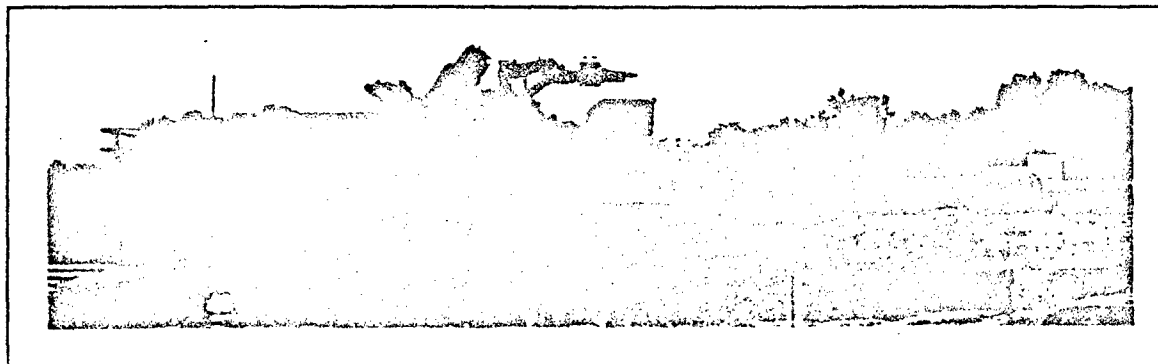


Figure 228
M1A1 at 10:00

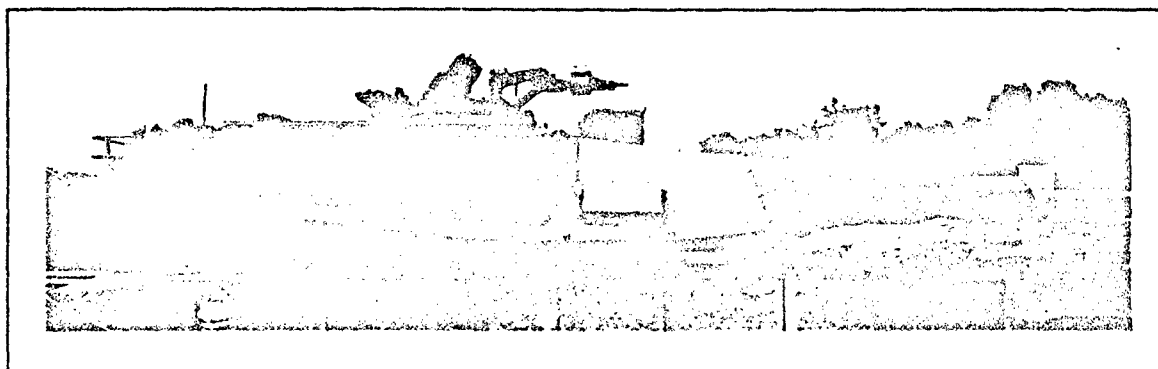


Figure 229
M1A1 at 10:30

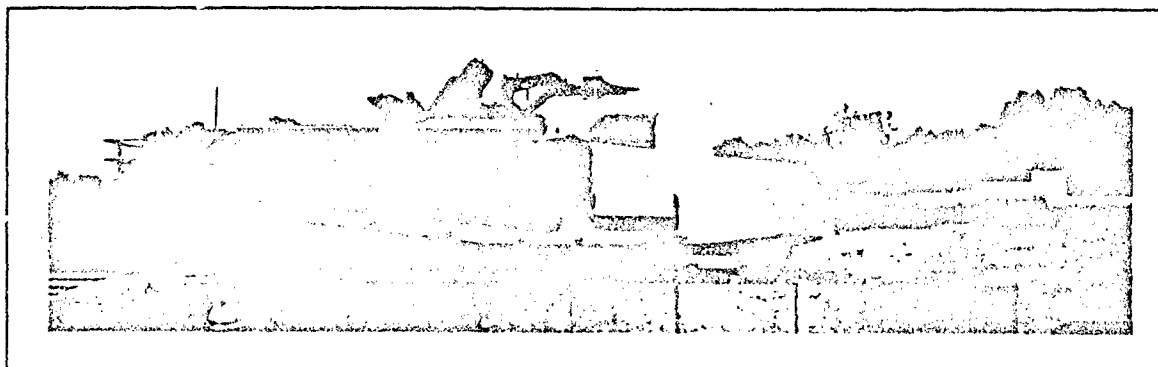


Figure 230
M1A1 at 11:00

M1 on 20 June, 1991. Clear Skies. M1 Positioned North-South. Metering West.

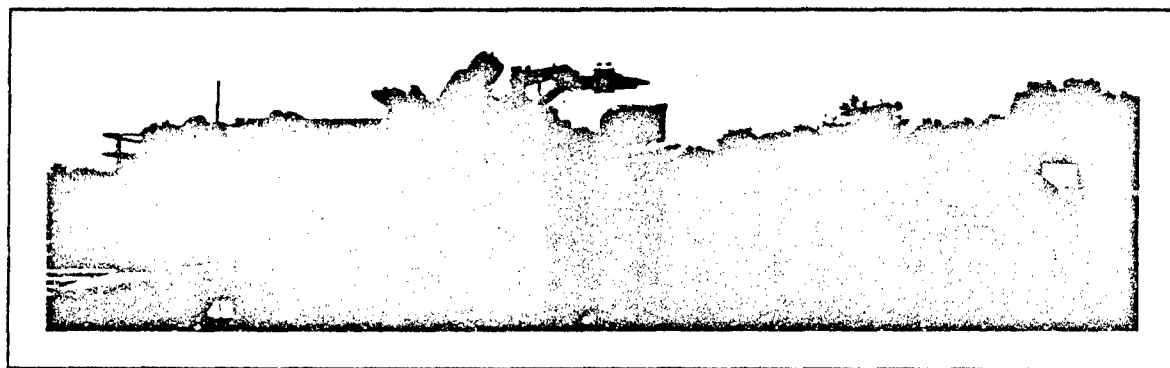


Figure 231
M1A1 at 11:30



Figure 232
M1A1 at 12:00

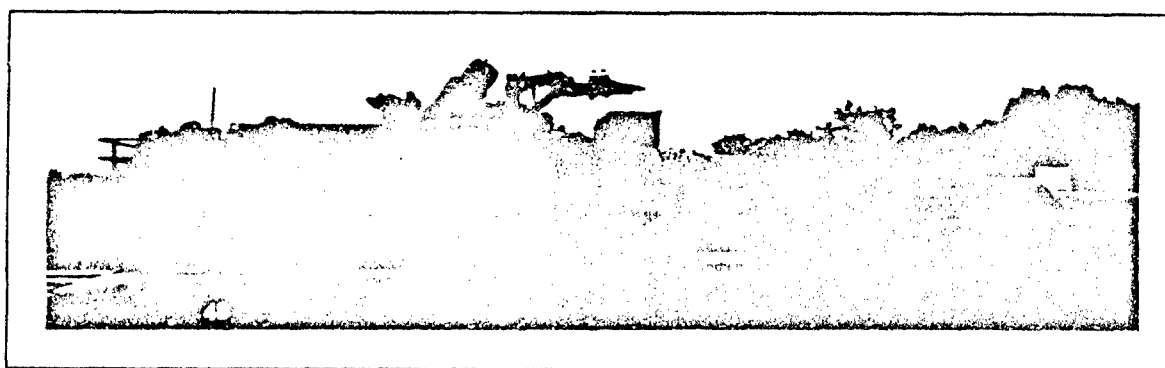


Figure 233
M1A1 at 12:30

M1 on 20 June, 1991. Clear Skies. M1 Positioned North-South. Metering West.

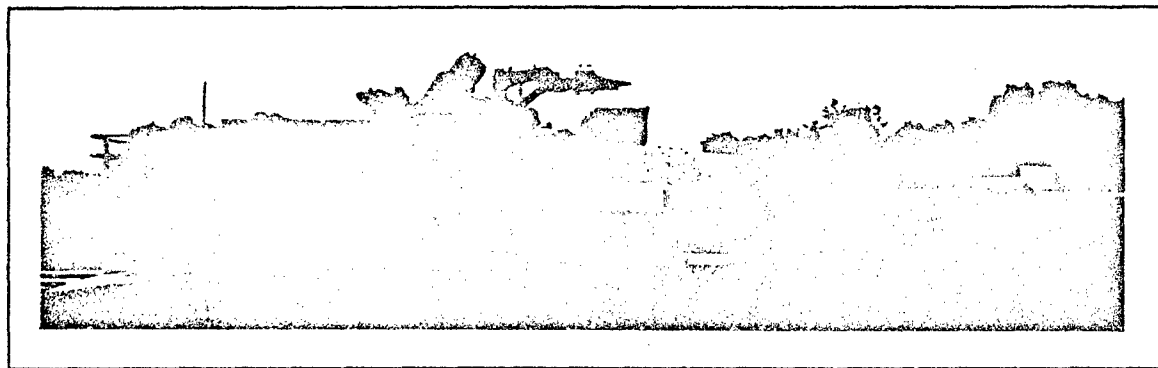


Figure 234
M1A1 at 13:00

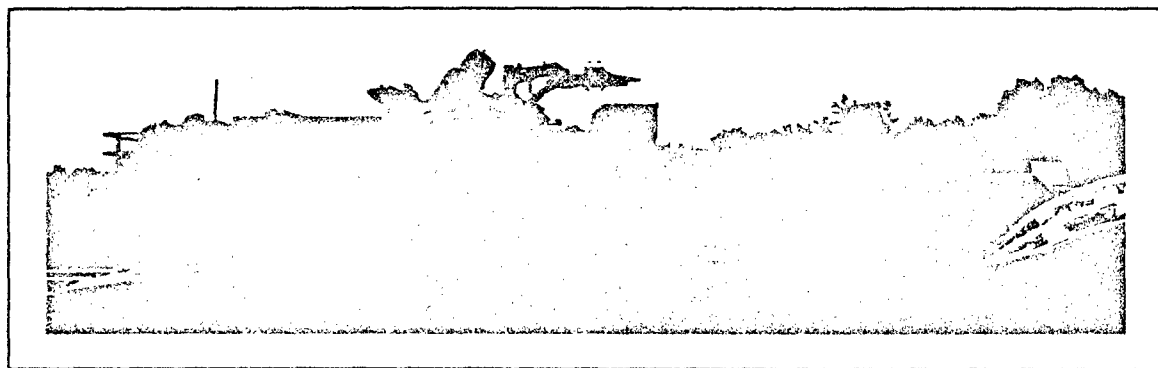


Figure 235
M1A1 at 13:30

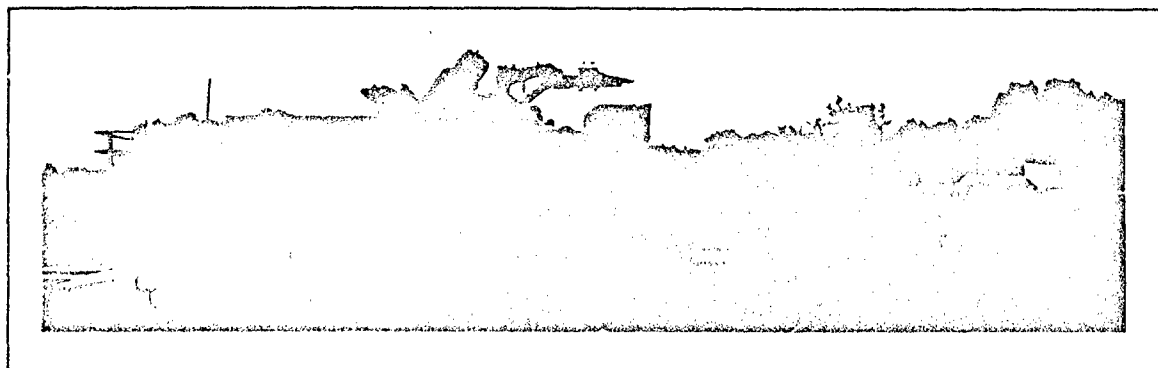


Figure 236
M1A1 at 14:00

M1 on 20 June, 1991. Clear Skies. M1 Positioned North-South. Metering West.

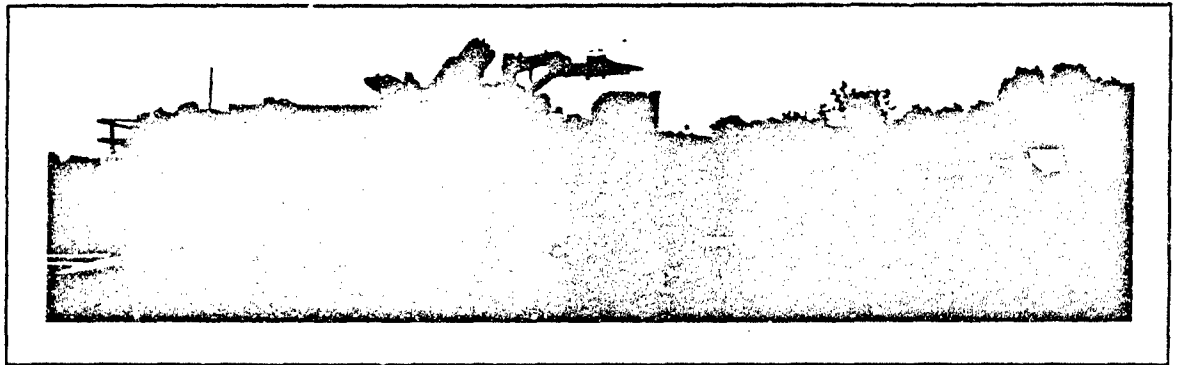


Figure 237
M1A1 at 14:30



Figure 238
M1A1 at 15:00

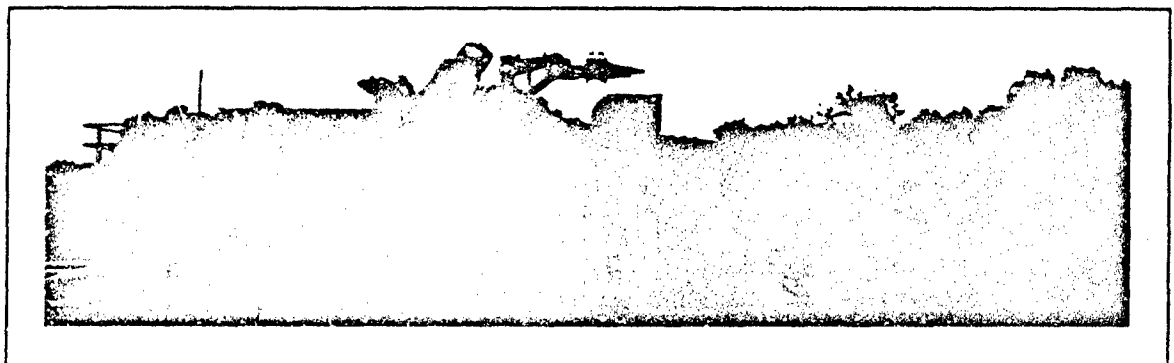


Figure 239
M1A1 at 15:30

M1 on 20 June, 1991. Clear Skies. M1 Positioned North-South. Metering West.

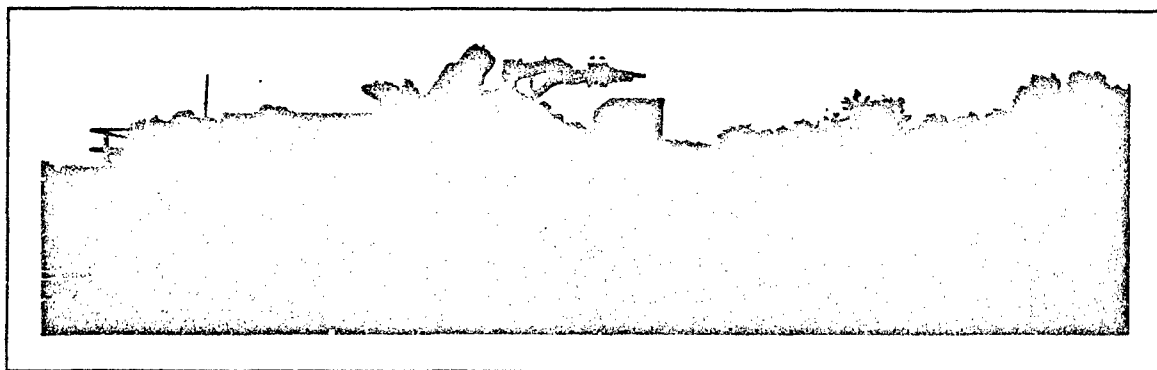


Figure 240
M1A1 at 16:00

Table 50, Table 51 and Table 52 give the results of the diurnal luminance readings.

Ln represents the luminance reading acquired when no polarizer was used.

Lv represents the luminance reading acquired when the transmission axis of the polarizer was was vertical.

Lh represents the luminance reading acquired when the transmission axis of the polarizer was was horizontal.

Table 50. M1A1 Luminance Ln (No Polarizer) on 20 June, 1991. Clear Skies 8:30 - 16:00
M1A1 Positioned North-South. Metering toward the West.

Area #	08:30	09:00	09:30	10:00	10:30	11:00	11:30	12:00
1	2115	2374	2406	2723	2466	2735	2316	2701
2	2124	2271	2339	2270	2199	2086	1799	1557
3	2201	2302	2431	2410	2367	2210	1834	1536
4	2216	2360	2495	2440	2370	2247	1931	1533
5	1657	1866	2051	1971	1970	1700	1152	1250
6	2270	2422	2493	2467	2386	2240	1897	1709
7	2110	2277	2332	2309	2210	2063	1732	1549
8	2247	2299	2475	2426	2305	2127	1761	1551
9	2186	2346	2507	2438	2280	2150	1742	1512
10	2324	2754	2349	2969	2905	1696	1017	1550
11	2415	3252	3447	3520	2918	3523	2748	2993
12	3021	3297	3456	3532	3667	3603	3297	3411
13	2860	3035	3144	3138	3080	3031	2661	2681
14	2496	2842	2793	2493	1587	2216	3157	2814
15	3023	3183	3288	3216	3115	2934	2534	2325

Area #	12:30	13:00	13:30	14:00	14:30	15:00	15:30	16:00
1	2748	2577	2227	1999	1171	1396	763	606
2	1189	958	692	631	624	623	623	615
3	1135	912	651	607	601	619	617	601
4	1098	870	612	575	586	608	603	586
5	1195	1027	833	664	553	471	436	439
6	1347	951	599	544	527	557	523	525
7	1178	877	675	581	586	609	605	588
8	1210	938	655	597	588	610	600	588
9	1174	865	628	588	590	603	594	576
10	987	962	525	572	512	461	464	374
11	2973	2730	2386	2293	1935	1456	738	579
12	3213	3076	2760	2364	1969	1522	833	656
13	2540	2357	2184	1969	1786	1698	1551	1457
14	1395	1849	857	1959	1021	753	1192	554
15	1874	1346	819	785	761	747	710	664

Table 51. Luminance Lv (Polarizer's Transmission Axis Vertical) on 20 June, 1991.
Clear Skies 8:30 - 16:00. M1A1 Positioned North-South. Metering West.

Area #	08:30	09:00	09:30	10:00	10:30	11:00	11:30	12:00
1	530	553	583	643	570	601	543	531
2	533	560	566	552	520	475	429	358
3	538	580	576	560	529	481	435	347
4	550	583	591	578	535	482	457	345
5	375	474	421	460	457	433	331	332
6	563	597	600	586	560	515	467	412
7	529	556	559	545	516	473	428	359
8	544	585	574	565	544	496	436	361
9	553	582	583	583	559	481	447	357
10	492	642	681	686	584	599	508	317
11	653	779	730	744	772	690	756	711
12	727	789	803	816	812	781	756	716
13	701	730	739	734	704	671	619	577
14	666	562	551	573	613	614	546	522
15	736	771	777	770	730	673	597	525

Area #	12:30	13:00	13:30	14:00	14:30	15:00	15:30	16:00
1	574	515	485	414	411	358	297	307
2	285	254	211	215	234	262	304	327
3	270	233	194	202	228	254	296	316
4	273	228	186	191	219	242	287	306
5	290	281	209	195	203	208	242	270
6	317	243	189	188	213	235	278	303
7	287	229	204	192	224	250	293	302
8	294	234	193	187	222	246	285	301
9	286	235	187	182	216	236	274	288
10	235	187	193	163	191	210	222	239
11	656	510	533	384	420	345	252	277
12	660	621	561	458	439	375	276	290
13	531	515	472	411	426	424	432	437
14	380	341	343	267	236	193	263	264
15	424	341	235	207	236	247	268	275

The graphs of Figure 241, Figure 242,...Figure 256 show all the measurements graphically.

To ascertain the degree of vertical and horizontal polarization from the M1A1, the ratios L_v/L_n and L_h/L_n were calculated for all measurement areas and for all the measurement times. The results are given in Table 53 and Table 54. These ratios are a measure of the transmittance of the polarizer. The graphs of Figure 257, Figure 258,...Figure 286 show the results graphically.

Table 52. LUMINANCE L_h (Polarizer's Transmission Axis Horizontal) on 20 June, 1991.
Clear Skies 8:30 - 16:00. M1A1 Positioned North-South. Metering West.

Area #	08:30	09:00	09:30	10:00	10:30	11:00	11:30	12:00
1	559	608	634	693	656	708	698	763
2	562	597	609	618	604	575	520	469
3	563	611	642	660	627	574	521	460
4	574	621	650	661	650	590	551	452
5	488	512	506	484	568	491	452	430
6	608	642	673	677	671	647	582	517
7	550	589	613	614	609	563	524	462
8	571	611	629	634	620	577	532	466
9	582	621	657	662	642	576	525	477
10	643	711	763	816	771	743	749	505
11	759	841	892	880	830	845	686	960
12	765	838	901	962	971	972	970	967
13	717	765	821	838	836	813	784	764
14	642	587	654	688	751	746	651	660
15	745	807	851	830	835	781	725	653

Area #	12:30	13:00	13:30	14:00	14:30	15:00	15:30	16:00
1	735	713	645	545	571	484	356	357
2	379	332	288	249	293	321	368	374
3	366	306	263	235	275	308	339	351
4	350	299	241	217	262	288	315	326
5	374	355	319	237	263	268	291	383
6	434	360	308	243	324	347	399	328
7	370	291	248	221	273	293	322	333
8	372	297	239	221	265	284	315	327
9	351	287	231	213	251	276	300	315
10	278	350	243	208	226	256	258	276
11	894	729	722	570	576	476	294	317
12	911	872	796	595	604	512	316	339
13	719	685	635	514	550	538	519	518
14	621	462	614	443	260	292	311	257
15	526	402	277	245	275	290	297	300

M1 LUMINANCE AT 08:30
METERING WEST AT 36 FEET
20 JUNE, 1991; CLEAR SKIES

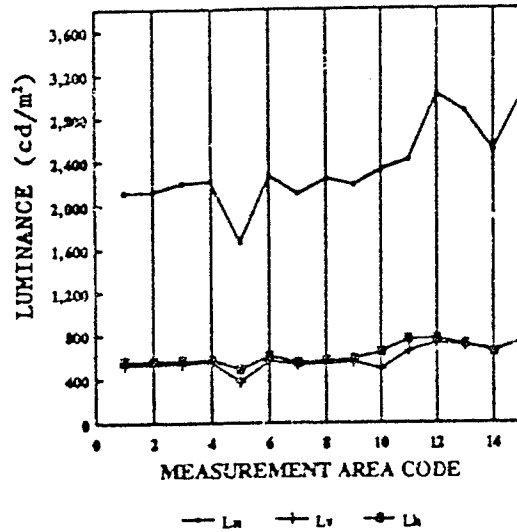


Figure 241

M1 LUMINANCE AT 09:00
METERING WEST AT 36 FEET
20 JUNE, 1991; CLEAR SKIES

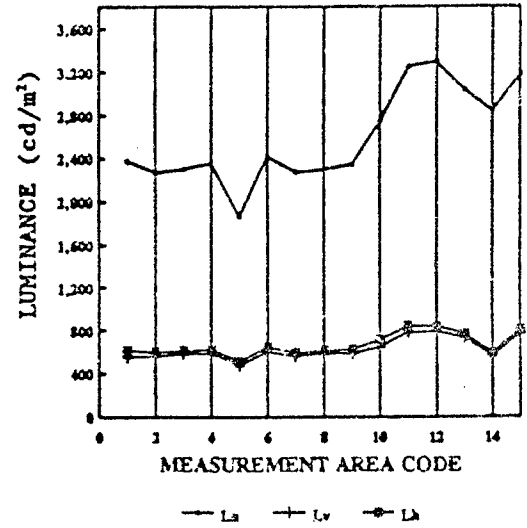


Figure 242

M1 LUMINANCE AT 09:30
METERING WEST AT 36 FEET
20 JUNE, 1991; CLEAR SKIES

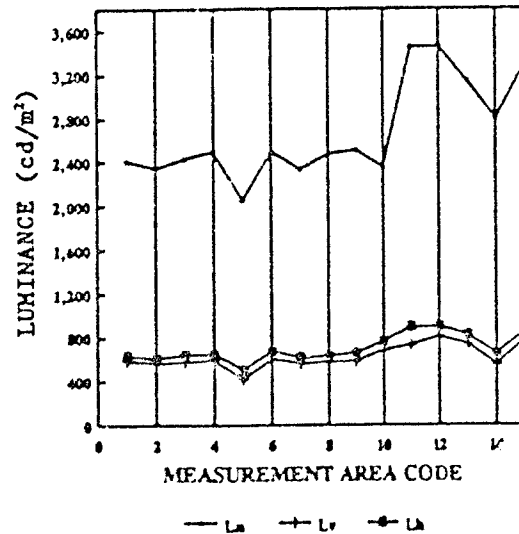


Figure 243

M1 LUMINANCE AT 10:00
METERING WEST AT 36 FEET
20 JUNE, 1991; CLEAR SKIES

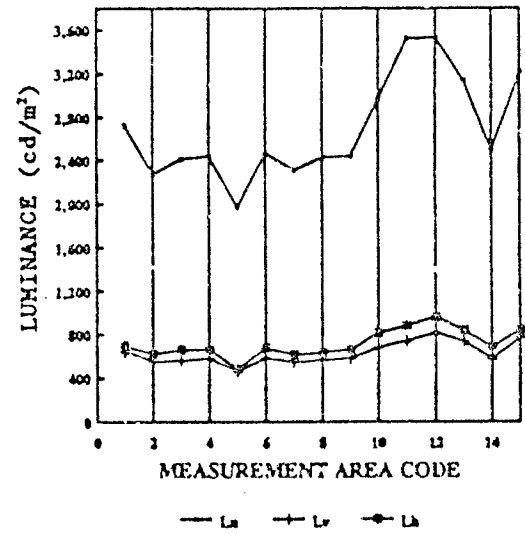


Figure 244

M1 LUMINANCE AT 10:30
METERING WEST AT 36 FEET
20 JUNE, 1991; CLEAR SKIES

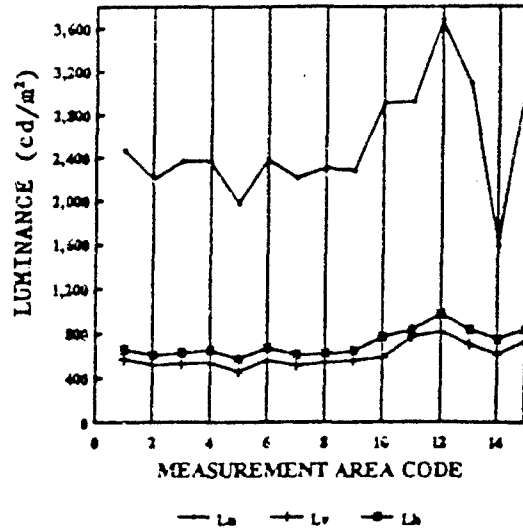


Figure 245

M1 LUMINANCE AT 11:00
METERING WEST AT 36 FEET
20 JUNE, 1991; CLEAR SKIES

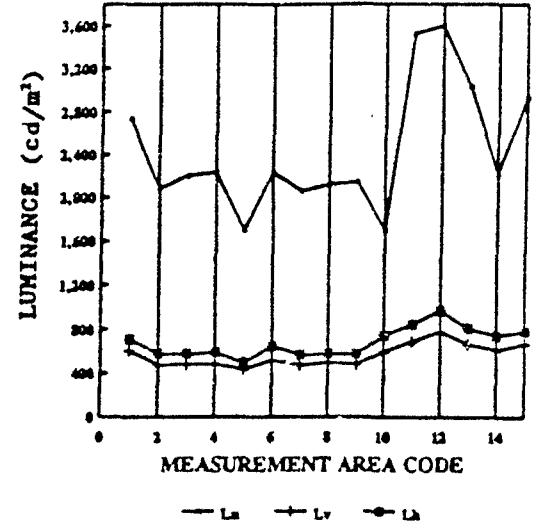


Figure 246

M1 LUMINANCE AT 11:30
METERING WEST AT 36 FEET
20 JUNE, 1991; CLEAR SKIES

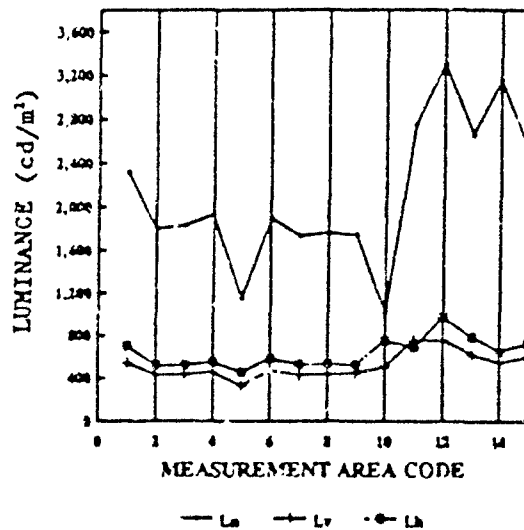


Figure 247

M1 LUMINANCE AT 12:00
METERING WEST AT 36 FEET
20 JUNE, 1991; CLEAR SKIES

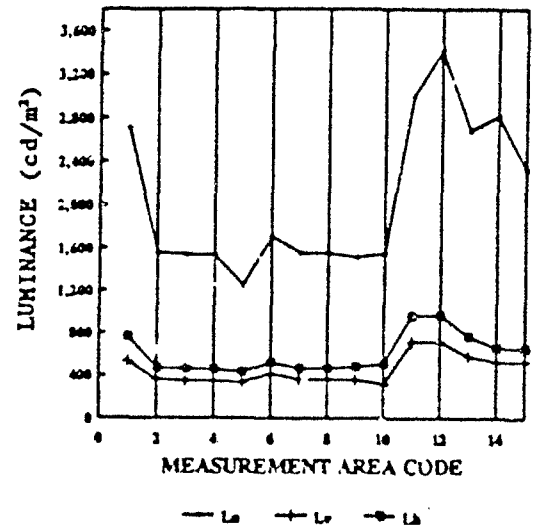


Figure 248

M1 LUMINANCE AT 12:30
METERING WEST AT 36 FEET
20 JUNE, 1991; CLEAR SKIES

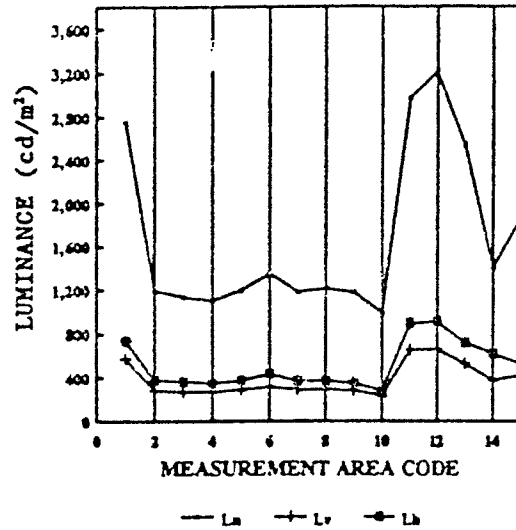


Figure 249

M1 LUMINANCE AT 13:00
METERING WEST AT 36 FEET
20 JUNE, 1991; CLEAR SKIES

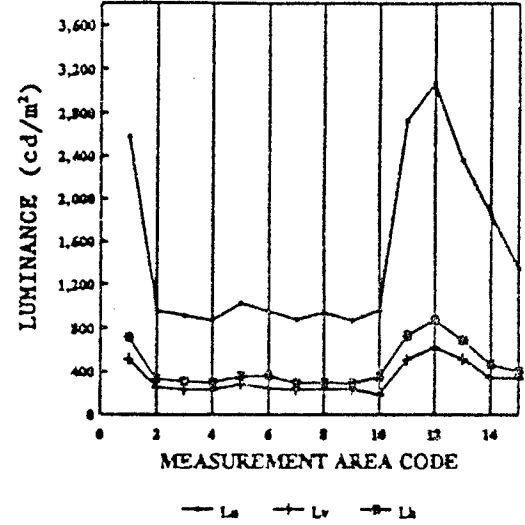


Figure 250

M1 LUMINANCE AT 13:30
METERING WEST AT 36 FEET
20 JUNE, 1991; CLEAR SKIES

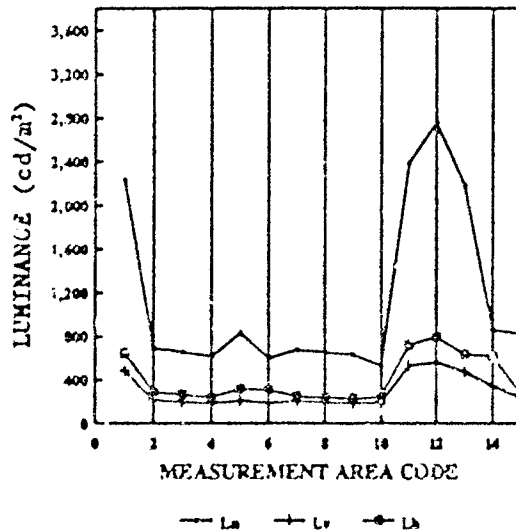


Figure 251

M1 LUMINANCE AT 14:00
METERING WEST AT 36 FEET
20 JUNE, 1991; CLEAR SKIES

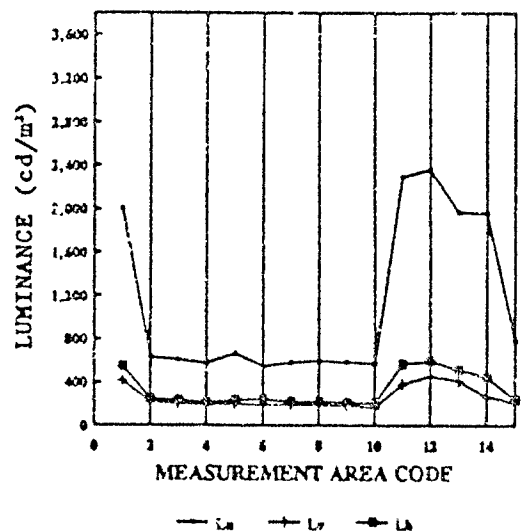


Figure 252

M1 LUMINANCE AT 14:30
METERING WEST AT 36 FEET
20 JUNE, 1991; CLEAR SKIES

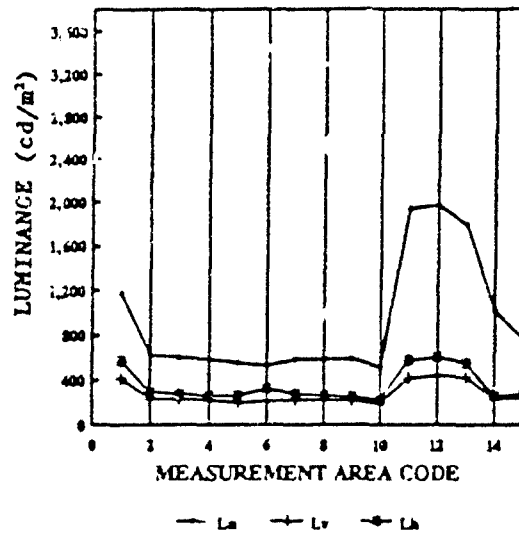


Figure 253

M1 LUMINANCE AT 15:00
METERING WEST AT 36 FEET
20 JUNE, 1991; CLEAR SKIES

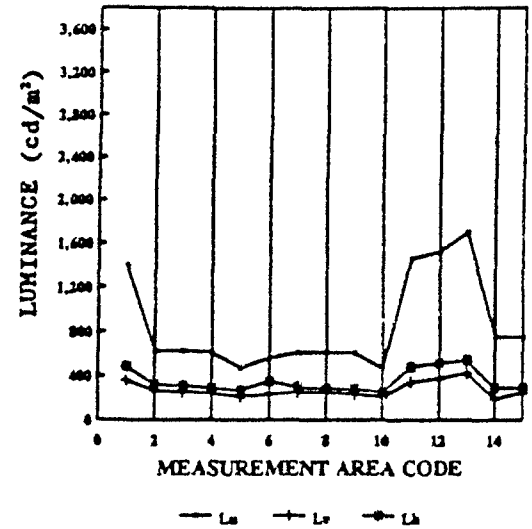


Figure 254

M1 LUMINANCE AT 15:30
METERING WEST AT 36 FEET
20 JUNE, 1991; CLEAR SKIES

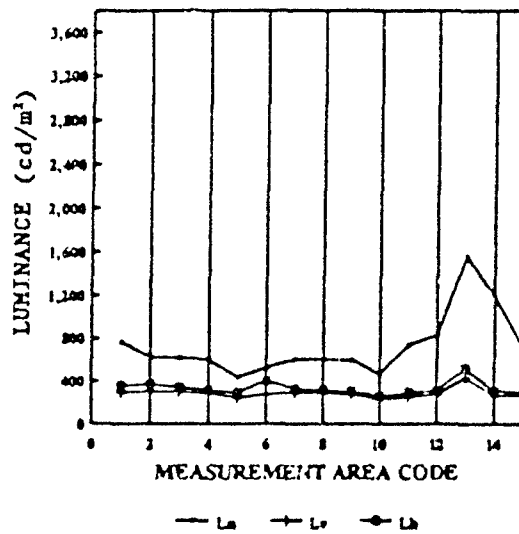


Figure 255

M1 LUMINANCE AT 16:00
METERING WEST AT 36 FEET
20 JUNE, 1991; CLEAR SKIES

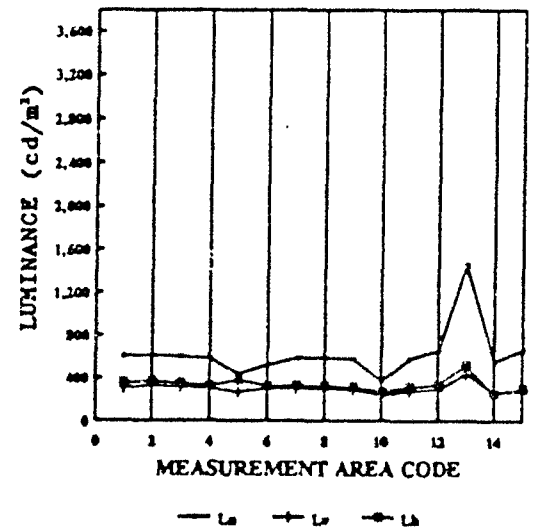


Figure 256

Table 53. Luminance Ratio (Lv/Ln).

Area #	08:30	09:00	09:30	10:00	10:30	11:00	11:30	12:00
1	0.25	0.23	0.24	0.24	0.23	0.22	0.23	0.20
2	0.25	0.25	0.24	0.24	0.24	0.23	0.24	0.23
3	0.24	0.25	0.24	0.23	0.22	0.22	0.24	0.23
4	0.25	0.25	0.24	0.24	0.23	0.21	0.24	0.23
5	0.23	0.25	0.21	0.23	0.23	0.25	0.29	0.27
6	0.25	0.25	0.24	0.24	0.23	0.23	0.25	0.24
7	0.25	0.24	0.24	0.24	0.23	0.23	0.25	0.23
8	0.24	0.25	0.23	0.23	0.24	0.23	0.25	0.23
9	0.25	0.25	0.23	0.24	0.24	0.22	0.26	0.24
10	0.21	0.23	0.29	0.23	0.20	0.35	0.50	0.20
11	0.27	0.24	0.21	0.21	0.26	0.20	0.28	0.24
12	0.24	0.24	0.23	0.23	0.22	0.22	0.23	0.21
13	0.24	0.24	0.23	0.23	0.23	0.22	0.23	0.22
14	0.27	0.20	0.20	0.23	0.39	0.28	0.17	0.19
15	0.24	0.24	0.24	0.24	0.23	0.23	0.24	0.23

Area #	12:30	13:00	13:30	14:00	14:30	15:00	15:30	16:00
1	0.21	0.20	0.22	0.21	0.35	0.26	0.39	0.51
2	0.24	0.26	0.31	0.34	0.38	0.42	0.49	0.53
3	0.24	0.26	0.30	0.33	0.38	0.41	0.48	0.53
4	0.25	0.26	0.30	0.33	0.37	0.40	0.48	0.52
5	0.24	0.27	0.25	0.29	0.37	0.44	0.56	0.62
6	0.24	0.25	0.32	0.35	0.40	0.42	0.53	0.58
7	0.24	0.26	0.30	0.33	0.38	0.41	0.48	0.51
8	0.24	0.25	0.29	0.31	0.38	0.40	0.47	0.51
9	0.24	0.27	0.30	0.31	0.37	0.39	0.46	0.50
10	0.24	0.19	0.37	0.28	0.37	0.45	0.48	0.64
11	0.22	0.19	0.22	0.17	0.22	0.24	0.34	0.48
12	0.21	0.20	0.20	0.19	0.22	0.25	0.33	0.44
13	0.21	0.22	0.22	0.21	0.24	0.25	0.28	0.30
14	0.27	0.18	0.40	0.14	0.23	0.26	0.22	0.48
15	0.23	0.25	0.29	0.26	0.31	0.33	0.38	0.41

Area #	MINIMUM	MAXIMUM	DIFF	STD
1	0.20	0.51	0.31	0.08
2	0.23	0.53	0.30	0.10
3	0.22	0.53	0.31	0.10
4	0.21	0.52	0.31	0.09
5	0.21	0.62	0.41	0.12
6	0.23	0.58	0.35	0.11
7	0.23	0.51	0.28	0.09
8	0.23	0.51	0.28	0.09
9	0.22	0.50	0.28	0.08
10	0.19	0.64	0.45	0.13
11	0.17	0.48	0.31	0.07
12	0.19	0.44	0.25	0.06
13	0.21	0.30	0.09	0.02
14	0.14	0.48	0.34	0.09
15	0.23	0.41	0.19	0.06

Note: MINIMUM refers to the smallest transmittance obtained between 08:30 and 16:00.
 MAXIMUM refers to the largest transmittance obtained between 08:30 and 16:00.
 DIFFERENCE refers to the difference between MAXIMUM and MINIMUM.
 STD refers to the standard deviation of transmittance for each measurement area.

LUMINANCE RATIO (L_v/L_n)
MEASUREMENT AREA #1
METERING WEST; CLEAR SKIES

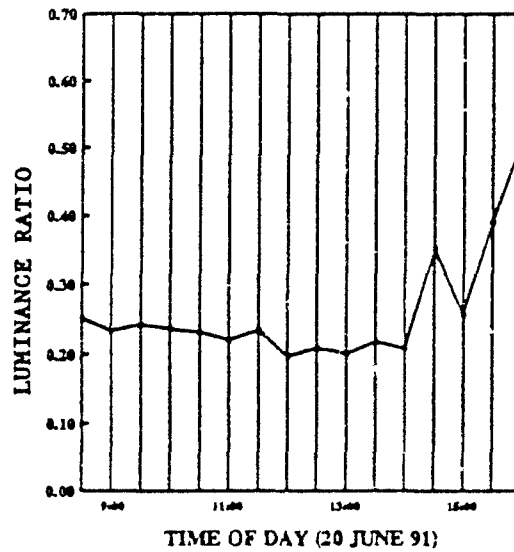


Figure 257

LUMINANCE RATIO (L_v/L_n)
MEASUREMENT AREA #2
METERING WEST; CLEAR SKIES

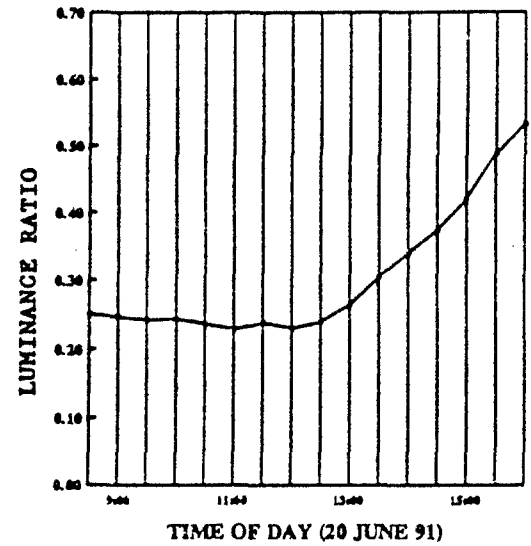


Figure 258

LUMINANCE RATIO (L_v/L_n)
MEASUREMENT AREA #3
METERING WEST; CLEAR SKIES

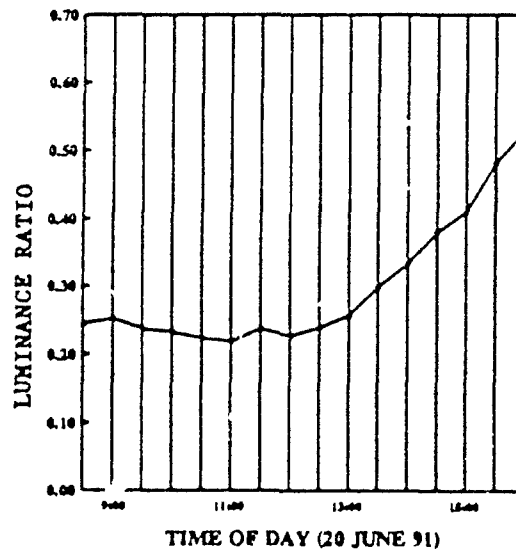


Figure 259

LUMINANCE RATIO (L_v/L_n)
MEASUREMENT AREA #4
METERING WEST; CLEAR SKIES

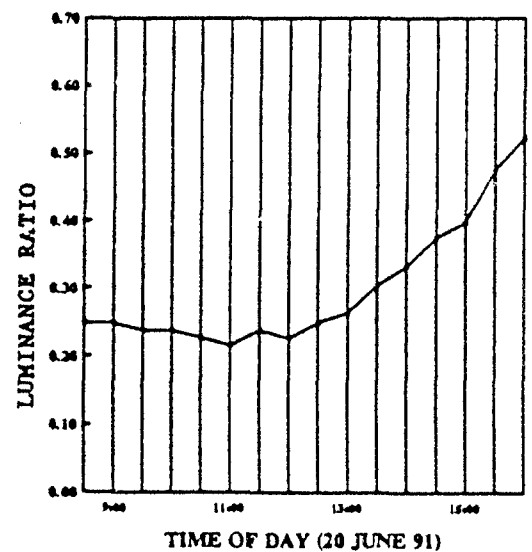


Figure 260

LUMINANCE RATIO (L_v/L_n)
MEASUREMENT AREA #5
METERING WEST; CLEAR SKIES

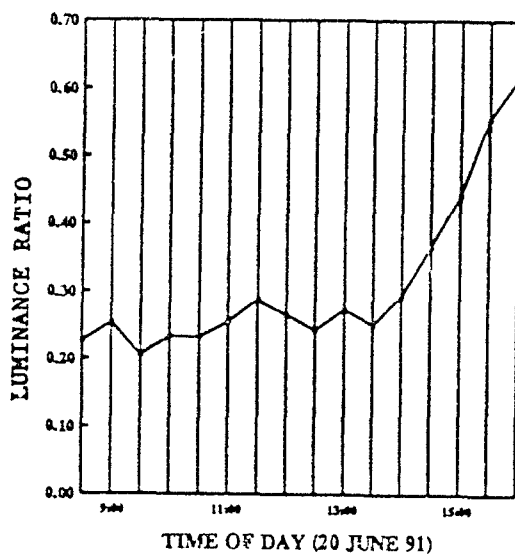


Figure 261

LUMINANCE RATIO (L_v/L_n)
MEASUREMENT AREA #6
METERING WEST; CLEAR SKIES

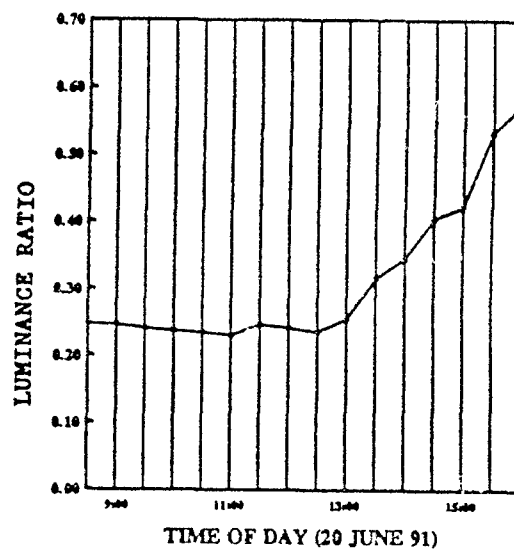


Figure 262

LUMINANCE RATIO (L_v/L_n)
MEASUREMENT AREA #7
METERING WEST; CLEAR SKIES

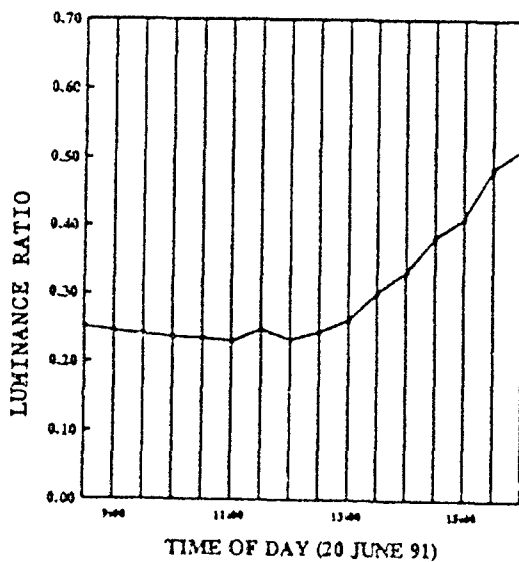


Figure 263

LUMINANCE RATIO (L_v/L_n)
MEASUREMENT AREA #8
METERING WEST; CLEAR SKIES

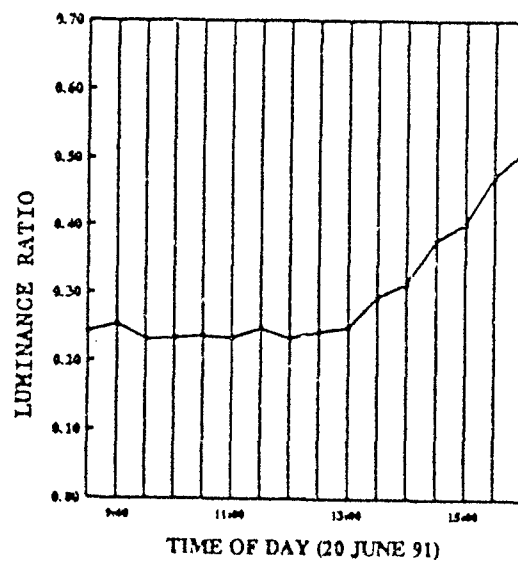


Figure 264

LUMINANCE RATIO (L_v/L_n)
MEASUREMENT AREA #9
METERING WEST; CLEAR SKIES

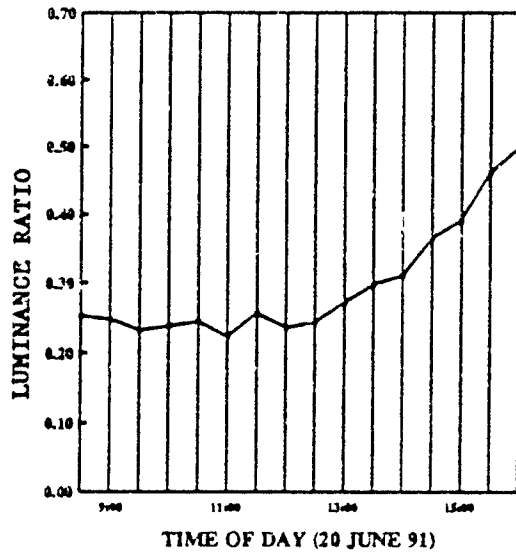


Figure 265

LUMINANCE RATIO (L_v/L_n)
MEASUREMENT AREA #10
METERING WEST; CLEAR SKIES

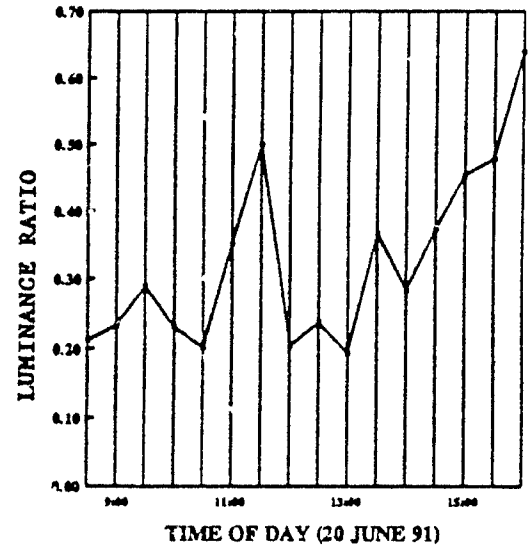


Figure 266

LUMINANCE RATIO (L_v/L_n)
MEASUREMENT AREA #11
METERING WEST; CLEAR SKIES

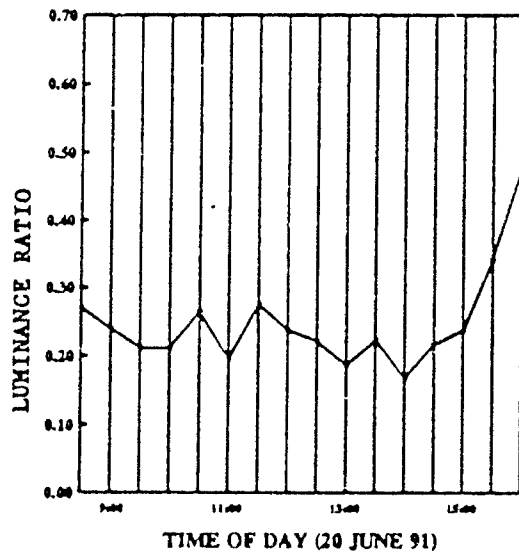


Figure 267

LUMINANCE RATIO (L_v/L_n)
MEASUREMENT AREA #12
METERING WEST; CLEAR SKIES

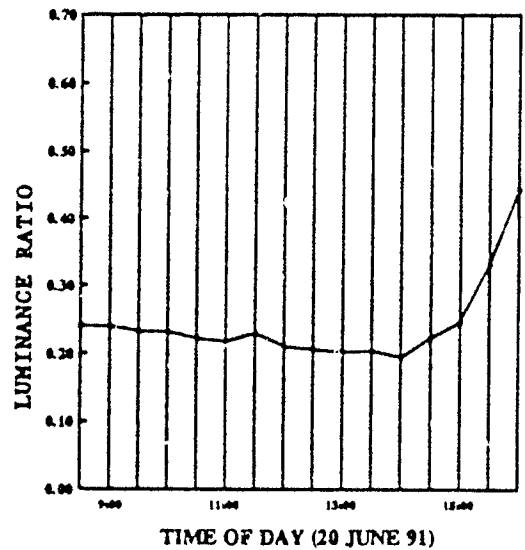


Figure 268

LUMINANCE RATIO (L_v/L_n)
MEASUREMENT AREA #13
METERING WEST; CLEAR SKIES

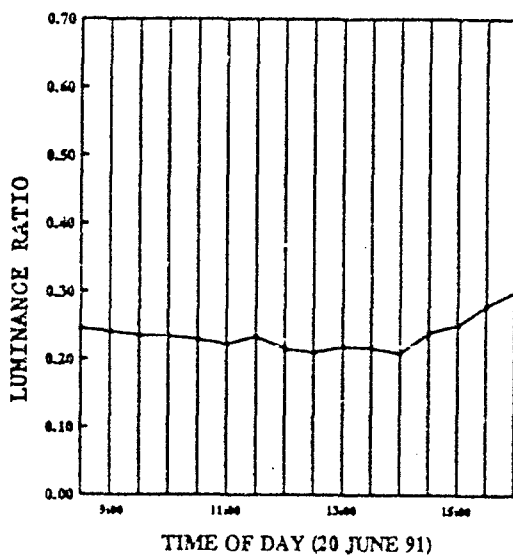


Figure 269

LUMINANCE RATIO (L_v/L_n)
MEASUREMENT AREA #14
METERING WEST; CLEAR SKIES

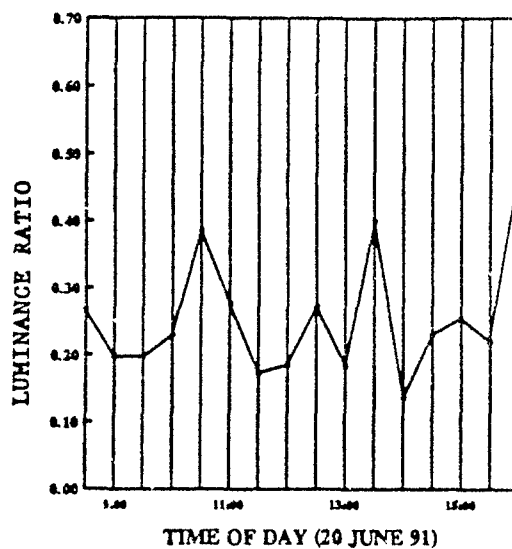


Figure 270

LUMINANCE RATIO (L_v/L_n)
MEASUREMENT AREA #15
METERING WEST; CLEAR SKIES

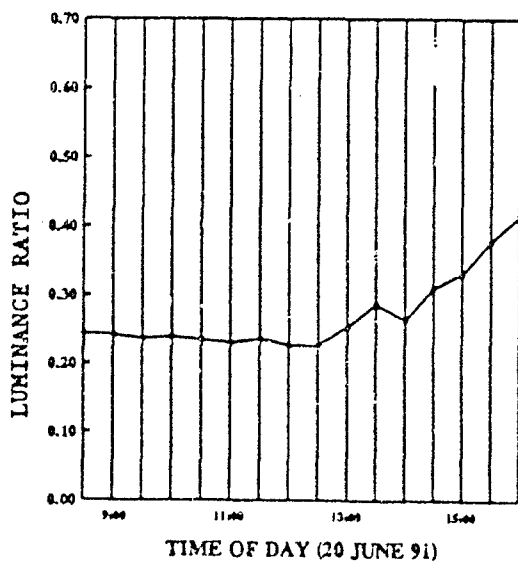


Figure 271

Table 54. Luminance Ratio (Lh/Ln).

Area #	08:30	09:00	09:30	10:00	10:30	11:00	11:30	12:00
1	0.26	0.26	0.26	0.25	0.27	0.26	0.30	0.28
2	0.26	0.26	0.26	0.27	0.27	0.28	0.29	0.30
3	0.26	0.27	0.26	0.27	0.26	0.26	0.28	0.30
4	0.26	0.26	0.26	0.27	0.27	0.26	0.29	0.29
5	0.29	0.7	0.25	0.25	0.29	0.29	0.39	0.34
6	0.27	0.27	0.27	0.27	0.28	0.29	0.31	0.30
7	0.26	0.26	0.26	0.27	0.28	0.27	0.30	0.30
8	0.25	0.27	0.25	0.26	0.27	0.27	0.30	0.30
9	0.27	0.26	0.26	0.27	0.28	0.27	0.30	0.32
10	0.28	0.26	0.32	0.27	0.27	0.44	0.74	0.33
11	0.31	0.26	0.26	0.25	0.28	0.24	0.25	0.32
12	0.25	0.25	0.26	0.27	0.26	0.27	0.29	0.28
13	0.25	0.25	0.26	0.27	0.27	0.27	0.29	0.28
14	0.26	0.21	0.23	0.28	0.47	0.34	0.21	0.23
15	0.25	0.25	0.26	0.26	0.27	0.27	0.29	0.28

Area #	12:30	13:00	13:30	14:00	14:30	15:00	15:30	16:00
1	0.27	0.28	0.29	0.27	0.49	0.35	0.47	0.59
2	0.32	0.35	0.42	0.39	0.47	0.51	0.59	0.61
3	0.32	0.34	0.40	0.39	0.46	0.50	0.55	0.58
4	0.32	0.34	0.39	0.38	0.45	0.47	0.52	0.56
5	0.31	0.35	0.38	0.36	0.47	0.57	0.67	0.87
6	0.32	0.38	0.51	0.45	0.62	0.62	0.76	0.63
7	0.31	0.33	0.37	0.38	0.47	0.48	0.52	0.57
8	0.31	0.32	0.37	0.37	0.45	0.47	0.52	0.56
9	0.30	0.33	0.37	0.36	0.43	0.46	0.50	0.55
10	0.28	0.36	0.46	0.36	0.44	0.55	0.56	0.74
11	0.30	0.27	0.30	0.25	0.30	0.33	0.40	0.55
12	0.28	0.28	0.29	0.25	0.31	0.34	0.38	0.52
13	0.28	0.29	0.29	0.26	0.31	0.32	0.33	0.36
14	0.44	0.25	0.72	0.23	0.25	0.39	0.26	0.45
15	0.28	0.30	0.34	0.31	0.36	0.39	0.42	0.45

Area #	MINIMUM	MAXIMUM	DIFF	STD
1	0.25	0.59	0.33	0.10
2	0.26	0.61	0.35	0.12
3	0.26	0.58	0.33	0.11
4	0.26	0.56	0.30	0.10
5	0.25	0.87	0.63	0.17
6	0.27	0.76	0.50	0.16
7	0.26	0.57	0.31	0.10
8	0.25	0.56	0.30	0.10
9	0.26	0.55	0.29	0.09
10	0.26	0.74	0.48	0.15
11	0.24	0.55	0.31	0.07
12	0.25	0.52	0.27	0.04
13	0.25	0.36	0.10	0.03
14	0.21	0.72	0.51	0.13
15	0.25	0.45	0.21	0.06

Note: MINIMUM refers to the smallest transmittance obtained between 08:30 and 16:00.
 MAXIMUM refers to the largest transmittance obtained between 08:30 and 16:00.
 DIFFERENCE refers to the difference between MAXIMUM and MINIMUM.
 STD refers to the standard deviation of transmittance for each measurement area.

LUMINANCE RATIO (L_h/L_n)
MEASUREMENT AREA #1
METERING WEST; CLEAR SKIES

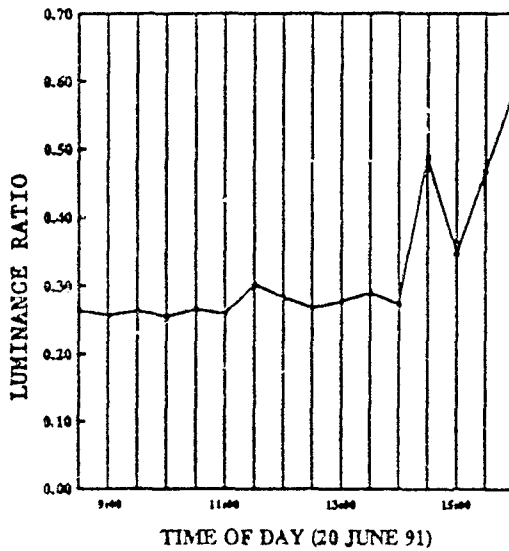


Figure 272

LUMINANCE RATIO (L_h/L_n)
MEASUREMENT AREA #2
METERING WEST; CLEAR SKIES

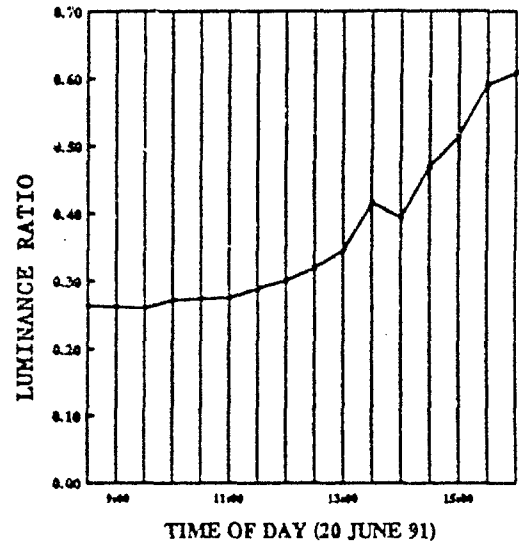


Figure 273

LUMINANCE RATIO (L_h/L_n)
MEASUREMENT AREA #3
METERING WEST; CLEAR SKIES

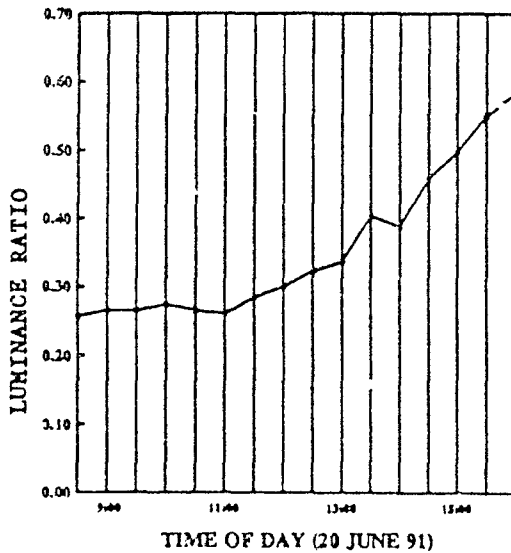


Figure 274

LUMINANCE RATIO (L_h/L_n)
MEASUREMENT AREA #4
METERING WEST; CLEAR SKIES

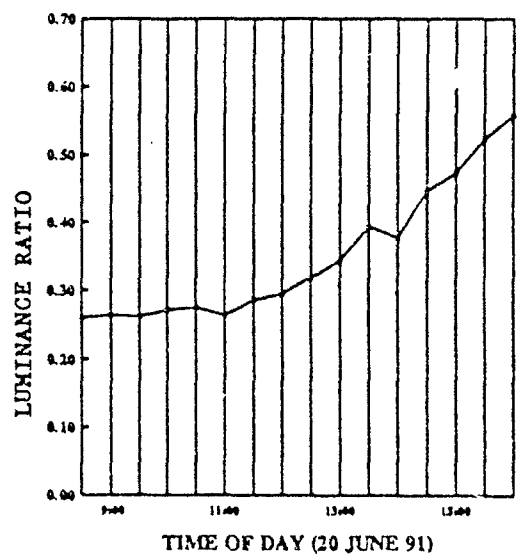


Figure 275

LUMINANCE RATIO (L_h/L_n)
MEASUREMENT AREA #5
METERING WEST; CLEAR SKIES

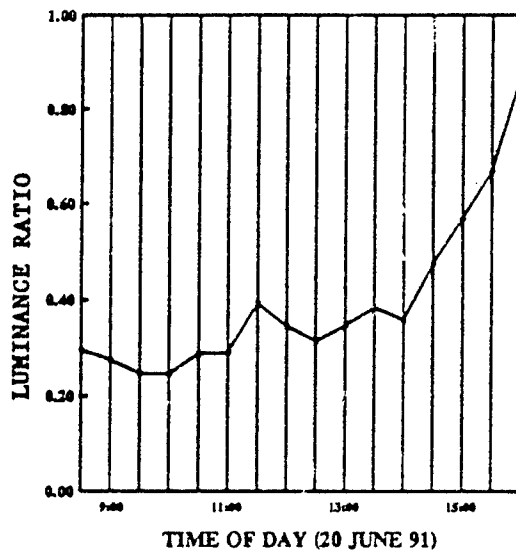


Figure 276

LUMINANCE RATIO (L_h/L_n)
MEASUREMENT AREA #6
METERING WEST; CLEAR SKIES

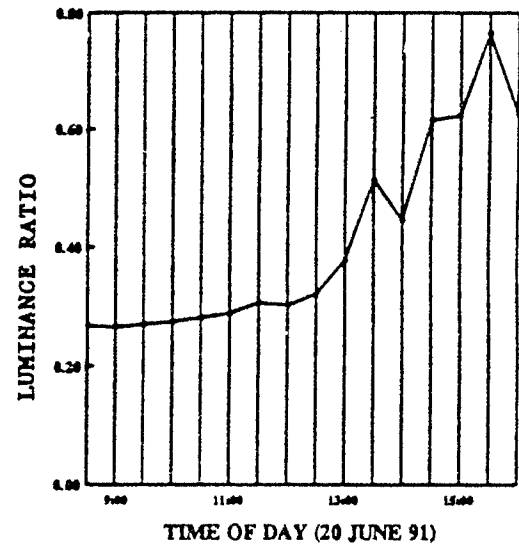


Figure 277

LUMINANCE RATIO (L_h/L_n)
MEASUREMENT AREA #7
METERING WEST; CLEAR SKIES

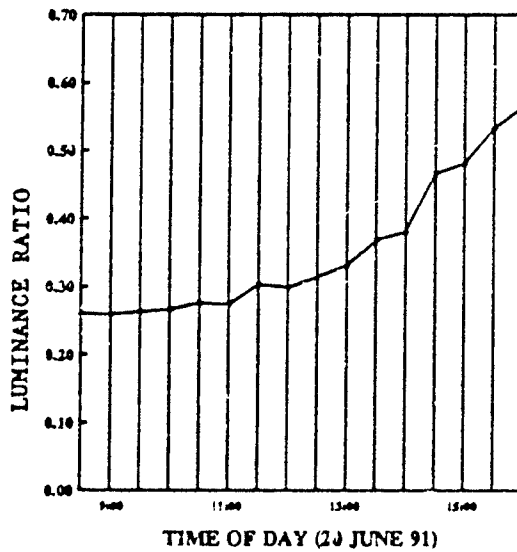


Figure 278

LUMINANCE RATIO (L_h/L_n)
MEASUREMENT AREA #8
METERING WEST; CLEAR SKIES

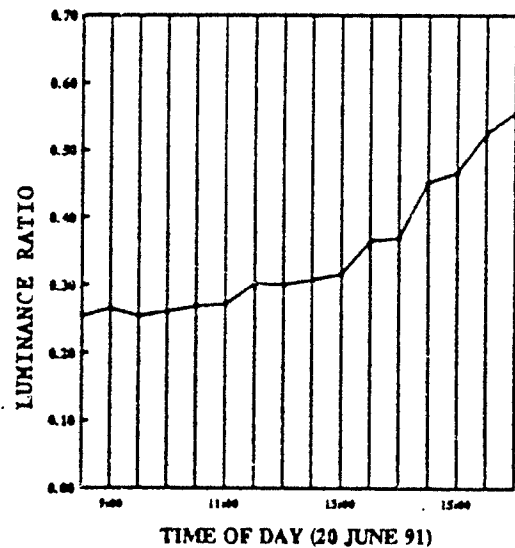


Figure 279

LUMINANCE RATIO (Lh/Ln)
MEASUREMENT AREA #9
METERING WEST; CLEAR SKIES

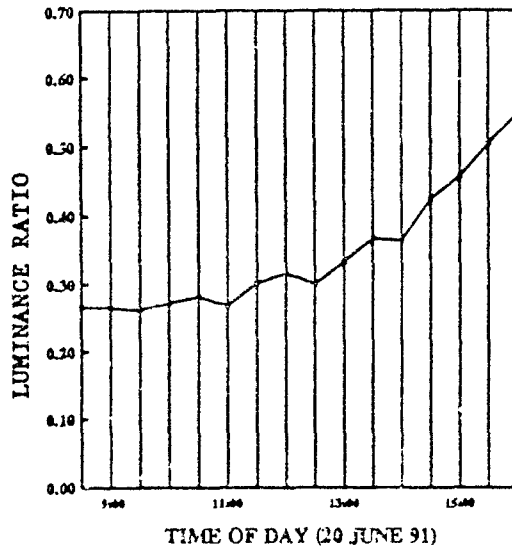


Figure 280

LUMINANCE RATIO (Lh/Ln)
MEASUREMENT AREA #10
METERING WEST; CLEAR SKIES

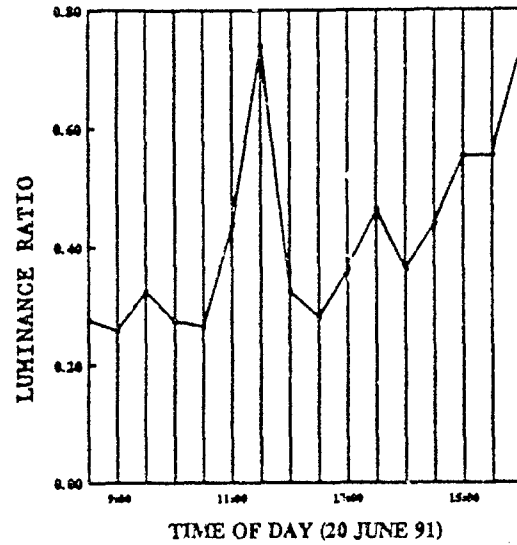


Figure 281

LUMINANCE RATIO (Lh/Ln)
MEASUREMENT AREA #11
METERING WEST; CLEAR SKIES

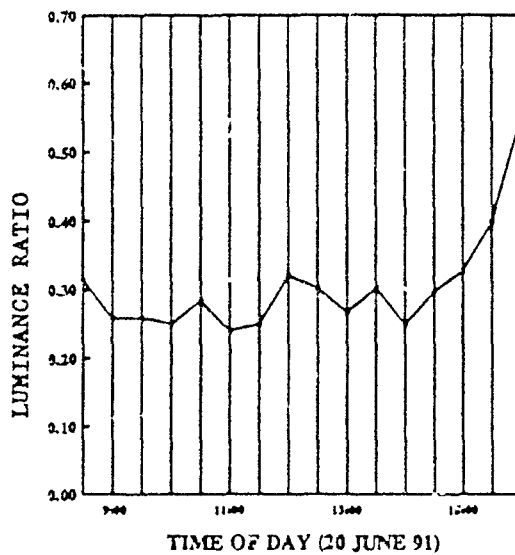


Figure 282

LUMINANCE RATIO (Lh/Ln)
MEASUREMENT AREA #12
METERING WEST; CLEAR SKIES

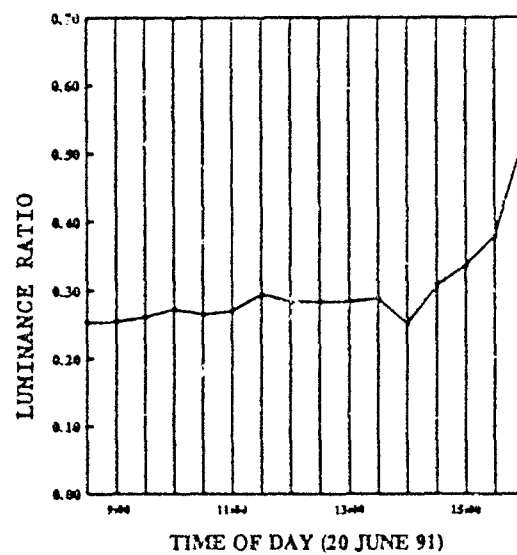


Figure 283

LUMINANCE RATIO (Lh/Ln)
MEASUREMENT AREA #13
METERING WEST; CLEAR SKIES

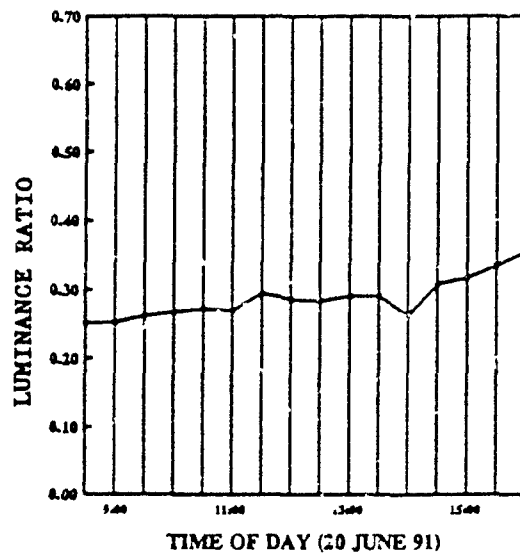


Figure 284

LUMINANCE RATIO (Lh/Ln)
MEASUREMENT AREA #14
METERING WEST; CLEAR SKIES

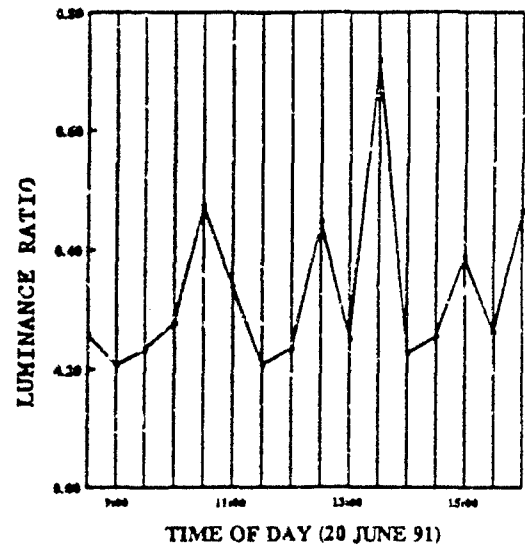


Figure 285

LUMINANCE RATIO (Lh/Ln)
MEASUREMENT AREA #15
METERING WEST; CLEAR SKIES

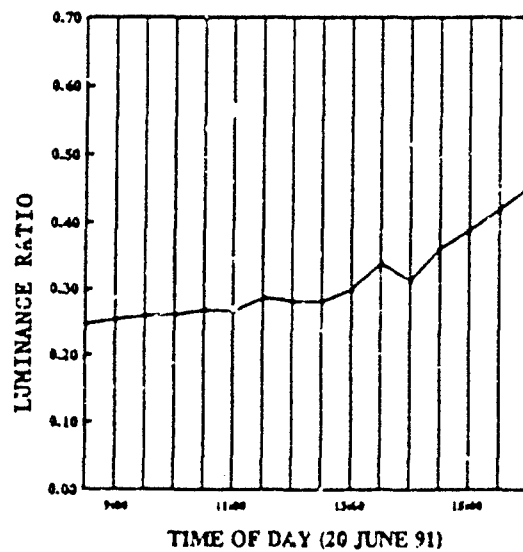


Figure 286

Table 55 shows the difference in the amount of vertical and horizontal polarization. The graphs of Figure 287, Figure 288,...Figure 304 show the results graphically.

Table 55. Luminance Difference (Lh - Lv).

Area #	08:30	09:00	09:30	10:00	10:30	11:00	11:30	12:00
1	29	55	50	50	87	106	155	233
2	29	37	43	66	83	100	92	111
3	25	31	66	100	98	93	87	113
4	24	37	59	83	115	108	94	107
5	113	38	85	23	112	58	121	98
6	45	45	73	91	111	132	115	105
7	21	33	55	69	93	91	96	103
8	26	26	56	69	76	81	96	105
9	29	40	73	79	84	95	78	120
10	151	69	82	130	187	144	241	188
11	106	61	162	136	58	155	-70	249
12	38	50	98	146	159	191	214	251
13	16	36	82	104	132	142	164	187
14	-24	25	103	116	138	132	105	138
15	9	36	75	68	105	109	128	127

Area #	12:30	13:00	13:30	14:00	14:30	15:00	15:30	16:00
1	161	198	159	130	160	126	59	50
2	94	78	77	34	59	58	64	47
3	95	73	68	33	48	54	43	35
4	77	71	55	26	42	46	29	20
5	85	74	110	41	60	60	49	113
6	117	117	118	57	111	112	122	26
7	82	61	45	29	49	43	29	31
8	78	63	46	33	43	38	30	27
9	65	52	44	31	36	40	26	27
10	43	163	51	46	34	46	36	36
11	238	219	190	186	157	131	42	41
12	251	251	235	137	165	136	40	49
13	188	171	162	103	123	114	87	81
14	240	121	271	175	24	99	48	-7
15	102	62	42	38	39	43	30	25

Area #	MINIMUM	MAXIMUM	DIFF	STD
1	29	233	204	59
2	29	111	82	24
3	25	113	88	28
4	20	115	95	31
5	23	121	98	30
6	26	132	106	32
7	21	103	83	27
8	26	105	79	25
9	26	120	95	27
10	34	241	206	66
11	-70	249	319	83
12	38	251	214	76
13	16	188	172	49
14	-24	271	295	79
15	9	128	119	37

Note: MINIMUM refers to the smallest difference obtained between 08:30 and 16:00.
 MAXIMUM refers to the largest difference obtained between 08:30 and 16:00.
 DIFFERENCE refers to the difference between MAXIMUM and MINIMUM.
 STD refers to the standard deviation of difference for each measurement area.

LUMINANCE DIFFERENCE ($L_h - L_v$)
MEASUREMENT AREA #1
METERING WEST; CLEAR SKIES

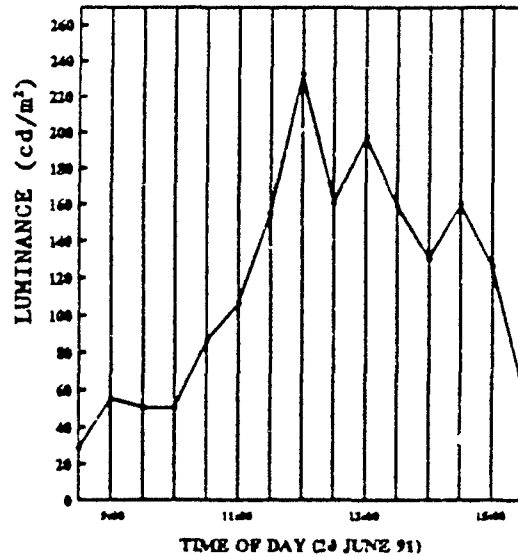


Figure 287

LUMINANCE DIFFERENCE ($L_h - L_v$)
MEASUREMENT AREA #2
METERING WEST; CLEAR SKIES

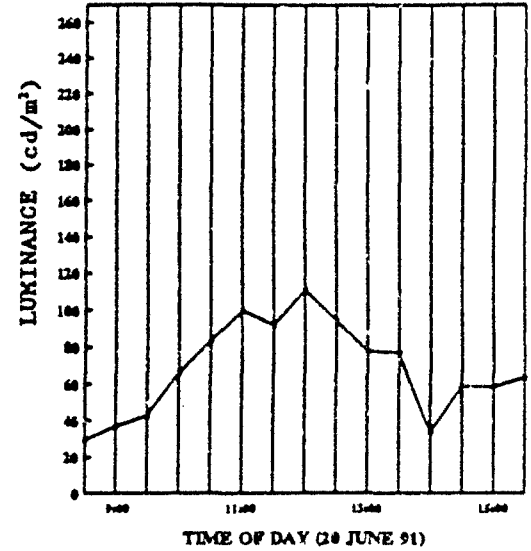


Figure 288

LUMINANCE DIFFERENCE ($L_h - L_v$)
MEASUREMENT AREA #3
METERING WEST; CLEAR SKIES

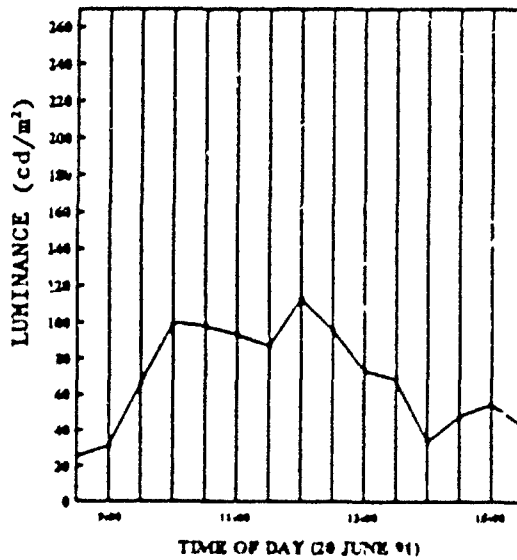


Figure 289

LUMINANCE DIFFERENCE ($L_h - L_v$)
MEASUREMENT AREA #4
METERING WEST; CLEAR SKIES

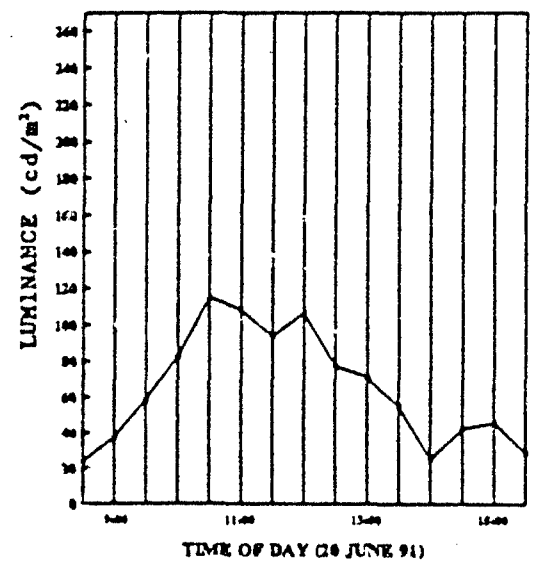


Figure 290

LUMINANCE DIFFERENCE ($L_h - L_v$)
MEASUREMENT AREA #5
METERING WEST; CLEAR SKIES

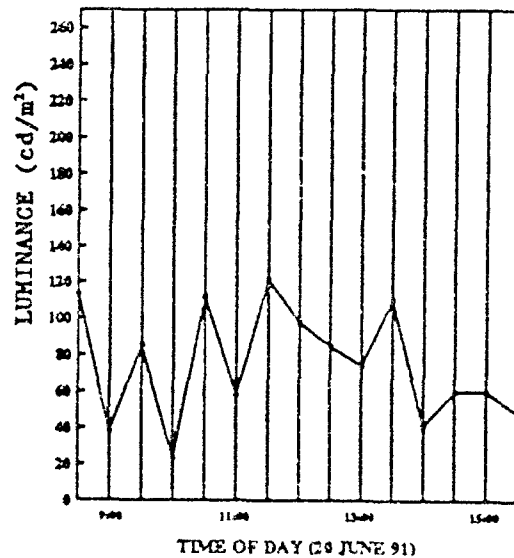


Figure 291

LUMINANCE DIFFERENCE ($L_h - L_v$)
MEASUREMENT AREA #6
METERING WEST; CLEAR SKIES

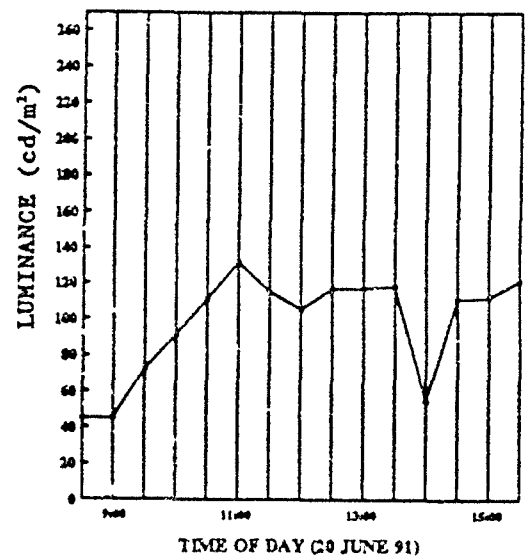


Figure 292

LUMINANCE DIFFERENCE ($L_h - L_v$)
MEASUREMENT AREA #7
METERING WEST; CLEAR SKIES

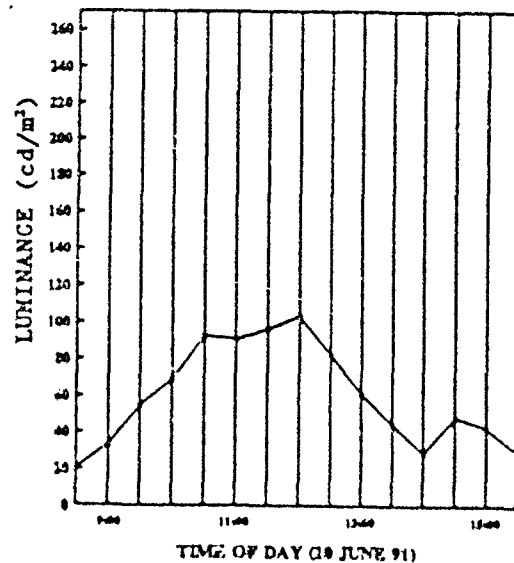


Figure 293

LUMINANCE DIFFERENCE ($L_h - L_v$)
MEASUREMENT AREA #8
METERING WEST; CLEAR SKIES

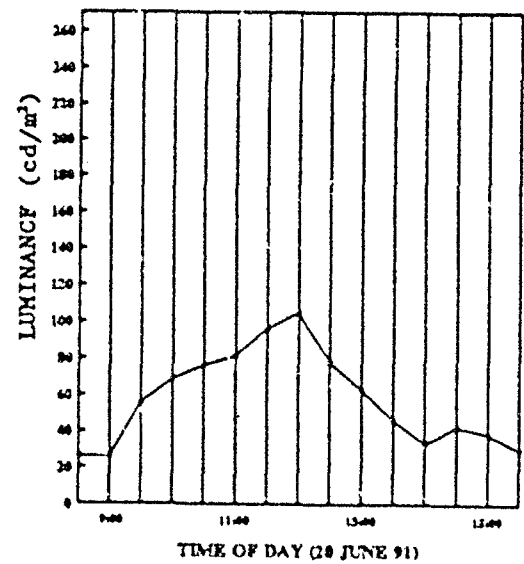


Figure 294

LUMINANCE DIFFERENCE ($L_h - L_v$)
MEASUREMENT AREA #9
METERING WEST; CLEAR SKIES

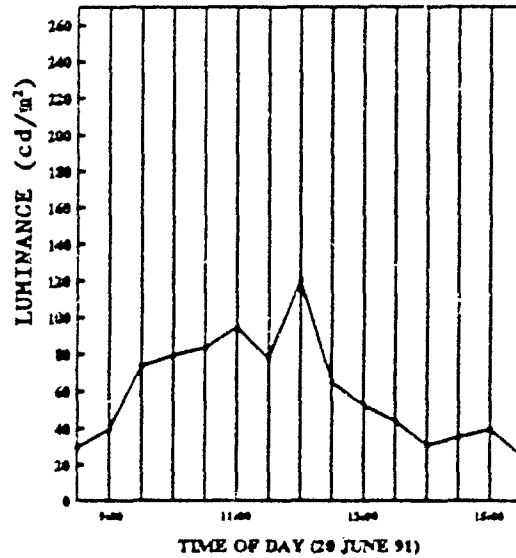


Figure 295

LUMINANCE DIFFERENCE ($L_h - L_v$)
MEASUREMENT AREA #10
METERING WEST; CLEAR SKIES

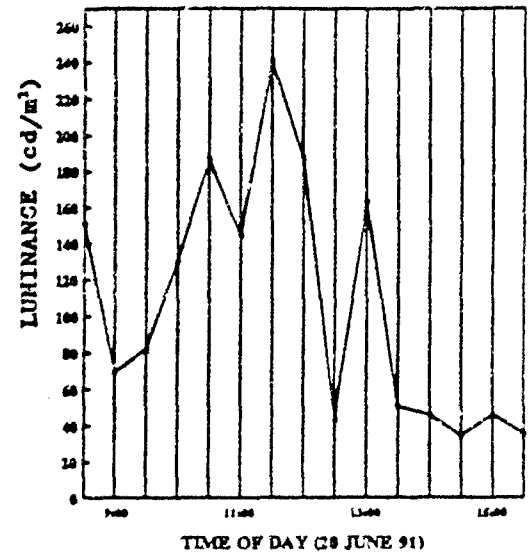


Figure 296

LUMINANCE DIFFERENCE ($L_h - L_v$)
MEASUREMENT AREA #11
METERING WEST; CLEAR SKIES

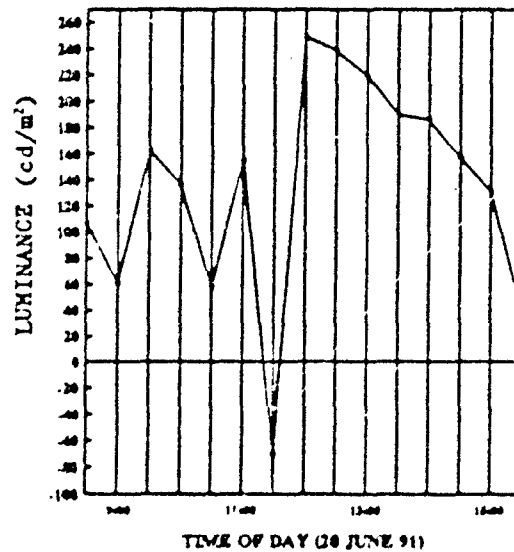


Figure 297

LUMINANCE DIFFERENCE ($L_h - L_v$)
MEASUREMENT AREA #12
METERING WEST; CLEAR SKIES

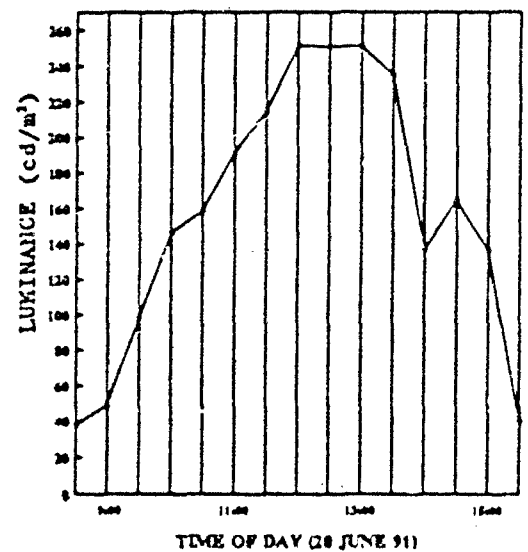


Figure 298

LUMINANCE DIFFERENCE ($L_h - L_v$)
MEASUREMENT AREA #13
METERING WEST; CLEAR SKIES

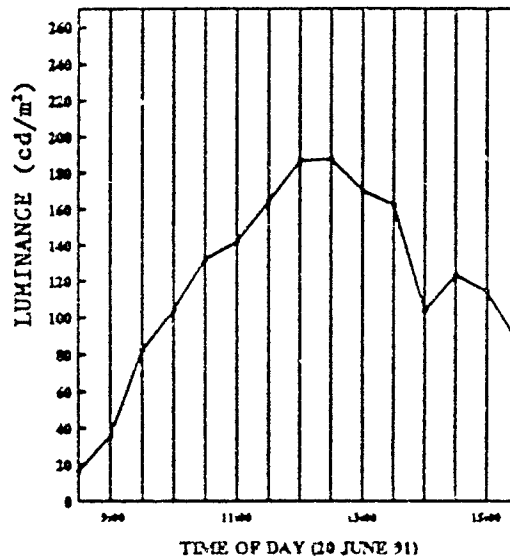


Figure 299

LUMINANCE DIFFERENCE ($L_h - L_v$)
MEASUREMENT AREA #14
METERING WEST; CLEAR SKIES

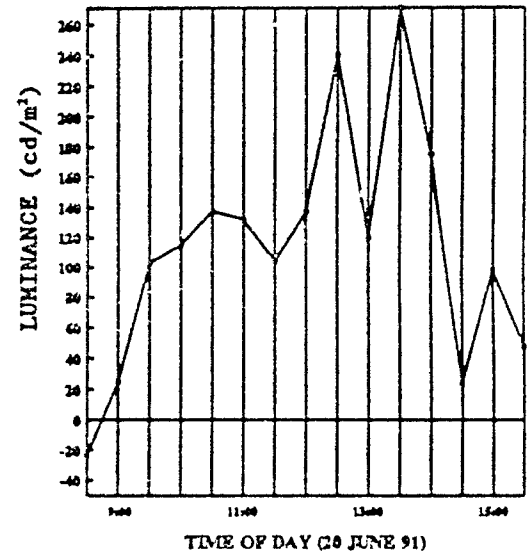


Figure 300

LUMINANCE DIFFERENCE ($L_h - L_v$)
MEASUREMENT AREA #15
METERING WEST; CLEAR SKIES

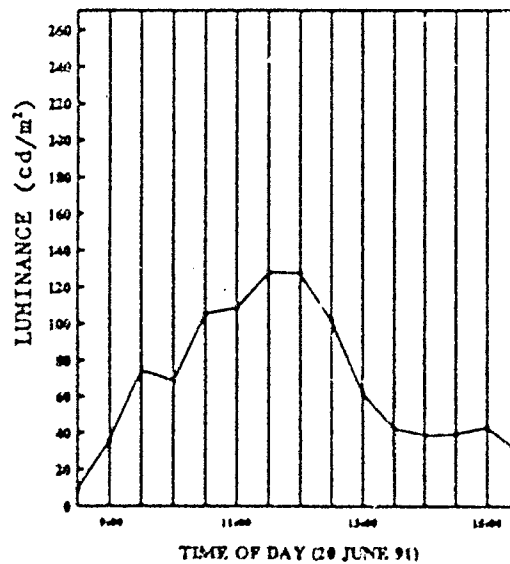


Figure 301

LUMINANCE DIFFERENCE ($L_h - L_v$)
LEFT SIDE OF M1 TURRET
METERING WEST; CLEAR SKIES

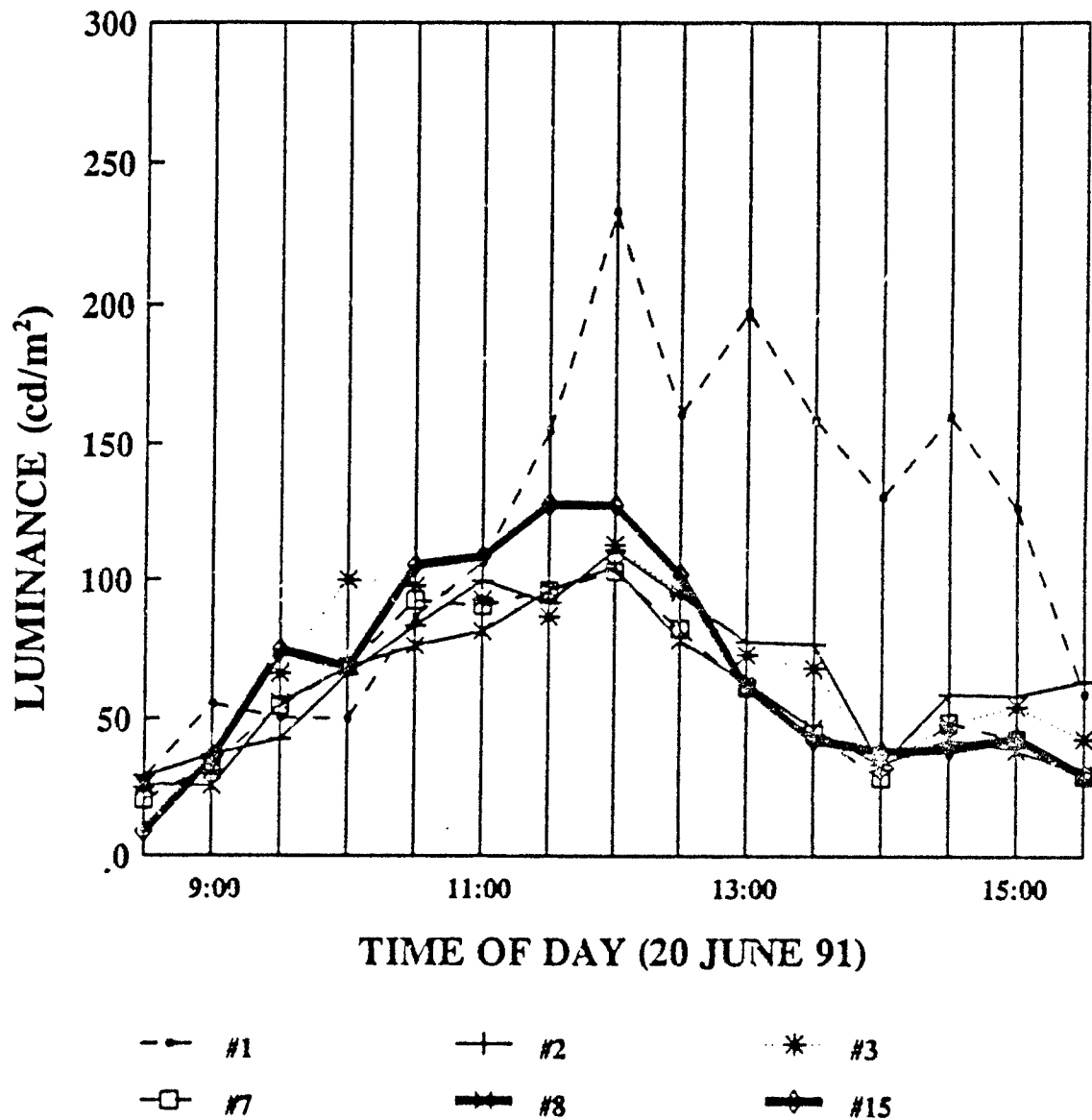


Figure 302

LUMINANCE DIFFERENCE (Lh - Lv)
MIDDLE OF M1 TURRET
METERING WEST; CLEAR SKIES

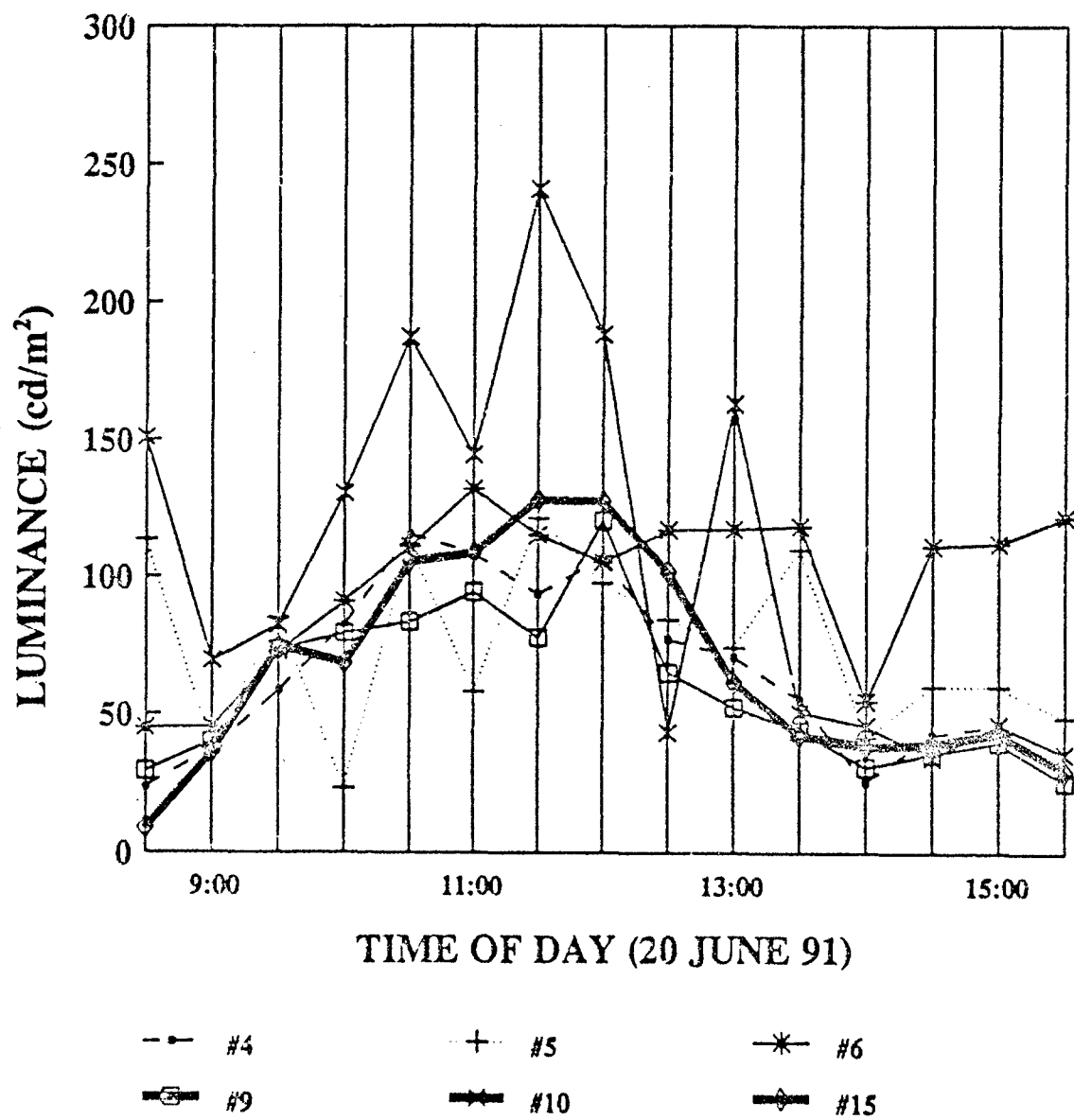


Figure 303

**LUMINANCE DIFFERENCE ($L_h - L_v$)
RIGHT SIDE OF M1 TURRET
METERING WEST; CLEAR SKIES**

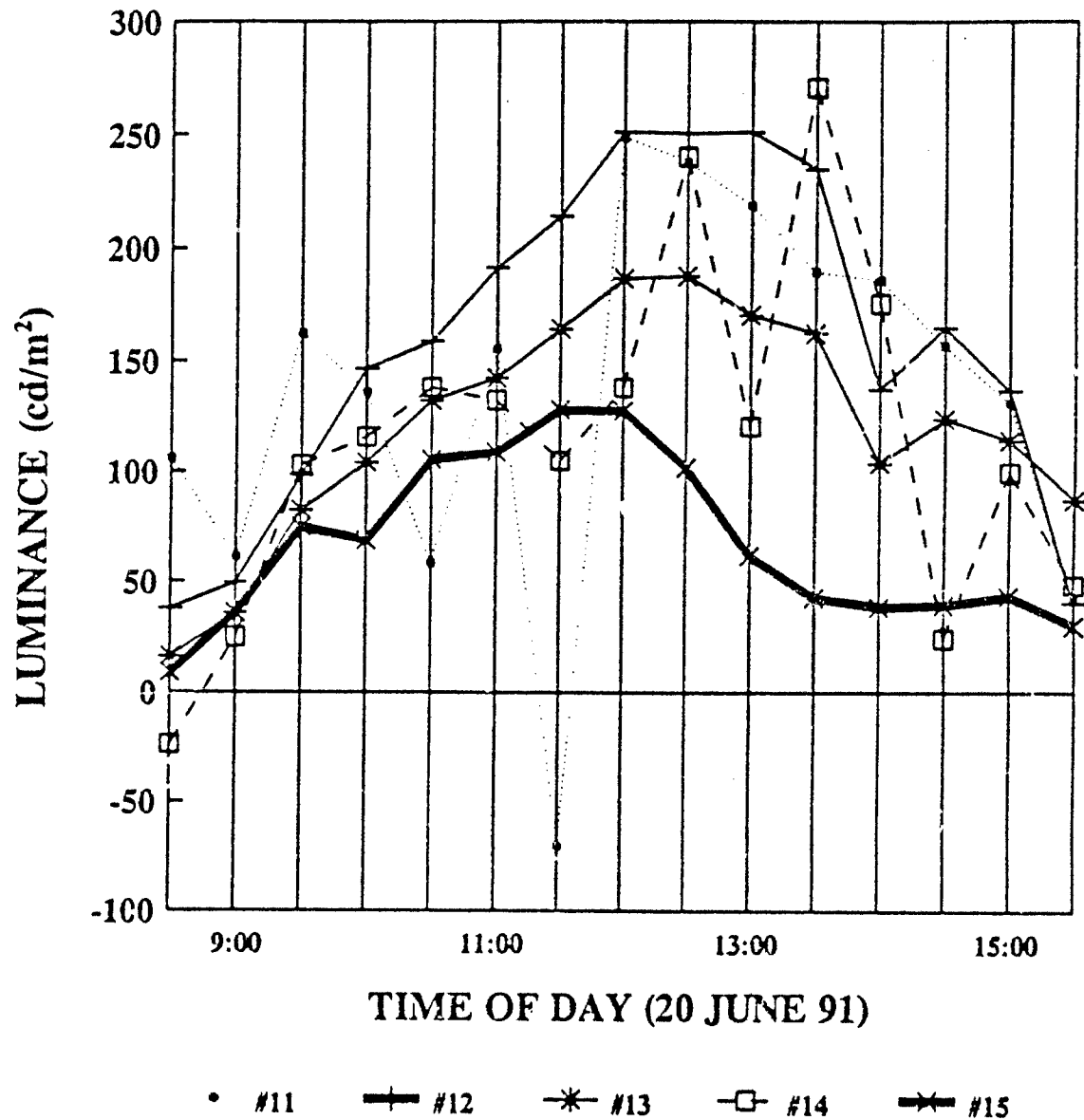


Figure 304

ANALYSIS OF 20 JUNE, 1991 STUDY

An interesting photograph of the diurnal photographic study (Figure 225, Figure 226,..., Figure 240) is Figure 235. This photograph shows the M1A1 at 13:30. As Table 56 indicates, this is approximately the time the sun crosses the meridian (sun due south). Since the M1A1 was positioned along a north-south line, the angle of incidence of the sun's rays on the skirt areas (Area #15, slope 90°, azimuth 270°) is 90°. The sun does not radiate its energy directly on the skirt area shortly after 13:30. This explains why all the vertical areas oriented along a north-south line on the M1A1 give low luminance readings after 13:30. The luminance of these areas after 13:30 is due to skylight (and to a lesser extent other sources) and is approximately 700 cd/m² (Table 50, Figure 251, Figure 252,..., Figure 256).

The sun's rays make an angle of incidence of 90° with Area #12 (Figure 224, slope 60°, azimuth 270°) shortly after 15:30. The sun's rays make an angle of incidence of 90° with Area #13 (Figure 224, slope 60°, azimuth 204°) shortly after 16:00.

Table 56. Sun's Position and Angles of Incidence for 20 June, 1991

				Area #12	Area #13	Area #15
				Slope	Slope	Slope
				60	60	90
				Azimuth	Azimuth	Azimuth
				270	204	270
EDST	Hour	Altitude	Azimuth	<1	<1	<1
08:30	284.0	20.6	267.7	9.1	50.0	27.1
09:00	219.5	26.1	272.8	3.9	52.3	31.4
09:30	299.0	31.6	278.2	6.7	54.9	36.7
10:00	306.5	37.0	284.0	13.1	57.6	42.5
10:30	314.0	42.3	290.4	19.8	60.5	48.7
11:00	321.5	47.4	297.7	26.7	63.4	55.2
11:30	329.0	52.1	306.2	33.6	66.3	61.8
12:00	336.5	56.2	316.3	40.5	69.2	68.6
12:30	344.0	59.6	328.4	47.3	72.0	75.4
13:00	351.5	61.9	342.5	54.2	74.7	82.3
13:30	359.0	62.9	358.0	60.9	77.3	89.1
14:00	6.5	62.3	13.68	67.7	79.7	----
14:30	14.0	60.3	28.20	74.4	81.9	----
15:00	21.6	57.2	40.78	81.0	83.9	----
15:30	29.1	53.2	51.37	87.5	85.6	----
16:00	36.5	48.6	60.27	----	87.0	----

NOTE: SOUTH - 0°, WEST - 90°, NORTH - 180°, EAST - 270°

At 8:30, the luminance of Area #12 and Area #15 are nearly equal, 3021 cd/m^2 and 3023 cd/m^2 respectfully, and the contrast between these two areas is zero. However, at 13:30, the luminance of Area #12 and Area #15 is 2760 cd/m^2 and 819 cd/m^2 respectfully and the contrast between these two areas is 2.4.

An important consequence of the shading of selected areas on a vehicle is contrast variation between different areas of the vehicle. The increase in contrast between Area #12 of the M1A1 (turret facet) and Area #15 of the M1A1 (skirt) at 13:30 compared to 8:30 increases the visibility of the vehicle and produces a visible signature.

At the conclusion of this study, it was initially thought that the polarization data of this study would be of little value. The vertical and horizontal positions of the transmission axis do not necessarily correspond to the minimum and maximum polarization readings. However, in a later study conducted on 15 July, 1991, it was found that the minimum and maximum polarization angles correspond very closely to the vertical and horizontal positions of the polarizer (Figure 305 and Figure 306). Also, there is a wealth of information contained in this polarization data that does not relate to minimum and maximum polarization angles.

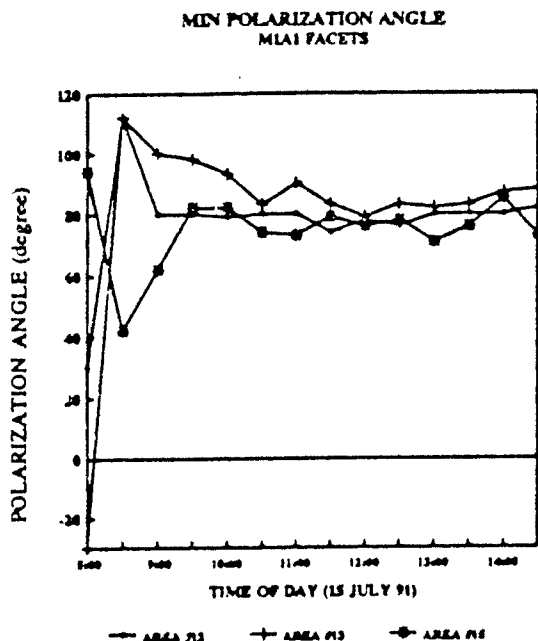


Figure 305

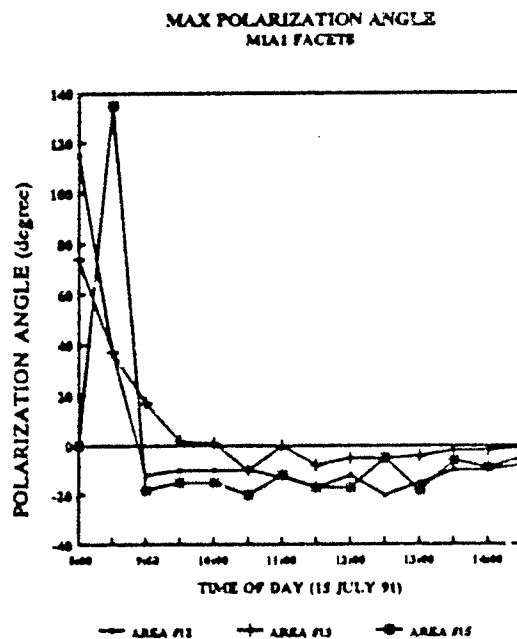


Figure 306

The optical density of the polarizer used for this study was determined, using unpolarized light from a Macbeth TD 502 Densitometer, to be 0.60. This corresponds to a transmittance of 0.25. (See Appendix A for a discussion of optical density and transmittance.) However, the transmittance can be greater than 0.25 if polarized light is incident on the polarizer. As a matter of fact, if the transmittance is found to be greater than 0.25, it is reasonably certain that some of the light entering the polarizer is polarized light.

The ratio of a luminance reading with a polarizer in front of the meter to the luminance reading without a polarizer in front of the meter is equal to the transmittance of the polarizer. Any ratio greater than 0.25 corresponds to polarized light entering the polarizer.

For example, virtually all the luminance ratios L_v/L_n (transmittance with the transmission axis of the polarizer vertical) for all fifteen areas of the M1A1 studied are 0.25 up to a time of 13:30. The ratios L_v/L_n at 13:00 and after are generally greater than 0.25 (Table 53, Figure 257, Figure 258,..., Figure 270). Since the transmittance is greater than 0.25 at 13:30 and after, the amount of polarized light entering the polarizer increases after 13:30. But most of the M1A1 areas studied do not receive light directly from the sun after 13:30! The only other reasonable source for this polarized light is sky light.

The nature of the ratios L_h/L_n (transmittance with the transmission axis of the polarizer horizontal) are similar to the ratios L_v/L_n . However, there are two distinct differences:

1. With a few minor exceptions, the ratios L_h/L_n , for all fifteen areas studied, are greater than L_v/L_n for all times between 8:30 and 16:00 (Table 53, Table 54, Figure 257, Figure 258,..., Figure 286).
2. Unlike L_v/L_n , which has a near constant value of 0.25 from 8:30 to 13:30 and then increases after 13:30, L_h/L_n slowly increases from 8:30 to 13:30. The ratio L_h/L_n increases at a greater rate after 13:30 than it does before 13:30.

When the M1A1 is oriented along a north-south line and viewing of the M1A1 is toward the west, the azimuth range of the sky which can affect polarization measurements of the M1A1 is from 180° to 360° (south = 0°). In other words, only light from the eastern hemispherical region of the sky can affect polarization measurements.

The photographs of Figure 307 show how the polarization of light from the sky for this region changes with time from 10:30 to 16:00. These photographs were obtained by placing a polarization axis finder in front of a 100 mm macro lens fitted with an extension tube attached to a 35 mm Canon A1 camera. The darker and broader the two opposing wedges appear, the greater the intensity of the polarized incident light. The polarization axis is along a line drawn through the center of the wedges. Appendix B gives a description of the polarization axis finder.

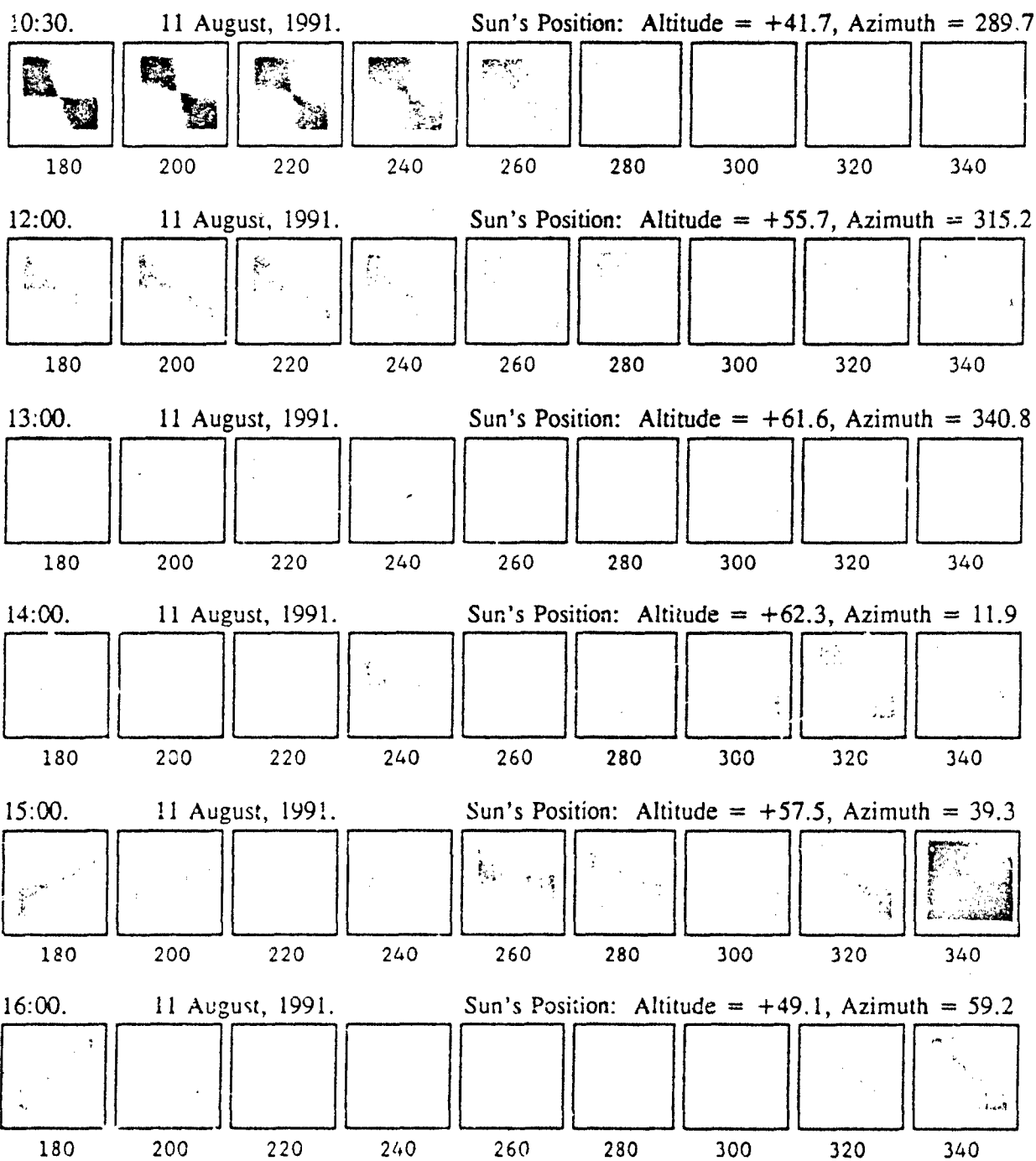


Figure 307

The Eastern Hemispherical Sky at 30° Altitude as Seen Through a Polarization Axis Finder

Note: Azimuth angles are displayed below the photographs.

The sky photographs of Figure 307 illustrate clearly that the eastern hemispherical region of the sky produces an increasing amount of polarized light from 10:30 to 16:00. At 10:30, the polarization of this region is particularly strong to the north and very weak to the south. As the sun's position advances to the west, the polarization of the southern portion of the sky's eastern hemisphere increases.

Another trend in the polarization data of this study relates to the diurnal difference $\Delta L = L_h - L_v$. In general, for most of the M1A1 areas studied, ΔL increases from 8:30 to approximately 11:30 then decreases from 12:00 to 13:30. Although this phenomenon is on a small scale, ($\Delta L = 150 \text{ cd/m}^2$) it definitely exists and it is interesting because it appears to be related to the altitude of the sun and the polarization axis of sky light.

The maximum deviation of the polarization axis of sky light from the horizontal occurs at 90° to the sun's direction and is equal to the complement of the sun's altitude. The sun's altitude is approximately 45° at 11:00 (Table 56) and increases to a maximum 63° at 13:30.

SUMMARY OF 20 JUNE, 1991 STUDY

The following are the highlights of this study:

1. The maximum luminance acquired for the M1A1 was 3667 cd/m^2 (10:30, Area #12, slope 60° , azimuth 270°).
2. Large scale shading occurs when the sun's position creates a 90° angle of incidence for the skirt area of the M1A1 (13:30, Area #15, slope 90° , azimuth 270°). This causes contrast variation (0 to 2.4), and increases the visibility of the vehicle and produces a visible signature.
3. The minimum and maximum polarization angles for light reflected from different areas of the M1A1 correspond closely to the vertical and horizontal positions of the transmission axis of a linear polarizer.
4. The transmittance of a polarizer is greater for polarized light than it is for unpolarized light.
5. The greatest degree of polarization from the M1A1 occurs when no direct light from the sun reaches its surfaces.
6. Sky light, which is partially polarized due to Rayleigh scattering, is a source of polarized light.
7. The degree of polarization of sky light for the eastern hemispherical sky increases from 8:30 to 16:00 from north to south.
8. The horizontal component of polarized light from the M1A1 is greater than the vertical component for almost every M1A1 area studied. The maximum difference occurs at approximately 11:30.

LUMINANCE, POLARIZATION AND CHROMATICITY STUDY ON 15 JULY, 1991

This study is similar to the 20 June, 1991 study with the following differences:

1. Only three M1A1 areas were metered, Area #12, Area #13 and Area #15 (Figure 224).
2. A linear polarizer (O.D. = 0.5) was rotated in front of the LS-100 luminance meter until a minimum reading was acquired. The polarization angle and luminance were both recorded.
3. The same polarizer was rotated in front of the LS-100 luminance meter until a maximum reading was acquired. The polarization angle and luminance were both recorded.
4. A Minolta CS-100 luminance meter was also used to acquire the three coordinates for the CIE Chromaticity Diagram. The same M1A1 areas (Figure 224, Area #12, Area #13 and Area #15) were metered with the CS-100 as with the LS-100. Also, a grass area (circle in Figure 309) and three different tree areas (numbered areas in Figure 310) were metered with the CS-100.

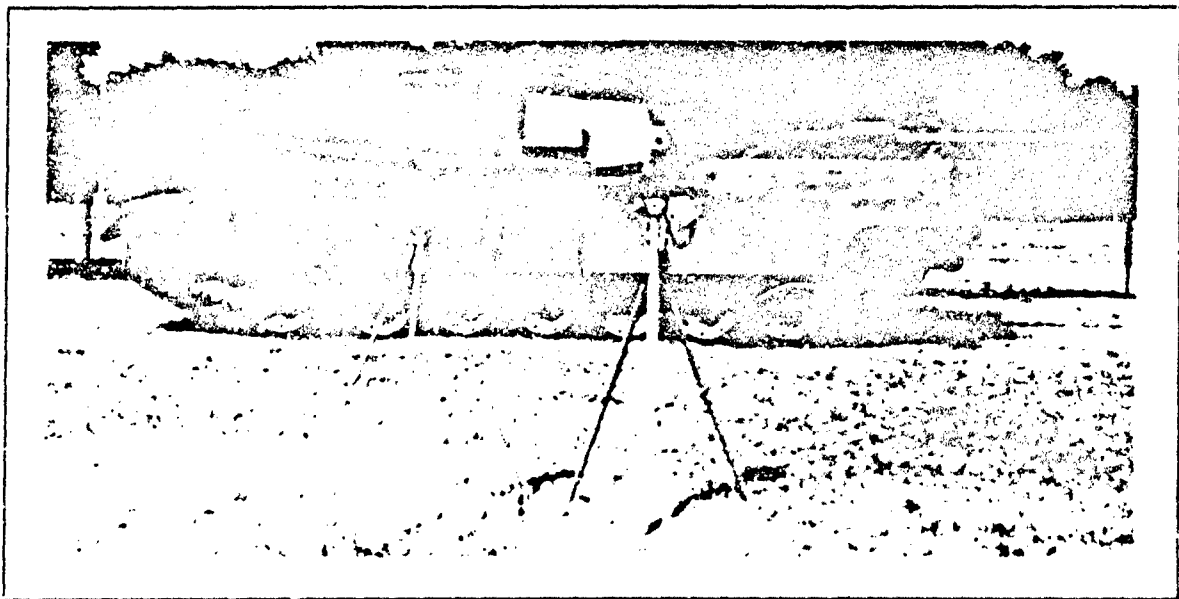


Figure 308
M1A1, LS-100 (right) and CS-100 (left) Positions for 15 July, 1991 Study

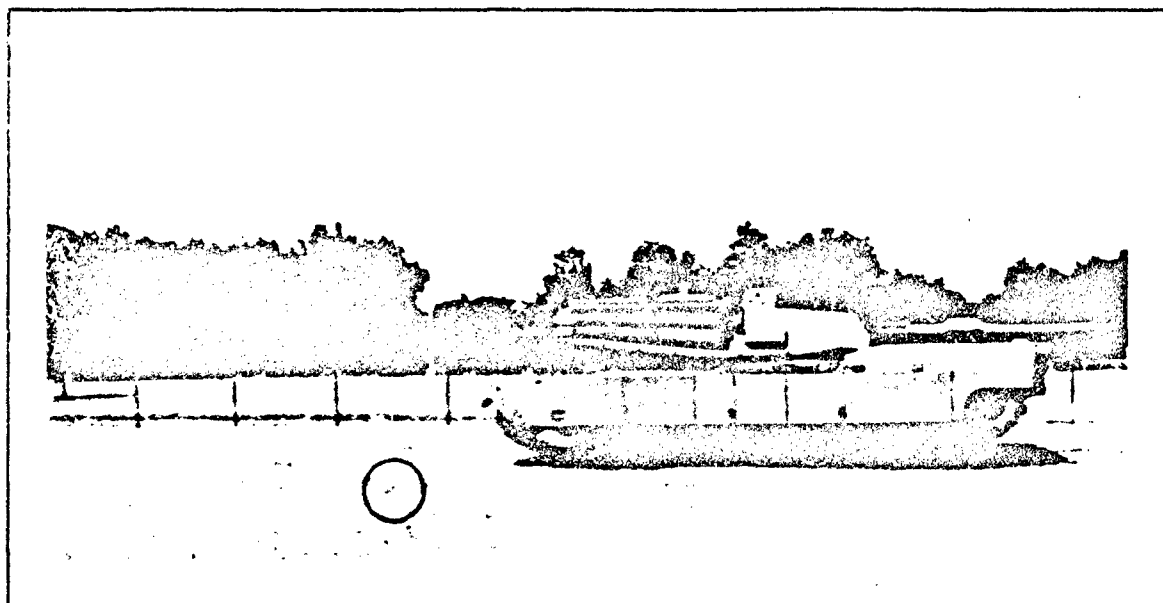


Figure 309
Location of the Grass Area Metered on 15 July, 1991

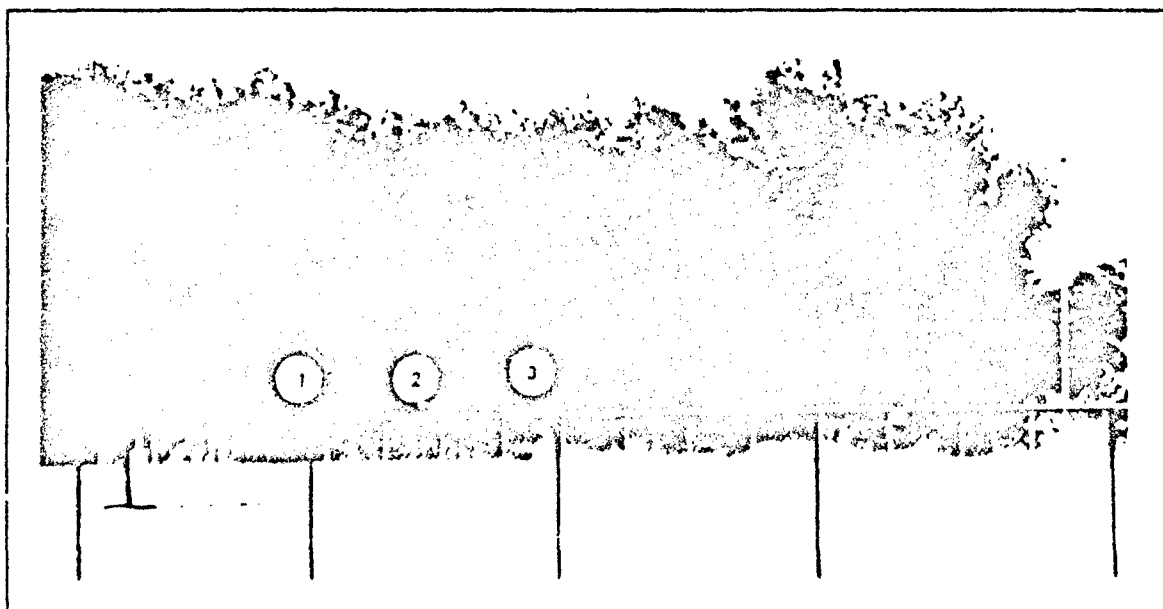


Figure 310
Location of the Three Tree Areas Metered on 15 July, 1991

Table 57. M1A1 Luminance and Polarization Data for Area #12 on 15 July, 1991

TIME	Ln	Lmin	Lmax	<min	<max
08:00	3065	890	907	30	115
08:30	3308	971	988	112	37
09:00	3442	1012	1069	80	-12
09:30	3617	1039	1142	80	-10
10:00	3649	1033	1196	79	-10
10:30	3617	998	1190	80	-10
11:00	3659	972	1228	80	-13
11:30	3574	945	1235	74	-17
12:00	3533	916	1247	78	-12
12:30	3533	903	1275	76	-20
13:00	3292	859	1236	80	-15
13:30	2922	742	1090	80	-10
14:00	2520	658	1008	80	-10
14:45	1872	534	820	82	-8

Table 58. M1A1 Luminance and Polarization Data for Area #13 on 15 July, 1991

TIME	Ln	Lmin	Lmax	<min	<max
08:00	2735	793	814	-30	74
08:30	2785	835	859	112	37
09:00	2796	836	878	100	17
09:30	2807	829	891	98	2
10:00	2728	802	890	93	1
10:30	2608	737	855	83	-10
11:00	2505	700	845	90	0
11:30	2413	667	829	83	-8
12:00	2351	634	802	79	-5
12:30	2350	640	818	83	-5
13:00	2211	625	773	82	-4
13:30	1966	565	713	83	-2
14:00	1851	545	646	87	-2
14:45	1685	480	581	88	-1

NOTES: Range - 36 feet. Minolta LS-100 Luminance meter

Clear Skies Until 12:00 (Light Overcast & Cloudy After 12:00)

Optical Density of linear polarizer - 0.50

Ln - Luminance reading with no polarizer

Lmin - Luminance reading with polarizer rotated to produce a minimum reading

Lmax - Luminance reading with polarizer rotated to produce a maximum reading

MIN < - The polarization angle which produces a minimum luminance reading

MAX < - The polarization angle which produces a maximum luminance reading

Table 59. M1A1 Luminance and Polarization Data for Area #15 on 15 July, 1991

TIME	Ln	Lmin	Lmax	<min	<max
08:00	3169	971	996	94	0
08:30	3313	1022	1037	42	135
09:00	3280	1036	1070	62	-18
09:30	3321	995	1056	82	-15
10:00	3205	910	1014	82	-15
10:30	3011	841	971	74	-20
11:00	2742	788	945	73	-12
11:30	2524	702	854	79	-17
12:00	2209	614	760	76	-17
12:30	1902	520	649	78	-5
13:00	1097	339	403	71	-18
13:30	637	209	229	76	-6
14:00	612	206	230	85	-9
14:45	641	188	221	73	-5

LUMINANCE OF AREA #12 M1A1 FACETS

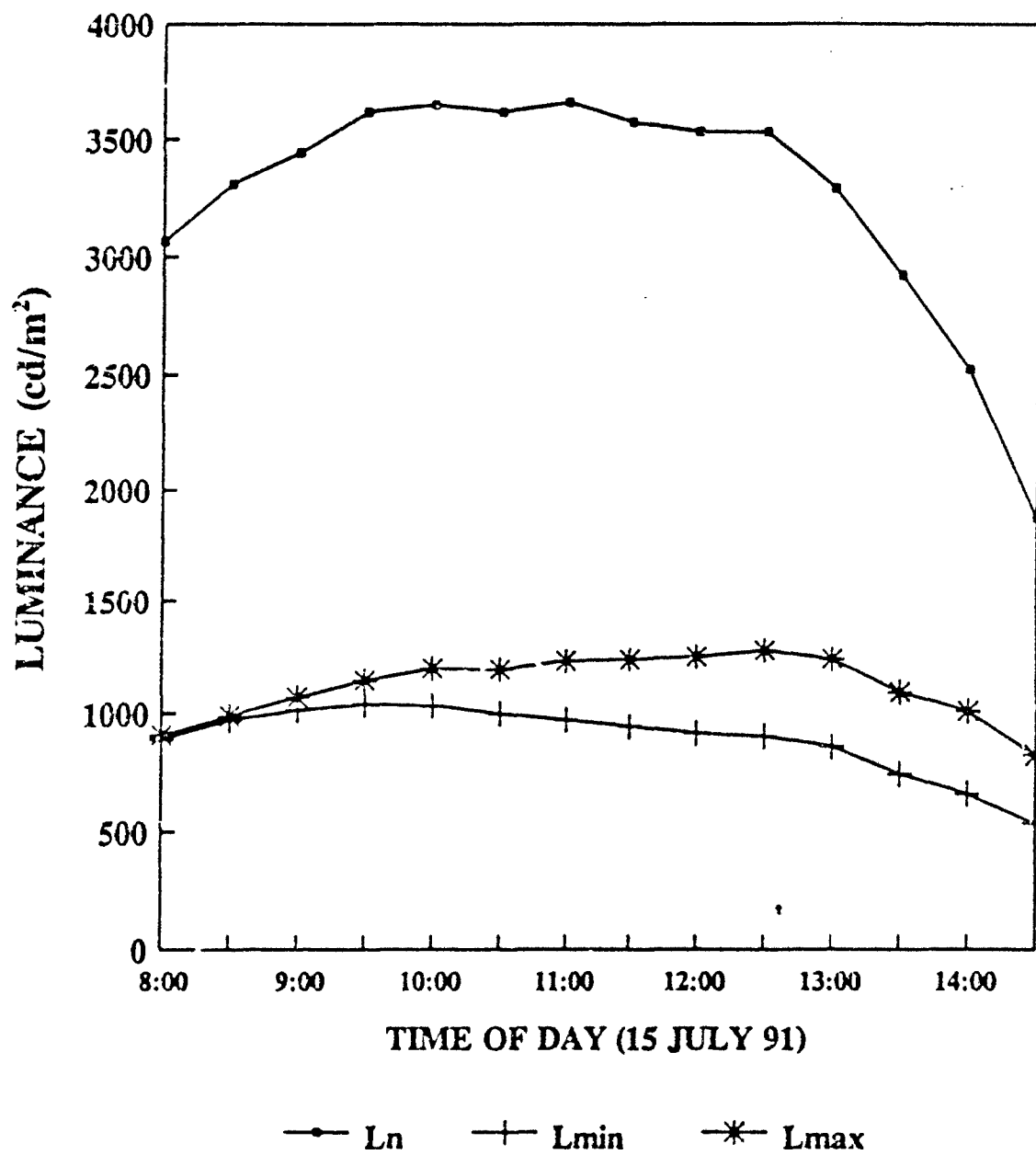


Figure 311

LUMINANCE OF AREA #13 M1A1 FACETS

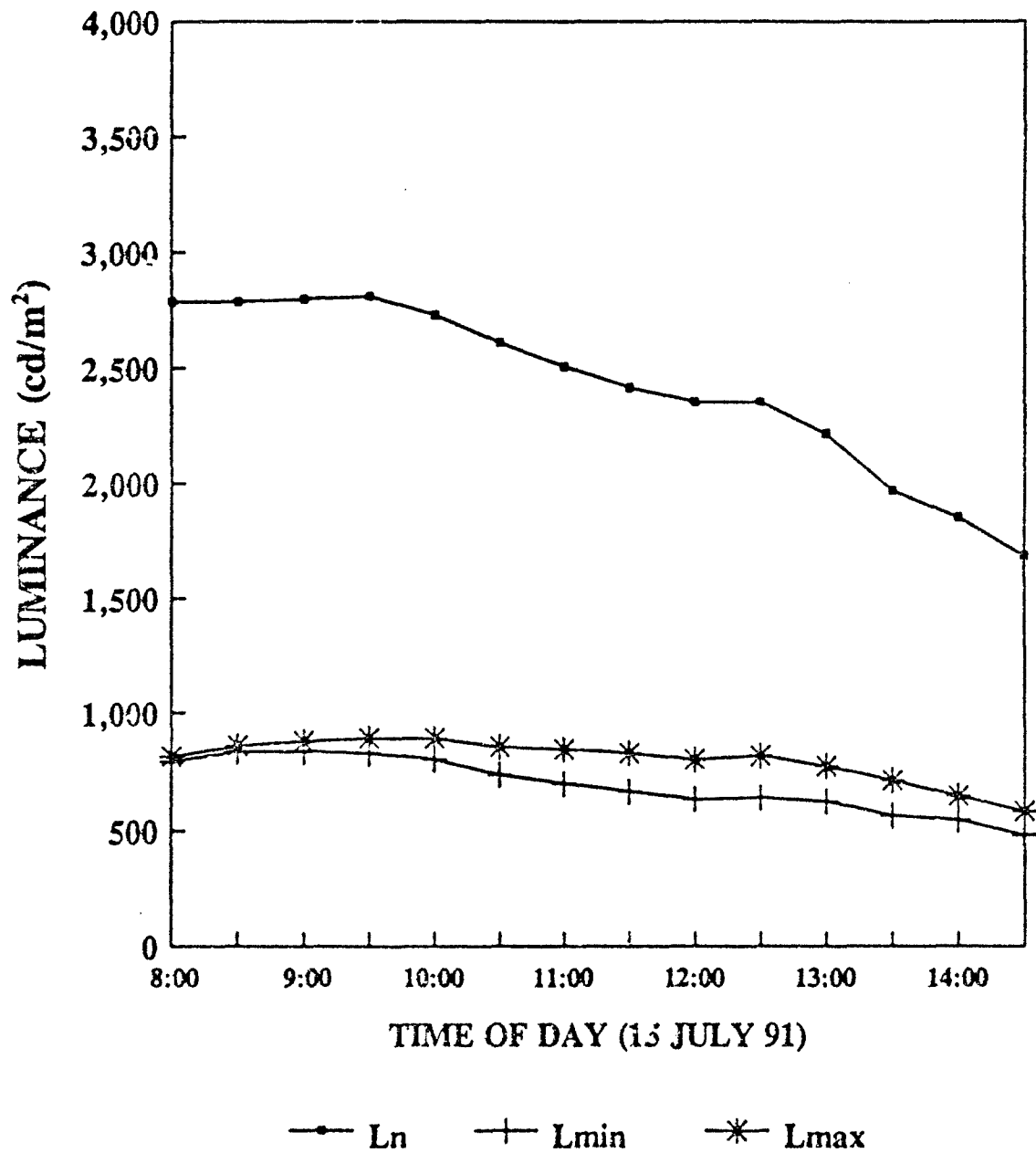


Figure 312

LUMINANCE OF AREA #15 M1A1 FACETS

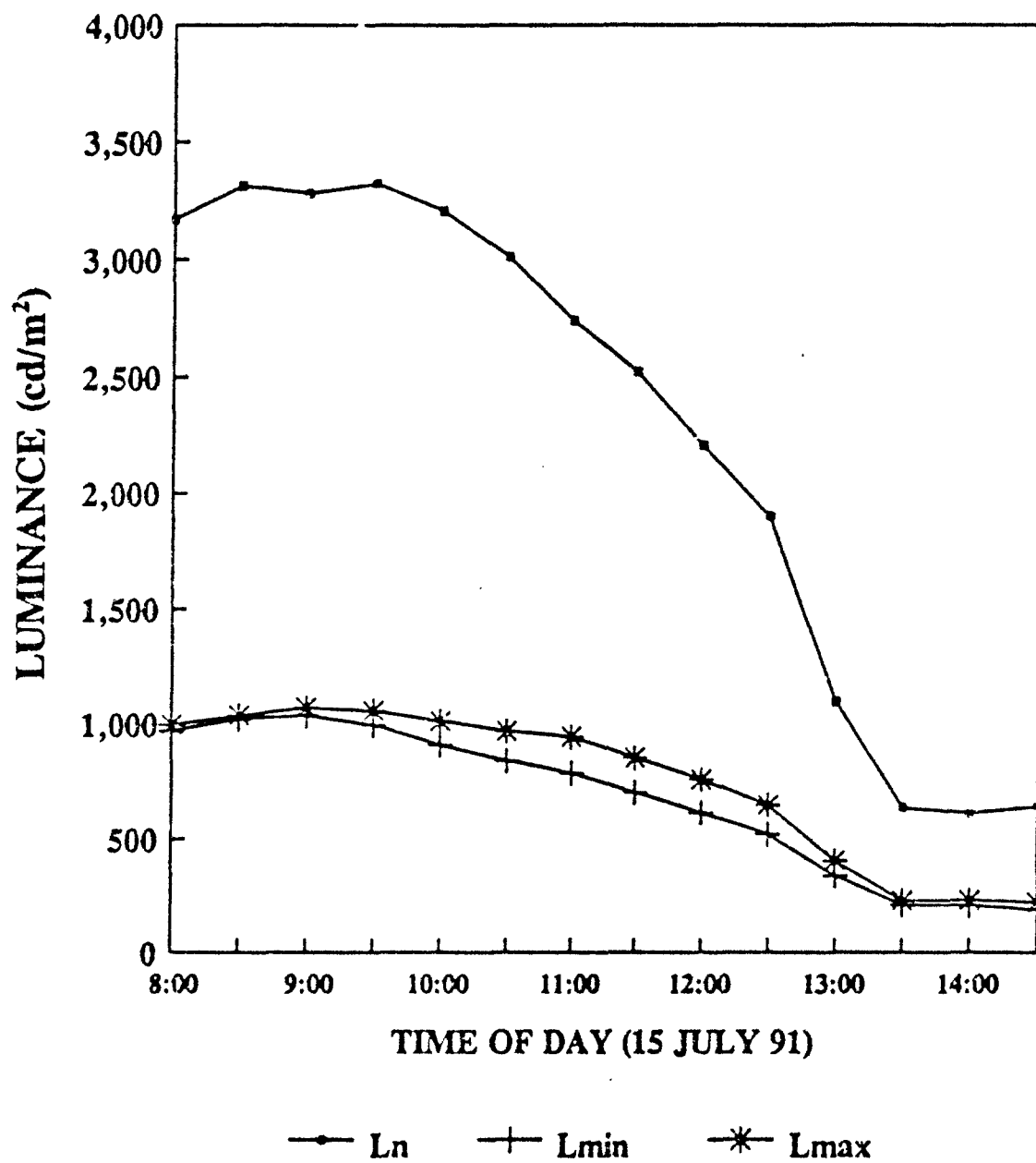


Figure 313

LUMINANCE OF M1A1 FACETS
CLEAR SKIES UNTIL 12:00
LIGHT OVERCAST & CLOUDY AFTER 12:00

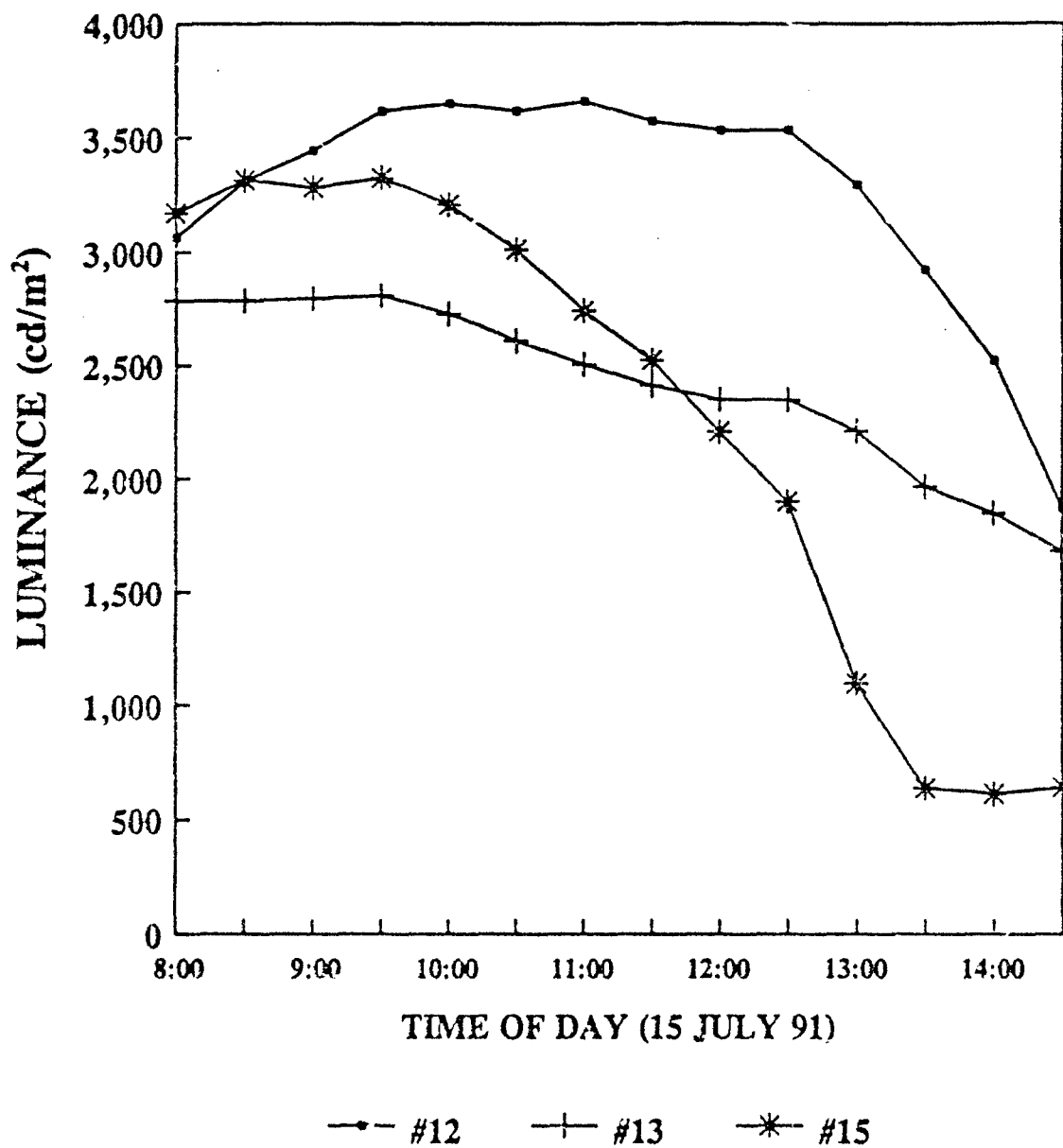


Figure 314

MIN POLARIZATION ANGLE M1A1 FACETS

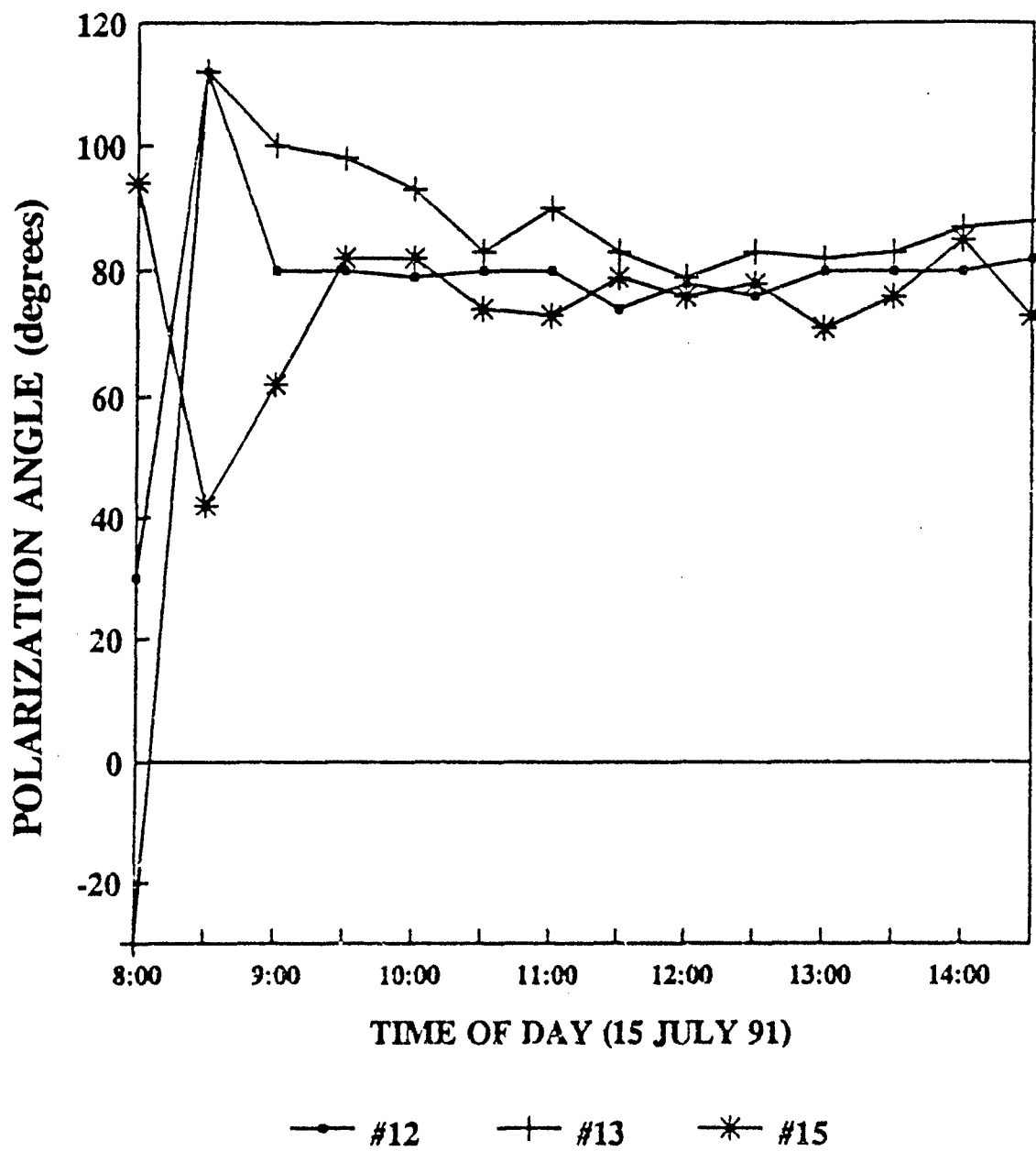


Figure 315

MAX POLARIZATION ANGLE M1A1 FACETS

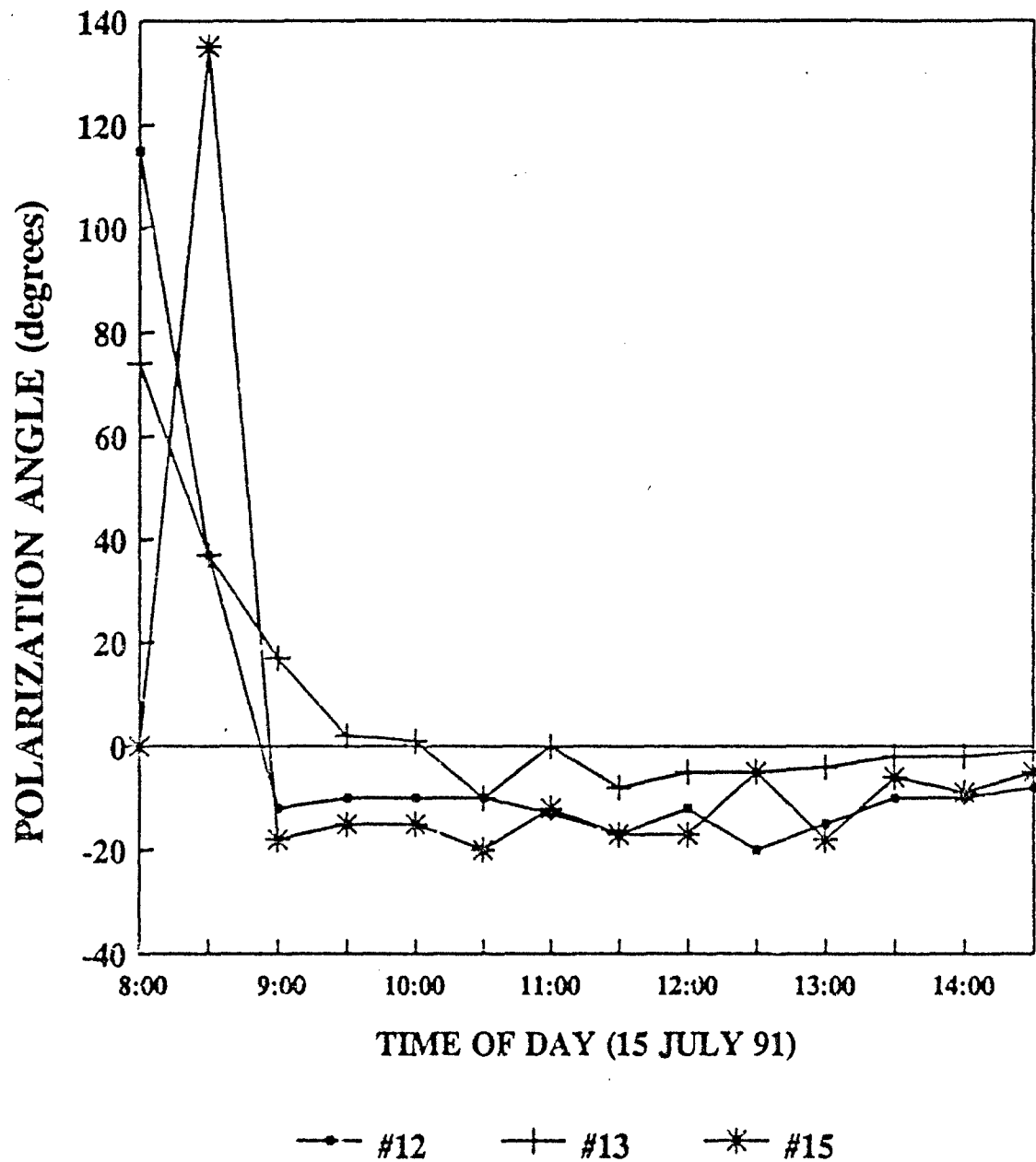


Figure 316

Table 60. M1A1 Luminance and Polarization Calculations for Area #12 on 15 July, 1991

TIME	Lmin-Lmax	Lmin/Lmax	Lmin/Ln	Lmax/Ln	<Diff	Deg of Polar
08:00	17	0.981	0.290	0.296	-85	0.009
08:30	17	0.983	0.294	0.299	75	0.009
09:00	57	0.947	0.294	0.311	92	0.027
09:30	103	0.910	0.287	0.316	90	0.047
10:00	163	0.864	0.283	0.328	89	0.073
10:30	192	0.839	0.276	0.329	90	0.088
11:00	256	0.792	0.266	0.336	93	0.116
11:30	290	0.765	0.264	0.346	91	0.133
12:00	331	0.735	0.259	0.353	90	0.153
12:30	372	0.708	0.256	0.361	96	0.171
13:00	377	0.695	0.261	0.375	95	0.180
13:30	348	0.681	0.254	0.373	90	0.190
14:00	350	0.653	0.261	0.400	90	0.210
14:45	286	0.651	0.285	0.438	90	0.211

Table 61. M1A1 Luminance and Polarization Calculations for Area #13 on 15 July, 1991

TIME	Lmin-Lmax	Lmin/Lmax	Lmin/Ln	Lmax/Ln	<Diff	Deg of Polar
08:00	21	0.974	0.285	0.292	-104	0.013
08:30	24	0.972	0.300	0.308	75	0.014
09:00	42	0.952	0.299	0.314	83	0.025
09:30	62	0.930	0.295	0.317	96	0.036
10:00	88	0.901	0.294	0.326	92	0.052
10:30	118	0.862	0.283	0.328	93	0.074
11:00	145	0.828	0.279	0.337	90	0.094
11:30	162	0.805	0.276	0.344	91	0.108
12:00	168	0.791	0.270	0.341	84	0.117
12:30	178	0.782	0.272	0.348	88	0.122
13:00	148	0.809	0.283	0.350	86	0.106
13:30	148	0.792	0.287	0.363	85	0.116
14:00	101	0.844	0.294	0.349	89	0.085
14:45	101	0.826	0.285	0.345	89	0.095

NOTES:

Lmx-Lnn - Difference between maximum and minimum luminance readings (Lmax - Lmin)
using a rotated polarizer

Lnn/Lmx - Ratio Lmin/Lmax

Lnn/Ln - Ratio Lmin/Ln

Lmx/Ln - Ratio Lmax/Ln

< Diff - Difference between MAX < and MIN <

Deg. of Polar = (Lmax - Lmin)/(Lmax + Lmin)

Table 62. M1A1 Luminance and Polarization Calculations for Area #15 on 15 July, 1991

TIME	Lmin-Lmax	Lmin/Lmax	Lmin/Ln	Lmax/Ln	<Diff	Deg of Polar
08:00	25	0.975	0.306	0.314	94	0.013
08:30	15	0.986	0.308	0.313	-93	0.007
09:00	34	0.968	0.316	0.326	80	0.016
09:30	61	0.942	0.300	0.318	97	0.030
10:00	104	0.897	0.284	0.316	97	0.054
10:30	130	0.866	0.279	0.322	94	0.072
11:00	157	0.834	0.287	0.345	85	0.091
11:30	152	0.822	0.278	0.338	96	0.098
12:00	146	0.808	0.278	0.344	93	0.106
12:30	129	0.801	0.273	0.341	83	0.110
13:00	64	0.841	0.309	0.367	89	0.086
13:30	20	0.913	0.328	0.359	82	0.046
14:00	24	0.896	0.337	0.376	94	0.055
14:45	33	0.851	0.293	0.345	78	0.081

**L_{min}/L_n POLARIZATION RATIO
M1A1 FACETS**

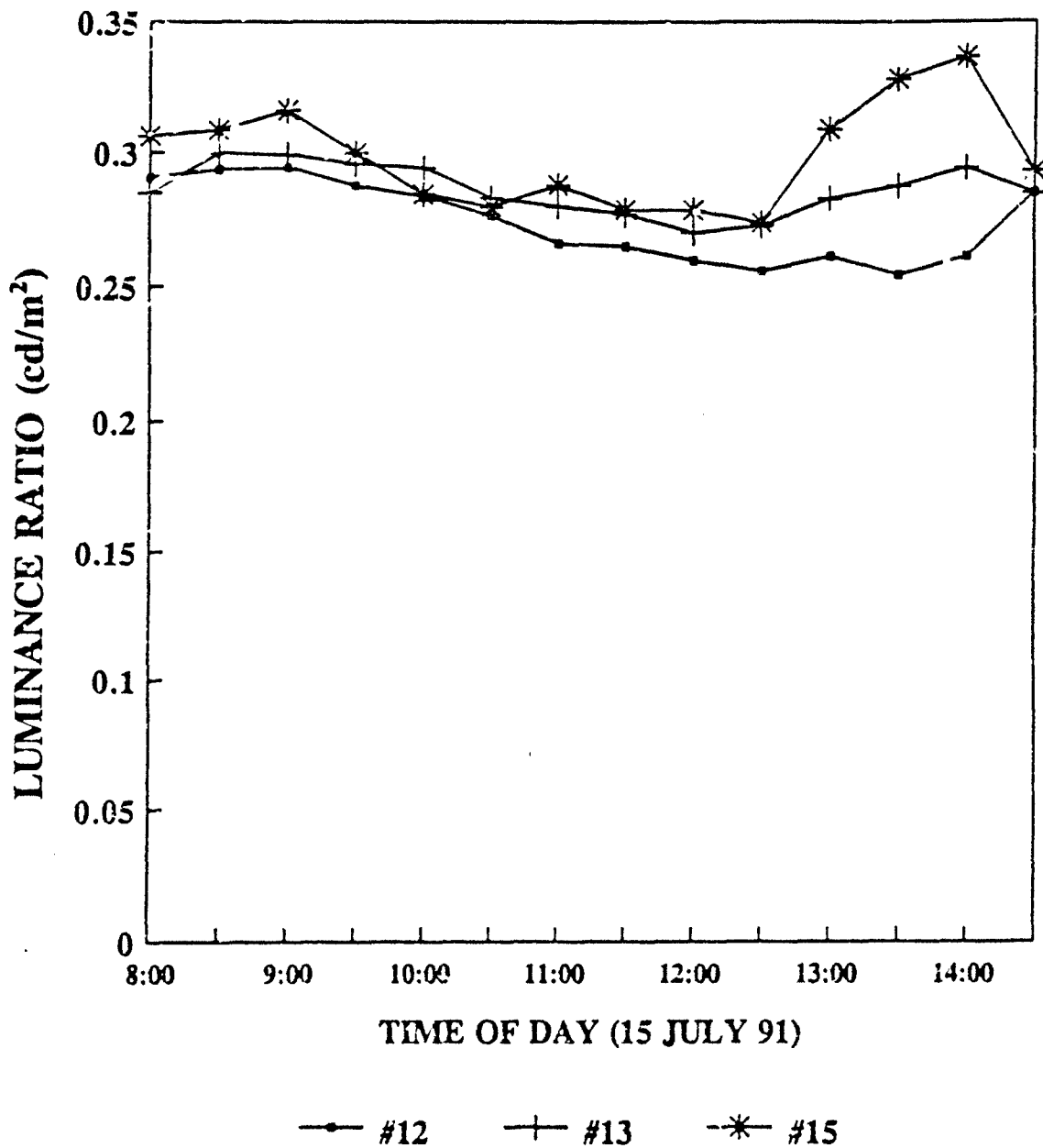


Figure 317

L_{max}/I_n POLARIZATION RATIO
M1A1 FACETS

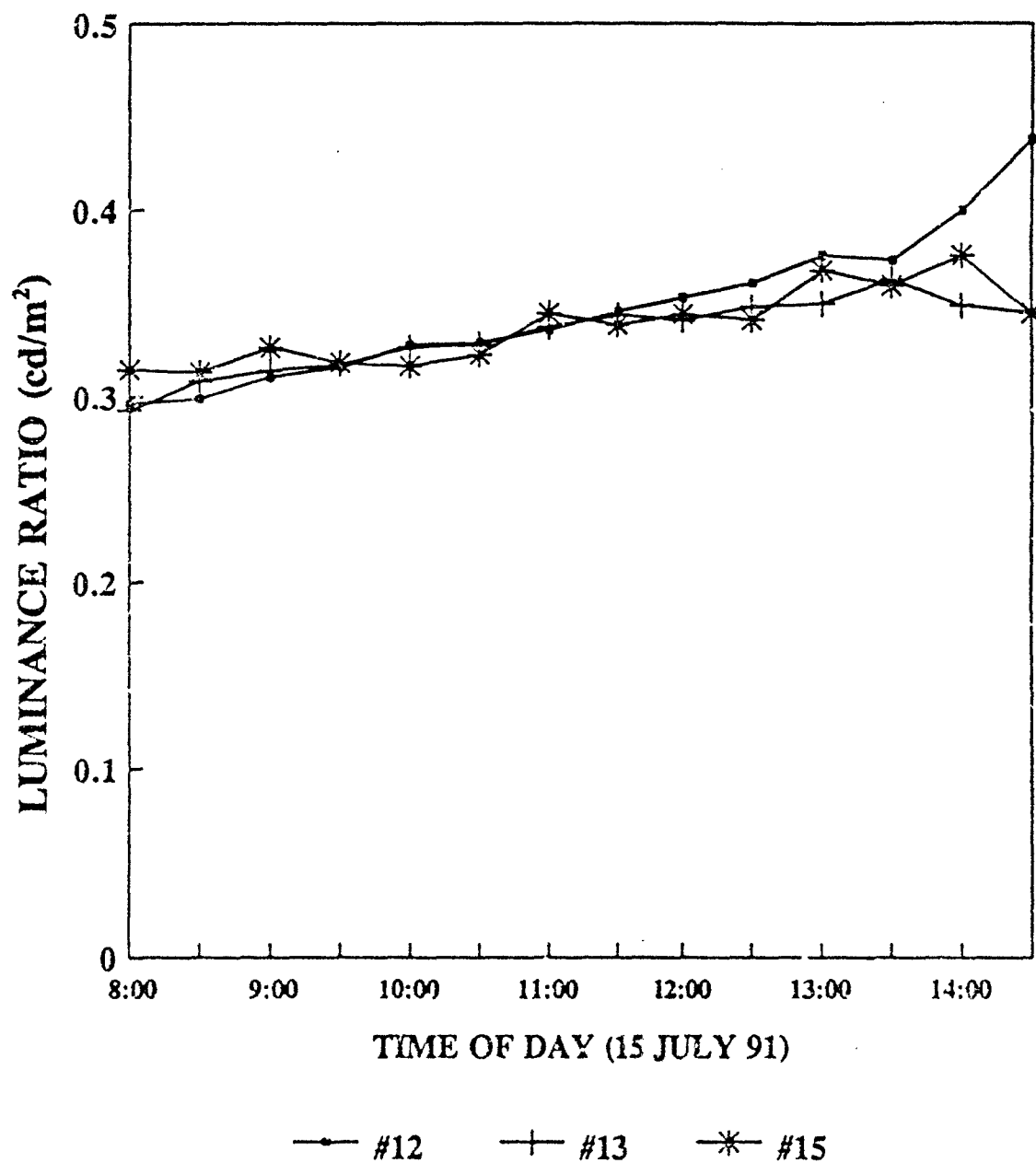


Figure 318

Lmin/Lmax POLARIZATION RATIO
M1A1 FACETS

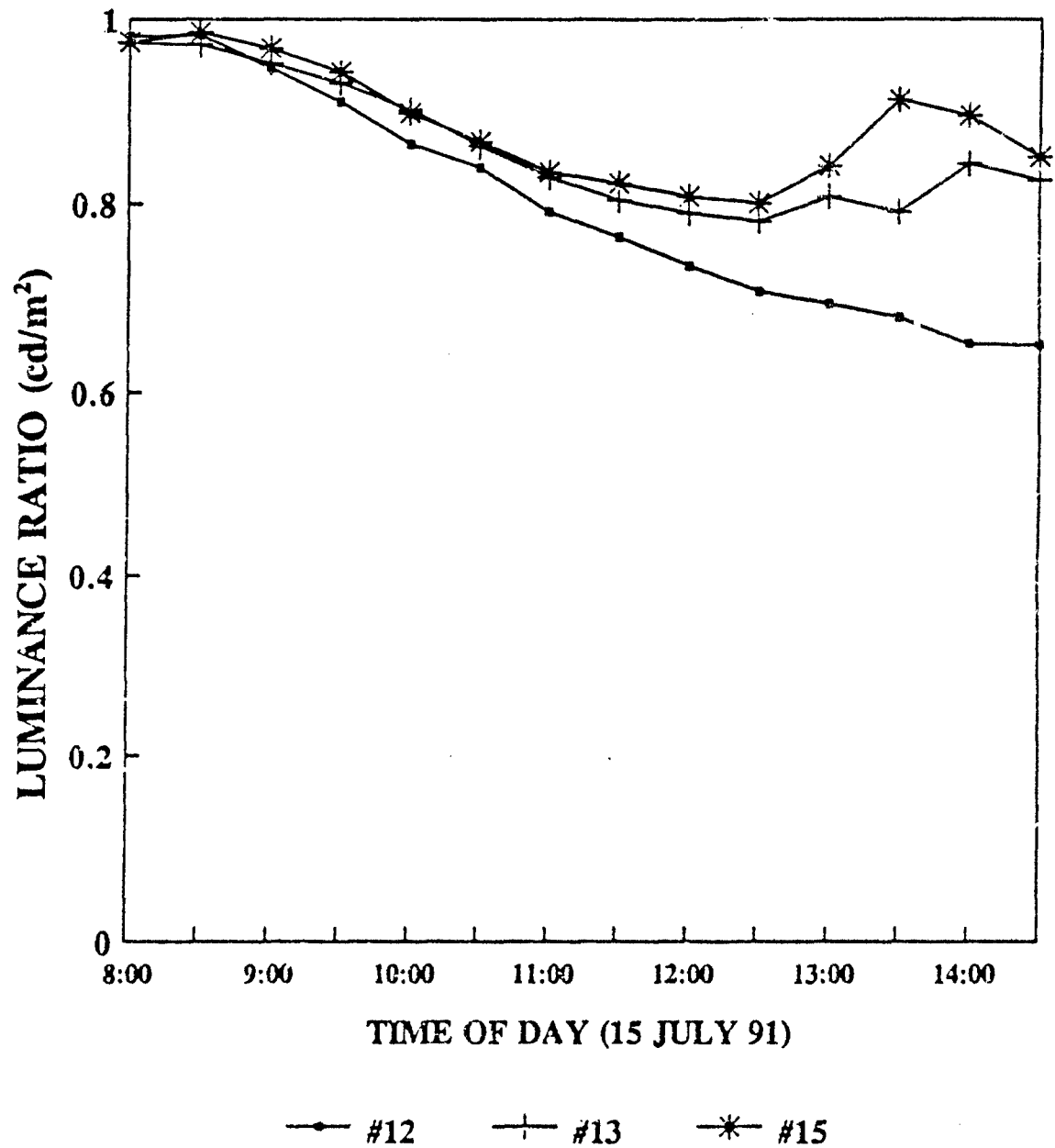


Figure 319

DEGREE OF POLARIZATION M1A1 FACETS

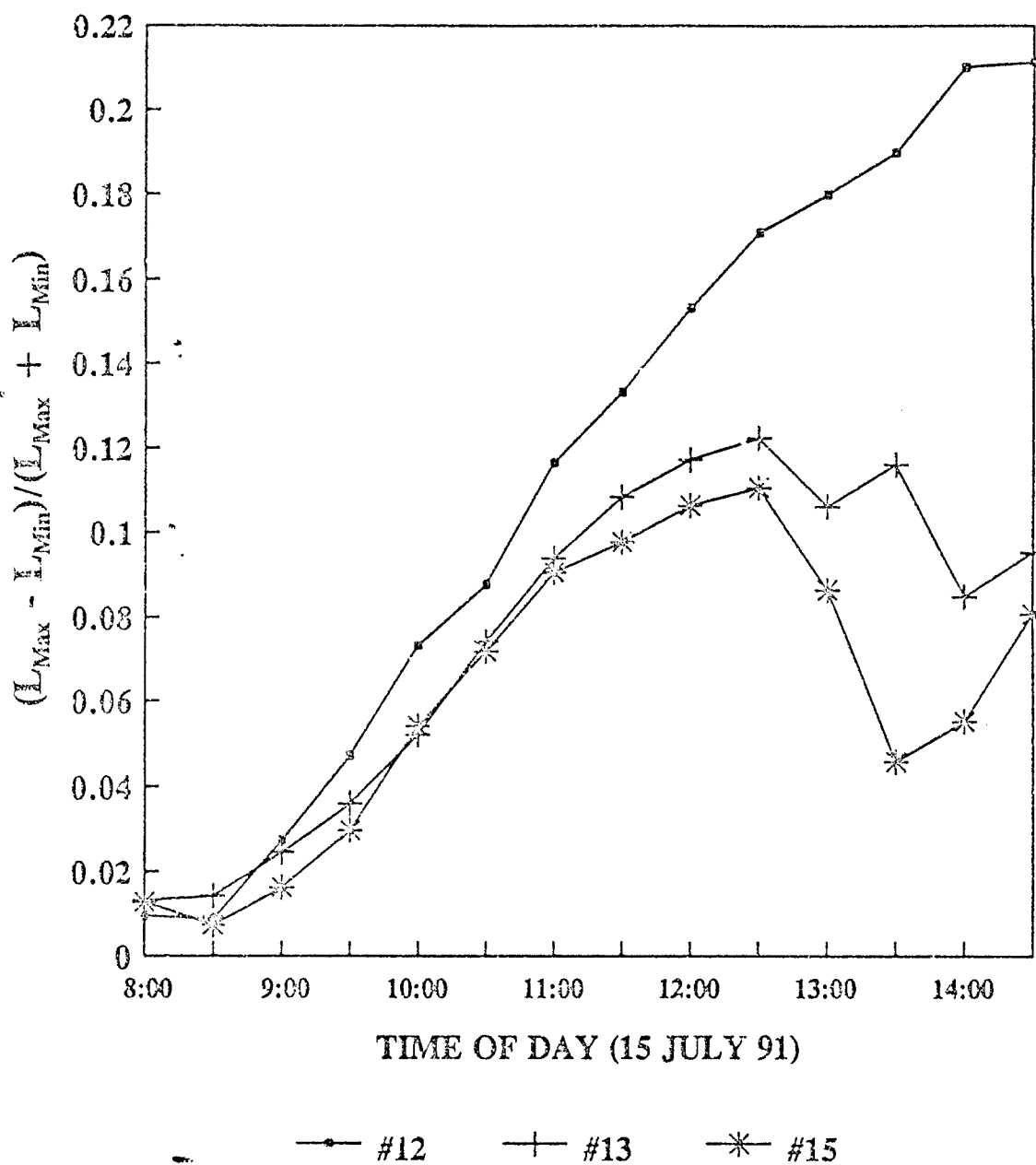


Figure 320

POLARIZATION MIN-MAX DIFFERENCE
M1A1 FACETS

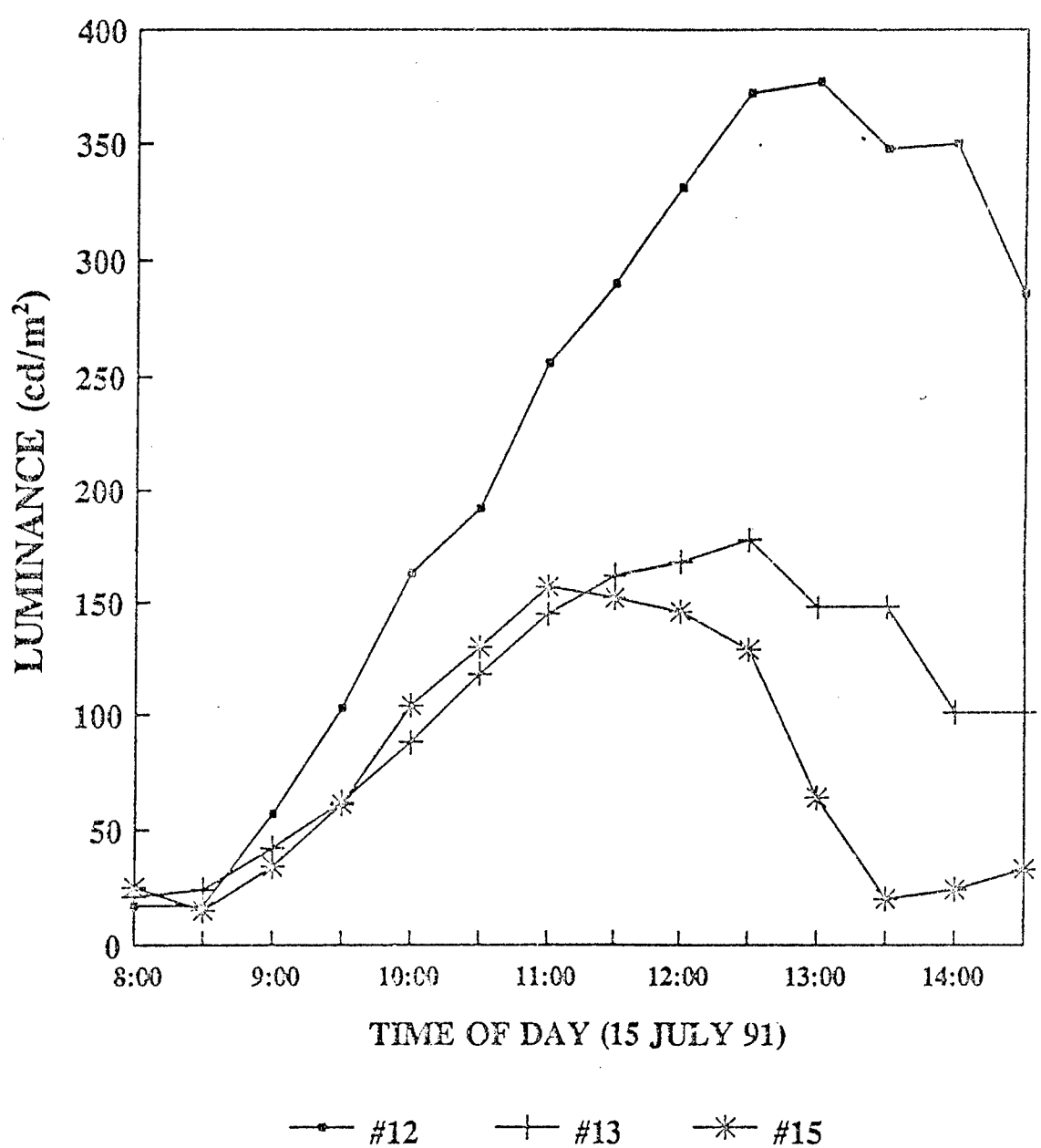


Figure 321

MIN-MAX POLARIZATION ANGLE DIFFERENCE
M1A1 FACETS

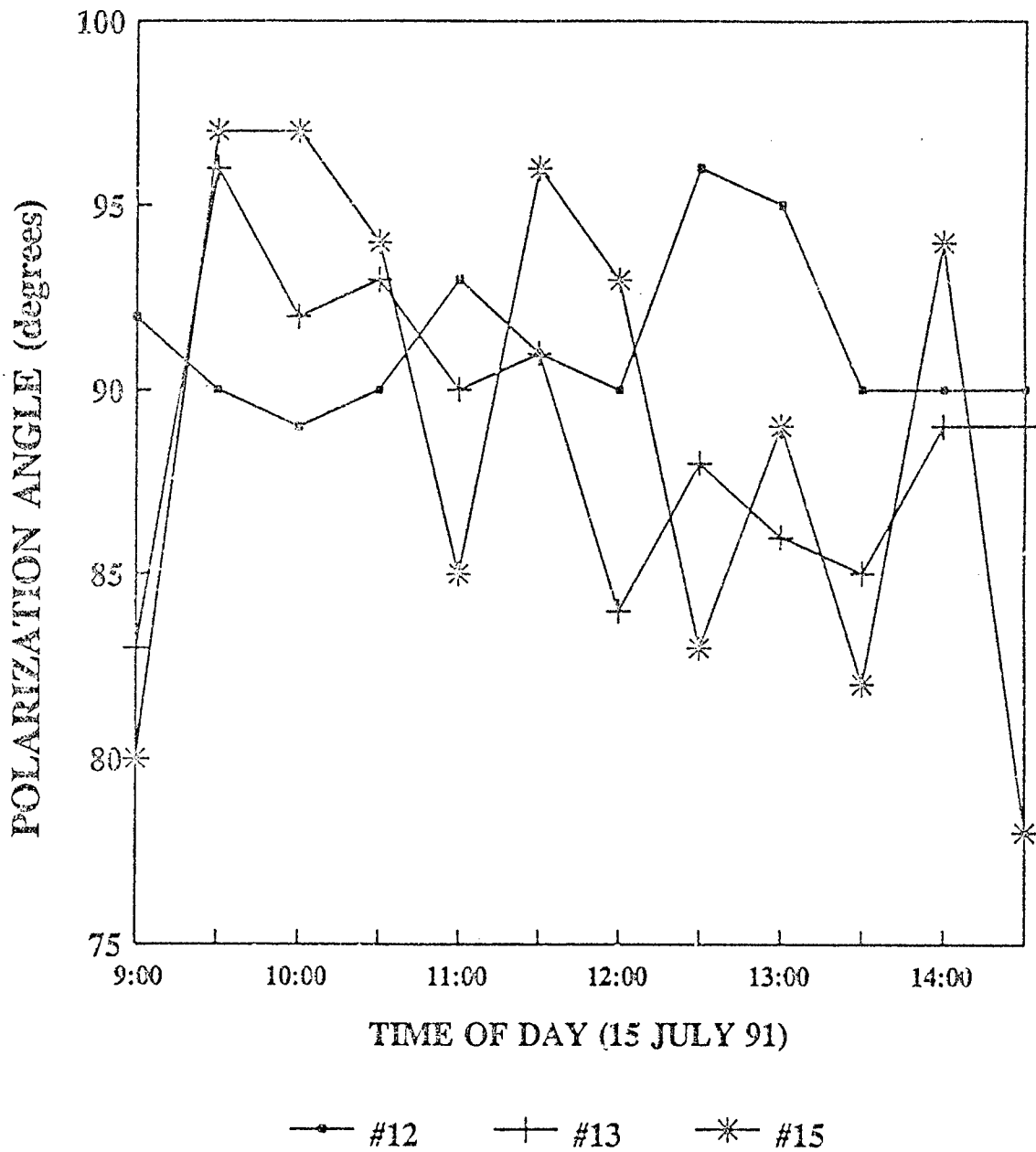


Figure 322

MIN-MAX POLARIZATION ANGLE DIFFERENCE
M1A1 FACETS

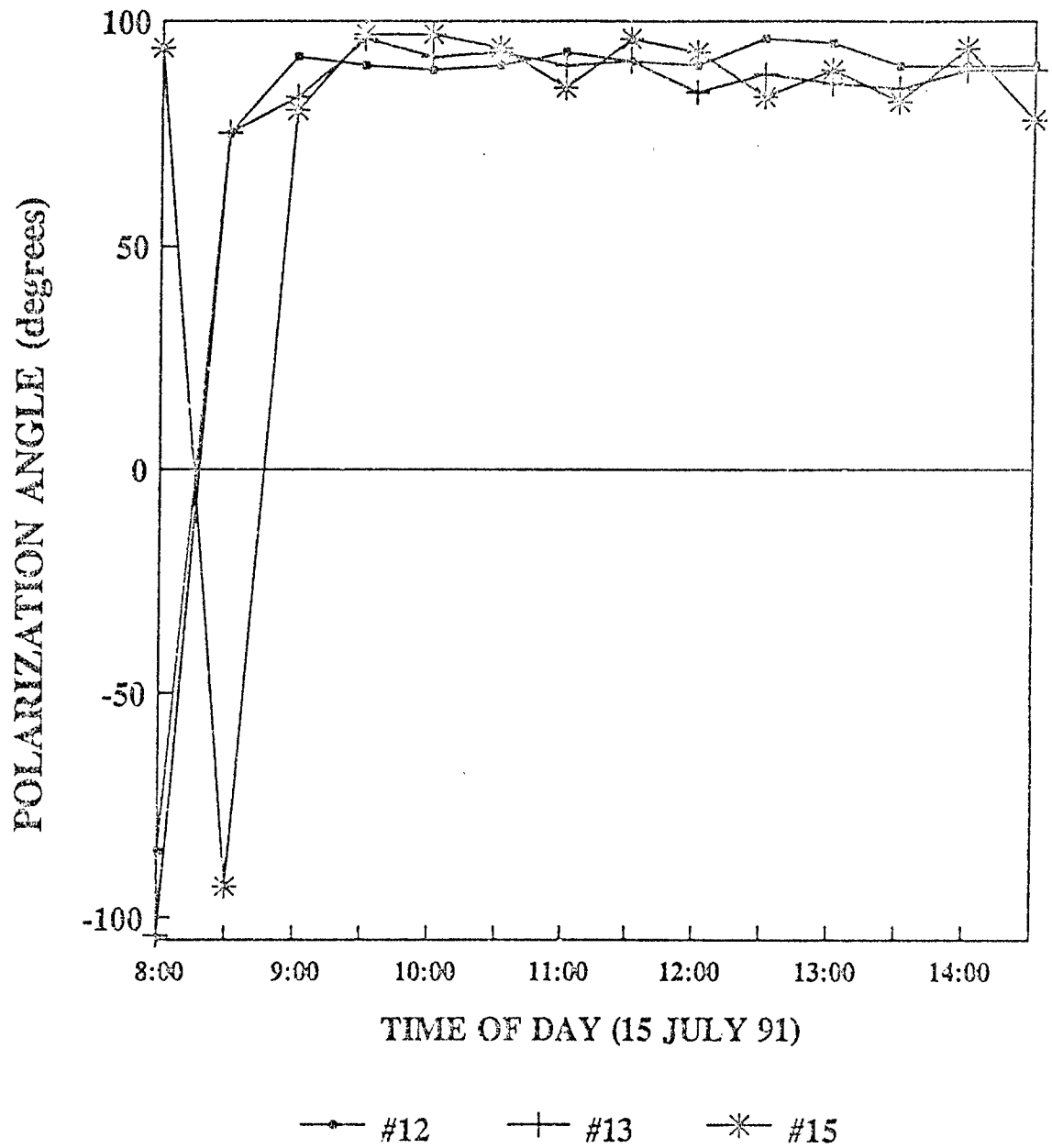


Figure 323

Table 63 Sun's Position and Angles of Incidence on 15 July, 1991

Clear Skies until 12:00, Light Overcast after 12:00

				AREA #12	AREA #13	AREA #15
				SLOPE	SLOPE	SLOPE
				60	60	90
LONGITUDE	83			AZIMUTH	AZIMUTH	AZIMUTH
LATITUDE	42.5			-90	-156	-90
				(270)	(204)	(270)
EDST	ALTITUDE	AZIMUTH	AZIMUTH	<i	<i	<i
08:00	18.4	-102.92	257.08	16.5	49.4	22.3
08:30	23.8	-98.24	261.76	9.6	51.4	25.1
09:00	29.3	-93.45	266.55	3.1	53.6	29.5
09:30	34.8	-88.43	271.57	5.0	56.2	34.9
10:00	40.3	-83.05	276.95	11.8	58.9	40.8
10:30	45.8	-77.08	282.92	18.7	61.7	47.2
11:00	51.1	-70.26	289.74	25.7	64.6	53.8
11:30	56.2	-62.16	297.84	32.7	67.5	60.5
12:00	60.8	-52.19	307.81	39.6	70.4	67.3
12:30	64.8	-39.63	320.37	46.6	73.2	74.2
13:00	67.7	-23.85	336.15	53.5	76.0	81.2
13:30	69.1	-5.22	354.78	60.3	78.6	88.1
14:00	68.7	14.18	14.18	67.1	81.1	95.1
14:30	66.5	31.63	31.63	73.9	83.3	102.1
15:00	63.0	45.87	45.87	80.6	85.3	109.0

NOTES:

<i - angle between sun's rays and the normal to an M1A1 facet (#12, #13 and #15)

The facet represented by Area #15 was facing east. Azimuth is zero for a south orientation. Negative angles represent rotations eastward.

The surface slopes represent angular displacements upward from the horizontal.

Table 64. Angles from Coordinate Axis for M1A1 Area #12 on 15 July, 1991

CLEAR SKIES UNTIL 12:00, LIGHT OVERCAST AFTER 12:00

AREA #12

FACET SLOPE: 60°

FACET AZIMUTH: -90° (EAST)

EDST	INCIDENT RAY			REFLECTED RAY			ANGLE BETWEEN	ANGLE BETWEEN
	+X	+Y	+Z	+X	+Y	+Z	I & L	R & L
08:00	157.7	102.2	71.6	137.3	77.8	49.9	22.3	42.7
08:30	154.9	97.5	66.2	143.4	82.5	54.4	25.1	36.6
09:00	150.5	93.0	60.7	149.2	87.0	59.4	29.5	30.8
09:30	145.1	88.7	55.2	154.8	91.3	64.8	34.9	25.2
10:00	139.2	84.7	49.7	159.9	95.3	70.6	40.8	20.1
10:30	132.8	81.0	44.2	163.9	99.0	76.7	47.2	16.1
11:00	126.2	77.8	38.9	165.8	102.2	82.9	53.8	14.2
11:30	119.5	74.9	33.8	164.9	105.1	89.4	60.5	15.1
12:00	112.7	72.6	29.2	161.6	107.4	95.9	67.3	18.4
12:30	105.8	70.8	25.2	156.8	109.2	102.5	74.2	23.2
13:00	98.8	69.7	22.3	151.4	110.3	109.3	81.2	28.6
13:30	91.9	69.2	20.9	145.6	110.8	116.0	88.1	34.4
14:00	84.9	69.4	21.3	139.7	110.6	122.9	95.1	40.3
14:30	77.9	70.2	23.5	133.6	109.8	129.8	102.1	46.4
15:00	71.0	71.6	27.0	127.5	108.4	136.7	109.0	52.5

NOTES:

X, Y and Z refer to the angles between the incident or reflected rays and the X (west), Y (south) and Z (up) axes.

The angles between I and L or R and L refer to the angles between the incident or reflected rays and the LS-100 luminance meter. The LS-100 was pointing west when measurements were acquired.

Table 65. Angles from Coordinate Axis for M1A1 Area #13 on 15 July, 1991

CLEAR SKIES UNTIL 12:00, LIGHT OVERCAST AFTER 12:00

AREA #13

FACET SLOPE: 60°

FACET AZIMUTH: -156° (204)

EDST	INCIDENT RAY			REFLECTED RAY			ANGLE	ANGLE
	+X	+Y	+Z	+X	+Y	+Z	BETWEEN I & L	BETWEEN R & L
08:00	157.7	102.2	71.6	62.2	144.9	70.4	22.3	117.8
08:30	154.9	97.5	66.2	62.3	149.0	77.2	25.1	117.7
09:00	150.5	93.0	60.7	63.1	152.3	84.1	29.5	116.9
09:30	145.1	88.7	55.2	64.6	154.6	90.8	34.9	115.4
10:00	139.2	84.7	49.7	66.9	155.6	97.5	40.8	113.1
10:30	132.8	81.0	44.2	69.8	155.0	104.0	47.2	110.2
11:00	126.2	77.8	38.9	73.2	153.1	110.4	53.8	106.8
11:30	119.5	74.9	33.8	77.1	150.0	116.6	60.5	102.9
12:00	112.7	72.6	29.2	81.4	146.1	122.5	67.3	98.6
12:30	105.8	70.8	25.2	86.1	141.7	128.0	74.2	93.9
13:00	98.8	69.7	22.3	91.0	136.9	133.1	81.2	89.0
13:30	91.9	69.2	20.9	96.1	131.9	137.4	88.1	83.9
14:00	84.9	69.4	21.3	101.5	126.8	140.9	95.1	78.5
14:30	77.9	70.2	23.5	106.9	121.6	143.2	102.1	73.1
15:00	71.0	71.6	27.0	112.5	116.4	144.1	109.0	67.5

Table 66. Angles from Coordinate Axis for M1A1 Area #15 on 15 July, 1991

CLEAR SKIES UNTIL 12:00, LIGHT OVERCAST AFTER 12:00

AREA #15

FACET SLOPE: 90°

FACET AZIMUTH: -90° (270)

EDST	INCIDENT RAY			REFLECTED RAY			ANGLE	ANGLE
	+X	+Y	+Z	+X	+Y	+Z	BETWEEN I & L	BETWEEN R & L
08:00	157.7	102.2	71.6	157.7	77.8	108.4	22.3	22.3
08:30	154.9	97.5	66.2	154.9	82.5	113.8	25.1	25.1
09:00	150.5	93.0	60.7	150.5	87.0	119.3	29.5	29.5
09:30	145.1	88.7	55.2	145.1	91.3	124.8	34.9	34.9
10:00	139.2	84.7	49.7	139.2	95.3	130.3	40.8	40.8
10:30	132.8	81.0	44.2	132.8	99.0	135.8	47.2	47.2
11:00	126.2	77.8	38.9	126.2	102.2	141.1	53.8	53.8
11:30	119.5	74.9	33.8	119.5	105.1	146.2	60.5	60.5
12:00	112.7	72.6	29.2	112.7	107.4	150.8	67.3	67.3
12:30	105.8	70.8	25.2	105.8	109.2	154.8	74.2	74.2
13:00	98.8	69.7	22.3	98.8	110.3	157.7	81.2	81.2
13:30	91.9	69.2	20.9	91.9	110.8	159.1	88.1	88.1
14:00	NA	NA	NA	NA	NA	NA	95.1	NA
14:30	NA	NA	NA	NA	NA	NA	102.1	NA
15:00	NA	NA	NA	NA	NA	NA	109.0	NA

ALTITUDE AND AZIMUTH
EDST. LONG. = 83 W. LAT. = 42.5 N

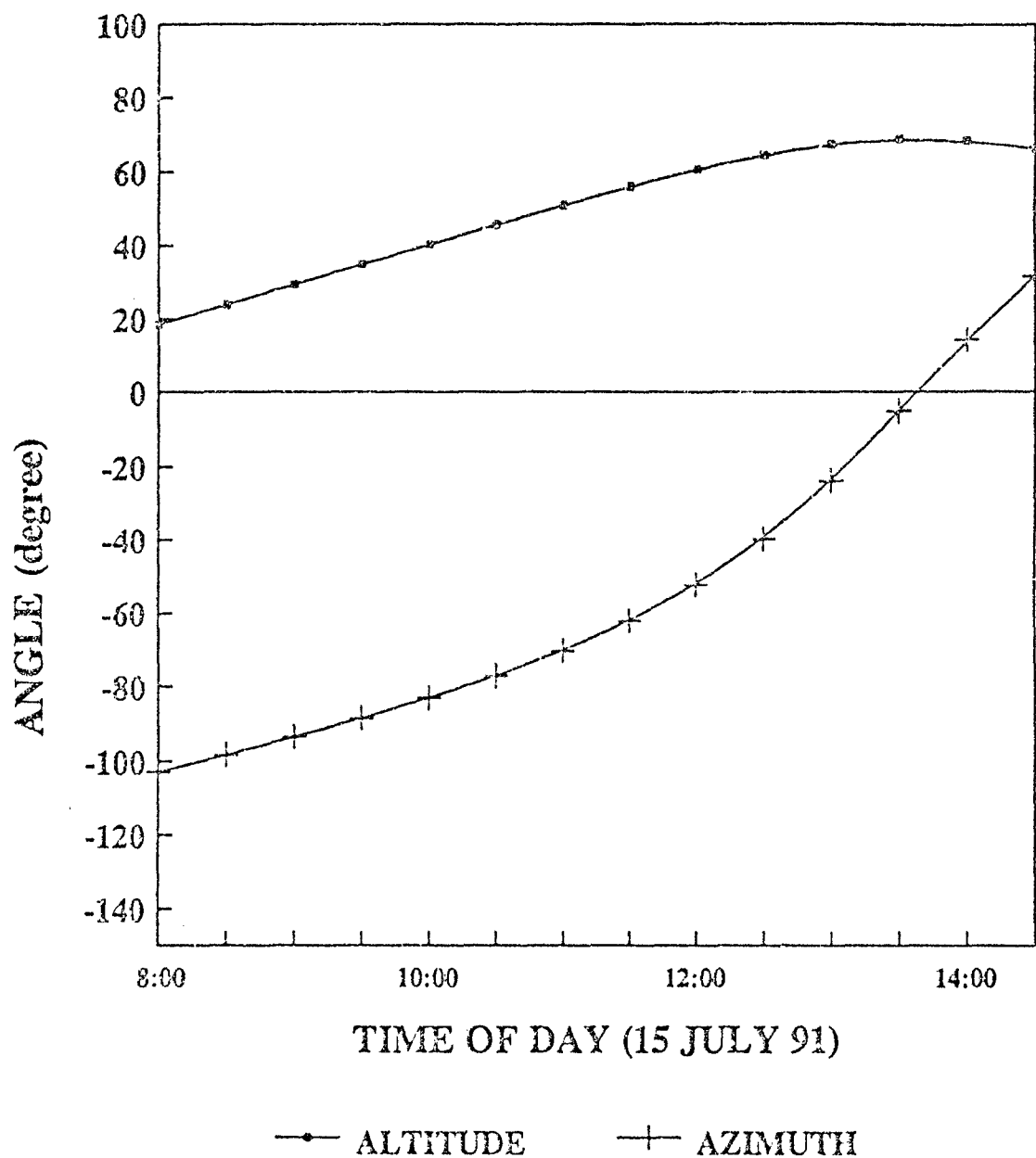


Figure 324

ANGLE BETWEEN I AND METER
EDST. LONG. = 83 W. LAT. = 42.5 N

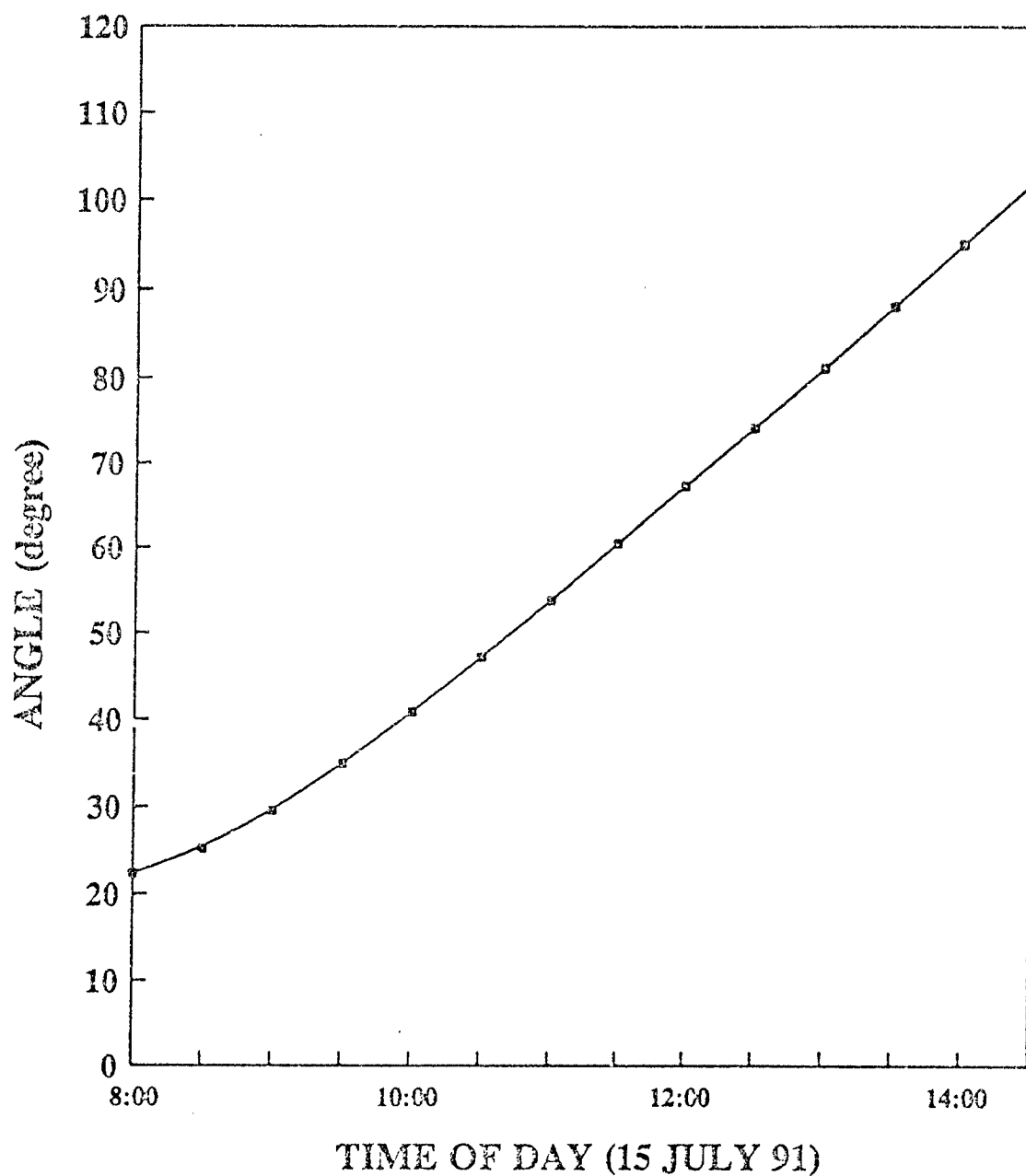


Figure 325

DIURNAL CHANGES IN $\angle i$ AND $\angle RL$
 AREA #12: SLOPE = 60° , AZIMUTH = -90°
 EDST. LONG. = 83° W LAT. = 42.5° N

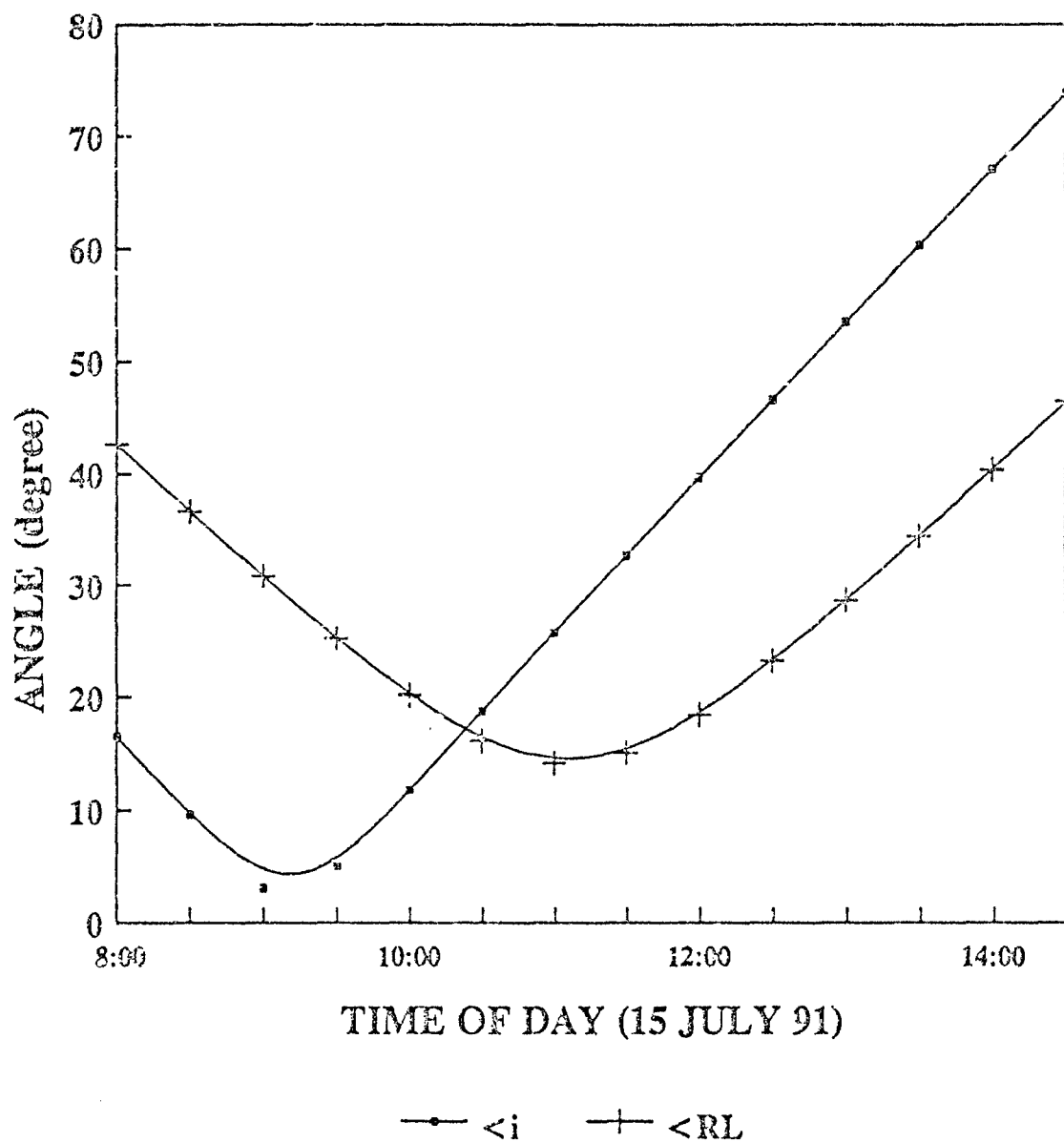


Figure 326

DIURNAL CHANGES IN $\angle i$ AND $\angle RL$
 AREA #13: SLOPE = 60, AZIMUTH = -156
 EDST. LONG. = 83 W LAT. = 42.5 N

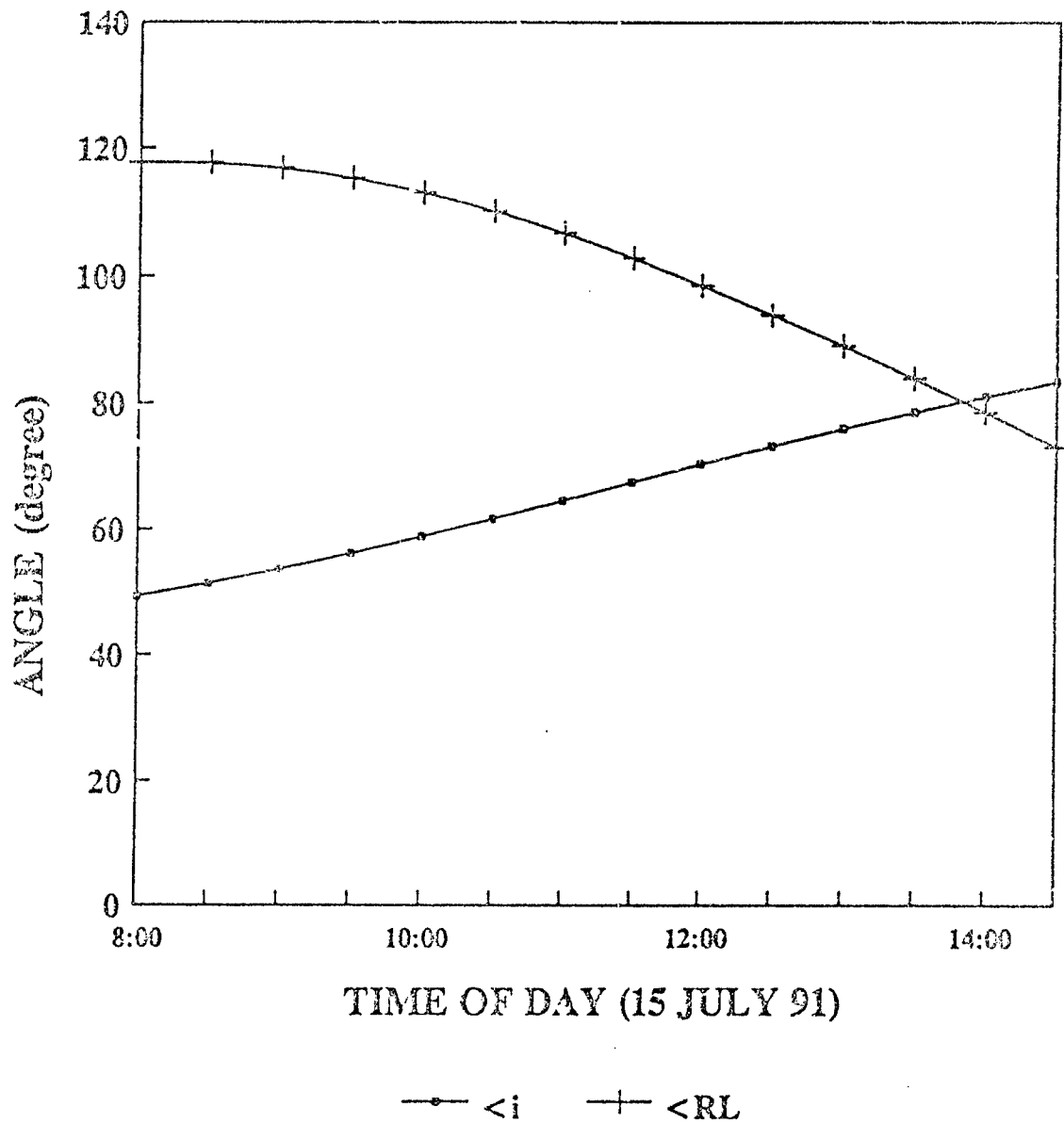


Figure 327

DIURNAL CHANGES IN $\angle i$ AND $\angle RL$
AREA #15: SLOPE = 90, AZIMUTH = -90
EDST. LONG. = 83 W. LAT. = 42.5 N

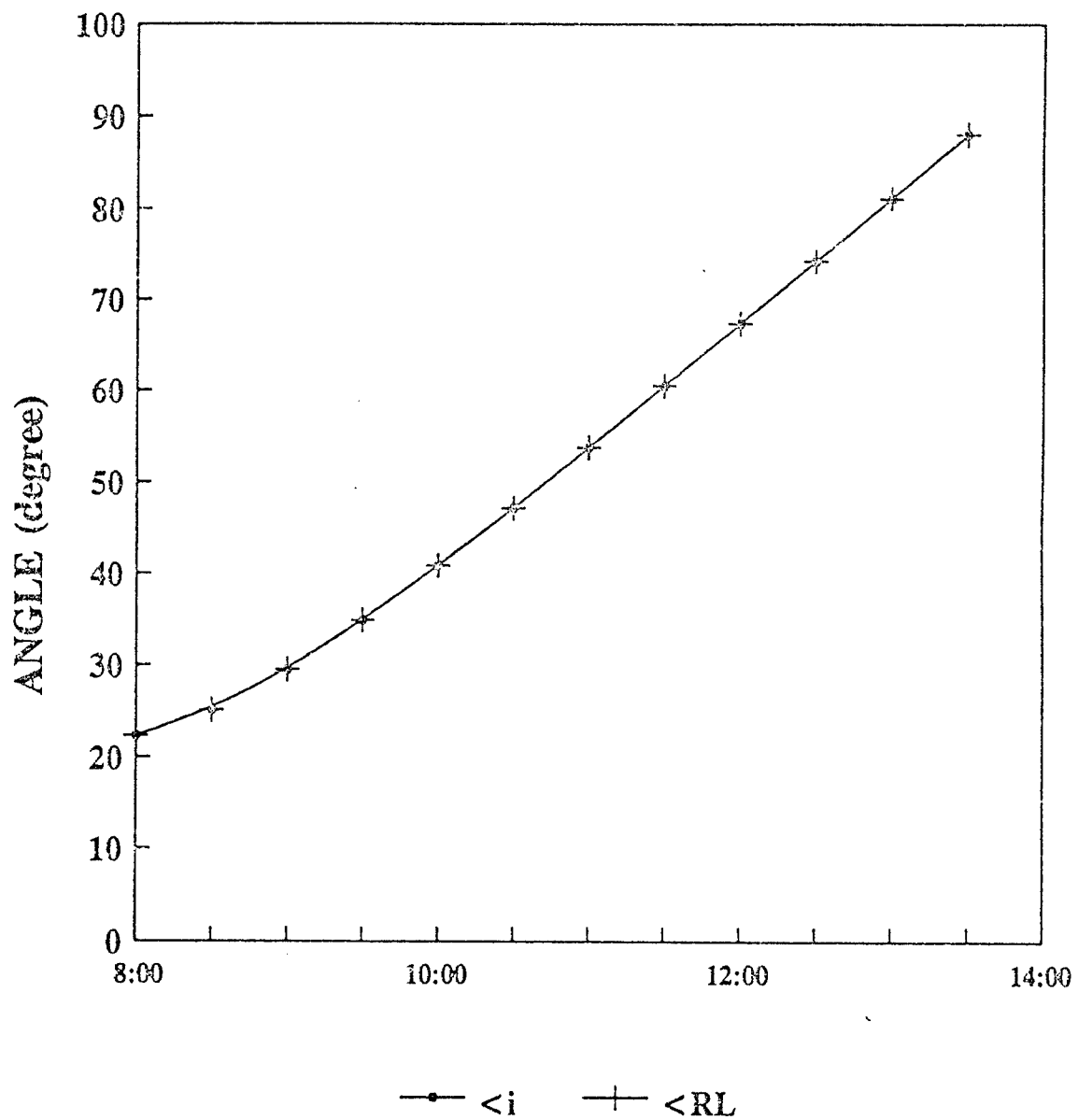


Figure 328

LUMINANCE vs ANGLE RL
M1A1 AREAS; 8:00 - 14:00
15 JULY, 1991; CLEAR SKIES

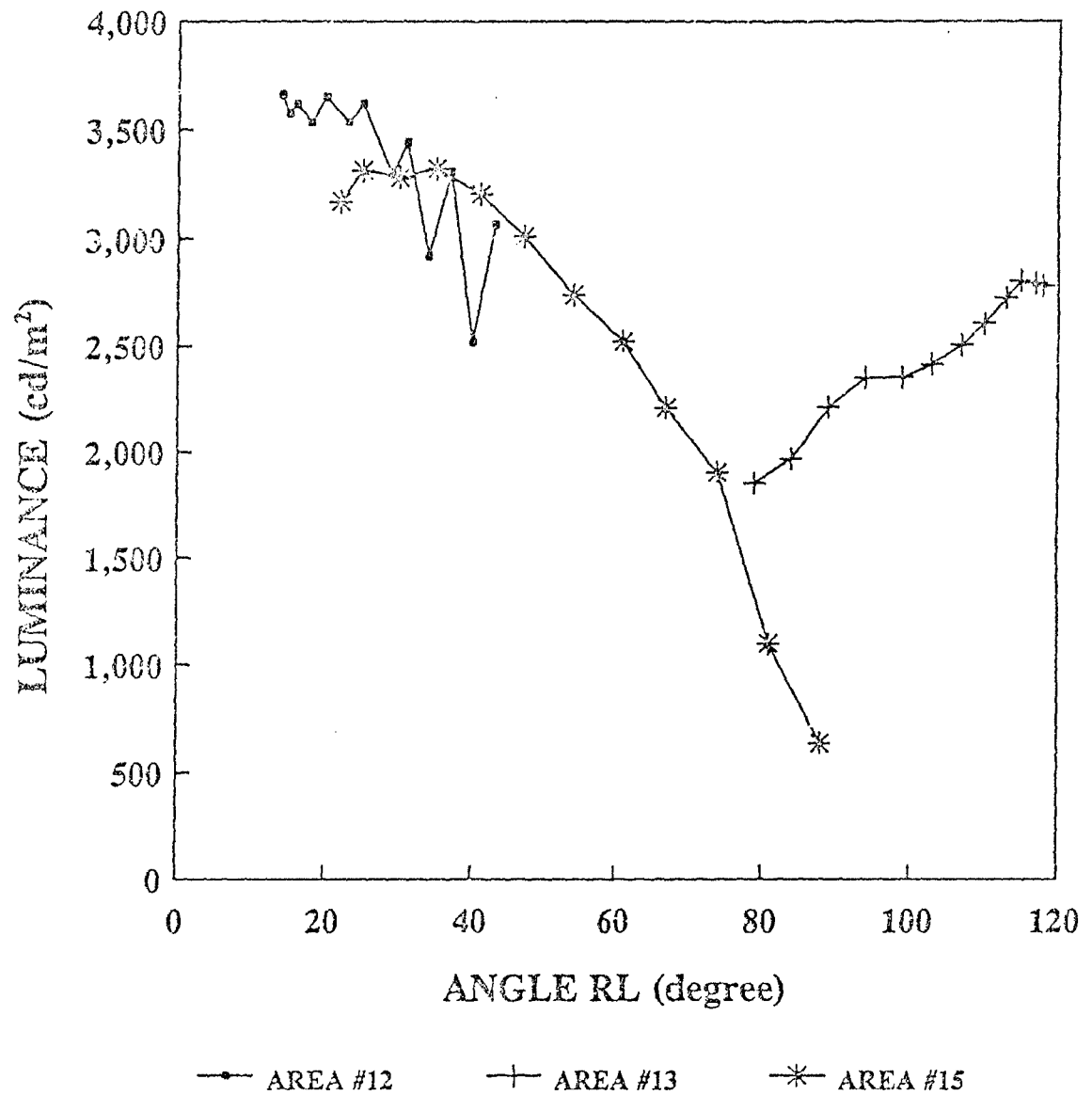


Figure 329

LUMINANCE VS SUN-METER ANGLE

M1A1 AREAS; 8:00 - 14:00
15 JULY, 1991; CLEAR SKIES

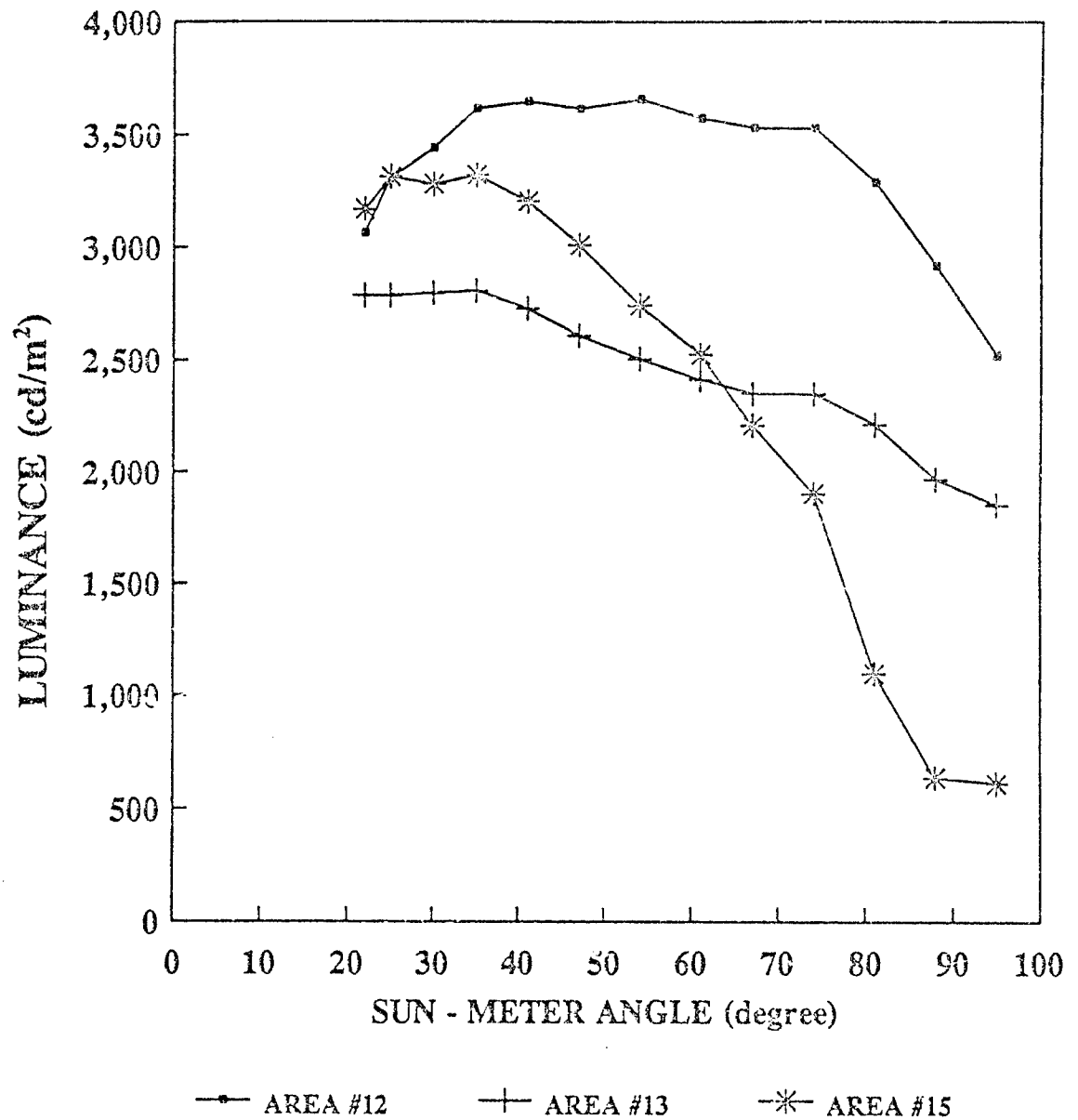


Figure 330

LUMINANCE vs ANGLE OF INCIDENCE M1A1 AREAS; 8:00 - 14:00 15 JULY 91; CLEAR SKIES

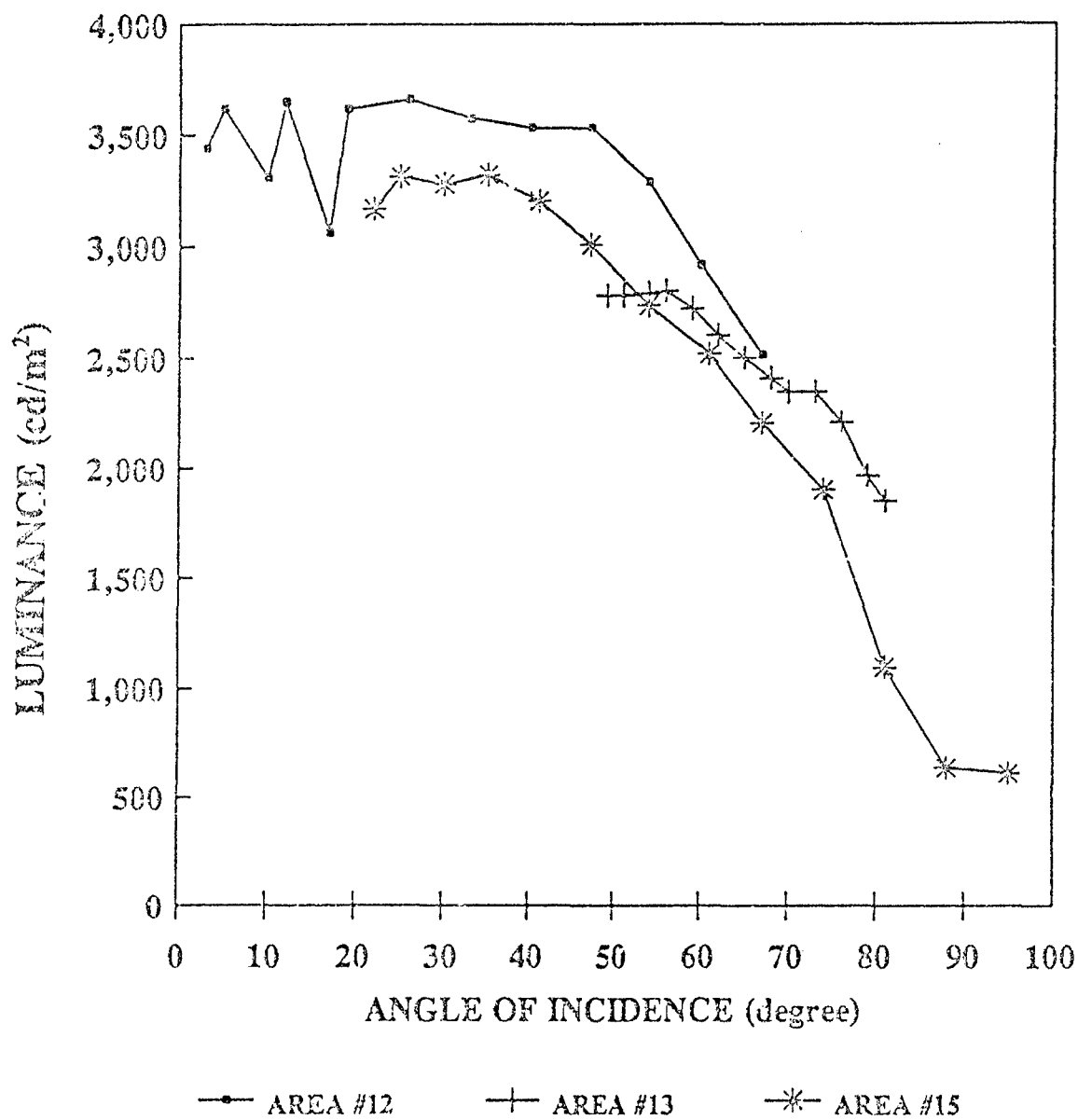


Figure 331

LUMINANCE vs COS i
M1A1 AREAS; 8:00 - 14:00
15 JULY 91; CLEAR SKIES

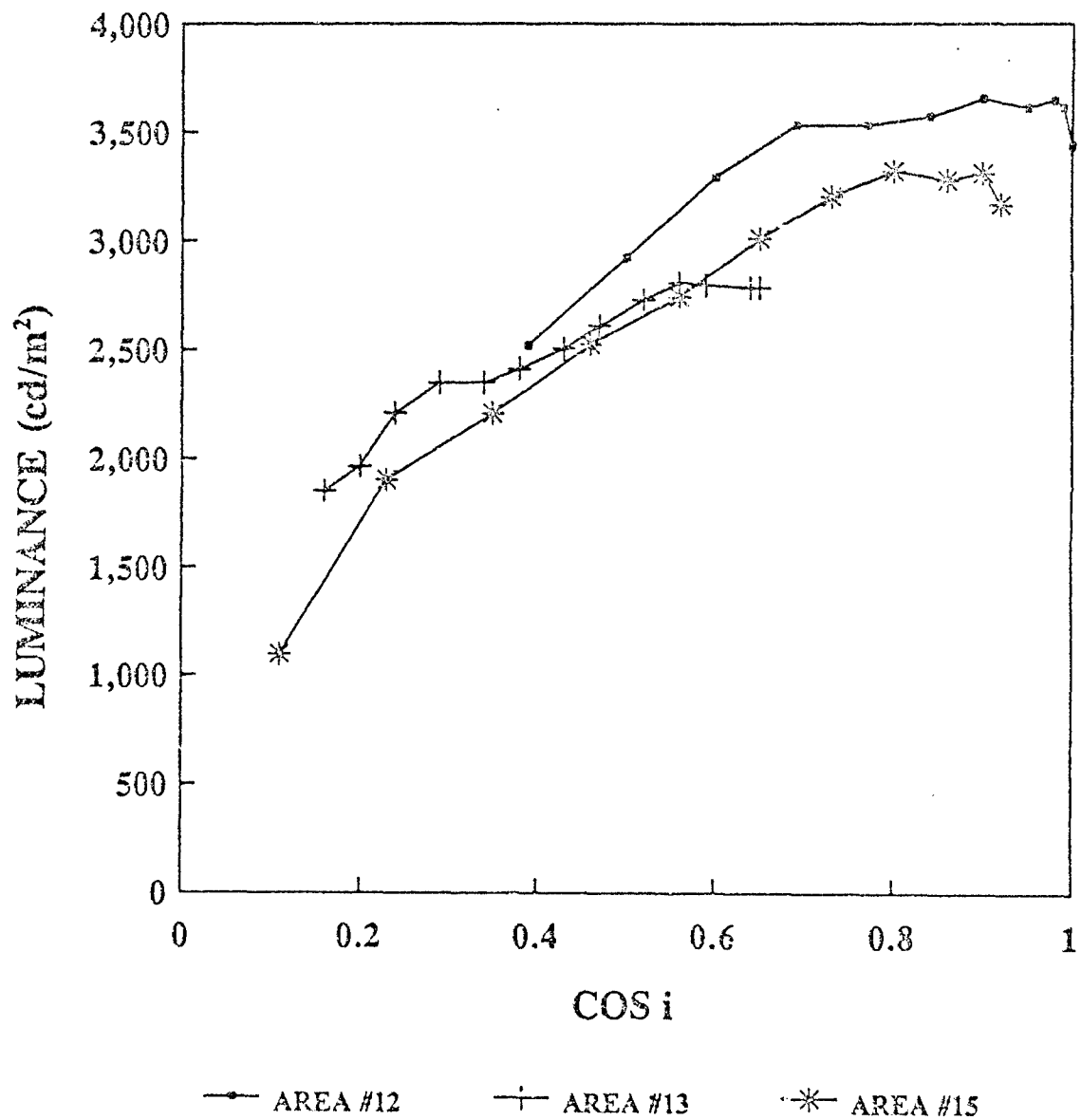


Figure 332

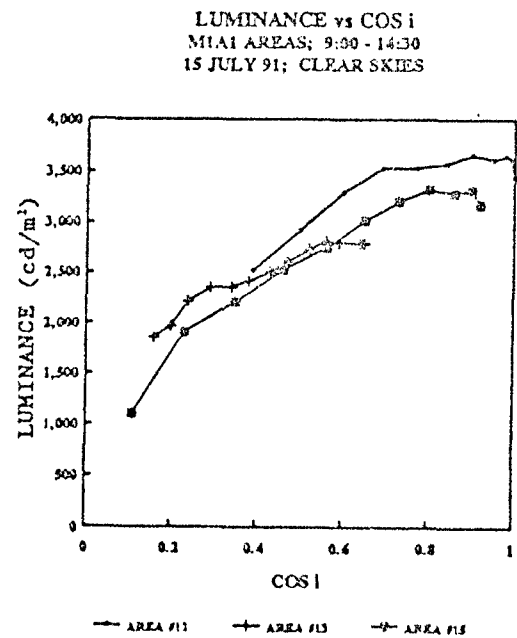
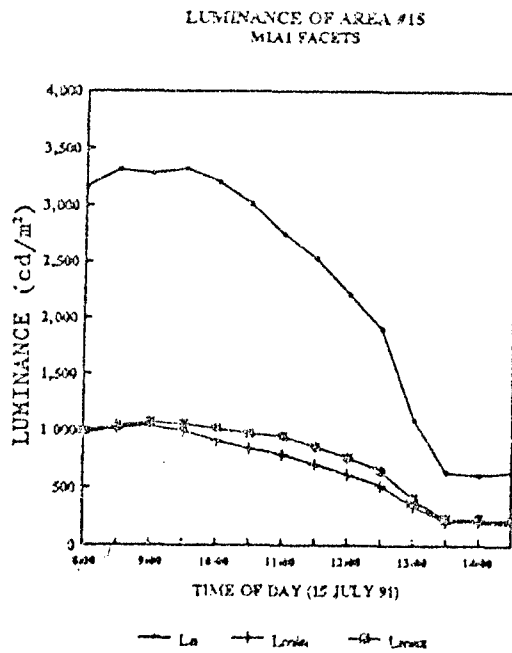
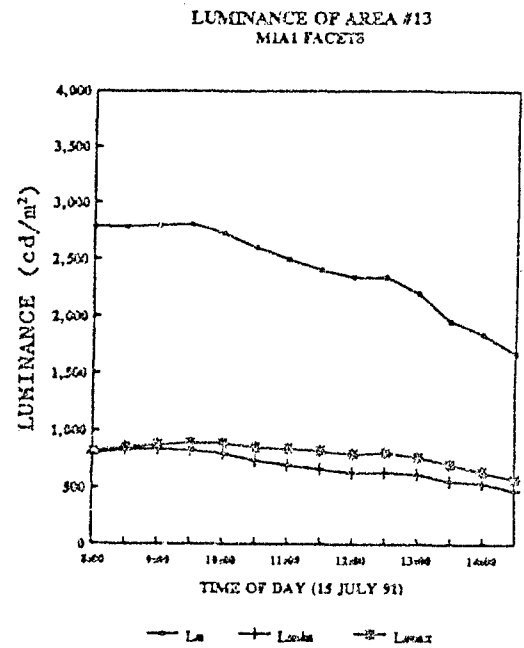
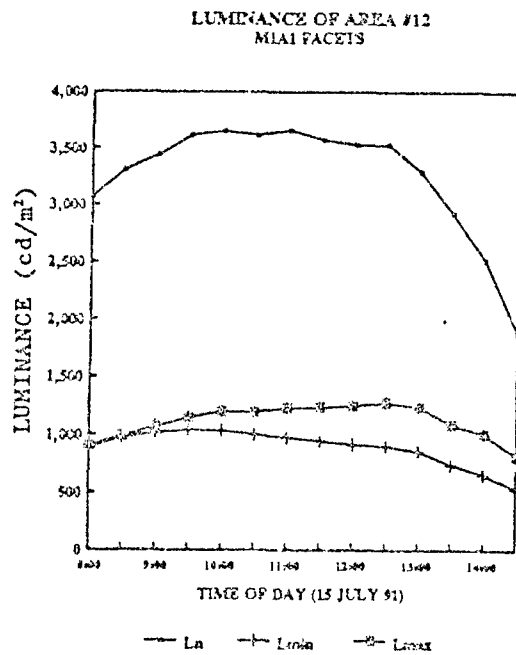


Figure 333

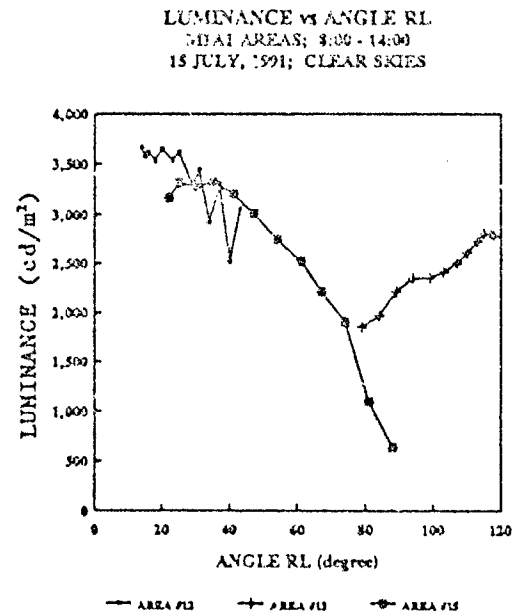
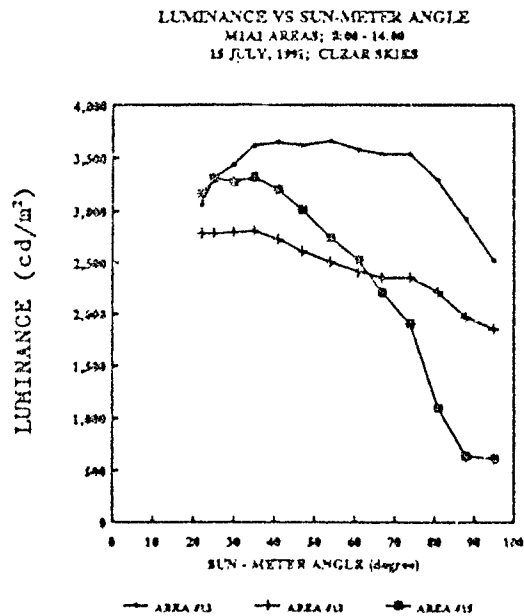
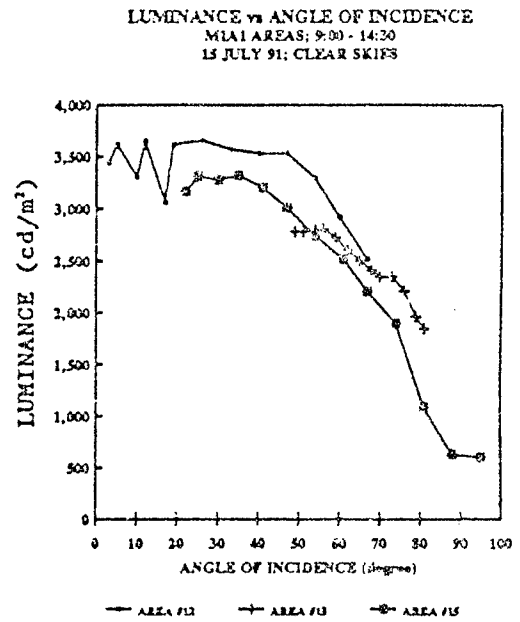
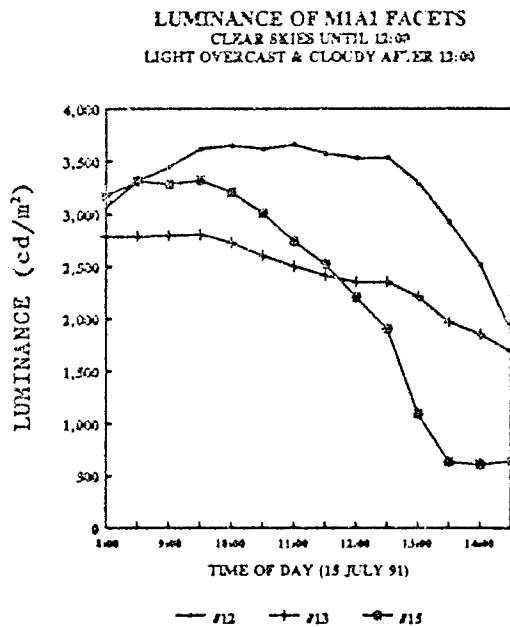


Figure 334

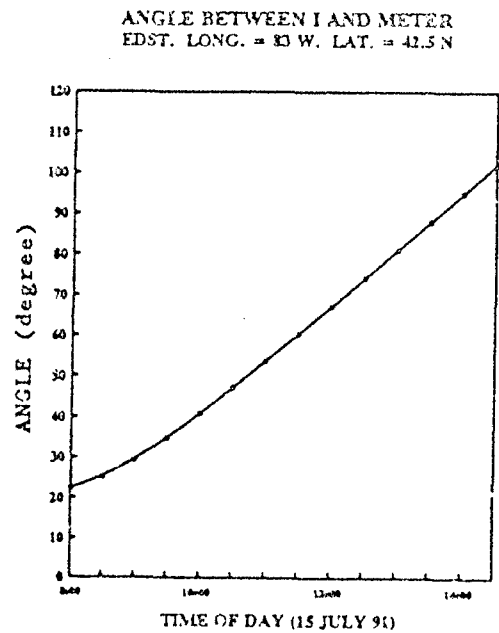
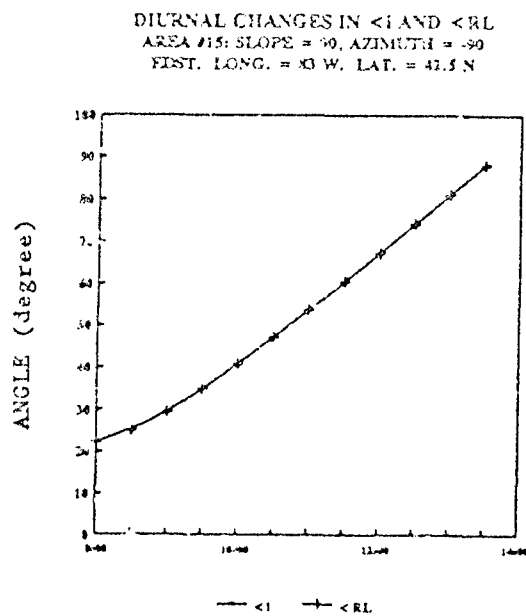
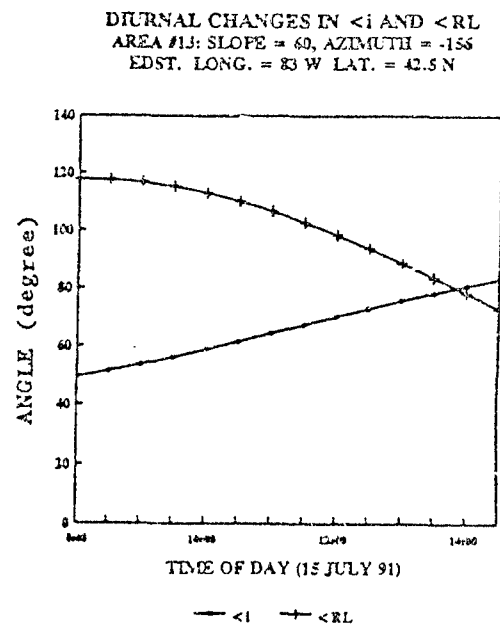
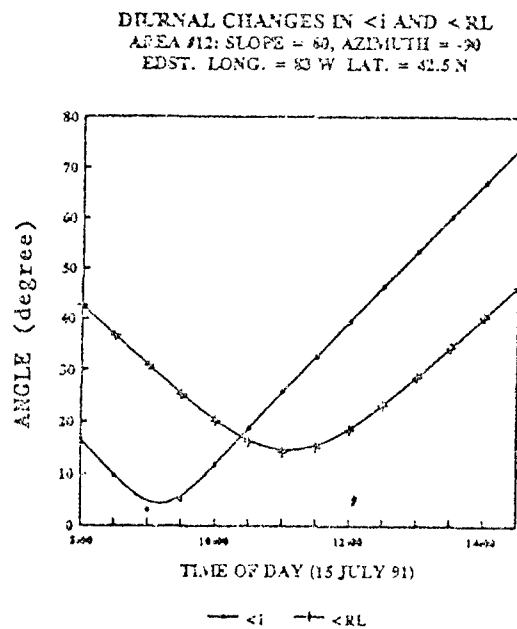


Figure 335

Table 67. CIE Coordinates for M1A1 Facets on 15 July, 1991

TIME	M1A1 AREA #12			M1A1 AREA #13		
	L	X	Y	L	X	Y
08:00	2740	0.354	0.383	2500	0.347	0.376
08:30	3080	0.347	0.378	2770	0.341	0.371
09:00	3280	0.344	0.375	2850	0.338	0.368
09:30	3480	0.342	0.373	2900	0.336	0.366
10:00	3560	0.341	0.372	2830	0.335	0.365
10:30	3520	0.341	0.371	2720	0.334	0.364
11:00	3490	0.340	0.370	2630	0.333	0.363
11:30	3490	0.339	0.368	2520	0.332	0.362
12:00	3480	0.338	0.366	2420	0.331	0.360
12:30	3520	0.336	0.364	2440	0.329	0.358
13:00	3280	0.336	0.363	2310	0.329	0.356
13:30	2950	0.334	0.381	2100	0.327	0.354
14:00	2560	0.332	0.359	1990	0.325	0.352
14:45	1870	0.330	0.356	1770	0.323	0.349

TIME	M1A1 AREA #15		
	L	X	Y
08:00	2910	0.360	0.378
08:30	3270	0.352	0.372
09:00	3310	0.349	0.369
09:30	3370	0.346	0.367
10:00	3210	0.345	0.366
10:30	3010	0.345	0.366
11:00	2780	0.343	0.364
11:30	2580	0.343	0.363
12:00	2200	0.342	0.362
12:30	1950	0.340	0.360
13:00	1330	0.338	0.358
13:30	740	0.330	0.351
14:00	574	0.327	0.350
14:45	621	0.331	0.353

NOTES:

Readings from Minolta CS-100.

Clear Skies Until 12:00. Light Overcast & Cloudy After 12:00.

L - Luminance; X,Y - CIE Coordinates.

M1A1 Range - 36 Feet. Grass Range - 40 Feet. Height - 5 Feet.

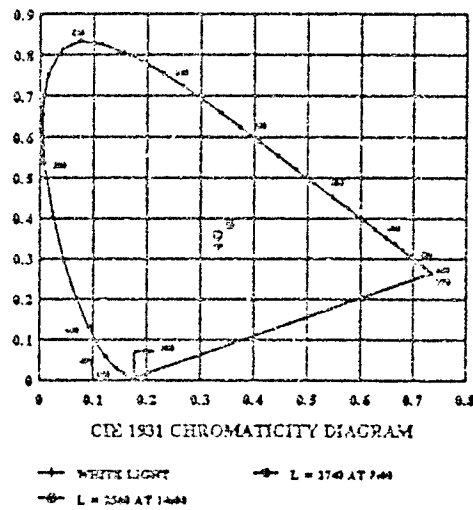
TEST CARD (FRESHLY PAINTED WITH 4 COATS OF WHITE TEMPRA PAINT):
L - 18,700 cd/m² X - 0.327 Y - 0.343

Table 68. CIE Coordinates for Grass and Trees on 15 July, 1991

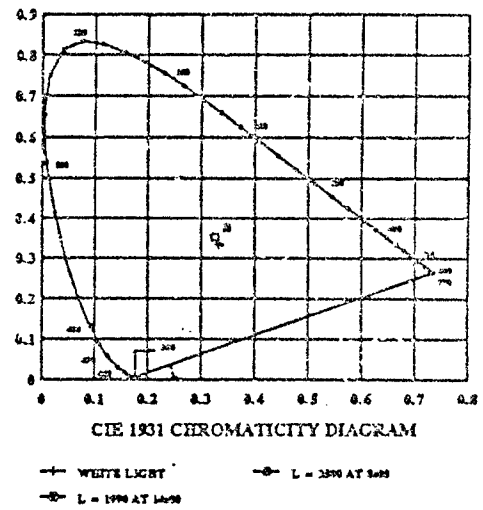
TIME	GRASS			TREE #1		
	L	X	Y	L	X	Y
08:00	2650	0.387	0.426	738	0.356	0.421
08:30	3120	0.382	0.426	743	0.349	0.414
09:00	3300	0.380	0.424	698	0.344	0.410
09:30	3530	0.378	0.425	688	0.343	0.408
10:00	3400	0.379	0.421	616	0.340	0.403
10:30	3340	0.378	0.425	528	0.337	0.398
11:00	3350	0.377	0.425	459	0.332	0.396
11:30	3170	0.378	0.423	466	0.332	0.395
12:00	2200	0.342	0.362	441	0.329	0.391
12:30	3330	0.378	0.419	392	0.324	0.380
13:00	3200	0.379	0.423	359	0.321	0.378
13:30	3110	0.379	0.415	334	0.316	0.372
14:00	3040	0.380	0.423	277	0.308	0.350
14:45	3070	0.383	0.428	287	0.303	0.345

TIME	TREE #2			TREE #3		
	L	X	Y	L	X	Y
08:00	844	0.357	0.425	851	0.360	0.430
08:30	827	0.353	0.417	864	0.354	0.422
09:00	794	0.351	0.412	788	0.352	0.416
09:30	734	0.350	0.409	732	0.348	0.413
10:00	731	0.347	0.406	674	0.346	0.408
10:30	652	0.346	0.404	563	0.343	0.403
11:00	532	0.344	0.399	397	0.338	0.396
11:30	430	0.339	0.394	307	0.331	0.386
12:00	378	0.333	0.380	266	0.322	0.378
12:30	339	0.330	0.382	236	0.320	0.376
13:00	325	0.321	0.377	281	0.317	0.371
13:30	304	0.318	0.371	280	0.316	0.369
14:00	300	0.314	0.364	311	0.316	0.364
14:45	290	0.307	0.350	320	0.311	0.355

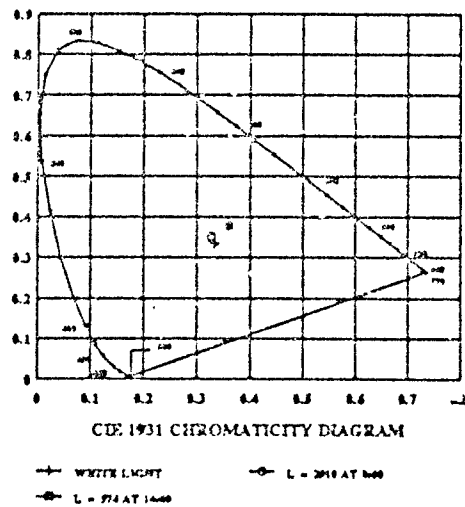
MIAI AREA #12
15 JULY, 1991
8:00 AND 14:00



MIAI AREA #13
15 JULY, 1991
8:00 AND 14:00



MIAI AREA #15
15 JULY, 1991
8:00 AND 14:00



GRASS AREA
15 JULY, 1991
8:00 AND 14:00

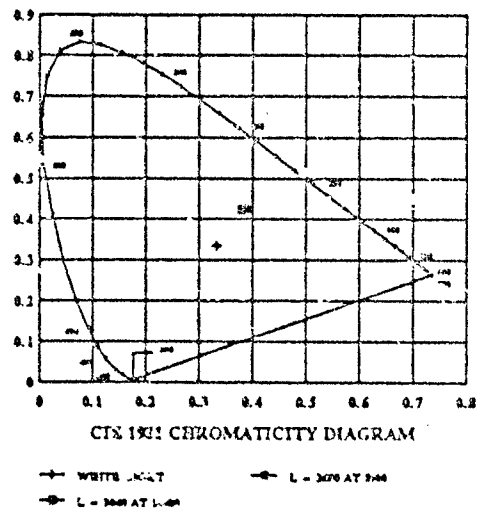
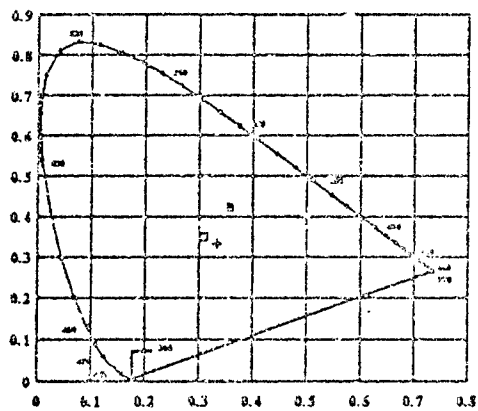


Figure 336

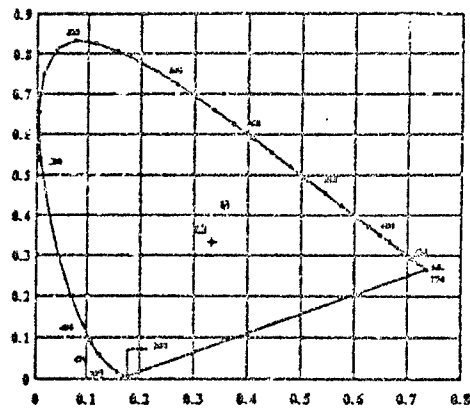
TREE AREA #1
15 JULY, 1991
8:00 AND 14:00



CIE 1931 CHROMATICITY DIAGRAM

—+— WHITE LIGHT —●— L = 75 AT 8:00
—○— L = 27 AT 14:00

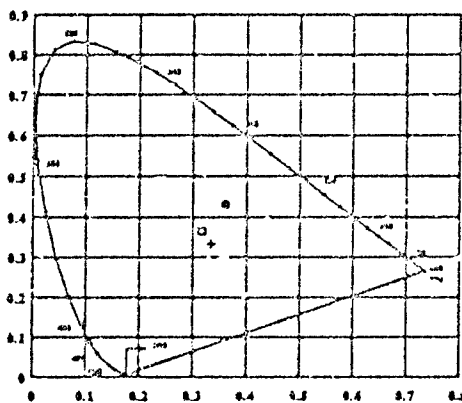
TREE AREA #2
15 JULY, 1991
8:00 AND 14:00



CIE 1931 CHROMATICITY DIAGRAM

—+— WHITE LIGHT —●— L = 54 AT 8:00
—○— L = 36 AT 14:00

TREE AREA #2
15 JULY, 1991
8:00 AND 14:00



CIE 1931 CHROMATICITY DIAGRAM

—+— WHITE LIGHT —●— L = 54 AT 8:00
—○— L = 36 AT 14:00

Figure 337

ANALYSIS OF 15 JULY, 1991 STUDY

Table 69 lists the maximum luminance reading acquired for each of the three M1A1 facets measured and the times for which these maximums occur. These values are comparable to those obtained in other studies (Table 50).

As was found in the 20 June, 1991 study, with the M1A1 oriented along a north-south line, large scale shading occurs for all vertical facets (skirt area)

also oriented along a north-south line when the sun crosses the meridian (13:30 EDST). The contrast variation produced by this shading, between Area #12 (turret) and Area #15 (skirt), ranges from -0.03 at 8:00 to 3.59 at 13:30 (Table 57 and Table 59). This contrast variation increases the visibility of the vehicle and produces a visual signature.

The axis of polarization which produced a minimum luminance reading had an orientation of approximately 80° from the horizontal. In other words, the transmission axis of the polarizer was nearly vertical for minimum readings. This was found to be true for all three M1A1 facets studied and for all times during the day except during the early morning hours (8:00 - 9:00) when the sun was in the eastern sky (Figure 315). Since the region of the sky near the sun produces little polarized light (Figure 307), the sunlight reflected from a north-south oriented vehicle during the times 8:00 to 10:00 EDST is mostly unpolarized light. This accounts for the difficulty in determining minimum and maximum polarization angles during this time of the day.

The axis of polarization which produced a maximum luminance reading had an orientation of approximately -10° from the horizontal. In other words, the transmission axis of the polarizer was nearly horizontal for maximum readings. This was found to be true for all three M1A1 facets studied and for all times during the day except during the early morning hours (8:00 - 9:00) when the sun was in the eastern sky (Figure 316).

Table 60, Table 61 and Figure 320 give the calculated degree of polarization obtained for the three M1A1 surface areas studied. The degree of polarization is given by

$$\frac{L_{MAX} - L_{MIN}}{L_{MAX} + L_{MIN}}$$

where L_{MAX} and L_{MIN} are the maximum and minimum luminance readings obtained while rotating a linear polarizer in front of the luminance meter.

Table 69. Maximum Luminance

Area #	L_{MAX}	Time
12	3659	11:00
13	2807	9:30
15	3321	9:30

For turret Area #12, the degree of polarization increased from 0.01 to 0.21 during the time interval from 8:00 to 14:00.

For turret Area #13, the degree of polarization increased from 0.01 to 0.12 during the time interval from 8:00 to 12:30. It then decreased from 0.12 to 0.09 during the time interval from 12:30 to 14:00.

For skirt Area #15, the degree of polarization increased from 0.01 to 0.11 during the time interval from 8:00 to 12:30. It then decreased from 0.11 to 0.05 during the one hour time interval from 12:30 to 13:30; rising again after the sun crossed the meridian (13:30 EDST) to a value of .08 at 14:45.

The sky polarization photographs of Figure 307 illustrate why the amount of linear polarized light reflected from a north-south oriented M1A1 should increase after 8:00. The eastern hemispherical sky is the only sky region which can affect western polarization readings from a north-south oriented M1A1. Therefore, since the amount of polarized light from this sky region increases from sunset to solar noon (Figure 307), the degree of polarized light reflected from the M1A1 also increases during this same period.

To discover when and where the greatest degree of polarized light can be detected from a vehicle, a circuit was constructed to operate a small d.c. motor at 32 RPM. A linear polarizer was positioned on the motor shaft. The entire unit was then positioned in front of a camcorder as shown in Figure 338.

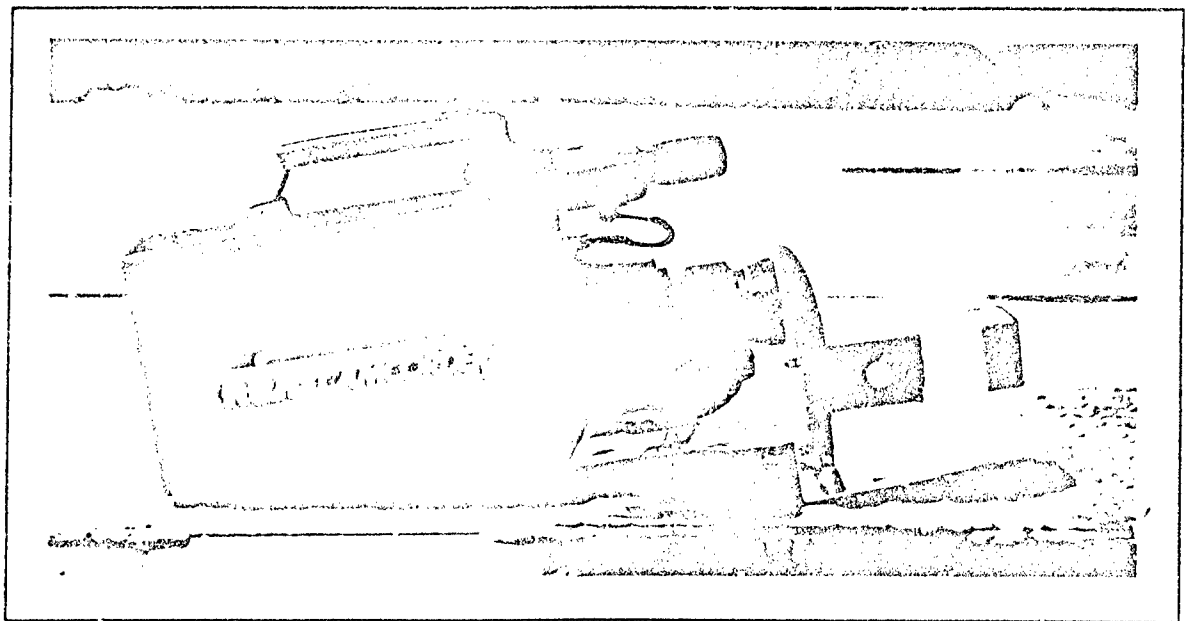


Figure 338

As the transmission axis of the linear polarizer rotated in front of the camcorder lens, polarized light entering the camcorder was observed to "flicker" in unison with the phase angle between the polarized incident light and the rotating analyzer.

A video tape was created using the arrangement described above. The video includes 360° views of an M1A1, M60, skylight and objects along the horizon. There is one dramatic feature of this video that stands out above all others. An outstanding amount of "flicker" (reflected polarized light) can be detected from surfaces which receive no light directly from the sun. Shadowed areas were observed to blink on and off like flashing neon signs. Rounded surfaces, like the M60 turret, fence posts, car hoods and windows, produced a considerable amount of "flicker" when illuminated by direct sun light. Flat surfaces, like the skirt area of the M1A1, showed very little "flicker" when illuminated by direct sun light. But these same flat surfaces flashed on and off as soon as sky light became the only source of illumination.

Initial attempts at finding a curve fit for luminance readings acquired from different M1A1 facets are not completely satisfactory. The closest curve fit achieved to date is shown in Figure 332. This graph shows luminance plotted as a function of $\cos i$ (i = angle of incidence). The curves for the three facets are nearly straight lines and coincident for the time interval 12:30 to 14:00. The horizontal tapering at the upper part of the curves for Area #13 and Area #15 correspond to the time interval 8:00 to 9:30 for both curves. The horizontal tapering of the upper part of the Area #15 curve corresponds to the time interval 8:00 to 12:00. Deviations from a linear relation between luminance and $\cos i$ appear to occur during the earlier times of the day.

Two factors have yet to be explored: (1) diurnal changes in the sun's power output, (2) the bidirectional reflectance distribution function for CARC-painted surfaces. These two factors will be explored at a later date.

SUMMARY OF CHROMATICITY STUDY

1. The CIE coordinates of the three different facets measured on the M1A1 shift slightly toward the white light coordinate as the sun moves westward from 8:00 to 14:00 (Table 19). Figure 126 shows the CIE coordinate placement of Area #12, Area #13, Area 15 and grass at 8:00 and 14:00
2. There is virtually no change in the CIE coordinates for grass from 8:00 to 14:00 (Table 20 and Figure 126).
3. The CIE coordinates measured for the three different tree areas have virtually the same behavior. The value of both the X and Y coordinates continuously decrease from 8:00 to 14:00 (Table 20). The trees have a greater saturation of green than the M1A1 and they show a greater shift toward the white light coordinate from 8:00 to 14:00 (Figure 127).

LUMINANCE OF NEW AND OLD CARC PAINTED SURFACES

The paint plant painted a small steel plate in the same fashion as an M1A1. The steel plate was first sandblasted and then chemically cleaned. The same epoxy primer and green CARC paint was applied to the steel plate as would be used for an M1A1.

The CARC plate was then alternately placed adjacent to Area #12 and Area #15 as shown in Figure 339 and Figure 340. The CARC plate was positioned so that it would have the same slope and azimuth as Area #12 and Area #15.

Diurnal measurements of the luminance from Area #12, Area #15 and the CARC plate positioned adjacent to these areas is given in Table 70. The results of this study are shown graphically in Figure 341, Figure 342 and Figure 343.

Table 70. Luminance of M1A1 Areas (#12 & #15) and CARC Painted Steel Plate

DATA:					CALCULATIONS:	
TIME	L #12	L #12'	L #15	L #15'	L12/L12'	L15/L15'
08:00	3020	2399	2858	2257	1.26	1.27
09:00	3274	2616	2958	2360	1.25	1.25
09:30	3456	2771	2996	2448	1.25	1.22
10:00	3560	2955	3046	2401	1.20	1.27
10:30	3633	2985	2842	2344	1.22	1.21
11:00	3597	2954	2630	2158	1.22	1.24
11:30	3563	2939	2466	1961	1.21	1.26
12:00	3463	2855	2080	1699	1.21	1.22
12:30	3294	2678	1668	1394	1.23	1.20
13:00	3103	2467	1144	1005	1.26	1.14
13:30	2797	2190	580	624	1.28	0.93
14:00	2468	1921	553	515	1.28	1.07
14:30	2043	1552	524	463	1.32	1.13
15:00	1433	1094	503	396	1.31	1.27

Notes: Date: 31 July, 1991
 Sky Conditions: Clear Skies
 Range - 36 Feet
 Readings from Minolta LS-100

L #12 refers to the luminance reading acquired from Area #12 on the M1A1.
 L #12' refers to the luminance reading acquired from the CARC painted steel plate when it was positioned adjacent to Area #12 on the M1A1.

L #15 refers to the luminance reading acquired from Area #15 on the M1A1.
 L #15' refers to the luminance reading acquired from the CARC painted steel plate when it was positioned adjacent to Area #15 on the M1A1.

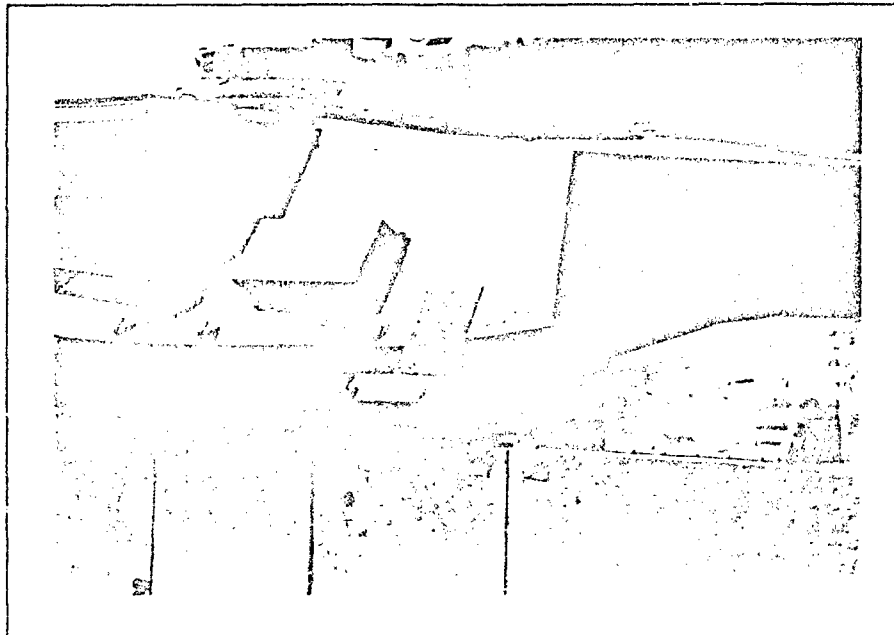


Figure 339
Position of CARC-Painted Steel Plate (#12') Near Area #12

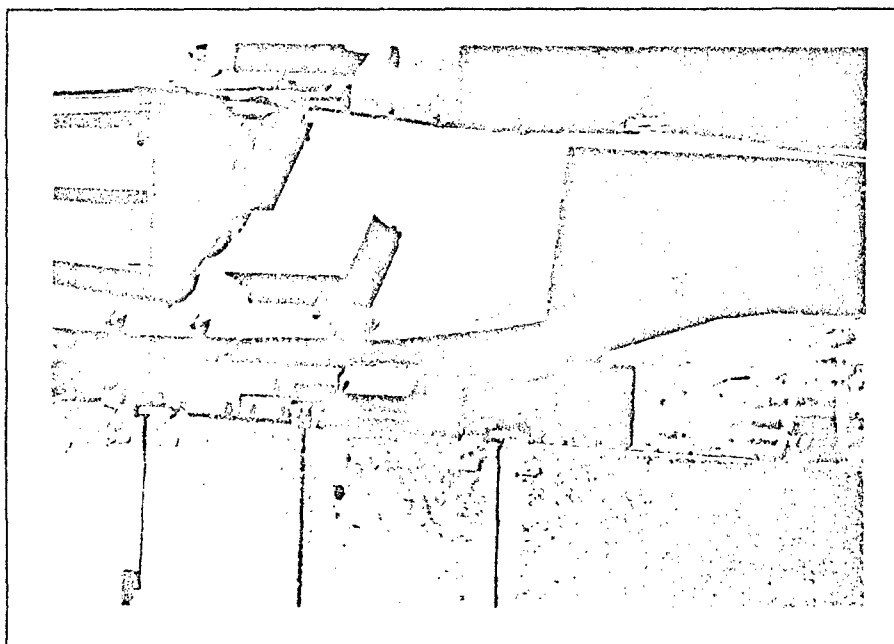


Figure 340
Position of CARC-Painted Steel Plate (#15') Near Area #15

LUMINANCE OF AREA #12
M1A1 AND CARC-PAINTED STEEL PLATE

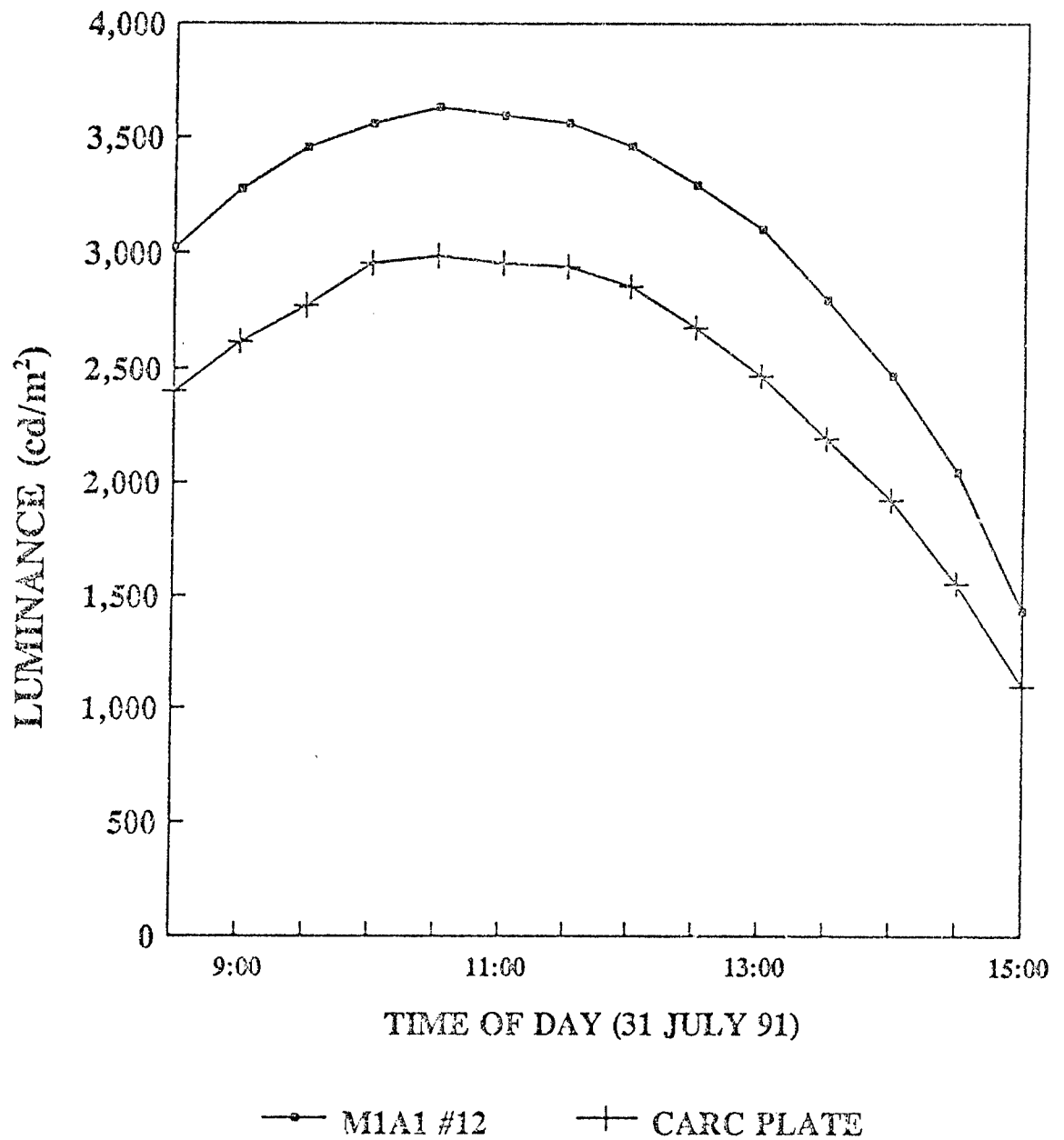
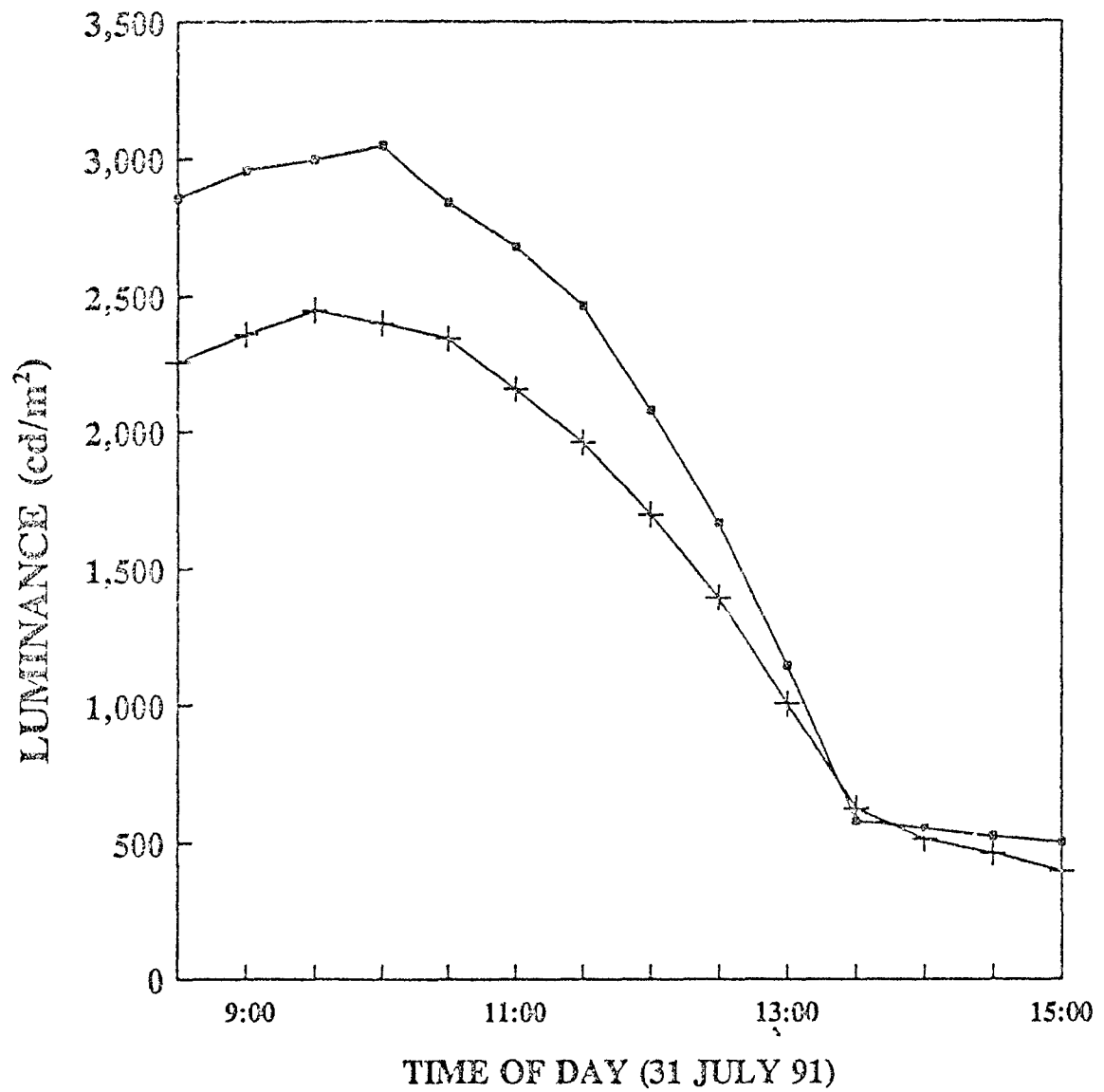


Figure 341

LUMINANCE OF AREA #15
M1A1 AND CARC-PAINTED STEEL PLATE



—●— M1A1 #15 —+— CARC PLATE

Figure 342

LUMINANCE RATIOS
M1A1 / CARC-PAINTED STEEL PLATE

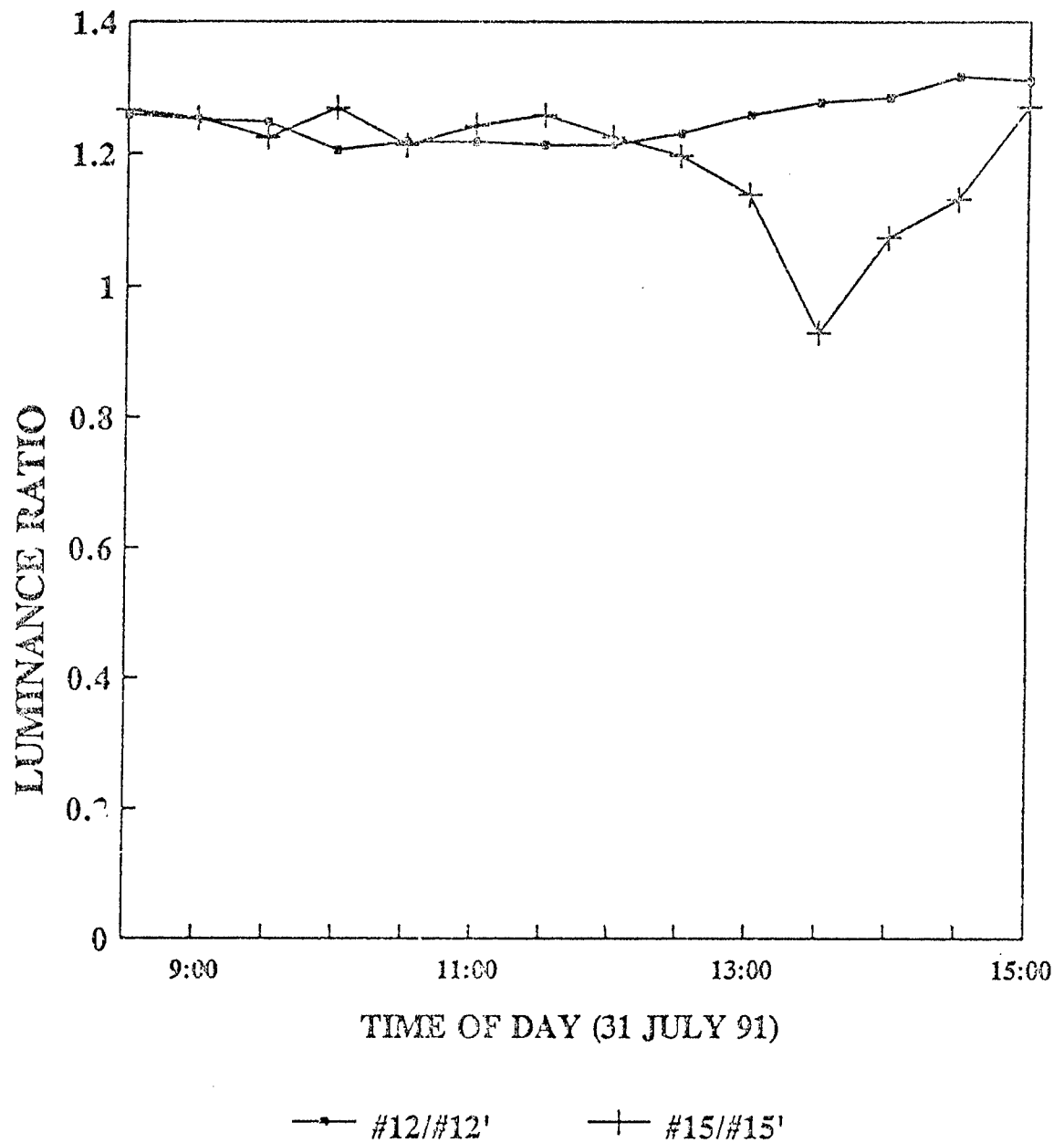


Figure 343

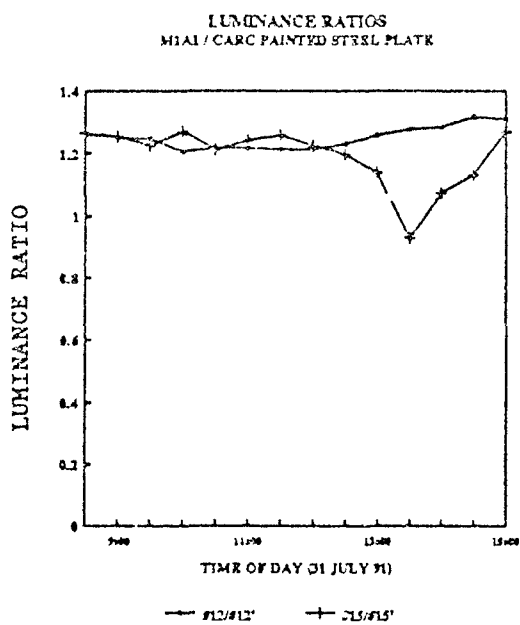
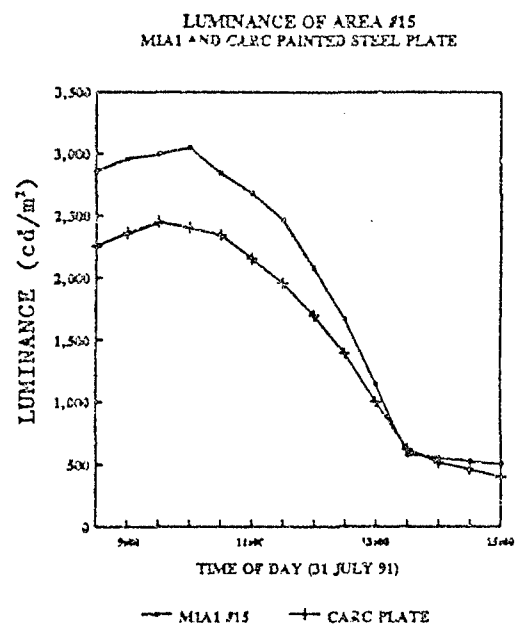
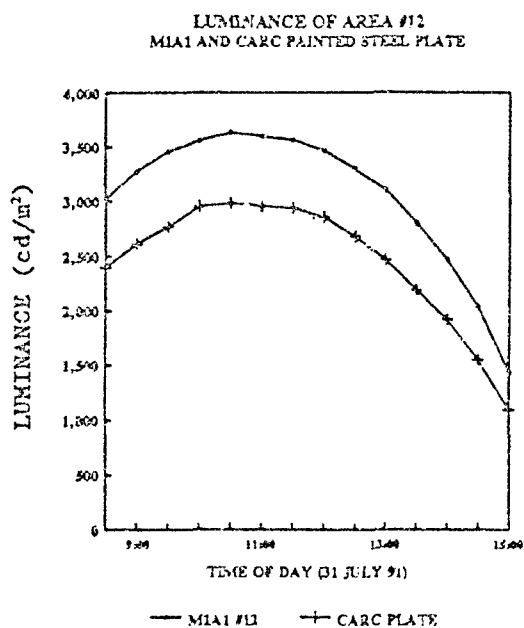


Figure 344

ANALYSIS AND SUMMARY OF NEW/OLD CARC SURFACE STUDY

The diurnal luminance graphs (Figure 341 and Figure 342) for the weathered M1A1 CARC-painted surfaces and the newly painted CARC surface look very similar. However, the luminance of the weathered surface was always greater than the newly painted CARC surface. The graph of the luminance ratio of the weathered CARC painted surface to the newly painted CARC surface (Figure 343) shows a nearly straight horizontal line for each of two different facets metered on the M1A1. The luminance ratios, L_{12}/L_{12} and L_{15}/L_{15} (weathered/new) is approximately 1.25. In other words, the weathered CARC painted surface is 25 percent brighter than a newly painted CARC surface.

The dip in the graph for Area #15 at 13:30 is due to shading. In hind sight, the position selected adjacent to Area #15 for the CARC plate was a poor choice. The plate rested on a ledge recessed two inches from the plane of Area #15. This position became shaded by turret areas before adjacent Area #15.

GONIOPHOTOMETRIC STUDIES OF A CARC-PAINTED SURFACE

AZIMUTHAL STUDY

PURPOSE

The purpose of this study was to acquire information on the light-distributing properties of a CARC (Chemical Agent Resistant Coating) painted sample illuminated by sunlight; in particular, to determine how luminance readings are affected by changes in azimuthal viewing angle when the altitude of the viewing angle is constant.

PROCEDURE

1. A five foot radius circle was drawn on a horizontal concrete parking lot.
2. A north-south line, determined by a compass, was drawn through the center of the circle.
3. The circumference of the circle was divided into eighteen equal arc lengths.
4. A CARC painted surface was positioned horizontally at the center of the circle.
5. Two metal rods were positioned vertically 12 inches apart in a block of wood.
6. The rods were positioned on one of the azimuth marks so that the shadows cast by the two rods were coincident.

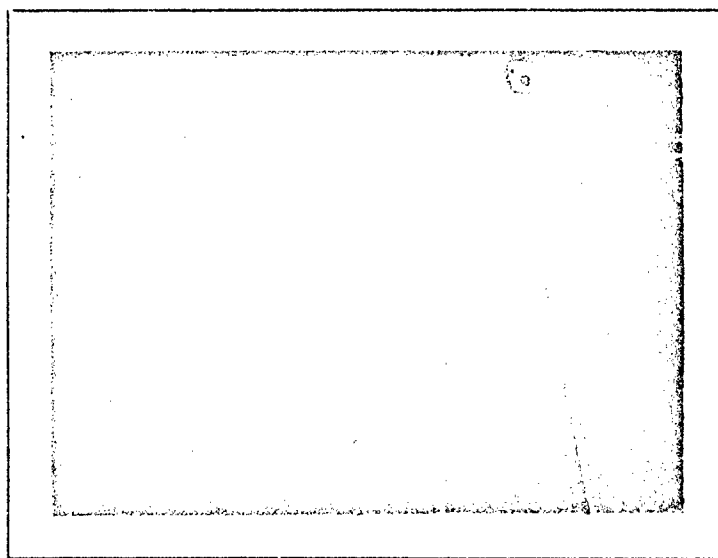


Figure 345.
Experimental Setup For Azimuth Study.

Table 71.
Data. 12:00 EDST

Azimuth (degree)	Luminance (cd/m ²)
0	3565
20	3313
40	3130
60	3044
80	2977
100	2939
120	2936
140	3005
160	2970
180	2968
200	2999
220	2964
240	3022
260	3170
280	3394
300	3643
320	3874
340	3975
360	3703

**GONIOPHOTOMETRIC RECORD
CARC-PAINTED STEEL PLATE
ILLUMINATION FROM SUN**

CARC PLATE SLOPE = 0°; METER SLOPE = 30°

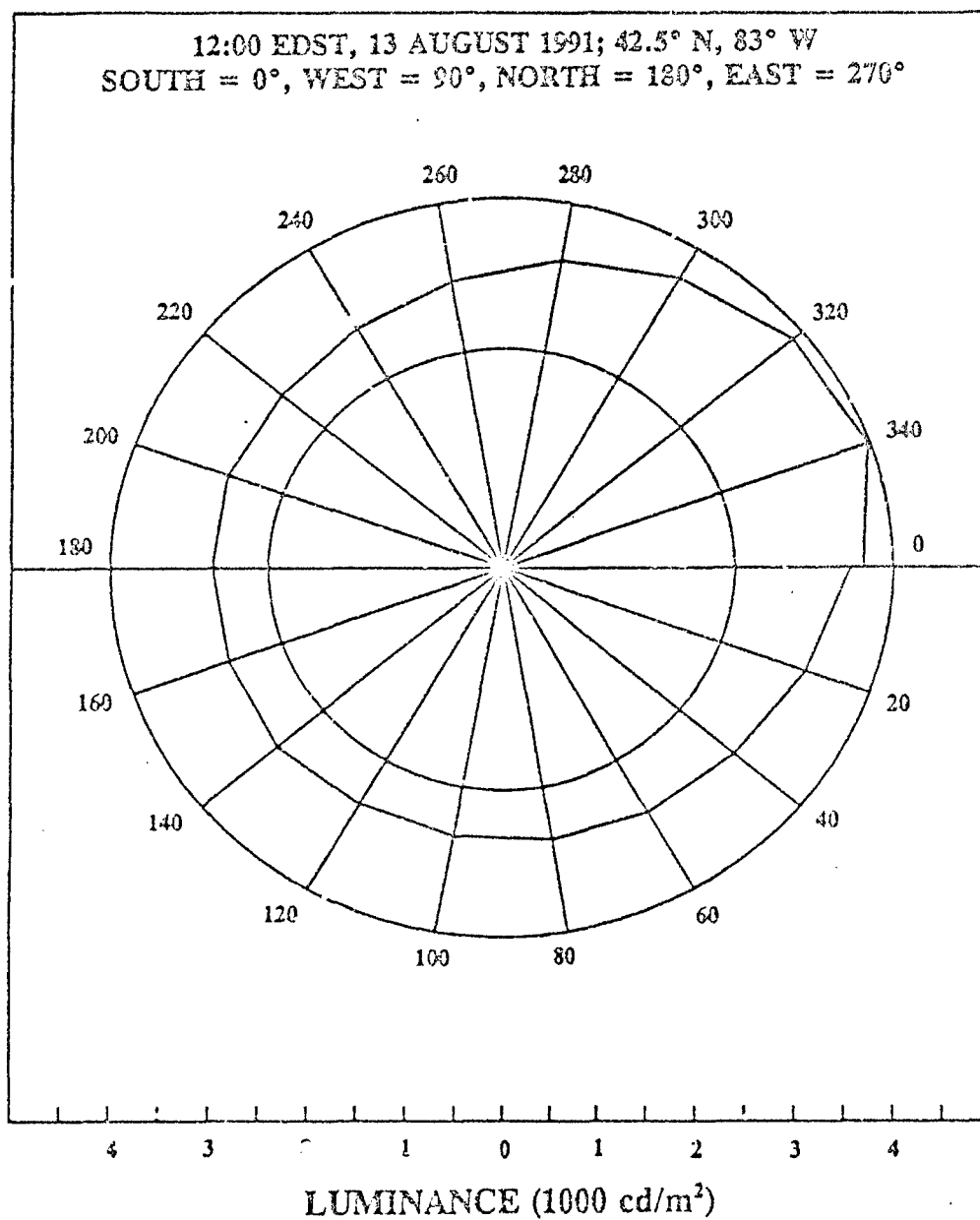


Figure 346.

7. The LS-100 Minolta Luminance Meter was positioned, with the aid of an angle level, on a tripod at a 30° angle with the horizontal.
8. The luminance meter was positioned so that the two rods appeared as one when sighting through the meter view finder.
9. The positioning of the rods and luminance meter was repeated for each of the eighteen azimuth marks along the perimeter of the circle.

Metering was toward the south when the azimuth was 0° . Azimuth was measured clockwise from the south point.

The time to acquire the data shown in Table 71 was 21 minutes.

The sun's altitude and azimuth on 13 August, 1991 at 12:00 EDT was $+55.6^\circ$ and 315.3° respectfully. The sun's altitude and azimuth on 13 August, 1991 at 12:30 EDT was $+59.1^\circ$ and 327.2° respectfully.

Skies were clear during data acquisition.

SUMMARY

The gloss of a surface is the degree it approaches a mirror surface. The two extreme cases of glossiness occur for Lambertian and specular surfaces. By definition, a Lambertian surface is a perfect reflecting diffuser. The luminance of a Lambertian surface is constant and has no dependence on angle of view. Incident light is distributed equally in every direction. It is the ideal surface of zero gloss. A purely specular surface produces a nonzero luminance value only at the angle of mirror reflection.

Table 71 and Figure 346 illustrate that the CARC painted sample exhibits approximately Lambertian properties for azimuth angles from 60° to 240° . Luminance readings varied by only 108 cd/m^2 (3.6%) for this range of azimuth angles. This range corresponds to the hemisphere opposite the sun and at right angles to the plane of incidence.

The sample showed intermediate light-distributing properties between Lambertian and specular for azimuth angles from 240° to 60° . The difference between the maximum luminance reading and the minimum luminance reading acquired was 1039 cd/m^2 (30.1%). As would be expected from a semi-gloss surface, the largest luminance reading acquired (3975 cd/m^2) corresponded approximately to an azimuth angle equal to the sun's azimuth.

Figure 346 also illustrates azimuthal symmetry in the sample's light-distributing properties. A line parallel to the incident plane, approximately the 160° - 340° line in Figure 346, is the approximate axis of symmetry.

GONIOPHOTOMETRIC READINGS IN THE PLANE OF INCIDENCE

PURPOSE

The purpose of this study was to acquire information on the light distributing properties of a CARC (Chemical Agent Resistant Coating) painted sample illuminated by sunlight; in particular, to determine how luminance readings are affected by changes in the surface altitude of the viewing angle for readings in the plane of incidence.

PROCEDURE

1. A magnet was attached to a camera tripod mount, which, in turn, was attached to a goniometric stand, as shown in Figure 347 below.
2. A CARC-painted steel plate was attached to the magnet, as shown in Figure 348 below.
3. An angle level (Figure 348) was used to set the slope of the CARC-painted sample.
4. A metal rod was attached to a magnet so that the rod was normal to the sample when the magnet was placed on the sample (Figure 348).
5. Two metal rods were positioned vertically, 12 inches apart, in a block of wood (Figure 348).
6. The rods were positioned so that the shadows cast by the two rods were coincident.
7. The CARC-painted sample was rotated until the shadows cast by the two vertical rods were coincident with the shadow cast by the rod normal to the sample's surface (Figure 4).



Figure 347.
Goniometric Support

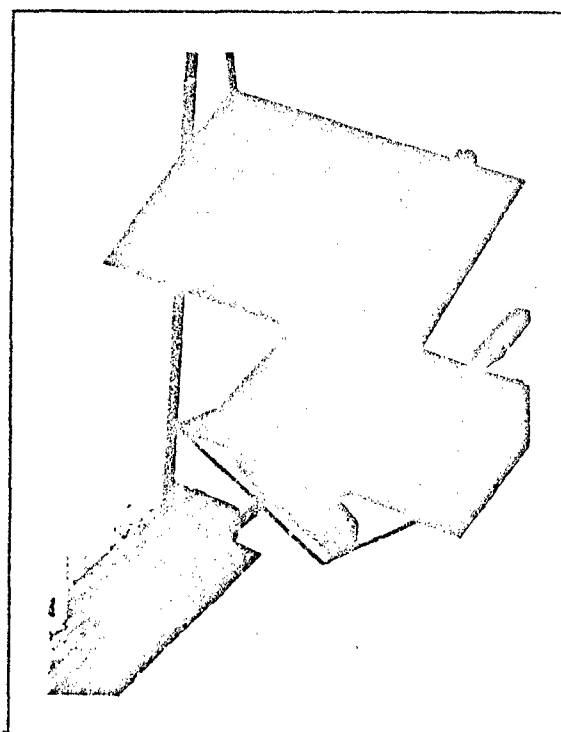


Figure 348.
Alignment to the Plane of Incidence

8. The LS-100 Minolta Luminance Meter was positioned, with the aid of an angle level, on a tripod at a 20° angle with the horizontal. Figure 349 shows all the equipment used to collect data for this study.
9. The luminance meter was positioned so that the two vertical rods and the rod normal to the sample's surface appeared as one when sighting through the meter's view finder.
10. The sample was rotated by 5° increments, in the plane of incidence, for as many angles as allowed by the altitude of the sun and the 20° slope of the luminance meter. This procedure was followed every 30 minutes from 08:00 to 12:30.

The time to acquire data for each 30-minute interval varied between 5 and 15 minutes. The duration depended on the number of measurements available. Frequent adjustments were made to the position of the vertical rods as the sun changed its position relative to the sample. Skies were clear during data acquisition.

Table 72 gives the sun's altitude and azimuth on 12 August, 1991 for the times data was collected. The data tables; Table 72, Table 73,...Table 79; were constructed by filtering out data pertaining to the same CARC slope for each of the time intervals data was acquired. Positive CARC slopes refer to tilts toward the sun. Negative CARC slopes refer to tilts away from the sun (Figure 350).

The calculation of the angle of incidence of the sun's rays on the CARC painted surface is shown in Figure 352, $\angle i = 90^\circ - (\text{Sun's Altitude} + \text{CARC Slope})$.

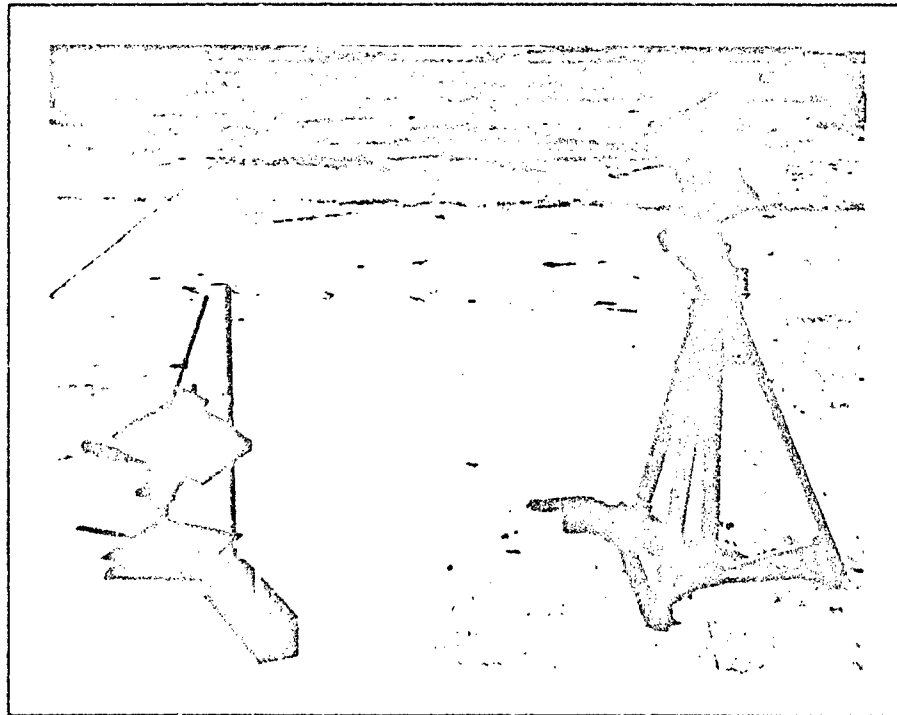


Figure 349.
Goniometric Equipment for Readings in the Plane of Incidence

Table 72. Luminance Readings When Metering Parallel to the Incident Plane.
Slope of CARC-Painted Sample = 0°. Luminance Meter Slope = 20°.

Date: 8-12-91 Longitude: 83° west Latitude: 42.5° north

EDST	Sun's Azimuth	Sun's Altitude	<i	Cos i	Luminance (cd/m ²)
08:30	267.4	19.7	70.3	0.337	5937
09:00	272.4	25.2	64.8	0.426	5631
09:30	277.8	30.7	59.3	0.511	6383
10:00	283.5	36.2	53.8	0.590	5855
10:30	289.9	41.5	48.5	0.662	5154
11:00	297.0	46.5	43.5	0.726	4812
11:30	305.4	51.3	38.7	0.780	4807
12:00	315.3	55.5	34.5	0.824	4456
12:30	327.1	59.0	31.0	0.857	4341

< i - the angle of incidence of the sun's rays on the CARC painted sample.

Table 73. Luminance Readings When Metering Parallel to the Incident Plane.
Slopes of CARC-Painted Sample = 5° and 10°. Luminance Meter Slope = 20°.

CARC Slope = 5°				CARC Slope = 10°			
EDST	<i	Cos i	Luminance (cd/m ²)	<i	Cos i	Luminance (cd/m ²)	
08:30	65.3	0.418	7036	60.3	0.496	7291	
09:00	59.8	0.504	6575	54.8	0.577	6989	
09:30	54.3	0.584	6435	49.3	0.653	6503	
10:00	48.8	0.658	5955	43.8	0.721	6238	
10:30	43.5	0.725	5357	38.5	0.782	5668	
11:00	38.5	0.783	5080	33.5	0.834	5328	
11:30	33.7	0.832	5061	28.7	0.877	5291	
12:00	29.5	0.870	4688	24.5	0.910	4894	
12:30	26.0	0.898	4528	21.0	0.933	4690	

Table 74. Luminance Readings When Metering Parallel to the Incident Plane.
Slopes of CARC-Painted Sample = 15° and -5°. Luminance Meter Slope = 20°.

CARC Slope = 15°				CARC Slope = -5°			
EDST	<i	Cos i	Luminance (cd/m ²)	<i	Cos i	Luminance (cd/m ²)	
08:30	55.3	0.569	7195	75.3	0.254	5015	
09:00	49.8	0.646	6943	69.8	0.346	5353	
09:30	44.3	0.716	6690	64.3	0.434	5230	
10:00	38.8	0.779	6345	58.8	0.518	5926	
10:30	33.5	0.834	5782	53.5	0.594	4994	
11:00	28.5	0.879	5561	48.5	0.663	4723	
11:30	23.7	0.915	5177	43.7	0.723	4644	
12:00	19.5	0.943	4997	39.5	0.771	4244	
12:30	16.0	0.961	4674	36.0	0.809	4099	

Table 75. Luminance Readings When Metering Parallel to the Incident Plane.
Slopes of CARC Painted Sample = -10° and -15° . Luminance Meter Slope = 20° .

CARC Slope = -10°				CARC Slope = -15°			
EDST	$\langle i$	$\cos i$	Luminance (cd/m^2)	$\langle i$	$\cos i$	Luminance (cd/m^2)	
08:30	80.3	0.169	3010	85.3	0.082	1693	
09:00	74.8	0.263	3865	79.8	0.178	2565	
09:30	69.3	0.354	4507	74.3	0.271	3177	
10:00	63.8	0.441	5340	68.8	0.361	3967	
10:30	58.5	0.522	5095	63.5	0.446	4047	
11:00	53.5	0.595	4899	58.5	0.523	4116	
11:30	48.7	0.660	4588	53.7	0.592	4787	
12:00	44.5	0.713	4028	49.5	0.649	3863	
12:30	41.0	0.754	3860	46.0	0.694	3582	

Table 76. Luminance Readings When Metering Parallel to the Incident Plane.
Slopes of CARC Painted Sample = -20° and -25° . Luminance Meter Slope = 20° .

CARC Slope = -20°				CARC Slope = -25°			
EDST	$\langle i$	$\cos i$	Luminance (cd/m^2)	$\langle i$	$\cos i$	Luminance (cd/m^2)	
08:30	90.0	0.000	661	NA	NA	NA	
09:00	84.8	0.091	1464	89.8	0.004	619	
09:30	79.3	0.186	2309	84.3	0.100	1366	
10:00	73.8	0.279	2995	78.8	0.194	2073	
10:30	68.5	0.366	2960	73.5	0.283	2210	
11:00	63.5	0.447	2968	68.5	0.367	2323	
11:30	58.7	0.519	3431	63.7	0.443	2849	
12:00	54.5	0.581	3502	59.5	0.507	2890	
12:30	51.0	0.629	3320	56.0	0.559	2855	

Table 77. Luminance Readings When Metering Parallel to the Incident Plane.
Slopes of CARC Painted Sample = -30° and -35° . Luminance Meter Slope = 20° .

CARC Slope = -30°				CARC Slope = -35°			
EDST	$\langle i$	$\cos i$	Luminance (cd/m^2)	$\langle i$	$\cos i$	Luminance (cd/m^2)	
08:30	NA	NA	NA	NA	NA	NA	
09:00	NA	NA	NA	NA	NA	NA	
09:30	89.3	0.013	827	NA	NA	NA	
10:00	83.8	0.108	1403	88.8	0.020	728	
10:30	78.5	0.199	1640	83.5	0.113	1118	
11:00	73.5	0.285	1964	78.5	0.200	1505	
11:30	68.7	0.363	2277	73.7	0.280	1705	
12:00	64.5	0.430	2319	69.5	0.350	1924	
12:30	61.0	0.484	2277	66.0	0.406	2108	

Table 78. Luminance Readings When Metering Parallel to the Incident Plane.
Slopes of CARC Painted Sample = -40° and -45° . Luminance Meter Slope = 20° .

CARC Slope = -40°				CARC Slope = -45°			
EDST	$\angle i$	$\cos i$	Luminance (cd/m^2)	$\angle i$	$\cos i$	Luminance (cd/m^2)	
08:30	NA	NA	NA	NA	NA	NA	
09:00	NA	NA	NA	NA	NA	NA	
09:30	NA	NA	NA	NA	NA	NA	
10:00	NA	NA	NA	NA	NA	NA	
10:30	88.5	0.026	419	NA	NA	NA	
11:00	83.5	0.114	1100	88.5	0.027	633	
11:30	78.7	0.195	1329	83.7	0.109	986	
12:00	74.5	0.267	1626	79.5	0.182	1228	
12:30	71.0	0.325	1769	76.0	0.241	1429	

Table 79. Luminance Readings When Metering Parallel to the Incident Plane.
Slopes of CARC Painted Sample = -50° and -55° . Luminance Meter Slope = 20° .

CARC Slope = -50°				CARC Slope = -55°			
EDST	$\angle i$	$\cos i$	Luminance (cd/m^2)	$\angle i$	$\cos i$	Luminance (cd/m^2)	
08:30	NA	NA	NA	NA	NA	NA	
09:00	NA	NA	NA	NA	NA	NA	
09:30	NA	NA	NA	NA	NA	NA	
10:00	NA	NA	NA	NA	NA	NA	
10:30	NA	NA	NA	NA	NA	NA	
11:00	NA	NA	NA	NA	NA	NA	
11:30	88.7	0.022	606	NA	NA	NA	
12:00	84.5	0.096	807	89.5	0.009	443	
12:30	81.0	0.156	1054	86.0	0.069	672	

Because of small sun altitudes in the early morning hours and a meter slope of 20° , a number of luminance readings were not available.

The range of positive slopes was restricted to values between 5° and 15° because of the 20° meter slope.

The range of negative slopes was restricted by the sun's altitude.

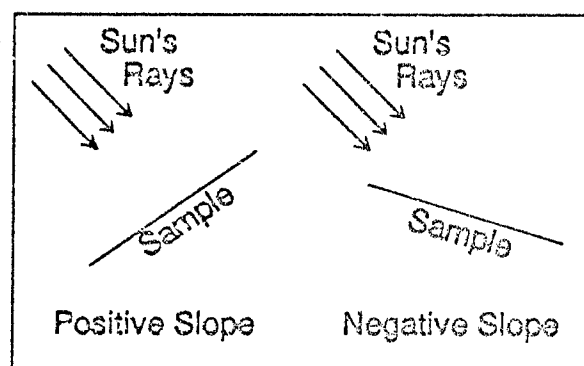
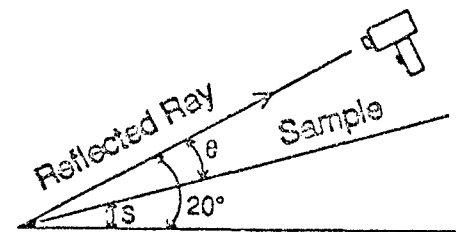


Figure 350.
Positive and Negative CARC Slopes

Table 80. Luminance Readings When Metering Parallel to the Incident Plane.
Data Arranged According to Metering Angle θ . Luminance Meter Slope = 20° .

EDST	i	Luminance	COS i	θ	EDST	i	Luminance	COS i	θ
12:00	89.5	443	0.009	75	08:30	90.0	661	0.000	40
12:30	86.0	679	0.069	75	09:00	84.8	1464	0.091	40
11:30	88.7	606	0.022	70	09:30	79.3	2309	0.186	40
12:00	84.5	807	0.096	70	10:00	73.8	2995	0.279	40
12:30	81.0	1054	0.156	70	10:30	68.5	2960	0.366	40
11:00	88.5	633	0.027	65	11:00	63.5	2968	0.447	40
11:30	83.7	986	0.109	65	11:30	58.7	3431	0.519	40
12:00	79.5	1228	0.182	65	12:00	54.5	3502	0.581	40
12:30	76.0	1429	0.241	65	12:30	51.0	3320	0.629	40
10:30	88.5	419	0.026	60	08:30	85.3	1693	0.082	35
11:00	83.5	1100	0.114	60	09:00	79.8	2565	0.178	35
11:30	78.7	1329	0.195	60	09:30	74.3	3177	0.271	35
12:00	74.5	1626	0.267	60	10:00	68.8	3967	0.361	35
12:30	71.0	1709	0.325	60	10:30	63.5	4047	0.446	35
10:00	88.8	728	0.020	55	11:00	58.5	4116	0.523	35
10:30	83.5	1118	0.113	55	11:30	53.7	4787	0.592	35
11:00	78.5	1505	0.200	55	12:00	49.5	3863	0.649	35
11:30	73.7	1705	0.280	55	12:30	46.0	3582	0.694	35
12:00	69.5	1924	0.350	55	08:30	80.3	3010	0.169	30
12:30	66.0	2108	0.406	55	09:00	74.8	3865	0.263	30
09:30	89.3	827	0.013	50	09:30	69.3	4507	0.354	30
10:00	83.8	1403	0.108	50	10:00	63.8	5340	0.441	30
10:30	78.5	1640	0.199	50	10:30	58.5	5095	0.522	30
11:00	73.5	1964	0.285	50	11:00	53.5	4899	0.595	30
11:30	68.7	2277	0.363	50	11:30	48.7	4538	0.660	30
12:00	64.5	2319	0.430	50	12:00	44.5	4028	0.713	30
12:30	61.0	2277	0.484	50	12:30	41.0	3860	0.754	30
09:00	89.8	619	0.004	45					
09:30	84.3	1366	0.100	45					
10:00	78.8	2073	0.194	45					
10:30	73.5	2210	0.283	45					
11:00	68.5	2323	0.367	45					
11:30	63.7	2849	0.443	45					
12:00	59.5	2890	0.507	45					
12:30	56.0	2855	0.559	45					



s = slope of CARC sample

θ = Angle between Meter and Sample

$$\theta = 20^\circ - s$$

Figure 351.
Calculation of Meter Angle θ

Table 81. Luminance Readings Parallel to the Incident Plane Continued.
Data Arranged According to Metering Angle θ . Luminance Meter Slope = 20° .

EDST	i	Luminance	COS i	θ	EDST	i	Luminance	COS i	θ
08:30	75.3	5016	0.254	25	08:30	60.3	7291	0.496	10
09:00	69.8	5353	0.346	25	09:00	54.8	6989	0.577	10
09:30	64.3	6230	0.434	25	09:30	49.3	6503	0.653	10
10:00	58.8	5926	0.518	25	10:00	43.8	6238	0.721	10
10:30	53.5	4994	0.594	25	10:30	38.5	5668	0.782	10
11:00	48.5	4723	0.663	25	11:00	33.5	5328	0.834	10
11:30	43.7	4644	0.723	25	11:30	28.7	5291	0.877	10
12:00	39.5	4244	0.771	25	12:00	24.5	4894	0.910	10
12:30	36.0	4099	0.809	25	12:30	21.0	4690	0.933	10
08:30	70.3	5937	0.337	20	08:30	55.3	7195	0.569	05
09:00	64.8	5631	0.426	20	09:00	49.8	6943	0.646	05
09:30	59.3	6383	0.511	20	09:30	44.3	6690	0.716	05
10:00	53.8	5855	0.590	20	10:00	38.8	6345	0.779	05
10:30	48.5	5154	0.662	20	10:30	33.5	5782	0.834	05
11:00	43.5	4812	0.726	20	11:00	28.5	5561	0.879	05
11:30	38.7	4807	0.780	20	11:30	23.7	5177	0.915	05
12:00	34.5	4456	0.824	20	12:00	19.5	4997	0.943	05
12:30	31.0	4341	0.857	20	12:30	16.0	4674	0.961	05
08:30	65.3	7291	0.418	15					
09:00	59.8	6989	0.504	15					
09:30	54.3	6503	0.584	15					
10:00	48.8	6238	0.658	15					
10:30	43.5	5668	0.725	15					
11:00	38.5	5328	0.783	15					
11:30	33.7	5291	0.832	15					
12:00	29.5	4894	0.870	15					
12:30	26.0	4690	0.898	15					

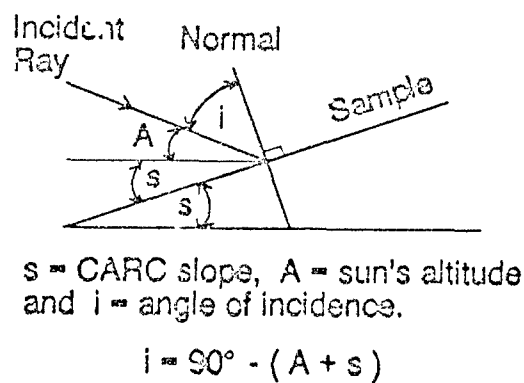


Figure 352.
Calculation of the Angle of Incidence

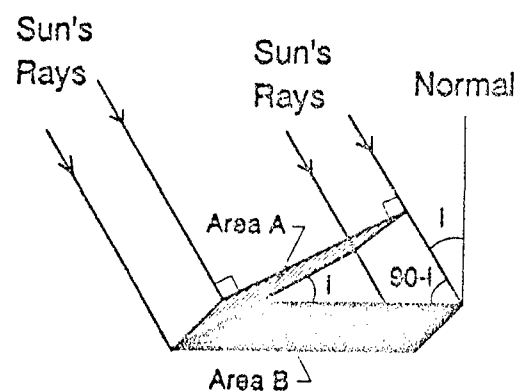


Figure 353.
 $\text{Area B} = \text{Area A} / \cos i$

SUN'S RAYS ON CARC-PAINTED SURFACE
METERING AT 20 DEGREES FROM HORIZONTAL
AND TOWARD SUN

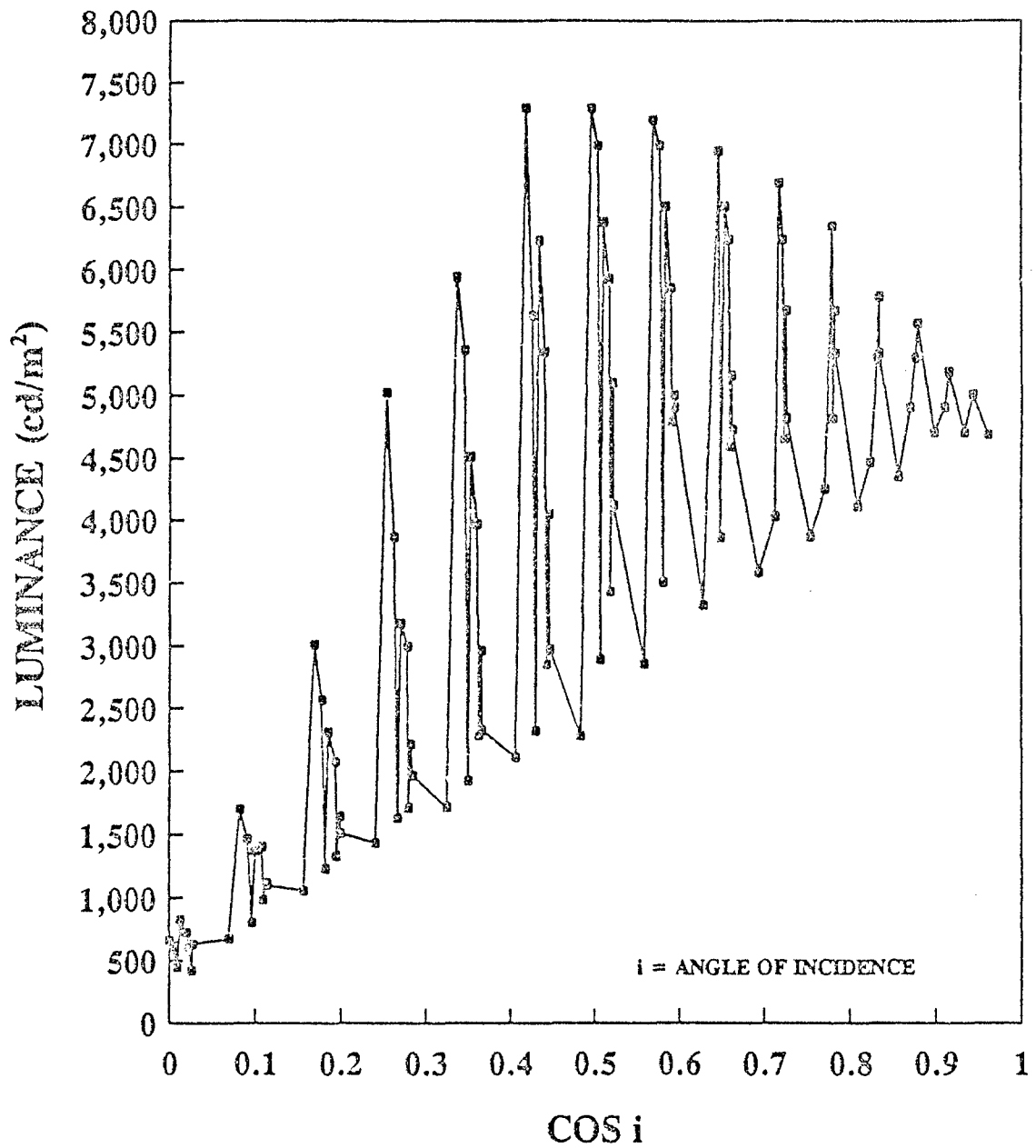


Figure 354.

SUN'S RAYS ON CARC PAINTED SURFACE
METERING AT 28 DEGREES FROM HORIZONTAL
AND TOWARD SUN

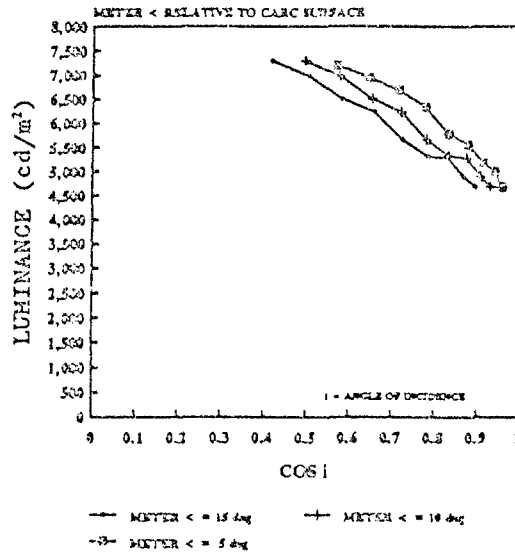


Figure 355

SUN'S RAYS ON CARC PAINTED SURFACE
METERING AT 28 DEGREES FROM HORIZONTAL
AND TOWARD SUN

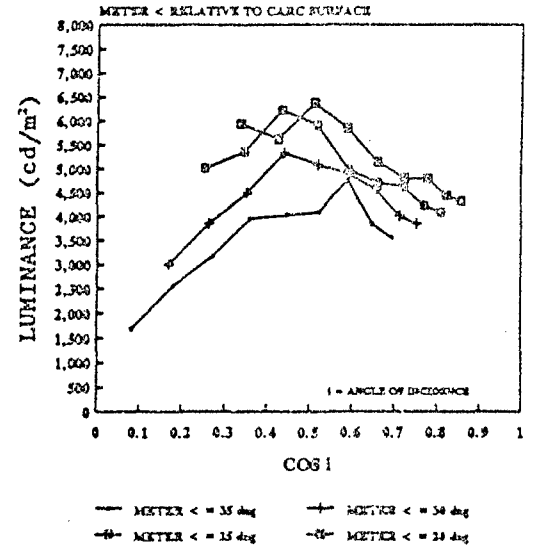


Figure 356

SUN'S RAYS ON CARC PAINTED SURFACE
METERING AT 28 DEGREES FROM HORIZONTAL
AND TOWARD SUN

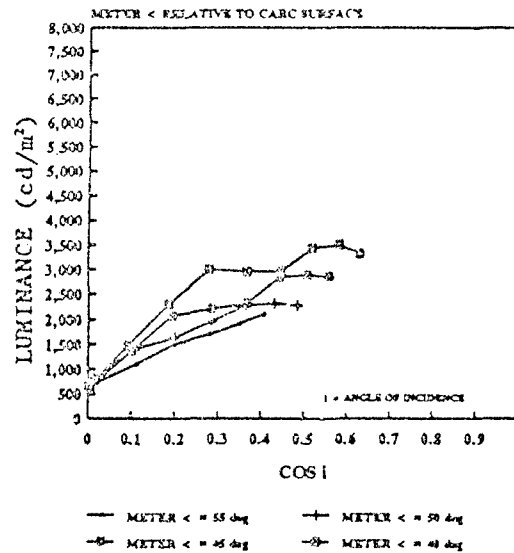


Figure 357

SUN'S RAYS ON CARC PAINTED SURFACE
METERING AT 28 DEGREES FROM HORIZONTAL
AND TOWARD SUN

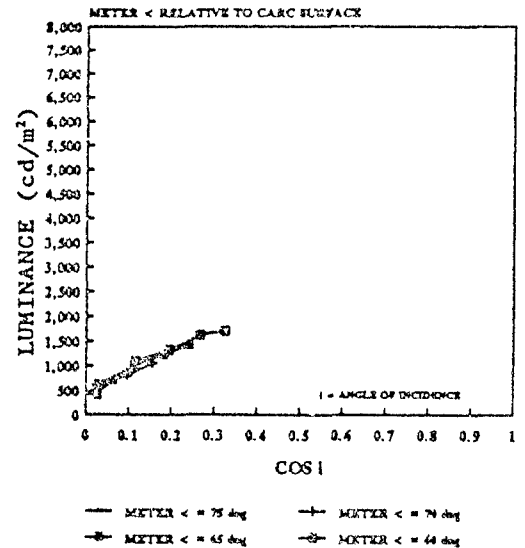


Figure 358

GONIOPHOTOMETRIC RECORD
Sun's Rays Incident on CARC Paint
Metering in the Plane of Incidence

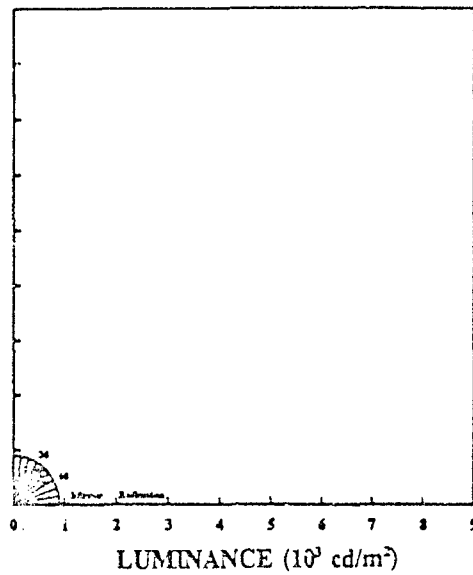


Figure 359

GONIOPHOTOMETRIC RECORD
Sun's Rays Incident on CARC Paint
Metering in the Plane of Incidence

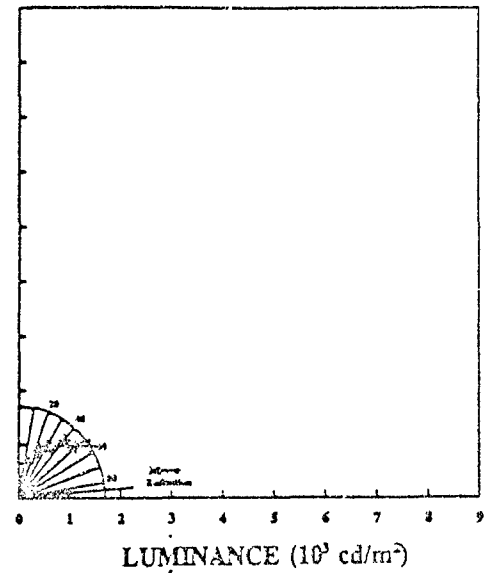


Figure 360

GONIOPHOTOMETRIC RECORD
Sun's Rays Incident on CARC Paint
Metering in the Plane of Incidence

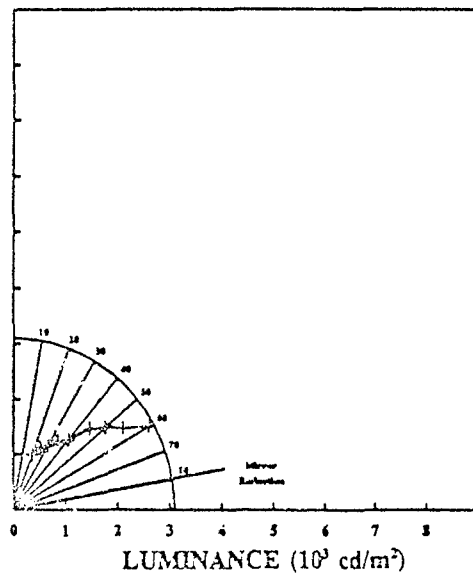


Figure 361

GONIOPHOTOMETRIC RECORD
Sun's Rays Incident on CARC Paint
Metering in the Plane of Incidence

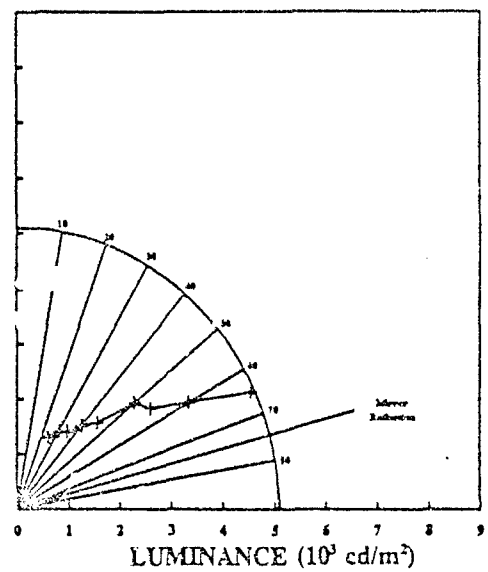


Figure 362

GONIOPHOTOMETRIC RECORD
Sun's Rays Incident on CARC Paint
Metering in the Plane of Incidence

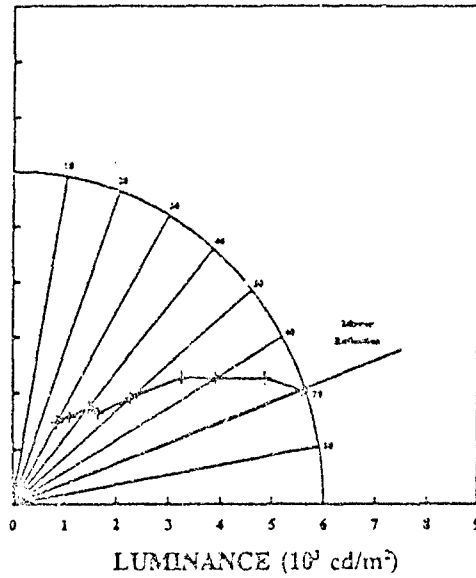


Figure 363

GONIOPHOTOMETRIC RECORD
Sun's Rays Incident on CARC Paint
Metering in the Plane of Incidence

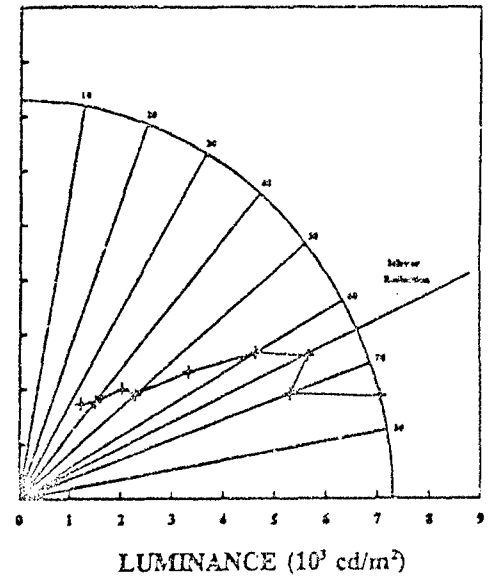


Figure 364

GONIOPHOTOMETRIC RECORD
Sun's Rays Incident on CARC Paint
Metering in the Plane of Incidence

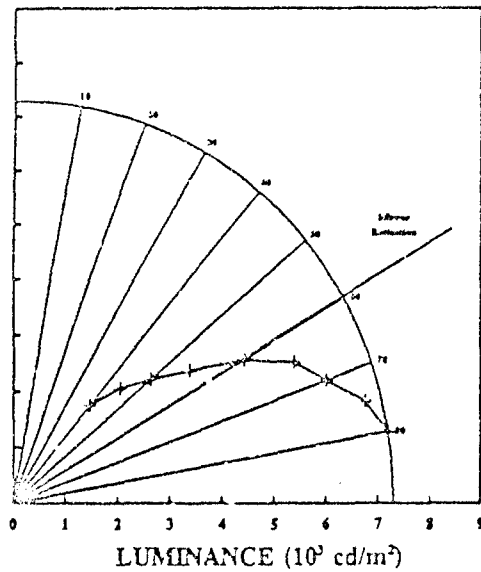


Figure 365

GONIOPHOTOMETRIC RECORD
Sun's Rays Incident on CARC Paint
Metering in the Plane of Incidence

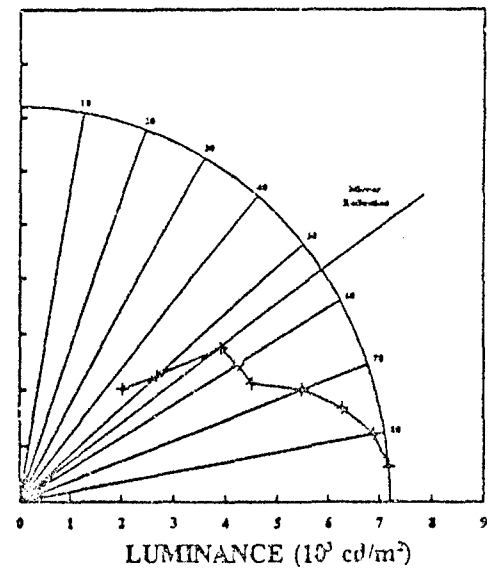


Figure 366

GONIOPHOTOMETRIC RECORD
Sun's Rays Incident on CARC Paint
Metering in the Plane of Incidence

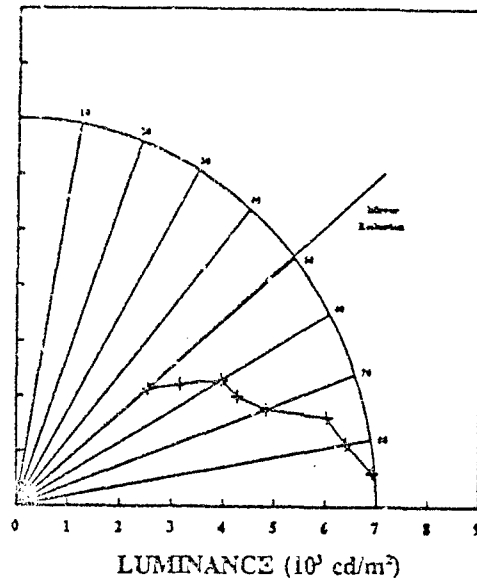


Figure 367

GONIOPHOTOMETRIC RECORD
Sun's Rays Incident on CARC Paint
Metering in the Plane of Incidence

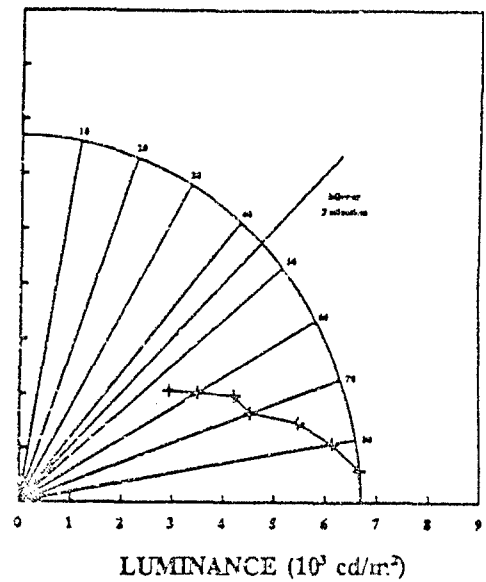


Figure 368

GONIOPHOTOMETRIC RECORD
Sun's Rays Incident on CARC Paint
Metering in the Plane of Incidence

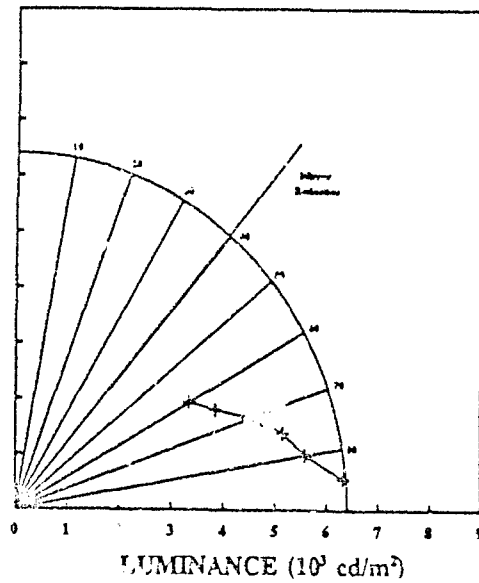


Figure 369

GONIOPHOTOMETRIC RECORD
Sun's Rays Incident on CARC Paint
Metering in the Plane of Incidence

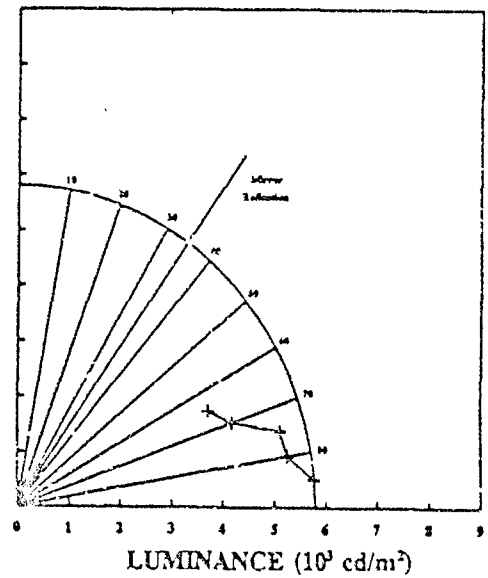


Figure 370

SUMMARY

The luminance readings for reflected sunlight from a Lambertian surface for the same metering angle from the surface would all be identical. However, the luminance readings should be different for different metering angles. For a Lambertian surface, luminance should be directly proportional to the cosine of the angle of incidence. Figure 353 illustrates how the light energy from the sun per unit area decreases with an increase in the angle of incidence. The energy per unit area is directly proportional to the cosine of the angle of incidence. This is the same principle which produces the seasons. Figure 354 is a plot of all the luminance readings acquired as a function of $\cos i$. Since this graph does not plot as a straight line, the surface of the CARC sample is not perfectly Lambertian.

Table 80 and Table 81 show the data from Table 72, Table 73, ...Table 79, arranged according to metering angle θ . Figure 351 shows how these metering angles were calculated. The graphs of Figure 355, Figure 356, Figure 357 and Figure 358 consist of sets of points which correspond to the same metering angle. For luminance readings in the plane of incidence, these four graphs suggest a surface microstructure which produces an increase in luminance for angles of incidence from 90° to 60° but a decrease in luminance for angles of incidence from 60° to 0° . These results are a bit peculiar since the light energy per unit area should increase with a decrease in the angle of incidence (Figure 353). Also, luminance readings are higher for smaller metering angles; metering closer to the surface.

The graphs of Figure 359, Figure 360, ...Figure 370 show luminance as a function of metering angle from the CARC-painted surface for similar angles of incidence (within a few degrees). The circular plots correspond to goniophotometric records of a Lambertian surface. The line extending outward from the origin past the Lambertian record indicates the approximate angle of incidence for which the data applies. The graphs of Figure 364, Figure 365, ...Figure 370 dramatically show that higher luminance readings are acquired for smaller metering angles; metering closer to the surface; rather than in the direction of mirror reflection when metering is in the plane of incidence.

There was no control over the source of illumination, the sun. The sun continuously changed its azimuth and altitude and time was required to move the meter so that it was always close to being in the plane of incidence. Little time was available to also change the 20° meter slope. Therefore, many gaps occur in the data. In particular, it would be helpful to have goniophotometric data for angles of incidence from 60° to 90° with corresponding meter angles from 5° to 15° and angles of incidence from 0° to 60° with corresponding metering angles from 40° to 90° .

GONIOPHOTOMETRIC READINGS PERPENDICULAR TO THE PLANE OF INCIDENCE

PURPOSE

The purpose of this study was to acquire information on the light distributing properties of a CARC- (Chemical Agent Resistant Coating) painted sample illuminated by sunlight; in particular, to determine how luminance readings are affected by changes in the surface altitude of the viewing angle for readings perpendicular to the plane of incidence.

PROCEDURE

1. A magnet was attached to a camera tripod mount, which, in turn, was attached to a goniometric stand (Figure 347).
2. A CARC-painted steel plate was attached to the magnet (Figure 348).
3. An angle level (Figure 348) was used to set the slope of the CARC-painted sample.
4. A metal rod was attached to a magnet so that the rod was normal to the sample when the magnet was placed on the sample (Figure 348).
5. Two metal rods were positioned vertically, 12 inches apart, in a block of wood (Figure 348).
6. The rods were positioned so that the shadows cast by the two rods were coincident.
7. The CARC painted sample was rotated until the shadows cast by the two vertical rods were coincident with the shadow cast by the rod normal to the sample's surface (Figure 348).
8. A long, straight metal tube was placed on the ground parallel to the two rods used to establish the plane of incidence.
9. The wood block holding the two rods was repositioned perpendicular to the metal tube (perpendicular to the sun's rays).
10. The LS-100 Minolta Luminance Meter was positioned, with the aid of an angle level, on a tripod at a 20° angle with the horizontal. Figure 349 shows all the equipment used to collect data for this study.
11. The luminance meter was positioned so that the two vertical rods appeared as one when sighting through the meter's view finder.
12. The sample was rotated by 5° increments, in the plane of incidence, for as many angles as allowed by the altitude of the sun and the 20° slope of the luminance meter. This procedure was followed every 30 minutes from 08:00 to 12:30.

The time to acquire data for each 30 minute interval varied between five minutes and 15 minutes. The duration depended on the number of measurements available. Frequent adjustments were made to the position of the vertical rods as the sun changed its position relative to the sample.

Skies were clear during data acquisition.

Table 72 gives the sun's altitude and azimuth on 12 August, 1991 for the times data was collected. The data tables, Table 82, Table 83 and Table 84, were constructed by filtering out data pertaining to the same CARC slope for each of the time intervals data was acquired.

Positive CARC slopes refer to tilts toward the sun. Negative CARC slopes refer to tilts away from the sun (Figure 350). The calculation of the angle of incidence of the sun's rays on the CARC-painted surface is shown in Figure 352, $\angle i = 90^\circ - (\text{Sun's Altitude} + \text{CARC Slope})$.

Table 82. Luminance Readings When Metering Perpendicular to the Incident Plane.
CARC Surface Slopes: $\phi = 0^\circ, 5^\circ, 10^\circ, 15^\circ, 20^\circ$ and 25° .
Luminance Meter Slope = 20° .

Date: 8-12-91

Longitude: 83°

Latitude: 42.5°

$\phi = 0^\circ$

EDST	$\angle i$	$\cos i$	Luminance (cd/m^2)
08:30	70.3	0.337	1441
09:00	64.8	0.426	1835
09:30	59.3	0.511	2113
10:00	53.8	0.590	2399
10:30	48.5	0.662	2636
11:00	43.5	0.725	2943
11:30	38.7	0.780	3099
12:00	34.5	0.824	3169
12:30	31.0	0.857	3238

$\phi = 5^\circ$

EDST	$\angle i$	$\cos i$	Luminance (cd/m^2)
08:30	65.3	0.418	1629
09:00	59.8	0.504	2022
09:30	54.3	0.584	2338
10:00	48.8	0.658	2626
10:30	43.5	0.725	2793
11:00	38.5	0.783	3111
11:30	33.7	0.832	3240
12:00	29.5	0.870	3271
12:30	26.0	0.898	3444

$\phi = 10^\circ$

EDST	$\angle i$	$\cos i$	Luminance (cd/m^2)
08:30	60.3	0.496	1813
09:00	54.8	0.577	2186
09:30	49.3	0.653	2511
10:00	43.8	0.721	2781
10:30	38.5	0.782	2955
11:00	33.5	0.834	3274
11:30	28.7	0.877	3355
12:00	24.5	0.910	3412
12:30	21.0	0.933	3583

$\phi = 15^\circ$

EDST	$\angle i$	$\cos i$	Luminance (cd/m^2)
08:30	55.3	0.569	1958
09:00	49.8	0.646	2343
09:30	44.3	0.716	2655
10:00	38.8	0.779	2983
10:30	33.5	0.834	3061
11:00	28.5	0.879	3386
11:30	23.7	0.915	3430
12:00	19.5	0.943	3549
12:30	16.0	0.961	3700

$\phi = 20^\circ$

EDST	$\angle i$	$\cos i$	Luminance (cd/m^2)
08:30	50.3	0.639	2142
09:00	44.8	0.710	2526
09:30	39.3	0.774	2844
10:00	33.8	0.831	3134
10:30	28.5	0.879	3134
11:00	23.5	0.917	3495
11:30	18.7	0.947	3569
12:00	14.5	0.968	3612
12:30	11.0	0.981	3651

$\phi = 25^\circ$

EDST	$\angle i$	$\cos i$	Luminance (cd/m^2)
08:30	45.3	0.703	2298
09:00	39.8	0.769	2672
09:30	34.3	0.826	3002
10:00	28.8	0.876	3288
10:30	23.5	0.917	3707
11:00	18.5	0.949	3562
11:30	13.7	0.971	3536
12:00	9.5	0.986	3618
12:30	6.0	0.994	3703

Table 83. Luminance Readings When Metering Perpendicular to the Incident Plane.
 CARC Surface Slopes: $\phi = 30^\circ, 35^\circ, 0^\circ, -5^\circ, -10^\circ$, and -15° .
 Luminance Meter Slope = 20° .

$\phi = 30^\circ$				$\phi = 35^\circ$			
EDST	<1	Cos i	Luminance (cd/m ²)	<1	Cos i	Luminance (cd/m ²)	
08:30	40.3	0.763	2614	35.3	0.816	NA	
09:00	34.8	0.821	2772	29.8	0.868	NA	
09:30	29.3	0.872	3133	24.3	0.912	3205	
10:00	23.8	0.915	3378	18.8	0.946	3505	
10:30	18.5	0.948	3485	13.5	0.972	3554	
11:00	13.5	0.973	3599	8.5	0.989	3732	
11:30	8.7	0.988	3608	3.7	0.998	3699	
12:00	4.5	0.997	3669	0.5	1.000	3694	
12:30	1.0	1.000	3720	4.0	0.998	3758	
$\phi = 0^\circ$				$\phi = -5^\circ$			
EDST	<1	Cos i	Luminance (cd/m ²)	<1	Cos i	Luminance (cd/m ²)	
08:30	70.3	0.337	NA	75.3	0.254	1281	
09:00	64.8	0.425	1905	69.8	0.346	1677	
09:30	59.3	0.511	2156	64.3	0.434	1847	
10:00	53.8	0.590	2425	58.8	0.518	2205	
10:30	48.5	0.662	2706	53.5	0.594	2532	
11:00	43.5	0.726	3010	48.5	0.663	2843	
11:30	38.7	0.780	3144	43.7	0.723	3001	
12:00	34.5	0.824	3229	39.5	0.771	3127	
12:30	31.0	0.857	3331	36.0	0.809	3231	
$\phi = -10^\circ$				$\phi = -15^\circ$			
EDST	<1	Cos i	Luminance (cd/m ²)	<1	Cos i	Luminance (cd/m ²)	
08:30	80.3	0.169	1095	25.3	0.082	872	
09:00	74.8	0.263	1525	79.8	0.178	1219	
09:30	69.3	0.354	1705	74.3	0.271	1491	
10:00	63.8	0.441	2041	68.8	0.361	1811	
10:30	58.5	0.522	2415	63.5	0.446	2074	
11:00	53.5	0.595	2698	58.5	0.53	2500	
11:30	48.7	0.660	2860	53.7	0.592	2738	
12:00	44.5	0.713	3021	49.5	0.649	2888	
12:30	41.0	0.754	3077	46.0	0.694	3027	

Note: An explanation of ϕ is given in Figure 350.

Table 84. Luminance Readings When Metering Perpendicular to the Incident Plane.
CARC Surface Slopes: $\phi = -20^\circ, -25^\circ, -30^\circ, -35^\circ, -40^\circ, -45^\circ, -50^\circ$ and -55° .
Luminance Meter Slope = 20° .

$\phi = -20^\circ$				$\phi = -25^\circ$			
EDST	$\angle i$	$\cos i$	Luminance (cd/m^2)	$\angle i$	$\cos i$	Luminance (cd/m^2)	
09:00	84.8	0.091	994	89.8	0.004	772	
09:30	79.3	0.186	1237	84.3	0.100	982	
10:00	73.8	0.279	1642	78.8	0.194	1375	
10:30	68.5	0.366	2031	73.5	0.263	1799	
11:00	63.5	0.447	2274	68.5	0.367	2067	
11:30	58.7	0.519	2640	63.7	0.443	2509	
12:00	54.5	0.581	2685	59.5	0.507	2550	
12:30	51.0	0.629	2949	56.0	0.559	2632	
$\phi = -30^\circ$				$\phi = -35^\circ$			
EDST	$\angle i$	$\cos i$	Luminance (cd/m^2)	$\angle i$	$\cos i$	Luminance (cd/m^2)	
09:30	89.3	0.013	686				
10:00	83.8	0.108	1104	88.8	0.020	828	
10:30	78.5	0.199	1626	83.5	0.113	1261	
11:00	73.5	0.285	1364	78.5	0.200	1621	
11:30	68.7	0.363	2369	73.7	0.280	2216	
12:00	64.5	0.430	2399	69.5	0.350	2270	
12:30	61.0	0.484	2476	66.0	0.406	2280	
$\phi = -40^\circ$				$\phi = -45^\circ$			
EDST	$\angle i$	$\cos i$	Luminance (cd/m^2)	$\angle i$	$\cos i$	Luminance (cd/m^2)	
10:30	88.5	0.026	982				
11:00	83.5	0.114	1390	88.5	0.027	1022	
11:30	78.7	0.195	1945	83.7	0.109	1780	
12:00	74.5	0.267	2041	79.5	0.182	1927	
12:30	71.0	0.325	2249	76.0	0.241	2094	
$\phi = -50^\circ$				$\phi = -55^\circ$			
EDST	$\angle i$	$\cos i$	Luminance (cd/m^2)	$\angle i$	$\cos i$	Luminance (cd/m^2)	
11:30	88.7	0.022	1451				
12:00	84.5	0.096	1542	89.5	0.009	1284	
12:30	81.0	0.156	1925	86.0	0.069	1588	

CALCULATION OF METER ANGLE θ

As the CARC sample was rotated through angle ϕ , the angle θ (meter angle) between the meter direction and the CARC surface varied. Figure 371 illustrates the geometry of the situation. The derivation of the meter angle θ follows:

ϕ is the angle the CARC sample is rotated about the x-axis.

\vec{M} is a unit vector representing a reflected ray of sun light toward the luminance meter.

$$\vec{M} = \cos 20^\circ \vec{i} + \sin 20^\circ \vec{k}$$

\vec{N} is a vector normal to the CARC sample and through the tip of the unit vector \vec{M} .

\vec{R} is a position vector to point B.

The coordinates of the points A and C are $A(\cos 20^\circ, 0, \sin 20^\circ)$ and $C(\cos 20^\circ, 0, 0)$.

Since $AC = \sin 20^\circ$ and $CB = \sin 20^\circ \sin \phi$, the coordinates of point B are $B(\cos 20^\circ, \sin 20^\circ \sin \phi \cos \phi, \sin 20^\circ \sin^2 \phi)$. Therefore,

$$\vec{R} = \cos 20^\circ \vec{i} + \sin 20^\circ \sin \phi \cos \phi \vec{j} + \sin 20^\circ \sin^2 \phi \vec{k}$$

$$\text{Since } \vec{R} \cdot \vec{M} = |\vec{R}| |\vec{M}| \cos \theta = \cos^2 20^\circ + \sin^2 20^\circ \sin^2 \phi,$$

$$\cos \theta = (\cos^2 20^\circ + \sin^2 20^\circ \sin^2 \phi)^{1/2}$$

Table 85.

ϕ	θ
0	20.0
5	19.9
10	19.7
15	19.3
20	18.8
25	18.1
30	17.2
35	16.3
40	15.2
45	14.0
50	12.7
55	11.3

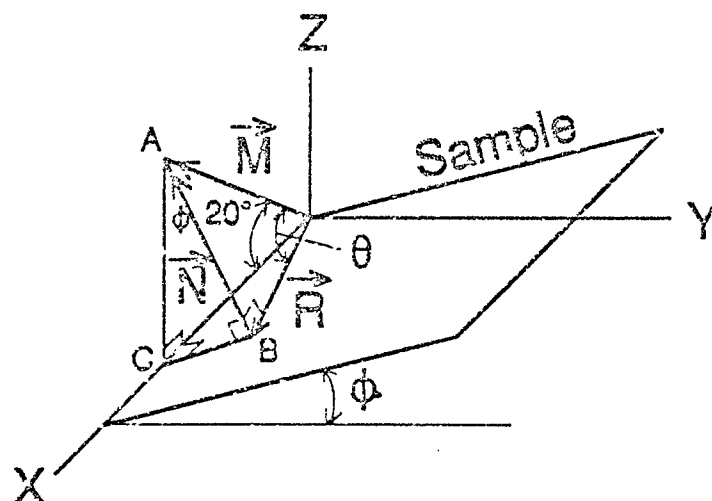


Figure 371.
Geometry for Calculating Meter Angle θ

SUN'S RAYS ON CARC-PAINTED SURFACE METERING AT 20 DEGREES FROM HORIZONTAL AND PERPENDICULAR TO SUN'S AZIMUTH

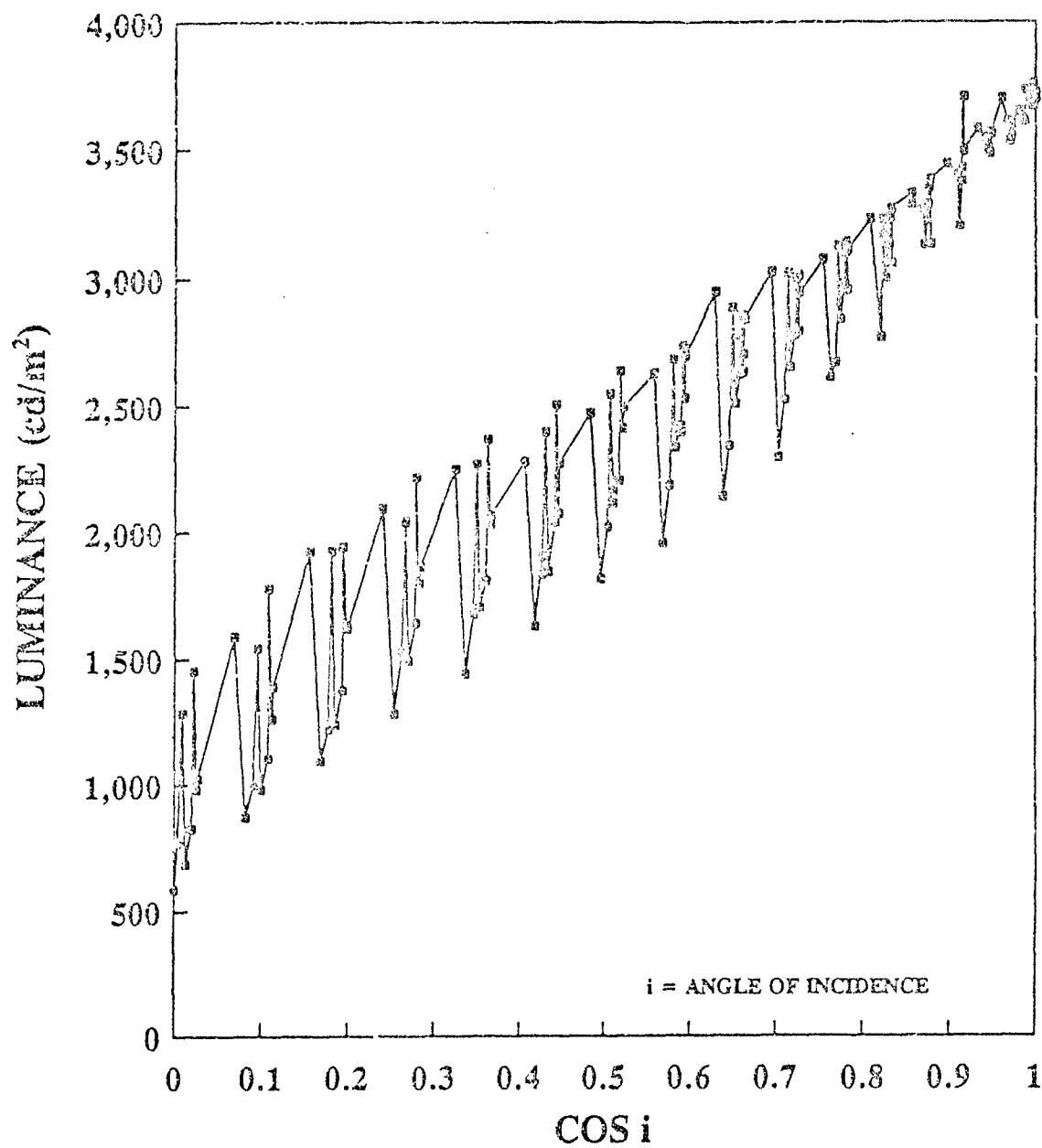


Figure 372.

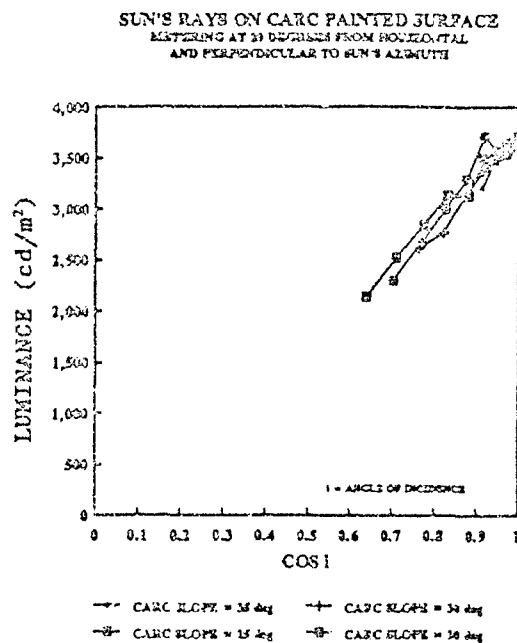


Figure 373.

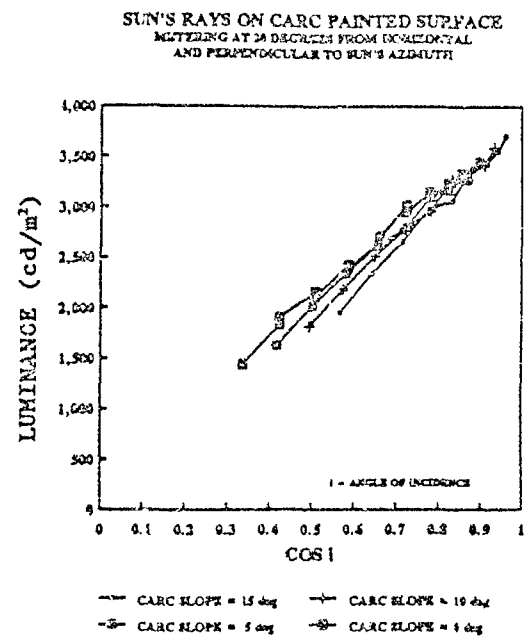


Figure 374.

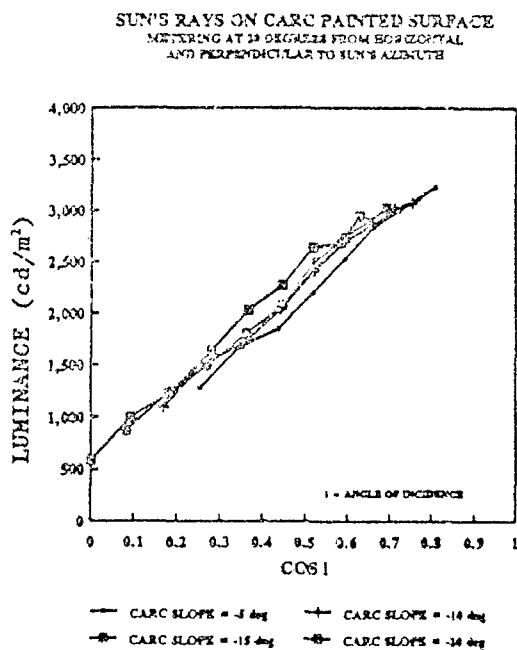


Figure 375.

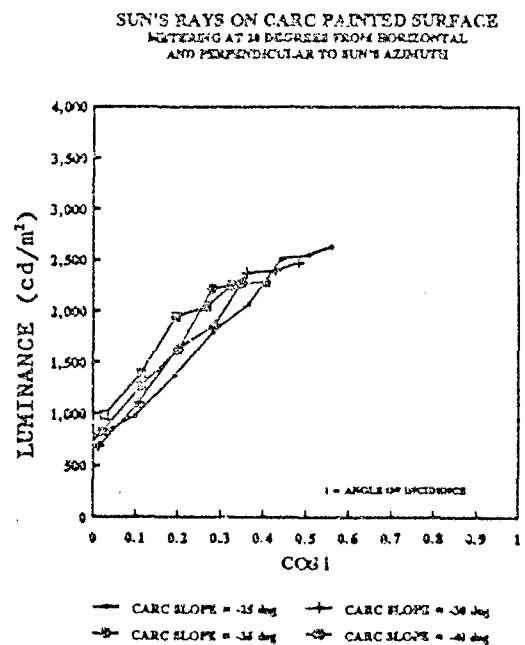


Figure 376.

SUMMARY

Figure 372 is a plot of all the luminance readings acquired as a function of $\cos i$ when metering was perpendicular to the plane of incidence. The graphs of Figure 373, Figure 374,...Figure 377 consist of sets of points from Figure 372 which correspond to the same CARC surface slope ϕ . Each set of points for each CARC surface slope plots nearly as a straight line. This suggests a Lambertian type surface when metering perpendicular to the plane of incidence.

As the CARC sample was rotated, the angle between the sample and the metering direction changed (Figure 371). As ϕ increased, θ decreased (Table 85). In general, slightly larger luminance readings were acquired for larger CARC surface slopes (for $\phi = 0^\circ$ to $\phi = -55^\circ$). This corresponds to smaller metering angles θ (Table 85). Similar results, but more dramatic, were obtained when metering in the plane of incidence.

Luminance readings are higher than what would be predicted for a Lambertian surface when metering closer to the surface of the CARC sample.

In the previous study, where metering was in the plane of incidence, a decrease in luminance was observed for decreasing angles of incidence from 60° to 0° for the same metering angle. This observation is the opposite of what would be expected, since a decrease in the angle of incidence produces more energy per area. This peculiar behavior was not observed when metering perpendicular to the incident plane.

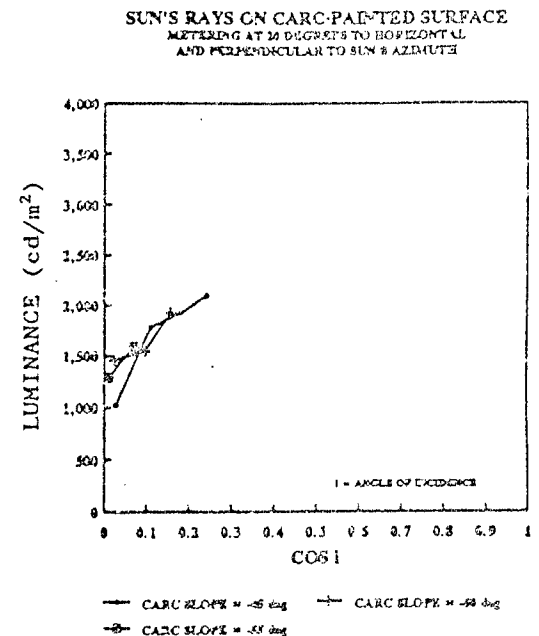


Figure 377.

LUMINANCE FROM A CARC PAINTED SAMPLE USING XENON LIGHT

PURPOSE

The purpose of this study was to acquire information on the light-distributing properties of a CARC-(Chemical Agent Resistant Coating) painted sample illuminated by an artificial Xenon light source; in particular, to determine how luminance readings are affected by changes in the angle of incidence. Additionally, this study determines how luminance readings are affected by changes in the meter-sample angle.

PROCEDURES

1. A Xenon light source was mounted at one end of a wood board.
2. A three inch diameter lens was clamped at the other end of the board so that light leaving the lens was collimated.
3. The wood board was mounted on a tripod and adjusted, with the aid of an angle level, to produce a 40° slope (Figure 378 and Figure 379, $\gamma = 40^\circ$).
4. A contact print of an 8" diameter protractor was made on an 8" X 10" sheet of photographic paper.
5. The protractor print was positioned on a horizontal, granite, holographic table (Figure 379).
6. Two vertical rods were placed on the protractor print; one at the 0° mark and the other at the 180° mark.
7. The protractor print was rotated so that collimated light from the Xenon source produced coincident shadows of the two vertical rods. The protractor print was taped to the table in this position.
8. One of the two vertical rods was positioned on the 40° mark and the other was positioned on the 220° mark.

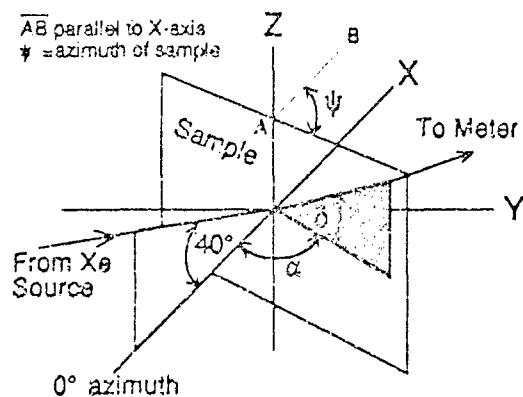


Figure 378

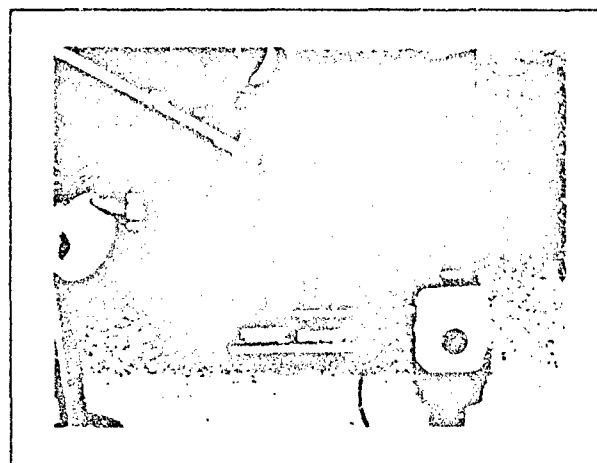


Figure 379

9. The LS-100 luminance meter, secured to a tripod, was positioned so that the two rods appeared as one rod while sighting through the meter's view finder.
10. A CARC-painted steel plate was positioned vertically on the protractor print along various lines through the center of the protractor while luminance readings were acquired.

Table 86. Luminance Readings from a CARC-painted Sample using a Xenon Light Source. Linear polarizer in front of source. Polarization axis horizontal. O.D. = 0.50 Xenon light source slope = 40°. Xenon Azimuth = 0°. $\alpha = 40^\circ$.

ψ	i	Cos i	$\delta = 0^\circ$ cd/m ²	$\delta = 10^\circ$ cd/m ²	$\delta = 20^\circ$ cd/m ²	$\delta = 30^\circ$ cd/m ²
10	82.4	0.133	0.956	0.906	0.951	0.995
20	74.8	0.262	1.654	1.626	1.716	1.750
30	67.5	0.383	2.252	2.225	2.331	2.374
40	60.5	0.492	2.792	2.778	2.865	2.905
50	54.1	0.587	3.466	3.276	3.330	3.380
60	48.4	0.663	3.892	3.684	3.744	3.792
70	44.0	0.720	4.259	4.006	4.079	4.183
80	41.0	0.754	4.409	4.163	4.252	4.377
90	40.0	0.766	4.463	4.438	4.434	4.522

Table 87. Luminance Readings from a CARC-painted Sample using a Xenon Light Source. Unpolarized light. Xenon light source slope = 0°. Xe Azimuth = 0°. $\delta = 0^\circ$.

ψ	i	Cos i	$\alpha = 40^\circ$ cd/m ²	$\alpha = 60^\circ$ cd/m ²
10	80.0	0.174	4.110	4.028
20	70.0	0.342	7.345	7.455
30	60.0	0.500	9.985	10.640
40	50.0	0.643	12.320	13.740
50	40.0	0.766	14.720	16.730
60	30.0	0.866	17.020	19.650
70	20.0	0.940	19.930	19.770
80	10.0	0.985	19.820	20.050
90	0.0	1.000	19.650	20.430

DERIVATION OF ANGLE OF INCIDENCE i

Let N represent a unit vector normal to the sample:

$$N = \sin \psi \, i + \cos \psi \, j.$$

Let I represent a unit vector in the direction of an incident Xenon light ray:

$$I = \cos 40^\circ \, i + \sin 40^\circ \, j.$$

$N \cdot I = \cos i = \cos 40^\circ \sin \psi$, where angle i is the angle of incidence.

$$\cos i = \cos 40^\circ \sin \psi$$

DERIVATION OF METER SAMPLE ANGLE β

Let R represent a unit position vector in the plane of the sample and with the same slope as the meter (Figure 380 and Figure 381):

$$R = -\cos \delta \cos \psi \, i + \cos \delta \sin \psi \, j + \sin \delta \, k$$

Let L represent a unit position vector in the direction of the luminance readings:

$$L = \cos \delta \cos \alpha \, i + \cos \delta \sin \alpha \, j + \sin \delta \, k$$

$$R \cdot L = \cos \beta = -\cos^2 \delta \cos \psi \cos \alpha + \cos^2 \delta \sin \psi \sin \alpha + \sin^2 \delta$$

$$\cos \beta = -\cos^2 \delta \cos (180 - [\psi + \alpha]) + \sin^2 \delta$$

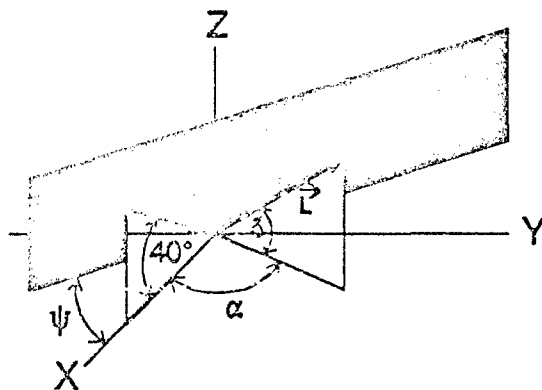


Figure 380

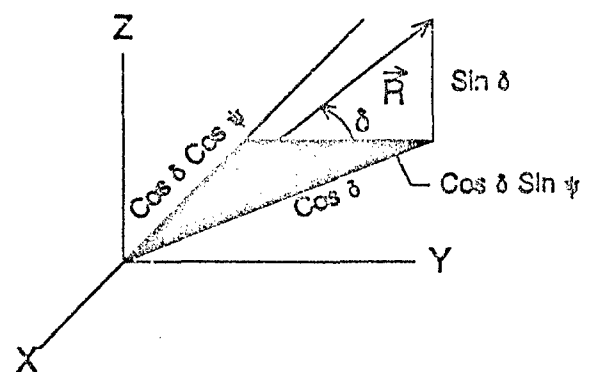


Figure 381

Table 58. Angles (β) Between Meter and Sample

	$\alpha = 40^\circ$ $\delta = 0^\circ$	$\alpha = 40^\circ$ $\delta = 10^\circ$	$\alpha = 40^\circ$ $\delta = 20^\circ$	$\alpha = 40^\circ$ $\delta = 30^\circ$	$\alpha = 60^\circ$ $\delta = 0^\circ$
ψ	β	β	β	β	β
10	130	126.4	116.8	103.4	110
20	120	117.1	108.9	97.2	100
30	110	107.6	100.7	90.4	90
40	100	97.9	92.1	83.1	80
50	90	88.3	83.3	75.5	70
60	80	78.5	74.3	67.7	60
70	70	68.8	65.2	59.6	50
80	60	59.0	56.0	51.3	40
90	50	49.2	46.8	42.9	30

SUMMARY

The importance of this study arises from the fact that sky conditions do not influence the final results. Data was acquired in a darkroom setting with a Xenon light source as the only source of illumination. Light reflected from the apparatus and the room's walls were the only other source of radiation. Also, the range of luminance readings acquired in this study (1 cd/m^2 - 24 cd/m^2), using a Xenon light source, were considerably smaller than those acquired in other studies (400 cd/m^2 - 7000 cd/m^2) using the sun as a source of light.

There were two parts to this study. In the first, measurements were made outside the plane of incidence. In the second, measurements were made in the plane of incidence.

Table 86 and the graph of Figure 383 summarize the results obtained when metering was outside the plane of incidence (sample in a vertical plane; Xe source slope = 40° , azimuth = 0° ; meter slopes of 0° , 10° , 20° and 30° with azimuth = 40°). The graph of Figure 383 shows a near-perfect direct proportion between luminance and the cosine of the angle of incidence for the CARC-painted sample. This graph does not suggest any luminance dependence on the meter-sample angle β . Even though the range of β is from 40° to 130° (Table 88), there is no observable deviation in the direct proportion between the luminance and $\cos i$. The sets of points for each of the four meter slopes, 0° , 10° , 20° and 30° , are nearly all coincident.

These results support the following conclusions when metering outside the plane of incidence:

1. The light-distributing properties of the CARC-painted sample produces luminance readings which would be obtained from a Lambertian type surface when metering is outside the plane of incidence.
2. Light energy per unit area is directly proportional to the cosine of the angle of incidence for a collimated light beam incident on the CARC-painted sample, just as it would be for a perfect diffuse reflector (Lambertian surface).

In the second part of this study, luminance measurements were made in the plane of incidence. Changes in the angle of incidence were made by rotating the sample in a horizontal plane while keeping the direction of the Xenon light source and the direction of the luminance meter constant. Figure 382 shows the geometry used for these measurements.

Table 87 and the graph of Figure 384 summarize the results obtained when metering was in the plane of incidence (sample in a vertical plane; Xenon source slope = 0° , azimuth = 0° ; LS-100 meter slope = 0° , azimuth = 40° and 60°). The two plots of Figure 384 (meter azimuth = 40° and 60°) are straight lines except for measurements acquired near the mirror reflection angle ($\psi = 60^\circ$, see Table 83). The CARC-painted sample has light-distributing properties similar to a Lambertian surface when luminance measurements are away from the direction of mirror reflection. However, it has light-distributing properties similar to a semi-gloss surface when luminance measurements are near the direction of mirror reflection. If the CARC-painted sample was a perfect diffuser, the two plots of Figure 384 would be straight lines and the plots would also be coincident.

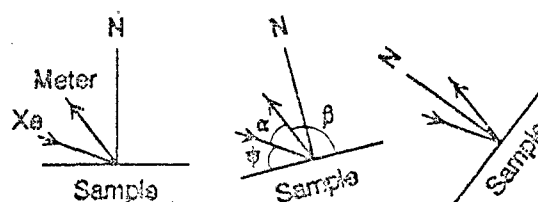


Figure 382.

GONIOPHOTOMETRIC STUDY CARC-PAINTED SAMPLE POLARIZED Xe LIGHT SOURCE

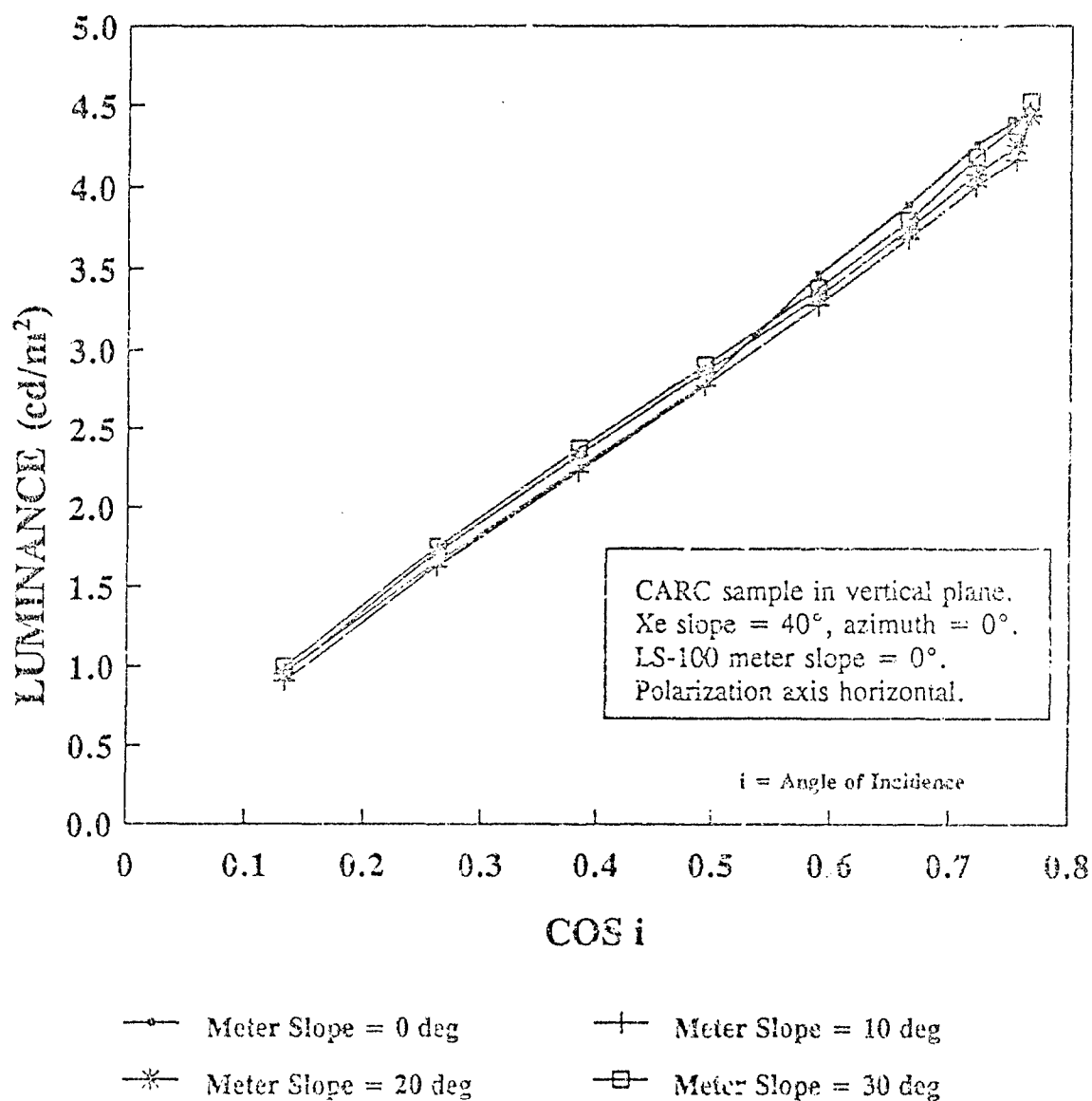
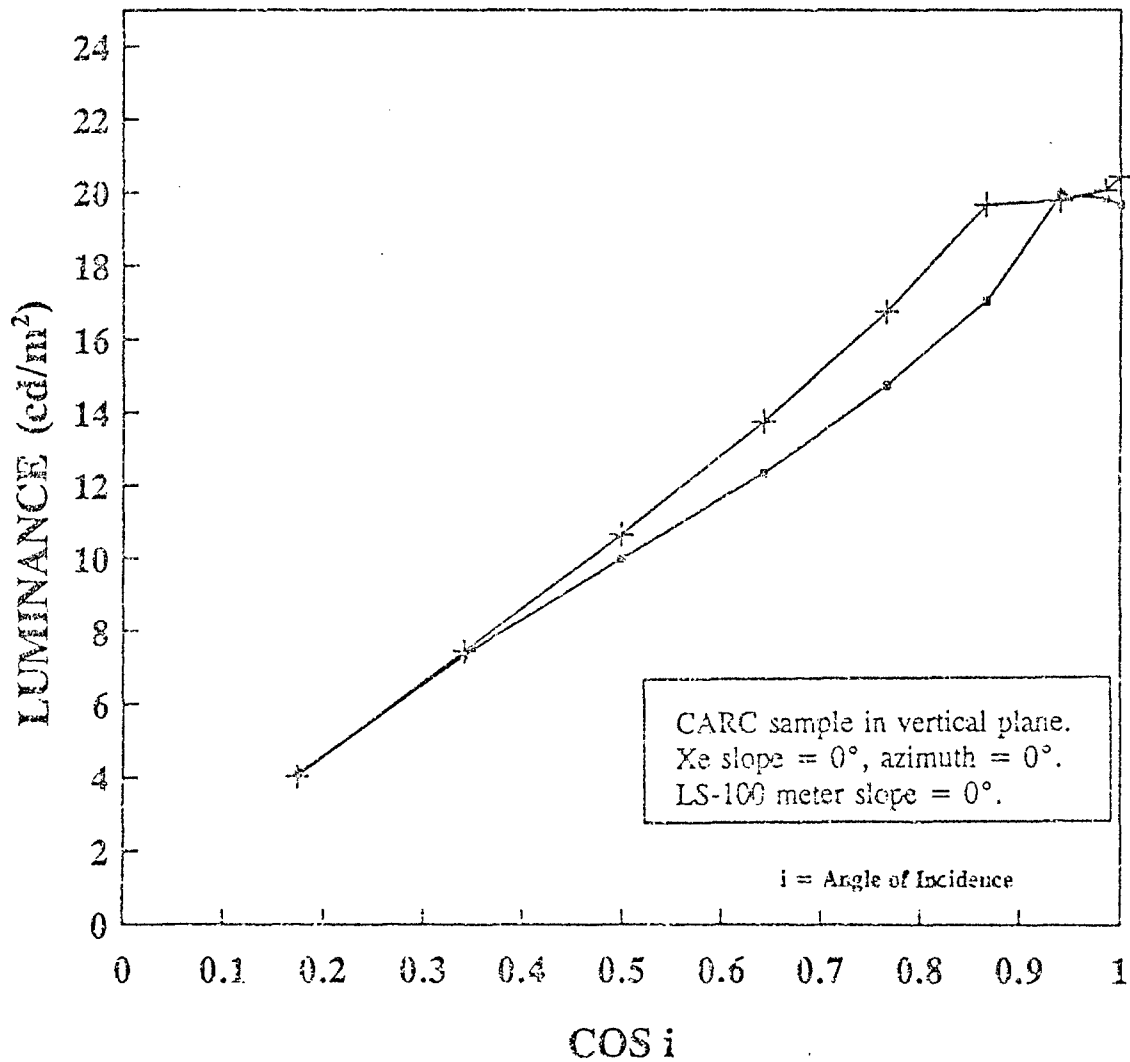


Figure 383.

GONIOPHOTOMETRIC STUDY CARC-PAINTED SAMPLE UNPOLARIZED Xe LIGHT SOURCE



—○— Meter Azimuth = 40

—+— Meter Azimuth = 60

Figure 384.

POLARIZATION AXIS OF REFLECTED WHITE LIGHT FROM A CARC-PAINTED SAMPLE

PURPOSE

The purpose of this study was to acquire information on the polarization properties of a CARC- (Chemical Agent Resistant Coating) painted sample illuminated by a collimated Xenon light source; in particular, to determine how the degree of polarization and the polarization angle are affected by changes in azimuthal viewing angle when the altitude of the viewing angle is constant.

PROCEDURES

1. A Xenon light source was mounted at one end of a wood board.
2. A three inch diameter lens was clamped at the other end of the board so that light leaving the lens was collimated.
3. A linear polarizer attached to an adjustable ring, to change the polarization angle θ , was positioned in front of the collimating lens.
4. The wood board was mounted on a tripod and adjusted, with the aid of an angle level, to produce a 40° slope (Figure 385 and Figure 386, $\gamma = 40^\circ$).
5. A contact print of an eight inch diameter protractor was made on an 8" X 10" sheet of photographic paper.
6. The protractor print was positioned on a horizontal, granite, holographic table (Figure 379).
7. Two vertical rods were placed on the protractor print; one at the 0° mark and the other at the 180° mark.
8. The protractor print was rotated so that collimated light from the Xenon source produced coincident shadows of the two vertical rods. The protractor print was taped to the table in this position.

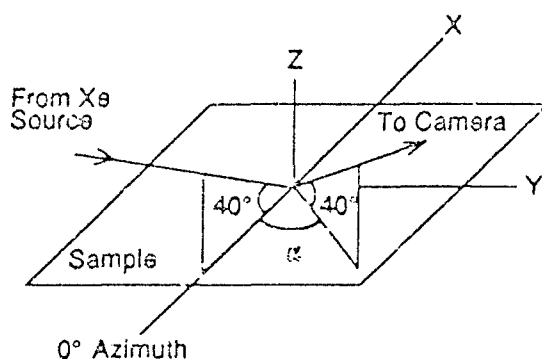


Figure 385

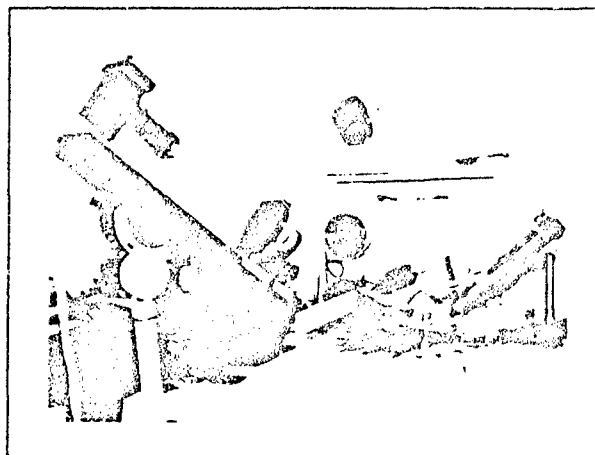


Figure 386

9. A 3/4" X 2" X 3' wooden board was placed across the protractor print at 20° intervals and pieces of tape were positioned on the table at opposite ends of the board.
10. A six inch tube with a polarization axis finder at one end was mounted on a 35 mm camera. A 4" X 1" mirror was taped to the top of the tube as shown in Figure 388 and Figure 389
11. The azimuth angle α (Figure 385) of the camera's line of sight was obtained through the use of the mirror (Figure 388 and Figure 389). The block of wood was positioned at the desired azimuth. The camera was then positioned so that the image of the edge of the wood and the wood edge were coincident, as shown in Figure 389.
12. The azimuth angle α was varied from 180° to 20°.
13. The transmission axis of the linear polarizer was horizontal when $\theta = 0^\circ$ (Figure 387). The linear polarizer was rotated clockwise, when looking toward the Xenon light source, in 10° increments from 0° to 90° for each azimuth angle α .

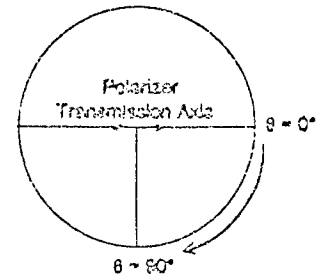


Figure 387.

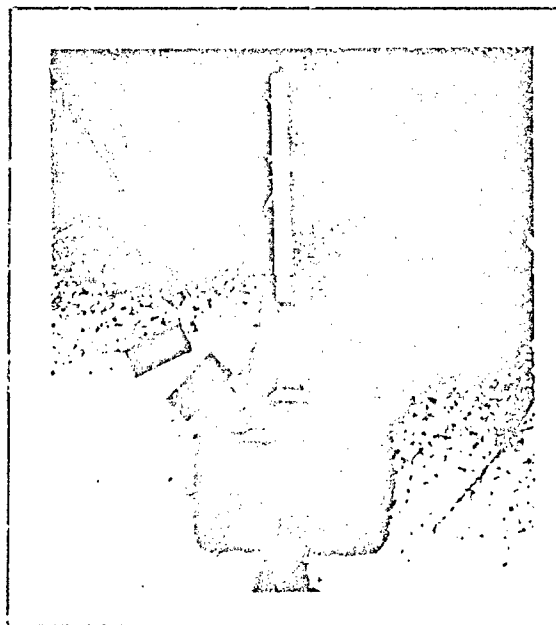


Figure 388

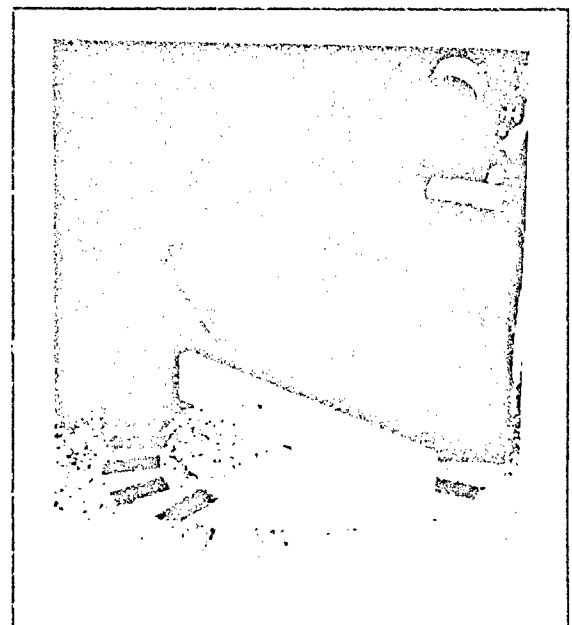


Figure 389

Figure 390, Figure 391,... Figure 394 show the results of this study. See Appendix B for an interpretation of the wedge shaped patterns.

CARC-Painted Sample Viewed Through a Polarization Axis Finder Using Xenon Light Source.
 Xe Slope = 40° , Camera Slope = 40° and CARC-Painted Sample in a Horizontal Plane.

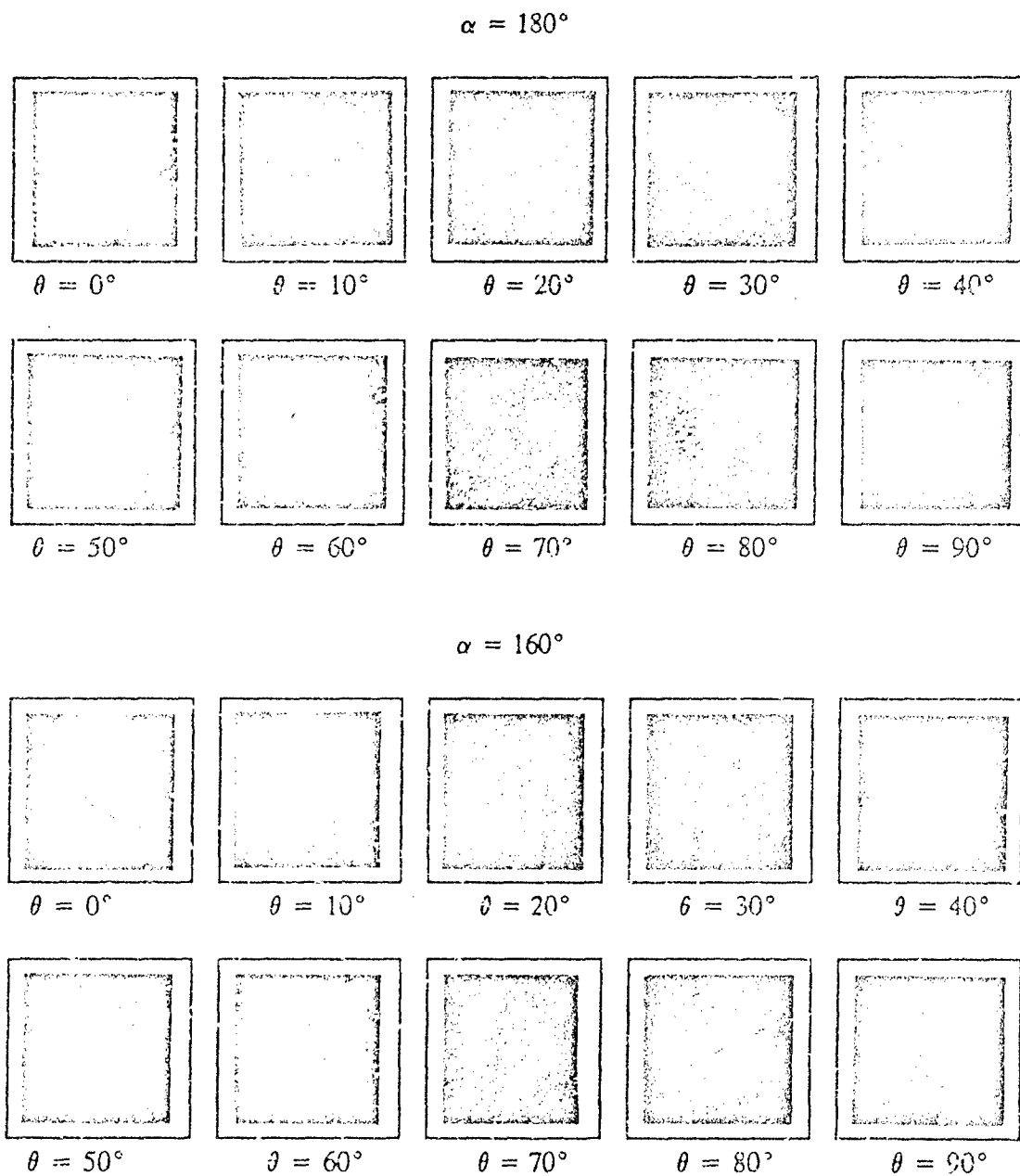


Figure 390.

CARC-Painted Sample Viewed Through a Polarization Axis Finder Using Xenon Light Source.
 Xe Slope = 40° , Camera Slope = 40° and CARC-Painted Sample in a Horizontal Plane.

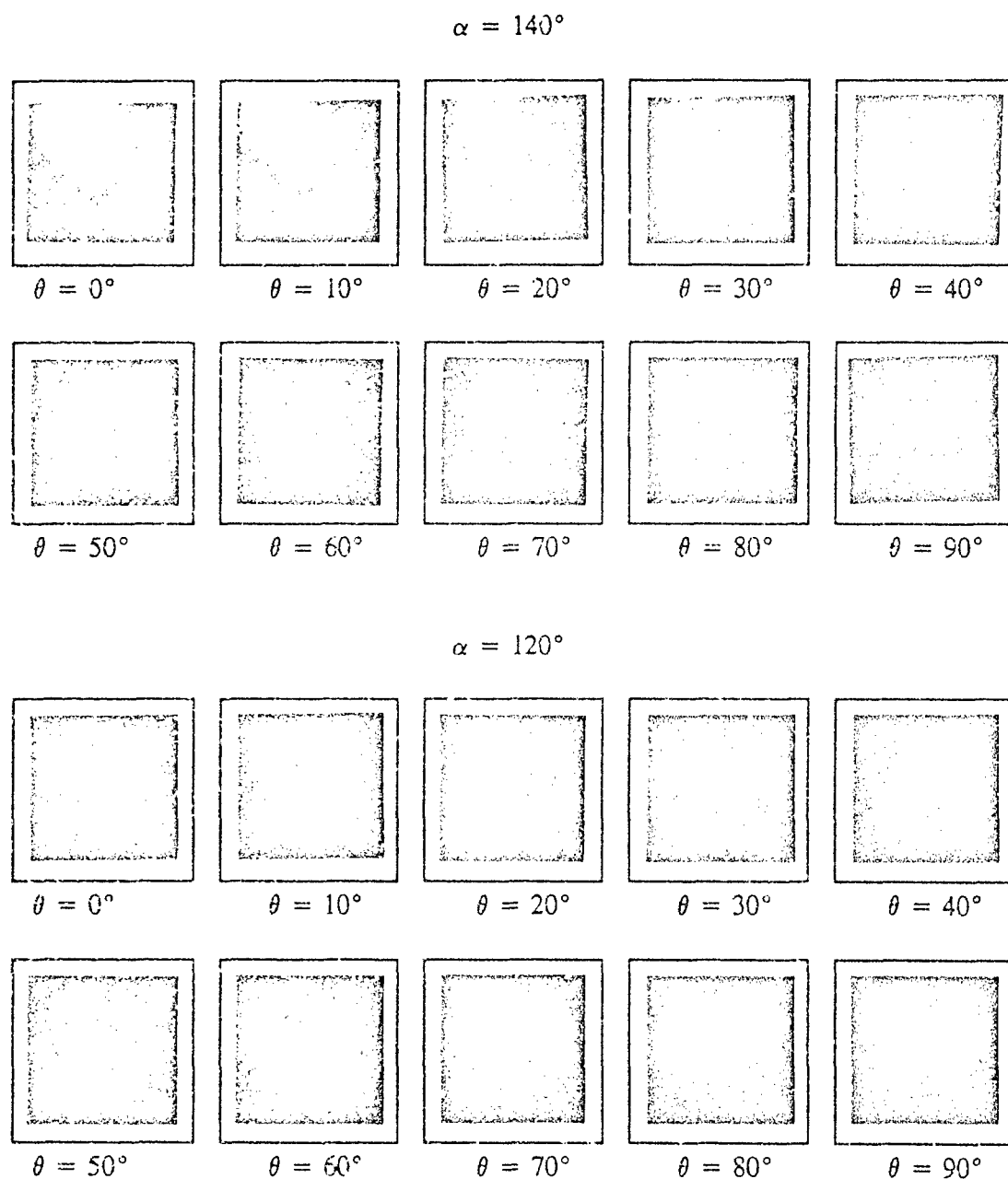


Figure 391.

CARC-Painted Sample Viewed Through a Polarization Axis Finder Using Xenon Light Source.
 Xe Slope = 40° , Camera Slope = 40° and CARC-Painted Sample in a Horizontal Plane.

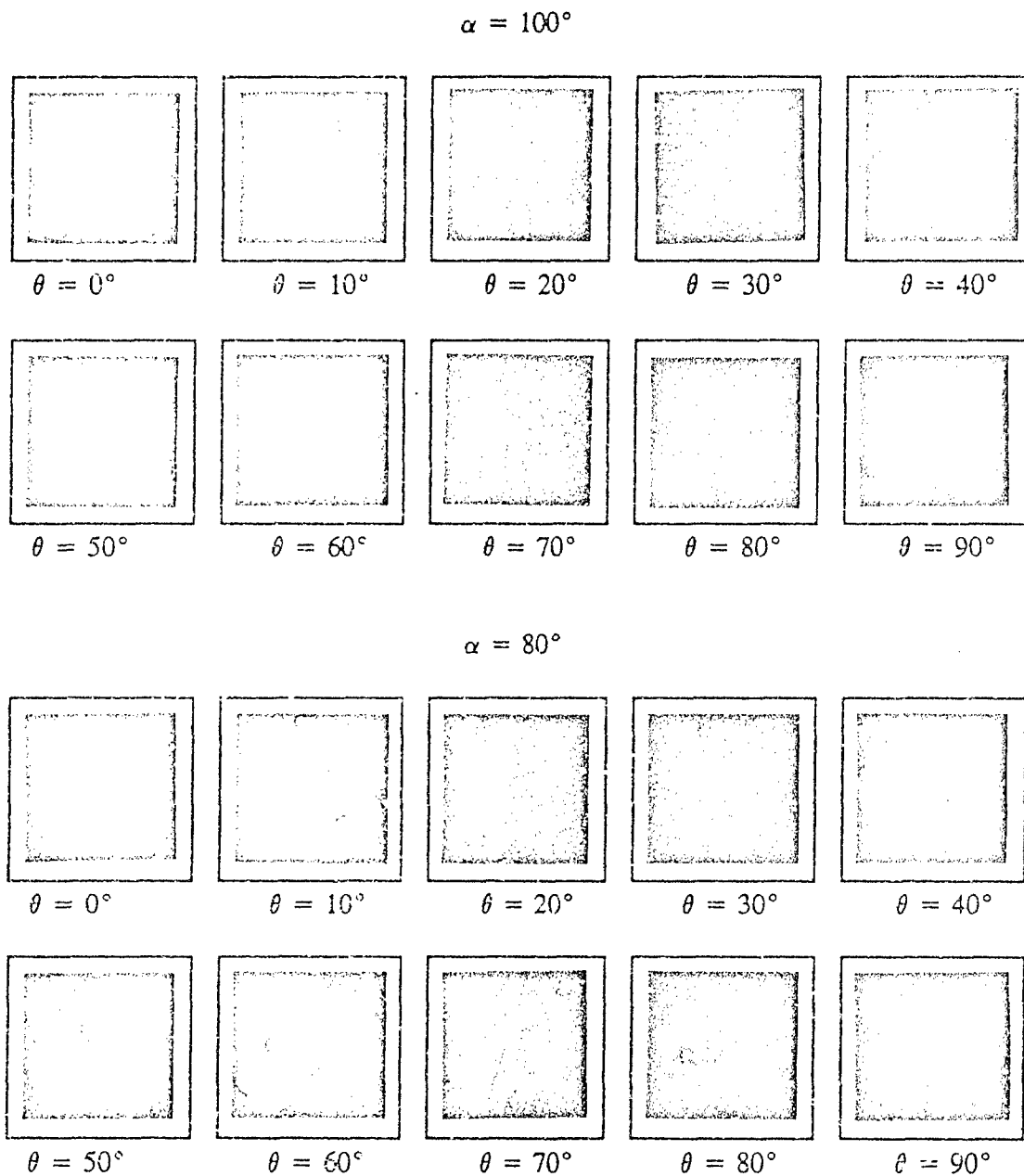


Figure 392.

CARC-Painted Sample Viewed Through a Polarization Axis Finder Using Xenon Light Source.
 Xe Slope = 40° , Camera Slope = 40° and CARC-Painted Sample in a Horizontal Plane.

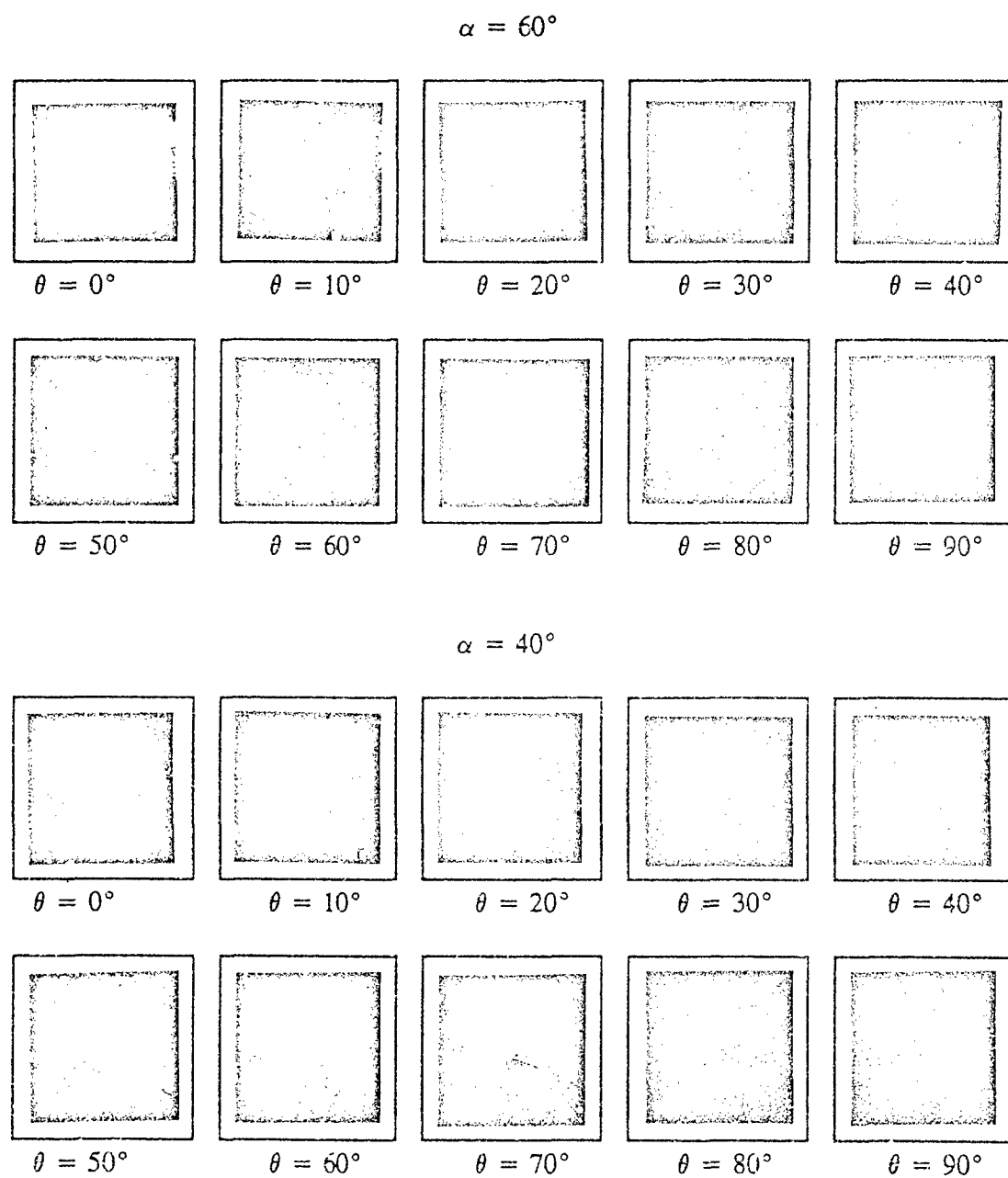


Figure 393.

CARC-Painted Sample Viewed Through a Polarization Axis Finder Using Xenon Light Source.
Xe Slope = 40° , Camera Slope = 40° and CARC-Painted Sample in a Horizontal Plane.

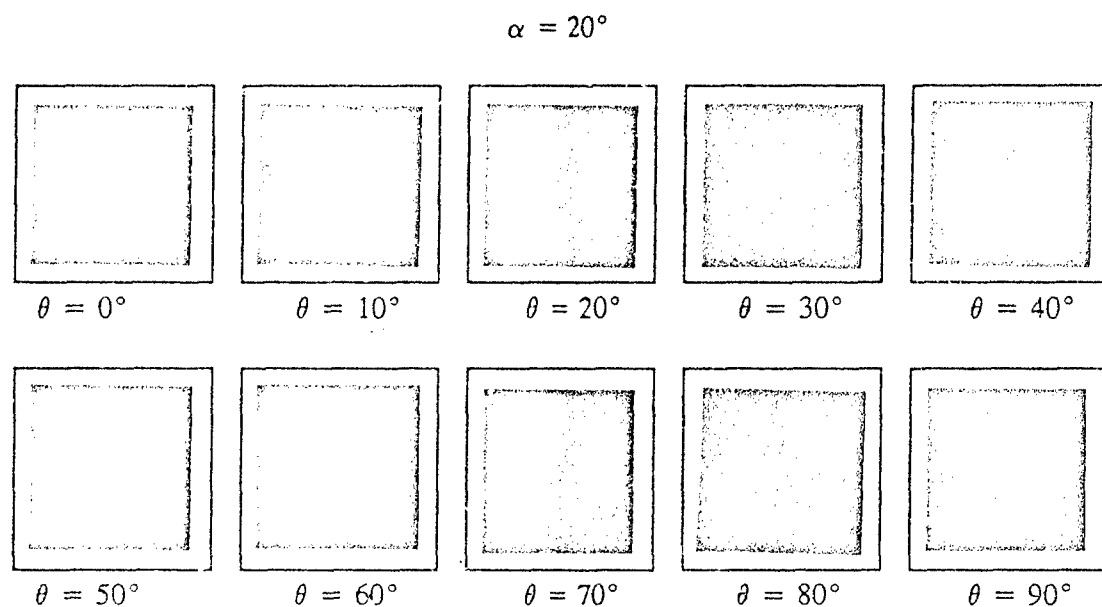


Figure 394.

Table 89. Orientation of Polarization Axis for Reflected Xe Light from CARC-Painted Surface. Degree of Polarization is near zero for $\alpha = 140^\circ$ and $\theta = 40^\circ$.

$\alpha \backslash \theta$	0	10	20	30	40	50	60	70	80	90
180	—	—	—	—	—	—	—	—		
160	—	—	—	—	—	—				
140	/	/	/	/		\	\	\	\	\
120	/	/	/		\	\	\	\	\	—
100	/		\	\	\	\	\	—	—	/
80	\	\	\	\	\	—	—	—	/	/
60	\	\	\	—	—	—	—	/	/	/
40	\	\	—	—	—	/	/	/	/	/
20	\	—	—	—	/	/	/	/	/	/

Table 90. Degrees of polarization axis from horizontal, ψ , for reflected Xe light from CARC painted surface. Angles are positive when orientations are clockwise from horizontal and negative for orientations counterclockwise from horizontal.

$\alpha \backslash \theta$	0	10	20	30	40	50	60	70	80	90
180	3	3	3	3	3	3	3	3	-87	-87
160	-7	-8	-9	-8	-9	-7	80	79	81	82
140	-30	-30	-30	-30		60	60	60	60	40
120	-44	-51	-69	87	70	55	52	35	20	0
100	-78	90	73	56	46	34	23	6	-6	-20
80	76	65	47	35	28	16	2	-5	-17	-36
60	57	45	35	17	7	0	-9	-20	-30	-42
40	37	29	18	7	0	-9	-22	-34	-45	-55
20	24	13	4	-5	-13	-24	-36	-45	-59	-67

FRESNEL MODEL

Fresnel's laws of reflection, derived from the elastic solid theory, are as follows:

$$\frac{R_s}{E_s} = - \frac{\sin(\phi - \phi')}{\sin(\phi + \phi')} \quad \frac{R_p}{E_p} = \frac{\tan(\phi - \phi')}{\tan(\phi + \phi')} \quad (1)$$

$$\frac{E'_s}{E_s} = \frac{2 \sin \phi' \cos \phi}{\sin(\phi + \phi')} \quad \frac{E'_p}{E_p} = \frac{2 \sin \phi' \cos \phi}{\sin(\phi + \phi') \cos(\phi - \phi')} \quad (2)$$

E, R and E' refer to the amplitudes of the electric vectors in the incident, reflected and refracted light respectively.

The subscripts s and p denote two planes of vibration; p vibrations are parallel to the plane of incidence and s vibrations are perpendicular to the plane of incidence.

The angles ϕ and ϕ' are the angles of incidence and refraction respectively.

$$\frac{R_p}{R_s} = - \frac{F_p}{E_s} \frac{\cos(\phi + \phi')}{\cos(\phi - \phi')} \quad (3)$$

The ratio $\frac{R_p}{R_g}$ is the tangent of the angle ψ , the angle between R and R_g (Figure 11).

The ratio $\frac{E_p}{E_s}$ is the tangent of the angle θ , the angle between E and E_s (Figure 11).

In general, equation (3) is only valid for reflected polarized light in the plane of incidence. The plane of incidence is normally taken to be the plane containing the incident and reflected rays of light and the normal to the surface. The only data collected for this condition (azimuth angle $\alpha = 180^\circ$, Figure 385) is shown in Figure 399. The graph of Figure 399 shows very good agreement between experimental data and predicted results using equation (3) with $n = 1.2$.

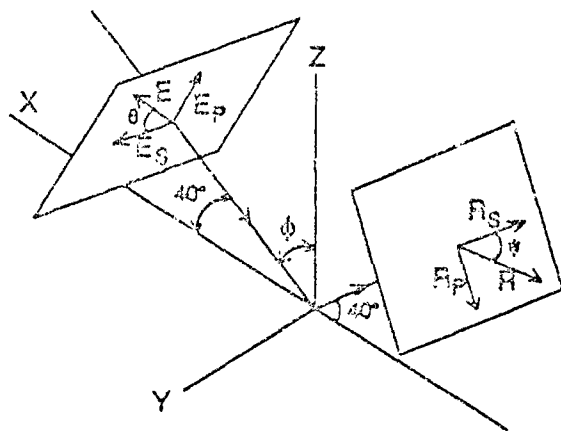


Figure 395.

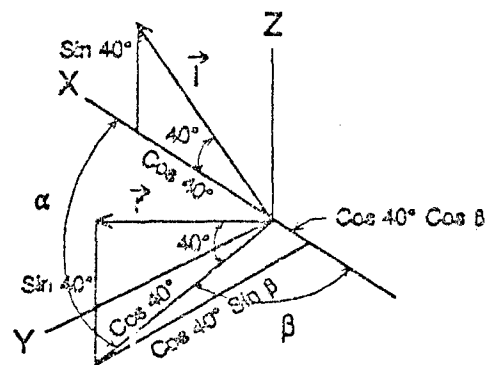


Figure 396.

The CARC-painted surface is not a mirror reflector but reflects light out of the plane of incidence. As a first step at explaining the nature of the reflected light out of the plane of incidence, the following ideas were incorporated into equation (3):

1. The plane passing through the incident ray and the reflected ray was taken to be the new plane of incidence.
2. The angle of incidence was assumed to be one half the angle between the incident ray and the reflected ray.
3. E_p was replaced with its projection onto a unit vector (vector D , Figure 398) perpendicular to I and in the new incident plane. E_s was replaced with its projection onto a unit vector (vector $-C$, Figure 393) perpendicular to the incident ray I and also to the new incident plane.
4. The angle between R and R_s (ψ), obtained from equation (3), was decreased (clockwise rotation) by the angle ϵ , the angle between the plane containing I and r and the plane containing r and the normal to the CARC-painted surface (N). Vertical lines in the photographs were in the plane containing r and N .

Let I equal a unit vector opposite in direction to an incident ray of light (Figure 396).

$$I = \cos 40^\circ i + \sin 40^\circ k$$

Let r equal a unit vector in the direction of the reflected ray of light (Figure 396).

$$r = -\cos 40^\circ \cos \beta i + \cos 40^\circ \sin \beta j + \sin 40^\circ k$$

From Figure 395 and Figure 397:

$$E = -\sin 40^\circ \sin \theta i + \cos \theta j + \cos 40^\circ \sin \theta k$$

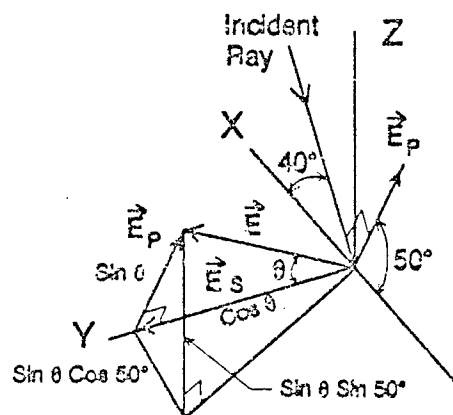


Figure 397.

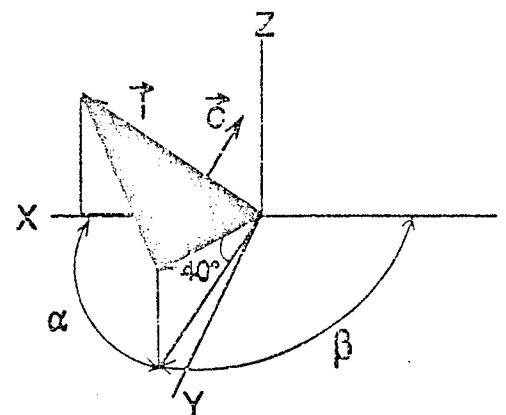


Figure 398.

From Figure 397: $E_s = \cos \theta \mathbf{j}$ and $E_p = -\sin 40 \sin \theta \mathbf{i} + \cos 40 \sin \theta \mathbf{k}$

$$-\mathbf{C} = \frac{\mathbf{r} \times \mathbf{I}}{|\mathbf{r} \times \mathbf{I}|} = \frac{\sin 40 \sin \beta \mathbf{i} + \sin 40 (1 + \cos \beta) \mathbf{j} - \cos 40 \sin \beta \mathbf{k}}{\sqrt{\sin^2 \beta + \sin^2 40 (1 + \cos \beta)^2}}$$

Unit vector $\mathbf{D} = x \mathbf{i} + y \mathbf{j} + z \mathbf{k}$ satisfies the following conditions:

$$1. \ x^2 + y^2 + z^2 = 1 \quad 2. \ \mathbf{D} \cdot \mathbf{I} = 0 \quad 3. \ \mathbf{D} \cdot \mathbf{C} = 0$$

$$\mathbf{D} = \frac{-\sin^2 40 (1 + \cos \beta) \mathbf{i} + \sin \beta \mathbf{j} + \sin 40 \cos 40 (1 + \cos \beta) \mathbf{k}}{\sqrt{\sin^2 \beta + \sin^2 40 (1 + \cos \beta)^2}}$$

E_s' is the projection of \mathbf{E} onto $-\mathbf{C}$. E_p' is the projection of \mathbf{E} onto \mathbf{D} .

$$E_s' = \mathbf{E} \cdot (-\mathbf{C}) = \frac{\sin 40 \cos \theta (1 + \cos \beta) - \sin \beta \sin \theta}{\sqrt{\sin^2 \beta + \sin^2 40 (1 + \cos \beta)^2}}$$

$$E_p' = \mathbf{E} \cdot \mathbf{D} = \frac{\sin 40 \sin \theta (1 + \cos \beta) + \sin \beta \cos \theta}{\sqrt{\sin^2 \beta + \sin^2 40 (1 + \cos \beta)^2}}$$

The angle ϵ between the plane containing \mathbf{r} and \mathbf{I} and the plane containing \mathbf{r} and \mathbf{N} ($\mathbf{N} = \mathbf{k}$) is found by determining the angle between their normals.

The unit vector \mathbf{N}' , normal to the plane containing \mathbf{r} and \mathbf{N} , is

$$\mathbf{N}' = \frac{\mathbf{N} \times \mathbf{r}}{|\mathbf{N} \times \mathbf{r}|} = -\sin \beta \mathbf{i} - \cos \beta \mathbf{j}$$

Since \mathbf{C} is a unit vector normal to the plane containing \mathbf{I} and \mathbf{r} ,

$$\mathbf{C} \cdot \mathbf{N}' = \frac{\sin 40 (1 + \cos \beta)}{\sqrt{\sin^2 \beta + \sin^2 40 (1 + \cos \beta)^2}} = \cos \epsilon$$

Table 91. Calculations. $C+/C- = \cos(\phi + \phi')/\cos(\phi - \phi')$. $\psi' = \psi - \epsilon$.
Exp. = Experimental values for ψ . Diff. = $\psi' - \text{Exp.}$

$\alpha = 180$ $\beta = 0$		$\phi = 50.00$ $\phi' = 39.67$		$n = 1.2$ $C+/C- = -0.01$		$\epsilon = 0.00$			
θ	Es'	Ep'	Ep'/Es'	θ'	Rp/Rs	ψ	ψ'	Exp.	Diff.
0.00	1.00	0.00	0.00	0.00	0.00	0.00	0.00	3.00	3.00
10.00	0.98	0.17	0.18	10.00	0.00	-0.06	-0.06	3.00	3.06
20.00	0.94	0.34	0.36	20.00	0.00	-0.12	-0.12	3.00	3.12
30.00	0.87	0.50	0.58	30.00	0.00	-0.19	-0.19	3.00	3.19
40.00	0.77	0.64	0.84	40.00	0.00	-0.28	-0.28	3.00	3.28
50.00	0.64	0.77	1.19	50.00	-0.01	-0.40	-0.40	3.00	3.40
60.00	0.50	0.87	1.73	60.00	-0.01	-0.58	-0.58	3.00	3.58
70.00	0.34	0.94	2.75	70.00	-0.02	-0.92	-0.92	3.00	3.92
80.00	0.17	0.98	5.67	80.00	-0.03	-1.90	-1.90	-87.00	85.10
90.00	0.00	1.00	∞	90.00	∞	-90.00	-90.00	-87.00	3.00

$\alpha = 180$ $\beta = 0$		$\phi = 50.00$ $\phi' = 26.78$		$n = 1.70$ $C+/C- = -0.25$		$\epsilon = 0.00$			
θ	Es'	Ep'	Ep'/Es'	θ'	Rp/Rs	ψ	ψ'	Exp.	Diff.
0.00	1.00	0.00	0.00	0.00	0.00	0.00	0.00	3.00	3.00
10.00	0.98	0.17	0.18	10.00	-0.04	-2.51	-2.51	3.00	5.51
20.00	0.94	0.34	0.36	20.00	-0.09	-5.17	-5.17	3.00	8.17
30.00	0.87	0.50	0.58	30.00	-0.14	-8.17	-8.17	3.00	11.17
40.00	0.77	0.64	0.84	40.00	-0.21	-11.79	-11.79	3.00	14.79
50.00	0.64	0.77	1.19	50.00	-0.30	-16.51	-16.51	3.00	19.51
60.00	0.50	0.87	1.73	60.00	-0.43	-23.31	-23.31	3.00	26.31
70.00	0.34	0.94	2.75	70.00	-0.68	-34.35	-34.35	3.00	37.35
80.00	0.17	0.98	5.67	80.00	-1.41	-54.67	-54.67	-87.00	32.33
90.00	0.00	1.00	∞	90.00	∞	-90.00	-90.00	-87.00	3.00

$\alpha = 160$ $\beta = 20$		$\phi = 48.97$ $\phi' = 38.95$		$n = 1.2$ $C+/C- = -0.04$		$\epsilon = 15.34$			
θ	Es'	Ep'	Ep'/Es'	θ'	Rp/Rs	ψ	ψ'	Exp.	Diff.
0.00	0.96	0.26	0.27	15.34	-0.01	-0.58	-15.92	-7.00	8.92
10.00	0.90	0.43	0.47	25.34	-0.02	-1.00	-16.34	-8.00	8.34
20.00	0.82	0.58	0.71	35.34	-0.03	-1.49	-16.83	-9.00	7.83
30.00	0.70	0.71	1.01	45.34	-0.04	-2.13	-17.47	-8.00	9.47
40.00	0.57	0.82	1.45	55.34	-0.05	-3.04	-18.38	-9.00	9.38
50.00	0.42	0.91	2.18	65.34	-0.08	-4.58	-19.92	-7.00	12.92
60.00	0.25	0.97	3.82	75.34	-0.14	-8.00	-23.34	80.00	76.66
70.00	0.08	1.00	12.27	85.34	-0.45	-24.27	-39.61	79.00	61.39
80.00	-0.09	1.00	-10.70	-84.66	0.39	21.47	6.13	81.00	74.87
90.00	-0.26	0.96	-3.65	-74.66	0.13	7.63	-7.71	82.00	89.71
$\alpha = 160$ $\beta = 20$		$\phi = 48.97$ $\phi' = 26.34$		$n = 1.7$ $C+/C- = -0.27$		$\epsilon = 15.34$			
θ	Es'	Ep'	Ep'/Es'	θ'	Rp/Rs	ψ	ψ'	Exp.	Diff.
0.00	0.96	0.26	0.27	15.34	-0.08	-4.31	-19.65	-7.00	12.65
10.00	0.90	0.43	0.47	25.34	-0.13	-7.41	-22.75	-8.00	14.75
20.00	0.82	0.58	0.71	35.34	-0.19	-11.02	-26.36	-9.00	17.36
30.00	0.70	0.71	1.01	45.34	-0.28	-15.53	-30.87	-8.00	22.87
40.00	0.57	0.82	1.45	55.34	-0.40	-21.66	-37.00	-9.00	28.00
50.00	0.42	0.91	2.18	65.34	-0.60	-30.88	-46.22	-7.00	39.22
60.00	0.25	0.97	3.82	75.34	-1.05	-46.39	-61.73	80.00	38.27
70.00	0.08	1.00	12.27	85.34	-3.37	-73.47	-88.81	79.00	12.19
80.00	-0.09	1.00	-10.70	-84.66	2.94	71.20	55.86	81.00	25.14
90.00	-0.26	0.96	-3.65	-74.66	1.00	45.03	29.69	82.00	52.31

$\alpha = 140$ $\beta = 40$		$\phi = 46.04$ $\phi' = 36.86$		$n = 1.2$ $C+/C- = -0.13$		$\epsilon = 29.52$			
θ	Es'	Ep'	Ep'/Es'	θ'	Rp/Rs	ψ	ψ'	Exp.	Diff.
0.00	0.87	0.49	0.57	29.52	-0.07	-4.05	-33.57	-30.00	3.57
10.00	0.77	0.64	0.82	39.52	-0.10	-5.89	-35.41	-30.00	5.41
20.00	0.65	0.76	1.17	49.52	-0.15	-8.34	-37.86	-30.00	7.86
30.00	0.51	0.86	1.70	59.52	-0.21	-12.01	-41.53	-30.00	11.53
40.00	0.35	0.94	2.68	69.52	-0.34	-18.53	-48.05	60.00	71.95
50.00	0.18	0.98	5.41	79.52	-0.68	-34.08	-63.60	60.00	56.40
60.00	0.01	1.00	119.40	89.52	-14.94	-86.17	64.31	60.00	4.31
70.00	-0.17	0.99	-5.96	-80.48	0.75	36.73	7.21	60.00	52.79
80.00	-0.33	0.94	-2.82	-70.48	0.35	19.45	-10.07	60.00	70.07
90.00	-0.49	0.87	-1.77	-60.48	0.22	12.46	-17.06	40.00	57.06
$\alpha = 140$ $\beta = 40$		$\phi = 46.04$ $\phi' = 25.05$		$n = 1.7$ $C+/C- = -0.35$		$\epsilon = 29.52$			
θ	Es'	Ep'	Ep'/Es'	θ'	Rp/Rs	ψ	ψ'	Exp.	Diff.
0.00	0.87	0.49	0.57	29.52	-0.20	-11.12	-40.64	-30.00	10.64
10.00	0.77	0.64	0.82	39.52	-0.29	-15.98	-45.50	-30.00	15.50
20.00	0.65	0.76	1.17	49.52	-0.41	-22.13	-51.65	-30.00	21.65
30.00	0.51	0.86	1.70	59.52	-0.59	-30.53	-60.05	-30.00	30.05
40.00	0.35	0.94	2.68	69.52	-0.93	-42.90	-72.42	60.00	47.58
50.00	0.18	0.98	5.41	79.52	-1.88	-61.94	88.54	60.00	28.54
60.00	0.01	1.00	119.40	89.52	-41.44	-88.62	61.86	60.00	1.86
70.00	-0.17	0.99	-5.96	-80.48	2.07	64.21	34.69	60.00	25.31
80.00	-0.33	0.94	-2.82	-70.48	0.98	44.39	14.87	60.00	45.13
90.00	-0.49	0.87	-1.77	-60.48	0.61	31.50	1.98	40.00	38.02

$\alpha = 120$ $\beta = 60$		$\phi = 41.56$ $\phi' = 33.56$		$n = 1.2$ $C+/C- = -0.26$		$\epsilon = 41.93$			
θ	Es'	Ep'	Ep'/Es'	θ'	Rp/Rs	ψ	ψ'	Exp.	Diff.
0.00	0.74	0.67	0.90	41.93	-0.23	-13.11	-55.04	-44.00	11.04
10.00	0.62	0.79	1.28	51.93	-0.33	-18.32	-60.25	-51.00	9.25
20.00	0.47	0.88	1.88	61.93	-0.49	-25.93	-67.86	-68.00	0.14
30.00	0.31	0.95	3.06	71.93	-0.79	-38.47	-80.40	87.00	12.60
40.00	0.14	0.99	7.05	81.93	-1.83	-61.33	76.74	70.00	6.74
50.00	-0.03	1.00	-29.67	-88.07	7.69	82.59	40.66	55.00	14.34
60.00	-0.21	0.98	-4.73	-78.07	1.23	50.82	8.89	52.00	43.11
70.00	-0.37	0.93	-2.48	-68.07	0.64	32.78	-9.15	35.00	44.15
80.00	-0.53	0.85	-1.60	-58.07	0.42	22.59	-19.34	20.00	39.34
90.00	-0.67	0.74	-1.11	-48.07	0.29	16.10	-25.83	0.00	25.83
$\alpha = 120$ $\beta = 60$		$\phi = 41.56$ $\phi' = 22.97$		$n = 1.7$ $C+/C- = -0.45$		$\epsilon = 41.93$			
θ	Es'	Ep'	Ep'/Es'	θ'	Rp/Rs	ψ	ψ'	Exp.	Diff.
0.00	0.74	0.67	0.90	41.93	-0.41	-22.17	-64.10	-44.00	20.10
10.00	0.62	0.79	1.28	51.93	-0.58	-30.08	-72.01	-51.00	21.01
20.00	0.47	0.88	1.88	61.93	-0.85	-40.39	-82.32	-68.00	14.32
30.00	0.31	0.95	3.06	71.93	-1.39	-54.28	83.79	87.00	3.21
40.00	0.14	0.99	7.05	81.93	-3.20	-72.65	65.42	70.00	4.58
50.00	-0.03	1.00	-29.67	-88.07	13.46	85.75	43.82	55.00	11.18
60.00	-0.21	0.98	-4.73	-78.07	2.15	65.03	23.10	52.00	28.90
70.00	-0.37	0.93	-2.48	-68.07	1.13	48.41	6.48	35.00	28.52
80.00	-0.53	0.85	-1.60	-58.07	0.73	36.06	-5.87	20.00	25.87
90.00	-0.67	0.74	-1.11	-48.07	0.51	26.80	-15.13	0.00	15.13

$\alpha = 100$ $\beta = 80$		$\phi = 35.93$ $\phi' = 29.28$		$n = 1.2$ $C+/C- = -0.42$		$\epsilon = 52.55$			
θ	Es'	Ep'	Ep'/Es'	θ'	Rp/Rs	ψ	ψ'	Exp.	Diff.
0.00	0.61	0.79	1.31	52.55	-0.55	-28.86	-81.41	-78.00	3.41
10.00	0.46	0.89	1.92	62.55	-0.81	-39.10	88.36	90.00	1.64
20.00	0.30	0.95	3.18	72.55	-1.34	-53.32	74.13	73.00	1.13
30.00	0.13	0.99	7.64	82.55	-3.23	-72.78	54.67	56.00	1.33
40.00	-0.04	1.00	-22.49	-87.45	9.49	83.99	31.44	46.00	14.56
50.00	-0.22	0.98	-4.49	-77.45	1.90	62.20	9.66	34.00	24.34
60.00	-0.38	0.92	-2.41	-67.45	1.02	45.48	-7.07	23.00	30.07
70.00	-0.54	0.84	-1.57	-57.45	0.66	33.48	-19.06	6.00	25.06
80.00	-0.68	0.74	-1.09	-47.45	0.46	24.70	-27.85	-6.00	21.85
90.00	-0.79	0.61	-0.77	-37.45	0.32	17.92	-34.63	-20.00	14.63
$\alpha = 100$ $\beta = 80$		$\phi = 35.93$ $\phi' = 20.19$		$n = 1.7$ $C+/C- = -0.58$		$\epsilon = 52.55$			
θ	Es'	Ep'	Ep'/Es'	θ'	Rp/Rs	ψ	ψ'	Exp.	Diff.
0.00	0.61	0.79	1.31	52.55	-0.76	-37.09	-89.63	-78.00	11.63
10.00	0.46	0.89	1.92	62.55	-1.11	-48.10	79.35	90.00	10.65
20.00	0.30	0.95	3.18	72.55	-1.84	-61.50	65.95	73.00	7.05
30.00	0.13	0.99	7.64	82.55	-4.43	-77.27	50.18	56.00	5.82
40.00	-0.04	1.00	-22.49	-87.45	13.02	85.61	33.06	46.00	12.94
50.00	-0.22	0.98	-4.49	-77.45	2.60	68.98	16.43	34.00	17.57
60.00	-0.38	0.92	-2.41	-67.45	1.39	54.36	1.82	23.00	21.18
70.00	-0.54	0.84	-1.57	-57.45	0.91	42.22	-10.33	6.00	16.33
80.00	-0.68	0.74	-1.09	-47.45	0.63	32.25	-20.30	-6.00	14.30
90.00	-0.79	0.61	-0.77	-37.45	0.44	23.92	-28.62	-20.00	8.62

$\alpha = 80$ $\beta = 100$		$\phi = 29.50$ $\phi' = 24.23$		$n = 1.2$ $C+/C- = -0.59$		$\epsilon = 61.66$			
θ	Es'	Ep'	Ep'/Es'	θ'	Rp/Rs	ψ	ψ'	Exp.	Diff.
0.00	0.47	0.88	1.85	61.66	-1.10	-47.77	70.57	76.00	5.43
10.00	0.31	0.95	3.02	71.66	-1.79	-60.84	57.50	65.00	7.50
20.00	0.15	0.99	6.82	81.66	-4.05	-76.14	42.20	47.00	4.80
30.00	-0.03	1.00	-34.52	-83.34	20.51	87.21	25.55	35.00	9.45
40.00	-0.20	0.98	-4.85	-78.34	2.88	70.85	9.19	28.00	18.81
50.00	-0.37	0.93	-2.52	-68.34	1.50	56.24	-5.42	16.00	21.42
60.00	-0.52	0.85	-1.62	-58.34	0.96	43.94	-17.72	2.00	19.72
70.00	-0.66	0.75	-1.12	-48.34	0.67	33.74	-27.92	-5.00	22.92
80.00	-0.78	0.62	-0.79	-38.34	0.47	25.17	-36.49	-17.00	19.49
90.00	-0.88	0.47	-0.54	-28.34	0.32	17.77	-43.89	-36.00	7.89
$\alpha = 80$ $\beta = 100$		$\phi = 29.50$ $\phi' = 16.84$		$n = 1.7$ $C+/C- = -0.71$		$\epsilon = 61.66$			
θ	Es'	Ep'	Ep'/Es'	θ'	Rp/Rs	ψ	ψ'	Exp.	Diff.
0.00	0.47	0.88	1.85	61.66	-1.31	-52.69	65.66	76.00	10.34
10.00	0.31	0.95	3.02	71.66	-2.13	-64.90	53.44	65.00	11.56
20.00	0.15	0.99	6.82	81.66	-4.83	-78.29	40.05	47.00	6.95
30.00	-0.03	1.00	-34.52	-83.34	24.43	87.66	26.00	35.00	9.00
40.00	-0.20	0.98	-4.85	-78.34	3.43	73.74	12.08	28.00	15.92
50.00	-0.37	0.93	-2.52	-68.34	1.78	60.70	-0.96	16.00	16.96
60.00	-0.52	0.85	-1.62	-58.34	1.15	48.93	-12.73	2.00	14.73
70.00	-0.66	0.75	-1.12	-48.34	0.80	38.50	-23.16	-5.00	18.16
80.00	-0.78	0.62	-0.79	-38.34	0.56	29.23	-32.42	-17.00	15.42
90.00	-0.88	0.47	-0.54	-28.34	0.38	20.89	-40.77	-36.00	4.77

$\alpha = 60$ $\beta = 120$		$\phi = 22.52$ $\phi' = 18.61$		$n = 1.2$ $C+/C- = -0.75$		$\epsilon = 69.64$			
θ	Es'	Ep'	Ep'/Es'	θ'	Rp/Rs	ψ	ψ'	Exp.	Diff.
0.00	0.35	0.94	2.69	69.64	-2.03	-63.82	46.54	57.00	10.46
10.00	0.18	0.98	5.47	79.64	-4.13	-76.39	33.97	45.00	11.03
20.00	0.01	1.00	158.90	89.64	-119.96	-89.52	20.84	35.00	14.16
30.00	-0.17	0.99	-5.89	-80.36	4.44	77.32	7.68	17.00	9.32
40.00	-0.34	0.94	-2.80	-70.36	2.12	64.70	-4.94	7.00	11.94
50.00	-0.49	0.87	-1.76	-60.36	1.33	52.99	-16.65	0.00	16.65
60.00	-0.64	0.77	-1.21	-50.36	0.91	42.34	-27.30	-9.00	18.30
70.00	-0.76	0.65	-0.85	-40.36	0.64	32.68	-36.96	-20.00	16.96
80.00	-0.86	0.51	-0.59	-30.36	0.44	23.86	-45.78	-30.00	15.78
90.00	-0.94	0.35	-0.37	-20.36	0.28	15.65	-53.99	-42.00	11.96

$\alpha = 60$ $\beta = 120$		$\phi = 22.52$ $\phi' = 13.02$		$n = 1.7$ $C+/C- = -0.83$		$\epsilon = 69.64$			
θ	Es'	Ep'	Ep'/Es'	θ'	Rp/Rs	ψ	ψ'	Exp.	Diff.
0.00	0.35	0.94	2.69	69.64	-2.22	-65.78	44.58	57.00	12.42
10.00	0.18	0.98	5.47	79.64	-4.51	-77.51	32.86	45.00	12.14
20.00	0.01	1.00	158.90	89.64	-131.09	-89.56	20.80	35.00	14.20
30.00	-0.17	0.99	-5.89	-80.36	4.86	78.37	8.73	17.00	8.27
40.00	-0.34	0.94	-2.80	-70.36	2.31	66.61	-3.03	7.00	10.03
50.00	-0.49	0.87	-1.76	-60.36	1.45	55.41	-14.23	0.00	14.23
60.00	-0.64	0.77	-1.21	-50.36	1.00	44.88	-24.76	-9.00	15.76
70.00	-0.76	0.65	-0.85	-40.36	0.70	35.04	-34.60	-20.00	14.60
80.00	-0.86	0.51	-0.59	-30.36	0.48	25.79	-43.85	-30.00	13.85
90.00	-0.94	0.35	-0.37	-20.36	0.31	17.02	-52.62	-42.00	10.62

$\alpha = 40$ $\beta = 140$		$\phi = 15.19$ $\phi' = 12.61$		$n = 1.2$ $C+/C- = -0.89$		$\epsilon = 76.83$			
θ	Es'	Ep'	Ep'/Es'	θ'	Rp/Rs	ψ	ψ'	Exp.	Diff.
0.00	0.23	0.97	4.27	76.83	-3.78	-75.20	27.97	37.00	9.03
10.00	0.06	1.00	18.07	86.83	-16.00	-86.42	16.74	29.00	12.26
20.00	-0.12	0.99	-8.35	-83.17	7.39	82.29	5.46	18.00	12.54
30.00	-0.29	0.96	-3.31	-73.17	2.93	71.14	-5.70	7.00	12.70
40.00	-0.45	0.89	-1.98	-63.17	1.75	60.26	-16.57	0.00	16.57
50.00	-0.60	0.80	-1.34	-53.17	1.18	49.77	-27.06	-9.00	18.06
60.00	-0.73	0.68	-0.94	-43.17	0.83	39.71	-37.12	-22.00	15.12
70.00	-0.84	0.55	-0.65	-33.17	0.58	30.06	-46.77	-34.00	12.77
80.00	-0.92	0.39	-0.43	-23.17	0.38	20.75	-56.08	-45.00	11.08
90.00	-0.97	0.23	-0.23	-13.17	0.21	11.70	-65.13	-55.00	10.13

$\alpha = 40$ $\beta = 140$		$\phi = 15.19$ $\phi' = 8.87$		$n = 1.7$ $C+/C- = -0.92$		$\epsilon = 76.83$			
θ	Es'	Ep'	Ep'/Es'	θ'	Rp/Rs	ψ	ψ'	Exp.	Diff.
0.00	0.23	0.97	4.27	76.83	-3.93	-75.71	27.45	37.00	9.55
10.00	0.06	1.00	18.07	86.83	-16.60	-86.55	16.62	29.00	12.38
20.00	-0.12	0.99	-8.35	-83.17	7.67	82.57	5.74	18.00	12.26
30.00	-0.29	0.96	-3.31	-73.17	3.04	71.77	-5.06	7.00	12.06
40.00	-0.45	0.89	-1.98	-63.17	1.82	61.16	-15.67	0.00	15.67
50.00	-0.60	0.80	-1.34	-53.17	1.23	50.81	-26.02	-9.00	17.02
60.00	-0.73	0.68	-0.94	-43.17	0.86	40.75	-36.08	-22.00	14.08
70.00	-0.84	0.55	-0.65	-33.17	0.60	30.98	-45.85	-34.00	11.85
80.00	-0.92	0.39	-0.43	-23.17	0.39	21.46	-55.37	-45.00	10.37
90.00	-0.97	0.23	-0.23	-13.17	0.21	12.13	-64.70	-55.00	9.70

$\alpha = 20$ $\beta = 160$		$\phi = 7.64$ $\phi' = 6.36$		$n = 1.2$ $C+/C- = -0.97$		$\epsilon = 83.53$			
θ	Es'	Ep'	Ep'/Es'	θ'	Rp/Rs	ψ	ψ'	Exp.	Diff.
0.00	0.11	0.99	8.82	83.53	-8.56	-83.34	13.13	24.00	10.87
10.00	-0.06	1.00	-16.19	-86.47	15.72	86.36	2.83	13.00	10.17
20.00	-0.23	0.97	-4.15	-76.47	4.03	76.07	-7.46	4.00	11.46
30.00	-0.40	0.92	-2.30	-66.47	2.23	65.83	-17.70	-5.00	12.70
40.00	-0.55	0.83	-1.51	-56.47	1.46	55.67	-27.86	-13.00	14.86
50.00	-0.69	0.72	-1.05	-46.47	1.02	45.61	-37.92	-24.00	13.92
60.00	-0.80	0.59	-0.74	-36.47	0.72	35.65	-47.88	-36.00	11.88
70.00	-0.90	0.45	-0.50	-26.47	0.48	25.79	-57.75	-45.00	12.75
80.00	-0.96	0.28	-0.30	-16.47	0.29	16.01	-67.53	-58.00	9.53
90.00	-0.99	0.11	-0.11	-6.47	0.11	6.28	-77.26	-67.00	10.26

$\alpha = 20$ $\beta = 160$		$\phi = 7.64$ $\phi' = 4.49$		$n = 1.7$ $C+/C- = -0.98$		$\epsilon = 83.53$			
θ	Es'	Ep'	Ep'/Es'	θ'	Rp/Rs	ψ	ψ'	Exp.	Diff.
0.00	0.11	0.99	8.82	83.53	-8.64	-83.40	13.07	24.00	10.93
10.00	-0.06	1.00	-16.19	-86.47	15.86	86.39	2.86	13.00	10.14
20.00	-0.23	0.97	-4.15	-76.47	4.07	76.19	-7.34	4.00	11.34
30.00	-0.40	0.92	-2.30	-66.47	2.25	66.02	-17.51	-5.00	12.51
40.00	-0.55	0.83	-1.51	-56.47	1.48	55.91	-27.63	-13.00	14.63
50.00	-0.69	0.72	-1.05	-46.47	1.03	45.86	-37.67	-24.00	13.67
60.00	-0.80	0.59	-0.74	-36.47	0.72	35.89	-47.64	-36.00	11.64
70.00	-0.90	0.45	-0.50	-26.47	0.49	25.99	-57.55	-45.00	12.55
80.00	-0.96	0.28	-0.30	-16.47	0.29	16.14	-67.39	-58.00	9.39
90.00	-0.99	0.11	-0.11	-6.47	0.11	6.33	-77.20	-67.00	10.20

Fresnel Model

Azimuth Angle = 180

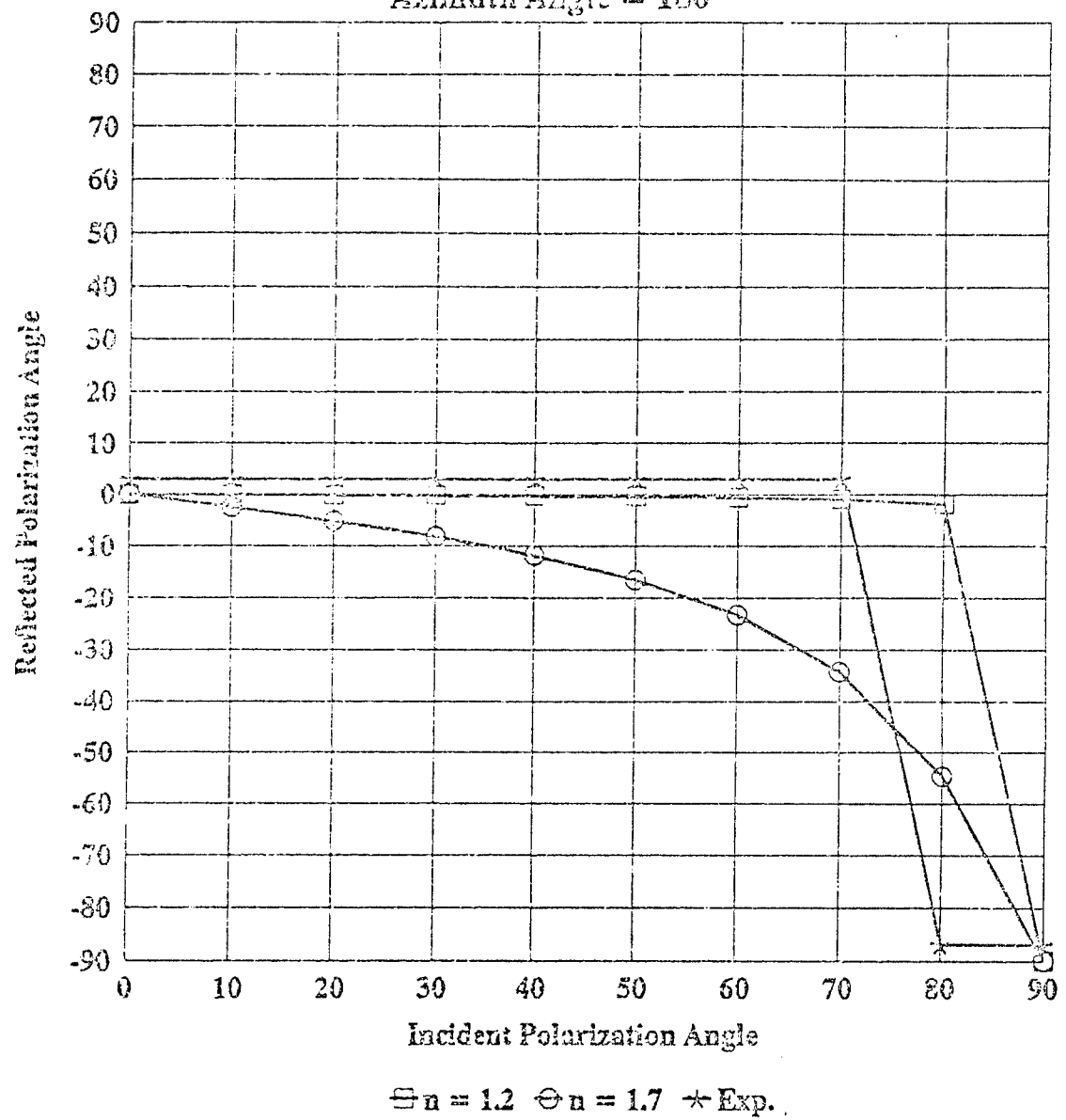


Figure 399. ψ' vs θ for $\alpha = 180$.

Fresnel Model

Azimuth Angle = 160

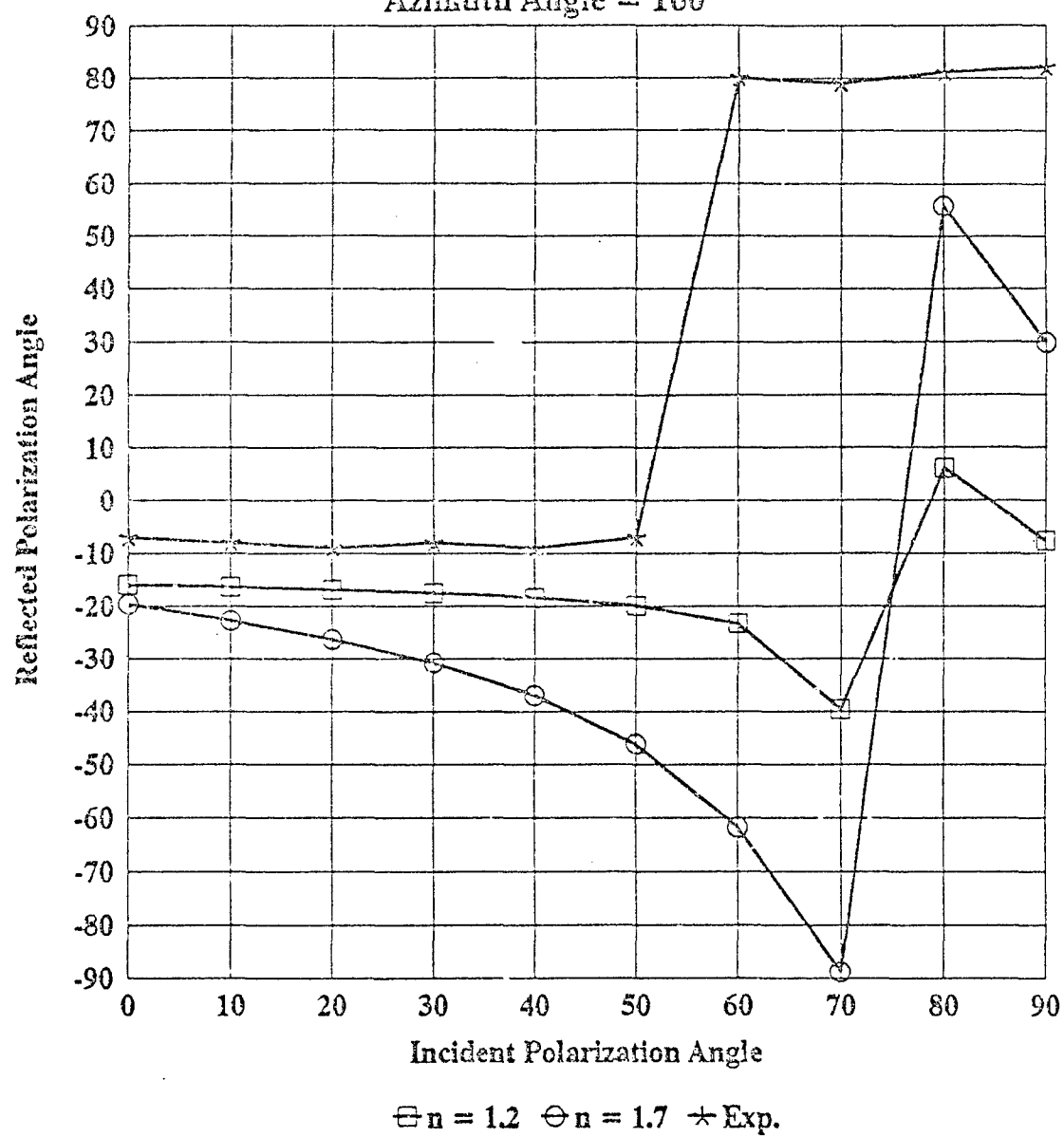


Figure 400. ψ' vs θ for $\alpha = 160$.

Fresnel Model

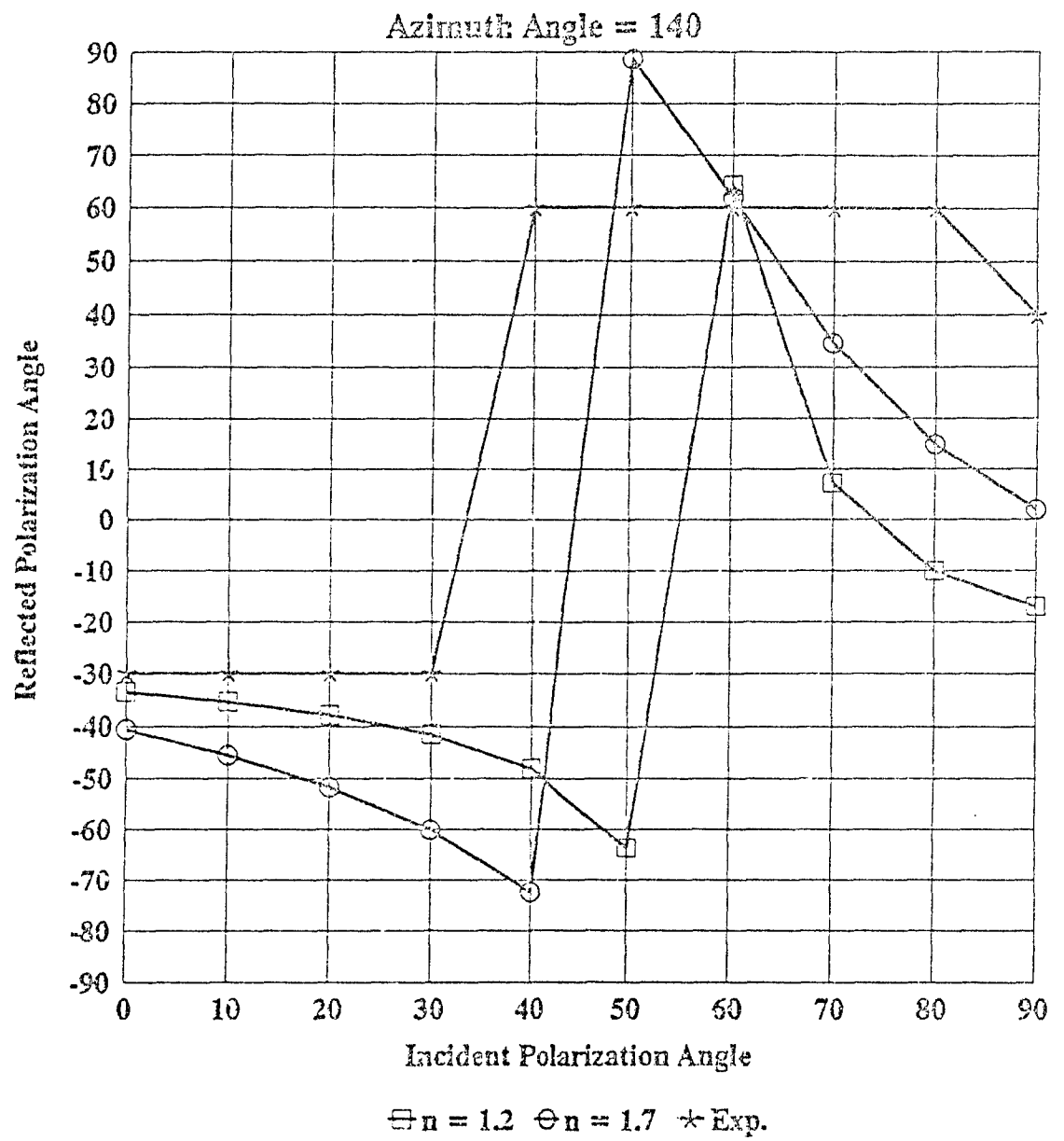
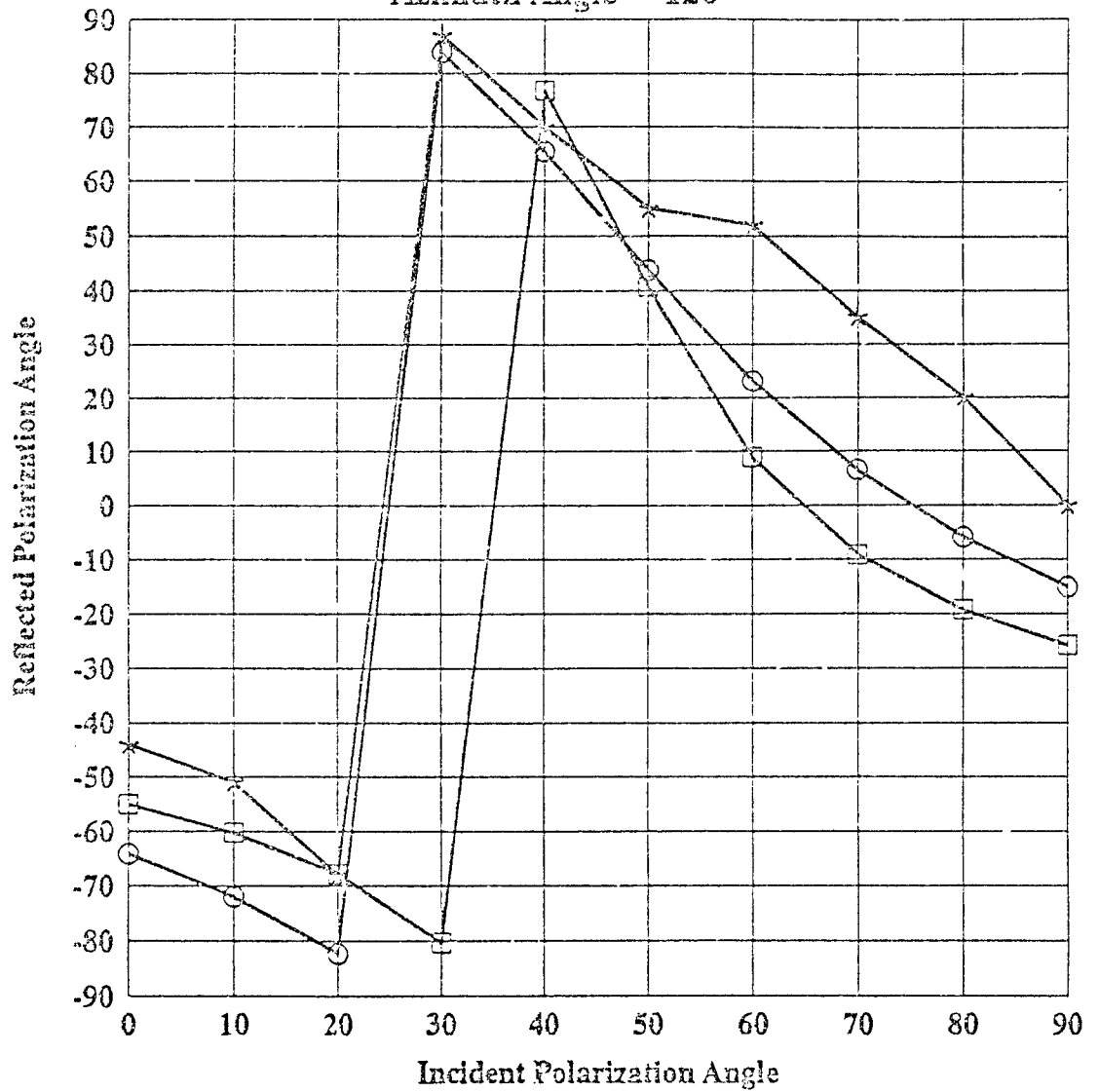


Figure 401. ψ' vs θ for $\alpha = 140$.

Fresnel Model

Azimuth Angle = 120



$\square n = 1.2$ $\circ n = 1.7$ \star Exp.

Figure 402. ψ' vs θ for $\alpha = 120$.

Fresnel Model

Azimuth Angle = 100

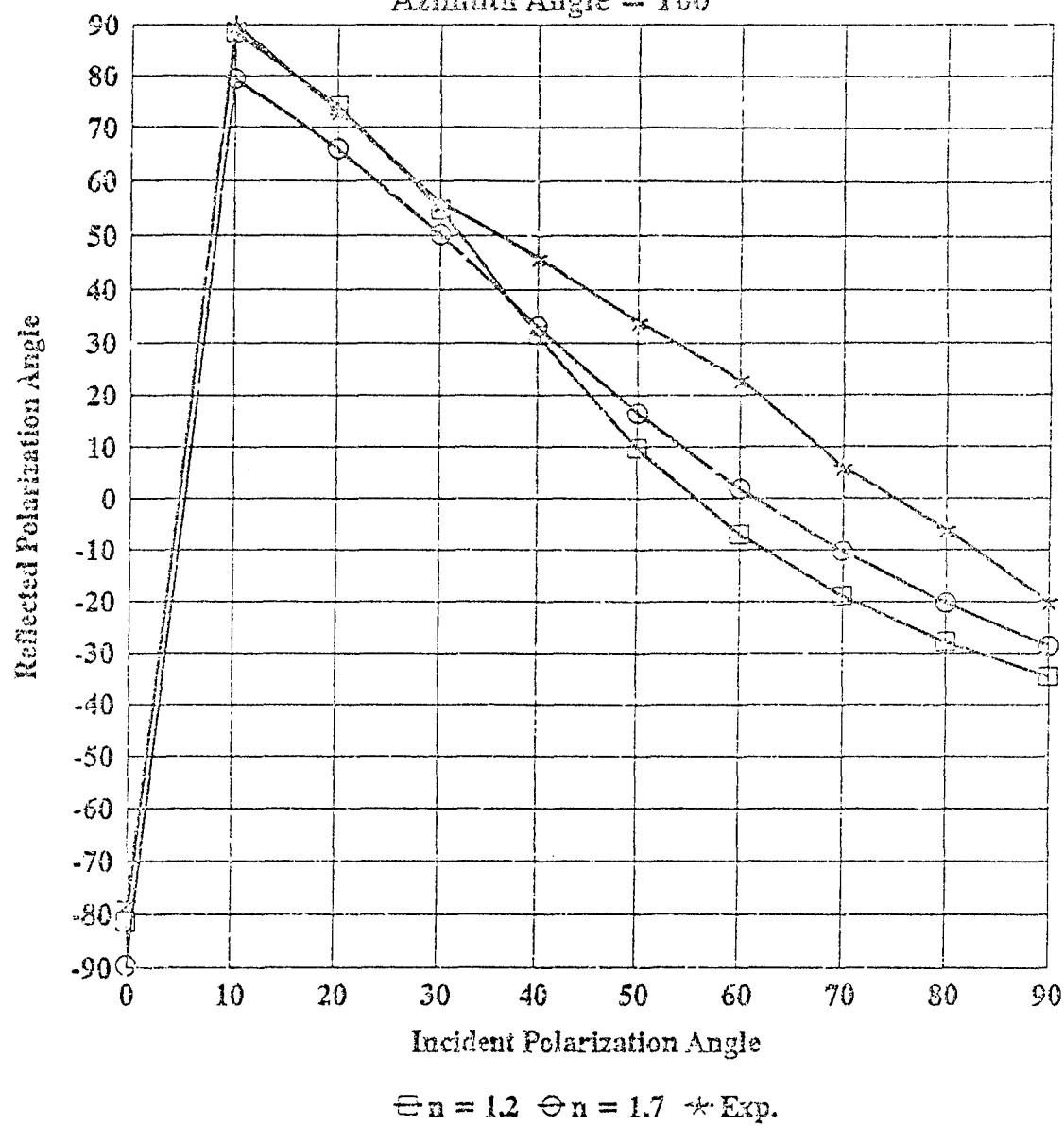
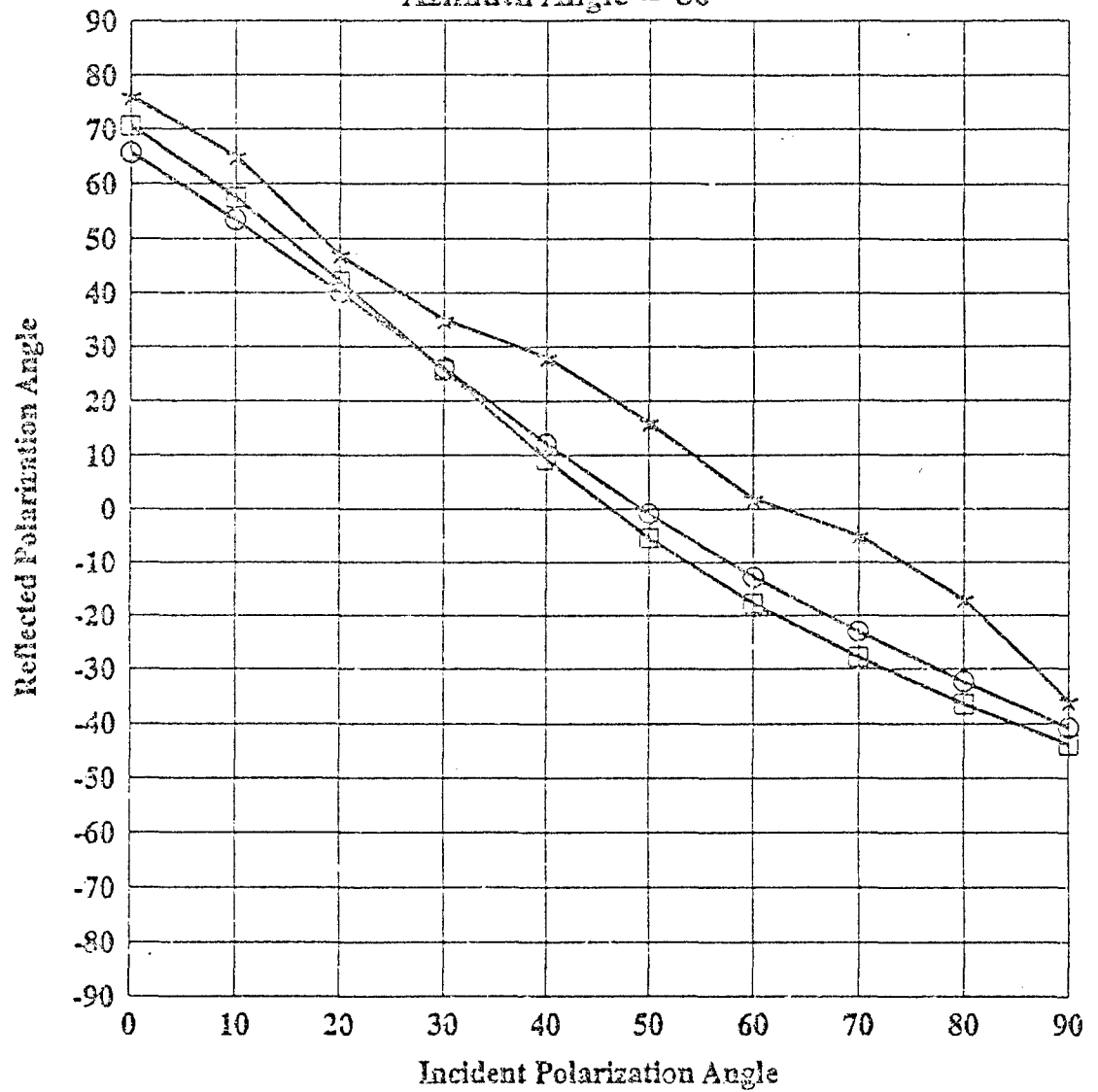


Figure 403. ψ' vs θ for $\alpha = 100$.

Fresnel Model

Azimuth Angle = 80



$\square n = 1.2$ $\circ n = 1.7$ \star Exp.

Figure 404. ψ' vs θ for $\alpha = 80$.

Fresnel Model

Azimuth Angle = 60

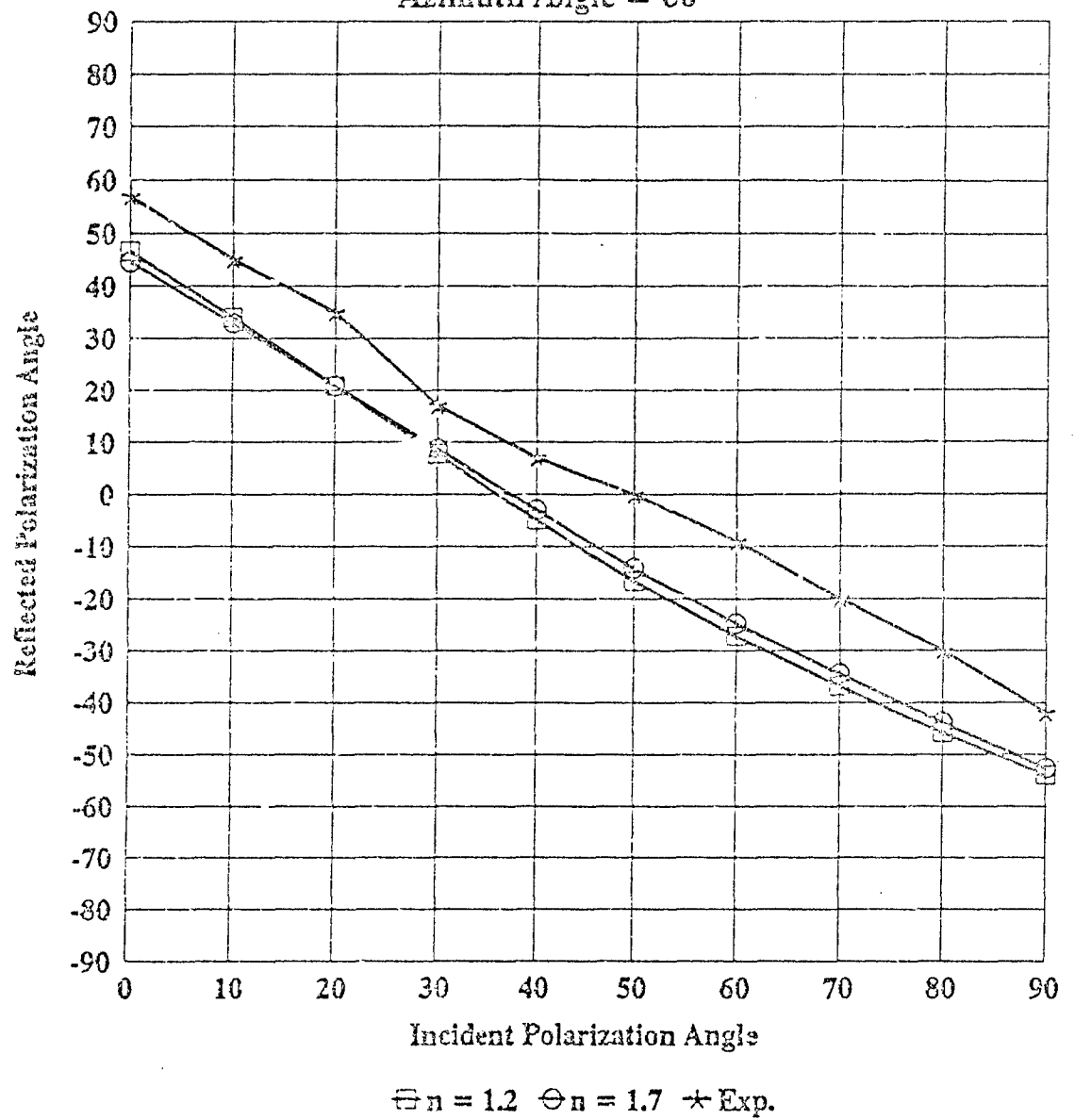
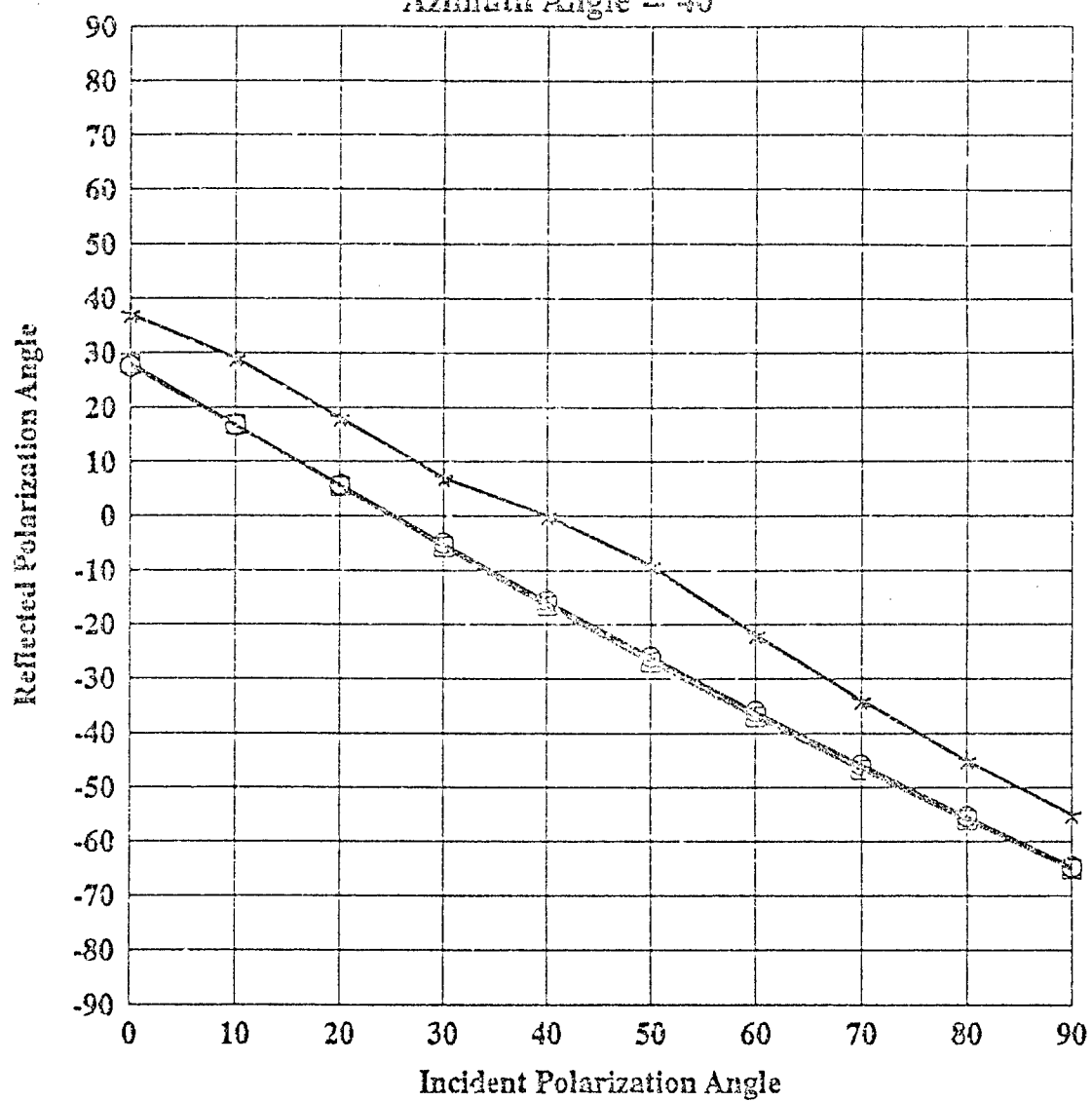


Figure 405. ψ' vs θ for $\alpha = 60$.

Fresnel Model

Azimuth Angle = 40



$\square n = 1.2$ $\circ n = 1.7$ \star Exp.

Figure 406. ψ' vs θ for $\alpha = 40$.

Fresnel Model

Azimuth Angle = 20

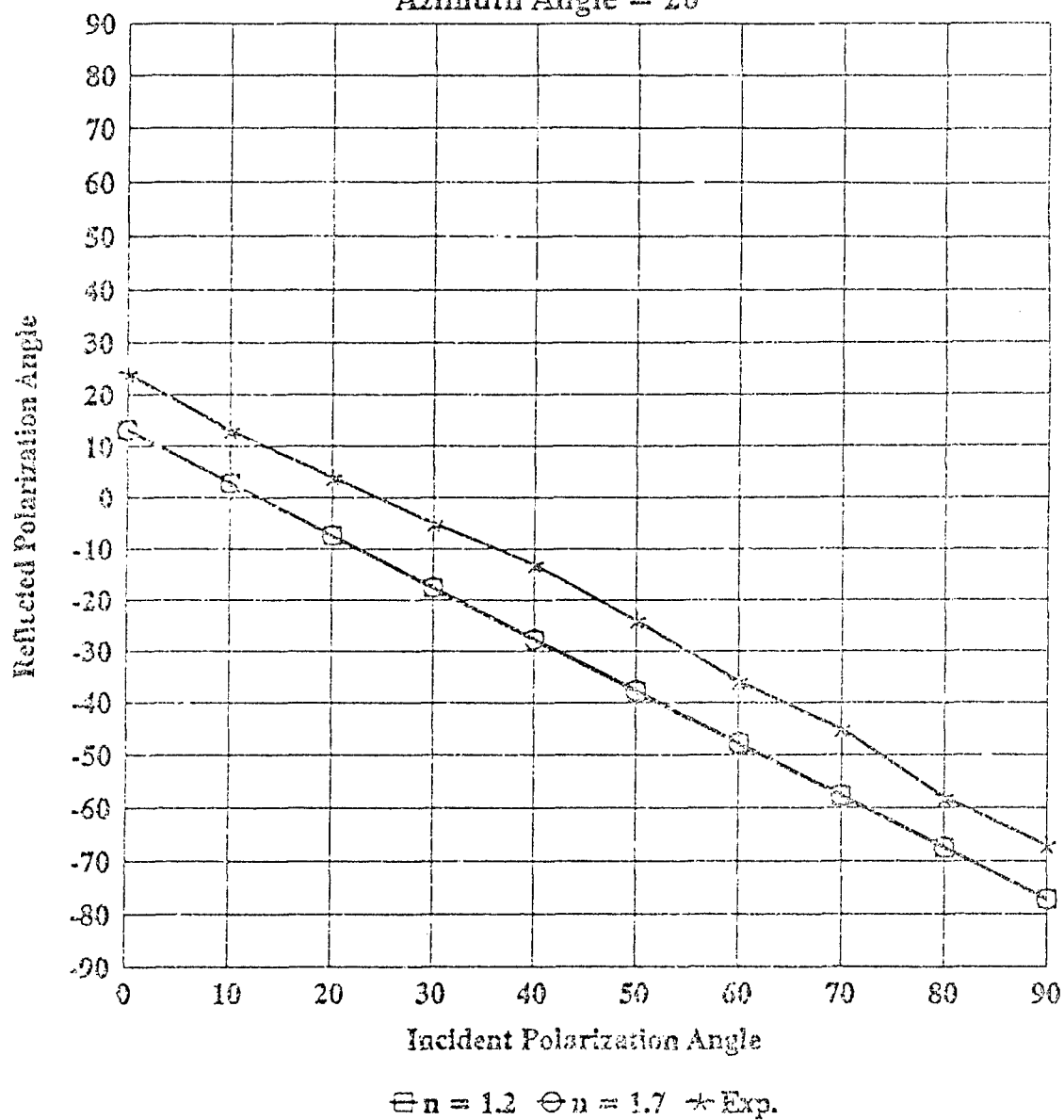


Figure 407. ψ' vs θ for $\alpha = 20$.

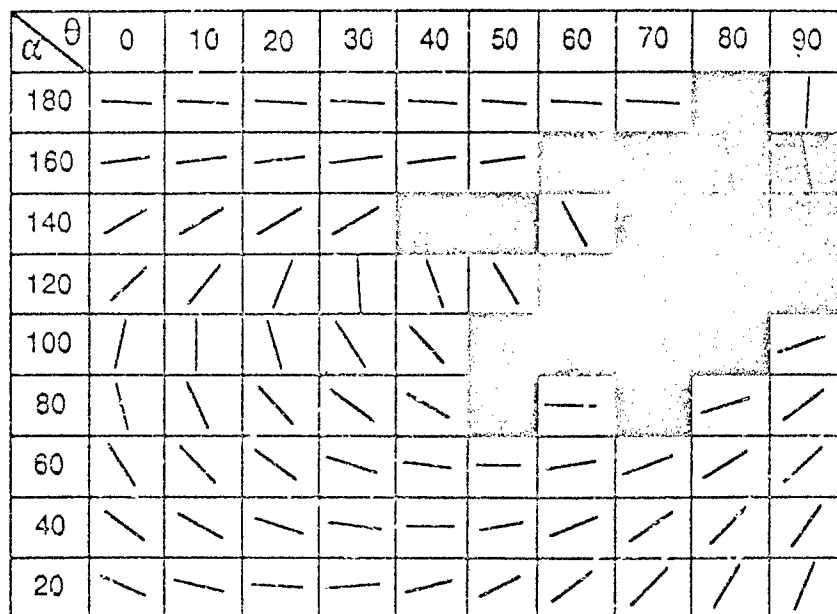


Figure 408.

Experimental polarization axes of reflected light from CARC sample. Shaded areas indicate conditions where predicted polarization axes deviate by more than 20° from experimental values.

$\alpha \backslash \theta$	0	10	20	30	40	50	60	70	80	90
180	3	3	3	3	3	3	4	4		3
160	9	8	8	9	9	13				
140	4	5	8	12			4			
120	11	9	0	13	7	14				
100	3	2	1	1	15					15
80	5	8	5	9	19		20		19	8
60	10	11	14	9	12	17	18	17	16	12
40	9	12	13	13	17	18	15	13	11	10
20	11	10	11	13	15	14	12	13	9	10

Figure 409.

Angular difference between predicted and experimental polarization axes of reflected light from CARC sample using the Fresnel model.

The graphs of Figure 399, Figure 400, ... Figure 407 and the charts of Figure 408 and Figure 409 indicate that the modified laws of reflection of Fresnel closely fit over 75 percent of the collected data. The greatest deviations occur within 60° of the plane containing the incident ray, the reflected ray and the normal to the surface and for $\theta > 40^\circ$.

RELATIVE INTENSITIES

The components R_s and R_p of the amplitude R of the electric vector for reflected light is obtained from equation (3)

$$R_s = - \frac{\sin(\phi - \phi')}{\sin(\phi + \phi')} E_s \quad R_p = \frac{\tan(\phi - \phi')}{\tan(\phi + \phi')} E_p$$

where R_s is the component perpendicular to the plane of incidence, R_p is the component parallel to the plane of incidence and $R = \sqrt{R_p^2 + R_s^2}$

By definition, $R' = \frac{R}{R_{\max}}$

R'^2 represents the relative intensities of the reflected light.

Table 92 shows the calculations of R'^2 for an index of refraction $n = 1.2$. Table 93 shows the calculations of R'^2 for an index of refraction $n = 1.7$. The graphs of Figure 410, Figure 411, . . . Figure 413 show the results graphically.

Table 92. Calculations of Relative Intensities for Reflected Light from CARC Sample
for $n = 1.2$

$\alpha = 180$					
θ	R_p	R_s	R	R'	R'^2
0	0.00000	0.17931	0.17931	1.0000	1.00
10	0.00018	0.17659	0.17659	0.98481	0.97
20	0.00036	0.16850	0.16850	0.93969	0.88
30	0.00052	0.15529	0.15529	0.86603	0.75
40	0.00067	0.13736	0.13736	0.76605	0.59
50	0.00080	0.11526	0.11526	0.64280	0.41
60	0.00091	0.08966	0.08966	0.50003	0.25
70	0.00099	0.06133	0.06134	0.34206	0.12
80	0.00103	0.03114	0.03115	0.17374	0.03
90	0.00105	0.00000	0.00105	0.00585	0.00
$\alpha = 160$					
θ	R_p	R_s	R	R'	R'^2
0	0.00169	0.16793	0.16793	0.93654	0.88
10	0.00274	0.15737	0.15740	0.87779	0.77
20	0.00370	0.14204	0.14209	0.79242	0.63
30	0.00455	0.12240	0.12248	0.68305	0.47
40	0.00526	0.09903	0.09917	0.55304	0.31
50	0.00582	0.07265	0.07289	0.40647	0.17
60	0.00619	0.04407	0.04450	0.24818	0.06
70	0.00638	0.01415	0.01552	0.08655	0.01
80	0.00637	-0.01620	0.01741	0.09711	0.01
90	0.00617	-0.04610	0.04648	0.25919	0.07

$\alpha = 140$					
θ	R_p	R_s	R	R'	R'^2
0	0.00992	0.13991	0.14026	0.78223	0.61
10	0.01281	0.12403	0.12469	0.69538	0.48
20	0.01531	0.10438	0.10550	0.58833	0.35
30	0.01734	0.08156	0.08338	0.46500	0.22
40	0.01885	0.05626	0.05933	0.33088	0.11
50	0.01979	0.02925	0.03531	0.19693	0.04
60	0.02012	0.00135	0.02017	0.11248	0.01
70	0.01985	-0.02660	0.03318	0.18506	0.03
80	0.01897	-0.05370	0.05698	0.31774	0.10
90	0.01751	-0.07920	0.08114	0.45249	0.20
$\alpha = 120$					
θ	R_p	R_s	R	R'	R'^2
0	0.02494	0.10711	0.10997	0.61331	0.38
10	0.02939	0.08878	0.09351	0.52150	0.27
20	0.03294	0.06775	0.07533	0.42009	0.18
30	0.03549	0.04466	0.05704	0.31809	0.10
40	0.03696	0.02021	0.04212	0.23491	0.06
50	0.03731	-0.00480	0.03762	0.20979	0.04
60	0.03652	-0.02980	0.04711	0.26273	0.07
70	0.03463	-0.05380	0.06395	0.35666	0.13
80	0.03168	-0.07610	0.08247	0.45993	0.21
90	0.02777	-0.09620	0.10013	0.55842	0.31

$\alpha = 100$					
θ	R_p	R_s	R	R'	R'^2
0	0.04279	0.07764	0.08365	0.49438	0.24
10	0.04783	0.05886	0.07584	0.42296	0.18
20	0.05142	0.03829	0.06411	0.35753	0.13
30	0.05344	0.01656	0.05595	0.31203	0.10
40	0.05385	-0.00570	0.05414	0.30195	0.09
50	0.05261	-0.02770	0.05947	0.33167	0.11
60	0.04978	-0.04900	0.06982	0.38935	0.15
70	0.04543	-0.06870	0.08235	0.45926	0.21
80	0.03971	-0.08630	0.09502	0.52993	0.28
90	0.03278	-0.10140	0.10652	0.59404	0.35
$\alpha = 80$					
θ	R_p	R_s	R	R'	R'^2
0	0.05961	0.0541	0.08051	0.44899	0.20
10	0.06429	0.0359	0.07362	0.41056	0.17
20	0.06701	0.0165	0.06902	0.38493	0.15
30	0.0677	-0.0033	0.06778	0.37801	0.14
40	0.06633	-0.0230	0.07022	0.39160	0.15
50	0.06295	-0.0421	0.07571	0.42224	0.18
60	0.05765	-0.0598	0.08309	0.46335	0.21
70	0.0506	-0.0758	0.09111	0.50812	0.26
80	0.04202	-0.0894	0.09879	0.55092	0.30
90	0.03215	-0.1003	0.10535	0.58754	0.35

$\alpha = 60$					
θ	R_p	R_s	R	R'	R'^2
0	0.07331	0.0360	0.08169	0.45560	0.21
10	0.07693	0.0186	0.07915	0.44140	0.19
20	0.07820	0.0006	0.0782	0.43612	0.19
30	0.07710	-0.0173	0.07902	0.44070	0.19
40	0.07365	-0.0348	0.08147	0.45432	0.21
50	0.06797	-0.0512	0.08511	0.47466	0.23
60	0.06022	-0.0661	0.08941	0.49861	0.25
70	0.05064	-0.0789	0.09378	0.52300	0.27
80	0.03953	-0.0894	0.09773	0.54503	0.30
90	0.02721	-0.0971	0.10086	0.56245	0.32
$\alpha = 40$					
θ	R_p	R_s	R	R'	R'^2
0	0.08314	0.0220	0.08599	0.47957	0.23
10	0.08525	0.0053	0.08542	0.47638	0.23
20	0.08478	-0.0115	0.08555	0.47710	0.23
30	0.08173	-0.0279	0.08636	0.48164	0.23
40	0.07619	-0.0435	0.08775	0.48935	0.24
50	0.06834	-0.0578	0.08951	0.49918	0.25
60	0.05841	-0.0703	0.09143	0.50986	0.26
70	0.04671	-0.0807	0.09326	0.52009	0.27
80	0.03359	-0.0887	0.09480	0.52870	0.28
90	0.01945	-0.0939	0.09589	0.53474	0.29

$\alpha = 20$					
θ	R_p	R_s	R	R'	R'^2
0	0.08898	0.0104	0.08958	0.49959	0.25
10	0.08938	-0.0057	0.08956	0.49945	0.25
20	0.08706	-0.0216	0.08970	0.50024	0.25
30	0.0821	-0.0368	0.08999	0.50184	0.25
40	0.07464	-0.0510	0.09039	0.50407	0.25
50	0.06492	-0.0636	0.09085	0.50665	0.26
60	0.05322	-0.0742	0.09132	0.50926	0.26
70	0.03991	-0.0826	0.09174	0.51159	0.26
80	0.02538	-0.0885	0.09205	0.51337	0.26
90	0.01008	-0.0917	0.09224	0.51438	0.26

Table 93. Calculations of Relative Intensities for Reflected Light from CARC Sample for $n = 1.7$

$\alpha = 180$					
θ	R_p	R_s	R	R'	R'^2
0	0.00000	0.4049	0.40494	1.00000	1.00
10	0.01749	0.3988	0.39917	0.98575	0.97
20	0.03446	0.3805	0.38208	0.94354	0.89
30	0.05037	0.3507	0.35429	0.87491	0.77
40	0.06476	0.3102	0.31689	0.78256	0.61
50	0.07717	0.2603	0.27149	0.67045	0.45
60	0.08725	0.2025	0.22047	0.54445	0.30
70	0.09467	0.1385	0.16776	0.41428	0.17
80	0.09921	0.0703	0.12160	0.30030	0.09
90	0.10074	0.0000	0.10074	0.24878	0.06

$\alpha = 160$					
θ	R_p	R_s	R	R'	R'^2
0	0.02889	0.3836	0.38467	0.94993	0.90
10	0.04674	0.3595	0.36251	0.89521	0.80
20	0.06317	0.3245	0.33055	0.81630	0.67
30	0.07769	0.2796	0.29017	0.71658	0.51
40	0.08984	0.2262	0.24339	0.60105	0.36
50	0.09926	0.1660	0.19337	0.47754	0.23
60	0.10566	0.1007	0.14594	0.36040	0.13
70	0.10886	0.0323	0.11355	0.28042	0.08
80	0.10874	-0.0370	0.11487	0.28368	0.08
90	0.10533	-0.1052	0.14888	0.36766	0.14
$\alpha = 140$					
θ	R_p	R_s	R	R'	R'^2
0	0.06475	0.1399	0.15417	0.38072	0.14
10	0.01281	0.1240	0.12469	0.30792	0.09
20	0.01531	0.1044	0.10550	0.26052	0.07
30	0.01734	0.0816	0.08338	0.20591	0.04
40	0.01885	0.0563	0.05933	0.14652	0.02
50	0.01979	0.0292	0.03531	0.08720	0.01
60	0.02012	0.0013	0.02017	0.04981	0.00
70	0.01985	-0.0266	0.03318	0.08195	0.01
80	0.01897	-0.0537	0.05698	0.14070	0.02
90	0.01751	-0.0792	0.08114	0.20037	0.04

$\alpha = 120$					
θ	R_p	R_s	R	R'	R'^2
0	0.10706	0.2627	0.28369	0.70058	0.49
10	0.12613	0.2177	0.25164	0.62143	0.39
20	0.14137	0.1662	0.21817	0.53877	0.29
30	0.15232	0.1095	0.18761	0.46331	0.21
40	0.15863	0.0496	0.16620	0.41043	0.17
50	0.16013	-0.0119	0.16057	0.39653	0.16
60	0.15676	-0.0730	0.17292	0.42703	0.18
70	0.14853	-0.1319	0.19870	0.49070	0.24
80	0.13598	-0.1868	0.23102	0.57051	0.33
90	0.11920	-0.2360	0.26437	0.65286	0.43
$\alpha = 100$					
θ	R_p	R_s	R	R'	R'^2
0	0.15019	0.1987	0.24905	0.61504	0.38
10	0.16788	0.1506	0.22555	0.55699	0.31
20	0.18048	0.0980	0.20536	0.50715	0.26
30	0.18759	0.0424	0.19232	0.47493	0.23
40	0.18900	-0.0145	0.18956	0.46812	0.22
50	0.18467	-0.0710	0.19784	0.48856	0.24
60	0.17473	-0.1253	0.21499	0.53093	0.28
70	0.15948	-0.1758	0.23733	0.58608	0.34
80	0.13938	-0.2209	0.26121	0.64505	0.42
90	0.11505	-0.2594	0.28372	0.70066	0.49

$\alpha = 80$					
θ	R_p	R_s	R	R'	R'^2
0	0.18372	0.1438	0.23729	0.53599	0.34
10	0.20353	0.0953	0.22476	0.55503	0.31
20	0.21215	0.0429	0.21666	0.53504	0.29
30	0.21433	-0.0028	0.21451	0.52973	0.28
40	0.21000	-0.0612	0.21874	0.54019	0.29
50	0.19928	-0.1118	0.22852	0.56433	0.32
60	0.18251	-0.1590	0.24208	0.59782	0.36
70	0.16020	-0.2014	0.25735	0.63552	0.40
80	0.13301	-0.2377	0.27235	0.67257	0.45
90	0.10179	-0.2667	0.28545	0.70493	0.50
$\alpha = 60$					
θ	R_p	R_s	R	R'	R'^2
0	0.21961	0.0988	0.24081	0.59467	0.35
10	0.23043	0.0511	0.23602	0.58284	0.34
20	0.23424	0.0018	0.23425	0.57847	0.33
30	0.23094	-0.0475	0.23578	0.58226	0.34
40	0.22062	-0.0954	0.24037	0.59360	0.35
50	0.20359	-0.1404	0.24732	0.61076	0.37
60	0.18039	-0.1811	0.25563	0.63129	0.40
70	0.15170	-0.2164	0.26423	0.65253	0.43
80	0.11840	-0.2450	0.27210	0.67196	0.45
90	0.08150	-0.2662	0.27839	0.68748	0.47

$\alpha = 40$					
θ	R_p	R_s	R	R'	R'^2
0	0.24172	0.0615	0.24944	0.61598	0.38
10	0.24787	0.0149	0.24832	0.61322	0.38
20	0.24649	-0.0321	0.24857	0.61385	0.38
30	0.23761	-0.0782	0.25016	0.61778	0.38
40	0.22152	-0.1220	0.25288	0.62448	0.39
50	0.19870	-0.1620	0.25635	0.63307	0.40
60	0.16984	-0.1971	0.26016	0.64246	0.41
70	0.13581	-0.2262	0.26382	0.65151	0.42
80	0.09767	-0.2484	0.26692	0.65917	0.43
90	0.05655	-0.2631	0.26911	0.66456	0.44
$\alpha = 20$					
θ	R_p	R_s	R	R'	R'^2
0	0.25489	0.0295	0.25660	0.63367	0.40
10	0.25604	-0.0161	0.25655	0.63354	0.40
20	0.24940	-0.0613	0.25683	0.63424	0.40
30	0.23519	-0.1046	0.25740	0.63566	0.40
40	0.21383	-0.1447	0.25821	0.63764	0.41
50	0.18597	-0.1805	0.25913	0.63993	0.41
60	0.15247	-0.2107	0.26007	0.64225	0.41
70	0.11433	-0.2345	0.26091	0.64433	0.42
80	0.07271	-0.2512	0.26155	0.64591	0.42
90	0.02889	-0.2603	0.26192	0.64681	0.42

Reflection From CARC-Painted Surface

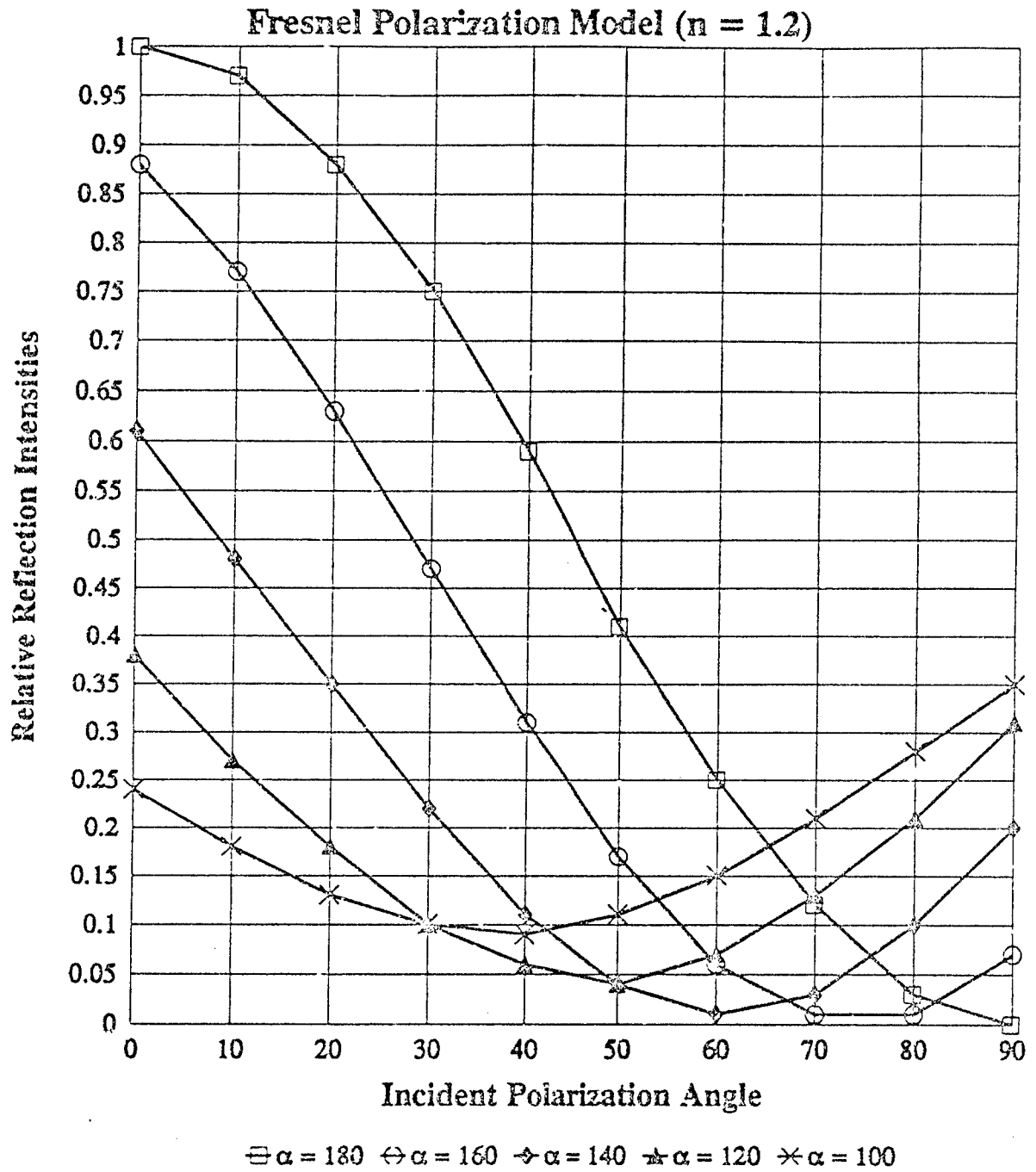


Figure 410.
Relative Reflection Intensities

Reflection From CARC-Painted Surface

Fresnel Polarization Model ($n = 1.2$)

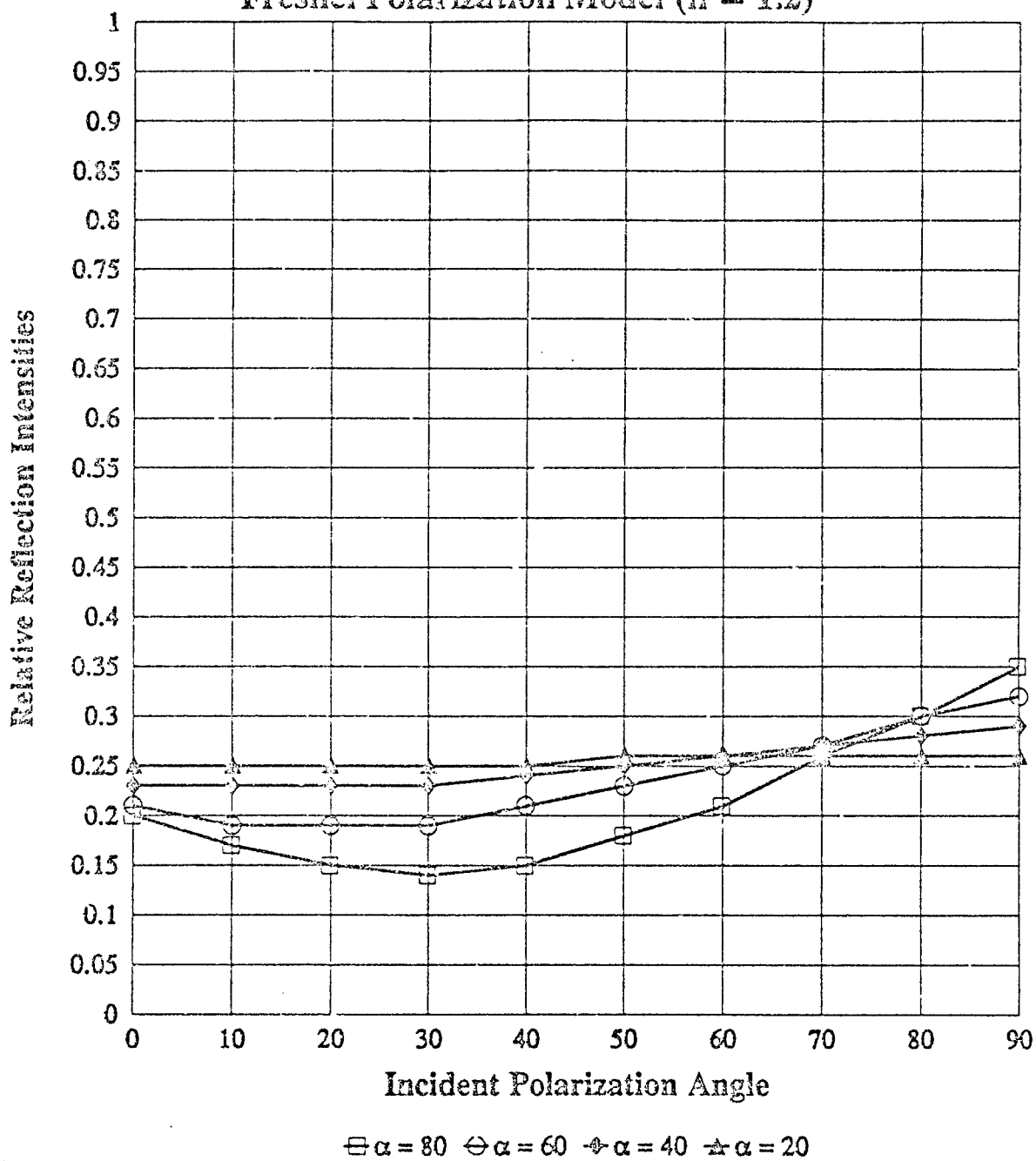


Figure 411.
Relative Reflection Intensities

Reflection From CARC-Painted Surface

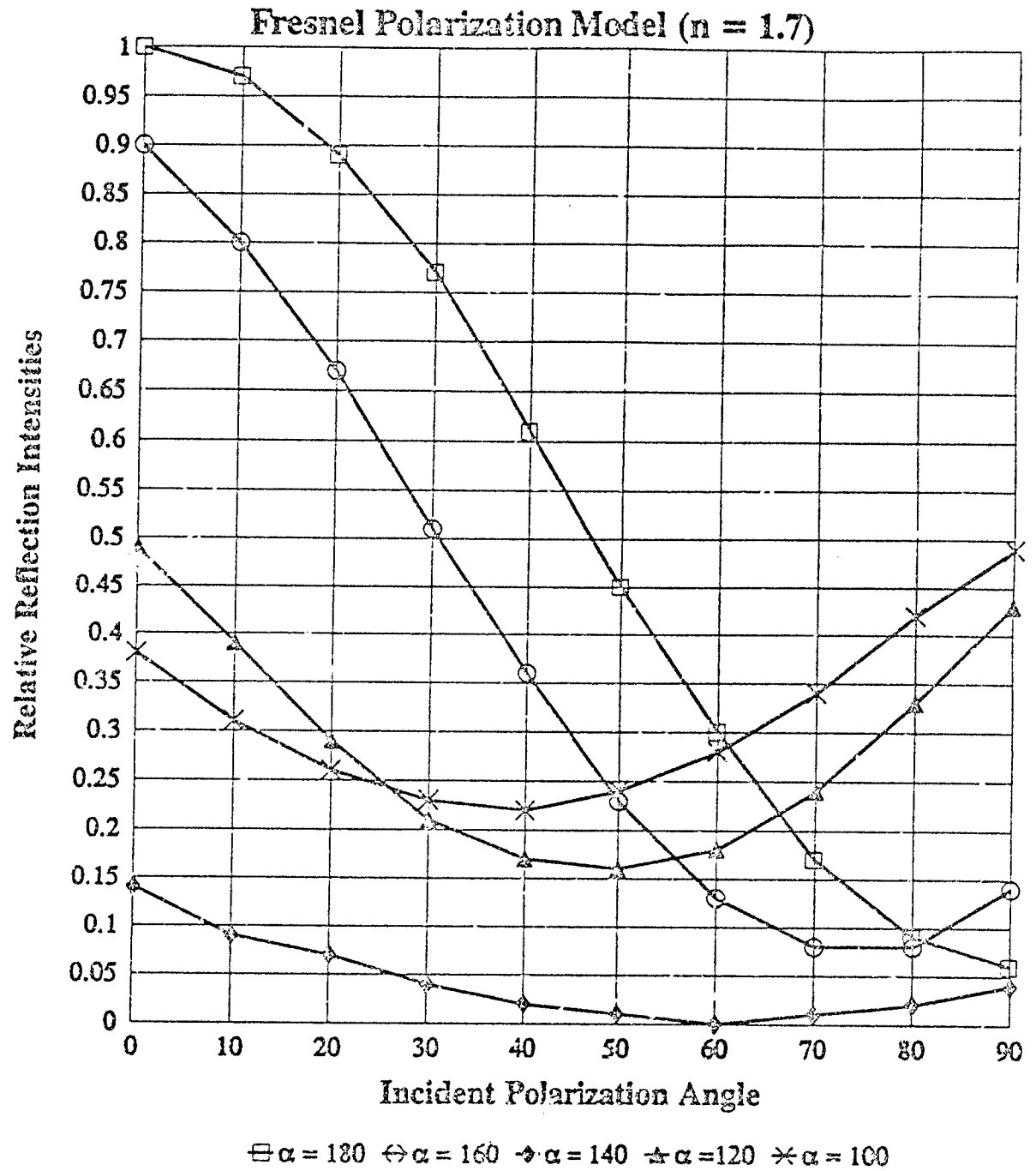


Figure 412.
Relative Reflection Intensities

Reflection From CARC-Painted Surface

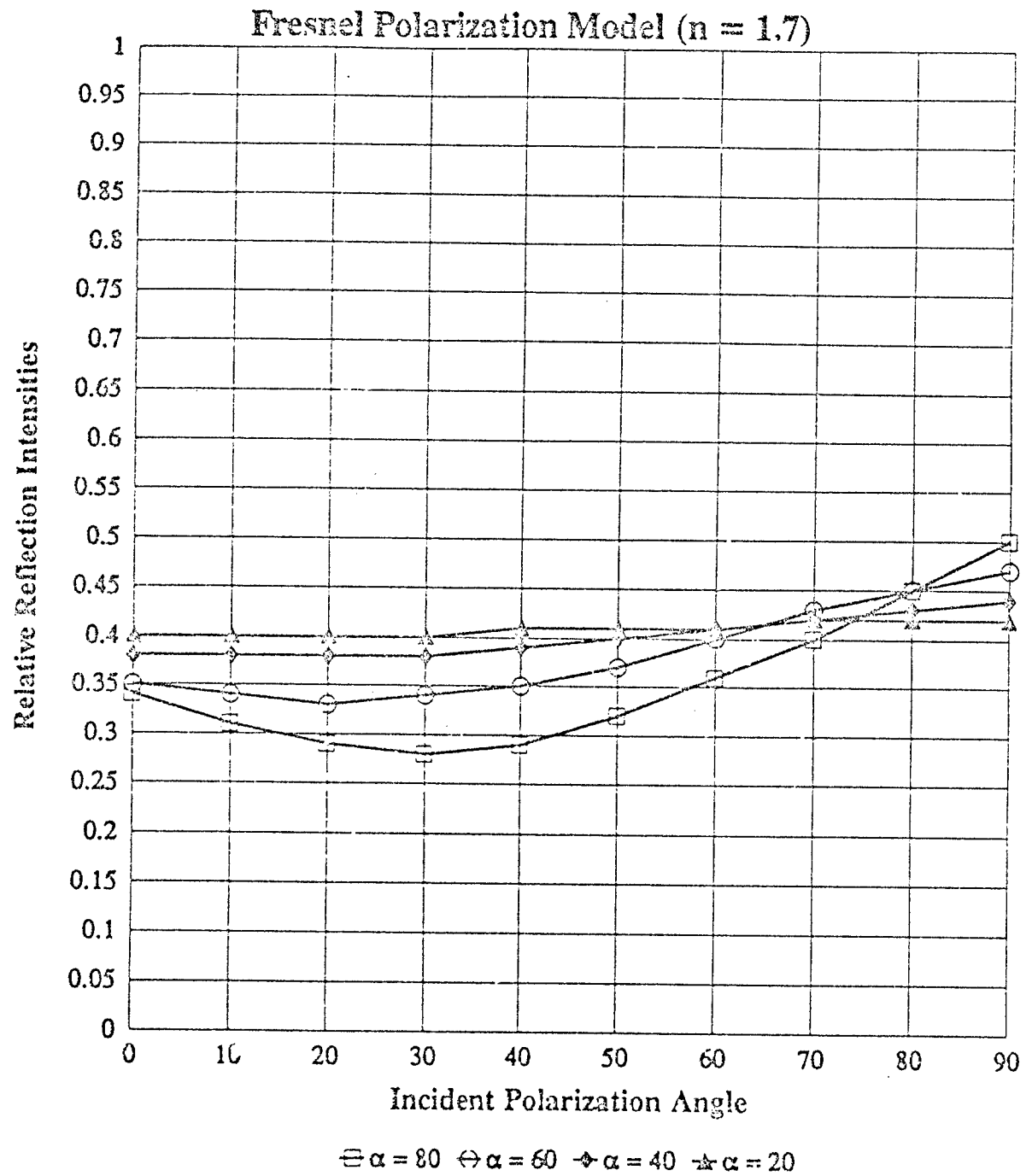


Figure 413.
Relative Reflection Intensities

SUMMARY

Polarization Axis

By using a modified definition of the plane of incidence, it has been demonstrated that the Fresnel equations for reflection are useful in predicting the angle of polarization for linear polarized light reflected from a CARC-painted sample. The results are shown in Figure 408 and Figure 409. The theory used fits over 75 percent of the collected data. Most of the deviation from theory occurs for azimuth angles between $\alpha = 160^\circ$ and $\alpha = 100^\circ$ and for incident polarization angles θ greater than 50° . This is an interesting development since this range agrees closely to the azimuth angles found in a previous study, "Goniophotometric Studies of a CARC-Painted Surface", 13 Aug., 1991, to correspond to a semi-gloss surface. The azimuth angles for which the modified Fresnel equations work best correspond to viewing angles for which the CARC surface acts as a diffuse reflector (Figure 346).

The photographs of Figure 390 for $\alpha = 180^\circ$ ($i = 50^\circ$) and the graph of Figure 399 suggest an index of refraction close to $n = 1.2$ for the CARC-paint layer. The selected light source slope and camera slope of 40° produced an angle of incidence of 50° for $\alpha = 180^\circ$. This is, coincidentally, close to the Brewster angle since the condition for the Brewster angle is given by $\tan i = n$ and $\tan 50^\circ = 1.19$. Unpolarized light incident on a dielectric at the Brewster angle produces reflected light that is plane-polarized parallel to the surface of the dielectric. The photographs of Figure 390 for $\alpha = 180^\circ$ ($i = 50^\circ$) and Table 89 illustrate that the reflected light was nearly plane-polarized parallel to the CARC-painted surface for all incident polarization angles $\theta = 0^\circ$ to $\theta = 80^\circ$. Also, light vibrating in the plane of incidence ($\theta = 90^\circ$) is not reflected at the Brewster angle. The photographs of Figure 390 for $\alpha = 180^\circ$ show very low intensities for the reflected light when the incident polarization angle was close to 90° .

Intensity

Since all the data collected for this study was in the form of photographs, intensity measurements are at best semi-quantitative. However, various trends can be identified in the collection of photographs which can be compared to theoretical predictions.

The trends in relative intensities shown in Figure 410 and Figure 411 for an index of refraction $n = 1.2$ more closely match the intensities shown in the polarization axis finder photographs than do the trends shown in Figure 412 and Figure 413 for $n = 1.7$. Figure 399 also supports the idea that the CARC paint layer has an index of refraction closer to 1.2 than to 1.7.

The plots of relative intensity from Figure 411 correspond to the photographs of Figure 392, Figure 393 and Figure 394. This graph and corresponding photographs are for azimuth angles $\alpha = 20^\circ$ to $\alpha = 100^\circ$. There is close agreement between theory and experimental data for this range of azimuth angles. The predicted values appear to be lower than the photographs indicate. However, theory predicts that the relative intensities are nearly constant for all incident polarization angles θ and this is the trend indicated in the photographs for this range of azimuth angles. Once again, theory and experimental data are in close agreement for viewing azimuth angles for which the CARC surface acts as a diffuse reflector.

The modified Fresnel equations, for azimuth angles $\alpha = 120^\circ$ to $\alpha = 180^\circ$, predict a continuous decrease in relative intensity which, after reaching zero, is accompanied by an increase in relative intensity. All the corresponding photographs show this same trend. However, the incident polarization angles for which the zero intensity values are reached differ by approximately 20° .

Limitations

Since this study was primarily phenomenological in nature, restrictions were imposed regarding space, available equipment and time. The slope of the light source and camera were limited to 40° . This limited the range of angles of incidence and reflectances as shown in Table 94.

Table 94. Range of Angles of Incidence i , Angles of Refraction r and Reflectances r_p and r_s .

α	$\angle i$	$n = 1.2$			$n = 1.7$		
		$\angle r$	r_p	r_s	$\angle r$	r_p	r_s
180.00	50.00	39.67	0.00000	0.03215	26.78	0.01015	0.16398
160.00	48.97	38.95	0.00004	0.03031	26.34	0.01193	0.15819
140.00	46.04	36.86	0.00041	0.02585	25.05	0.01727	0.14335
120.00	41.56	33.56	0.00139	0.02073	22.97	0.02567	0.12470
100.00	35.93	29.27	0.00291	0.01630	20.19	0.03580	0.10673
80.00	29.50	24.23	0.00459	0.01299	16.84	0.04597	0.09182
60.00	22.52	18.61	0.00612	0.01073	13.02	0.05487	0.08062
40.00	15.19	12.61	0.00729	0.00930	8.87	0.06163	0.07301
20.00	7.64	6.36	0.00802	0.00851	4.49	0.06581	0.06864

The diameter of the aperture of the polarization axis finder was two inches. The tube it was connected to was approximately 12 inches long. This geometry allows for an approximately 10° solid angle of reflected light to be incident on the film plane.

The centers of the wedges in the photographs were determined to within two degrees. This introduces an approximately two degree error in determining the polarization axis of the reflected light.

CONCLUSIONS

LUMINANCE

The largest luminance readings for sunlight reflected from three ground combat vehicles, the M60 tank, the M1 Abrahams tank and the Marine Corps amphibious Light Armored Vehicle (LAV25), were obtained from the turret areas of the vehicles. The highest luminance reading from these vehicles ($16,600 \text{ cd/m}^2$) was obtained from the top of the turret of the M60 and is due to specular reflection. Specular reflection is enhanced by (1) smooth surfaces, (2) elevated positions, (3) beveled or rounded shapes, and (4) gloss and semi-gloss painted surfaces. Luminance readings for the M60 decreased, in general, for areas closer to the ground because specular reflections for these regions are frequently below the ground plane.

Specular reflection is reduced or eliminated by overcast sky conditions. Dense, overcast skies tend to make the luminance ratios more constant. Openings in cloud cover contribute to variance in luminance. Cumulus clouds near the direction of the sun were observed to increase the luminance readings of ground vehicles. These clouds reflected more light onto a target area than would be produced by light coming directly from the sun alone.

The M1 has three distinguishing luminance areas: the turret, the skirt and the track and suspension areas. These areas remain distinguishing features despite orientation, time of day or sky condition. The average luminance obtained from the skirt area is approximately 70 percent of the average luminance obtained from the turret areas. The average luminance obtained from the track and suspension areas is approximately 30 percent of the average luminance obtained from the turret areas. The largest luminance reading obtained from a M1 turret area was $4,618 \text{ cd/m}^2$; acquired at 10:00 on 1 August 1990 during clear skies. The M1 turret areas also showed the greatest variance in luminance (as great as 50 percent of the average turret value) compared to other areas (maximum variance for skirt: 18 percent of the average; maximum variance for track and suspension: 16 percent of the average). Although large variances in luminance occur for individual points on the turret, the average luminance of the turret changed less than the other areas. During clear skies, the average luminance of the turret decreased at the approximate rate of $600 \text{ cd/m}^2/\text{hr}$ from 11:00 to 15:00. The average luminance of the skirt (11:00 to 14:00) and track and suspension areas (10:00 to 12:00) decreased at approximately $1,000 \text{ cd/m}^2/\text{hr}$.

The largest luminance reading acquired from the LAV25 ($3,300 \text{ cd/m}^2$) was obtained from a turret area. In terms of luminance, the LAV25 is a bisectonal vehicle. The wheel areas are separated from the upper beveled regions of the vehicle by a horizontal joint running the entire length of the vehicle. When the vehicle is positioned on the ground, the wheel areas make up nearly 50 percent of the vehicle's side surface area. Significant diurnal shading occurs in this area. In the early morning hours, with the vehicle positioned along a north-south line and metering to the west, the luminance of the road wheels and the areas

immediately above them are nearly the same. However, diurnal shading in the wheel areas produces variation in the luminance ratio of these two areas. During clear skies, the ratio of the average luminance of the wheel areas to the average luminance of the areas above them decreased at the approximate rate of 0.15 per hour.

During clear skies, there are extended periods of time for which the average luminance of the M1, the LAV25, grass and trees can be expressed by linear equations. Table 95 gives a summary of the equations for the approximate average luminance for these targets and backgrounds. Average luminance L is expressed in cd/m^2 and time t is in hours. These equations are valid for times 10:00 to 15:00 with $t = 0$ at 10:00.

Table 95. Approx. Average Luminance.

M1	$L = 3,000 - 500 t$
LAV25	$L = 1,700 - 200 t$
Grass	$L = 3,400 - 250 t$
Trees	$L = 1,200 - 80 t$

The best curve fit, during clear skies, for diurnal luminance readings of sunlight reflected from plane surface facets was obtained when luminance was plotted as a function of the cosine of the angle of incidence. This is the same principle which produces the seasons. Light energy from the sun per unit area decreases with an increase in the angle of incidence. The curves are nearly straight lines for the time interval 12:30 to 14:00. Deviations from a linear relationship between luminance and the cosine of the angle of incidence occurred before 12:30. These deviations are a result of the diurnal changes in the sun's power output. However, luminance was found to be directly proportional to the cosine of the angle of incidence when luminance readings were acquired from a CARC-(Chemical Agent Resistant Coating) painted flat surface using a collimated white light source in a dark room.

There is a significant difference between the luminance readings from a newly CARC painted surface and those from a weathered CARC-painted surface. A weathered CARC-painted surface was found to be approximately 25 percent brighter than a newly CARC-painted surface. This result was obtained during clear skies using three different M1 facets during the time interval 8:00 to 15:00.

The gloss of a surface is the degree it approaches a mirror surface. The two extreme cases of glossiness occur for Lambertian and specular surfaces. By definition, a Lambertian surface is a perfect reflecting diffuser. The luminance of a Lambertian surface is constant and has no dependence on angle of view. Incident light is distributed equally in every direction. It is the ideal surface of zero gloss. A purely specular surface produces a non-zero luminance value only at the angle of mirror reflection.

The newly CARC-painted surface was found to exhibit approximately Lambertian properties for azimuth angles from 60° to 240° . Luminance readings varied by only $108 \text{ cd}/\text{m}^2$ (3.6 percent) for this range of azimuth angles. This range corresponds to the hemisphere opposite the sun and at right angles to the plane of incidence.

The sample showed intermediate light-distributing properties between Lambertian and specular for azimuth angles from 60° to 240° . The difference between the maximum luminance reading and the minimum luminance reading acquired was 1039 cd/m^2 (30.1 percent). As would be expected from a semi-gloss surface, the largest luminance reading acquired (3975 cd/m^2) corresponded approximately to an azimuth angle equal to the sun's azimuth.

Goniophotometric records obtained for the CARC-painted sample show that higher luminance readings are acquired for smaller metering angles; metering closer to the surface; rather than in the direction of mirror reflection when metering is in the plane of incidence. This is in agreement with Fresnel's laws of reflection for polarized light reflected from a dielectric parallel to the plane of incidence. Also, the records show a decrease in luminance for angles of incidence between 0° and 60° but an increase in luminance for angles of incidence between 60° and 90° when metering was in the plane of incidence. This is also in agreement with Fresnel's laws for polarized reflected light parallel to the plane of incidence.

CONTRAST

Contrast is one of many factors which influences the ability to detect targets. All successful models that predict the probability of detecting targets will contain a contrast term. Contrast values for the M60 varied considerably, both the contrast for a given area and the average contrast for the entire vehicle. Using grass as a background, the largest contrast value for a single area and the largest variation in contrast ($+0.84$ to $+3.80$) was obtained from the top of the M60 turret. When considering the contrast of the M60 as a whole, using a grass background, the range of contrast extends from -0.95 to $+3.80$. The range of contrast, using trees as background, extends from -0.24 to $+2.50$.

During clear skies, the average M1 contrast using tree and grass backgrounds can be expressed as linear equations for extended periods of time; examples are given in Table 96. The equations of Table 96 are valid for the times 10:00 to 15:00. The correlation coefficients for these equations are greater than 0.98. Contrast is represented by C ; the time t is in hours with $t = 0$ at 10:00. The data from which these equations were derived was acquired for a M1 orientation along a north-south line and metering toward the west. There is a small change in the rate at which average contrast decreases when the range increases. This is due to more recessed areas being included in the measurement area at greater ranges.

Table 96. Average M1 Contrast Using Tree and Grass Backgrounds on 1 August, 1990.

Range	Contrast/Trees	Contrast/Grass
36 feet	$C = 2.06 - 0.49 t$	$C = 0.38 - 0.20 t$
100 feet	$C = 1.53 - 0.38 t$	$C = 0.02 - 0.14 t$
200 feet	$C = 1.34 - 0.35 t$	$C = -0.11 - 0.12 t$
300 feet	$C = 1.21 - 0.33 t$	$C = -0.03 - 0.12 t$

An important consequence of the shading of selected areas on a vehicle is contrast variation between different areas of the vehicle. This contrast variation increases the visibility of the vehicle and produces a visual signature. Also, high contrast areas increase vehicle detectability and can become prominent cue features for threat observers. Significant contrast occurs between M1 turret areas and the M1 skirt areas due to diurnal shading of the skirt area. The luminance of the turret areas was observed to be as much as five times greater than the luminance of skirt areas (14:00, 1 August, 1990).

During clear skies, the average LAV25 contrast using tree and grass backgrounds can be expressed as linear equations for extended periods of time; examples are given in Table 97. The equations of Table 97 are valid for the times 9:30 to 14:30. The correlation coefficients for these equations range from 0.87 to 0.99. Contrast is represented by C ; the time t is in hours with $t = 0$ at the beginning of the time interval. The data from which these equations were derived was acquired for a LAV25 orientation along a north-south line and metering toward the west. The negative contrast values obtained using a grass background indicate that the luminance of the grass was greater than the average luminance of the LAV25. The change in the description of contrast after 12:30 is due to shading of the LAV25 wheels.

Table 97. Average LAV25 Contrast Using Tree and Grass Backgrounds on 1 August, 1990.

Range	Time Interval	Contrast/Trees	Contrast/Grass
36 feet	9:30 - 12:30	$C = 0.55$	$C = -0.31$
36 feet	12:30 - 14:30	$C = 0.57 - 0.31 t$	$C = -0.31 - 0.16 t$
100 feet	9:30 - 14:30	$C = 0.33 - 0.11 t$	$C = -0.41 - 0.06 t$
200 feet	9:30 - 14:30	$C = 0.25 - 0.09 t$	$C = -0.56 - 0.03 t$
300 feet	9:30 - 14:30	$C = 0.27 - 0.10 t$	$C = -0.47 - 0.04 t$

When two nonparallel surfaces of a vehicle meet, a rounded edge is formed. This edge may be formed by a single metal plate, a weld joint or a bend. Under the right conditions, an edge may appear as a white line. These white lines are produced by specular reflection. Because of the roundness of the edge, there are many different angles of incidence for an edge surface for any given sun position. Hence, the white outline can be observed from many different directions, especially for edges near the top of the vehicle. Different colors of paint have little effect on the degree of glare. White lines were observed on edges painted with three different colors; one of the colors being flat black. Since the entire illuminated edge appeared white, the white line is associated with light that has not interacted with the paint pigments; there is little absorption by the pigment materials.

An important consequence of the edge effect is to increase the contrast between the edge and surrounding surfaces. This increase in contrast increases the visibility of the vehicle. A linear polarizer is effective in reducing glare because the specularly reflected light from the edges is linearly polarized to a considerable extent. The degree of glare extinction depends on the angle between the transmission axis of the polarizer and the plane of polarization of the reflected light. Controlling edge contrast is important for limiting recognition and identification of threat observers.

POLARIZATION

Sunlight reflected from three different M1 facets was found to be partially polarized. The degree of polarization depends on the time of day, sky conditions, and facet orientations. However, the reflected light was nearly horizontally polarized for all three M1 facets studied and for all times during the day except during early morning hours (8:00 to 10:00) when the sun was in the eastern sky. Since the region of the sky near the sun produces little polarized light, sunlight reflected from a north-south oriented vehicle during the times 8:00 to 10:00 (Eastern Daylight Standard Time) is mostly unpolarized light. This accounts for the small degree of polarization during this time of the day.

For the turret area with a slope of 60° and an azimuth of 270° , the degree of polarization increased continuously from 0.01 to 0.21 during the time interval from 8:00 to 14:00. For the turret area with a slope of 60° and an azimuth of 204° , the degree of polarization increased from 0.01 to 0.12 during the time interval from 8:00 to 12:30. It then decreased from 0.12 to 0.09 during the time interval from 12:30 to 14:00. For the skirt area, the degree of polarization increased from 0.01 to 0.11 during the time interval from 8:00 to 12:30. It then decreased from 0.11 to 0.05 during the one hour time interval from 12:30 to 13:30; rising again after the sun crossed the meridian (13:30 EDST) to a value of .08 at 14:45.

Sky polarization photographs were obtained by placing a polarization axis finder in front of the lens of a 35 mm camera. These photographs illustrate why the amount of linear polarized light reflected from a north-south oriented M1 should increase after 8:00. The eastern hemispherical sky is the only sky region which can affect western polarization readings from a north-south oriented M1. Therefore, since the amount of polarized light from this sky region increases from sunset to solar noon, the degree of polarized light reflected from the M1 also increases during this same period.

A video tape was created from a camcorder with a rotating linear polarizer in front of the camcorder lens. As the transmission axis of the linear polarizer rotated in front of the camcorder lens, polarized light entering the camcorder was observed to "flicker" in unison with the phase angle between the polarized incident light and the rotating analyzer. The video includes 360° views of an M1, M60, skylight and objects along the horizon.

There is one dramatic feature of this video that stands out above all others. An outstanding amount of "flicker" (reflected polarized light) can be detected from surfaces which receive no light directly from the sun. Shadowed areas were observed to blink on and off like flashing neon signs. Rounded surfaces, like the M60 turret, fence posts, car hoods and windows, produced a considerable amount of "flicker" when illuminated by direct sunlight. Flat surfaces, like the skirt area of the M1, showed very little "flicker" when illuminated by direct sunlight. But these same flat surfaces flashed on and off as soon as sky light became the only source of illumination. This "flicker" phenomenon, as it relates to polarized light reflected from ground combat vehicles, has capabilities of being used as a detection device. Ground combat vehicles, shielded from direct sunlight, might be detected because of polarized sky light reflected from their surfaces.

By using a modified definition of the plane of incidence, it has been demonstrated that the Fresnel equations for reflection are useful in predicting the angle of polarization for linear polarized light reflected from a CARC-painted sample. The theory used fits over 75 percent of collected in-house data relating to collimated, plane polarized, xenon light reflected from a CARC painted sample. Most of the deviation from theory occurs for azimuth angles between 60° and 100° and for incident polarization angles greater than 50°. The azimuth angles for which the modified Fresnel equations work best correspond to viewing angles for which the CARC surface acts as a diffuse reflector.

Unpolarized light incident on a dielectric at the Brewster angle ϕ ($\tan \phi$ = index of refraction) produces reflected light that is plane-polarized parallel to the surface of the dielectric. Experimental results indicate that the reflected xenon light was nearly plane-polarized parallel to the CARC-painted surface for all incident polarization angles 0° to 80° when the angle of incidence was 50°. These results suggest an index of refraction close to 1.2 for the CARC paint layer. Analysis also shows very low intensities for the reflected light when the incident polarization angle was close to 90°.

The modified Fresnel equations, for azimuth angles 120° to 180° , predict a continuous decrease in relative intensity which, after reaching zero, is accompanied by an increase in relative intensity. All photographic data for the in-house study show this same trend. However, the incident polarization angles for which the zero intensity values are reached differ by approximately 20° .

CHROMATICITY

The three coordinates for the CIE Chromaticity Diagram were measured for three different M1 facets, three different tree areas and a grass area. Measurements were made from 8:00 to 14:45. Clear skies prevailed until 12:00; light overcast and cloudy conditions existed after 12:00. The CIE coordinates of the three different M1 facets shifted slightly toward the white light coordinate as the sun moved westward from 8:00 to 14:00. There was virtually no change in the CIE coordinates for grass from 8:00 to 14:00. There was little difference in the behavior of the CIE coordinates for the three different tree areas measured. The value of both the X and Y tree coordinates continuously decreased from 8:00 to 14:00. The tree areas had a greater saturation of green than the M1 and they showed a greater shift toward the white light coordinate from 8:00 to 14:00.

RECOMMENDATIONS

Preliminary investigations have identified sky illumination as the principle source of polarized reflected light from ground combat vehicles. Since this source of illumination produces a unique visual signature of ground vehicles, it is desirable to obtain a mathematical description of this source of illumination. Ideally, the model should be able to predict the polarization axis and the relative intensity of polarized light for any point in the sky at any time of the day for which sky illumination is the principle source of polarized light. Hopefully, this model can be integrated with a second model which predicts the degree of polarization and the polarization axis of reflected light from the surfaces of ground vehicles. This second model should produce acceptable results for any surface orientation. Presently, only a framework has been established from which these models can be derived.

One of the limitations of the diurnal luminance and contrast studies relates to an inability to spot measure the entire surface area of a ground vehicle in a reasonable amount of time. New technological advances in digital cameras could remedy this limitation. With the click of a button, the entire exposed surface area of a vehicle can be digitally recorded for computer analysis. Since these digital cameras have color capabilities, vehicle signatures could be studied in terms of diurnal color changes.

APPENDIX A

OPTICAL DENSITY AND TRANSMITTANCE

Optical Density is defined as the logarithm to the base ten of the ratio of the power of the incident beam to that of the exiting beam.

$$D = \log_{10} \frac{I_o}{I_T} = -\log_{10} T$$

Where:

D = Optical Density, I_o = Incident power and I_T = Transmitted power

The transmittance, T, is $\frac{I_T}{I_o}$ and is given by

$$T = 10^{-D}$$

Suppose that a luminance reading from the Minolta LS-100 luminance meter is L. If a polarizer of optical density 0.5 (transmittance = 0.316) is placed in front of the Minolta LS-100 luminance meter, the luminance reading should never be greater than 0.316 L. However, data collected using polarized light with a polarizer of optical density 0.5 placed in front of the LS-100 produced luminance readings greater than 0.316 L. Luminance readings as high as 0.6 L were obtained.

Figure 414, Figure 415 and Figure 416 describe a simple experiment to obtain the luminance from a source of unpolarized light. The optical density of the neutral density filter and the polarizer P_1 were measured using a densitometer; both were found to be 0.50. The results are given in Table 98. The transmittance through the neutral density filter and the polarizer are both close to the predicted value of 0.316.

Figure 418, Figure 419 and Figure 420 describe a simple experiment to obtain the luminance from a source of polarized light. The linear polarizer P_0 polarizes the light from the frosted glass plate. Linear polarizer P_1 serves as an analyzer. Table 99 gives a summary of the results.

When polarized light was transmitted through a neutral density filter positioned in front of the LS-100, the transmittance through the neutral density filter was found to be close to the predicted value of 0.316.

The results obtained from the arrangement shown in Figure 420, however, illustrate that there are clearly angles between the transmission axes of the polarizers that produce transmittance greater than 0.316. When the angle between the transmission axes of the polarizers is varied from 0° to 180° , the transmittance increases from 0.00 to 0.59 and then decrease to 0.00. Figure 421 and Figure 422 show the results graphically. From the Law of Malus, the transmittance should be directly proportional to $\text{Cos}^2 \theta$.

Although the collected data for the crossed polarizers agrees with the Law of Malus, $L_1 = 857 \text{ Cos}^2 \theta$, the expected values for the luminance, considering that the transmittance of the polarizer is 0.316, should fit the equation $L_1 = .0316 L_0 \text{ Cos}^2 \theta$. The ratio of the experimental luminance readings to the expected luminance readings is a constant, 1.87, for light passing through crossed polarizers and incident on the Minolta LS-100.

Obviously, the optical density of 0.5 (transmittance 0.316), measured with the densitometer, is only appropriate for unpolarized light.

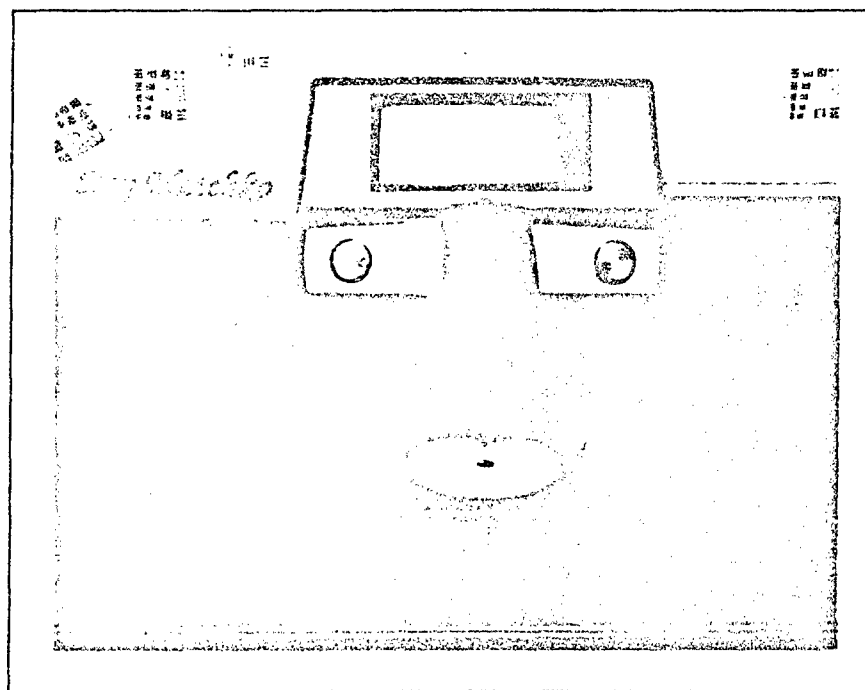
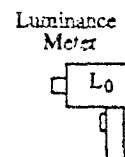
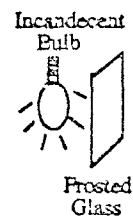


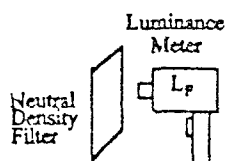
Figure 414
Macbeth TD 502 Densitometer

Table 98. Luminance (L) and luminance ratios using polarized and unpolarized light with the Minolta LS-100 luminance meter.

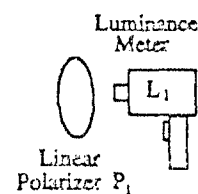
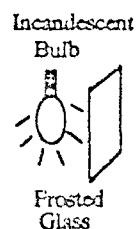
L_0	L_F	L_1
5833	1921	1730
$L_F / L_0 = 0.330$		
$L_1 / L_0 = 0.297$		



Note: All luminance (L) values are in cd/m^2 .
Figure A-1



Optical Density of Filter = 0.50
Transmittance of Filter = 0.316



Optical Density of P_1 = 0.50
Transmittance of P_1 = 0.316

Figure 415

Figure 416

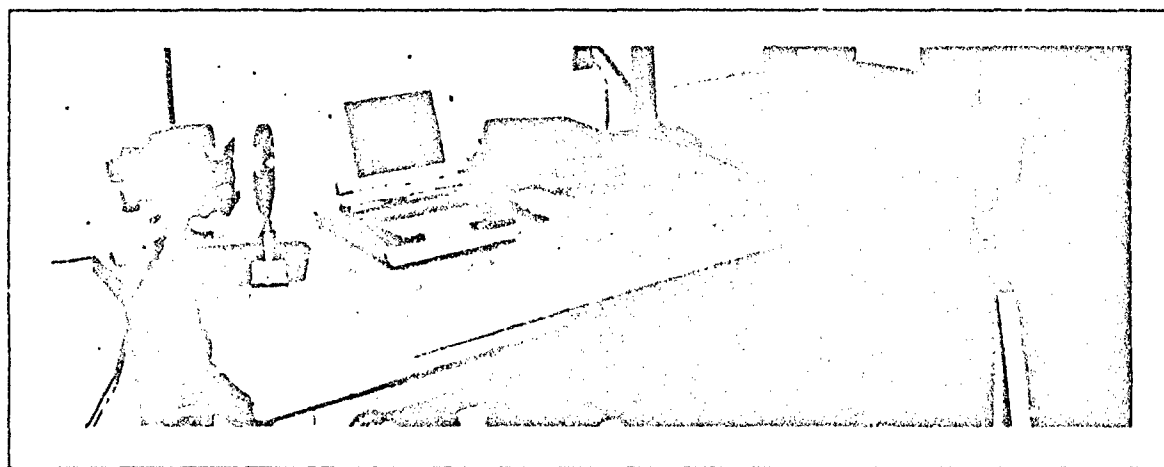


Figure 417
Experimental setup for measuring luminance of polarized light with the Minolta LS-100

Table 99. Luminance (L) and luminance ratios using polarized light with the Minolta LS-100 luminance meter.

$L_0 = 1447; L_F = 478; \theta_0 = 90^\circ$			
$L_0 / L_F = 0.330$			
θ_1	$\theta = \theta_1 - \theta_0$	L_1	L_1 / L_0
0	-90	1	0.001
10	-80	18	0.012
20	-70	82	0.057
30	-60	185	0.128
40	-50	318	0.220
50	-40	464	0.321
60	-30	610	0.422
70	-20	730	0.504
80	-10	813	0.561
90	0	857	0.592
100	10	848	0.586
110	20	779	0.538
120	30	673	0.465
130	40	535	0.370
140	50	378	0.261
150	60	247	0.170
160	70	125	0.086
170	80	36	0.025
180	90	3	0.002

Note: All luminance (L) values are in cd/m^2 .

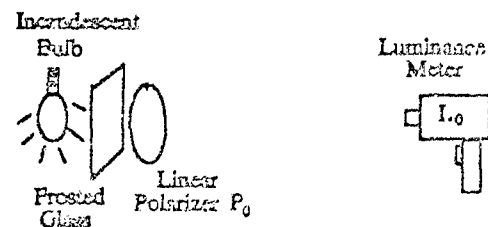


Figure 418

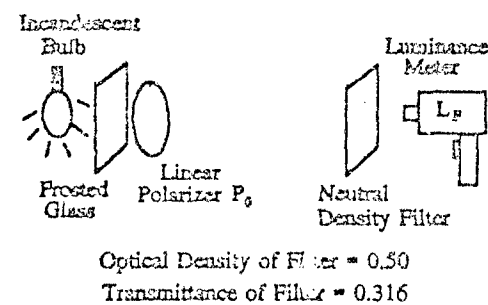


Figure 419

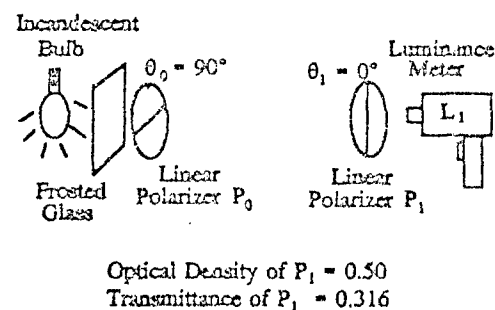


Figure 420

LUMINANCE USING CROSSED POLARIZERS METERING FROM MINOLTA LS-100

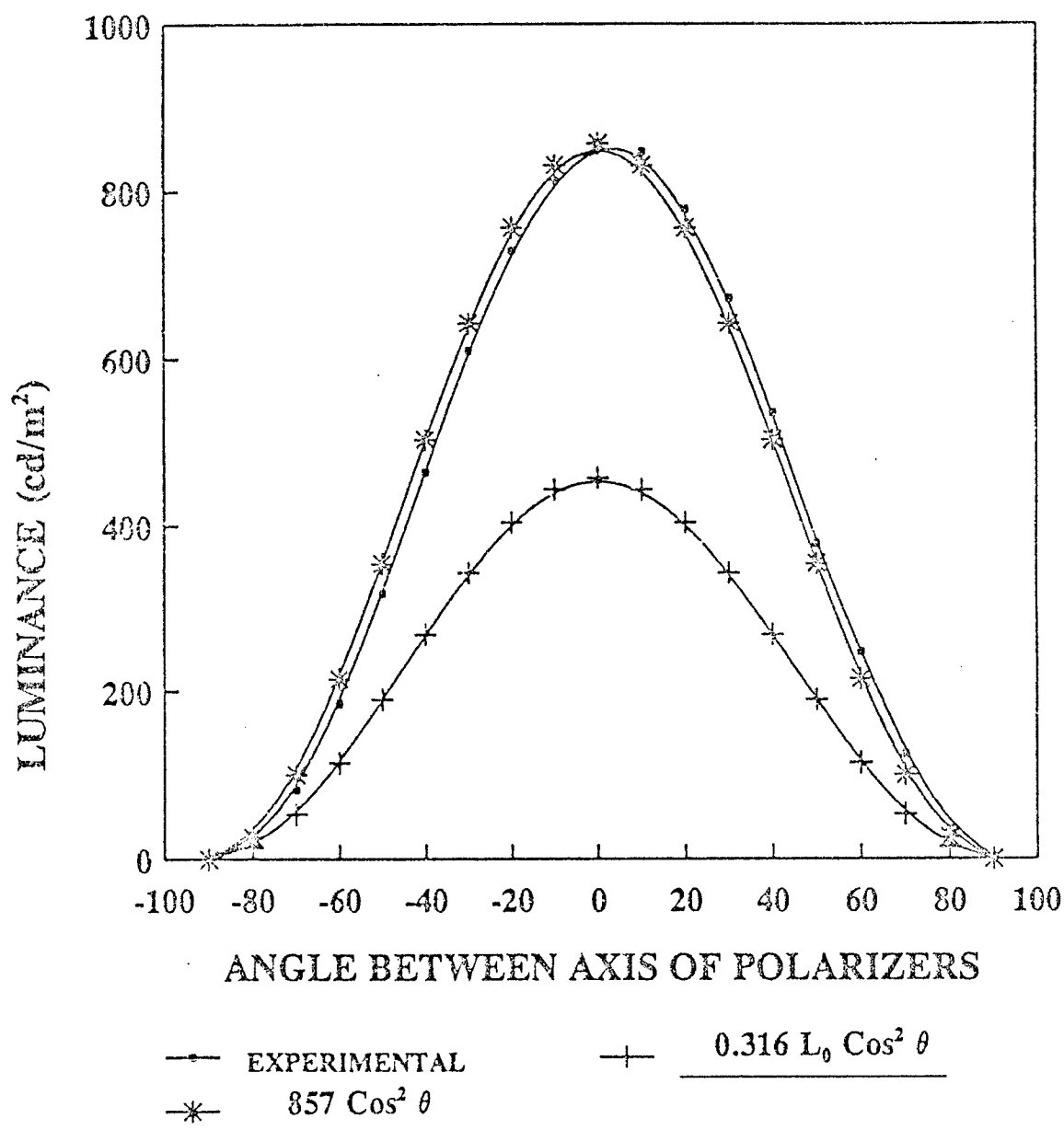


Figure 421

LUMINANCE RATIOS USING CROSSED POLARIZERS METERING FROM MINOLTA LS-100

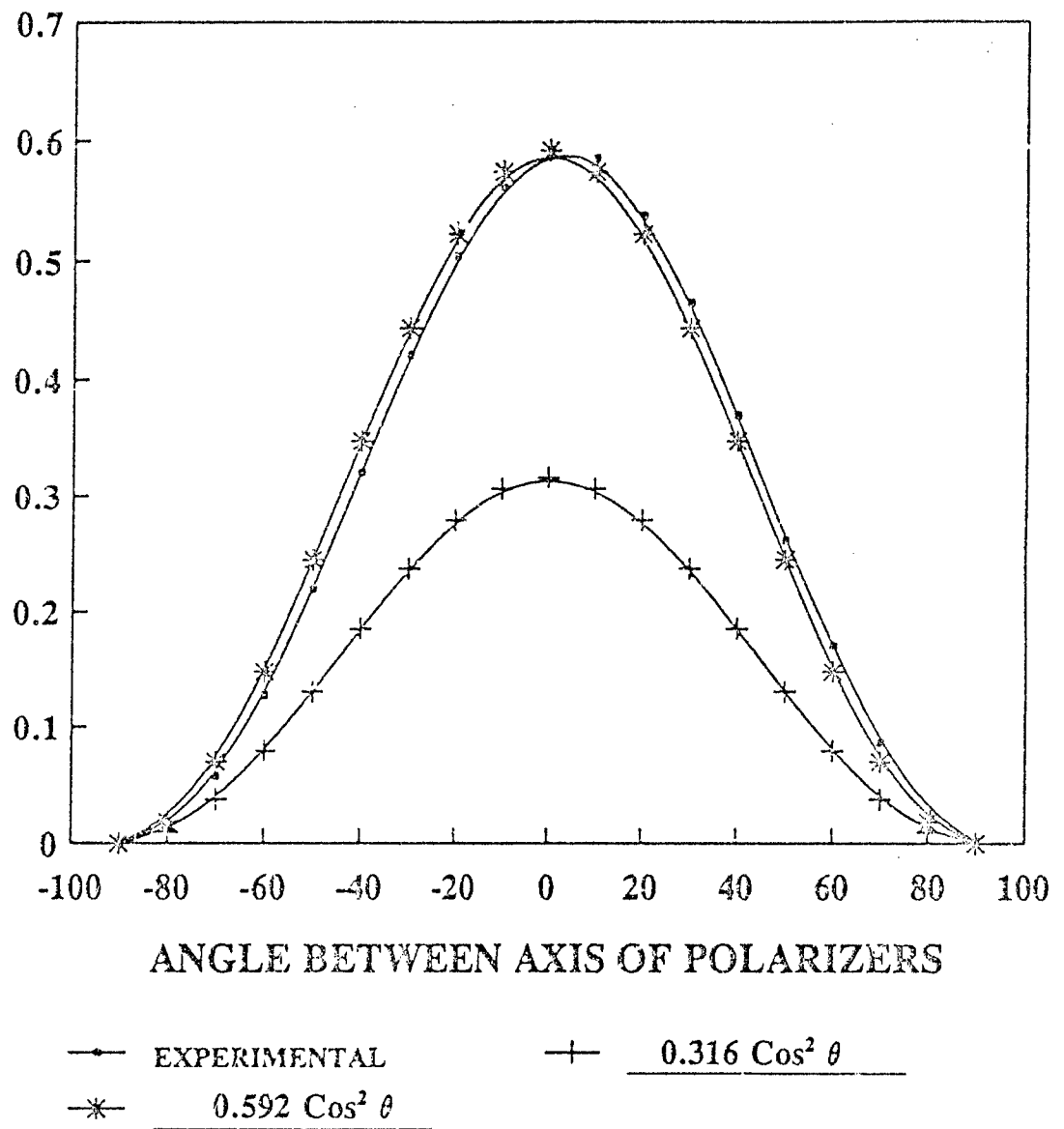


Figure 422

APPENDIX B

POLARIZATION AXIS FINDER

This device finds the polarization axis of linear polarized light and visually indicates the intensity of polarization. The circular lens element is polarized concentrically about the center. Each tiny area is a linear polarizer, with the direction of the transmission axis perpendicular to the radius. This arrangement causes a blackout (two dark opposing wedges) of polarized light in direct alignment with the axis of polarity of the incident light. The polarization axis is along a line through the center of the two dark opposing wedges. The darker and broader these wedges appear, the greater the intensity of the polarization of the incident light.

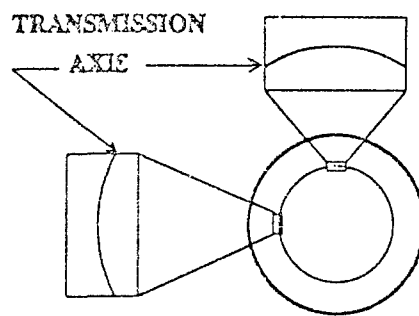


Figure 423

The axis finder is a polarizer with circular concentric transmission axes.

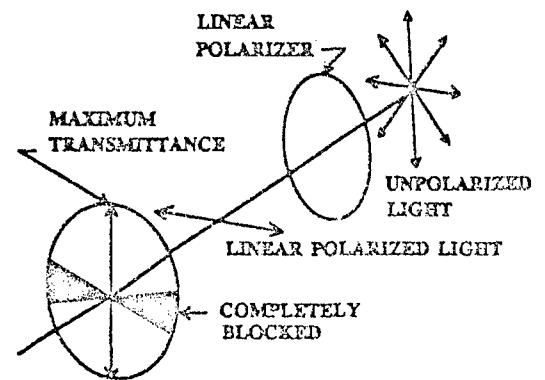


Figure 424

Axis finder used to locate the transmission axis of a linear polarizer

APPENDIX C THE ASTRONOMICAL TRIANGLE

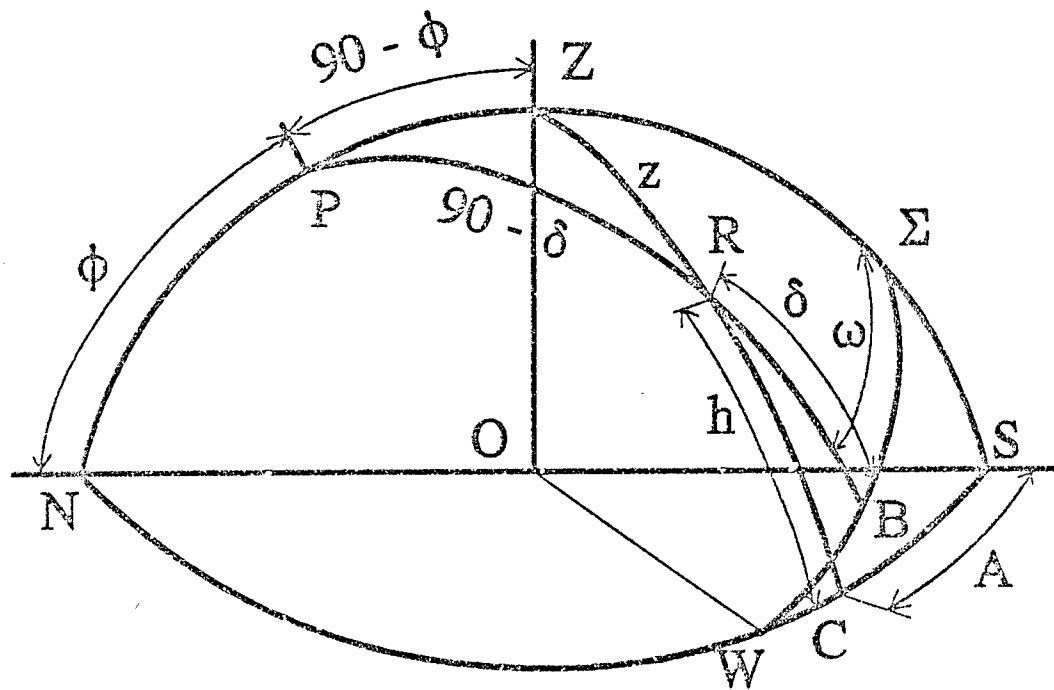


Figure 425
The Astronomical Triangle ZRP.

Vertices: North Pole P, Zenith Z and Heavenly Body R.

Sides:
 $PZ = 90 - \text{Latitude } (\phi)$
 $ZR = z = 90 - \text{Altitude } (h)$
 $PR = 90 - \text{Declination } (\delta)$

Angles:
 $\angle P = \text{hour angle } (\omega)$
 $\angle Z = 180 - \text{Azimuth } (A)$

Σ is the intersection of the meridian and the equator.
 N is north. S is south. W is west.

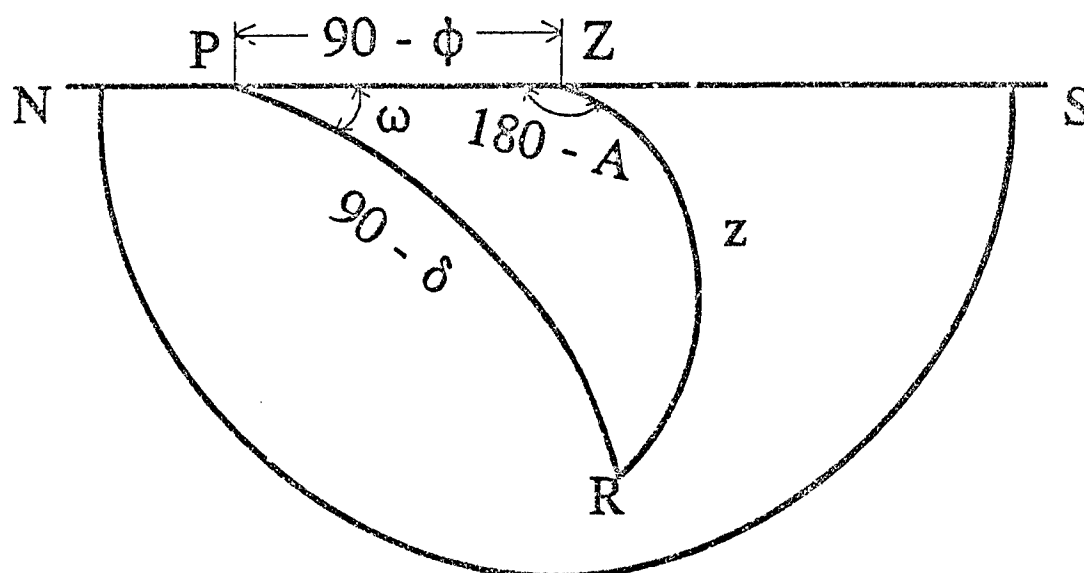


Figure 426
Astronomical Triangle, with heavenly body R west of meridian.

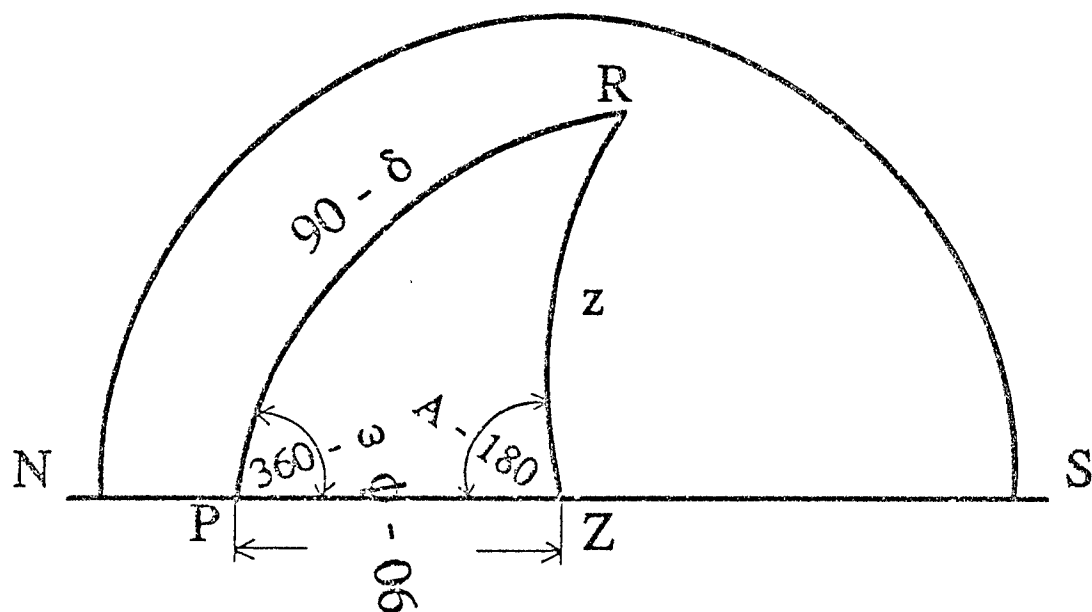


Figure 427
Astronomical Triangle, with heavenly body R east of meridian.

FORMULAS FOR SPHERICAL TRIANGLES

Law of Sines:

$$\frac{\sin a}{\sin A} = \frac{\sin b}{\sin B} = \frac{\sin c}{\sin C} \quad (1)$$

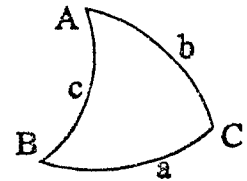


Figure 428

Law of Cosines:

$$\cos a = \cos b \cos c + \sin b \sin c \cos A \quad (2)$$

$$\cos b = \cos a \cos c + \sin a \sin c \cos B \quad (3)$$

$$\cos c = \cos a \cos b + \sin a \sin b \cos C \quad (4)$$

$$\cos A = -\cos B \cos C + \sin B \sin C \cos a \quad (5)$$

$$\cos B = -\cos A \cos C + \sin A \sin C \cos b \quad (6)$$

$$\cos C = -\cos A \cos B + \sin A \sin B \cos c \quad (7)$$

Relation between Two Angles and Three Sides:

$$\sin a \cos B = \sin c \cos b - \cos c \sin b \cos A \quad (8)$$

Half-Angle Formulas:

$$\tan \frac{A}{2} = \frac{p}{\sin(s-a)} \quad \tan \frac{B}{2} = \frac{p}{\sin(s-b)} \quad (9)$$

$$\tan \frac{C}{2} = \frac{p}{\sin(s-c)} \quad \text{where} \quad s = \frac{a+b+c}{2}$$

$$\text{and} \quad p = \sqrt{\frac{\sin(s-a) \sin(s-b) \sin(s-c)}{\sin s}}$$

FORMULAS FOR THE ASTRONOMICAL TRIANGLE

From (1)

$$\sin \omega \cos \delta = \sin z \sin A \quad (10)$$

From (2)

$$\cos z = \sin \phi \sin \delta + \cos \phi \cos \delta \cos \omega \quad (11)$$

From (3)

$$\sin \delta = \sin \phi \cos z - \cos \phi \sin z \cos A \quad (12)$$

From (8)

$$\sin z \cos A = \sin \phi \cos \delta \cos \omega - \cos \phi \sin \delta \quad (13)$$

From (9)

$$\tan \frac{\omega}{2} = \pm \sqrt{\frac{\sin \frac{[z - (\phi - \delta)]}{2} \sin \frac{[z + (\phi - \delta)]}{2}}{\cos \frac{[z - (\phi + \delta)]}{2} \cos \frac{[z + (\phi + \delta)]}{2}}} \quad (14)$$

From (8)

$$\cos \delta \cos \omega = \cos \phi \cos z + \sin \phi \sin z \cos A \quad (15)$$

APPENDIX D

ANGLE BETWEEN SUN'S RAYS AND PLANE

If \mathbf{r} is a unit vector,

$$Z = \cos \beta \quad (16)$$

$$X = W \sin \alpha \quad (17)$$

$$Y = W \cos \alpha \quad (18)$$

$$W = \sin \beta \quad (19)$$

$$X = \sin \beta \sin \alpha \quad (20)$$

$$Y = \sin \beta \cos \alpha \quad (21)$$

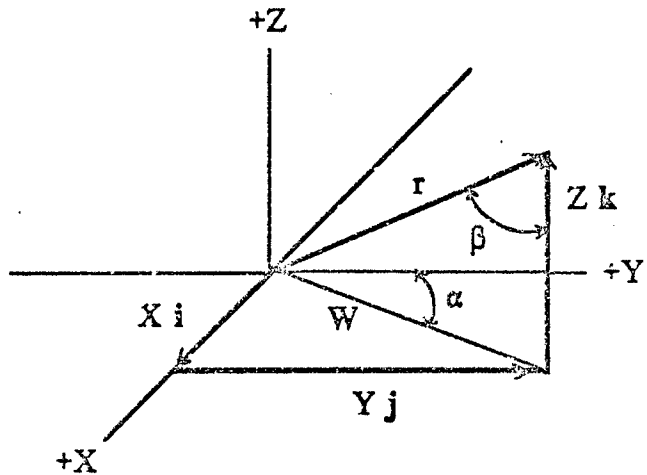


Figure 429

$$\mathbf{r} = X \mathbf{i} + Y \mathbf{j} + Z \mathbf{k} \quad (22)$$

$$\mathbf{r} = \sin \beta \sin \alpha \mathbf{i} + \sin \beta \cos \alpha \mathbf{j} + \cos \beta \mathbf{k} \quad (23)$$

If \mathbf{r} is a unit vector opposite in direction to an incident sun ray, then

β = zenith distance of sun (z) and α = azimuth of sun (A).

$$\mathbf{r} = \sin z \sin A \mathbf{i} + \sin z \cos A \mathbf{j} + \cos z \mathbf{k} \quad (24)$$

The azimuth of the sun is measured westward from south and is zero when the sun is on the meridian.

Let \mathbf{n} be a unit vector in the direction of a normal to a plane surface. Then

$$\mathbf{n} = \sin s \sin \gamma \mathbf{i} + \sin s \cos \gamma \mathbf{j} + \cos s \mathbf{k} \quad (25)$$

where s is the slope of the plane and γ is the azimuth of the plane.

The azimuth of the plane is measured westward from south and is zero when the normal to the plane points south.

The vector dot product can be used to find the angle between r and n :

$$r \cdot n = |r| |n| \cos i \quad (26)$$

where i is the angle between r and n .

Angle i is the angle of incidence the sun's rays make with the normal to the surface.

Since r and n are unit vectors

$$\cos i = \frac{r \cdot n}{|r| |n|} = r \cdot n \quad (27)$$

$$\begin{aligned} \cos i = \sin z \sin A \sin s \sin \gamma + \sin z \cos A \sin s \cos \gamma \\ + \cos z \cos s \end{aligned} \quad (28)$$

Using the expression for $\sin z \sin A$ from (10), the expression for $\cos z$ from (11) and the expression for $\sin z \cos A$ from (13), equation (28) can be rewritten as:

$$\begin{aligned} \cos i = \sin \omega \cos \delta \sin s \sin \gamma + \sin \phi \cos \delta \cos \omega \sin s \cos \gamma \\ - \cos \phi \sin \delta \sin s \cos \gamma + \sin \phi \sin \delta \cos s \\ + \cos \phi \cos \delta \cos \omega \cos s \end{aligned}$$

(29)

APPENDIX E

EQUATIONS FOR REFLECTED SUN RAY

The following is a derivation of the equation for the direction of a reflected sun ray from any plane surface.

Let z = zenith angle of sun

Let A = azimuth of sun

Let \mathbf{I} be a unit vector opposite in direction to an incident sun ray.

From (24):

$$\mathbf{I} = \sin z \sin A \mathbf{i} + \sin z \cos A \mathbf{j} + \cos z \mathbf{k} \quad (30)$$

Let s = slope of plane surface

Let γ = azimuth of plane surface (south = 0)

Let \mathbf{N} be a unit vector normal to a plane surface P .

From (25):

$$\mathbf{N} = \sin s \sin \gamma \mathbf{i} + \sin s \cos \gamma \mathbf{j} + \cos s \mathbf{k} \quad (31)$$

Let \mathbf{R} be a unit vector in the direction of the reflected sun ray from P .

$$\mathbf{R} = X \mathbf{i} + Y \mathbf{j} + Z \mathbf{k} \quad (32)$$

Since vector \mathbf{R} is a unit vector, X , Y and Z are the direction cosines of vector \mathbf{R} .

Find X, Y, Z .

Let i = angle of incidence.

From the laws of reflection:

A. I, N and R are coplanar

$$R \cdot (I \times N) = 0 \quad (33)$$

B. The angle of incidence equals the angle of reflection

$$N \cdot R = \cos i \quad (34)$$

$$I \cdot R = \cos 2i \quad (35)$$

Let

$$I_1 = \sin z \sin A \quad (36)$$

$$I_2 = \sin z \cos A \quad (37)$$

$$I_3 = \cos z \quad (38)$$

$$N_1 = \sin s \sin \gamma \quad (39)$$

$$N_2 = \sin s \cos \gamma \quad (40)$$

$$N_3 = \cos s \quad (41)$$

Also, from (28)

$$\cos i = I_1 N_1 + I_2 N_2 + I_3 N_3 \quad (42)$$

$$\cos 2i = 2(I_1 N_1 + I_2 N_2 + I_3 N_3)^2 - 1 \quad (43)$$

Equations (30) and (31) become

$$I = I_1 i + I_2 j + I_3 k \quad (44)$$

$$N = N_1 i + N_2 j + N_3 k \quad (45)$$

Equation (33) can be written as

$$R \cdot (I \ X \ N) = \begin{vmatrix} X & Y & Z \\ I_1 & I_2 & I_3 \\ N_1 & N_2 & N_3 \end{vmatrix} = 0 \quad (46)$$

Expanding the determinant in (46)

$$(I_2 N_3 - I_3 N_2) X + (I_3 N_1 - I_1 N_3) Y + (I_1 N_2 - I_2 N_1) Z = 0 \quad (47)$$

From (34)

$$N_1 X + N_2 Y + N_3 Z = \cos i \quad (48)$$

From (35)

$$I_1 X + I_2 Y + I_3 Z = \cos 2i \quad (49)$$

Using the following matrices,

$$M = \begin{pmatrix} (I_2 N_3 - I_3 N_2) & (I_3 N_1 - I_1 N_3) & (I_1 N_2 - I_2 N_1) \\ N_1 & N_2 & N_3 \\ I_1 & I_2 & I_3 \end{pmatrix}$$

$$Q = \begin{pmatrix} X \\ Y \\ Z \end{pmatrix} \quad \text{and} \quad K = \begin{pmatrix} 0 \\ \cos i \\ \cos 2i \end{pmatrix}$$

equations (47), (48) and (49) become

$$M Q = K \quad (50)$$

Solving for Q

$$Q = K M^{-1} \quad (51)$$

By definition

$$M^{-1} = \frac{\text{adj } M}{\det M} \quad (52)$$

Combining (51) and (52)

$$Q = \frac{K \text{adj } M}{\det M} \quad (53)$$

The adjoint matrix of M (adj M) is found by replacing each element of M by its cofactor and then transposing. The signed minor $(-1)^{i+j} m_{ij}$ is called the cofactor of the element a_{ij} .

Replacing each element of M by its cofactor

adj M = transpose of

$$\begin{pmatrix} (I_3 N_2 - I_2 N_3) & (I_1 N_3 - I_3 N_1) & (I_2 N_1 - I_1 N_2) \\ (I_1 I_3 N_3 - I_3^2 N_1 + I_1 I_2 N_2 - I_2^2 N_1) & (I_2 I_3 N_3 - I_3^2 N_2 - I_1^2 N_2 + I_1 I_2 N_1) & (I_2 I_3 N_2 - I_2^2 N_3 + I_1 I_3 N_1 - I_1^2 N_3) \\ (I_3 N_1 N_3 - I_1 N_3^2 - I_1 N_2^2 + I_2 N_1 N_2) & (I_3 N_2 N_3 - I_2 N_3^2 + I_1 N_1 N_2 - I_2 N_1^2) & (I_2 N_2 N_3 - I_3 N_2^2 - I_3 N_1^2 + I_1 N_1 N_3) \end{pmatrix} \quad (54)$$

adj M =

$$\begin{pmatrix} (I_3 N_2 - I_2 N_3) & (I_1 I_3 N_3 - I_3^2 N_1 + I_1 I_2 N_2 - I_2^2 N_1) & (I_3 N_1 N_3 - I_1 N_3^2 - I_1 N_2^2 + I_2 N_1 N_2) \\ (I_1 N_3 - I_3 N_1) & (I_2 I_3 N_3 - I_3^2 N_2 - I_1^2 N_2 + I_1 I_2 N_1) & (I_3 N_2 N_3 - I_2 N_3^2 + I_1 N_1 N_2 - I_2 N_1^2) \\ (I_2 N_1 - I_1 N_2) & (I_2 I_3 N_2 - I_2^2 N_3 + I_1 I_3 N_1 - I_1^2 N_3) & (I_2 N_2 N_3 - I_3 N_2^2 - I_3 N_1^2 + I_1 N_1 N_3) \end{pmatrix} \quad (55)$$

K adj M =

$$\begin{pmatrix} (I_1 I_3 N_3 - I_3^2 N_1 + I_1 I_2 N_2 - I_2^2 N_1) \cos i + (I_3 N_1 N_3 - I_1 N_3^2 - I_1 N_2^2 + I_2 N_1 N_2) \cos 2i \\ (I_2 I_3 N_3 - I_3^2 N_2 - I_1^2 N_2 + I_1 I_2 N_1) \cos i + (I_3 N_2 N_3 - I_2 N_3^2 + I_1 N_1 N_2 - I_2 N_1^2) \cos 2i \\ (I_2 I_3 N_2 - I_2^2 N_3 + I_1 I_3 N_1 - I_1^2 N_3) \cos i + (I_2 N_2 N_3 - I_3 N_2^2 - I_3 N_1^2 + I_1 N_1 N_3) \cos 2i \end{pmatrix} \quad (56)$$

The determinant of M (det M) =

$$\begin{vmatrix} (I_2 N_3 - I_3 N_2) & (I_3 N_1 - I_1 N_3) & (I_1 N_2 - I_2 N_1) \\ N_1 & N_2 & N_3 \\ I_1 & I_2 & I_3 \end{vmatrix} \\ = - (I_2 N_3 - I_3 N_2)^2 - (I_1 N_3 - I_3 N_1)^2 - (I_1 N_2 - I_2 N_1)^2 \quad (57)$$

$$\begin{pmatrix} X \\ Y \\ Z \end{pmatrix} = \frac{\begin{pmatrix} (I_2^2 N_1 - I_1 I_2 N_2 - I_1 I_3 N_3 + I_3^2 N_1) \cos i + (I_1 N_2^2 - I_2 N_1 N_2 - I_3 N_1 N_3 + I_1 N_3^2) \cos 2i \\ (I_1^2 N_2 - I_1 I_2 N_1 - I_2 I_3 N_3 + I_3^2 N_2) \cos i + (I_2 N_1^2 - I_1 N_1 N_2 - I_3 N_2 N_3 + I_2 N_3^2) \cos 2i \\ (I_1^2 N_3 - I_1 I_3 N_1 - I_2 I_3 N_2 + I_2^2 N_3) \cos i + (I_3 N_1^2 - I_1 N_1 N_3 - I_2 N_2 N_3 + I_3 N_2^2) \cos 2i \end{pmatrix}}{(I_1 N_2 - I_2 N_1)^2 + (I_2 N_3 - I_3 N_2)^2 + (I_1 N_3 - I_3 N_1)^2} \quad (58)$$

$$X = \frac{(I_2^2 N_1 - I_1 I_2 N_2 - I_1 I_3 N_3 + I_3^2 N_1) \cos i + (I_1 N_2^2 - I_2 N_1 N_2 - I_3 N_1 N_3 + I_1 N_3^2) \cos 2i}{(I_1 N_2 - I_2 N_1)^2 + (I_2 N_3 - I_3 N_2)^2 + (I_1 N_3 - I_3 N_1)^2} \quad (59)$$

$$Y = \frac{(I_1^2 N_2 - I_1 I_2 N_1 - I_2 I_3 N_3 + I_3^2 N_2) \cos i + (I_2 N_1^2 - I_1 N_1 N_2 - I_3 N_2 N_3 + I_2 N_3^2) \cos 2i}{(I_1 N_2 - I_2 N_1)^2 + (I_2 N_3 - I_3 N_2)^2 + (I_1 N_3 - I_3 N_1)^2} \quad (60)$$

$$Z = \frac{(I_1^2 N_3 - I_1 I_3 N_1 - I_2 I_3 N_2 + I_2^2 N_3) \cos i + (I_3 N_1^2 - I_1 N_1 N_3 - I_2 N_2 N_3 + I_3 N_2^2) \cos 2i}{(I_1 N_2 - I_2 N_1)^2 + (I_2 N_3 - I_3 N_2)^2 + (I_1 N_3 - I_3 N_1)^2} \quad (61)$$

CASE 1: HORIZONTAL SURFACE ($S = \gamma = 0$):

If the slope (s) and azimuth (γ) of the surface are both zero (surface is horizontal), then from (39), (40) and (41): $N_1 = N_2 = 0$ and $N_3 = 1$.

The direction cosines of R (X , Y , and Z) from (59), (60) and (61) become

$$X = \frac{I_1(\cos 2i - I_3 \cos i)}{I_1^2 + I_2^2} = \frac{\sin A(\cos 2i - \cos z \cos i)}{\sin z} \quad (62)$$

$$Y = \frac{I_2(\cos 2i - I_3 \cos i)}{I_1^2 + I_2^2} = \frac{\cos A(\cos 2i - \cos z \cos i)}{\sin z} \quad (63)$$

$$Z = \cos i \quad (64)$$

Equation (28) with $s = \gamma = 0$ becomes

$$\cos i = \cos z \quad (65)$$

Substituting (65) and the identity $\cos 2i = 2 \cos^2 i - 1$ into (62), (63) and (64) and using $\sin^2 i + \cos^2 i = 1$, (32) becomes

$$R = -\sin z \sin A i - \sin z \cos A j + \cos z k \quad (66)$$

From (30), a unit vector in the direction of an incident sun ray is

$$-I = -\sin z \sin A i - \sin z \cos A j - \cos z k \quad (67)$$

Note: The direction cosines for the X and Y axis of (66) and (67) are equal but the direction cosines for the Z axis are supplementary.

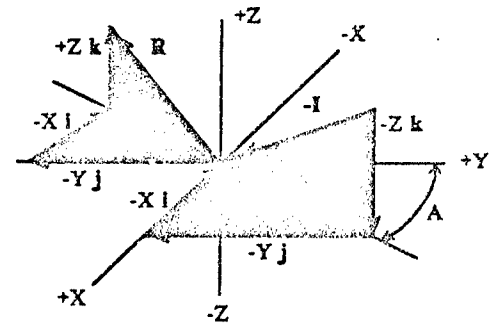


Figure 430

CASE 2: VERTICAL SURFACE FACING SOUTH ($S = 90^\circ$, $\gamma = 0$):

If the slope (s) of the reflecting surface is 90° and the azimuth (γ) of the surface is zero (surface is vertical and facing south), then from (36), (37)...,(43):

$$I_1 = \sin z \sin A$$

$$I_2 = \sin z \cos A, I_3 = \cos z$$

$$N_1 = 0, N_2 = 1, N_3 = 0,$$

$$\cos i = \sin z \cos A$$

$$\cos 2i = 2 \sin^2 z \cos^2 z - 1$$

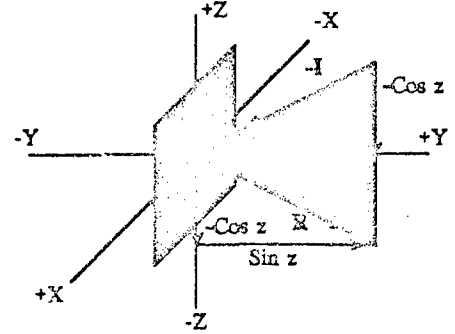


Figure 431

The direction cosines of R (X , Y , and Z) from (59), (60) and (61) become

$$X = 0 \quad (68)$$

$$Y = \frac{\cos^2 z \sin z}{\cos^2 z} = \sin z \quad (69)$$

$$Z = \frac{-\sin^2 z \cos z + \cos z (2\sin^2 z - 1)}{\cos^2 z} = -\cos z \quad (70)$$

Equation (32) becomes

$$R = \sin z \mathbf{j} - \cos z \mathbf{k} \quad (71)$$

From (30), a unit vector in the direction of an incident sun ray is

$$-I = -\sin z \mathbf{j} - \cos z \mathbf{k} \quad (72)$$

DISTRIBUTION LIST

	Copies
Commander Defense Technical Information Center Bldg. 5, Cameron Station ATTN: DDAC Alexandria, VA 22304-9990	2
Manager Defense Logistics Studies Information Exchange ATTN: AMXMC-D Fort Lee, VA 23801-6044	2
Commander U.S. Army Tank-Automotive Command ATTN: ASQNC-TAC-DIT (Technical Library) Warren, MI 48397-5000	2
Commander U.S. Army Tank-Automotive Command ATTN: AMSTA-CF Warren, MI 48397-5000	1
Director U.S. Army Material Systems Analysis Activity ATTN: AMXSY-D (Mr. Kramer) Aberdeen Proving Ground, MD 21005-5071	1
Commander U.S. Army Tank-Automotive Command ATTN: SFAE-ASM -SS (MAJ S. Cooper) Warren, MI 48397-5000	1
Commander U.S. Army Combined Arms Center ATTN: ATZL-CDE-D (Mr. A. Hauschild) Ft. Leavenworth, KS 66027	1